THE ROLE OF EPIGENETIC MODIFICATIONS IN CANCER PROGRESSION VOLUME II

EDITED BY: Hailong Pei, Lei Chang, Hongquan Zhang and Atsushi Fujimura
PUBLISHED IN: Frontiers in Oncology and Frontiers in Cell and Developmental Biology

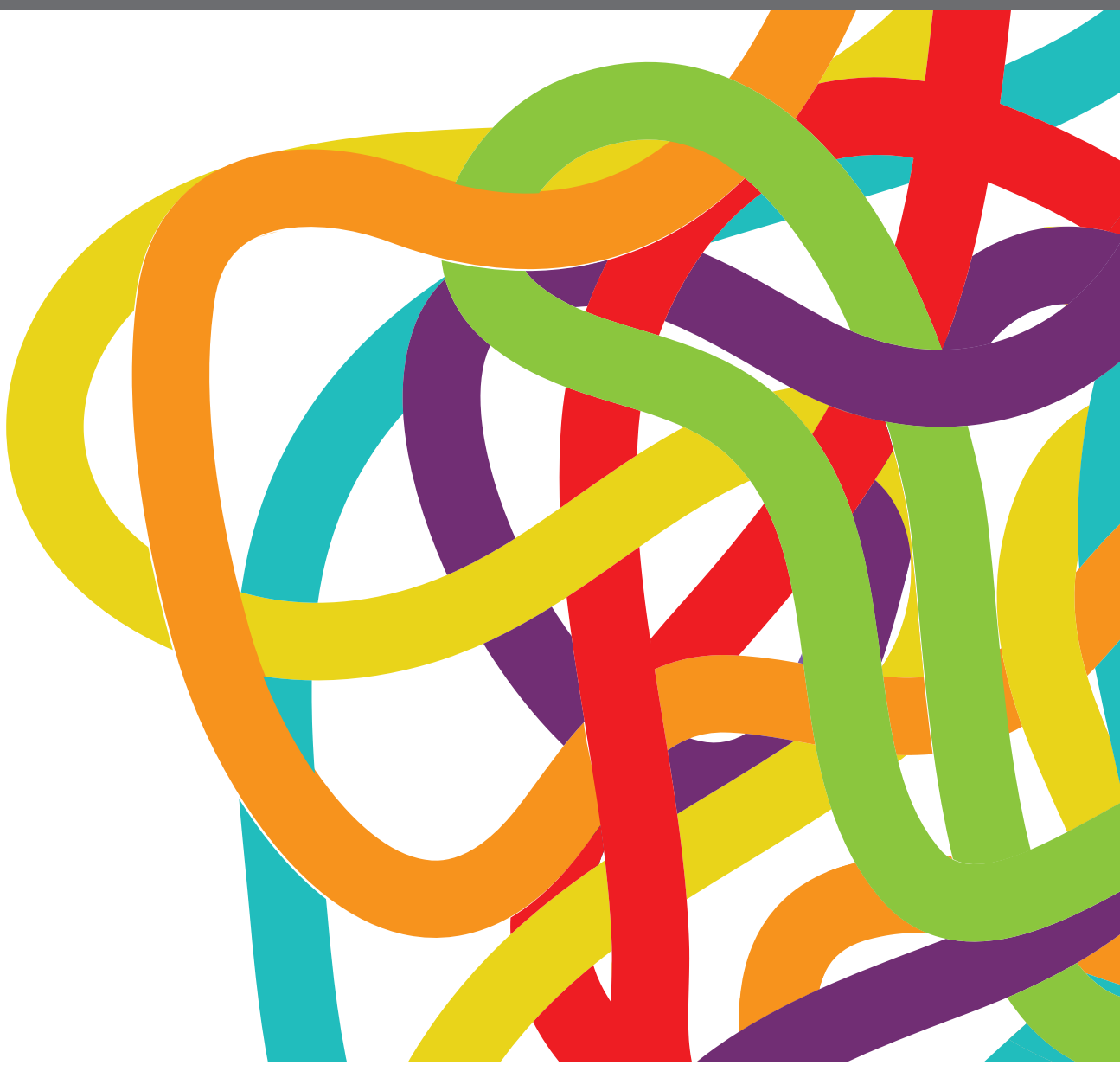

frontiers Research Topics

frontiers

ISSN 1664-8714
ISBN 978-2-88976-299-6
DOI 10.3389/978-2-88976-299-6

About Frontiers

Frontiers is more than just an open-access publisher of scholarly articles: it is a pioneering approach to the world of academia, radically improving the way scholarly research is managed. The grand vision of Frontiers is a world where all people have an equal opportunity to seek, share and generate knowledge. Frontiers provides immediate and permanent online open access to all its publications, but this alone is not enough to realize our grand goals.

Frontiers Journal Series

The Frontiers Journal Series is a multi-tier and interdisciplinary set of open-access, online journals, promising a paradigm shift from the current review, selection and dissemination processes in academic publishing. All Frontiers journals are driven by researchers for researchers; therefore, they constitute a service to the scholarly community. At the same time, the Frontiers Journal Series operates on a revolutionary invention, the tiered publishing system, initially addressing specific communities of scholars, and gradually climbing up to broader public understanding, thus serving the interests of the lay society, too.

Dedication to Quality

Each Frontiers article is a landmark of the highest quality, thanks to genuinely collaborative interactions between authors and review editors, who include some of the world's best academicians. Research must be certified by peers before entering a stream of knowledge that may eventually reach the public - and shape society; therefore, Frontiers only applies the most rigorous and unbiased reviews.
Frontiers revolutionizes research publishing by freely delivering the most outstanding research, evaluated with no bias from both the academic and social point of view. By applying the most advanced information technologies, Frontiers is catapulting scholarly publishing into a new generation.

What are Frontiers Research Topics?

Frontiers Research Topics are very popular trademarks of the Frontiers Journals Series: they are collections of at least ten articles, all centered on a particular subject. With their unique mix of varied contributions from Original Research to Review Articles, Frontiers Research Topics unify the most influential researchers, the latest key findings and historical advances in a hot research area! Find out more on how to host your own Frontiers Research Topic or contribute to one as an author by contacting the Frontiers Editorial Office: frontiersin.org/about/contact

THE ROLE OF EPIGENETIC MODIFICATIONS IN CANCER PROGRESSION VOLUME II

Topic Editors:
Hailong Pei, Soochow University, China
Lei Chang, Soochow University Medical College (SUMC), China
Hongquan Zhang, Peking University, China
Atsushi Fujimura, Okayama University, Japan

Citation: Pei, H., Chang, L., Zhang, H., Fujimura, A., eds. (2022). The Role of Epigenetic Modifications in Cancer Progression Volume II.
Lausanne: Frontiers Media SA. doi: 10.3389/978-2-88976-299-6

Table of Contents

04 ***HPV-Related Promoter Methylation-Based Gene Signature Predicts Clinical Prognosis of Patients With Cervical Cancer***
Ran Zhou, Zhuo Chen, Zuo-Run Xiao, Shou-Li Wang and Chao Rong

13 ***Non-Coding RNAs Associated With Radioresistance in Triple-Negative Breast Cancer***
Alberto Aranza-Martínez, Julio Sánchez-Pérez, Luis Brito-Elias, César López-Camarillo, David Cantú de León, Carlos Pérez-Plasencia and Eduardo López-Urrutia

28 ***Methyltransferase-Like 3-Mediated m6A Methylation of Hsa_circ_0058493 Accelerates Hepatocellular Carcinoma Progression by Binding to YTH Domain-Containing Protein 1***
Anqi Wu, Yuhao Hu, Yao Xu, Jing Xu, Xinyue Wang, Aiting Cai, Ruoyu Liu, Lin Chen and Feng Wang

40 ***Long Non-coding RNAs LINC01679 as a Competitive Endogenous RNAs Inhibits the Development and Progression of Prostate Cancer via Regulating the miR-3150a-3p/SLC17A9 Axis***
Yuan-yuan Mi, Chuan-yu Sun, Li-feng Zhang, Jun Wang, Hong-bao Shao, Feng Qin, Guo-wei Xia and Li-jie Zhu

58 ***Value of Contrast-Enhanced Ultrasound in the Preoperative Evaluation of Papillary Thyroid Carcinoma Invasiveness***
Lei Chen, Luzeng Chen, Zhenwei Liang, Yuhong Shao, Xiuming Sun and Jinghua Liu

66 ***An Overview of Epigenetic Methylation in Pancreatic Cancer Progression***
Yuhao Zhao, Mao Yang, Shijia Wang, Sk Jahir Abbas, Junzhe Zhang, Yongsheng Li, Rong Shao and Yingbin Liu

78 ***Gene Promoter-Methylation Signature as Biomarker to Predict Cisplatin-Radiotherapy Sensitivity in Locally Advanced Cervical Cancer***
Carlos Contreras-Romero, Eloy-Andrés Pérez-Yépez, Antonio Daniel Martinez-Gutierrez, Alma Campos-Parra, Alejandro Zentella-Dehesa, Nadia Jacobo-Herrera, César López-Camarillo, Guillermo Corredor-Alonso, Jaime Martínez-Coronel, Mauricio Rodríguez-Dorantes, David Cantu de León and Carlos Pérez-Plasencia

88 ***The Status and Prospects of Epigenetics in the Treatment of Lymphoma***
Jiaxin Liu, Jia-nan Li, Hongyu Wu and Panpan Liu

111 ***CpG Site-Specific Methylation-Modulated Divergent Expression of* PRSS3 *Transcript Variants Facilitates Nongenetic Intratumor Heterogeneity in Human Hepatocellular Carcinoma***
Shuye Lin, Hanli Xu, Mengdi Pang, Xiaomeng Zhou, Yuanming Pan, Lishu Zhang, Xin Guan, Xiaoyue Wang, Bonan Lin, Rongmeng Tian, Keqiang Chen, Xiaochen Zhang, Zijiang Yang, Fengmin Ji, Yingying Huang, Wu Wei, Wanghua Gong, Jianke Ren, Ji Ming Wang, Mingzhou Guo and Jiaqiang Huang

128 ***Chk1 Inhibition Hinders the Restoration of H3.1K56 and H3.3K56 Acetylation and Reprograms Gene Transcription After DNA Damage Repair***
Nan Ding, Zhiang Shao, Fangyun Yuan, Pei Qu, Ping Li, Dong Lu, Jufang Wang and Qianzheng Zhu

frontiers in Oncology

ORIGINAL RESEARCH
published: 21 October 2021
doi: 10.3389/fonc.2021.753102

HPV-Related Promoter Methylation-Based Gene Signature Predicts Clinical Prognosis of Patients With Cervical Cancer

Ran Zhou[1†], Zhuo Chen[2†], Zuo-Run Xiao[3], Shou-Li Wang[3] and Chao Rong[3*]*

[1] Department of Pharmacy, The First Affiliated Hospital of USTC, Division of Life Sciences and Medicine, University of Science and Technology of China, Hefei, China, [2] Department of Pathology, The First Affiliated Hospital of USTC, Division of Life Sciences and Medicine, University of Science and Technology of China, Hefei, China, [3] Department of Pathology, School of Biology & Basic Medical Sciences, Soochow University, Suzhou, China

OPEN ACCESS

Edited by:
Atsushi Fujimura, Okayama University, Japan

Reviewed by:
Yara Lucia Furtado, Federal University of Rio de Janeiro, Brazil
Vineeta Batra, University of Delhi, India

***Correspondence:**
Shou-Li Wang
wangshouli@suda.edu.cn
Chao Rong
chaorong@suda.edu.cn

[†]These authors have contributed equally to this work

Specialty section:
This article was submitted to Molecular and Cellular Oncology, a section of the journal Frontiers in Oncology

Received: *04 August 2021*
Accepted: *06 October 2021*
Published: *21 October 2021*

Citation:
Zhou R, Chen Z, Xiao Z-R, Wang S-L and Rong C (2021) HPV-Related Promoter Methylation-Based Gene Signature Predicts Clinical Prognosis of Patients With Cervical Cancer. Front. Oncol. 11:753102. doi: 10.3389/fonc.2021.753102

Persistent high-risk HPV infection drives tumorigenesis in various human malignancies, including cervical, oropharyngeal, anal, and vulvar carcinomas. Although HPV-related tumors arise in several different sites, they share many common genetic and epigenetic events. Complex and heterogeneous genomic aberrations and mutations induced by high-risk HPV contribute to the initiation and progression of cervical cancer (CC). However, the associations between high-risk HPV infection and DNA methylation have not been clearly investigated. In the present study, HPV-related gene promoter methylation signature was comprehensively analyzed using multiple interactive platforms. CC patients were successfully classified into high-risk and low-risk groups with significant differences in clinical outcomes based on the HPV-related gene promoter methylation signature. Moreover, the protein levels of ALDH1A2 and clinical prognostic value were confirmed in the CC patients cohort. In summary, our study provides compelling evidence that HPV-related gene promoter methylation signature serves as a strong prognostic signature for CC patients. Clinical investigations in large CC patient cohorts are greatly needed to pave the way to implement epigenetic biomarkers into better clinical management.

Keywords: cervical cancer, human papillomavirus (HPV), DNA methylation, prognostic biomarkers, gene signature

INTRODUCTION

Cervical cancer (CC) is one of the most prevalent and lethal human malignancies worldwide. It is widely recognized that persistent infection with high-risk types of the human papillomavirus (HPV) leads to transformation from cervical intraepithelial neoplasia (CIN) to neoplasms (1, 2). Although improvements have been achieved in early cytomorphological screening, vaccines against HPV, advanced treatment strategies, the incidence and mortality have increased over the past decades, especially in developing countries (3, 4). In China, 140,000 new cases and 80,000 women deaths from CC occur annually, which affected youth trends more clearly (5). Consequently, better therapy and

stratification of patients with CC at high risk of treatment failure remains a significant challenge, and there is urgently needed to identify promising diagnostic and prognostic biomarkers.

Complex and heterogeneous genomic aberrations and mutations induced by high-risk HPV contribute to the initiation and progression of CC (6–8). However, the association between high-risk HPV infection and DNA methylation has not been investigated. A growing number of studies suggest that epigenetic abnormalities such as aberrant DNA hypermethylation within gene promoters in various tumor entities, including CC (9, 10). For example, well-known tumor suppressors or tumor-related genes (*CDH1, CDKN2A, DAPK*, etc.) are silenced by promoter methylation in CC (11). High-risk HPV infection has been demonstrated to regulate DNA methylation in HPV-related cancers. Both E6 and E7 viral oncogene were reported to affect DNA methyltransferase activity, which increased our understanding of molecular principles underlying the pathogenesis of HPV-related cancers (12–14). In the past, an HPV-related gene promoter methylation signature of 5 genes (*ALDH1A2, OSR2, GRIA4, GATA4,* and *IRX4*) was identified in HPV-driven head and neck squamous carcinoma (HNSCC) by a genome-wide array approach (15). The significant correlation between promoter hypermethylation and suppressed gene expression indicated a vital role of candidate genes in HPV-related cancers.

The promising prediction value of HPV-related gene promoter methylation signature raised the attractive question of whether the gene signature could be employed as a reliable prognosticator for clinical staging and prognosis of CC. In the present study, HPV-related gene promoter methylation signature was comprehensively analyzed using multiple interactive platforms, including cBioPortal, GEPIA2, UALCAN (16–18). In addition, HPV-related methylation-based gene signature and clinical prognosis of patients with CC were examined in The Cancer Genome Atlas (TCGA) database (19). Finally, the correlation of ALDH1A2 protein expression and clinical prognostic value was confirmed in the CC patient cohort.

RESULTS

Comprehensive Analysis of the HPV-Related Gene Signature in Multiple Cancer Types

To evaluate the differentially expressed HPV-related gene signature between tumor and normal tissues, the online web server GEPIA2 was applied to analyze the gene expression data from TCGA cohorts and GTEx projects. Differential signature score analysis revealed that the HPV-related gene signature was significantly reduced in the tumor tissues of eight cancer cohorts as compared to the expression levels in corresponding non-tumor tissues, including Cervical squamous cell carcinoma and endocervical adenocarcinoma (CESC), Breast invasive carcinoma (BRCA), Acute Myeloid Leukemia (LAML), Ovarian serous cystadenocarcinoma (OV), Skin Cutaneous Melanoma (SKCM), Testicular Germ Cell Tumors (TGCT), Uterine Corpus Endometrial Carcinoma (UCEC), Uterine Carcinosarcoma (UCS). In the cohort of CESC, 306 tumor tissues and 13 normal tissues were compared (**Figure 1A**). A pan-cancer analysis with 10,967 tumor samples in 32 TCGA cohorts revealed that a low frequency of *ALDH1A2* (1.4%), *OSR2* (5%), *GRIA4* (3%), *GATA4* (4%), and *IRX4* (5%) was genetically altered. The high frequency of genetic alterations in the five genes was observed in several cancers, including esophageal adenocarcinoma (30.77%), bladder urothelial carcinoma (29.68%), uterine carcinosarcoma (28.07%), lung adenocarcinoma (27.56%), lung squamous cell carcinoma (27.52%) (**Figure 1B**). 13.8% of 297 cervical squamous cell carcinoma cases revealed that genetic alterations in the five-gene signature with a low frequency of *ALDH1A2* (1.3%), *OSR2* (1%), *GRIA4* (4%), *GATA4* (1%), and *IRX4* (7%) (**Figure 1C**). Together, the gene expression level of HPV-related gene signature was significantly lower in cervical cancer as compared to the level of normal tissues. In contrast, a rather low frequency of genetic alterations was observed.

Promoter Methylation of HPV-Related Gene Signature in Cervical Cancer

To investigate the promoter methylation data of HPV-related gene signature in cervical cancer, we applied an interactive web-portal UALCAN to perform analyses for TCGA-CESC. Box whisker plots revealed that promoter DNA methylation levels (average beta values) of *ALDH1A2, GATA4, GRIA4*, and *IRX4* were significantly elevated in primary tumors as compared to normal tissues (**Figure 2A**). It is generally accepted that gene promoter hypermethylation may downregulate transcription of the affected gene. We observed a significant inverse correlation between gene promoter methylation and relative transcript levels for *ALDH1A2, OSR2*, and *IRX4* (**Figure 2B**). Differential expression analysis revealed that the levels of *ALDH1A2* and *OSR2* were significantly reduced in the tumor tissues as compared to the normal tissues (**Figure 2C**). Thus, our findings suggest that *ALDH1A2*, *OSR2* gene transcription is regulated by gene promoter methylation, which is suppressed in the primary tumors. In addition, promoter DNA methylation levels (average beta values) of *ALDH1A2, OSR2, GATA4, GRIA4*, and *IRX4* were compared among the patients with different clinical stages. Box whisker plots showed that promoter DNA methylation levels of *ALDH1A2* in tumor clinical stage IV were significantly elevated than any other subgroup with stage I/II/III (**Figure 3A**). Concerning average beta values of *GATA4, GRIA4*, and *IRX4*, the patients with tumor stage IV had the highest level as compared to the subgroup patients with stage I/II/III tumor (**Figures 3C–E**). By contrast, *OSR2* promoter DNA methylation level in patients with stage I tumors was significantly higher as compared to the patients with stage III/IV tumors (**Figure 3B**). In summary, promoter methylation of HPV-related gene signature is significantly associated with the CC clinical stage.

HPV-Related Methylation-Based Gene Signature Was Significantly Associated With the Clinical Prognosis of Patients With Cervical Cancer

Next, we asked whether HPV-related methylation-based gene signature is associated with the clinical prognosis of patients with

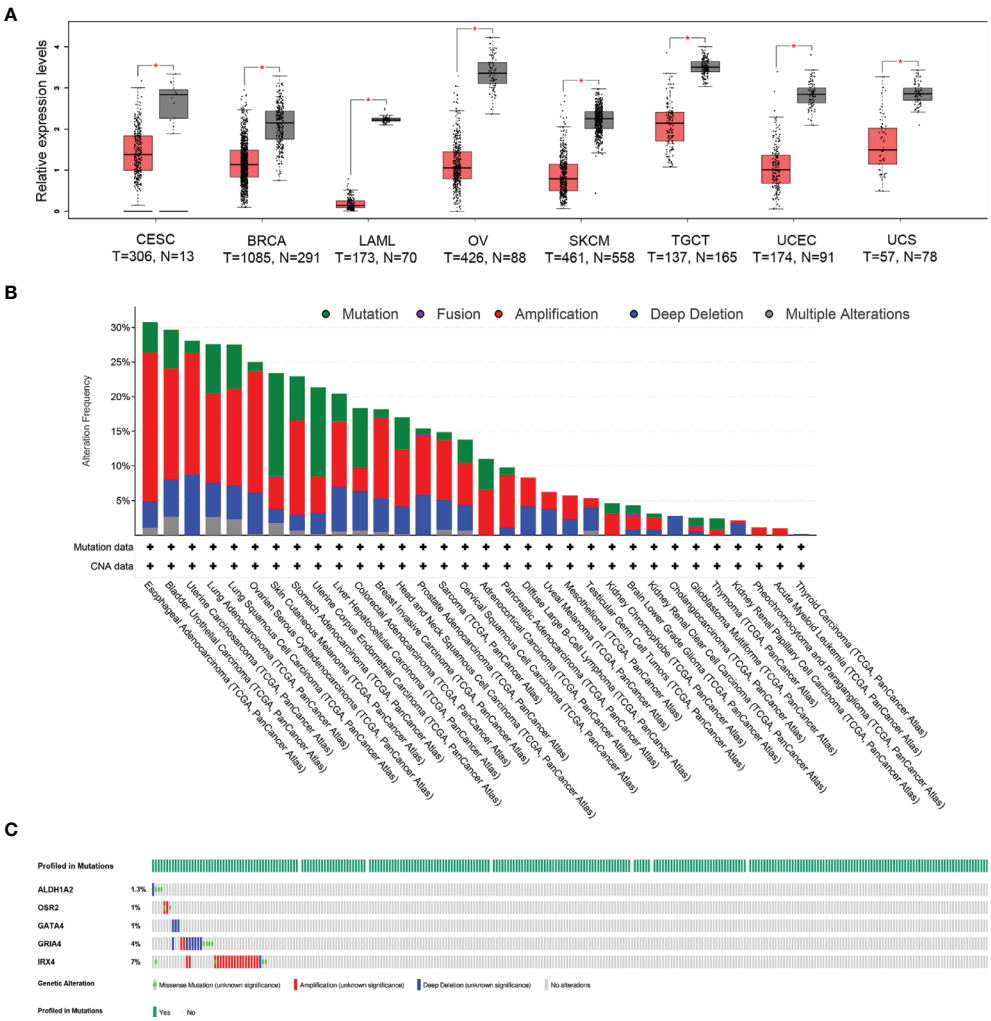

FIGURE 1 | Different expression and mutational landscape of HPV-related gene signature in multiple TCGA-cohorts. **(A)** The significantly different expression profile of HPV-related gene signature between tumor and normal tissues (GTEx database) was identified in eight TCGA-cohorts, including Cervical squamous cell carcinoma and endocervical adenocarcinoma (CESC), Breast invasive carcinoma (BRCA), Acute Myeloid Leukemia (LAML), Ovarian serous cystadenocarcinoma (OV), Skin Cutaneous Melanoma (SKCM), Testicular Germ Cell Tumors (TGCT), Uterine Corpus Endometrial Carcinoma (UCEC), Uterine Carcinosarcoma (UCS), *$P < 0.05$. **(B)** Genetic alterations of HPV-related gene signature from 32 TCGA-cohorts were presented. **(C)** Oncoprint shows genetic alterations of the five-gene signature in the cohort of CESC.

cervical cancer. A heat map based on *ALDH1A2*, *OSR2*, *GATA4*, *GRIA4*, and *IRX4* transcript levels were generated by the *SurvExpress* web tool, and two clusters with either low or high prognostic risk were defined by prognostic index (PI) and Cox fitting (20, 21) (**Figure 4A**). The expression level of the five genes was compared between the high-risk group (n=86) and the low-risk group (n=175), which revealed the levels of the five genes were significantly reduced in the high-risk group (**Figure 4B**). As expected, the age of patients and the number of death events in the high-risk group are significantly higher as compared to the low-risk group (**Figures 4C, D**). Chi-square analysis showed the low-risk group is significantly associated with younger age (P=0.002) and lower T status (p=0.006) (**Supplementary Table S1**). Furthermore, the Kaplan-Meier plot and Log-Rank analysis exhibited a significant difference in overall survival between the high and low-risk groups (**Figure 4E**; Log-rank = 16.446, $P < 0.001$). In summary, these findings demonstrated that HPV-related methylation-based gene signature predicts the clinical outcome for CC patients.

The Protein Levels of ALDH1A2 in Cervical Cancer Were Correlated With Clinical Outcomes

To confirm the prognostic value of the candidate gene *ALDH1A2* in the protein level, we determined ALDH1A2 protein levels by immunohistochemical (IHC) staining in primary tumor tissues from patients with cervical cancer, and we found the heterogeneous cytoplasmic expression of ALDH1A2 in tumor tissues (**Figure 5A**). The patients were divided into two subgroups depending on different immunoreactivity scores (IRS) with $ALDH1A2^{high}$ (n =

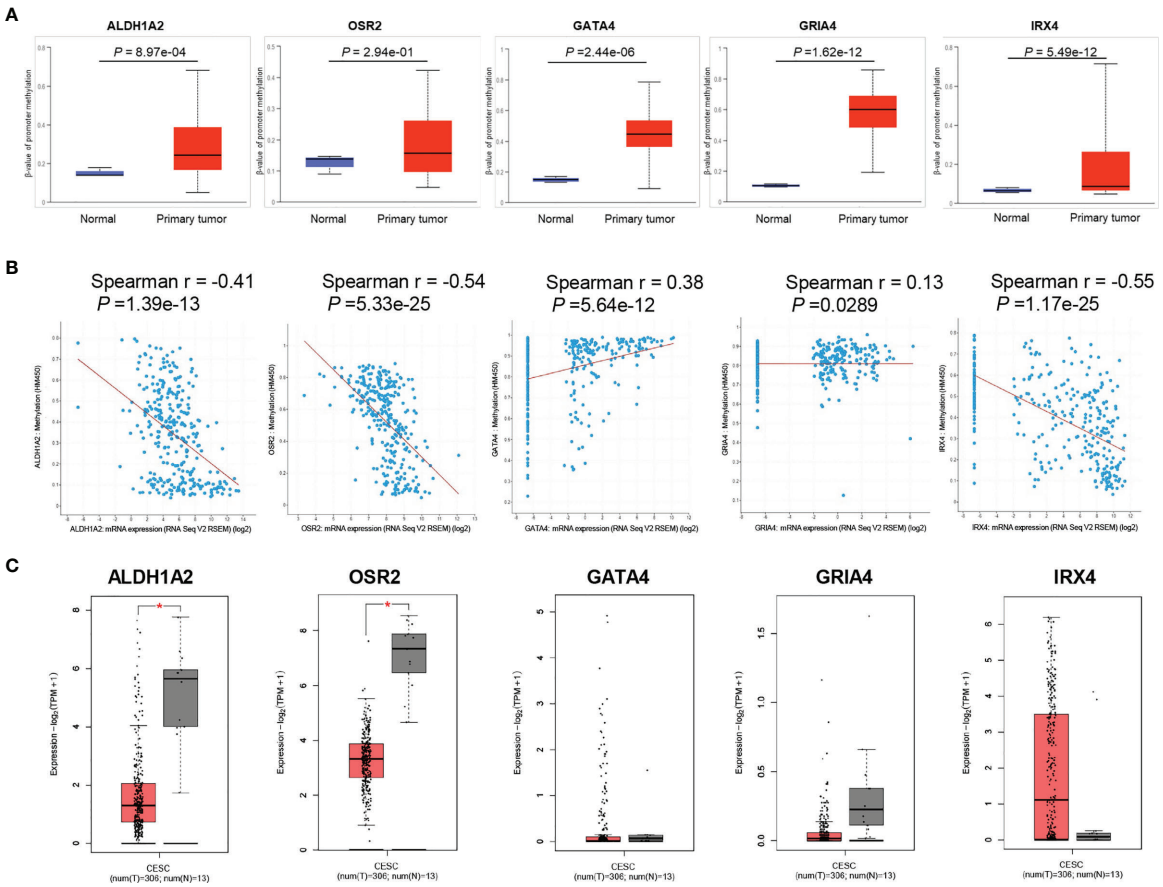

FIGURE 2 | Promoter methylation analysis of HPV-related gene signature in TCGA-CESC cohort. **(A)** Box and whisker plots revealed methylation β-values of HPV-related gene signature between tumor and normal tissues, *P* values were presented for each gene. **(B)** Spearman correlation analysis between gene promoter methylation and relative transcript levels for each gene were performed by the cBioPortal tool, *P* values were presented for each gene. **(C)** The significantly different expression level of each gene was presented by boxplots, $^{*}P < 0.05$.

13) and ALDH1A2^{low} (n = 37) for further analysis. The patients with clinical stage I/II had a statistically higher IRS of ALDH1A2 as compared to the patients with stage III/IV (**Figure 5B**), which was in line with our *in silico* analysis findings. Survival analysis revealed that patients with ALDH1A2^{low} expression tumors had a significantly worse disease-specific survival (DSS) as compared to the patients with ALDH1A2^{high} expression pattern (**Figure 5C**). Taken together, our results showed low expression of ALDH1A2 serves as an unfavorable risk factor and a prognosticator to identify patients with cervical cancer at high risk for treatment failure.

DISCUSSION

Persistent high-risk HPV infection drives tumorigenesis in various types of human malignancies, including cervical, oropharyngeal, anal, and vulvar carcinomas (22–24). Although HPV-related tumors arise in several different sites, they share many common genetic and epigenetic events. As one of the most significant epigenetic modifications, aberrant DNA methylation is a fundamental epigenetic event for HPV-related carcinogenesis. DNA methylation signatures have been proven to predict the clinical prognosis in a variety of cancers (25–29). In the past, HPV-related alterations in the DNA methylome of patients with oropharyngeal squamous cell carcinoma (OPSCC) were screened, and a methylation score based on the five-gene promoter methylation pattern was identified for a reliable prognostic factor (15). The significant correlation between promoter hypermethylation and suppressed gene-level indicated the critical function of candidate genes in HPV-driven carcinogenesis and the response to treatment.

In this study, we performed the first comprehensive analysis of HPV-related gene promoter methylation signature of five-gene (*ALDH1A2, OSR2, GRIA4, GATA4*, and *IRX4*) in TCGA database. We found the total expression level of HPV-related gene signature was significantly lower in cervical cancer as compared to the level of normal tissues, whereas a rather low frequency of genetic alterations was observed. In addition, promoter DNA methylation levels (average beta values) of *ALDH1A2*, *GATA4*, *GRIA4*, and *IRX4* were significantly

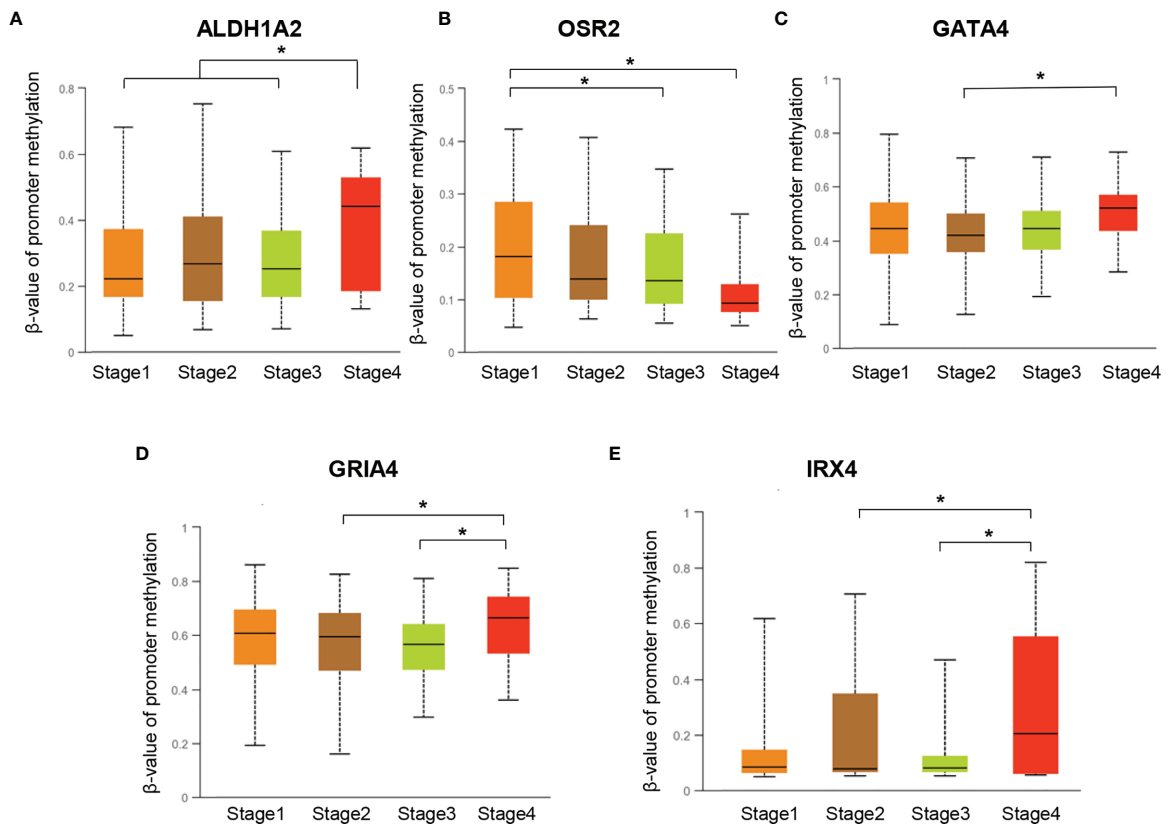

FIGURE 3 | Promoter DNA methylation levels of ALDH1A2 **(A)**, OSR2 **(B)**, GATA4 **(C)**, GRIA4 **(D)**, and IRX4 **(E)** were compared among the patients with different clinical-stages, *$P < 0.05$.

elevated in primary cervical carcinoma as compared to normal tissues. As expected, differential expression analysis revealed that the levels of *ALDH1A2* and *OSR2* were significantly reduced in the tumor tissues as compared to the normal tissues. Elevated promoter DNA methylation level of *ALDH1A2* was observed in the advanced clinical stage, suggesting that *ALDH1A2* gene expression was associated with the clinical outcome in cervical cancer patients. Despite aberrant promoter hypermethylation of *ALDH1A2*, *OSR2*, *GATA4*, and *GRIA4* have already been reported in several human tumor cell lines or tumor tissues. To the best of our knowledge, there is no study focusing on the methylation signature of five genes in cervical cancer. To highlight the prognostic value of HPV-related methylation signature, a risk-scoring model was established, and the risk scores were calculated based on *ALDH1A2*, *OSR2*, *GATA4*, *GRIA4*, and *IRX4* transcript levels as well as the regression coefficient of each gene. We found the ages, cancer-related death events, T status were significantly different between patients in high-risk and low-risk subgroups. We also observed the significantly different overall survival between two risk groups, which was evaluated by Kaplan-Meier analysis and log-rank test. A previous study reported that CC patients could be divided into three heterogeneous clusters base on HPV-related methylation sites, which supports that DNA methylation sites can serve as biomarkers for subgroup identification and prognostic risk stratification (30). Despite these promising achievements, heterogeneous clusters based on the HPV-related methylation sites turned out to be a limitation for the potential translation into clinical practice.

So far, our study investigated the one gene-encoded protein expression, *ALDH1A2*, in the primary tumor tissues from patients with cervical carcinoma. We excluded the *GATA4*, *GRIA4*, and *IRX4* genes due to no significant difference between the tumor tissues and the normal tissues in cervical carcinoma based on the TCGA-CESC data. Promoter DNA methylation levels (average beta values) of *OSR2* revealed no significant changes between primary tumors and normal tissues. Moreover, low cancer specificity of *OSR2* was found based on the literature review. Our presented data indicate that the expression and function of the *ALDH1A2* gene are more relevant for the clinical prognosis of CC patients. The gene *ALDH1A2* encodes aldehyde dehydrogenase one family member A2 (ALDH1A2), which is a rate-limiting enzyme involved in the cellular synthesis of retinoic acid. Previous studies have demonstrated ALDH1A2 to be a candidate tumor suppressor in several human malignancies, including prostate, head and neck, ovarian cancer (15, 31–33). However, it had not been determined whether reduced ALDH1A2 protein expression is relevant to the prognosis of CC patients. Therefore, ALDH1A2, promisingly

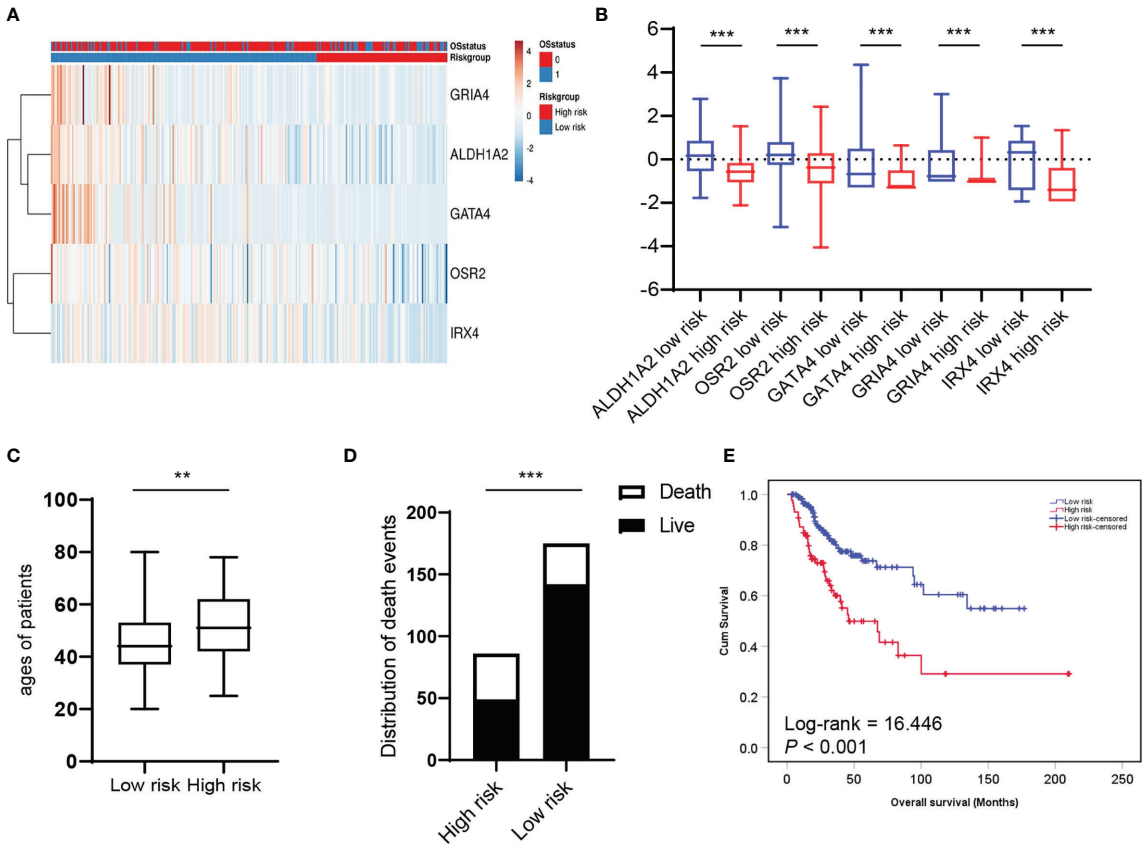

FIGURE 4 | HPV-related methylation-based gene signature is associated with the clinical prognosis of patients with cervical cancer. **(A)** Heatmap represented HPV-related gene signature expression values (rows) and tumor samples (columns) in low and high-risk groups by supervised clustering. **(B)** Box and whisker plots of HPV-related gene signature expression values were compared between two risk groups by *t*-test. The average ages **(C)** and the distribution of death events **(D)** between two risk groups were compared. **(E)** Overall survival of two risk groups was evaluated by Kaplan–Meier survival plot and Log-Rank test. $^{**}P < 0.01$, $^{***}P < 0.001$.

suitable for the clinical prognosis of CC patients, was selected to determine protein levels by immunohistochemical (IHC) staining in primary tumor tissues from patients with cervical cancer. In line with the previous studies, our results showed that the expression of ALDH1A2 at an advanced stage is lower than that at an early tumor stage. Furthermore, a low expression level of ALDH1A2 protein is significantly associated with unfavorable clinical outcomes of CC patients, which indicates that abnormal expression of ALDH1A2 might play a critical role in CC carcinogenesis and prognostic value. However, the detailed mechanism underlying the association between *ALDH1A2* gene methylation and the progression of CC requires further investigation. Moreover, we will certainly increase the number of patient cohorts and will investigate the protein expressions of four other HPV-related tumor suppressor genes in cervical cancer.

CONCLUSION

In summary, our study provides compelling evidence that HPV-related gene promoter methylation and expression successfully classify CC patients into high-risk and low-risk groups with significant differences in prognosis. The five methylated-differentially expressed genes signature was promising for the translation from bench to bedside to evaluate the prognosis of CC patients, which offers a novel strategy to identify patients at high risk for treatment failure. Moreover, encoded proteins regulated by the gene promoter methylation might serve as reliable markers for early diagnosis, risk stratification, and innovative cancer treatment.

MATERIALS AND METHODS

Bioinformatics Analysis

Mutation and CNA analyses were conducted on the TGCA PanCanAtlas datasets using the cBioPortal database version 3.6.12 (Center for Molecular Oncology at MSK, New York, NY, USA). DNA methylation data and gene expression data from TCGA-CESC were accessed through cBioPortal tool. Correlation analysis was performed between methylation beta values and log-base-2-transformed gene expression data with Pearson's correlation with a Bonferroni correction to the *P*-values.

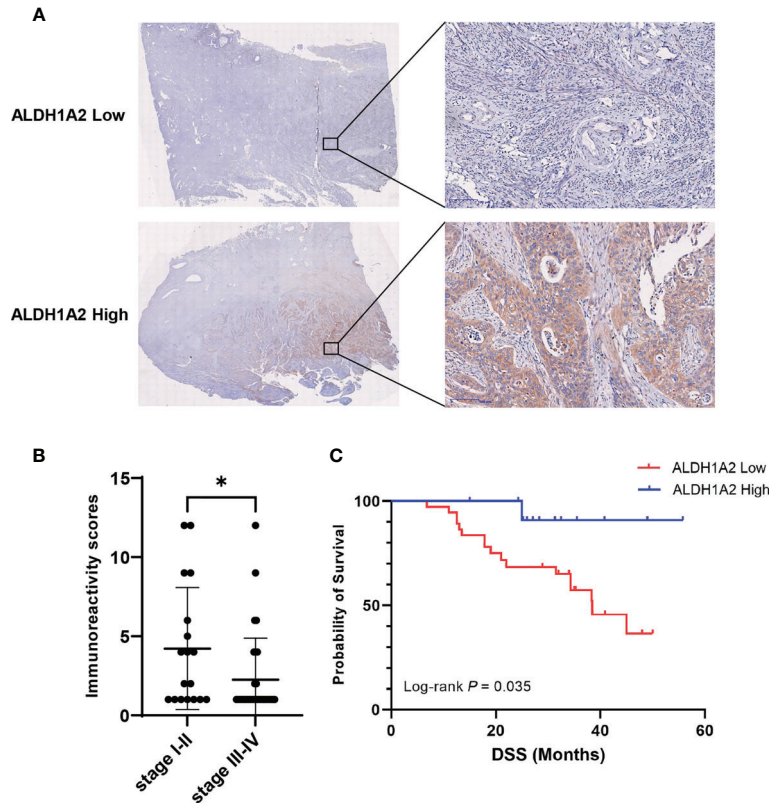

FIGURE 5 | Correlation between ALDH1A2 protein levels and clinical prognosis of patients with cervical cancer. **(A)** Representative pictures of IHC stained primary tumor sections with different expression of ALDH1A2 protein levels (brown signal). Counterstaining with hematoxylin. Scale bars:100μm. **(B)** Immunoreactivity scores were compared between the low clinical stage (I/II) (n=18) and the high clinical stage (III/IV) (n=32). Bars depict mean values ± SEM of IRS, *$P < 0.05$. **(C)** Disease-specific survival of patients with cervical cancer separated by high versus low ALDH1A2 expression. *P*-value was derived by log-rank test.

Expression in various cancers and their normal tissue counterparts were analyzed using the Gene Expression Profiling Analysis (GEPIA) (Beijing, China). GEPIA2 provides RNA sequencing data from TCGA of tumor samples with paired adjacent TCGA and Genotype-Tissue Expression (GTEx) normal tissue samples. TCGA and GTEx RNA-Seq expression datasets in GEPIA are based on the UCSC (University of California, Santa Cruz) Xena project (34), which are recomputed based on a uniform bioinformatic pipeline to eliminate batch effects. To compare expression data, data are normalized by quantile-normalization or other two additional normalization strategies. UALCAN database (http://ualcan.path.uab.edu) was used to compare the promoter methylation of HPV-related gene signature between normal and primary CC tissues, as well as methylation beta values of each gene among different tumor stages.

We downloaded the five genes expression profile of TCGA-CESC from cBio Cancer Genomics Portal (http://cbioportal.org) in December 2020. Low-risk and high-risk groups of patients with CC were generated depending on the prognostic index (PI) and Cox fitting. A heat map representation of the five genes expression values was made by supervised clustering with *ClustVis* (21), a freely available web server at http://biit.cs.ut.ee/clustvis/.

Patient Tissue Specimens

Patients with primary CC diagnosed and treated between 2015 and 2020 were comprised in the retrospective study cohort. Tumor tissue sections from formalin-fixed paraffin-embedded (FFPE) were obtained at the Department of Pathology, The First Affiliated Hospital of University of Science and Technology of China after approval by the ethics committee. Biopsies of non-surgically treated patients, as well as samples of patients who underwent tumor surgery, were included. All subjects gave written informed consent for data collection as it is a standard procedure in our department. Patients with suspicious clinical findings who underwent diagnostic endoscopy and/or patients before tumor surgery with a histologically confirmed diagnosis of CC were asked to consent. The protocol was approved by the Ethics Committee of the First Affiliated Hospital of USTC (Ethic No 2021/BLK02) in accordance with the declaration of Helsinki. Experimental treatment procedures were not part of this study. The patients were treated according to the guidelines for cervical cancer. The final analysis was based on 50 patients with CC (**Supplementary Table S2**). Clinical and therapeutic follow-up of the cohort was assessed retrospectively. The cohort did not include recurrences or specimens from surgery.

Immunohistochemical Staining and Pathological Scoring

Immunohistochemical staining was carried out in paraffin-embedded tissue from patients with primary CC. Tissue sections were deparaffinized and rehydrated by the following our previous study (35) and incubated with primary antibody ALDH1A2 (1:500, HPA010022, Sigma-Aldrich) at 4°C overnight. Tissue sections were incubated with a biotinylated anti-rabbit secondary antibody (Boster) for 2 h. Streptavidin-HRP (Boster) and Peroxidase Substrate (DAB) solution (MXB Biotechnologies, Fuzhou, China) were added to the tissue sections for signal development. Tissue slides were scanned using the DMS-10 Scan System (D-metrix, Suzhou). Three experienced pathologists analyzed scanned slides by using the D-metrix Viewer software (version 1.0.0). Semiquantitative analysis was performed according to the number of stained tumor cells (score A; 1, no positive cells; 2, less than 33% positive cells; 3, between 34% and 66% positive cells; 4, more than 66% positive cells), and according to the staining intensity (score B; 1, no staining; 2, weak staining; 3, moderate staining; 4, high staining). Both values were multiplied to calculate the final immunoreactivity score (IRS) for defined subgroups (final expression scores ranged 1-16).

Statistical Analysis

All statistical analysis was done using GraphPad Prism version 9.1 (GraphPad Software, USA) and IBM SPSS Statistics version 22. Differences of clinicopathological features between the low-risk and high-risk groups were compared using Chi-square Test or Fisher's exact test. Significance of the difference was calculated by student's *t*-test. Disease-specific survival (DSS) was estimated as the time from the date of primary tumor diagnosis to the date of CC-related death within the follow-up period (events) or to the date of CC unrelated death or without progression (censored). Survival difference was assessed by Kaplan-Meier plot and Log-Rank analysis. A P-value <0.05 was considered statistically significant.

DATA AVAILABILITY STATEMENT

Publicly available datasets were analyzed in this study. This data can be found here: http://cbioportal.org.

ETHICS STATEMENT

The studies involving human participants were reviewed and approved by Ethics Committee of the First Affiliated Hospital of USTC (Ethic No 2021/BLK02). The patients/participants provided their written informed consent to participate in this study.

AUTHOR CONTRIBUTIONS

CR and S-LW conceived and guided the study. RZ, ZC, and Z-RX performed the experiments. RZ, ZC and CR analyzed and interpreted the data. RZ and CR contributed to the writing and data presentation of the manuscript. All authors contributed to the article and approved the submitted version.

FUNDING

This study was supported by the grants from the Natural Science Foundation of Jiangsu Province (No. BK20200878), the Natural Science Foundation of the Jiangsu Higher Education Institutions of China (No. 20KJB310014), and the Priority Academic Program Development of Jiangsu Higher Education Institutions (PAPD).

ACKNOWLEDGMENTS

We gratefully acknowledge Ms. Yue Wu (Suzhou Cancercell Medical Testing Co., Ltd.) for excellent technical assistance.

SUPPLEMENTARY MATERIAL

The Supplementary Material for this article can be found online at: https://www.frontiersin.org/articles/10.3389/fonc.2021.753102/full#supplementary-material

REFERENCES

1. Crosbie EJ, Einstein MH, Franceschi S, Kitchener HC. Human Papillomavirus and Cervical Cancer. *Lancet* (2013) 382(9895):889–99. doi: 10.1016/S0140-6736(13)60022-7
2. Cohen PA, Jhingran A, Oaknin A, Denny L. Cervical Cancer. *Lancet* (2019) 393(10167):169–82. doi: 10.1016/S0140-6736(18)32470-X
3. Lei J, Ploner A, Elfstrom KM, Wang J, Roth A, Fang F, et al. HPV Vaccination and the Risk of Invasive Cervical Cancer. *N Engl J Med* (2020) 383(14):1340–8. doi: 10.1056/NEJMoa1917338
4. Ferreira da Silva I, Ferreira da Silva I, Koifman RJ. Cervical Cancer Treatment Delays and Associated Factors in a Cohort of Women From a Developing Country. *J Glob Oncol* (2019) 5:1–11. doi: 10.1200/JGO.18.00199
5. Chen W, Zheng R, Baade PD, Zhang S, Zeng H, Bray F, et al. Cancer Statistics in China, 2015. *CA Cancer J Clin* (2016) 66(2):115–32. doi: 10.3322/caac.21338
6. Schiffman M, Doorbar J, Wentzensen N, de Sanjose S, Fakhry C, Monk BJ, et al. Carcinogenic Human Papillomavirus Infection. *Nat Rev Dis Primers* (2016) 2:16086. doi: 10.1038/nrdp.2016.86
7. Saavedra KP, Brebi PM, Roa JC. Epigenetic Alterations in Preneoplastic and Neoplastic Lesions of the Cervix. *Clin Epigenet* (2012) 4(1):13. doi: 10.1186/1868-7083-4-13
8. Johannsen E, Lambert PF. Epigenetics of Human Papillomaviruses. *Virology* (2013) 445(1-2):205–12. doi: 10.1016/j.virol.2013.07.016
9. von Knebel Doeberitz M, Prigge ES. Role of DNA Methylation in HPV Associated Lesions. *Papillomavirus Res* (2019) 7:180–3. doi: 10.1016/j.pvr.2019.03.005
10. Zhu H, Zhu H, Tian M, Wang D, He J, Xu T. DNA Methylation and Hydroxymethylation in Cervical Cancer: Diagnosis, Prognosis and Treatment. *Front Genet* (2020) 11:347. doi: 10.3389/fgene.2020.00347
11. Bouras E, Karakioulaki M, Bougioukas KI, Aivaliotis M, Tzimagiorgis G, Chourdakis M. Gene Promoter Methylation and Cancer: An Umbrella Review. *Gene* (2019) 710:333–40. doi: 10.1016/j.gene.2019.06.023
12. Jeon S, Lambert PF. Integration of Human Papillomavirus Type 16 DNA Into the Human Genome Leads to Increased Stability of E6 and E7 mRNAs: Implications for Cervical Carcinogenesis. *Proc Natl Acad Sci U S A* (1995) 92(5):1654–8. doi: 10.1073/pnas.92.5.1654

13. Reuschenbach M, Huebbers CU, Prigge ES, Bermejo JL, Kalteis MS, Preuss SF, et al. Methylation Status of HPV16 E2-Binding Sites Classifies Subtypes of HPV-Associated Oropharyngeal Cancers. *Cancer* (2015) 121(12):1966–76. doi: 10.1002/cncr.29315
14. Steenbergen RD, Snijders PJ, Heideman DA, Meijer CJ. Clinical Implications of (Epi)Genetic Changes in HPV-Induced Cervical Precancerous Lesions. *Nat Rev Cancer* (2014) 14(6):395–405. doi: 10.1038/nrc3728
15. Kostareli E, Holzinger D, Bogatyrova O, Hielscher T, Wichmann G, Keck M, et al. HPV-Related Methylation Signature Predicts Survival in Oropharyngeal Squamous Cell Carcinomas. *J Clin Invest* (2013) 123(6):2488–501. doi: 10.1172/JCI67010
16. Gao J, Aksoy BA, Dogrusoz U, Dresdner G, Gross B, Sumer SO, et al. Integrative Analysis of Complex Cancer Genomics and Clinical Profiles Using the Cbioportal. *Sci Signal* (2013) 6(269):pl1. doi: 10.1126/scisignal.2004088
17. Tang Z, Kang B, Li C, Chen T, Zhang Z. GEPIA2: An Enhanced Web Server for Large-Scale Expression Profiling and Interactive Analysis. *Nucleic Acids Res* (2019) 47(W1):W556–60. doi: 10.1093/nar/gkz430
18. Chandrashekar DS, Bashel B, Balasubramanya SAH, Creighton CJ, Ponce-Rodriguez I, Chakravarthi B, et al. UALCAN: A Portal for Facilitating Tumor Subgroup Gene Expression and Survival Analyses. *Neoplasia* (2017) 19 (8):649–58. doi: 10.1016/j.neo.2017.05.002
19. Cancer Genome Atlas N. Comprehensive Genomic Characterization of Head and Neck Squamous Cell Carcinomas. *Nature* (2015) 517(7536):576–82. doi: 10.1038/nature14129
20. Aguirre-Gamboa R, Gomez-Rueda H, Martinez-Ledesma E, Martinez-Torteya A, Chacolla-Huaringa R, Rodriguez-Barrientos A, et al. SurvExpress: An Online Biomarker Validation Tool and Database for Cancer Gene Expression Data Using Survival Analysis. *PLoS One* (2013) 8(9):e74250. doi: 10.1371/journal.pone.0074250
21. Metsalu T, Vilo J. ClustVis: A Web Tool for Visualizing Clustering of Multivariate Data Using Principal Component Analysis and Heatmap. *Nucleic Acids Res* (2015) 43(W1):W566–70. doi: 10.1093/nar/gkv468
22. Scarth JA, Patterson MR, Morgan EL, Macdonald A. The Human Papillomavirus Oncoproteins: A Review of the Host Pathways Targeted on the Road to Transformation. *J Gen Virol* (2021) 102(3). doi: 10.1099/jgv.0.001540
23. Moody CA, Laimins LA. Human Papillomavirus Oncoproteins: Pathways to Transformation. *Nat Rev Cancer* (2010) 10(8):550–60. doi: 10.1038/nrc2886
24. Sabatini ME, Chiocca S. Human Papillomavirus as a Driver of Head and Neck Cancers. *Br J Cancer* (2020) 122(3):306–14. doi: 10.1038/s41416-019-0602-7
25. Xu Z, Gujar H, Fu G, Ahmadi H, Bhanvadia S, Weisenberger DJ, et al. A Novel DNA Methylation Signature as an Independent Prognostic Factor in Muscle-Invasive Bladder Cancer. *Front Oncol* (2021) 11:614927. doi: 10.3389/fonc.2021.614927
26. van der Zee RP, van Noesel CJM, Martin I, Ter Braak TJ, Heideman DAM, de Vries HJC, et al. DNA Methylation Markers Have Universal Prognostic Value for Anal Cancer Risk in HIV-Negative and HIV-Positive Individuals. *Mol Oncol* (2021). doi: 10.1002/1878-0261.12926
27. Thuijs NB, Berkhof J, Ozer M, Duin S, van Splunter AP, Snoek BC, et al. DNA Methylation Markers for Cancer Risk Prediction of Vulvar Intraepithelial Neoplasia. *Int J Cancer J Int du Cancer* (2021). doi: 10.1002/ijc.33459
28. Schotten LM, Darwiche K, Seweryn M, Yildiz V, Kneuertz PJ, Eberhardt WEE, et al. DNA Methylation of PTGER4 in Peripheral Blood Plasma Helps to Distinguish Between Lung Cancer, Benign Pulmonary Nodules and Chronic Obstructive Pulmonary Disease Patients. *Eur J Cancer* (2021) 147:142–50. doi: 10.1016/j.ejca.2021.01.032
29. Pan H, Renaud L, Chaligne R, Bloehdorn J, Tausch E, Mertens D, et al. Discovery of Candidate DNA Methylation Cancer Driver Genes. *Cancer Discov* (2021). doi: 10.1158/2159-8290.CD-20-1334
30. Yang S, Wu Y, Wang S, Xu P, Deng Y, Wang M, et al. HPV-Related Methylation-Based Reclassification and Risk Stratification of Cervical Cancer. *Mol Oncol* (2020) 14(9):2124–41. doi: 10.1002/1878-0261.12709
31. Kim H, Lapointe J, Kaygusuz G, Ong DE, Li C, van de Rijn M, et al. The Retinoic Acid Synthesis Gene ALDH1a2 Is a Candidate Tumor Suppressor in Prostate Cancer. *Cancer Res* (2005) 65(18):8118–24. doi: 10.1158/0008-5472.CAN-04-4562
32. Seidensaal K, Nollert A, Feige AH, Muller M, Fleming T, Gunkel N, et al. Impaired Aldehyde Dehydrogenase 1 Subfamily Member 2a-Dependent Retinoic Acid Signaling is Related With a Mesenchymal-Like Phenotype and an Unfavorable Prognosis of Head and Neck Squamous Cell Carcinoma. *Mol Cancer* (2015) 14:204. doi: 10.1186/s12943-015-0476-0
33. Choi JA, Kwon H, Cho H, Chung JY, Hewitt SM, Kim JH. ALDH1A2 Is a Candidate Tumor Suppressor Gene in Ovarian Cancer. *Cancers (Basel)* (2019) 11(10). doi: 10.3390/cancers11101553
34. Goldman MJ, Craft B, Hastie M, Repecka K, McDade F, Kamath A, et al. Visualizing and Interpreting Cancer Genomics Data *via* the Xena Platform. *Nat Biotechnol* (2020) 38(6):675–8. doi: 10.1038/s41587-020-0546-8
35. Rong C, Muller MF, Xiang F, Jensen A, Weichert W, Major G, et al. Adaptive ERK Signalling Activation in Response to Therapy and in Silico Prognostic Evaluation of EGFR-MAPK in HNSCC. *Br J Cancer* (2020) 123(2):288–97. doi: 10.1038/s41416-020-0892-9

Conflict of Interest: The authors declare that the research was conducted in the absence of any commercial or financial relationships that could be construed as a potential conflict of interest.

Publisher's Note: All claims expressed in this article are solely those of the authors and do not necessarily represent those of their affiliated organizations, or those of the publisher, the editors and the reviewers. Any product that may be evaluated in this article, or claim that may be made by its manufacturer, is not guaranteed or endorsed by the publisher.

frontiers in Oncology

REVIEW
published: 04 November 2021
doi: 10.3389/fonc.2021.752270

Non-Coding RNAs Associated With Radioresistance in Triple-Negative Breast Cancer

Alberto Aranza-Martínez[1†], Julio Sánchez-Pérez[1†], Luis Brito-Elias[1], César López-Camarillo[2], David Cantú de León[3], Carlos Pérez-Plasencia[1,4] and Eduardo López-Urrutia[1*]*

[1] Laboratorio de Genómica Funcional, Facultad de Estudios Superiores Iztacala Universidad Nacional Autónoma de México (UNAM), Tlalnepantla, Mexico, [2] Posgrado en Ciencias Genómicas, Universidad Autónoma de la Ciudad de México, Mexico City, Mexico, [3] Dirección de Investigación, Instituto Nacional de Cancerología (INCan), Mexico City, Mexico, [4] Laboratorio de Genómica, Instituto Nacional de Cancerología (INCan), Mexico City, Mexico

OPEN ACCESS

Edited by:
Hailong Pei,
Soochow University, China

Reviewed by:
Jianming Tang,
Zhejiang Provincial People's Hospital, China
Reem Amr Assal,
Heliopolis University for Sustainable Development, Egypt

***Correspondence:**
Carlos Pérez-Plasencia
carlos.pplas@gmail.com
Eduardo López-Urrutia
e_urrutia@unam.mx

[†]These authors have contributed equally to this work

Specialty section:
This article was submitted to Molecular and Cellular Oncology, a section of the journal Frontiers in Oncology

Received: 02 August 2021
Accepted: 06 October 2021
Published: 04 November 2021

Citation:
Aranza-Martínez A, Sánchez-Pérez J, Brito-Elias L, López-Camarillo C, Cantú de León D, Pérez-Plasencia C and López-Urrutia E (2021) Non-Coding RNAs Associated With Radioresistance in Triple-Negative Breast Cancer. Front. Oncol. 11:752270. doi: 10.3389/fonc.2021.752270

The resistance that Triple-Negative Breast Cancer (TNBC), the most aggressive breast cancer subtype, develops against radiotherapy is a complex phenomenon involving several regulators of cell metabolism and gene expression; understanding it is the only way to overcome it. We focused this review on the contribution of the two leading classes of regulatory non-coding RNAs, microRNAs (miRNAs) and long non-coding RNAs (lncRNAs), against ionizing radiation-based therapies. We found that these regulatory RNAs are mainly associated with DNA damage response, cell death, and cell cycle regulation, although they regulate other processes like cell signaling and metabolism. Several regulatory RNAs regulate multiple pathways simultaneously, such as miR-139-5p, the miR-15 family, and the lncRNA HOTAIR. On the other hand, proteins such as CHK1 and WEE1 are targeted by several regulatory RNAs simultaneously. Interestingly, the study of miRNA/lncRNA/mRNA regulation axes increases, opening new avenues for understanding radioresistance. Many of the miRNAs and lncRNAs that we reviewed here can be used as molecular markers or targeted by upcoming therapeutic options, undoubtedly contributing to a better prognosis for TNBC patients.

Keywords: breast cancer, triple negative breast-cancer, radioresistance, non-coding RNAs, long non-coding RNAs, microRNAs

INTRODUCTION

Breast cancer (BC) is the malignant tumor with the highest number of cases diagnosed worldwide and the most common cause of death in women (1). Although it is a heterogeneous disease, breast tumors can be classified based on the expression level of hormonal receptors for estrogen (ER), progesterone (PR), and human epidermal growth factor receptor 2 (HER2) in subtypes depending on the presence (+) or absence (–) of hormonal receptors, namely Luminal A (ER+, PR+/-, HER2-), Luminal B (ER+, PR+/-, HER2+), and HER2-enriched (ER -, PR -, HER2+). A fourth subtype that

lacks the expression of all the mentioned hormonal receptors is named Triple Negative (ER -, PR -, HER2-) or Basal-like (2).

Triple-Negative Breast Cancer (TNBC) is further classified into four subtypes; Basal-like 1 (BL1), Basal-like 2 (BL2), Mesenchymal (M), and Luminal Androgen Receptor positive (LAR), where each subtype considers cancerous stage, gene pattern expression, propagation, metastasis, histologic differences and response to common chemotherapeutic neoadjuvants (3). Among the breast cancer subtypes, TNBC is the most aggressive, has a poor prognosis and a high risk of recurrence and metastasis (4–6), and complicates targeted therapies in patients due to the absence of hormonal receptors (ER, PR, HER2) (6).

TNBC patients commonly receive systemic treatments such as chemotherapy or local therapies, including conventional surgery and radiotherapy either in isolation or in combination with other types of treatments for increased effectiveness and prognosis after surgery (6–9).

Radiotherapy has proved efficient for breast cancer patients after mastectomy, at least in levels I and II, reducing recurrence and mortality (10). This type of therapy employs ionizing radiation (IR), e.g., X-rays, gamma rays, α, and β particles, ion carbon or electron, neutron, and proton beams (11, 12) to improve the diagnosis.

IR affects cells directly and indirectly. The direct effect is promoting DNA damage like single-strand breaks (SSBs), double-strand breaks (DSBs), also called clustered DNA lesions, genomic instability, and inducing apoptosis. On the other hand, the indirect effect is caused by reactive oxygen species (ROS) generated from the interconnection between IR and water, promoting complex DNA lesions that alter cell homeostasis, modifying proteins and lipids, eventually lead to cell death (13–15). Nevertheless, the implementation of radiotherapy is still controversial (16), and its efficacy may be limited by the presence of tumor cells resistant to ionizing radiation (17) due to alterations in the pathways and genes involved in the DNA damage response system (DDR).

The alteration of these elements that generally play an important role in preserving cell viability through the repairing genetic material modifies the response of tumor cells to radiotherapy (18).

Recently, it has been observed that not only the irradiated cells themselves react by modifying their metabolism, but that they communicate with neighboring, unirradiated cells through gap junctions and secreted small molecules in a mechanism known as 'radiation-induced bystander effect' (RIBE). Through RIBE, bystander cells can rescue irradiated cells, increasing their survival (19). It has been shown that angiogenesis, invasion, metastasis, and proliferative signaling maintenance can also be induced through RIBE, affecting the outcome of IR therapies and enhancing radioresistance (20).

Several groups have reported mechanisms that lead cells to resistance to TNBC therapies, such as hypoxia, cell cycle regulation (21), signaling pathways linked to radiosensitivity like mTOR (22) and EGFR/PI3K/Akt (23), among others. Here we want to highlight the role of two classes of non-coding RNAs (ncRNAs), microRNAs (miRNAs) and long non-coding RNAs (lncRNAs), in the development of radioresistance.

MicroRNAs are small, 21-25 nucleotide-long, single-stranded RNA molecules (24) that negatively regulate mRNA through binding their 3' UTR and blocking translation (25, 26). They are involved in virtually every cellular process: cell cycle control, differentiation, proliferation, apoptosis, autophagy, and DNA repair, among others, and thus have a role in cancer, either as oncogenes –dubbed oncomirs– or tumor suppressors (27).

Several studies show that miRNAs promote resistance to treatments in other cancer types (28); notably, they can promote radioresistance or radiosensitivity. For instance, miR-214 is upregulated in ovarian cancer, leading to PTEN mRNA degradation and PI3K/Akt activation, thus promoting radioresistance (29). miR-183-5p promotes radioresistance by decreasing ATG5 mRNA expression, interacting with downstream signaling genes from PI3K and Wnt signaling pathways, and upregulating them in colorectal cancer (30, 31). Likewise, miR-365 enhances radiosensitivity by inhibiting the CDC25A expression in non-small cell lung cancer cells, consequently improving the prognosis after IR treatment (32).

Long non-coding (lncRNAs) RNAs are 200+ nucleotide-long molecules (33), transcribed mainly by RNA pol II (34). There are recent reports of their involvement in the regulation of gene expression, metastasis, and invasion of cancer cells (33), miRNA silencing (35), apoptosis, autophagy, cell cycle regulation, and DNA repair (17, 36, 37). As the number of described lncRNAs increases (38), so does the number that regulates the biological processes mentioned above.

lncRNAs have been described in various cancer types. For example, NEAT1 is implicated in the DNA repair process by homologous recombination pathway regulating CHK1, CHK2, BRCA1, and RPA2 expression in multiple myeloma (39). FAM83H-AS1 promotes metastasis and proliferation by interacting and regulating HuR protein stability in ovarian cancer (40). ANRIL promotes proliferation, cell metastasis and inhibits apoptosis by suppressing miR-125a expression in nasopharyngeal carcinoma cells (41). POU3F3 inhibits autophagy signaling by decreasing SMAD4 in colorectal cancer and is involved in cell proliferation and migration (42). Finally, upregulated WTAPP1 promotes invasion and migration in non-small cell lung cancer by interacting with HAND2-S1 and decreasing its expression (43).

Most interestingly, these two classes of ncRNAs can interact with each other, adding to the complexity and importance of their regulation on mRNAs. Several lncRNAs have regions complementary to miRNA sequences that compete for their binding with the target mRNA. This binding sequesters miRNAs to complementary lncRNAs and prevents them from binding to their mRNA targets, turning lncRNAs into miRNA sponges, effective positive mRNA regulators (44, 45).

Interactions of this kind have been reported in diverse biological processes. lncRNA PCAT1 downregulates miR-128 in cervical cancer, promoting proliferation, migration, invasion and thus decreasing radiosensitivity (46). LncRNA *lnc-RI* competitively binds with miR-4727 regulating Non-Homologous End Joining (NHEJ) through LIG4 mRNA stabilization, affecting cell cycle and radiosensitivity in colorectal cancer (47). LncRNA

TRPM2-AS in gastric cancer serves as a sponge for miR-612, promoting radioresistance by upregulation of the DNA double-strand break repair protein FOXM1 (48). Several interactions like these have been reported in TNBC. For instance, lncRNA WEE-AS1promotes proliferation by downregulating miR-32-5p (49), while LINC00173 downregulates miR-490-3p and promotes a more aggressive phenotype (50). Recently, Yuan and colleagues identified MAL2 and NEAT1 as key miRNA regulators in TNBC through an in silico approach (51).

Both miRNAs (52) and lncRNAs (53) have been employed as radiotherapy response biomarkers; however, more research is needed to understand their role in radioresistance fully. A complete grasp of this process and its elements will provide a knowledge base for increasing radiotherapy's effectiveness in breast and other cancer types. This review describes the different miRNAs, lncRNAs, and their associations that regulate resistance against ionizing radiation-based therapies in breast cancer. We found that these ncRNAs are mainly involved in DNA damage response, but they are also involved in cell death, cell cycle regulation, and other functional aspects. In the following sections, we summarize the currently described ncRNAs involved in the alteration of these processes.

METHODS

We searched the Medline database for journal articles in English, published from 2001 to 2021, using combinations of the following keywords: lncRNA, miRNA, breast cancer, radiotherapy, radioresistance, and radiosensitivity.

We obtained 45 articles reporting the diverse roles of ncRNAs in radioresistance. We thoroughly read each paper and extracted data about the type of ncRNAs, targets, and pathways involved in cell radiosensitivity or radioresistance mechanisms, the type of cell line used in both *in vivo* or *in vitro* assays; subsequently, we constructed three ncRNA interaction networks using Cytoscape, available at NDEx. (https://www.ndexbio.org/#/). These networks correspond to those processes most regulated by ncRNAs: DNA damage, apoptosis and autophagy, and cell cycle.

ncRNAs INVOLVED IN DNA DAMAGE

DNA damage response system (DDR) is a complex network comprising several processes to locate and correct DNA damage to maintain genomic integrity. This extensive network includes mechanisms for damage detection, signal transduction, DNA repair tolerance processes, and cell cycle control. For detailed descriptions of the proteins that participate in these processes, please refer to Giglia-Mari et al. (54).

DNA is an intrinsically reactive molecule and is highly susceptible to damage or chemical alterations due to endogenous processes and factors, such as replication errors, spontaneous deamination of bases, oxidative damage by ROS and formation of abasic sites; or by exogenous agents, for example, DNA breaks by IR, alkylation of bases by chemical agents, modification of bases by ultraviolet (UV) radiation, among others (55, 56). The main repair mechanisms for these damages are nucleotide excision repair (NER), base excision repair (BER), homologous recombination (HR), non-homologous end junction (NHEJ), and mismatch repair (MMR). These processes are extensively explained by Christmann et al. (57).

DNA double-strand breaks (DSB) are the most predominant and damaging lesions caused by IR (58). The most common DSB repair mechanisms are the Homologous Recombination (HR) and the Non-Homologous End Joining (NHEJ) pathways (59). The cell cycle phase determines the triggering of one or the other, but in both cases, they require the intervention of other DDR proteins (54). In addition to the proteins involved in DDR, many ncRNAs are essential to the damage response mechanisms (60–62). Furthermore, these ncRNAs modulate the DDR elements' activity after irradiation, promoting radioresistant or radiosensitive phenotypes (9).

H2AX as an Indicator of Radiosensitivity

Phosphorylation of the histone variant H2AX is an early event in DDR and, thus, a reliable marker of ongoing DNA repair. However, H2AX foci decrease upon completion of the DNA repair process, so extended detection indicates radiosensitivity (63). The effect of multiple ncRNAs that target DDR proteins can be assessed through H2AX detection.

P. Zhang and collaborators (64) found BC cells that overexpress miR-205 exhibit persistent H2AX foci, indicating their low capacity to repair damage after IR. The authors suggest that ZEB1 mediates the effect of miR-205 by partially restoring repair. They demonstrated that miR-205 inhibition increases the expression levels of ZEB1 and Ubc13[u1] [u2]. Therefore, miR-205 radiosensitizes BC cells by inhibiting HR by targeting ZEB1 and Ubc13.

Similarly, Mei and colleagues (65) reported that BC cells transfected with the miR-15 family of mimics showed persistent higher levels of gamma-H2AX after irradiation, indicating unrepaired DNA damage. It is well-known that gamma-H2AX foci decrease shortly after radiation; these authors suggest that the miR-15 family be involved in inhibiting DNA repair, thus acting as radiosensitizers.

Masoudi-Khoram et al. (66) used gamma-H2AX and RAD51 as markers to evaluate DNA damage by IR in two BC-derived cell lines. They found that RAD51 expression increased post-radiation while gamma-H2AX expression reached a peak 4 hours after irradiation and then rapidly decreased. They identified miR-16-5p as a possible important mediator of radiation response and suggested that miR-16-5p could promote radiosensitive breast cancer cells to IR.

In a study with diverse cancer-derived cell lines, Koo and colleagues demonstrated that miR-200c overexpression in the breast cancer cell line, MDA-MB-468 provoked an increase of gamma-H2AX foci and prolonged focus formations after irradiation. This effect was associated with a discernible downregulation of p-DNA-PKcs involved in NHEJ repair (67).

Lin et al. (68) found that overexpression of miR-200c enhanced IR-induced DNA strand breaks in BC cell culture. They found a correlation between increased miR-200c expression and the presence of H2AX foci. Years later, Wang et al. (69) discovered that lncRNA LINC02582 is a downstream target of miR-200c. LINC02582 interacts with USP7 to deubiquitinate and stabilize CHK1, a critical effector in response to DNA damage that facilitates DNA repair, promoting radioresistance (70). However, their results demonstrated that miR-200c expression reduced the CHK1 protein level since it targets LINC02582. They suggest the miR-200c/LINC02582/USP7/CHK1 signaling axis as a potential target to improve breast cancer response to radiation therapy.

In another study with diverse cancer cell types, including BC cells, Lee et al. (71) described miR-7 as a radiosensitizer. Its overexpression causes downregulation of EGFR, AKT, ERK, and STAT3. They inhibited miR-7, which led to positive regulation of EGFR and its downstream effectors to validate these results. Besides, they reported that ectopic overexpression of the miR-7 caused marked prolongation of radiation-induced gamma-H2AX foci formation. The authors associated this phenomenon with a decrease in DNA-PKcs phosphorylation with an activated EGFR-associated signaling pathway.

Zhang et al. (72) found a positive correlation between the expression of LINP1, Ku80, and DNA-PKcs after IR and identified that the lncRNA LINP1 binds Ku80 and DNA-PKcs, promoting radioresistance. They hinted that DSB repair is enhanced by LINP1 across the NHEJ pathway due LINP1 to providing a scaffold for Ku80 and DNA-Pkcs. The authors confirmed this by measuring DNA damage through gamma-H2AX. When LINP1 was removed, gamma-H2AX foci were more persistent. Besides, they discovered that activation of EGFR upregulates LINP1 transcription through activation of the RAS-MEK-ERK pathway; in this manner, cells with EGFR activation improve DNA repair through the LINP1/Ku80/DNA PKcs axis. Also, they identified a negative feedback mechanism where p53 and miR-29 are involved. P53 regulates the expression of miR-29 directly, and, in turn, this negatively regulates LIPN1; this is an uncommon miRNA-lncRNA interaction since lncRNAs sponge miRNAs in most of the currently described instances.

ncRNAs That Target HR Proteins

RAD51, catalyzes the strand transfer between a broken sequence and its homolog to re-synthesize the damaged region (73). Gasparini et al. (74), demonstrated that miR-155 effectively reduces HR repair by targeting RAD51 directly; thus, miR-155 contributes to increased sensitivity to IR. These findings were established both *in vivo* and *in vitro*. They found that miR-155 overexpression is associated with lower RAD51 expression; besides, they found a higher survival rate in a TNBC patient cohort due to the anti-correlation between miR-155 overexpression and its target RAD51.

Another study (75) demonstrated that miR-302a downregulation confers radioresistance and that restoration of its expression sensitizes breast cancer cells to radiotherapy since miR-302a targets RAD52, an essential participant in HR repair, and AKT1 (76). Chai et al. (77) show that miR-185 was downregulated in radioresistant BC cells and that there is an inverse correlation with the expression of AKT1 and RAD52. Besides, induced overexpression of miR-185 decreases the expression of AKT1, RAD52, and Bcl-2.

In another work that involved alteration of HR participants, Troschel and collaborators (78) reported that miR-142-3p can sensitize breast cancer cells to radiotherapy by downregulating BRCA1 and BRCA2, two proteins that mediate DSB repair by HR. BRCA1 and BRCA2 play a role as mediators of recombination, promote ssDNA resection, and are believed to be required for subnuclear assembly of RAD51 (79).

Another workgroup found that miR-671-5p was inversely correlated with FOXM1. Through HCR assay, the authors measured the DNA repair capability in breast cancer cell lines. In cells with miR-671-5p inhibited after IR, the HCR activity was significant compared to the control, and FOXM1 expression also increased. Their western blot results showed that miR-671-5p suppressed the expression of genes downstream from FOXM1 involved in the DNA repair pathway; these are RAD51 and BRIP1, the latter contributes to the DNA repair function of BRCA1 (80). Thus, their results hint that miR-671-5p radiosensitizes breast cancer cells by targeting the FOXM1 target, affecting downstream genes involved in DNA repair (81).

ncRNAs That Target Other DDR Proteins

The lncRNA HOTAIR has recently emerged as a multifunctional regulator. Quian et al. (82) demonstrated that HOTAIR could induce resistance to radiotherapy in breast cancer cells. They found that the Ku70 and Ku80 proteins, DNA-PKs, and ATM were upregulated due to HOTAIR overexpression, thus promoting repair and reducing IR sensitivity. In response to DSB, Ku70 and Ku80 associate with broken end chains and then recruit DNA-PKcs to the damage sites, i.e., Ku proteins act as a scaffold for other proteins that participate in the NHEJ pathway (83, 84).

Surprisingly, it was reported that miR-139-5p modulated resistance to radiation in breast cancer by affecting multiple genes involved in DDR. Five of its six confirmatory targets have roles in diverse DDR pathways essential for post-radiation damage repair. These pathways include microhomology-mediated end-junction (MMJE) with POLQ and XRCC5, BER in which miR-139-5 targets POLQ, NHEJ with XRCC5, HR for RAD54L. Additionally, it regulates DNA topology during repair targeting TOP2A and TOP1 and seems to have a ROS defense role by targeting MAT2AT (85).

The above findings are summarized in **Figure 1**, which shows the main elements involved in DDR and the ncRNAs that reportedly regulate them. We found it interesting that only one report involved ATM, one of the primary DNA-damage sensors; ATM responded to HOTAIR overexpression, as did the Ku proteins. There are, however, reports of several ncRNAs that target virtually every downstream pathway—notably, miR139-5p targets proteins that participate in HR, NER, and NHEJ. miR-200c is also multifunctional in DDR; it targets CHK1 through LINC02582 and the DNA PKcs involved in NHEJ. This repair pathway is also targeted by the LINP1 lncRNA, itself regulated by

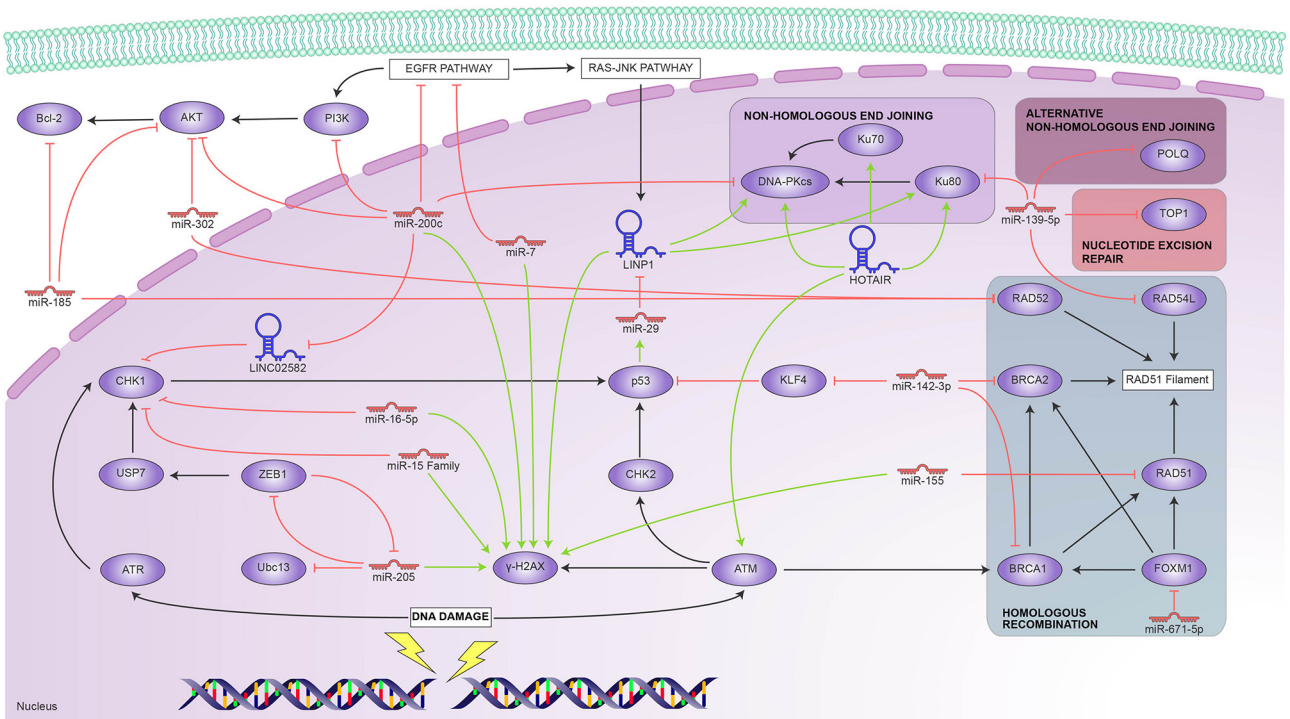

FIGURE 1 | Reported ncRNAs that regulate DNA damage response and their targets. Green arrowheads represent positive regulation and red bars, negative regulation.

P53 through miR-29; conversely, our search only yielded reports of HR being regulated by miRNAs, such as miR-155 and miR-142. All these ncRNAs are potential radioresistance markers and attractive targets towards induced radiosensitivity.

ncRNAs INVOLVED IN APOPTOSIS AND AUTOPHAGY

Dysregulation of cell death plays a key role during carcinogenesis. Multiple alterations occur within apoptotic pathways leading to an overall reduction of apoptosis in tumor cells and the rise of apoptosis-resistant phenotypes (86, 87).

Apoptosis

Apoptosis is the most common form of controlled cell death, in which the cell gradually collapses and ultimately dies. It can be triggered by the intrinsic pathway, initiated by either the absence or excess of growth factors, hormones, and cytokines, or by the extrinsic pathway, set off by interaction between death ligands and death receptors such as those from the Tumour Necrosis Factor (TNF) family. For further detail on apoptosis and its effectors, please refer to Cao & Tait (88).

Several ncRNAs regulate the apoptotic response to IR in BC. Yu and colleagues (89) observed an association between miR-144 overexpression and cell survival after irradiation. Subsequent experiments revealed that miR-144 overexpression increased Bcl2 levels and inhibited the pro-apoptotic protein Bax and caspase activity; meanwhile, PTEN and pAkt showed aberrant expression levels, suggesting that miR-144 regulate the radiation-induced apoptotic response by targeting the PTEN/Akt signaling pathway.

Overexpression of the multifunctional lncRNA HOTAIR was also observed in BC cells following irradiation; high expression of this lncRNA has been associated with radioresistance acquisition, even though the exact role of HOTAIR in this process remains unclear. In-vitro experiments showed alterations in the proliferative and apoptotic cells ratio, altered Akt expression, and downregulation of the pro-apoptotic Bad protein. These findings suggest that HOTAIR induces radioresistance by inhibiting apoptosis *via* the PI3K/Akt-Bad signaling pathway (90). A more recent study suggests another possible mechanism for HOTAIR-induced radioresistance. Knockdown of HOTAIR resulted in an increase of radiation-induced apoptosis, DNA damage, cell cycle arrest, and an upregulation of miR-218. Since miR-218 upregulation promoted cell apoptosis, this data suggests that the HOTAIR-miR-218 axis plays a critical role in radiation-induced apoptosis (36).

Other authors found an upregulation of the lncRNA CCAT1 in radioresistant BC tissues where miR-148b was found to be downregulated. The interaction between CCAT1 and miR-148b was confirmed through luciferase reporter assay. Downregulation

of CCAT1 increased radiosensitivity through inhibiting proliferation and promoting apoptosis, implying that the CCAT1-miR148b interaction regulates the acquisition of radioresistance in BC cells (91).

On the other hand, ncRNAs have also been found to sensitize BC cells to radiotherapy by inducing apoptosis. Zhu and colleagues (92) observed that the upregulation of miR-195 enhanced radiosensitivity in BC cells *via* increasing radiation-induced apoptosis by downregulation of Bcl2. More recently, Chai and colleagues (77) reported downregulation of miR-185 in radioresistant BC cells; conversely, overexpressed miR-185 radiosensitized BC cells. miR-185 overexpression led to Bcl2 downregulation, thus identifying Bcl2 as a downstream target of miR-185. Further experiments showed that Bcl2 silencing radiosensitized BC cells, confirming the role of the miR-185-Bcl2 axis in radioresistance.

In another study, miR-122-3p overexpression was found to sensitize BC cells to ionizing radiation. It was also found that miR-122-3p overexpression induced apoptosis after irradiation while suppressing migration and invasion. Additionally, the aberrant expression levels of PTEN/PI3K/AKT and EMT pathways proteins suggest that miR-122-3p might control radiation-induced apoptosis by regulating the PTEN/PI3K/AKT pathway (93).

Autophagy

Autophagy is a set of adaptations usually aimed at avoiding cell death by sequestering and recycling a portion of the cytoplasm and organelles. Still, it can be triggered to remove damaged or senescent organelles to maintain energy balance or as a result of nutrient deprivation, ultimately leading to cell death. Descriptions of the involved proteins and their functions can be found in reviews such as those by Doherty & Baehrecke (94), Kim & Lee (95), and Maiuri et al. (96). Autophagy plays a dual role during carcinogenesis, leading to cell death or promoting cell survival *via* inhibiting apoptosis (97).

Several workgroups have demonstrated that ncRNAs play a role in the regulation of autophagy in BC after irradiation. Yi and colleagues (98) observed that the overexpression of miR-199a-5p in MCF7 cells inhibited radiation-induced autophagy. Inhibition of Beclin1 and DRAM1 due to miR-199a-5p was also observed, identifying them as downstream targets and suggesting a potential mechanism for radiation-induced autophagy. However, experiments in the MDA-MB-231 cell line showed that miR-199a-5p overexpression upregulated Beclin1 and DRAM1, promoting radiation-induced autophagy. Further experiments showed that miR-199a-5p regulates cell cycle arrest after IR; additionally, it altered the radiation response of BC after IR. This evidence confirms a role for miR-199a-5p in radiation-induced autophagy through a still undetermined underlying molecular mechanism.

In the same way, miR-200c sensitized BC cells to IR. miR-200c overexpression inhibited radiation-induced autophagy in BC cells; moreover, UBQLN1, a protein associated with promoting autophagosome formation, was identified as a downstream target of miR-200c. This finding suggested that miR-200c enhances radiosensitivity in BC cells by suppressing radiation-induced autophagy through the regulation of UBQLN1 (99).

Luo and colleagues (100) found that the overexpression of miR-129-5p sensitized BC cells to IR, while autophagy acted as a protective response. Subsequently, miR-129-5p was found to inhibit autophagy during the early stages of autophagosome formation, promoting apoptosis. HMGB1 was identified as a potential downstream target for miR-129-5p using online databases. HMGB1 knockdown reduced cell survival and radiation-induced autophagy, suggesting that miR-129-5p may radiosensitize BC cells by inhibiting radiation-induced autophagy *via* directly targeting HMGB1.

Unsurprisingly, we found reports of several lncRNAs that induce radioresistance by blocking apoptosis and others that perform the opposite function, all of them represented in **Figure 2**. So far, the evidence appoints Bcl2 as the hub of this regulation; it is upregulated indirectly by miR144 and downregulated by miR-185 and miR-195. Meanwhile, the HOTAIR-miR-218, CCAT1-miR148b, and PCAT6-miR-185-5p axes block apoptosis through mechanisms still under study. Conflicting reports on the role of miR-199-5p show how much more there is to know about the role of ncRNAs in the delicate balance between apoptosis and autophagy in tumor development.

ncRNAs INVOLVED IN CELL CYCLE

The equilibrium between cell proliferation and death is tightly controlled by the cell cycle, a complex regulatory network that progresses through alternating cell growth, subcellular component synthesis, and cell division phases. Cell cycle progression is regulated primarily by a family of proteins called cyclins that bind and activate their effector counterparts, cyclin-dependent kinases, or CDKs. In an undisturbed cell, timely cyclin expression activates the necessary CDKs, which, in turn, phosphorylate multiple targets that control phase-specific processes. Cyclin D is expressed from early G1 and activates CDK6, both cyclin E in late G1-S and cyclin A in early S-G2 phase activate CDK2, and cyclin B activates CDK1 in G2-M. For additional details on these and other cell cycle regulators and their alterations in cancer, please refer to Foster (101).

Cell cycle checkpoints are, essentially, fail-safe mechanisms that prevent cell cycle progression in response to stimuli such as cell overgrowth, suboptimal chromosome segregation during mitosis, and, notably, DNA damage (102). The ATM/ATR–p53 signaling pathway, part of the DDR, induces G1 or G2 arrest, allowing for DNA repair prior to replication or preventing the cell from undergoing mitosis with a set of altered chromosomes, respectively. However, these mechanisms are dysregulated in cancer cells and let cells with accumulating mutations proliferate (103). In this way, several ncRNAs are upregulated in BC and BC-derived cell lines, associated with a radioresistant phenotype both in patients and cell cultures, suggesting active participation of ncRNAs in the modulation of the response to radiotherapy.

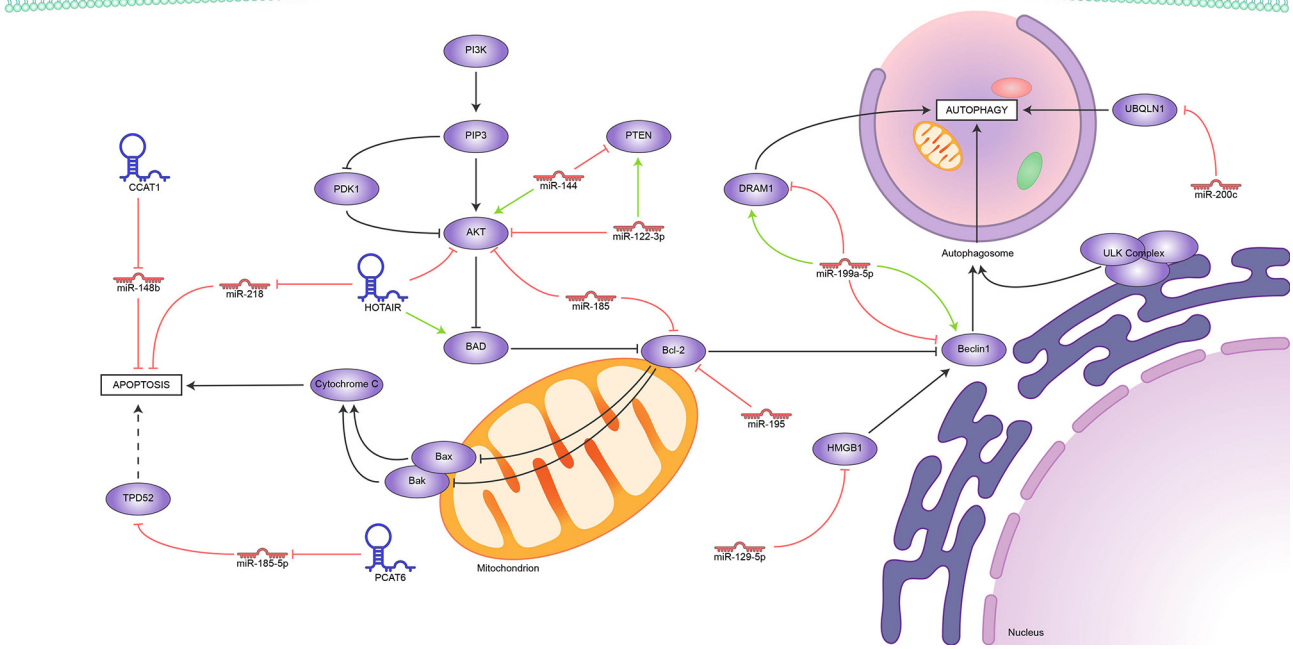

FIGURE 2 | Reported ncRNAs that regulate apoptosis, autophagy, and their targets. Green arrowheads represent positive regulation and red bars, negative regulation.

G1/S Checkpoint

Zhang and collaborators (104) found that LINC00963 expression led to the upregulation of the cell cycle regulatory proteins cyclin D1 and CDK6, leading to higher p27 levels and cell cycle progression. Furthermore, elevated LINC00963 expression was significantly associated with tumor size and metastasis. These authors searched for potential miRNA targets and found that LINC00963 sponged miR-324-3p and upregulated ACK1, which belongs to a family of non-receptor-tyrosine-kinases and functions as a driver of tumor progression.

Liu and colleagues (17) found a strong association between cell survival *in vitro* and increased LINC00511 expression, besides its significant over-expression in BC patients. Subsequent in-vitro experiments correlated its expression with radioresistance and a higher cell proliferation rate. These authors performed a bioinformatic search for miRNA targets and found that LINC00511 sponges miR-185 upregulating STXBP4. This protein has been proven to promote cell cycle progression through TP63 activation (105).

On the other hand, some ncRNAs were recently shown to increase radiosensitivity. For instance, the multifunctional lncRNA HOTAIR increased its expression in BC cells upon radiation exposure. Experimental HOTAIR knockdown increased DNA damage and led to cell cycle arrest. It was also observed that HOTAIR exerted its radiosensitizing effect through the downregulation of miR-218, although the corresponding upregulated target is still to be elucidated (36).

G2/M and Spindle Checkpoints

Mei and colleagues found that miR-15a, 15b, and 16 influence radiosensitivity of MCF7 and MDA-MB-231 breast cancer cells, observable through the enhanced duration of H2AX foci and release of the G2 arrest induced by radiation. They demonstrated the interaction between these miRNAs and the cell cycle regulator WEE1 and CHK1 mRNAs through luciferase assays, but they did not find the dramatic reduction they expected at the protein level, hinting at a more complex mechanism (65). In a differential miRNA expression study, miR-16-5p was upregulated in correlation with radiosensitivity in the radiosensitive T47D and the radioresistant MDA-MB-231cell lines. Through bioinformatic analyses, these authors predicted its interaction with targets such as WEE1, Chk1, and CDC27 (66). miR-16-5p had been previously observed to inhibit proliferation in prostate (106) and breast (107) cancers by targeting AKT.

Low CDC27, a component of the anaphase-promoting complex, is a radioresistance marker in TBNC (108). According to a study in MDA-MB-231 cells, this affects the corresponding miR-27a overexpression, which targets CDC27 and increases cell proliferation even under ionizing radiation (109).

According to these reports, ncRNAs mainly regulate the spindle checkpoint, as it is strongly controlled by the miR-15 family and the closely related miR-16; meanwhile, LINC00963 regulates the G1/S checkpoint, as seen in **Figure 3**. Interestingly, we found no reports of ncRNAs that influence the S or G2

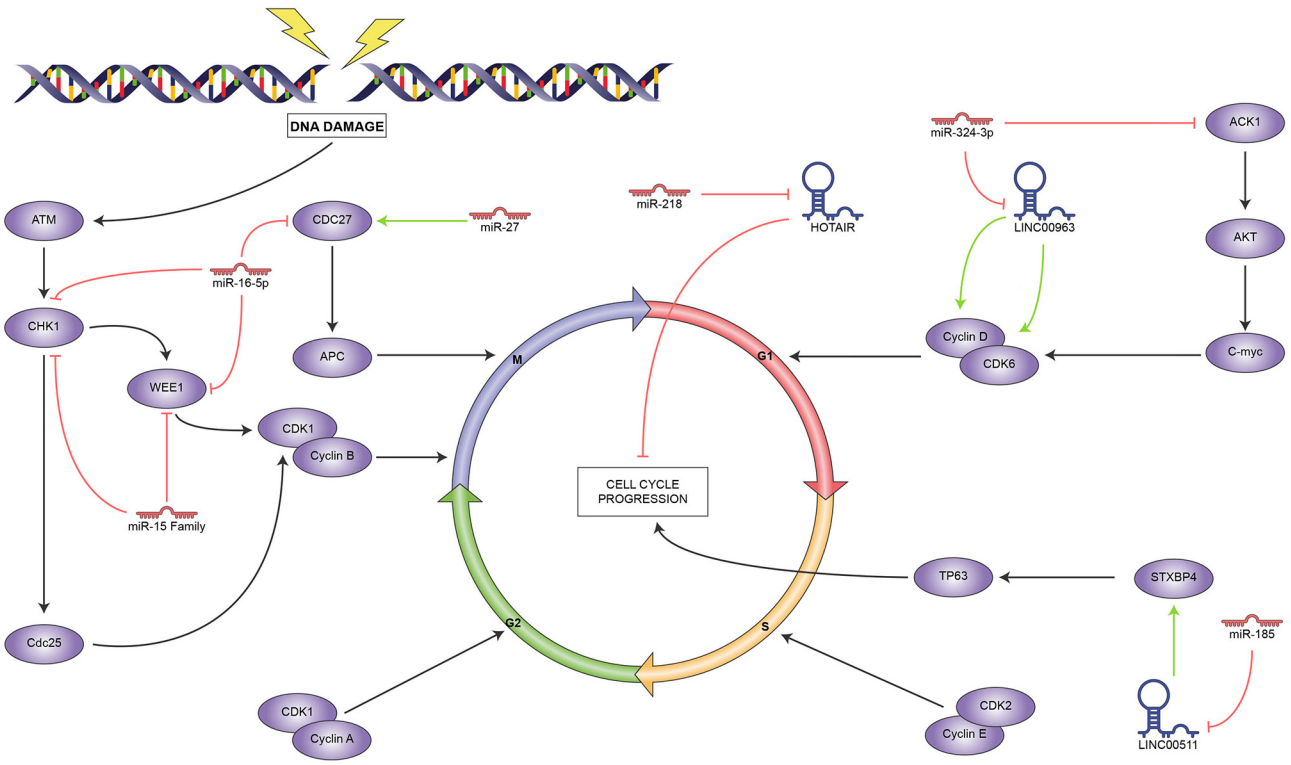

FIGURE 3 | Reported ncRNAs that regulate cell cycle and their targets. Green arrowheads represent positive regulation and red bars, negative regulation.

phases, which leaves ample room for research in this area, given the importance of cell cycle control in cancer. In this regard, the mechanisms employed by HOTAIR and LINC5011 to control cell proliferation are still to be determined.

OTHER ncRNA TARGETS

Besides those reviewed in the preceding sections, our search yielded reports on ncRNAs that induce either radioresistance or radiosensitivity by regulating processes such as cell signaling, metabolism, and inflammation, although these were not as abundant. We briefly summarize them in this section and **Table 1**, hoping to encourage further research in these aspects.

Cell Signaling

STAT3 is a transcription factor that regulates gene expression in response to several stimuli such as growth factors and interleukins. In breast cancer, it regulates several target oncogenes and participates in cancer progression, metastasis, apoptosis, and resistance to therapies (125), and it is targeted by ncRNAs modifying the response to radiotherapy in breast cancer.

miR-124 was negatively regulated in HER2-positive breast cancer cells; this miRNA directly targets STAT3, which regulates HER2 expression. So, miR-124 overexpression caused STAT3 downregulation and enhanced radiotherapy response by increasing cell death. The weak miR-124 expression could enhance STAT3 expression and promote radioresistance in HER2-positive breast cancer (116). Similarly, Yang and coworkers (110) observed that miR-634 was significantly decreased in breast cancer cell lines upon radiation. A miR-634 transfection assay showed an increase in apoptosis and a drastic decrease in cell survival capacity. They demonstrated that miR-634 suppresses breast cancer cells by targeting STAT3, increasing radiotherapy sensitivity.

The EGFR pathway is also associated with breast cancer progression since it regulates multiple tumorigenic processes (126). Fabris et al. (111) observed IR-induced miR-223 expression following BC mass removal. Further experiments revealed that miR-223 directly targets EGF, suggesting it may affect the activation of the EGFR pathway. Additionally, miR-223 overexpression was found to antagonize the pro-tumorigenic signals induced by wound fluids *via* negative regulation of EGF.

Overexpression of miR-122 was observed in therapy-induced radioresistant BC cells; additionally, it sensitized BC cells to IR. Contrastingly, miR-122 knockdown resulted in the acquisition of radioresistance in BC cells. Several proteins involved in diverse pathways such as the transcription factor ZNF611, the TNF pathway elements TNFRS21 and RIPK1, and the Ras-MAPK pathway mediators DUSP8 and HRAS were identified as miR-122 potential targets. These findings suggest that miR-122 may play a multifunctional role in acquiring radioresistance (117).

TABLE 1 | Reported ncRNAs that regulate cell signaling, cell metabolism, and inflammation.

ncRNA	Target	Pathway	Reference
ncRNA promoting radiosensitivity			
miR-634	STAT3	JAK-STAT signaling pathway	Yang et al. (110)
miR-223	EGFR	EGFR signaling pathway	Fabris et al. (111)
miR-7	EGFR, Akt	EGFR signaling pathway, PI3K-AKT signaling pathway	Lee et al. (71)
miR-125b	c-JUN	JNK signaling pathway	Metheerairut et al. (112)
miR-671-5p	FOXM1	Cellular senescence	Tan et al. (81)
Let-7	–	Embryonic development	Wang et al. (113)
miR-22	Sirt1	AMPK signaling pathway	Zhang et al. (114)
miR-770-5p	PBK (PDZ-binding kinase)	–	Lee et al. (115)
ncRNA promoting radiorensistance			
miR-124	STAT3	JAK-STAT signaling pathway	Fu et al. (116)
miR-122	ZNF611, ZNF304, RIPK1, HRAS, Dusp8, TNFRSF21	TNF signaling pathway, RAS-MAPK signaling pathway	Pérez-Añorve et al. (117)
miR-34	p53	p53 signaling pathway	Kato et al. (118)
miR-33a	ABCA1/ABCG1	Lipid metabolism	Wolfe et al. (119)
HOTAIR	miR-449b-5p, HSPA1A	JNK signaling pathway	Zhang et al. (120)
miR-210, miR-10b, miR-182, miR-142, miR-221, miR-21, miR-93, miR-15b	–	–	Grinan-Lison et al. (52)
miR-620	HPGD/PGE2	Metabolism of prostaglandins	Huang et al. (121)
PCAT6	miR-185-5p, TPD52	Membrane traffic	Shi et al. (122)
NEAT1	NOQ1	Oxidative stress	Lin et al. (123)
miR-668	IkB-alfa	NF-Kappa B signaling pathway	Luo et al. (124)

The JNK signaling pathway promoted cell survival in cancer by interacting with multiple pathways (127). Metheetrairut and colleagues (112) found that miR-125b sensitized BC cells to IR. miR-125b was also found to promote radiation-induced senescence in BC cells. Furthermore, c-JUN regulation by miR-125b was found to be involved in radiosensitivity in BC cells; additionally, members of the MAPK signaling pathway were targeted by miR-125b, suggesting that regulation of the MAPK-c-JUN axis by miR-125b might modulate radiosensitivity in BC cells.

Alterations in the p53 pathway play a key role during carcinogenesis (128). Kato and colleagues (118) observed radiation-induced expression of miR-34 mediated by p53 in BC cells. Furthermore, various BC cell lines showed differential miR-34 expression, and cell lines with low miR-34 levels were radiosensitive. Further experimentation revealed that miR-34 might prevent cells from radiation-induced cell death.

FOXM1 is a transcription factor necessary for many biological processes as cell proliferation, cell cycle progression, and cell differentiation. It is a master regulator of DNA damage response, and it is also associated with EMT phenotype in cancer; likewise, it promotes metastasis and tumor progression (129, 130). Tan et al. (81) demonstrated that miR-671-5p radio- and chemosensitize breast cancer cells by targeting FOXM1. They worked with 21T cells and found that miR-671-5p was decreased during breast cancer progression, contrary to FOXM1. In addition, they found that miR-671-5poverexpression reduces FOXM1 expression and affects the downstream genes involved in EMT (TGF-β and VEGF) and DNA repair during BC progression. This way, miR-671-5p inhibits cell proliferation and invasion and sensitizes breast cancer cells to IR.

Cell Metabolism

Cholesterol regulation has proven to be involved in cancer progression (131). Wolfe and colleagues (119) found that miR-33a expression regulates HDL-induced radioresistance through targeting ABCA1. miR-33a expression was found to be lower in irradiated BC cells than in non-irradiated BC cells. Additionally, the expression of the ABCA1 protein was inversely correlated with that of miR-33a. Furthermore, knockdown of miR-33a in BC cell lines with higher miR-33a expression levels resulted in radiosensitization, whereas miR-33a mimic transfection in BC cell lines with low miR-33a expression led to the inhibition of HDL-induced radiosensitization *via* regulation of ABCA1. miR-33a was also associated with an adverse outcome in BC patients.

The Lin28/Let-7 axis, primarily active during embryonic development, regulates multiple genes involved in several tumorigenic processes (132). It may also be involved in the regulation of radioresistance in BC. Cell lines expressing higher levels of the Lin28 protein showed increased survival compared to those expressing lower levels of Lin28. Meanwhile, Lin28 knockdown showed an increase in radiosensitivity. Lin28 was also associated with the regulation of apoptosis; on the other hand, Let7 was confirmed to be directly regulated by Lin28, thus suggesting possible mechanisms for acquiring radioresistance *via* Lin28 (113).

Sirt1 is a histone deacetylase that acts as a regulator in multiple physiological processes such as cell growth, apoptosis, DNA damage and, tumor development; in addition, it promotes tumorigenesis and is upregulated in breast cancer (133–135). Zhang and collaborators (114) reported that Sirt1 is a direct target of miR-22, and their expression is antagonistic, so miR-22 improves radiosensitivity to breast cancer cells by targeting Sirt1.

While miR-22 expression was downregulated in breast cancer cells after IR, Sirt1 was upregulated. However, they found that overexpression of miR-22 regulated Sirt1 expression negatively, blocking its function, such as suppressing tumorigenesis and enhancing the radiosensitivity of breast cancer.

Lee and colleagues (115) discovered that miR-770-5p radiosensitizes breast cancer cells by targeting PDZ-binding kinase (PBK). PBK is a serine-threonine kinase that has been reported to be upregulated in rapidly proliferating cells, as well as in a variety of tumors, furthermore, it was shown to promote transformation and has metastatic properties (136–138). In this study, miR-770-5p was shown to be upregulated by IR response and to be inversely correlated with PBK expression both *in vitro* and *in vivo*. Despite the oncogenic potential of PBK, the authors report that miR-770-5p can directly target PBK in radiation response, confers radiosensitivity to breast cancer.

In addition to the HOTAIR roles described in the previous sections, Zhang et al. (120) identified that it confers radioresistance to breast cancer cells through the HOTAIR/miR-449-5p/HSPA1A axis. HSPA1A is a chaperone overexpressed in a large variety of tumor lines, including breast cancer (139), and its expression exhibited a positive correlation with that of HOTAIR in irradiated breast cancer cells. Also, HOTAIR acts as a sponge for miR-449-5p, preventing it from exerting its role as a negative HSPA1 regulator, allowing the development of a radioresistant phenotype.

Cancer stem cells (CSCs) play a key role during tumor development (140). Griñán-Lisón and colleagues (52) identified several miRNAs that may modulate some CSCs properties, such as proliferation, metastasis, and response to IR. miR-142, miR-15b, miR-210, miR-21, miR-221, miR-10b, miR-182, and miR-93, involved in multiple pathways, showed aberrant expression in various BC cell lines and patients. Their results showed that IR affected BC cell lines differentially, decreasing stemness properties in MCF7 and SKBR3 cells and increasing them in the TNBC cell line MDA-MB-231, along with miR-10b, miR-210, and miR-221 expression. Similarly, miR-10b was overexpressed in patients positive for Ki67 that received IR, while miR-210 and miR-221 were detected in the only TNBC patient with recurrence in the study.

In the same way, the lncRNA PCAT6 was found to be upregulated in TNBC tissues. Subsequent experiments showed that PCAT6 knockdown promoted radiosensitivity in BC cells by inhibiting cell survival and promoting apoptosis. miR-185-5p was later identified as a potential target for PCAT6 and shown to be negatively regulated by it. Also, miR-185-5p was found to target TPD52 directly. Knockdown of both PCAT6 and TPD52 resulted in an increased radiosensitivity in TNBC cells, indicating PCAT6 plays a role in radioresistance *via* regulating the miR-185-5p-TPD52 axis (122).

Lin and colleagues (123) found that NQO1 expression and activity were higher in radioresistant BC-derived cells, modulated by the cancer stem cell-derived NEAT1 lncRNA instead of the more traditional JNK signaling. This finding suggested that the regulation of NEAT1 in NQO1 expression was potentially mediated by suppressing NQO1-targeting miRNAs because the mRNA level was not changed in the radioresistant MDA-MB-231 cells. Still, their results suggested that NEAT might regulate the protein stability of NOQ1 in 231-RR cells through a yet undescribed mechanism. At the time of writing, this is the only report of a lncRNA associated with radioresistance exerting its function through a pathway other than gene up-regulation through miRNA sponging.

Inflammation

Inflammation has also been related to cancer progression (141), and Huang and collaborators (121) found that ncRNAs can also regulate it. Mainly, miR-620 regulates 15-hydroxyprostaglandin dehydrogenase (15-PGDH/HPGD) negatively, which induces radioresistance driven by prostaglandin E2 (PGE2) accumulation, as 15-PGDH normally antagonizes COX-2 by degrading it.

Multiple inflammatory effects during carcinogenesis are mediated by the activation of the NF-κB pathway (142). M. Luo and colleagues (124) observed that increased expression levels of miR-668 in BC cells led to the acquisition of radioresistance while its knockdown sensitized resistant BC cells to IR. miR-668 inhibited lκBα, activating the NF-κB pathway and increasing intranuclear p65, which, in turn, enhances NF-κB binding activity. Thus, miR-668 might regulate radioresistance in BC cells by activating the NF-κB pathway.

CONCLUDING REMARKS

Breast cancer is the most common malignancy in women and one of the leading causes of cancer death worldwide. Fortunately, radiotherapy is an effective treatment that provides local tumor control, increases survival, and reduces mortality. However, the acquisition of radioresistant phenotypes can compromise the success of therapy. In this review, we summarize the ncRNAs that participate in conferring radioresistance to breast cancer.

Recently, ncRNAs have emerged as important regulators of multiple cellular processes, and resistance to cancer treatment is no exception; we found reports of ncRNAs involved mainly in the regulation of the DDR mechanisms, followed by cell death, cell cycle, and other processes where the role of ncRNAs is studied in the same depth. A significant number of these works concerned miRNAs, although the proportion of reports on lncRNAs is likely to grow in the upcoming years since lncRNAs have a lower research age. In addition, we observed a growing trend in the number of reports of the response to IR through lncRNA-miRNA-target axes. While it is probable that most of the ncRNAs that regulate radioresistance follow this model, there are other mechanisms of action to explore.

We found of particular interest that several of the reported ncRNAs exhibit a multi-modulator capacity, targeting genes involved in various pathways. Some of them even perform dual roles inducing either radiosensitivity or radioresistance in different contexts. For example, miR-139-5p modulates five different targets involved in four different DDR pathways and,

additionally, can regulate DNA topology during the repair process. miR-185 regulates AKT and BCL-2, involved in the regulation of apoptosis, and RAD52, involved in HR. The miR-15 family, comprising the closely related miR-15a, miR-15b, and miR-16, is also multifunctional; it targets CHK1, promoting the formation of the γH2AX foci, while also regulating the cell cycle by targeting WEE1. miR-200c targets multiple proteins involved in the DDR and is also involved in autophagy by regulating the UBQLN1 protein; additionally, it may participate in other major pathways such as the PI3K-AKT and the EGFR. As for lncRNAs, HOTAIR regulates proteins involved in NHEJ, and its overexpression promotes radiation-induced apoptosis, possibly by targeting the PTEN-AKT pathway and miR-218, suggesting it may be a hub where the regulation of DDR, apoptosis, and cell cycle converge.

Accumulating evidence highlights the importance of the interaction between miRNAs and lncRNA. We found reports of miRNA/lncRNA/mRNA axes with a role in BC radioresistance, such as miR-200c/LINC02582/CHK1 and HOTAIR/miR-449-5p/HSPA1A. Our findings point to an increase in this kind of report since mRNA targets are yet to be identified. For instance, miR-185 was identified as a downstream target of the lncRNA LINC00511, promoting cell cycle progression and modulating DDR by regulating unidentified mRNAs. We also found reports with solid association data between a given ncRNA and radioresistance, such as HOTAIR, NEAT1, and miR-199a-5p, whose targets and interactions are still to be determined.

On the other hand, the regulation exerted by multiple ncRNAs converges in some protein targets, evincing the importance of their roles in the acquisition of radioresistance. CHK1 was directly regulated by lncRNA LINC02582, miR-16-5p, and the miR-15 family, and WEE1 was found to be controlled by the miR-15 family and miR-16-5p. Similarly, γH2AX foci formation was induced by several ncRNAs, including miR-155, LINP1, miR-200c, miR-7, miR-16-5p, the miR-15 family, and miR-205.

Many of the ncRNAs mentioned in this review are molecular marker candidates and promising therapeutic targets. Strategies aimed at downregulating ncRNAs that confer radioresistance or re-establishing the expression of those that elicit radiosensitivity are evident possibilities for adjuvant therapies that improve the outcome of radiotherapy alone. However, to get to that point, we need to fully characterize the mechanisms these ncRNAs employ. We anticipate more profound studies on ncRNA function for the upcoming years, as more research groups aim to validate the soaring results that bioinformatic analyses yield through the use of *in vivo* and *in vitro* models. Overall, the study of ncRNAs has great potential in the development of adjuvant and targeted therapies in the quest for higher survival rates and better prognosis not only for BC patients but for all cancer patients.

AUTHOR CONTRIBUTIONS

EL-U conceived the review. AA-M, JS-P, CL-C, and LB-E searched and organized the information. AL-A, JS-P, LB-E, and EL-U wrote the manuscript. AL-A, JS-P, DL, and LB-E prepared the figures. CL-C contributed substantially over the discussion and revision of the manuscript. EL-U and CP-P edited the final version. All authors contributed to the article and approved the submitted version.

FUNDING

This study was funded by DGAPA-PAPIIT, Universidad Nacional Autónoma de México with Grant Number IA204620, awarded to EL-U.

ACKNOWLEDGMENTS

LB-E is a student from Posgrado en Ciencias Biológicas, Universidad Nacional Autónoma de México (UNAM) and received a fellowship from CONACYT.

REFERENCES

1. Sung H, Ferlay J, Siegel RL, Laversanne M, Soerjomataram I, Jemal A, et al. Global Cancer Statistics 2020: GLOBOCAN Estimates of Incidence and Mortality Worldwide for 36 Cancers in 185 Countries. *CA Cancer J Clin* (2021) 71:209–49. doi: 10.3322/caac.21660
2. Llombart-Cussac A, Cortés J, Paré L, Galván P, Bermejo B, Martínez N, et al. HER2-Enriched Subtype as a Predictor of Pathological Complete Response Following Trastuzumab and Lapatinib Without Chemotherapy in Early-Stage HER2-Positive Breast Cancer (PAMELA): An Open-Label, Single-Group, Multicentre, Phase 2 Trial. *Lancet Oncol* (2017) 18:545–54. doi: 10.1016/S1470-2045(17)30021-9
3. Lehmann BD, Jovanović B, Chen X, Estrada MV, Johnson KN, Shyr Y, et al. Refinement of Triple-Negative Breast Cancer Molecular Subtypes: Implications for Neoadjuvant Chemotherapy Selection. *PloS One* (2016) 11:1–22. doi: 10.1371/journal.pone.0157368
4. Ménard S, Fortis S, Castiglioni F, Agresti R, Balsari A. HER2 as a Prognostic Factor in Breast Cancer. *Oncology* (2001) 61:67–72. doi: 10.1159/000055404
5. Abulkhair O, Moghraby JS, Badri M, Alkushi A. Clinicopathologic Features and Prognosis of Triple-Negative Breast Cancer in Patients 40 Years of Age and Younger in Saudi Arabia. *Hematol Oncol Stem Cell Ther* (2012) 5:101–6. doi: 10.5144/1658-3876.2012.101
6. He MY, Rancoule C, Rehailia-Blanchard A, Espenel S, Trone JC, Bernichon E, et al. Radiotherapy in Triple-Negative Breast Cancer: Current Situation and Upcoming Strategies. *Crit Rev Oncol Hematol* (2018) 131:96–101. doi: 10.1016/j.critrevonc.2018.09.004
7. Lu L, Dong J, Wang L, Xia Q, Zhang D, Kim H, et al. Activation of STAT3 and Bcl-2 and Reduction of Reactive Oxygen Species (ROS) Promote Radioresistance in Breast Cancer and Overcome of Radioresistance With Niclosamide. *Oncogene* (2018) 37:5292–304. doi: 10.1038/s41388-018-0340-y
8. Waks AG, Winer EP. Breast Cancer Treatment: A Review. *JAMA - J Am Med Assoc* (2019) 321:288–300. doi: 10.1001/jama.2018.19323
9. Podralska M, Ciesielska S, Kluiver J, van den Berg A, Dzikiewicz-Krawczyk A, Slezak-Prochazka I. Non-Coding RNAs in Cancer Radiosensitivity: MicroRNAs and Lncrnas as Regulators of Radiation-Induced Signaling Pathways. *Cancers (Basel)* (2020) 12:1–27. doi: 10.3390/cancers12061662

10. McGale P, Taylor C, Correa C, Cutter D, Duane F, Ewertz M, et al. Effect of Radiotherapy After Mastectomy and Axillary Surgery on 10-Year Recurrence and 20-Year Breast Cancer Mortality: Meta-Analysis of Individual Patient Data for 8135 Women in 22 Randomised Trials. *Lancet* (2014) 383:2127–35. doi: 10.1016/S0140-6736(14)60488-8
11. Giulietti A. Laser-Driven Particle Acceleration for Radiobiology and Radiotherapy: Where We Are and Where We Are Going. *Med Appl Laser-Generated Beams Part IV Rev Prog Strateg Futur* (2017) 10239:1023904. doi: 10.1117/12.2270945
12. Malouff TD, Mahajan A, Mutter RW, Krishnan S, Hoppe BS, Beltran C, et al. Carbon Ion Radiation Therapy in Breast Cancer: A New Frontier. *Breast Cancer Res Treat* (2020) 181:291–6. doi: 10.1007/s10549-020-05641-2
13. Lomax ME, Folkes LK, O'Neill P. Biological Consequences of Radiation-Induced DNA Damage: Relevance to Radiotherapy. *Clin Oncol* (2013) 25:578–85. doi: 10.1016/j.clon.2013.06.007
14. Hatzi VI, Laskaratou DA, Mavragani IV, Nikitaki Z, Mangelis A, Panayiotidis MI, et al. Non-Targeted Radiation Effects *In Vivo*: A Critical Glance of the Future in Radiobiology. *Cancer Lett* (2015) 356:34–42. doi: 10.1016/j.canlet.2013.11.018
15. Sridharan DM, Asaithamby A, Bailey SM, Costes SV, Doetsch PW, Dynan WS, et al. Understanding Cancer Development Processes After HZE-Particle Exposure: Roles of ROS, DNA Damage Repair and Inflammation. *Radiat Res* (2015) 183:1–26. doi: 10.1667/RR13804.1
16. Yao Y, Chu Y, Xu B, Hu Q, Song Q. Radiotherapy After Surgery has Significant Survival Benefits for Patients With Triple-Negative Breast Cancer. *Cancer Med* (2019) 8:554–63. doi: 10.1002/cam4.1954
17. Liu L, Zhu Y, Liu AM, Feng Y, Chen Y. Long Noncoding RNA LINC00511 Involves in Breast Cancer Recurrence and Radioresistance by Regulating STXBP4 Expression via miR-185. *Eur Rev Med Pharmacol Sci* (2019) 23:7457–68. doi: 10.26355/eurrev_201909_18855
18. Nickoloff JA, Boss MK, Allen CP, LaRue SM. Translational Research in Radiation-Induced DNA Damage Signaling and Repair. *Transl Cancer Res* (2017) 6:S875–91. doi: 10.21037/tcr.2017.06.02
19. Chen S, Zhao Y, Han W, Chiu SK, Zhu L, Wu L, et al. Rescue Effects in Radiobiology: Unirradiated Bystander Cells Assist Irradiated Cells Through Intercellular Signal Feedback. *Mutat Res Fundam Mol Mech Mutagen* (2011) 706:59–64. doi: 10.1016/j.mrfmmm.2010.10.011
20. Heeran AB, Berrigan HP, O'Sullivan J. The Radiation-Induced Bystander Effect (RIBE) and its Connections With the Hallmarks of Cancer. *Radiat Res* (2019) 192:668–79. doi: 10.1667/RR15489.1
21. Wang H, Mu X, He H, Zhang XD. Cancer Radiosensitizers. *Trends Pharmacol Sci* (2018) 39:24–48. doi: 10.1016/j.tips.2017.11.003
22. Choi J, Yoon YN, Kim N, Park CS, Seol H, Park IC, et al. Predicting Radiation Resistance in Breast Cancer With Expression Status of Phosphorylated S6K1. *Sci Rep* (2020) 10:1–8. doi: 10.1038/s41598-020-57496-8
23. Kaidar-Person O, Lai C, Kuten A, Belkacemi Y. "The Infinite Maze" of Breast Cancer, Signaling Pathways and Radioresistance. *Breast* (2013) 22:411–8. doi: 10.1016/j.breast.2013.04.003
24. He L, Hannon GJ. MicroRNAs: Small RNAs With a Big Role in Gene Regulation. *Nat Rev Genet* (2004) 5:522–31. doi: 10.1038/nrg1379
25. Filipowicz W, Bhattacharyya SN, Sonenberg N. Mechanisms of Post-Transcriptional Regulation by microRNAs: Are the Answers in Sight? *Nat Rev Genet* (2008) 9:102–14. doi: 10.1038/nrg2290
26. Asiaf A, Ahmad ST, Arjumand W, Zargar MA. MicroRNAs in Breast Cancer: Diagnostic and Therapeutic Potential. *Methods Mol Biol* (2018) 1699:23–43. doi: 10.1007/978-1-4939-7435-1_2
27. Svoronos AA, Engelman DM, Slack FJ. OncomiR or Tumor Suppressor? The Duplicity of MicroRNAs in Cancer. *Cancer Res* (2016) 76:3666–70. doi: 10.1158/0008-5472.CAN-16-0359
28. Si W, Shen J, Zheng H, Fan W. The Role and Mechanisms of Action of microRNAs in Cancer Drug Resistance. *Clin Epigenet* (2019) 11:1–24. doi: 10.1186/s13148-018-0587-8
29. Zhang Q, Zhang S. MIR-214 Promotes Radioresistance in Human Ovarian Cancer Cells by Targeting PETN. *Biosci Rep* (2017) 37:1–8. doi: 10.1042/BSR20170327
30. Falzone L, Scola L, Zanghì A, Biondi A, Di Cataldo A, Libra M, et al. Integrated Analysis of Colorectal Cancer microRNA Datasets: Identification of microRNAs Associated With Tumor Development. *Aging (Albany NY)* (2018) 10:1000–14. doi: 10.18632/aging.101444
31. Zheng S, Zhong Y-F, Tan D-M, Xu Y, Chen H-X, Wang D. miR-183-5p Enhances the Radioresistance of Colorectal Cancer by Directly Targeting ATG5. *J Biosci* (2019) 44:92. doi: 10.1007/s12038-019-9918-y
32. Li H, Jiang M, Cui M, Feng G, Dong J, Li Y, et al. MiR-365 Enhances the Radiosensitivity of non-Small Cell Lung Cancer Cells Through Targeting CDC25A. *Biochem Biophys Res Commun* (2019) 512:392–8. doi: 10.1016/j.bbrc.2019.03.082
33. Bhan A, Soleimani M, Mandal SS. Long Noncoding RNA and Cancer: A New Paradigm. *Cancer Res* (2017) 77:3965–81. doi: 10.1158/0008-5472.CAN-16-2634
34. Prensner JR, Chinnaiyan AM. The Emergence of lncRNAs in Cancer Biology. *Cancer Discov* (2011) 1:391–407. doi: 10.1158/2159-8290.CD-11-0209
35. Sahu A, Singhal U, Chinnaiyan AM. Long Noncoding RNAs in Cancer: From Function to Translation. *Trends Cancer* (2015) 1:93–109. doi: 10.1016/j.trecan.2015.08.010
36. Hu X, Ding D, Zhang J, Cui J. Knockdown of lncRNA HOTAIR Sensitizes Breast Cancer Cells to Ionizing Radiation Through Activating miR-218. *Biosci Rep* (2019) 29:1–9. doi: 10.1042/BSR20181038
37. Su M, Wang H, Wang W, Wang Y, Ouyang L, Pan C, et al. LncRNAs in DNA Damage Response and Repair in Cancer Cells. *Acta Biochim Biophys Sin (Shanghai)* (2018) 50:433–9. doi: 10.1093/ABBS/GMY022
38. Chakraborty S, Deb A, Maji RK, Saha S, Ghosh Z. LncRBase: An Enriched Resource for lncRNA Information. *PloS One* (2014) 9:1–11. doi: 10.1371/journal.pone.0108010
39. Taiana E, Favasuli V, Ronchetti D, Todoerti K, Pelizzoni F, Manzoni M, et al. Long non-Coding RNA NEAT1 Targeting Impairs the DNA Repair Machinery and Triggers Anti-Tumor Activity in Multiple Myeloma. *Leukemia* (2020) 34:234–44. doi: 10.1038/s41375-019-0542-5
40. Dou Q, Xu Y, Zhu Y, Hu Y, Yan Y, Yan H. LncRNA FAM83H-AS1 Contributes to the Radioresistance, Proliferation, and Metastasis in Ovarian Cancer Through Stabilizing HuR Protein. *Eur J Pharmacol* (2019) 852:134–41. doi: 10.1016/j.ejphar.2019.03.002
41. Hu X, Jiang H, Jiang X. Downregulation of lncRNA ANRIL Inhibits Proliferation, Induces Apoptosis, and Enhances Radiosensitivity in Nasopharyngeal Carcinoma Cells Through Regulating miR-125a. *Cancer Biol Ther* (2017) 18:331–8. doi: 10.1080/15384047.2017.1310348
42. Shan TD, Xu JH, Yu T, Li JY, Zhao LN, Ouyang H, et al. Knockdown of Linc-POU3F3 Suppresses the Proliferation, Apoptosis, and Migration Resistance of Colorectal Cancer. *Oncotarget* (2016) 7:961–75. doi: 10.18632/ONCOTARGET.5830
43. Zhang L, Jin C, Yang G, Wang B, Hua P, Zhang Y. LncRNA WTAPP1 Promotes Cancer Cell Invasion and Migration in NSCLC by Downregulating lncRNA HAND2-As1. *BMC Pulm Med* (2020) 20:1–6. doi: 10.1186/s12890-020-01180-0
44. Chen X, Liang H, Zhang CY, Zen K. MiRNA Regulates Noncoding RNA: A Noncanonical Function Model. *Trends Biochem Sci* (2012) 37:457–9. doi: 10.1016/j.tibs.2012.08.005
45. Yang C, Wu D, Gao L, Liu X, Jin Y, Wang D, et al. Competing Endogenous RNA Networks in Human Cancer: Hypothesis, Validation, and Perspectives. *Oncotarget* (2016) 7:13479–90. doi: 10.18632/oncotarget.7266
46. Ge X, Gu Y, Li D, Jiang M, Zhao S, Li Z, et al. Knockdown of lncRNA PCAT1 Enhances Radiosensitivity of Cervical Cancer by Regulating miR-128/GOLM1 Axis. *Onco Targets Ther* (2020) 13:10373–85. doi: 10.2147/OTT.S263728
47. Liu R, Zhang Q, Shen L, Chen S, He J, Wang D, et al. Long Noncoding RNA lnc-RI Regulates DNA Damage Repair and Radiation Sensitivity of CRC Cells Through NHEJ Pathway. *Cell Biol Toxicol* (2020) 36:493–507. doi: 10.1007/s10565-020-09524-6
48. Xiao J, Lin L, Luo D, Shi L, Chen W, Fan H, et al. Long Noncoding RNA TRPM2-AS Acts as a microRNA Sponge of miR-612 to Promote Gastric Cancer Progression and Radioresistance. *Oncogenesis* (2020) 9:1–15. doi: 10.1038/s41389-020-0215-2
49. Wang R, Huang Z, Qian C, Wang M, Zheng Y, Jiang R, et al. LncRNA WEE2-AS1 Promotes Proliferation and Inhibits Apoptosis in Triple Negative Breast Cancer Cells *via* Regulating miR-32-5p/TOB1 Axis.

Biochem Biophys Res Commun (2020) 526:1005–12. doi: 10.1016/j.bbrc.2020.01.170
50. Fan H, Yuan J, Li X, Ma Y, Wang X, Xu B, et al. LncRNA LINC00173 Enhances Triple-Negative Breast Cancer Progression by Suppressing miR-490-3p Expression. *BioMed Pharmacother* (2020) 125:109987. doi: 10.1016/j.biopha.2020.109987
51. Huang Y, Wang X, Zheng Y, Chen W, Zheng Y, Li G, et al. Construction of an mRNA-miRNA-lncRNA Network Prognostic for Triple-Negative Breast Cancer. *Aging (Albany NY)* (2021) 13:1153–75. doi: 10.18632/aging.202254
52. Griñán-Lisón C, Olivares-Urbano MA, Jiménez G, López-Ruiz E, Val C, Morata-Tarifa C, et al. miRNAs as Radio-Response Biomarkers for Breast Cancer Stem Cells. *Mol Oncol* (2020) 14:556–70. doi: 10.1002/1878-0261.12635
53. Yao Z, Zhang Y, Xu D, Zhou X, Peng P, Pan Z, et al. Research Progress on Long non-Coding RNA and Radiotherapy. *Med Sci Monit* (2019) 25:5757–70. doi: 10.12659/MSM.915647
54. Giglia-Mari G, Zotter A, Vermeulen W. DNA Damage Response. *Cold Spring Harb Perspect Biol* (2011) 3:1–19. doi: 10.1101/cshperspect.a000745
55. Chatterjee N, Walker GC. Mechanisms of DNA Damage, Repair, and Mutagenesis. *Environ Mol Mutagen* (2017) 58:235–63. doi: 10.1002/em.22087
56. Sancar A, Lindsey-Boltz LA, Ünsal-Kaçmaz K, Linn S. Molecular Mechanisms of Mammalian DNA Repair and the DNA Damage Checkpoints. *Annu Rev Biochem* (2004) 73:39–85. doi: 10.1146/annurev.biochem.73.011303.073723
57. Christmann M, Tomicic MT, Roos WP, Kaina B. Mechanisms of Human DNA Repair: An Update. *Toxicology* (2003) 193:3–34. doi: 10.1016/S0300-483X(03)00287-7
58. Mladenov E, Magin S, Soni A, Iliakis G. DNA Double-Strand Break Repair as Determinant of Cellular Radiosensitivity to Killing and Target in Radiation Therapy. *Front Oncol* (2013) 3:113. doi: 10.3389/fonc.2013.00113
59. Scott SP, Pandita TK. The Cellular Control of DNA Double-Strand Breaks. *J Cell Biochem* (2006) 99:1463–75. doi: 10.1002/jcb.21067
60. Durut N, Mittelsten Scheid O. The Role of Noncoding RNAs in Double-Strand Break Repair. *Front Plant Sci* (2019) 10:1155. doi: 10.3389/fpls.2019.01155
61. Storici F, Tichon AE. RNA Takes Over Control of DNA Break Repair. *Nat Cell Biol* (2017) 19:1382–4. doi: 10.1038/ncb3645
62. Zhang C, Peng G. Non-Coding RNAs: An Emerging Player in DNA Damage Response. *Mutat Res Rev Mutat Res* (2015) 763:202–11. doi: 10.1016/j.mrrev.2014.11.003
63. Mah LJ, El-Osta A, Karagiannis TC. γh2AX: A Sensitive Molecular Marker of DNA Damage and Repair. *Leukemia* (2010) 24:679–86. doi: 10.1038/leu.2010.6
64. Zhang P, Wang L, Rodriguez-Aguayo C, Yuan Y, Debeb BG, Chen D, et al. MiR-205 Acts as a Tumour Radiosensitizer by Targeting ZEB1 and Ubc13. *Nat Commun* (2014) 5:1–10. doi: 10.1038/ncomms6671
65. Mei Z, Su T, Ye J, Yang C, Zhang S, Xie C. The miR-15 Family Enhances the Radiosensitivity of Breast Cancer Cells by Targeting G2 Checkpoints. *Radiat Res* (2015) 183:196–207. doi: 10.1667/RR13784.1
66. Masoudi-Khoram N, Abdolmaleki P, Hosseinkhan N, Nikoofar A, Mowla SJ, Monfared H, et al. Differential miRNAs Expression Pattern of Irradiated Breast Cancer Cell Lines Is Correlated With Radiation Sensitivity. *Sci Rep* (2020) 10:1–12. doi: 10.1038/s41598-020-65680-z
67. Koo T, Cho BJ, Kim DH, Park JM, Choi EJ, Kim HH, et al. MicroRNA-200c Increases Radiosensitivity of Human Cancer Cells With Activated EGFR-Associated Signaling. *Oncotarget* (2017) 8:65457–68. doi: 10.18632/oncotarget.18924
68. Lin J, Liu C, Gao F, Mitchel REJ, Zhao L, Yang Y, et al. MiR-200c Enhances Radiosensitivity of Human Breast Cancer Cells. *J Cell Biochem* (2013) 114:606–15. doi: 10.1002/jcb.24398
69. Wang B, Zheng J, Li R, Tian Y, Lin J, Liang Y, et al. Long Noncoding RNA LINC02582 Acts Downstream of miR-200c to Promote Radioresistance Through CHK1 in Breast Cancer Cells. *Cell Death Dis* (2019) 10:1–15. doi: 10.1038/s41419-019-1996-0
70. Chen Y, Sanchez Y. Chk1 in the DNA Damage Response: Conserved Roles From Yeasts to Mammals. *DNA Repair (Amst)* (2004) 3:1025–32. doi: 10.1016/j.dnarep.2004.03.003
71. Lee KM, Choi EJ, Kim IA. MicroRNA-7 Increases Radiosensitivity of Human Cancer Cells With Activated EGFR-Associated Signaling. *Radiother Oncol* (2011) 101:171–6. doi: 10.1016/j.radonc.2011.05.050
72. Zhang Y, He Q, Hu Z, Feng Y, Fan L, Tang Z, et al. Long Noncoding RNA LINP1 Regulates Repair of DNA Double-Strand Breaks in Triple-Negative Breast Cancer. *Nat Struct Mol Biol* (2016) 23:522–30. doi: 10.1038/nsmb.3211
73. Daboussi F, Dumay A, Delacôte F, Lopez BS. DNA Double-Strand Break Repair Signalling: The Case of RAD51 Post-Translational Regulation. *Cell Signal* (2002) 14:969–75. doi: 10.1016/S0898-6568(02)00052-9
74. Gasparini P, Lovat F, Fassan M, Casadei L, Cascione L, Jacob NK, et al. Protective Role of miR-155 in Breast Cancer Through RAD51 Targeting Impairs Homologous Recombination After Irradiation. *Proc Natl Acad Sci USA* (2014) 111:4536–41. doi: 10.1073/pnas.1402604111
75. Liang Z, Ahn J, Guo D, Votaw JR, Shim H. MicroRNA-302 Replacement Therapy Sensitizes Breast Cancer Cells to Ionizing Radiation. *Pharm Res* (2013) 30:1008–16. doi: 10.1007/s11095-012-0936-9
76. Symington LS. Role of RAD52 Epistasis Group Genes in Homologous Recombination and Double-Strand Break Repair. *Microbiol Mol Biol Rev* (2002) 66:630–70. doi: 10.1128/mmbr.66.4.630-670.2002
77. Chai Y, Yang X, Li Y, Qu Q. MicroRNA-185 Overexpression Sensitizes Breast Cancer Cells to Ionizing Radiation: A Potential Therapeutic Role in Breast Cancer. *Int J Clin Exp Pathol* (2017) 10:274–81.
78. Troschel FM, Böhly N, Borrmann K, Braun T, Schwickert A, Kiesel L, et al. miR-142-3p Attenuates Breast Cancer Stem Cell Characteristics and Decreases Radioresistance *In Vitro*. *Tumor Biol* (2018) 40:1–10. doi: 10.1177/1010428318791887
79. Zhang J. The Role of BRCA1 in Homologous Recombination Repair in Response to Replication Stress: Significance in Tumorigenesis and Cancer Therapy. *Cell Biosci* (2013) 3:1–14. doi: 10.1186/2045-3701-3-11
80. Cantor SB, Bell DW, Ganesan S, Kass EM, Drapkin R, Grossman S, et al. BACH1, a Novel Helicase-Like Protein, Interacts Directly With BRCA1 and Contributes to its DNA Repair Function. *Cell* (2001) 105:149–60. doi: 10.1016/S0092-8674(01)00304-X
81. Tan X, Li Z, Ren S, Rezaei K, Pan Q, Goldstein AT, et al. Dynamically Decreased miR-671-5p Expression Is Associated With Oncogenic Transformation and Radiochemoresistance in Breast Cancer. *Breast Cancer Res* (2019) 21:1–14. doi: 10.1186/s13058-019-1173-5
82. Qian L, Fei Q, Zhang H, Qiu M, Zhang B, Wang Q, et al. lncRNA HOTAIR Promotes DNA Repair and Radioresistance of Breast Cancer *via* EZH2. *DNA Cell Biol* (2020) 39:2166–73. doi: 10.1089/dna.2020.5771
83. Shrivastav M, De Haro LP, Nickoloff JA. Regulation of DNA Double-Strand Break Repair Pathway Choice. *Cell Res* (2008) 18:134–47. doi: 10.1038/cr.2007.111
84. Tomimatsu N, Tahimic CGT, Otsuki A, Burma S, Fukuhara A, Sato K, et al. Ku70/80 Modulates ATM and ATR Signaling Pathways in Response to DNA Double Strand Breaks. *J Biol Chem* (2007) 282:10138–45. doi: 10.1074/jbc.M611880200
85. Pajic M, Froio D, Daly S, Doculara L, Millar E, Graham PH, et al. miR-139-5p Modulates Radiotherapy Resistance in Breast Cancer by Repressing Multiple Gene Networks of DNA Repair and ROS Defense. *Cancer Res* (2018) 78:501–15. doi: 10.1158/0008-5472.CAN-16-3105
86. Kaczanowski S. Apoptosis: Its Origin, History, Maintenance and the Medical Implications for Cancer and Aging. *Phys Biol* (2016) 13:31001. doi: 10.1088/1478-3975/13/3/031001
87. Pistritto G, Trisciuoglio D, Ceci C, Garufi A, D'Orazi G. Apoptosis as Anticancer Mechanism: Function and Dysfunction of its Modulators and Targeted Therapeutic Strategies. *Aging (Albany NY)* (2016) 8:603–19. doi: 10.18632/aging.100934
88. Cao K, Tait SWG. Apoptosis and Cancer: Force Awakens, Phantom Menace, or Both? *Int Rev Cell Mol Biol* (2018) 337:135–52. doi: 10.1016/bs.ircmb.2017.12.003
89. Yu L, Yang Y, Hou J, Zhai C, Song Y, Zhang Z, et al. MicroRNA-144 Affects Radiotherapy Sensitivity by Promoting Proliferation, Migration and Invasion of Breast Cancer Cells. *Oncol Rep* (2015) 34:1845–52. doi: 10.3892/or.2015.4173
90. Zhou Y, Wang C, Liu X, Wu C, Yin H. Long non-Coding RNA HOTAIR Enhances Radioresistance in MDA-MB231 Breast Cancer Cells. *Oncol Lett* (2017) 13:1143–8. doi: 10.3892/ol.2017.5587

91. Lai Y, Chen Y, Lin Y, Ye L. Down-Regulation of LncRNA CCAT1 Enhances Radiosensitivity *via* Regulating miR-148b in Breast Cancer. *Cell Biol Int* (2018) 42:227–36. doi: 10.1002/cbin.10890
92. Zhu J, Ye Q, Chang L, Xiong W, He Q, Li W. Upregulation of miR-195 Enhances the Radiosensitivity of Breast Cancer Cells Through the Inhibition of BCL-2. *Int J Clin Exp Med* (2015) 8:9142–8. doi: 10.1007/s12038-019-9918-y
93. Zhang J, Cui Y, Lin X, Zhang G, Li Z. MiR-122-3p Sensitizes Breast Cancer Cells to Ionizing Radiation *via* Controlling of Cell Apoptosis, Migration and Invasion. *Int J Clin Exp Pathol* (2017) 10:215–23.
94. Doherty J, Baehrecke EH. Life, Death and Autophagy. *Nat Cell Biol* (2018) 20:1110–7. doi: 10.1038/s41556-018-0201-5
95. Kim KH, Lee M-S. Autophagy—a Key Player in Cellular and Body Metabolism. *Nat Rev Endocrinol* (2014) 10:322–37. doi: 10.1038/nrendo.2014.35
96. Maiuri MC, Zalckvar E, Kimchi A, Kroemer G. Self-Eating and Self-Killing: Crosstalk Between Autophagy and Apoptosis. *Nat Rev Mol Cell Biol* (2007) 8:741–52. doi: 10.1038/nrm2239
97. D'Arcy MS. Cell Death: A Review of the Major Forms of Apoptosis, Necrosis and Autophagy. *Cell Biol Int* (2019) 43:582–92. doi: 10.1002/cbin.11137
98. Yi H, Liang B, Jia J, Liang N, Xu H, Ju G, et al. Differential Roles of miR-199a-5p in Radiation-Induced Autophagy in Breast Cancer Cells. *FEBS Lett* (2013) 587:436–43. doi: 10.1016/j.febslet.2012.12.027
99. Sun Q, Liu T, Yuan Y, Guo Z, Xie G, Du S, et al. MiR-200c Inhibits Autophagy and Enhances Radiosensitivity in Breast Cancer Cells by Targeting UBQLN1. *Int J Cancer* (2015) 136:1003–12. doi: 10.1002/ijc.29065
100. Luo J, Chen J, He L. Mir-129-5p Attenuates Irradiation-Induced Autophagy and Decreases Radioresistance of Breast Cancer Cells by Targeting HMGB1. *Med Sci Monit* (2015) 21:4122–9. doi: 10.12659/MSM.896661
101. Foster I. Cancer: A Cell Cycle Defect. *Radiography* (2008) 14:144–9. doi: 10.1016/j.radi.2006.12.001
102. Barnum KJ, O'Connell MJ. Cell Cycle Regulation by Checkpoints. *Methods Mol Biol* (2014) 1170:29–40. doi: 10.1007/978-1-4939-0888-2_2
103. Kastan MB, Bartek J. Cell-Cycle Checkpoints and Cancer. *Nature* (2004) 432:316–23. doi: 10.1038/nature03097
104. Zhang N, Zeng X, Sun C, Guo H, Wang T, Wei L, et al. LncRNA LINC00963 Promotes Tumorigenesis and Radioresistance in Breast Cancer by Sponging miR-324-3p and Inducing ACK1 Expression. *Mol Ther Nucleic Acids* (2019) 18:871–81. doi: 10.1016/j.omtn.2019.09.033
105. Rokudai S, Li Y, Otaka Y, Fujieda M, Owens DM, Christiano AM, et al. STXBP4 Regulates APC/C-Mediated P63 Turnover and Drives Squamous Cell Carcinogenesis. *Proc Natl Acad Sci USA* (2018) 115:E4806–14. doi: 10.1073/pnas.1718546115
106. Wang F, Wang W, Lu L, Xie Y, Yan J, Chen Y, et al. MicroRNA-16-5p Regulates Cell Survival, Cell Cycle and Apoptosis by Targeting AKT3 in Prostate Cancer Cells. *Oncol Rep* (2020) 44:1282–92. doi: 10.3892/or.2020.7682
107. Ruan L, Qian X. MiR-16-5p Inhibits Breast Cancer by Reducing AKT3 to Restrain NF-κB Pathway. *Biosci Rep* (2019) 39(8):20191611. doi: 10.1042/BSR20191611
108. Talvinen K, Karra H, Pitkänen R, Ahonen I, Nykänen M, Lintunen M, et al. Low Cdc27 and High Securin Expression Predict Short Survival for Breast Cancer Patients. *APMIS* (2013) 121:945–53. doi: 10.1111/apm.12110
109. Ren YQ, Fu F, Han J. MiR-27a Modulates Radiosensitivity of Triple-Negative Breast Cancer (TNBC) Cells by Targeting CDC27. *Med Sci Monit* (2015) 21:1297–303. doi: 10.12659/MSM.893974
110. Yang B, Kuai F, Chen Z, Fu D, Liu J, Wu Y, et al. MiR-634 Decreases the Radioresistance of Human Breast Cancer Cells by Targeting STAT3. *Cancer Biother Radiopharm* (2020) 35:241–8. doi: 10.1089/cbr.2019.3220
111. Fabris L, Berton S, Citron F, D'Andrea S, Segatto I, Nicoloso MS, et al. Radiotherapy-Induced miR-223 Prevents Relapse of Breast Cancer by Targeting the EGF Pathway. *Oncogene* (2016) 35:4914–26. doi: 10.1038/onc.2016.23
112. Metheetrairut C, Adams BD, Nallur S, Weidhaas JB, Slack FJ. Cel-Mir-237 and its Homologue, hsa-miR-125b, Modulate the Cellular Response to Ionizing Radiation. *Oncogene* (2017) 36:512–24. doi: 10.1038/onc.2016.222
113. Wang L, Yuan C, Lv K, Xie S, Fu P, Liu X, et al. Lin28 Mediates Radiation Resistance of Breast Cancer Cells *via* Regulation of Caspase, H2A.X and Let-7 Signaling. *PloS One* (2013) 8:e67373. doi: 10.1371/journal.pone.0067373
114. Zhang X, Li Y, Wang D, Wei X. miR-22 Suppresses Tumorigenesis and Improves Radiosensitivity of Breast Cancer Cells by Targeting Sirt1. *Biol Res* (2017) 50:27. doi: 10.1186/s40659-017-0133-8
115. Lee HC, Her N-G, Kang D, Jung SH, Shin J, Lee M, et al. Radiation-Inducible miR-770-5p Sensitizes Tumors to Radiation Through Direct Targeting of PDZ-Binding Kinase. *Cell Death Dis* (2017) 8:e2693–3. doi: 10.1038/cddis.2017.116
116. Fu Y, Xiong J. MicroRNA-124 Enhances Response to Radiotherapy in Human Epidermal Growth Factor Receptor 2-Positive Breast Cancer Cells by Targeting Signal Transducer and Activator of Transcription 3. *Croat Med J* (2016) 57:457–64. doi: 10.3325/cmj.2016.57.457
117. Perez-Añorve IX, Gonzalez-De la Rosa CH, Soto-Reyes E, Beltran-Anaya FO, Del Moral-Hernandez O, Salgado-Albarran M, et al. New Insights Into Radioresistance in Breast Cancer Identify a Dual Function of miR-122 as a Tumor Suppressor and oncomiR. *Mol Oncol* (2019) 13:1249–67. doi: 10.1002/1878-0261.12483
118. Kato M, Paranjape T, Ullrich R, Nallur S, Gillespie E, Keane K, et al. The Mir-34 microRNA Is Required for the DNA Damage Response *In Vivo* in C. Elegans and *In Vitro* in Human Breast Cancer Cells. *Oncogene* (2009) 28:2419–24. doi: 10.1038/onc.2009.106
119. Wolfe AR, Bambhroliya A, Reddy JP, Debeb BG, Huo L, Larson R, et al. MiR-33a Decreases High-Density Lipoprotein-Induced Radiation Sensitivity in Breast Cancer. *Int J Radiat Oncol Biol Phys* (2016) 95:791–9. doi: 10.1016/j.ijrobp.2016.01.025
120. Zhang S, Wang B, Xiao H, Dong J, Li Y, Zhu C, et al. LncRNA HOTAIR Enhances Breast Cancer Radioresistance Through Facilitating HSPA1A Expression *via* Sequestering miR-449b-5p. *Thorac Cancer* (2020) 11:1801–16. doi: 10.1111/1759-7714.13450
121. Huang X, Taeb S, Jahangiri S, Korpela E, Cadonic I, Yu N, et al. miR-620 Promotes Tumor Radioresistance by Targeting 15-Hydroxyprostaglandin Dehydrogenase (HPGD). *Oncotarget* (2015) 6:22439–51. doi: 10.18632/oncotarget.4210
122. Shi R, Wu P, Liu M, Chen B, Cong L. Knockdown of lncRNA PCAT6 Enhances Radiosensitivity in Triple-Negative Breast Cancer Cells by Regulating miR-185-5p/TPD52 Axis. *Onco Targets Ther* (2020) 13:3025–37. doi: 10.2147/OTT.S237559
123. Lin LC, Lee H, Chien PJ, Huang YH, Chang MY, Lee YC, et al. Nad(P)h: Quinone Oxidoreductase 1 Determines Radiosensitivity of Triple Negative Breast Cancer Cells and Is Controlled by Long non-Coding Rna Neat1. *Int J Med Sci* (2020) 17:2214–24. doi: 10.7150/ijms.45706
124. Luo M, Ding L, Li Q, Yao H. miR-668 Enhances the Radioresistance of Human Breast Cancer Cell by Targeting IκBα. *Breast Cancer* (2017) 24:673–82. doi: 10.1007/s12282-017-0756-1
125. Ma JH, Qin L, Li X. Role of STAT3 Signaling Pathway in Breast Cancer. *Cell Commun Signal* (2020) 18:1–13. doi: 10.1186/s12964-020-0527-z
126. Masuda H, Zhang D, Bartholomeusz C, Doihara H, Hortobagyi GN, Ueno NT. Role of Epidermal Growth Factor Receptor in Breast Cancer. *Breast Cancer Res Treat* (2012) 136:331–45. doi: 10.1007/s10549-012-2289-9
127. Wu Q, Wu W, Fu B, Shi L, Wang X, Kuca K. JNK Signaling in Cancer Cell Survival. *Med Res Rev* (2019) 39:2082–104. doi: 10.1002/med.21574
128. Duffy MJ, Synnott NC, Crown J. Mutant P53 as a Target for Cancer Treatment. *Eur J Cancer* (2017) 83:258–65. doi: 10.1016/j.ejca.2017.06.023
129. Raychaudhuri P, Park HJ. FoxM1: A Master Regulator of Tumor Metastasis. *Cancer Res* (2011) 71:4329–33. doi: 10.1158/0008-5472.CAN-11-0640
130. Zona S, Bella L, Burton MJ, Nestal de Moraes G, Lam EWF. FOXM1: An Emerging Master Regulator of DNA Damage Response and Genotoxic Agent Resistance. *Biochim Biophys Acta - Gene Regul Mech* (2014) 1839:1316–22. doi: 10.1016/j.bbagrm.2014.09.016
131. Sharma B, Agnihotri N. Role of Cholesterol Homeostasis and its Efflux Pathways in Cancer Progression. *J Steroid Biochem Mol Biol* (2019) 191:105377. doi: 10.1016/j.jsbmb.2019.105377
132. Balzeau J, Menezes MR, Cao S, Hagan JP. The LIN28/let-7 Pathway in Cancer. *Front Genet* (2017) 8:31. doi: 10.3389/fgene.2017.00031
133. Lee H, Kim KR, Noh SJ, Park HS, Kwon KS, Park BH, et al. Expression of DBC1 and SIRT1 Is Associated With Poor Prognosis for Breast Carcinoma. *Hum Pathol* (2011) 42:204–13. doi: 10.1016/j.humpath.2010.05.023
134. Liu T, Liu PY, Marshall GM. The Critical Role of the Class III Histone Deacetylase SIRT1 in Cancer. *Cancer Res* (2009) 69:1702–5. doi: 10.1158/0008-5472.CAN-08-3365

135. Santolla MF, Avino S, Pellegrino M, De Francesco EM, De Marco P, Lappano R, et al. SIRT1 Is Involved in Oncogenic Signaling Mediated by GPER in Breast Cancer. *Cell Death Dis* (2015) 6:1–12. doi: 10.1038/cddis.2015.201
136. Ayllón V, O'Connor R. PBK/TOPK Promotes Tumour Cell Proliferation Through P38 MAPK Activity and Regulation of the DNA Damage Response. *Oncogene* (2007) 26:3451–61. doi: 10.1038/sj.onc.1210142
137. Dougherty JD, Garcia ADR, Nakano I, Livingstone M, Norris B, Polakiewicz R, et al. PBK/TOPK, a Proliferating Neural Progenitor-Specific Mitogen-Activated Protein Kinase Kinase. *J Neurosci* (2005) 25:10763–85. doi: 10.1523/JNEUROSCI.3207-05.2005
138. Joel M, Mughal AA, Grieg Z, Murrell W, Palmero S, Mikkelsen B, et al. Targeting PBK/TOPK Decreases Growth and Survival of Glioma Initiating Cells *In Vitro* and Attenuates Tumor Growth *In Vivo*. *Mol Cancer* (2015) 14:1–15. doi: 10.1186/s12943-015-0398-x
139. Vostakolaei MA, Hatami-Baroogh L, Babaei G, Molavi O, Kordi S, Abdolalizadeh J. Hsp70 in Cancer: A Double Agent in the Battle Between Survival and Death. *J Cell Physiol* (2021) 236:3420–44. doi: 10.1002/jcp.30132
140. Clara JA, Monge C, Yang Y, Takebe N. Targeting Signalling Pathways and the Immune Microenvironment of Cancer Stem Cells — a Clinical Update. *Nat Rev Clin Oncol* (2020) 17:204–32. doi: 10.1038/s41571-019-0293-2
141. Gupta SC, Kunnumakkara AB, Aggarwal S, Aggarwal BB. Inflammation, a Double-Edge Sword for Cancer and Other Age-Related Diseases. *Front Immunol* (2018) 9:2160. doi: 10.3389/fimmu.2018.02160
142. Aggarwal BB. Nuclear Factor-κB. *Cancer Cell* (2004) 6:203–8. doi: 10.1016/j.ccr.2004.09.003

Conflict of Interest: The authors declare that the research was conducted in the absence of any commercial or financial relationships that could be construed as a potential conflict of interest.

Publisher's Note: All claims expressed in this article are solely those of the authors and do not necessarily represent those of their affiliated organizations, or those of the publisher, the editors and the reviewers. Any product that may be evaluated in this article, or claim that may be made by its manufacturer, is not guaranteed or endorsed by the publisher.

frontiers in Cell and Developmental Biology

ORIGINAL RESEARCH
published: 23 November 2021
doi: 10.3389/fcell.2021.762588

Methyltransferase-Like 3-Mediated m6A Methylation of Hsa_circ_0058493 Accelerates Hepatocellular Carcinoma Progression by Binding to YTH Domain-Containing Protein 1

Anqi Wu[1†], Yuhao Hu[1†], Yao Xu[2†], Jing Xu[3], Xinyue Wang[3], Aiting Cai[1], Ruoyu Liu[1], Lin Chen[4] and Feng Wang[1]**

[1] Department of Laboratory Medicine, Affiliated Hospital of Nantong University, Nantong, China, [2] Department of Laboratory Medicine, The Second Affiliated Hospital of Nantong University, Nantong, China, [3] Department of Laboratory Medicine, School of Public Health, Nantong University, Nantong, China, [4] Department of Hepatology Laboratory, Nantong Third Hospital Affiliated to Nantong University, Nantong, China

Circular RNAs (circRNAs) are highly correlated with the progression and prognosis of hepatocellular carcinoma (HCC). In addition, mounting evidence has revealed that N6-methyladenosine (m6A) methylation, a common RNA modification, is involved in the progression of malignancies. In this research, a novel circRNA, hsa_circ_0058493, was proven to be upregulated in HCC, which was correlated with the prognosis of HCC patients. Experimentally, hsa_circ_0058493 knockdown suppressed the growth and metastasis of HCC cells *in vivo* and *in vitro*. On the contrary, the overexpression of hsa_circ_0058493 in HCC cells had the opposite effect *in vitro*. Mechanistic experiments revealed that hsa_circ_0058493 contained m6A methylation sites and that methyltransferase-like 3 (METTL3) mediated the degree of methylation modification of hsa_circ_0058493. Furthermore, YTH domain-containing protein 1 (YTHDC1) could bind to hsa_circ_0058493 and promote its intracellular localization from the nucleus to the cytoplasm. In addition, both si-METTL3 and si-YTHDC1 suppressed HCC cell growth and metastasis, whereas rescue experiments confirmed that overexpression of hsa_circ_0058493 inverted the inhibitory effects of si-METTL3 and si-YTHDC1 on HCC cells. Taken together, this study explored the oncogenic role of m6A-modified hsa_circ_0058493 and found to accelerate HCC progression via the METTL3-hsa_circ_0058493-YTHDC1 axis, indicating a potential therapeutic target for this deadly disease.

Keywords: circular RNA, HCC, N6-methyladenosine, hsa_circ_0058493, METTL3, YTHDC1

OPEN ACCESS

Edited by:
Lei Chang,
Soochow University Medical College (SUMC), China

Reviewed by:
Shukui Wang,
Nanjing Medical University, China
Jianxiang Chen,
Hangzhou Normal University, China

****Correspondence:***
Feng Wang
richardwangf@163.com
Lin Chen
xiaobei227@sina.com

[†] These authors have contributed equally to this work

Specialty section:
This article was submitted to Molecular and Cellular Oncology, a section of the journal Frontiers in Cell and Developmental Biology

Received: *22 August 2021*
Accepted: *12 October 2021*
Published: *23 November 2021*

Citation:
Wu A, Hu Y, Xu Y, Xu J, Wang X, Cai A, Liu R, Chen L and Wang F (2021) Methyltransferase-Like 3-Mediated m6A Methylation of Hsa_circ_0058493 Accelerates Hepatocellular Carcinoma Progression by Binding to YTH Domain-Containing Protein 1. Front. Cell Dev. Biol. 9:762588. doi: 10.3389/fcell.2021.762588

INTRODUCTION

Hepatocellular carcinoma (HCC), one of malignant tumors in the world with high incidence and mortality (Chen et al., 2019c; Lan et al., 2019). In addition, the high postoperative recurrence rate and metastasis rate lead to the poor prognosis of HCC patients (Zhang and Zhang, 2019; Wang et al., 2020d). Because of the scarcity of effective treatments, patients are often diagnosed with advanced HCC without receiving timely treatment (Zhang et al., 2018; Zhao et al., 2020). In view of the above, the clinical biomarkers used to diagnose HCC are not specific (Liu et al., 2021). To clarify the mechanism of the occurrence and development of HCC, it is necessary to seek biomarkers for the early diagnosis of HCC (Xu et al., 2020).

Circular RNAs (circRNAs) are a class of non-coding RNAs which have covalently closed circular structure. Furthermore, circular ribonucleic acid, without a 5′ end and 3′ tail structure, is more stable than the corresponding linear ribonucleic acid (Geng et al., 2018; Han et al., 2021). A growing number of studies have elucidated the mechanism of circRNAs in many malignant tumors (Latowska et al., 2020). For example, a potential diagnostic biomarker, circTMEM45A, may promote HCC progression through the miR-665/IGF2 axis by acting as a sponge for microRNA-665 (Zhang et al., 2020). In addition, circ-FBXW7 is an endogenous circRNA with translational function, and circ-FBXW7 and its encoded protein FBXW7-185aa have a certain prognostic value for glioblastoma (Yang et al., 2018). It is commonly known that circRNAs have high stability and can be used as new biomarkers for disease diagnosis or prognosis (Lei et al., 2020). However, the potential function of cyclic ribonucleic acid in HCC is still under investigation.

As a main modification in eukaryotic mRNA, N6-methyladenosine (m6A) plays vital roles in cancers (Li and Zhan, 2020; Chen et al., 2021). Many reports have proven that there are three players in m6A modification. These are the so-called m6A-related "writers," "erasers," and "readers" which mediate the methylation process, participate in the demethylation process and participate in RNA recognition, respectively (Qian et al., 2019; Pan et al., 2020). Methyltransferase-like 3 and 14 proteins (METTL3 and METTL14) are the "writers" of m6A. The relevant literature has reported that METTL3 is overexpressed in HCC, while METTL14 is underexpressed in HCC (Liu et al., 2020). Moreover, the YT521-B homology (YTH) domain family protein is a characteristic m6A reader (Xu et al., 2015). Research has shown that YTH domain-containing protein 1 (YTHDC1) promotes the nuclear export of circNSUN2 which bind to m6A motifs, ultimately promoting colorectal cancer progression (Chen et al., 2019a). Moreover, m6A modification also influences mRNA translation, splicing, export, degradation and processing (Wang et al., 2020a). However, the relationship between m6A modification and circRNAs in HCC needs to be further explored.

In the current research, we concluded that hsa_circ_0058493 was upregulated in HCC. Moreover, we have studied that hsa_circ_0058493 was regulated by m6A methylation and promoted the progression of HCC by binding to YTHDC1. In summary, hsa_circ_0058493 is expected to be a therapeutic target for HCC.

MATERIALS AND METHODS

Patient Tissue Specimens

Fifty-one pairs of HCC tissue and paired normal tissue were gathered from the Affiliated Hospital of Nantong University from January 2015 to December 2016. The clinical data of all patients was used with their informed consents. The Ethics Committee of the Affiliated Hospital of Nantong University authorized the agreement of the organization used for this study.

Cell Culture and Transfection

In this study, HCC cell lines (BEL-7404, HCCLM3, SK-Hep-1, SMMC-7721, and MHCC-97H) together with a normal liver cell line (LO2) were purchased from the Chinese Academy of Sciences. All cells were cultured in high glucose Dulbecco's Modified Eagle's Medium (Corning, NY, United States), which contained 10% fetal bovine serum (FBS, Gibco, Grand Island, NY, United States) and 1% penicillin-streptomycin-amphotericin B solution (Solarbio, Beijing, China), at 37°C with 5% CO_2 in an incubator. HCCLM3 and SMMC-7721 cells were treated with negative control (shNC) and sh-hsa_circ_0058493 (sh-circ-1, sh-circ-2) or negative control (oe-NC) and oe-hsa_circ_0058493 (oe-circ). The transfection plasmid was provided by Geneseed Biotech Co., Ltd. Cells were cultured for 48 h before transfection. When the cells have grown to 70–80% density of the six-well plate, we transfected the cells with Lipofectamine 3000. After 48 h of transfection, RT–qPCR assays were used to detect the transfection efficiency and carry out follow-up experiments. The sequences of the negative control (shNC) were TCACCAGAAGCGTACCATACTC, and the sequences of sh-hsa_circ_0058493 were ATACAGACGGCT GAACCCTGGTGAG (sh-circ-1) and ACAGACGGCTGAAC CCTGGTGAGAA (sh-circ-2). The sequences of si-METTL3 were GCACTTGGATCTACGGAA and the sequences of si-YTHDC1 were CAAGGAGTGTTATCTTAAT.

Animal Studies

All experiments were approved by the Institutional Animal Care and Utilization Committee of Nantong University. sh-hsa_circ_0058493 and its negative control cells were stably transfected into HCCLM3 cells. Approximately 1×10^7 cells were injected subcutaneously into the armpit of nude male mice (4 weeks old, 10 in total, divided into five mice per group). The growth of the tumor was recorded by measuring the size with a caliper every week. After 4–5 weeks, the tumors were removed from the mice and their volume and weight were recorded. Besides, the tumors were made into paraffin-embedded sections for HE staining and immunohistochemical examination (IHC).

Immunohistochemical Staining

After fixing the tumor with 4% paraformaldehyde, paraffin-embedded sections were prepared. After sectioning the tumor, the slices were degreased in xylene and then subjected to microwave heating treatment to extract the antigen. Next, the sections were incubated with PCNA, Ki67 and Bcl-2 and secondary antibody (Santa Cruz, CA, United States). After being

washed, the sections were stained with hematoxylin and 3,3′-diaminobenzidine (DAB). Finally, the slices were imaged and observed with an inverted microscope.

RNA Extraction, Reverse Transcription, and RT–qPCR

Total RNA was isolated by using TRIzol reagent (Invitrogen). Then, a reverse transcription kit was used to convert total RNA into cDNA (Thermo Fisher Science, United States). The expression levels of circRNAs and mRNAs were amplified on a LightCycler 480 qRT-PCR instrument (Roche, Germany) with Plus SYBR real-time PCR mixture (BioTeke, Beijing, China). Samples were subjected to reaction conditions of 15 s at 95°C, 30 s at 60°C, 30 s at 75°C, and 45 cycles. Each sample was repeated three times. The comparative cycle threshold values ($2^{-\Delta\Delta Ct}$) were calculated to analyze the expression level of circRNAs and mRNAs. The primer information is shown in **Table 1**.

Cell Proliferation and Clone Formation Assay

Cell proliferation ability was evaluated by a CCK-8 kit (MedChemExpress, Shanghai, China). The transfected cells were developed in 96-well plate at a density of 3,000 cells/well. At 24, 48, 72, 96, and 120 h after inoculation, after adding 10 μl of CCK-8 solution to each well, absorbance value was measured at 450 nm after 2 h of incubation. In the colony formation assay, approximately 1,000 cells per well of transfected cells were added into a six-well plate with 2 weeks' incubation. Next, the cells were fixed with 4% formaldehyde and stained with 0.1% crystal violet. Finally, clonal spots were photographed and counted.

Cell Migration and Invasion Assays

In cell migration experiment, 5×10^5/ml transfected cells were seeded into the upper chambers with DMEM without serum. In addition, the lower chambers were added with DMEM containing 10% FBS. Similarly, in cell invasion experiment, 7×10^5/ml transfected cells were cultured in chambers covered with 100 μl Matrigel (1:10 dilution; BD Biosciences). After incubation for 48 h, the chambers were fixed and stained as above. After wiping the upper chamber with a cotton swab, we used a microscope to count the number of migrated and invaded cells at the bottom of the chambers.

TABLE 1 | Sequence information for primers used in this study.

Gene	Sequence (5′-3′)
hsa_circ_0058493 (divergent primers)	F: TATCTGGCCATGCAACGGAG
	R: TCACCCTAGCAACTTTGGCC
hsa_circ_0058493 (convergent primers)	F: ATTCTCACCAGGGTTCAGCC
	R: CTCCGTTGCATGGCCAGATA
METTL3	F: CTTCAGTTCCTGAATTAGC
	R: ATGTTAAGGCCAGATCAGAGAG
YTHDC1	F: ATCTTCCGTTCGTGCTGT
	R: ACCATACACCCTTCGCTTT
18s	F: CGGCTACCACATCCAAGGAA
	R: GCTGGAATTACCGCGGCT

Cell Cycle Assay and Apoptosis Experiments

The treated cells were all collected and fixed with 70% ethanol. After removing the ethanol, the cells were washed three times with phosphate buffer. Fifty microliters of enzyme was added to each tube, which were incubated in a bath at 37°C. Then, 200 μl dye was added to each tube in the dark and incubated on ice. After the transfected cells were cultured, the cells and the dead cells in the six-well plate were collected. Cells were resuspended in PBS for collection and stained with Annexin V-Alexa Fluor 647/PI. Cell cycle assays and apoptosis experiments were performed by flow cytometry (BD Bioscience, United States). The results were statistically analyzed.

RNA Immunoprecipitation Assay

According to the instructions, the RIP experiment was performed with an RNA binding protein immunoprecipitation kit (Geneseed Biotech, Guangzhou, China). A total of 1×10^7 cells were added to the lysate, and 100 μl of the supernatant was used as a positive control. The magnetic beads were coated with 5 μg of anti-YTHDC1 (77422, Cell Signaling Technology), anti-m6A (56593, Cell Signaling Technology), and IgG (2729, Cell Signaling Technology) at 4°C for 2 h. The antibody surface-coated magnetic beads and cell lysate were incubated overnight at 4°C, and the magnetic bead-protein-RNA complex was washed with RIP washing buffer. Cell lysate was added to the magnetic bead complex-antibody to capture the antigen. After eluting the complex bound to the magnetic beads, the RNA was extracted with a filter column. The expression of hsa_circ_0058493 was determined by an RT–qPCR assay.

Nuclear and Cytoplasmic Extraction

Nuclear and cytoplasmic RNA were separated and extracted by nuclear and cytoplasmic protein extraction kits (Beyotime Biotechnology). Then, the expression of hsa_circ_0058493 in the cytoplasm and nucleus was analyzed by RT–qPCR assay.

Statistical Analysis

The data were analyzed with SPSS 21.0 statistical software. A $P < 0.05$ was regarded as statistically significant for two-sided analysis. All data was presented as the mean ± standard deviation. Comparisons between groups were analyzed by *t*-test or ANOVA.

RESULTS

Characterization and Detection of Hsa_circ_0058493 in Hepatocellular Carcinoma

We screened and detected the expression of 5 circRNAs in HCC from the GSE97332 database and GSE97508 database. Hsa_circ_0058493 expression in HCC tissues was

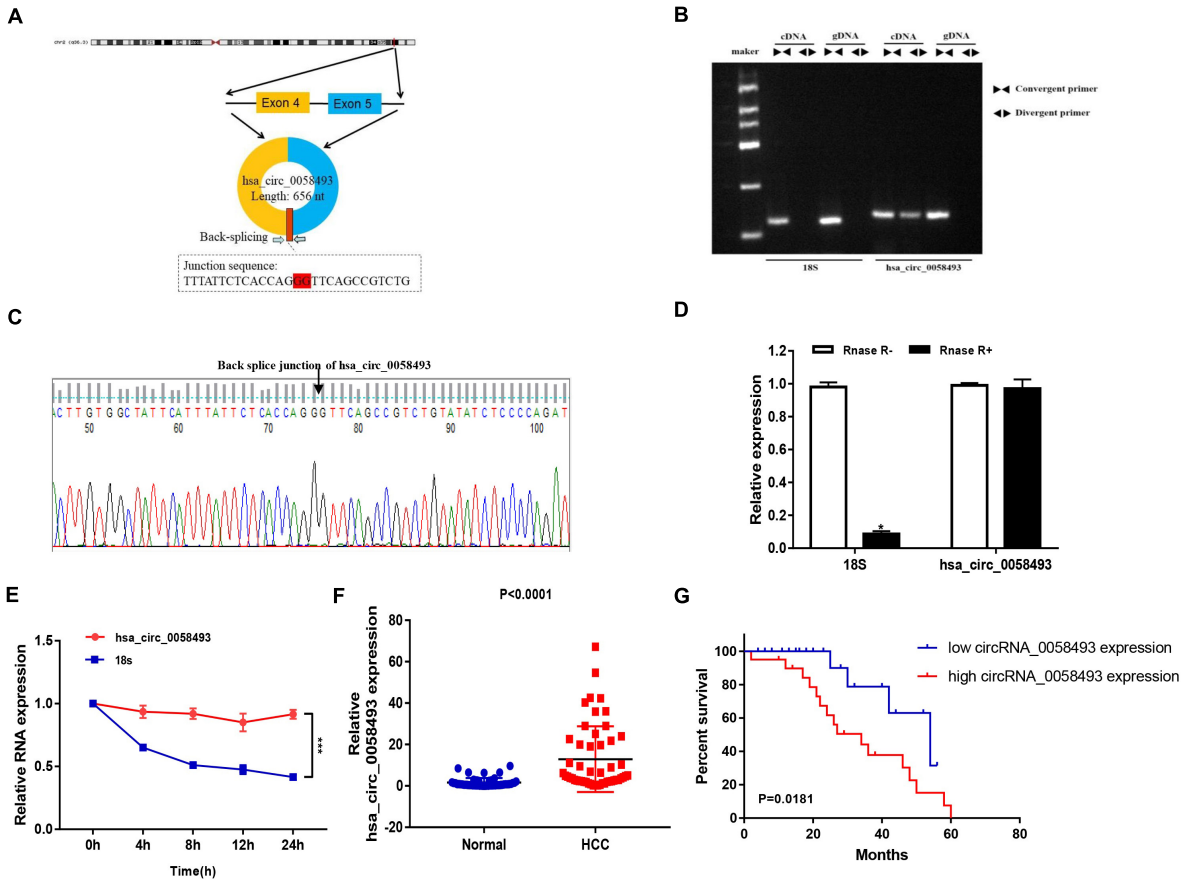

FIGURE 1 | (A) The circular structure of hsa_circ_0058493 showed that the hsa_circ_0058493 primer was derived from exons 4–5 of the RHBDD1 gene. Yellow represents exon4, blue represents exon5, and red represents the Back-splicing. **(B)** Gel electrophoresis results showed that the head-to-head primers can amplify products in both gDNA and cDNA, while the back-to-back primers can only amplify hsa_circ_0058493 in cDNA, which proved that hsa_circ_0058493 had a circular structure. **(C)** The reverse splicing junction of hsa_circ_0058493 was detected by Sanger sequencing. **(D)** The results of the RNase R enzyme digestion test showed that the expression of linear RNA decreased visibly after RNase R enzyme digestion, while the expression of hsa_circ_0058493 after RNase R enzyme treatment did not change clearly. **(E)** After treatment with actinomycin D in HCCLM3 cells, the relative RNA expression of hsa_circ_0058493 and mRNA were detected at different times. **(F)** Relative expression of hsa_circ_0058493 in 51 pairs of HCC and normal tissues. **(G)** The overall survival curve with low and high expression of hsa_circ_0058493 in HCC was analyzed by Kaplan–Meier. $^{*}P < 0.05$, $^{***}P < 0.001$ vs. control group.

distinctly increased, and we studied the circular structure of hsa_circ_0058493 and discovered hsa_circ_0058493 was derived from exons 4–5 of the RHBDD1 gene (**Figure 1A**). To characterize hsa_circ_0058493, we designed convergent primers and divergent primers. Also, agarose gel electrophoresis results showed that hsa_circ_0058493 was amplified from complementary DNA (cDNA) instead of genomic DNA (gDNA) (**Figure 1B**). Furthermore, Sanger sequencing confirmed that there was a back-splicing junction (**Figure 1C**). Additionally, RNase R specifically degrades linear RNAs rather than circRNAs, and we confirmed that hsa_circ_0058493 can resist the digestion of RNase R (**Figure 1D**). After treatment with actinomycin D, qRT-PCR results proved that hsa_circ_0058493 possessed a longer half-life than the mRNA. Hsa_circ_0058493 was more stable than mRNA due to its ring structure (**Figure 1E**). Next, we studied the expression profile of hsa_circ_0058493 in 51 pairs of tissues. The expression of hsa_circ_0058493 in HCC tissues was memorably upregulated (**Figure 1F**). Kaplan Meier analysis showed that HCC patients in hsa_circ_0058493 high expression group had a worse prognosis and shorter survival time (**Figure 1G**). In summary, these results indicated that hsa_circ_0058493 has a true ring structure and is generally upregulated in HCC tissues. Additionally, hsa_circ_0058493 was connected with the progression of HCC and may become a promising prognostic marker for HCC.

Hsa_circ_0058493 Promoted the Growth and Metastasis of Hepatocellular Carcinoma Cells

In order to discover the role of hsa_circ_0058493 in HCC cells, we first performed qRT-PCR assays to detect the expression of hsa_circ_0058493 in HCC cell lines (**Figure 2A**). Then, knockdown and overexpression plasmids were used to stably transfect HCC cell lines HCCLM3 and SMMC-7721, respectively, and a negative control was used (**Figure 2B**). The CCK-8 test

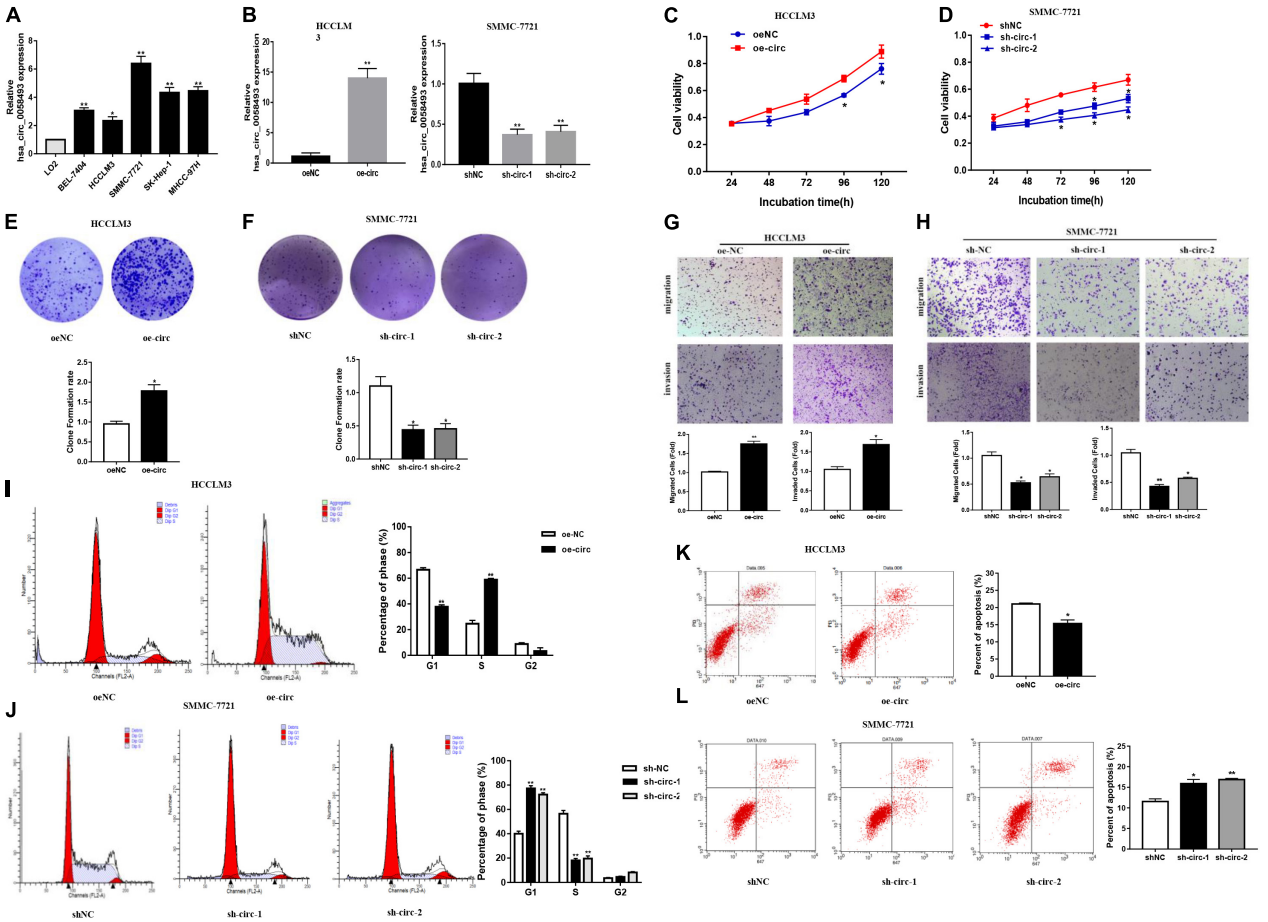

FIGURE 2 | (A) The expression of hsa_circ_0058493 in BEL-7404, HCCLM3, SMMC-7721, SK-Hep-1, MHCC-97H, and LO2 cells was detected by qRT–PCR assays. **(B)** The efficiency of transfecting the knockout plasmid and overexpression plasmid of hsa_circ_0058493 into HCC cells by qRT-PCR. **(C,D)** The CCK-8 test was used to analyze the proliferation of HCC cells with overexpression and knockdown of hsa_circ_0058493 (oe-circ and sh-circ-1, sh-circ-2). **(E,F)** Cloning experiments were tested to analyze the effect of oe-circ and sh-circ-1, sh-circ-2 on the proliferation of HCC cells. The colony formation rate was shown by a histogram. **(G,H)** The migration and invasion ability of HCC cells with oe-circ and sh-circ-1, sh-circ-2 was tested by the Transwell assay. The number of migrating and invading cells was counted. **(I,J)** Cell cycle assays were analyzed by flow cytometry. The histogram showed that hsa_circ_0058493 knockdown cells stagnated in G1 phase and that hsa_circ_0058493-overexpressing cells promoted cell proliferation. The triangle symbols are for discrimination of G1 vs. S and S vs. G2. **(K,L)** Apoptosis was detected by flow cytometry. The assay proved that the number of apoptotic cells detected in the samples transfected with the overexpression of hsa_circ_0058493 (oe-circ) was small, while the samples transfected with knockdown of hsa_circ_0058493 (sh-circ-1, sh-circ-2) had more apoptotic cells. $^{*}P < 0.05$, $^{**}P < 0.01$ vs. control group.

results displayed that overexpression of hsa_circ_0058493 (oe-circ) facilitated cell proliferation, alternatively knockdown of hsa_circ_0058493 (sh-circ-1, sh-circ-2) inhibited cell proliferation (**Figures 2C,D**). The clone formation experiment exhibited that compared with the negative control, the oe-circ raised the number of clones of HCCLM3 cells, nevertheless, sh-circ reduced the number of clones of SMMC-7721 cells (**Figures 2E,F**). The above results proved the proliferation ability of hsa_circ_0058493 in HCC. Furthermore, the Transwell assay confirmed that the migration and invasion ability of oe-circ cells was better than that of the negative control (oe-NC), whereas, the migration and invasion ability of sh-circ cells was worse than that of the negative control (sh-NC) (**Figures 2G,H**). Afterward, flow cytometry analysis showed that the number of oe-circ cells in S phase increased, while the percentage of sh-circ cells in G1 phase increased. The results proved that oe-circ in HCC cells rescued cell cycle arrest and promoted cell proliferation (**Figures 2I,J**). Moreover, cell apoptosis was detected by Annexin V and PI double staining kits. The results indicated that oe-circ subtracted apoptotic cells, while sh-circ increased the number of apoptotic cells (**Figures 2K,L**).

Downregulation of Hsa_circ_0058493 Inhibited the Growth of Hepatocellular Carcinoma Tumors *in vivo*

In nude mouse subcutaneous tumor formation experiments, we stably transfected hsa_circ_0058493 knockdown cells into the HCCLM3 cell line and inoculated the HCCLM3 cell line into the skin of nude mice. Then, we observed the growth of

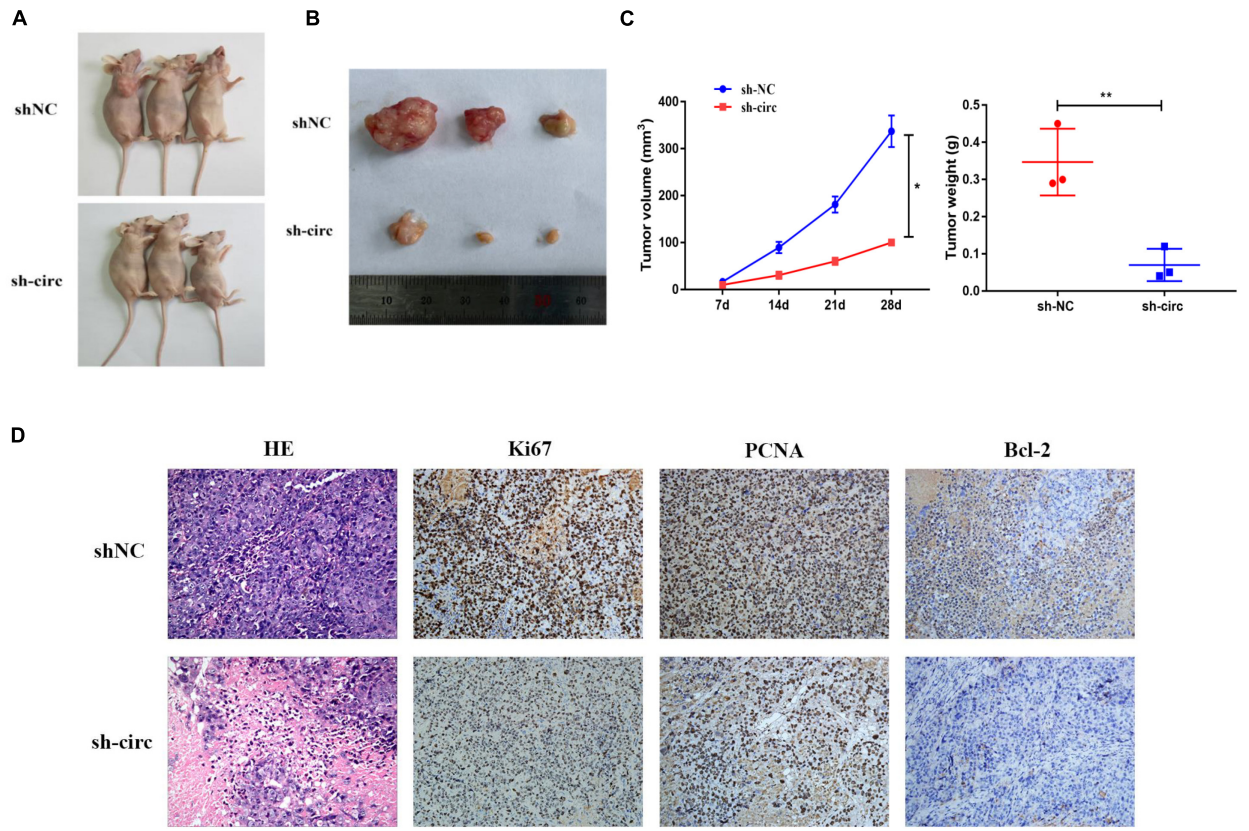

FIGURE 3 | (A) Image of nude mice 28 days after inoculation with sh-NC (control) and sh-circ plasmids. **(B)** Representative images of subcutaneous tumors in nude mice. **(C)** The tumor growth volume and weight measurements of nude mice showed that the growth of tumors was inhibited after hsa_circ_0058493 was knocked down. **(D)** The expression of Ki67, PCNA, and Bcl-2 (tumor proliferation marker and tumor apoptosis marker) in nude mice were detected by H&E staining and IHC staining. $^{*}P < 0.05$, $^{**}P < 0.01$ vs. control group.

subcutaneous tumors every week. Silencing of hsa_circ_0058493 significantly inhibited the growth of subcutaneous tumors (**Figures 3A,B**). In addition, the tumors injected with the transfected knockdown plasmid grew much slower than those injected with the negative control plasmid. Compared with sh-NC group, the tumor volume and weight of the sh-circ group were notably reduced (**Figure 3C**). Besides, the results of H&E and immunohistochemistry staining showed that in hsa_circ_0058493 knockdown group, the positive rate of Ki67, PCNA (tumor proliferation marker) and Bcl-2 (tumor apoptosis marker) *in vivo* was markedly reduced compared with sh-NC (**Figure 3D**). These experimental data indicated that hsa_circ_0058493 promoted the growth of HCC tumors *in vivo*.

Methyltransferase-Like 3 Catalyzed the m6A Modification of Hsa_circ_0058493

N6-methyladenosine is considered to be a common mRNA modification. It is known that circRNAs containing "RRm6ACH" (R = G or A, H = A, C or U) are more prone to m6A modification. We used the SRAMP database to predict the m6A site, and we found that it was close to the junction site of hsa_circ_0058493 (**Figure 4A**). To explore whether hsa_circ_0058493 contained m6A methylation, we performed a methylated RNA immunoprecipitation (MeRIP) test. Compared with the control IgG, the complex precipitated by the anti-m6A antibody was enriched in hsa_circ_0058493 (**Figure 4B**). Furthermore, the RNA-binding protein immunoprecipitation (RIP) assay proved that compared with oe-NC, the degree of methylation of hsa_circ_0058493 transfected with the oe-circ plasmid was increased (**Figure 4C**). Methyltransferase-like 3 (METTL3) is called an N6-methyladenosine "writer" and plays a vital role in catalyzing m6A modification. Studies have shown that METTL3 is upregulated in HCC. qRT-PCR experiments were used to verify that METTL3 was upregulated in HCC tissues (**Figure 4D**). Additionally, the qRT-PCR experimental data stated that the expression of METTL3 was positively relevant to hsa_circ_0058493 in HCC tissues (**Figure 4E**). Next, we constructed a METTL3 knockdown plasmid and performed a series of recovery experiments. The knockdown efficiency of the METTL3 plasmid reached more than 50% (**Figure 4F**). Subsequently, it was demonstrated by MeRIP that the methylation degree decreased in hsa_circ_0058493 after transfection of si-METTL3 compared with the control group si-NC (**Figure 4G**). Overall, hsa_circ_0058493 contains methylation sites, and

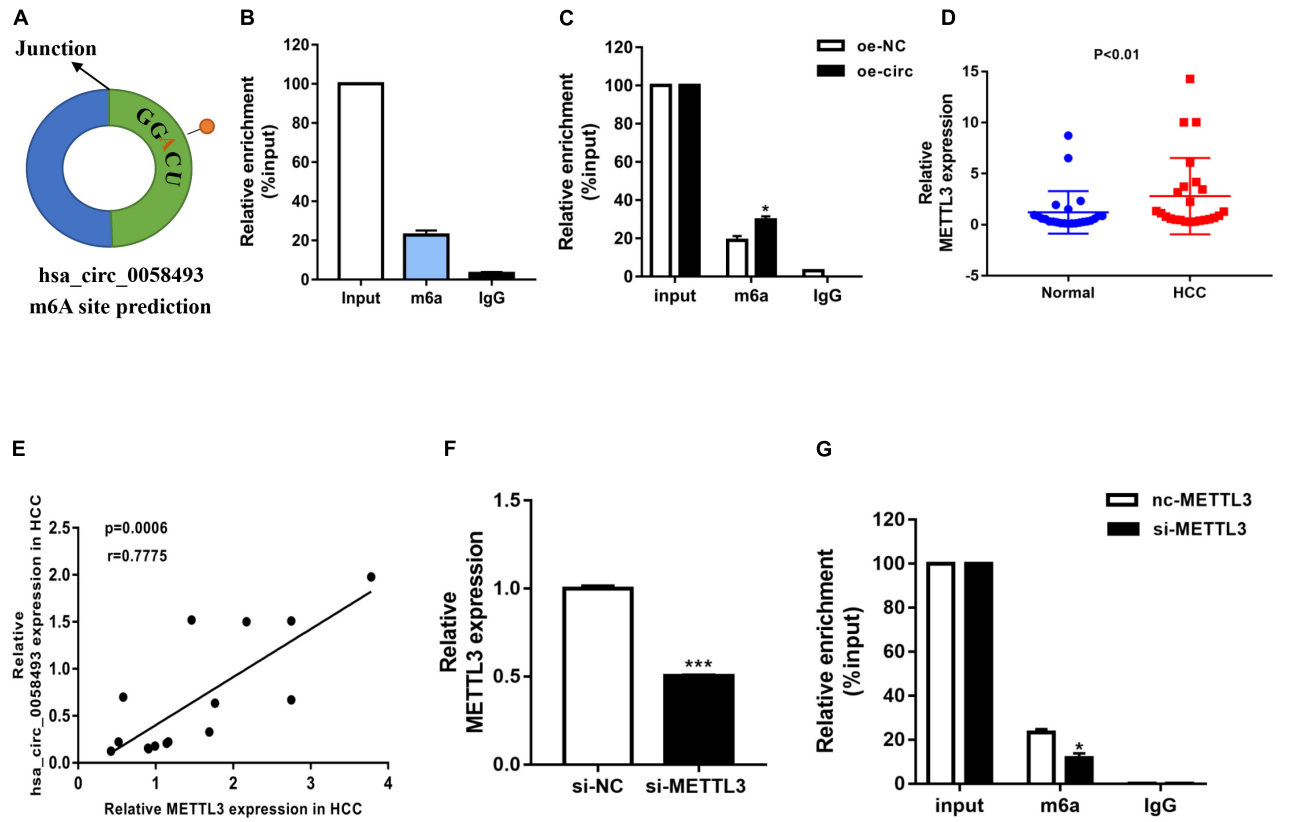

FIGURE 4 | (A) The SRAMP database predicted the GGACU m6A site in hsa_circ_0058493. **(B)** MeRIP experiment shows that circNSUN2 is relatively enriched in m6A antibody compared with control IgG antibody. **(C)** When the hsa_circ_0058493 overexpression plasmid was transfected, the MeRIP experiment proved that the m6A antibody was more enriched. **(D)** Relative expression of METTL3 in 12 pairs of HCC and adjacent tissues was detected by qRT-PCR. **(E)** Hsa_circ_0058493 was positively correlated with METTL3. The *P* value and correlation coefficient were calculated by Pearson correlation analysis. **(F)** The knockdown efficiency of the METTL3 knockdown plasmid was tested by qRT-PCR. **(G)** MeRIP experiment proved that after knocking down METTL3 in hsa_circ_0058493, the degree of m6A methylation decreased. $^{*}P < 0.05$, $^{***}P < 0.001$ vs. control group.

METTL3 promotes the extent of m6A modification in hsa_circ_0058493.

Methyltransferase-Like 3 Affected the Biological Activity of Hsa_circ_0058493 in Hepatocellular Carcinoma

After knocking down METTL3 (si-METTL3) and overexpressing hsa_circ_0058493 (oe-circ) in the SMMC-7721 cell line, the cell proliferation, migration and invasion abilities were tested. The CCK-8 and the clone formation experiments proved that after knocking down METTL3, the cell proliferation ability decreased parallel with control. However, the proliferation ability was rescued after overexpression of hsa_circ_0058493 (**Figures 5A,B**). Afterward, flow cytometry analysis demonstrated that cell cycle arrest increased and cell growth ability decreased after transfection of the METTL3 knockdown plasmid (si-METTL3) in the SMMC-7721 cell line, but transfection of the hsa_circ_0058493 overexpression plasmid (oe-circ) rescued cell cycle arrest and promoted cell growth ability (**Figure 5C**). Similarly, the Transwell assay confirmed that after the METTL3 knockdown plasmid (si-METTL3) was transfected into the SMMC-7721 cell line, the cell migration and invasion ability decreased, but after transfection with the hsa_circ_0058493 overexpression plasmid (oe-circ), the cell migration and invasion ability was restored (**Figure 5D**). Based on the above experimental results, we concluded that METTL3 can affect the extent of m6A modification of hsa_circ_0058493, which in turn affects the growth and metastasis of HCC in response to hsa_circ_0058493.

YTH Domain-Containing Protein 1 Interacted With Hsa_circ_0058493 and Promoted Cytoplasmic Export of Hsa_circ_0058493

Several researches have indicated that circular RNAs can perform a regulatory function by binding related proteins and have a carcinogenic effect in many cancers. We used the ENCORI and RBPDB databases for bioinformatics analysis and found that YTHDC1 may be a binding protein of hsa_circ_0058493 (**Figure 6A**). The qRT-PCR experiments validated that YTHDC1 expression was upregulated in HCC tissues (**Figure 6B**). We designed a point mutation in the binding sequence of

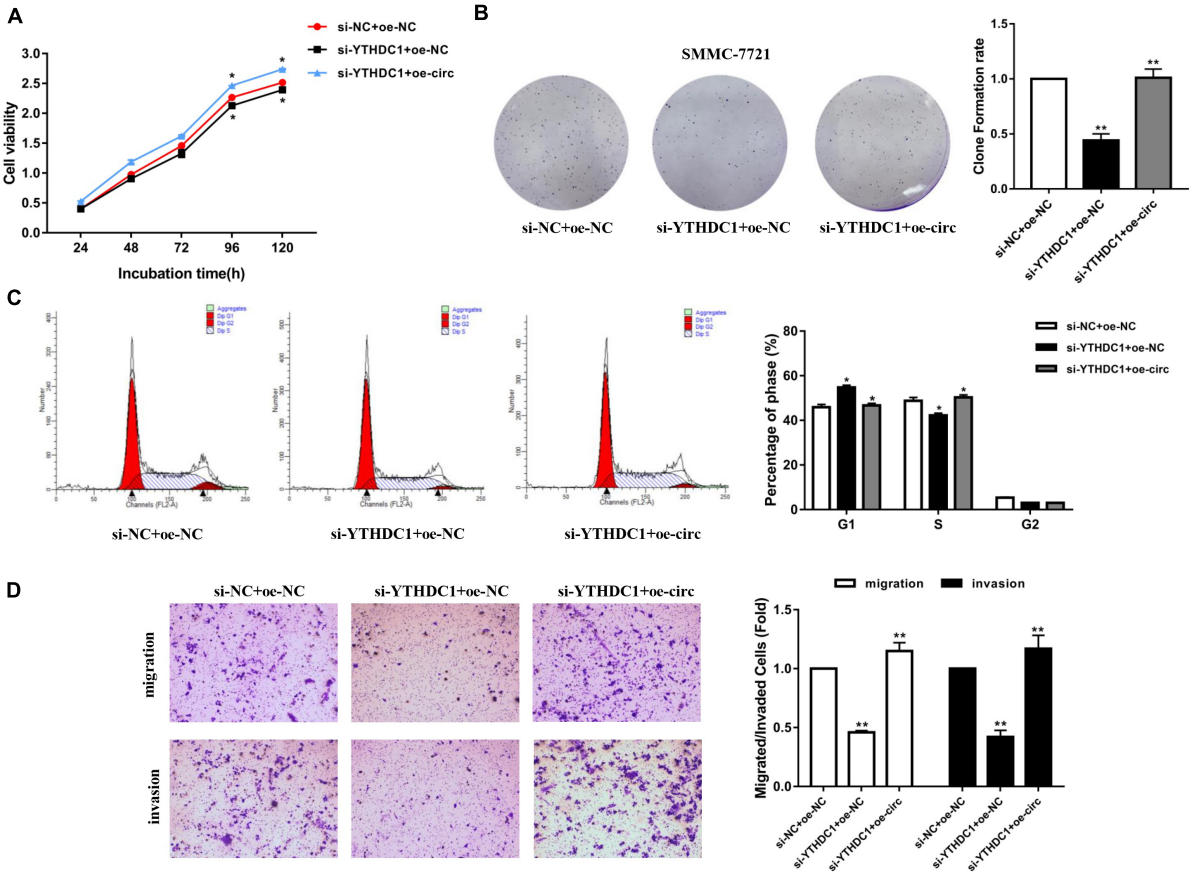

FIGURE 5 | (A) A CCK-8 assay was used to determine the proliferation of HCC cells after transfection with si-NC + oe-NC, si-YTHDC1 + oe-NC, and si-YTHDC1 + oe-circ. **(B)** A cloning assay was performed to detected proliferation ability of HCC cells with si-NC + oe-NC, si-YTHDC1 + oe-NC, and si-YTHDC1 + oe-circ. Colony formation rates are shown by histograms. **(C)** The cell cycle of HCC cells after transfection with si-NC + oe-NC, si-YTHDC1 + oe-NC, and si-YTHDC1 + oe-circ was determined by flow cytometry. As evident in the histogram, more cells arrested in the G1 phase were observed in si-YTHDC1 + oe-NC compared with si-NC + oe-NC. After cotransfection of si-YTHDC1 + oe-circ, the number of cells arrested in G1 phase decreased again compared with si-YTHDC1 + oe-NC. The triangle symbols are for discrimination of G1 vs. S and S vs. G2. **(D)** The invasion and migration abilities of HCC cells after transfection with si-NC + oe-NC, si-YTHDC1 + oe-NC, and si-YTHDC1 + oe-circ were assessed by Transwell assay. Histograms were used to show the number of invaded and migrated cells. $^{*}P < 0.05$, $^{**}P < 0.01$ vs. control group.

hsa_circ_0058493 and YTHDC1, and performed the RIP experiment with YTHDC1 antibody. Compared with the negative control IgG, we observed an obvious enrichment of hsa_circ_0058493 in the wild type (WT) group and there was almost not any enrichment rate in the mutant (Mut) group, which verified that YTHDC1 could bind to hsa_circ_0058493 at the prediction site (**Figure 6C**). We found that YTHDC1 mRNA expression decreased when hsa_circ_0058493 was knocked down, while the expression increased when hsa_circ_0058493 was overexpressed (**Figures 6D,E**). The qRT-PCR experimental data proved that YTHDC1 was positively correlated with hsa_circ_0058493 in HCC (**Figure 6F**). The location of hsa_circ_0058493 was detected by nuclear-cytoplasmic separation experiments which certified that U6 was present in the nucleus, 18S and hsa_circ_0058493 were present in the cytoplasm (**Figure 6G**). Next, we constructed a YTHDC1 knockdown plasmid and verified the knockdown efficiency of YTHDC1 (**Figure 6H**). When the YTHDC1 plasmid was knocked out, we found that hsa_circ_0058493 was transported from the cytoplasm to the nucleus (**Figure 6I**). Taken together, hsa_circ_0058493 is transported from the nucleus to the cytoplasm in a m6A-dependent manner by binding to YTHDC1.

Overexpression of Hsa_circ_0058493 Rescued the Carcinogenic Effect of YTH Domain-Containing Protein 1 Knockdown in Hepatocellular Carcinoma

After knocking down YTHDC1 (si-YTHDC1) and overexpressing hsa_circ_0058493 (oe-circ) in the SMMC-7721 cell line, the cell proliferation, migration and invasion abilities were determined. The CCK-8 experiment and the colony formation experiment proved that the cell proliferation ability decreased after knocking down YTHDC1. However, the proliferation ability was rescued after overexpression of hsa_circ_0058493 (**Figures 7A,B**). Afterward, flow cytometry

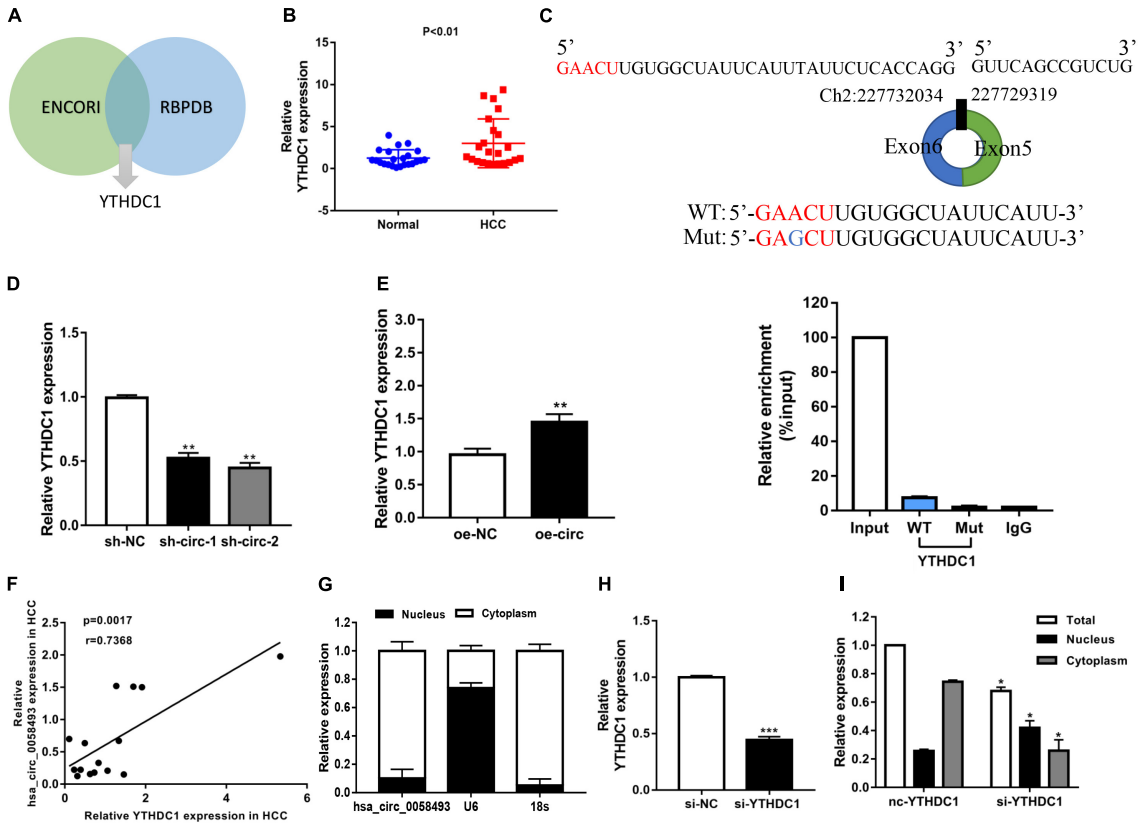

FIGURE 6 | (A) Through the intersection of the ENCORI and RBPDB databases, it was concluded that hsa_circ_0058493 may interact with YTHDC1. **(B)** Relative expression of YTHDC1 in 12 pairs of HCC and adjacent tissues was detected by qRT-PCR assays. **(C)** Top, a point mutation in the binding sequence of hsa_circ_0058493 and YTHDC1. Bottom, the RIP experiment proved that YTHDC1 interacted with hsa_circ_0058493 and IgG antibody was used as a control. **(D,E)** The expression of YTHDC1 mRNA was detected by qRT-PCR in cells with hsa_circ_0058493 knockdown plasmid or hsa_circ_0058493 overexpression plasmid. **(F)** Hsa_circ_0058493 was positively correlated with YTHDC1. The *P* value and correlation coefficient were calculated by Pearson correlation analysis. **(G)** Nuclear and cytoplasmic separation experiments showed that hsa_circ_0058493 was in the cytoplasm. U6 was used as a positive control in the nucleus while 18S was used as a positive control in the cytoplasm. **(H)** The knockdown efficiency of the YTHDC1 knockdown plasmid was tested by qRT-PCR. **(I)** The nucleoplasmic separation experiment showed that after knocking down YTHDC1, hsa_circ_0058493 was transported from the cytoplasm to the nucleus. $^{*}P < 0.05$, $^{**}P < 0.01$, $^{***}P < 0.001$ vs. control group.

analysis displayed that cell cycle arrest increased and cell growth ability decreased after transfection of the knockdown plasmid of YTHDC1 (si-YTHDC1), but transfection of the overexpression plasmid of hsa_circ_0058493 (oe-circ) rescued cell cycle arrest and promoted cell growth ability (**Figure 7C**). Similarly, the Transwell assay confirmed that after the knockdown plasmid of YTHDC1 (si-YTHDC1) was transfected into the SMMC-7721 cell line, the cell migration and invasion ability decreased which then was restored when the overexpression plasmid of hsa_circ_0058493 (oe-circ) was transfected, (**Figure 7D**). In summary, hsa_circ_0058493 promoted the growth and metastasis of HCC cells by binding to YTHDC1.

DISCUSSION

Hepatocellular carcinoma is a malignant tumor that occurs in the liver which has high mortality (Wang et al., 2020a). As one of malignant tumors, the pathogenesis of HCC, as well as its early diagnosis, treatment and prognosis in the clinic, has been of great interest (Wang et al., 2020b). In addition to surgical resection in HCC, alpha fetoprotein (AFP) is a currently known HCC diagnostic biomarker and widely used in the clinic (Wang and Wei, 2020; Zheng et al., 2020). However, early diagnosis by AFP is not available for all patients, and AFP is no longer recommended as a tool for HCC surveillance and diagnosis in recent HCC guidelines. Since the early diagnosis rate of HCC has not been satisfactory, the therapeutic effect of HCC has been poor (Wang and Zhang, 2020). Therefore, further analysis of the pathogenesis of HCC and search for new diagnostic- and prognostic-related markers has some significance for the treatment of HCC (Ozgor and Otan, 2020).

As a novel non-coding RNA that was first discovered many years ago, circRNA has a closed loop structure and is chiefly situated in the cytoplasm or existed in exosomes (Li et al., 2015). Most circRNAs are circularized from exons, or some have lasso structures circularized from introns (Xiao et al., 2020). Compared with linear RNA, circRNA is not affected by

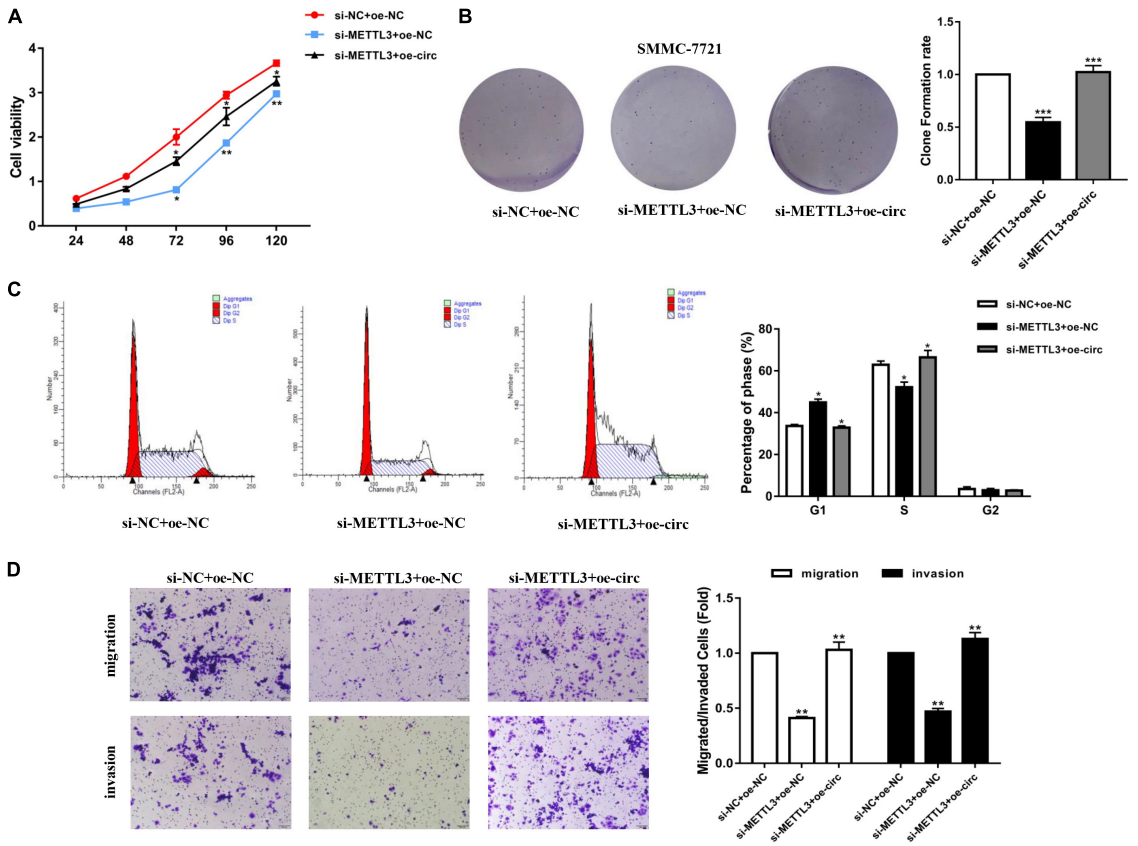

FIGURE 7 | (A) A CCK-8 assay was tested to determine the proliferation of HCC cells with si-NC + oe-NC, si-METTL3 + oe-NC, and si-METTL3 + oe-circ. **(B)** A cloning experiment was used to detected cell proliferation ability of HCC cells with si-NC + oe-NC, si-METTL3 + oe-NC, and si-METTL3 + oe-circ. Colony formation rates are shown by histograms. **(C)** The cell cycle of HCC cells after transfection with si-NC + oe-NC, si-METTL3 + oe-NC, and si-METTL3 + oe-circ was determined by flow cytometry. As evident in the histogram, more cells arrested in the G1 phase were observed in si-METTL3 + oe-NC compared with si-NC + oe-NC. After cotransfection of si-METTL3 + oe-circ, the number of cells arrested in G1 phase decreased again compared with si-METTL3 + oe-NC. The triangle symbols are for discrimination of G1 vs. S and S vs. G2. **(D)** The invasion and migration abilities of HCC cells after transfection with si-NC + oe-NC, si-METTL3 + oe-NC, and si-METTL3 + oe-circ were assessed by Transwell assay. Histograms were used to show the number of invaded and migrated cells. $^{*}P < 0.05$, $^{**}P < 0.01$, $^{***}P < 0.001$ vs. control group.

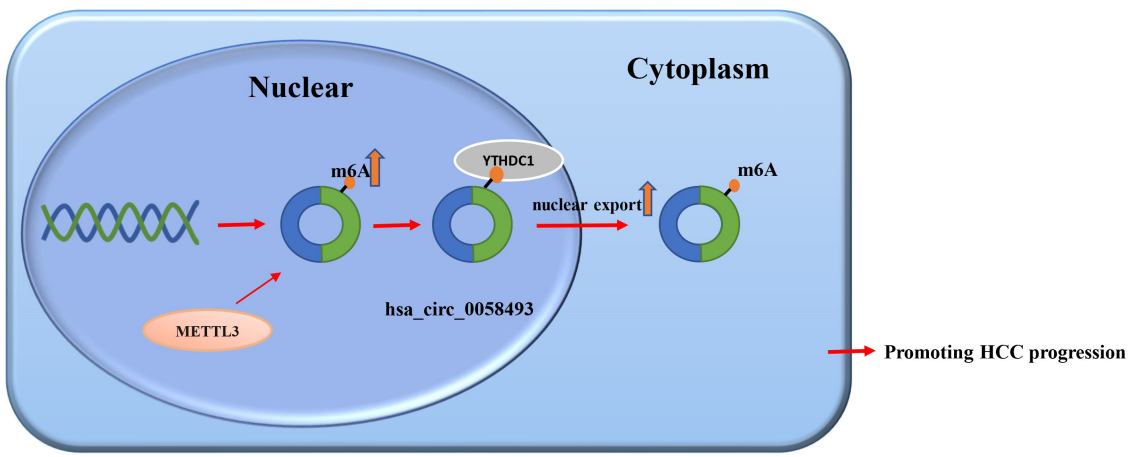

FIGURE 8 | The regulatory mechanism of hsa_circ_0058493 in HCC.

RNA exonuclease. Thus, circRNAs have more stable expressions and are not easily degraded (Verduci et al., 2019). With the advancement of contemporary sequencing technology, most circRNAs have been found in most eukaryotes. Recent studies have shown that circRNA is abnormally expressed in different diseases and plays a regulatory role in tumor development (Kong et al., 2020). For example, circRNA_0000285, with higher expression in cervical cancer (CC) than normal tissues, may promote the development of CC through FUS (Chen et al., 2019b). CircRNA_100876 expression was elevated in breast cancer (BC) and promoted the proliferation ability of BC cells (Yang et al., 2019). Hsa_circ_100395, with decreased expression in lung cancer tissues, inhibited the progression of lung cancer (Chen et al., 2018). With respect to our current study, we identified the cyclic structure of hsa_circ_0058493 and discovered that the expression of hsa_circ_0058493 was prominently upregulated in HCC. Afterward, survival curve analysis showed that hsa_circ_0058493 is a potential target for HCC. Hence, the promise of circRNAs for HCC treatment has been confirmed by numerous studies.

In this study, we investigated a new circular RNA, hsa_circ_0058493, and identified its circular structure. Subsequently, we conducted functional experiments to discuss the impact of hsa_circ_0058493 in the development of HCC. Some *in vivo* experiments verified that hsa_circ_0058493 can promote the growth and metastasis of HCC cells. In addition, hsa_circ_0058493 can also inhibit cell apoptosis. Similarly, *in vitro* nude mouse tumor formation experiments also proved that hsa_circ_0058493 can promote the growth of HCC tumors.

There are more than one hundred modifications of RNA, and N6-methyladenosine (m6A) modification is a common post-transcriptional modification of mRNA in mammals (Wang et al., 2020c). m6A methylation modification can affect many functions of mRNA, such as stability, splicing, export, translation and decay (Lee et al., 2020). Moreover, numerous documents have shown that m6A modification plays a crucial part in most cancers and that m6A modification exists in most non-coding RNAs (Huang et al., 2020).

Methyltransferase-like 3 is called the m6A methyltransferase "writer" and has been confirmed to be upregulated in HCC tissues. YTHDC1 possesses a YTH domain that has been generally accepted as a nuclear reader protein and preferentially binds m6A (Xu et al., 2014). In the present research, we discovered that METTL3 catalyzes m6A modification of hsa_circ_0058493, and the methylation site of hsa_circ_0058493 could bind to YTHDC1 and export it from the nucleus to the cytoplasm in a m6A-dependent manner, ultimately promoting HCC progression (**Figure 8**).

CONCLUSION

We experimentally demonstrated that hsa_circ_0058493 was a meaningful oncogenic circRNA and may be a biomarker of HCC. Hsa_circ_0058493 played effects in HCC progression by promoting HCC cell growth and metastasis through the m6A-hsa_circ_0058493-YTHDC1 axis. The above results suggest that hsa_circ_0058493 may become a promising target for HCC and provide a strategy for HCC treatment.

DATA AVAILABILITY STATEMENT

The raw data supporting the conclusions of this article will be made available by the authors, without undue reservation.

ETHICS STATEMENT

The studies involving human participants were reviewed and approved by the Ethics Committee of the Affiliated Hospital of Nantong University. The patients/participants provided their written informed consent to participate in this study. The animal study was reviewed and approved by the Ethics Committee of the Affiliated Hospital of Nantong University.

AUTHOR CONTRIBUTIONS

LC and FW conceived and designed the research. AW, YH, YX, XW, and AC performed the experiments. JX and RL analyzed the data. AW, YH, and YX wrote the manuscript. All authors reviewed and approved this version of manuscript.

FUNDING

This work was financially supported by the National Natural Science Foundation of China (81873978), Key Project of Social Development in Jiangsu Province (BE2019691), Chinese Postdoctoral Science Foundation (2018M642298), College Students' Innovation and Entrepreneurship Project of Jiangsu (202110304103Y), Foundation of Nantong Science and Technology Bureau (MS2019021 and MS22018010), and Postdoctoral Research Funding Project of Jiangsu Province (2021K012A).

REFERENCES

Chen, C., Yuan, W., Zhou, Q., Shao, B., Guo, Y., Wang, W., et al. (2021). N6-methyladenosine-induced circ1662 promotes metastasis of colorectal cancer by accelerating YAP1 nuclear localization. *Theranostics* 11, 4298–4315. doi: 10.7150/thno.51342

Chen, D., Ma, W., Ke, Z., and Xie, F. (2018). CircRNA hsa_circ_100395 regulates miR-1228/TCF21 pathway to inhibit lung cancer progression. *Cell Cycle* 17, 2080–2090. doi: 10.1080/15384101.2018.1515553

Chen, Y., Peng, C., Chen, J., Chen, D., Yang, B., He, B., et al. (2019c). WTAP facilitates progression of hepatocellular carcinoma via m6A-HuR-dependent epigenetic silencing of ETS1. *Mol. Cancer* 18:127.

Chen, R. X., Chen, X., Xia, L. P., Zhang, J. X., Pan, Z. Z., Ma, X. D., et al. (2019a). N(6)-methyladenosine modification of circNSUN2 facilitates cytoplasmic

export and stabilizes HMGA2 to promote colorectal liver metastasis. *Nat. Commun.* 10:4695. doi: 10.1038/s41467-019-12651-2

Chen, R. X., Liu, H. L., Yang, L. L., Kang, F. H., Xin, L. P., Huang, L. R., et al. (2019b). Circular RNA circRNA_0000285 promotes cervical cancer development by regulating FUS. *Eur. Rev. Med. Pharmacol. Sci.* 23, 8771–8778. doi: 10.26355/eurrev_201910_19271

Geng, Y., Jiang, J., and Wu, C. (2018). Function and clinical significance of circRNAs in solid tumors. *J. Hematol. Oncol.* 11:98. doi: 10.1186/s13045-018-0643-z

Han, J., Thurnherr, T., Chung, A. Y. F., Goh, B. K. P., Chow, P. K. H., Chan, C. Y., et al. (2021). Clinicopathological-associated regulatory network of deregulated circRNAs in hepatocellular carcinoma. *Cancers* 13:2772. doi: 10.3390/cancers13112772

Huang, H., Weng, H., and Chen, J. (2020). m(6)A modification in coding and non-coding RNAs: roles and therapeutic implications in cancer. *Cancer Cell* 37, 270–288. doi: 10.1016/j.ccell.2020.02.004

Kong, Z., Wan, X., Lu, Y., Zhang, Y., Huang, Y., Xu, Y., et al. (2020). Circular RNA circFOXO3 promotes prostate cancer progression through sponging miR-29a-3p. *J. Cell Mol. Med.* 24, 799–813. doi: 10.1111/jcmm.14791

Lan, T., Li, H., Zhang, D., Xu, L., Liu, H., Hao, X., et al. (2019). KIAA1429 contributes to liver cancer progression through N6-methyladenosine-dependent post-transcriptional modification of GATA3. *Mol. Cancer* 18:186. doi: 10.1186/s12943-019-1106-z

Latowska, J., Grabowska, A., Zarebska, Z., Kuczynski, K., Kuczynska, B., and Rolle, K. (2020). Non-coding RNAs in brain tumors, the contribution of lncRNAs, circRNAs, and snoRNAs to cancer development-their diagnostic and therapeutic potential. *Int. J. Mol. Sci.* 21:7001. doi: 10.3390/ijms21197001

Lee, Y., Choe, J., Park, O. H., and Kim, Y. K. (2020). Molecular mechanisms driving mRNA degradation by m6A modification. *Trends Genet.* 36, 177–188. doi: 10.1016/j.tig.2019.12.007

Lei, D., Wang, Y., Zhang, L., and Wang, Z. (2020). Circ_0010729 regulates hypoxia-induced cardiomyocyte injuries by activating TRAF5 via sponging miR-27a-3p. *Life Sci.* 262:118511. doi: 10.1016/j.lfs.2020.118511

Li, N., and Zhan, X. (2020). Identification of pathology-specific regulators of m(6)A RNA modification to optimize lung cancer management in the context of predictive, preventive, and personalized medicine. *EPMA J.* 11, 485–504. doi: 10.1007/s13167-020-00220-3

Li, Y., Zheng, Q., Bao, C., Li, S., Guo, W., Zhao, J., et al. (2015). Circular RNA is enriched and stable in exosomes: a promising biomarker for cancer diagnosis. *Cell Res.* 25, 981–984. doi: 10.1038/cr.2015.82

Liu, B., Tian, Y., Chen, M., Shen, H., Xia, J., Nan, J., et al. (2021). CircUBAP2 promotes MMP9-mediated oncogenic effect via sponging miR-194-3p in hepatocellular carcinoma. *Front. Cell. Dev. Biol.* 9:675043. doi: 10.3389/fcell.2021.675043

Liu, X., Qin, J., Gao, T., Li, C., Chen, X., Zeng, K., et al. (2020). Analysis of METTL3 and METTL14 in hepatocellular carcinoma. *Aging* 12, 21638–21659. doi: 10.18632/aging.103959

Ozgor, D., and Otan, E. (2020). HCC and tumor biomarkers: does one size fits all? *J. Gastrointest. Cancer* 51, 1122–1126. doi: 10.1007/s12029-020-00485-x

Pan, J., Xu, L., and Pan, H. (2020). Development and validation of an m6A RNA methylation regulator-based signature for prognostic prediction in cervical squamous cell carcinoma. *Front. Oncol.* 10:1444. doi: 10.3389/fonc.2020.01444

Qian, J. Y., Gao, J., Sun, X., Cao, M. D., Shi, L., Xia, T. S., et al. (2019). KIAA1429 acts as an oncogenic factor in breast cancer by regulating CDK1 in an N6-methyladenosine-independent manner. *Oncogene* 38, 6123–6141. doi: 10.1038/s41388-019-0861-z

Verduci, L., Strano, S., Yarden, Y., and Blandino, G. (2019). The circRNA-microRNA code: emerging implications for cancer diagnosis and treatment. *Mol. Oncol.* 13, 669–680. doi: 10.1002/1878-0261.12468

Wang, Y., Yao, R., Zhang, D., Chen, R., Ren, Z., and Zhang, L. (2020d). Circulating neutrophils predict poor survival for HCC and promote HCC progression through p53 and STAT3 signaling pathway. *J. Cancer* 11, 3736–3744. doi: 10.7150/jca.42953

Wang, M., Yang, Y., Yang, J., Yang, J., and Han, S. (2020a). circ_KIAA1429 accelerates hepatocellular carcinoma advancement through the mechanism of m(6)A-YTHDF3-Zeb1. *Life Sci.* 257:118082. doi: 10.1016/j.lfs.2020.118082

Wang, M., Yu, F., Chen, X., Li, P., and Wang, K. (2020b). The underlying mechanisms of noncoding RNAs in the chemoresistance of hepatocellular carcinoma. *Mol. Ther. Nucleic Acids* 21, 13–27. doi: 10.1016/j.omtn.2020.05.011

Wang, T., Kong, S., Tao, M., and Ju, S. (2020c). The potential role of RNA N6-methyladenosine in cancer progression. *Mol. Cancer* 19:88. doi: 10.1186/s12943-020-01204-7

Wang, T., and Zhang, K. H. (2020). New blood biomarkers for the diagnosis of AFP-negative hepatocellular carcinoma. *Front. Oncol.* 10:1316. doi: 10.3389/fonc.2020.01316

Wang, W., and Wei, C. (2020). Advances in the early diagnosis of hepatocellular carcinoma. *Genes Dis.* 7, 308–319. doi: 10.1016/j.gendis.2020.01.014

Xiao, M. S., Ai, Y., and Wilusz, J. E. (2020). Biogenesis and functions of circular RNAs come into focus. *Trends Cell Biol.* 30, 226–240. doi: 10.1016/j.tcb.2019.12.004

Xu, C., Liu, K., Ahmed, H., Loppnau, P., Schapira, M., and Min, J. (2015). Structural basis for the discriminative recognition of n6-methyladenosine RNA by the human YT521-B homology domain family of proteins. *J. Biol. Chem.* 290, 24902–24913. doi: 10.1074/jbc.M115.680389

Xu, C., Wang, X., Liu, K., Roundtree, I. A., Tempel, W., Li, Y., et al. (2014). Structural basis for selective binding of m6A RNA by the YTHDC1 YTH domain. *Nat. Chem. Biol.* 10, 927–929. doi: 10.1038/nchembio.1654

Xu, J., Wan, Z., Tang, M., Lin, Z., Jiang, S., Ji, L., et al. (2020). N(6)-methyladenosine-modified CircRNA-SORE sustains sorafenib resistance in hepatocellular carcinoma by regulating beta-catenin signaling. *Mol. Cancer* 19:163. doi: 10.1186/s12943-020-01281-8

Yang, C. Y., Zhang, F. X., He, J. N., and Wang, S. Q. (2019). CircRNA_100876 promote proliferation and metastasis of breast cancer cells through adsorbing microRNA-361-3p in a sponge form. *Eur. Rev. Med. Pharmacol. Sci.* 23, 6962–6970. doi: 10.26355/eurrev_201908_18736

Yang, Y., Gao, X., Zhang, M., Yan, S., Sun, C., Xiao, F., et al. (2018). Novel Role of FBXW7 Circular RNA in repressing glioma tumorigenesis. *J. Natl. Cancer Inst.* 110, 304–315. doi: 10.1093/jnci/djx166

Zhang, G., and Zhang, G. (2019). Upregulation of FoxP4 in HCC promotes migration and invasion through regulation of EMT. *Oncol. Lett.* 17, 3944–3951. doi: 10.3892/ol.2019.10049

Zhang, T., Jing, B., Bai, Y., Zhang, Y., and Yu, H. (2020). Circular RNA circTMEM45A acts as the sponge of MicroRNA-665 to promote hepatocellular carcinoma progression. *Mol. Ther. Nucleic Acids* 22, 285–297. doi: 10.1016/j.omtn.2020.08.011

Zhang, X., Xu, Y., Qian, Z., Zheng, W., Wu, Q., Chen, Y., et al. (2018). circRNA_104075 stimulates YAP-dependent tumorigenesis through the regulation of HNF4a and may serve as a diagnostic marker in hepatocellular carcinoma. *Cell Death Dis.* 9:1091. doi: 10.1038/s41419-018-1132-6

Zhao, T., Jia, L., Li, J., Ma, C., Wu, J., Shen, J., et al. (2020). Heterogeneities of site-specific N-glycosylation in HCC tumors with low and high AFP concentrations. *Front. Oncol.* 10:496. doi: 10.3389/fonc.2020.00496

Zheng, Y., Zhu, M., and Li, M. (2020). Effects of alpha-fetoprotein on the occurrence and progression of hepatocellular carcinoma. *J. Cancer Res. Clin. Oncol.* 146, 2439–2446. doi: 10.1007/s00432-020-03331-6

Conflict of Interest: The authors declare that the research was conducted in the absence of any commercial or financial relationships that could be construed as a potential conflict of interest.

Publisher's Note: All claims expressed in this article are solely those of the authors and do not necessarily represent those of their affiliated organizations, or those of the publisher, the editors and the reviewers. Any product that may be evaluated in this article, or claim that may be made by its manufacturer, is not guaranteed or endorsed by the publisher.

frontiers in Cell and Developmental Biology

ORIGINAL RESEARCH
published: 25 November 2021
doi: 10.3389/fcell.2021.737812

Long Non-coding RNAs LINC01679 as a Competitive Endogenous RNAs Inhibits the Development and Progression of Prostate Cancer via Regulating the miR-3150a-3p/SLC17A9 Axis

Yuan-yuan Mi[1†], Chuan-yu Sun[2†], Li-feng Zhang[3†], Jun Wang[1†], Hong-bao Shao[1], Feng Qin[1], Guo-wei Xia[2] and Li-jie Zhu[1*]*

[1] Department of Urology, Affiliated Hospital of Jiangnan University, Wuxi, China, [2] Department of Urology, Huashan Hospital, Fudan University, Shanghai, China, [3] Department of Urology, Affiliated Changzhou No. 2 People's Hospital of Nanjing Medical University, Changzhou, China

OPEN ACCESS

Edited by:
Hailong Pei,
Soochow University, China

Reviewed by:
Wen Xiao,
Huazhong University of Science and Technology, China
Sercan Ergun,
Ondokuz Mayıs University, Turkey
Kenichi Takayama,
Tokyo Metropolitan Institute of Gerontology, Japan

***Correspondence:**
Li-jie Zhu
zhulijiezlj6123@163.com
Guo-wei Xia
xiaguoweiurohs@163.com

† These authors have contributed equally to this work

Specialty section:
This article was submitted to Molecular and Cellular Oncology, a section of the journal Frontiers in Cell and Developmental Biology

Received: 07 July 2021
Accepted: 27 September 2021
Published: 25 November 2021

Citation:
Mi Y-y, Sun C-y, Zhang L-f, Wang J, Shao H-b, Qin F, Xia G-w and Zhu L-j (2021) Long Non-coding RNAs LINC01679 as a Competitive Endogenous RNAs Inhibits the Development and Progression of Prostate Cancer via Regulating the miR-3150a-3p/SLC17A9 Axis. Front. Cell Dev. Biol. 9:737812. doi: 10.3389/fcell.2021.737812

Long non-coding RNAs (lncRNAs) have been indicated as the candidate factors to predict cancer prognosis. However, it is still unknown whether lncRNA combinations may be utilized for predicting overall survival (OS) of prostate cancer (PCa). The present work focused on selecting the potent OS-related lncRNA signature for PCa and studying its molecular mechanism to enhance the prognosis prediction accuracy. Differentially expressed lncRNAs (DElncRNAs) or differentially expressed genes (DEGs) were obtained based on TCGA database by R software "edgeR" package. lncRNAs or mRNAs significantly related to PCa were screened through univariate as well as multivariate Cox regression, for the construction of the risk model for prognosis prediction. Moreover, this constructed risk model was validated through ROC analysis, univariate regression, and Kaplan–Meier (KM) analysis. Additionally, we built a lncRNA–miRNA–mRNA ceRNA network through bioinformatics analysis. Colony formation, CCK-8, flow cytometry, scratch, and Transwell assays were performed based on PCa cells subjected to small interfering RNA (siRNA) targeting LINC01679/SLC17A9 and vector expressing LINC01679/SLC17A9 transfection. Thereafter, the ceRNA mechanism was clarified *via* qRT-PCR, Western blotting (WB), RNA pull-down, and luciferase reporter assays. Nude mouse tumor xenograft was established to examine LINC01679's oncogenicity within PCa cells. According to our results, LINC01679 depletion promoted cell proliferation, metastasis, tumor growth, and inhibited cell apoptosis *in vivo* and *in vitro*, which was also associated with poor survival. LINC01679 regulated miR-3150a-3p level by sponging it. Importantly, miR-3150a-3p overexpression was related to the increased proliferation and decreased apoptosis of PCa cells. Rescue assays suggested that miR-3150a-3p mimics rescued the repression on PCa progression mediated by LINC01679 upregulation, but SLC17A9 downregulation reversed the miR-3150a-3p inhibitor-mediated repression on PC progression. Importantly, SLC17A9 downregulation rescued

the repression on PCa progression mediated by LINC01679 upregulation. LINC01679 and SLC17A9 are tightly associated with certain clinicopathological characteristics of PCa and its prognostic outcome. In addition, LINC01679 is the ceRNA that suppresses PCa development through modulating the miR-3150a-3p/SLC17A9 axis.

Keywords: LINC01679, miR-3150a-3p, SLC17A9, prostate cancer, ceRNA

INTRODUCTION

Prostate cancer (PCa) is the most common reproductive cancer in men. PCa ranks the second and fifth in terms of its morbidity and death-related cause among men worldwide (Wang G. et al., 2018). The occurrence and development of PCa is not achieved overnight; instead, it needs to go through a long evolutionary cycle. Generally, genomic mutations, changes in the cellular ecosystem, unhealthy living habits, and living environment can lead to the occurrence of PCa (Grozescu and Popa, 2017). Noteworthily, the transformation from normal prostate cells to tumor cells and further invasion and metastasis are a highly heterogeneous and extremely complex process (Chang et al., 2014). Therefore, in view of different development links, it is of important theoretical and clinical significance to use big data, cloud computing technology, and translational biomedical informatics methods to achieve accurate intervention, slow down, or even reverse the process of prostate cancerization through systematic analysis, integration, and identification of key elements. The interactions between biomolecules form the large-scale and complex biomolecule networks, including the protein–protein interaction (PPI) network (Athanasios et al., 2017), gene co-expression network (van Dam et al., 2018), miRNA–mRNA regulatory network (Lou et al., 2019), and ceRNA regulatory network (Jiang et al., 2020). Analyzing network structure and function is of crucial significance to understand complex biological problems. Therefore, it has always been an important issue in network science and systems biology to find the key sites or key role relationships in the network system, so as to measure or evaluate the stability of biological systems. Long non-coding RNAs (lncRNAs) are suggested in studies as the oncogenes or tumor suppressors for cancer (Wang J. et al., 2018; Wang et al., 2019; Zhuang et al., 2019). Competitive endogenous RNAs (ceRNAs), including mRNAs, pseudogenes, lncRNAs, and circRNAs, can bind competitively to miRNAs, thereby affecting miRNAs' effect on target genes (Qi et al., 2015). This study built a ceRNA network to find key sites affecting the stability of the network and system and their relationship, so as to provide theoretical reference for diagnosing and treating PCa and other cancers.

Long non-coding RNAs are RNAs that are more than 200 nucleotides (nt) long, which cannot encode proteins (Wang J. et al., 2018). Some lncRNAs can serve as the oncogenes or tumor suppressor genes of PCa (Lingadahalli et al., 2018; Shang et al., 2019; Wu M. et al., 2019). Their abnormal expression is closely related to PCa genesis and progression, which are the markers for diagnosing and targets for treating PCa. PCA3, an early discovered lncRNA molecule, is reported to be related to PCa (Soares et al., 2019). Its expression is prostate-specific and can be used in the clinical diagnosis and management of PCa. In PCa, PCAT1 can negatively regulate the functional defect of BRCA2-induced homologous recombination and promote PCa cell growth through increasing cMyc; as a result, it can be used as a prognostic marker of PCa (Prensner et al., 2014). At present, integrated analysis based on ceRNA competition mechanism is the mainstream method to identify the lncRNA markers for cancer. Many articles suggest that lncRNAs play the role of ceRNAs for regulating PCa development (Wu X. et al., 2019; Zhang Y. et al., 2019). Notably, lncRNA UCA1 is a ceRNA that can enhance PCa development through the sponge of miR-143 (Yu et al., 2020). lncRNA HCP5 enhances PCa cell growth through sponging miR-4656 for regulating CEMIP level (Hu and Lu, 2020). Moreover, after being activated by RAX5, lncRNA FOXP4-AS1 enhances PCa proliferation through the sequestration of miR-3184-5p for upregulating FOXP4 (Wu X. et al., 2019). However, the function of LINC01679 in tumor progression has not been studied yet.

This work focused on the role of LINC01679 in PCa and the related molecular mechanism. It was found that LINC01679 inhibited PCa genesis and development through sponging miR-3150a-3p and specifically targeting SLC17A9. Findings from this study help to diagnose and treat PCa.

MATERIALS AND METHODS

Patient Datasets and Processing of Long Non-coding RNAs and mRNAs

All data were obtained based on the TCGA database. We adopted the Data Transfer Tool (GDC Apps) to download clinical and gene expression profiling data from PCa cases[1]. Altogether, 540 PCa cases were later randomized as training and validation sets (ratio, 7:3) to carry out integrated analysis by the "caret" package. The sample inclusion criteria in both sets were as follows: (1) samples were randomized as training or test set; (2) comparable clinical characteristics of samples from both sets. All data were freely accessible, and approval by Ethics Committee was unnecessary. All data were processed according to relevant NIH TCGA human subject protection policies and data access policy[2].

The Illumina HiSeq RNASeq platform was adopted to obtain mRNA or lncRNA expression profiles in PCa cases, which were subsequently normalized according to TCGA. Thereafter, the "edgeR" function of the R package was utilized for detecting differentially expressed RNAs (DERNAs) and

[1]https://tcga-data.nci.nih.gov/

[2]http://cancergenome.nih.gov/publications/publicationguidelines

identifying differentially expressed lncRNAs (DElncRNAs) by adopting the thresholds of adjusted $p < 0.05$ and log2 fold change (FC) > 2.0.

Construction of the Long Non-coding RNAs or mRNA Signature

The associations between mRNA or lncRNA levels and patient overall survival (OS) were analyzed by the univariate Cox model. At the same time, univariate analysis was conducted to identify significant lncRNAs ($p < 0.05$). Later, LASSO regression was conducted to select and verify mRNAs or lncRNAs by the "glmnet" function of the R package. Last, this study established an mRNA- or lncRNA-based prognostic risk score according to summation of products of RNA expression multiplied by regression model (β), which was determined by the following formula: Risk_score = βlncRNA1 × lncRNA1 level + βlncRNA2 × lncRNA2 level + · ···· + βlncRNAn × lncRNAn level or βmRNA1 × mRNA1 level + βmRNA2 × mRNA2 level + · ···· + βmRNAn × mRNA level.

Confirmation of Long Non-coding RNAs or mRNA Signature

This study assigned the enrolled cases and the survival data based on risk score. In addition, all cases were classified into high- or low-risk group according to the median risk score. Thereafter, this study drew the Kaplan–Meier (KM) survival curves for estimating high or low risk of the enrolled cases. Later, this study carried out a univariate analysis using the Cox proportional hazards regression model. Afterward, the risk score was utilized to compare the sensitivity and specificity of survival prediction, whereas time-dependent receiver operating characteristic (t-ROC) curves were drawn for evaluating 5-year prognosis prediction accuracy. Additionally, multivariate analysis was carried out to examine the independent prediction performance of mRNA or lncRNA risk score compared with additional clinical features. The conditional inference tree was constructed by "party" "tree" function of R package to further illustrate our results. $p < 0.05$ (two-sided) indicated statistical significance. The R software was employed for all analyses.

Patient Specimens and Cell Culture

Altogether, 55 PCa samples and 55 matched non-carcinoma prostate samples were obtained from PCa cases treated at Affiliated Hospital of Jiangnan University from May 2013 to June 2018 (**Table 1**). All resected specimens were frozen within liquid nitrogen at once and stored under −80°C. Each subject provided written informed consent. The Research Ethics Committee of the Affiliated Hospital of Jiangnan University approved our study protocols carried out in line with the Declaration of Helsinki. Based on the median SLC17A9, LINC01679, or miR-3150a-3p expression, this study divided 55 PCa samples into a high- or a low-expression group. The human normal prostate epithelial RWPE-2 cells and human PCa cell lines (DU145, PC-3, LNCaP, C4-2B, and 22RV1) were provided by the American Type Culture Collection (ATCC, Rockville, MD, United States). All cell lines were cultivated within DMEM containing 10% fetal bovine serum (FBS, HyClone, Logan, UT, United States) as well as 1% penicillin-streptomycin (HyClone) under 37°C and 5% CO_2 conditions.

TABLE 1 | The Relationship between LINC01679 and clinicopathological characteristics in 55 patients with prostate cancer.

Parameters	No. of cases	LINC01679 expression		*p*-values
		Low	High	
Age (years)				0.218
≥60	28	15	13	
<60	27	10	17	
Differentiation				0.96
Poor	31	14	17	
Well/moderate	24	11	13	
PSA				0.004*
≥23.6	28	18	10	
<23.6	27	7	20	
Gleason score				0.002*
≥7	29	19	10	
<7	26	6	20	

*PSA, prostate-specific antigen; *p < 0.05.*

Bioinformatics Analysis

TargetScan database[3] and starBase V2.0[4] were applied in predicting miRNA target genes and lncRNA target miRNAs. Gene expression profiling interactive analysis (GEPIA) database[5] was used to determine SLC17A9 expression in PCa and the correlation of LINC01679 and SLC17A9. Oncomine[6] and UALCAN[7] databases were used to determine SLC17A9 expression in PCa.

Competitive Endogenous RNA Regulatory Network Establishment

Firstly, associations between those screened DElncRNAs and miRNAs and between those selected miRNAs and the selected differentially expressed genes (DEGs) were predicted by the starBase database. Thereafter, we adopted Cytoscape 3.5.1 software[8] to visually map results.

Cell Transfection

GenePharma was responsible for constructing vectors expressing LINC01679 [LINC01679-overexpression (OE); Shanghai, China] and vectors expressing SLC17A9 (SLC17A9-OE). Besides, we obtained empty vectors from GenePharma. The SLC17A9 or LINC01679-targeting small interfering RNA (siRNA) [SLC17A9- or LINC01679-knockdown (KD)], together with the corresponding negative control (NC), was provided by GenePharma (Shanghai, China). In the meantime, miR-3150a-3p

[3]http://www.targetscan.org/vert_72/

[4]http://starbase.sysu.edu.cn/starbase2/index.php

[5]http://gepia.cancer-pku.cn/

[6]https://www.oncomine.org/resource/login.html

[7]http://ualcan.path.uab.edu/

[8]http://www.cytoscape.org/

inhibitor and miR-3150a-3p mimic, along with scrambled NC miRNA (NC inhibitor/mimic), were provided by Sigma-Aldrich. Lipofectamine 2000 Reagent (Invitrogen, Carlsbad, CA, United States) was utilized in cell transfection strictly following specific protocols. After reaching 30–50% confluency, we utilized 40 nM miRNAs, 20 nM siRNAs, and 15 nM vectors to transfect cells, separately, for 48 h by the use of Lipofectamine 2000 (Life Technologies) following specific instructions.

Cell Counting Kit-8 Assay

Cells (4,000 cells/well) were inoculated into each well of the 96-well plates that contained 100 μl of culture medium. There were six wells set for each replicate. After 72 h of culture within the medium that contained 5% FBS, we inoculated cells within the 37°C incubator under 5% CO_2 atmosphere overnight. Later, each well was added with 10 μl of CCK-8 solution (5 mg/ml, Beyotime Institute of Biotechnology, Shanghai, China) at 0, 12, 24, and 48 h, respectively, for CCK-8 assay, followed by another 1 h of culture. For blank control group, CCK-8 solution and culture medium were added into each well. Thereafter, the microplate reader (Bio-Tek, VT, United States) was adopted to measure absorbance (OD) value at 450 nm (OD 450) compared with control.

Nuclear – Cytoplasmic Fractionation

This study utilized the NE-PER Cytoplasmic and Nuclear Extraction Reagents (Thermo Fisher Scientific) to separate the cytoplasmic fraction from the nuclear counterpart in line with specific protocols. Thereafter, total RNA was extracted by adopting the RNA Isolation Kit (Tiangen Biotech, Beijing, China). Afterward, the cytoplasmic-to-nuclear ratio of specific RNA expression was measured through qRT-PCR, with GAPDH being the cytoplasmic reference and U6 being the nuclear reference.

Colony Formation Assay

After incubation in six-well plates at 500/well, the formation of cell colonies was observed after 2 weeks. Then, colonies were subjected to methanol fixation as well as 0.1% crystal violet staining under ambient temperature. Finally, colonies that contained at least 50 cells were regarded as the positive colonies under the microscope.

Flow Cytometry

This study adopted the Annexin V-fluorescein isothiocyanate and propidium iodide (FITC/PI) kit (Beyotime Institute of Biotechnology, Shanghai, China) for detecting cell apoptosis through flow cytometric analysis in accordance with specific protocols.

Transwell Assay

After resuspending in serum-free medium, cells from diverse groups were digested with pancreatin. Afterward, 200 μl of the cell suspension that contained altogether 5×10^3 cells was added into the top Transwell chamber, whereas 500 μl of DMEM that contained 10% FBS was added into the bottom chamber for 24 h of incubation within a humidified incubator at 37°C. Subsequently, 4% formaldehyde was utilized to fix cells invading the Transwell chamber, and 0.1% crystal violet staining (Beyotime) was used to stain cells. Last, a microscope was utilized to detect cell invasion.

Scratch Assay

Cells (5×10^5/well) were inoculated into six-well plates. Later, we used the 200-μl pipette tip to create a wound on the confluent cell monolayer. Later, the inverted microscope was utilized to take images of wound closure at 0 and 24 h. Then, wound healing distance was examined.

Tumor Xenograft Model

The Animal Care Committee of Fudan University Shanghai Cancer Center (Shanghai, China) approved our study protocols. Treated cells were injected subcutaneously in the 20 male BALB nude mice (4 weeks old; $n = 5$) *via* the right flank. Body weight (BW, g) and tumor volume were determined at intervals of 3 days. Each animal was sacrificed after 4 weeks to collect tumor tissues, images were taken, and tumor volume was measured. To be specific, tumor volume was measured by the following formula: Volume (mm^3) = [width^2 (mm^2) × length (mm)]/2. The dissected tumor tissue was frozen within liquid nitrogen, followed by preservation under −80°C or 10% formalin fixation, paraffin embedding, sectioning, and staining.

Dual-Luciferase Reporter Assay

A luciferase construct containing wild-type (WT) and mutated (MUT) binding site vectors of LINC01679 3′ -untranslated region (3′UTR) or WT and MUT binding site vectors of SLC17A9 3′UTR (Promega, Madison, Wisconsin, United States) was co-transfected with scramble or miR-3150a-3p mimic/inhibitor into cells grown within 24-well plates by the use of Lipofectamine 3000 (Thermo Fisher Scientific, Inc). Later, we used a dual-luciferase assay system (Promega) to analyze luciferase activities of transfected cells in accordance with specific instructions.

A luciferase construct containing WT and MUT binding site vectors of SLC17A9 3′UTR (Promega, Madison, Wisconsin, United States) was co-transfected with NC/vector or LINC01679-KD/LINC01679-OE into cells grown within 24-well plates by the use of Lipofectamine 3000 (Thermo Fisher Scientific, Inc). Later, we used a dual-luciferase assay system (Promega) to analyze luciferase activities of transfected cells in accordance with specific instructions.

RNA Pull-Down Assay

Probe-ATB or probe-control was transcribed from ATB shRNA lentivector and labeled *in vitro* by Biotin RNA Labeling Mix (Roche, Basel, Switzerland) to carry out RNA pull-down assay. Secondary structure was formed through biotin-labeled RNAs by adopting the RNA structure buffer (Thermo Fisher Scientific, MA, United States). Then, RNA immunoprecipitation wash buffer (500 μl, Thermo Fisher Scientific) was utilized to rinse Streptavidin beads

(Thermo Fisher Scientific) thrice, while the beads were later mixed with biotinylated RNAs overnight under 4°C. Later, the magnetic field was applied to separate the overnight mixture to obtain the streptavidin bead–RNA complexes. Afterward, complexes were mixed with cell lysates before 1 h of incubation on the rotator under ambient temperature. Again, the magnetic field was applied to separate the mixture after incubation for obtaining streptavidin bead–RNA–protein complexes.

qRT-PCR

Quick-RNA^{TM} Microprep Kit (Zymo, CA, United States) was employed to extract the total cellular RNA. Meanwhile, the PrimeScript^{TM} RT Reagent Kit equipped with gDNA Eraser (TaKaRa, Shiga, Japan) was adopted to prepare cDNA in accordance with the manufacturer's instructions. Then, the TB Green Premix ExTaq II (Tli RNaseH Plus, TaKaRa) was applied for qRT-PCR, whereas the LightCycler® 96 Instrument (Roche, Switzerland) was employed for analysis. Then, we determined fold changes (FC) by the $\Delta\Delta$Ct approach, with U6 or GAPDH being the endogenous control. **Table 2** lists the primers used.

Western Blotting Analysis

After washing with PBS, cells were lysed with the pre-chilled lysis buffer. Later, the collected cell lysates were subjected to 15 min of centrifugation at 14,000 × *g* and 4°C and boiling with 5 × sample buffer (BSA; Thermo Fisher Scientific, Inc., CA, United States) after the protein content was measured. Afterward, WB assay was performed on those protein samples. To carry out WB, the 4%–20% precasting gel (Bio-Rad Laboratories) was used to transfer protein onto the nitrocellulose membranes, and then 5% skim milk was utilized to block the membranes (Bio-Rad Laboratories) for 1 h under ambient temperature. Later, specific antibodies (dilution, 1:1,000), including anti-SLC17A9, anti-VEGF, anti-Bax, anti-Ki67, anti-MTA1, anti-Bcl-2, anti-MMP-2, and GAPDH (Santa Cruz, CA, United States), were used to block membranes. Subsequently, secondary antibodies (Santa Cruz) were utilized to incubate membranes at ambient temperature for 1 h, followed by visualization using the ECL solution (Bio-Rad Laboratories). Finally, images were taken using the chemiluminescence imaging system (Mini HD9; UVitec, Cambridge, United Kingdom).

TABLE 2 | The primer sequence of qRT-PCR.

Gene	Sequence (5′-3′)
LINC01679	F: TGCCACTCGTGAGAACTGTCTA R: GATAGGCTCTGCAAGACACC
miR-3150a-3p	F: CCAGAGGGTCCACTCCAGTTTTCCAG R: GACTCAAGGGTGTCGTCT
SLC17A9	F: TGGGTTGTGGGGTCATGGG R: TACTTCTCTGTGGCATGATGGCT
GAPDH	F: GAACGAGCCGAGTGAAGCC R: CTTTGACTGCTTTCCCACCGG
U6	F: GCAGTGGACGACGAGTAGGA R: GCACACGAAGCAGGAAGCTA

Statistical Analysis

The relative change in LINC01679 expression > 0.8 (median value) was deemed as high expression. Correlations between LINC01679 level and clinicopathological factors were examined by chi-square test. Besides, a KM curve was drawn to analyze patient survival by log-rank test. Results were displayed as means ± standard deviation (SD). SPSS22.0 was employed to carry out statistical analysis. Data across diverse groups were compared through ANOVA and least significant difference (LSD) test, whereas those of two groups were examined through Student's *t*-test. A difference of $p < 0.05$ indicated statistical significance. Each experiment was conducted thrice.

RESULTS

Identification of Significant Differentially Expressed Long Non-coding RNAs for Prostate Cancer Prognosis

This study discovered DElncRNAs between cancer and non-carcinoma samples. Altogether, 2,974 DElncRNAs (namely, 1,598 with downregulation and 1,376 with upregulation) were discovered by the "edgeR" function of the R package. Thereafter, the identified DElncRNAs were incorporated in the construction of a volcano plot (**Figure 1A**) as well as a heat map showing the 200 most significant genes (**Figure 1B**). Among them, 11 PCa-related DElncRNAs were found to be markedly related to OS of TCGA-derived PCa cases ($p < 0.01$) through Cox proportional hazards analysis, which included five low-risk lncRNAs [LINC01679, SLC12A5-AS1, PRRT3-AS1, LINC01088, and LINC00668; hazard ratio (HR) < 1] and six high-risk ones (HOXB-AS3, LINC00908, SNHG12, LINC01694, LCMT1-SA2, and LINC00342; HR > 1) (**Figure 1C**). The above-identified 11 DElncRNAs were subsequently adopted to construct the best prognosis prediction nomogram for PCa-associated lncRNAs (**Figure 1D**). Risk score together with relevant survival of PCa cases was illustrated by risk curve and scatterplot. As a result, the greater risk score indicated the higher risk of mortality (**Figures 1E,F**). As revealed by KM survival analysis, high-risk cases showed reduced OS relative to low-risk patients ($p = 2.115e-03$; **Figure 1G**). Besides, time-dependent receiver operating characteristic (ROC) curve analysis showed that the area under the ROC (AUC) value for the survival-related lncRNA prognosis signature was 0.712 (**Figure 1H**).

Identification of Significant Prostate Cancer-Related Differentially Expressed Genes

This study obtained significant DEGs between cancer and non-carcinoma samples. Altogether, 1,938 DEGs (namely, 1,488 with downregulation and 450 with upregulation) were discovered by the "edgeR" function of the R package. The above DEGs were later incorporated into the construction of a volcano plot for

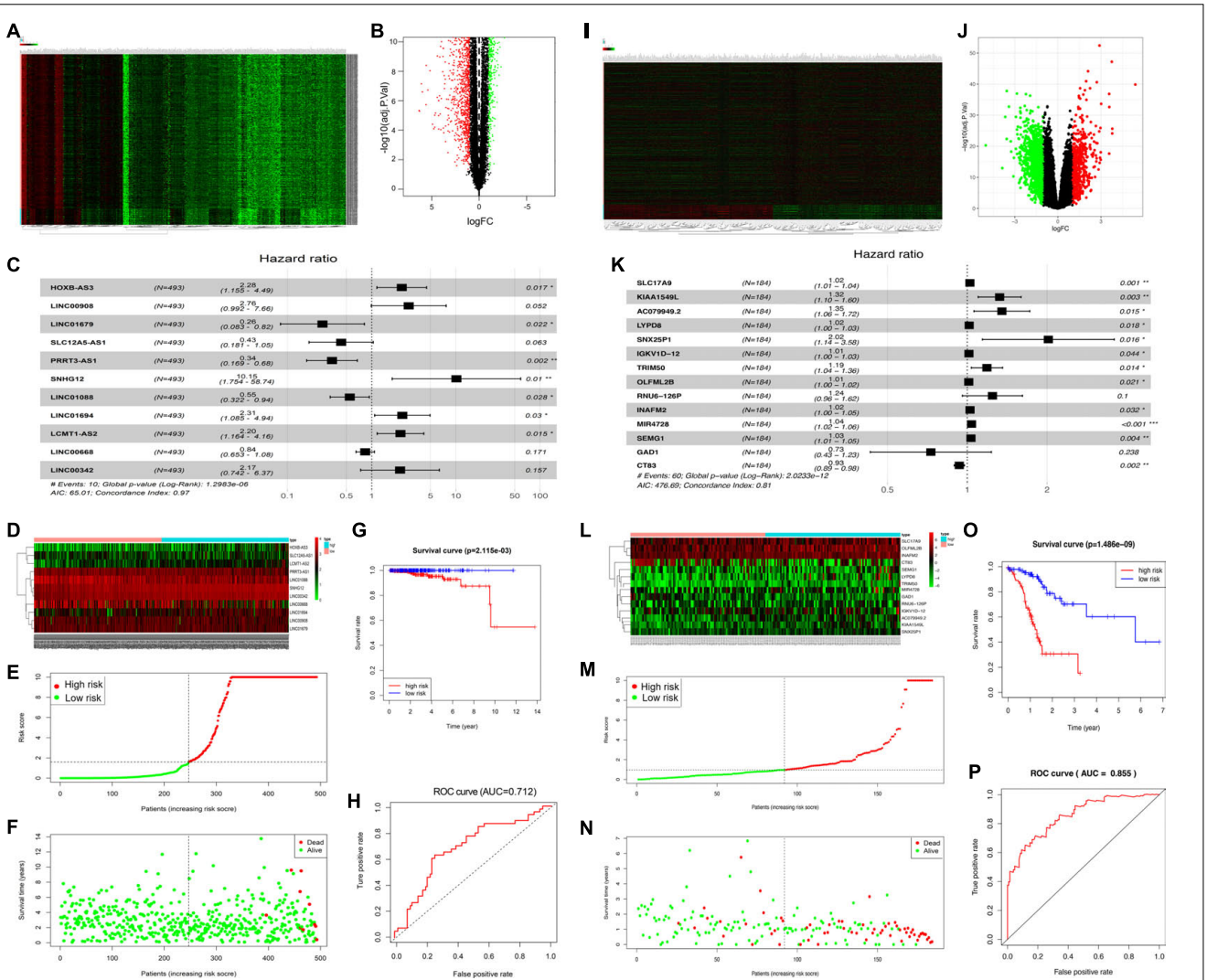

FIGURE 1 | Identification of significant PCa-related DElncRNAs and DEGs. Heat map demonstrating the DElncRNAs **(A)** and DEGs **(I)**. Volcano plot showing the DElncRNAs **(B)** and DEGs **(J)**, FC, fold change. **(C)** Forest map showing HRs (95% CIs) together with *p*-values for those screened DElncRNAs, and DEGs **(K)** by univariate Cox proportional hazards analysis. Heat map displaying the expression levels of OS-related DElncRNAs **(D)** and DEGs **(L)** in the high-risk and low-risk groups. **(E,M)** Risk curve plotted according to risk scores of all samples. **(F,N)** Scatterplot drawn according to patient survival status, where red and green dots denote death and survival, respectively. **(G,O)** KM curve showing the survival between low- and high-risk groups according to median risk score and risk model. **(H,P)** AUC values of clinical characteristics and risk score based on ROC curves.

DEGs (**Figure 1I**) together with a heat map for the 200 most significant genes (**Figure 1J**). Of these genes, 14 DEGs were found to be markedly related to OS of TCGA-derived PCa cases ($p < 0.01$) through Cox proportional hazards analysis, which included 2 low-risk DEGs (GAD1 and CT83; HR < 1) and 12 high-risk ones (SLC17A9, KIAA1549L, AC079949.2, LYPD8, SNX25P1, IGKV1D-12, TRIM50, OLFML2B, SEMG1, RNU6-126P, INAFM2, and MIR4728; HR > 1) (**Figure 1K**). These 14 DEGs were later included to construct the best prognosis prediction nomogram for DEGs related to PCa prognosis (**Figure 1L**). A greater risk score stood for the greater risk of mortality (**Figures 1M,N**). According to KM survival analysis, high-risk cases showed reduced OS relative to low-risk cases (p = 1.486e-09; **Figure 1O**). Besides, time-dependent ROC curve analysis showed that the AUC value for the survival-related mRNA prognosis signature was 0.855 (**Figure 1P**).

Competitive Endogenous RNA Regulatory Network Construction in Prostate Cancer

To further understand the role of DElncRNAs within PCa, the present work constructed the ceRNA regulatory network according to lncRNAs–miRNAs–mRNAs for PCa. Firstly, 14 DEGs and 11 DElncRNAs acquired in the previous section were utilized; then, 70,727 pairs of overlapped miRNAs and lncRNAs and 2,012,127 pairs of overlapped mRNAs and miRNAs were identified based on the starBase database. According to our

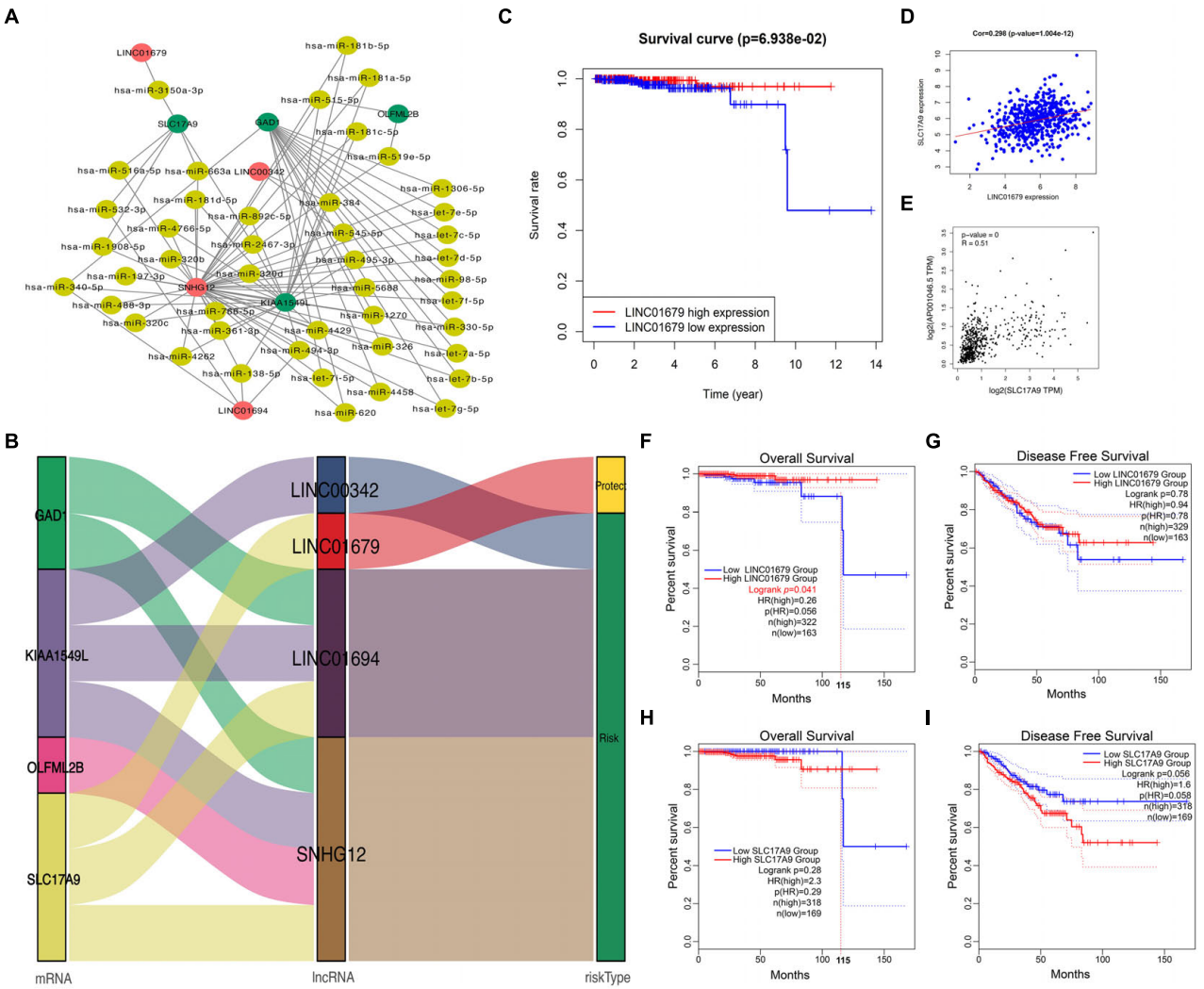

FIGURE 2 | Construction of a ceRNA regulatory network for PCa. **(A,B)** Construction of the four lncRNAs–mRNAs co-expression networks for predicting the OS of PCa, and network visualization by Sankey diagram and Cytoscape. **(C)** KM analysis on high and low LINC01679 levels. **(D)** Correlation analysis between LINC01679 expression and SLC17A9 expression based on TCGA database **(D)** and GEPIA database **(E)**. GEPIA database was used to analyze the role of LINC01679 in OS **(F)** and DFS **(G)** of PCa patients and the role of SLC17A9 in OS **(H)** and DFS **(I)** of PCa patients.

findings, four mRNAs were chosen to construct the ceRNA network. Last, the ceRNA network for PCa was established based on 4 DElncRNAs, 45 DEmiRNAs, and 4 DEmRNAs (**Figure 2A**). As observed from **Figure 2B**, LINC01679 (lncRNA)–SLC17A9 (mRNA) was the only pair of lncRNA–mRNA in the protection group. Furthermore, KM analysis revealed that cases showing low expression of LINC01679 had reduced OS relative to those with high expression (**Figure 2C**). LINC01679 was co-expressed with SLC17A9 in PCa, and LINC01679 expression was positively associated with SLC17A9 expression (**Figure 2D**). The GEPIA website pooled the data from TCGA and Genotype-Tissue Expression (GTEx) datasets. The GTEx dataset can complement the lack of control data in the TCGA dataset. The inclusion of GTEx data will make the results of the analysis more accurate. The results are shown in **Figure 2E**, which similarly suggested that LINC01679 expression was positively associated with SLC17A9 expression. In addition, we further analyze the role of LINC01679 and SLC17A9 in the OS and disease-free survival (DFS) of PCa based on the GEPIA database. The results showed that LINC01679 expression was significantly associated with OS of PCa (**Figure 2F**) and has not been significant to the DFS of PCa (**Figure 2G**). However, it was obvious from **Figure 2G** that the rate of the DFS for PCa patients with high LINC01679 expression was superior to that of PCa patients with low LINC01679 expression. In addition, SLC17A9 expression is not significant to the OS (**Figure 2H**) and the DFS of PCa (**Figure 2I**). When survival time exceeds 115 months, the survival rate of PCa patients with high SLC17A9 expression is significantly higher than that of PCa patients with low SLC17A9 expression. Next, LINC01679 expression was significantly related to PSA and gleason grade (**Table 1**).

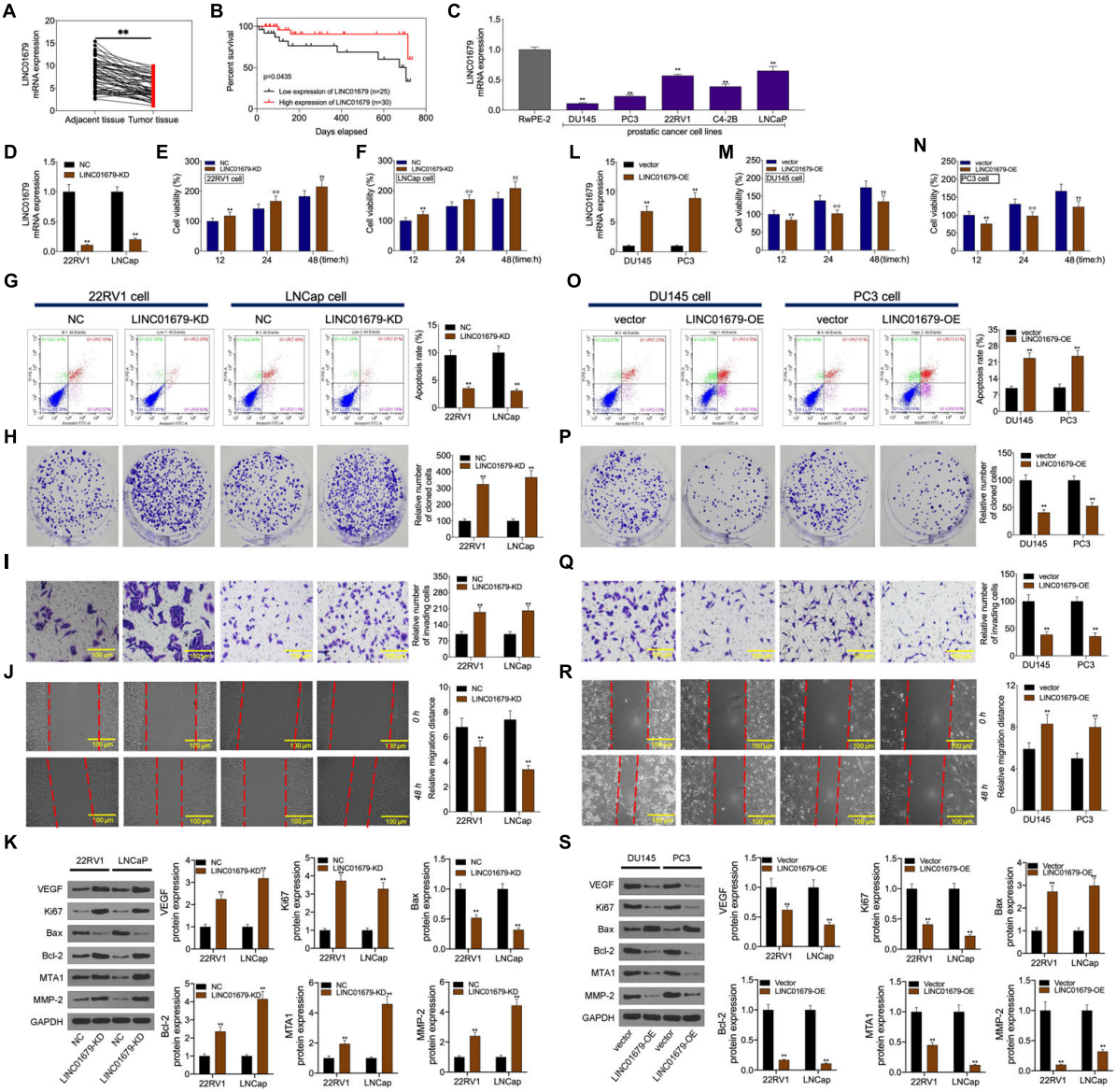

FIGURE 3 | LINC01679 regulated cell proliferation, apoptosis, migration, and invasion *in vitro.* **(A)** qRT-PCR assay was conducted to detect LINC01679 expression in PCa patients. **(B)** KM survival analysis on high and low LINC01679 expression. **(C)** LINC01679 levels within PCa cells measured by qRT-PCR assay. LINC01679 expression **(D,L)**, cell viability **(E,F,M,N)**, cell apoptosis **(G,O)**, proliferation **(H,P)**, invasion **(I,Q)**, migration **(J,R)**, and protein expression of VEGF, Ki67, Bax, Bcl-2, MTA1, and MMP-2 **(K,S)** of cells transfected with siRNA-LINC01679 or LINC01679-expressing vector determined by qRT-PCR, CCK-8, flow cytometry, colony formation, Transwell, scratch, and WB assays. The experiment was repeated thrice independently; ** vs. NC or vector group, $p < 0.01$; ✣ vs. vector at 24 h group; †† vs. vector at 48 h group.

LINC01679 was Correlated With Clinicopathologic Characteristics and Regulated Cell Proliferation, Invasion, Migration, Apoptosis, Tumorigenesis *in vitro and vivo*

Firstly, our results showed that low expression of LINC01679 was significantly correlated with high PSA level (≥23.6 ng/ml) and high Gleason score (≥7) ($P < 0.01$, **Table 1**). Then LINC01679 levels within cancer samples markedly reduced relative to matched non-carcinoma samples (**Figure 3A**). Patients in the low LINC01679 expression group displayed poor survival (**Figure 3B**). In addition, LINC01679 expression within PCa cells decreased significantly, relative to normal control cells (**Figure 3C**). After siRNA targeting LINC01679 was transfected into 22RV1 and LNCap cells, LINC01679 expression in the LINC01679-KD group decreased significantly (**Figure 3D**). Moreover, according to flow cytometric, CCK-8,

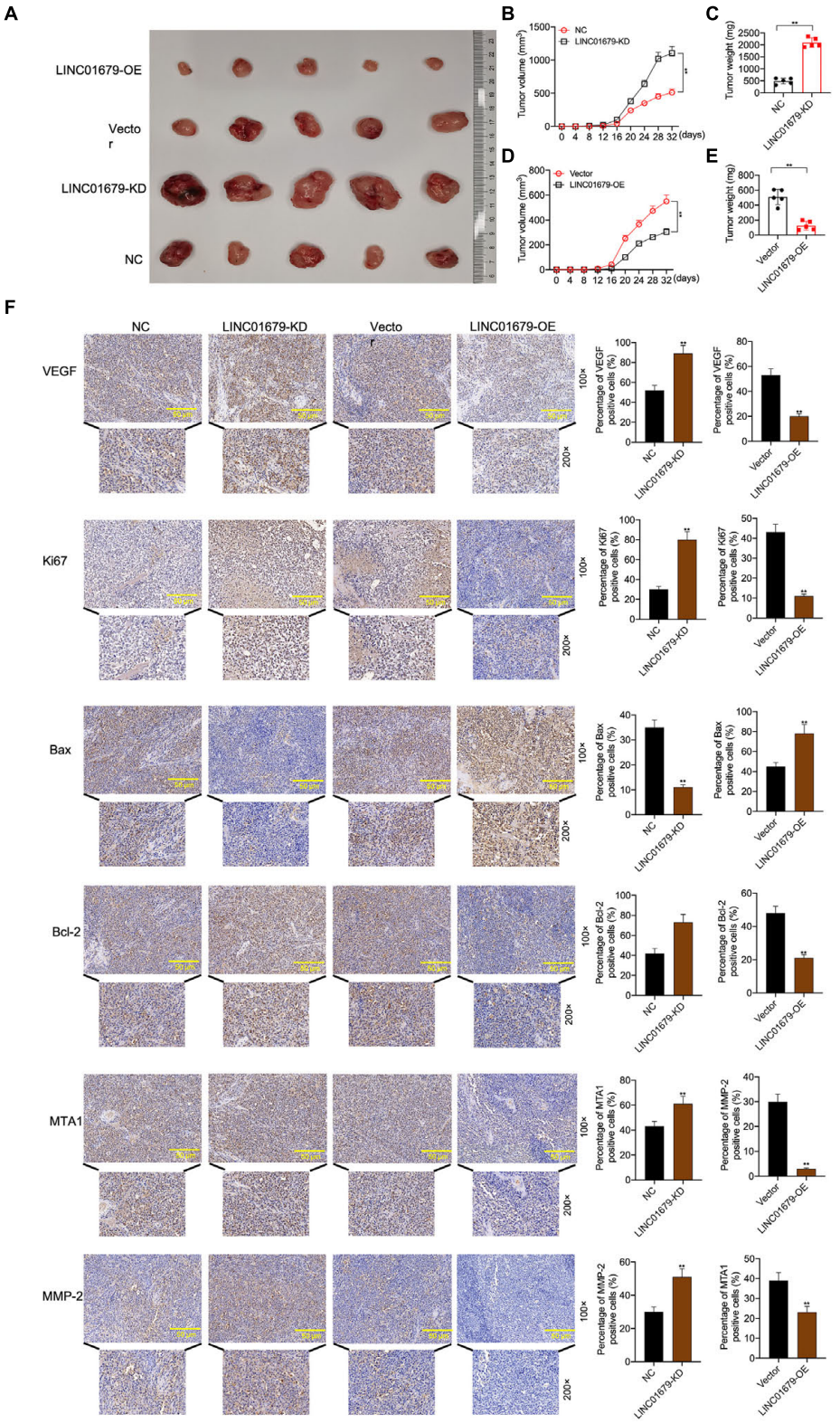

FIGURE 4 | LINC01679 regulated tumorigenesis *in vivo.* **(A)** The nude mouse tumor xenograft assay displaying the oncogenicity of LINC01679 inhibition or overexpression ($n = 5$). Quantitative analysis on tumor growth **(B)** and tumor weight **(C)** after siRNA-LINC01679 treatment. Quantitative analysis on tumor growth **(D)** and tumor weight **(E)** after LINC01679-expressing vector treatment. **(F)** Immunohistochemical staining of VEGF, Ki67, Bax, Bcl-2, MTA1, and MMP-2 in tumor tissues. The experiment was repeated thrice independently; ** vs. NC or vector group, $p < 0.01$.

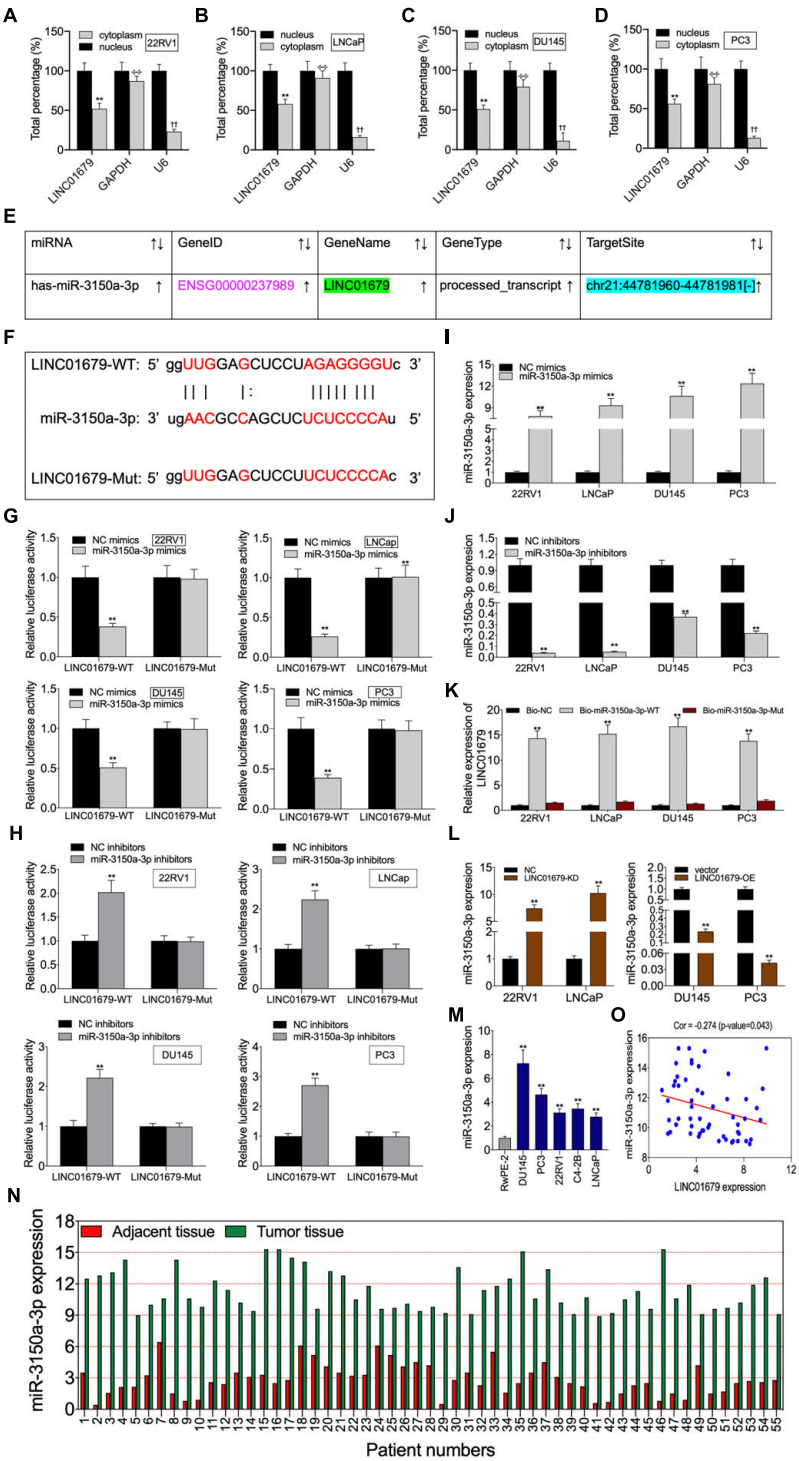

FIGURE 5 | LINC01679 acted as a sponge of miR-3150a-3p in PCa. **(A–D)** Nuclear–cytoplasmic fractionation was performed to investigate LINC01679 expression in the cytoplasm and nucleus of PCa cells. **(E)** miR-3150a-3p was predicted as a potential target of LINC01679 by the starBase website. **(F)** Specific binding regions between LINC01679 sequence and miR-3150a-3p sequence analyzed by the online analysis software. **(G,H)** Binding of LINC01679 to miR-3150a-3p verified by dual-luciferase reporter gene assay. **(I,J)** miR-3150a-3p expression in PCa cell lines after miR-3150a-3p mimics/or inhibitors treatment determined by qRT-PCR. **(K)** Dramatic enrichment of LINC01679 was detected in biotinylated miR-3150a-3p by RNA pull-down assay. **(L)** LINC01679 expression after siRNA-LINC01679 or LINC01679-expressing vector treatment determined by qRT-PCR. **(M,N)** LINC01679 expression in PCa cell lines and patients measured by qRT-PCR. **(O)** Spearman correlation analysis between LINC01679 expression and miR-3150a-3p expression. The experiment was repeated thrice independently; ** vs. NC or vector group, $p < 0.01$; ✣✣ vs. nucleus (GAPDH) group; †† vs. nucleus (U6) group.

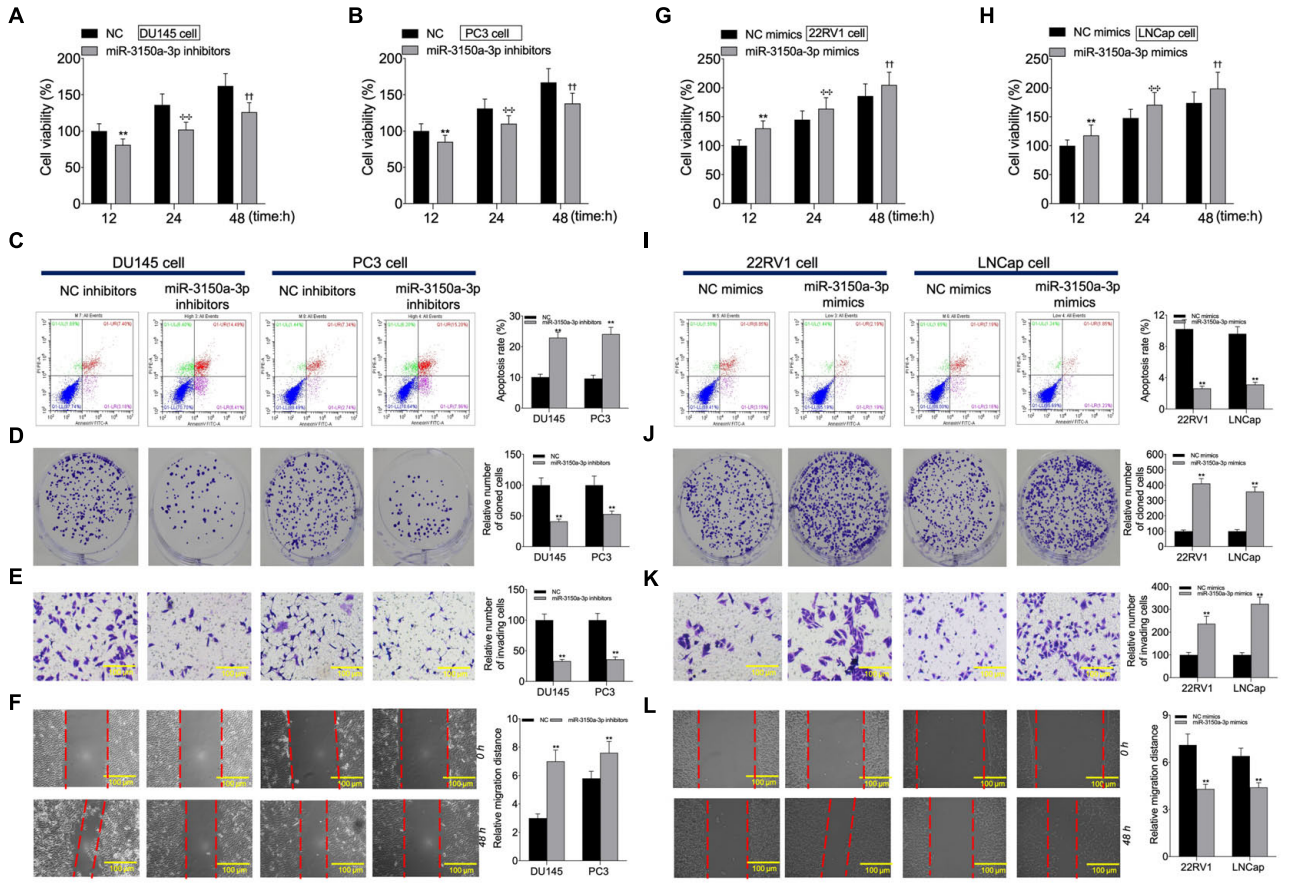

FIGURE 6 | miR-3150a-3p regulated cell proliferation, apoptosis, migration, and invasion *in vitro*. Cell viability **(A,B,G,H)**, cell apoptosis **(C,I)**, proliferation **(D,J)**, invasion **(E,K)**, and migration **(F,L)** of cells transfected with miR-3150a-3p inhibitors or miR-3150a-3p mimics determined by CCK-8, flow cytometry, colony formation, Transwell, and scratch assays. The experiment was repeated thrice independently; ** vs. NC inhibitors or NC mimics group, $p < 0.01$; ✣✣ vs. vector at 24 h group; †† vs. vector at 48 h group.

colony formation, scratch, and Transwell assays, LINC01679-KD enhanced cell growth, invasion, and migration, but suppressed their apoptosis *in vitro* (**Figures 3E–J**). Furthermore, LINC01679-KD upregulated the expression of VEGF, Ki67, Bcl-2, MTA1, and MMP2, while downregulating that of Bax at the protein level (**Figure 3K**). Meanwhile, LINC01679-expressing vector was transfected into DU145 and PC3 cells with low LINC01679 expression, so as to upregulate the LINC01679 levels (**Figure 3L**). As a result, cell viability was inhibited, cell apoptosis increased, and invasion and migration were attenuated (**Figures 3M–R**). Moreover, LINC01679-OE reduced VEGF, Ki67, Bcl-2, MTA1, and MMP2 levels, while increasing Bax expression at the protein level (**Figure 3S**).

The nude mouse tumor xenograft experiment showed that LINC01679-KD transfected 22RV1 cells had increased oncogenicity compared with untreated 22RV1 cells, whereas LINC01679-OE transfected PC3 cells had decreased oncogenicity relative to untreated PC3 cells (**Figures 4A–E**). VEGF, Ki67, Bax, Bcl-2, MTA1, and MMP2 expression in cancer tissues was consistent with those in cancer cells, as revealed by immunohistochemical staining (**Figure 4F**).

LINC01679 Played a Role of Sponging miR-3150a-3p in Prostate Cancer

To investigate the function of LINC01679 to sponge miRNA, we separated the nuclear fraction from the cytoplasmic counterpart. As a result, cytoplasmic localization of LINC01679 was mainly found (**Figures 5A–D**). Based on the starBase website, we predicted miR-3150a-3p as the candidate LINC01679 target (**Figure 5E**). Then, based on bioinformatics analysis, LINC01679 had a binding site for miR-3150a-3p (**Figure 5F**). To validate the direct interaction of LINC01679 with miR-3150a-3p, this study carried out a luciferase reporter assay. As observed, miR-3150a-3p mimics remarkably decreased the LINC01679-WT reporter luciferase activity, but the difference was not significant compared with the LINC01679-Mut reporter (**Figure 5G**); by contrast, miR-3150a-3p inhibitors dramatically elevated LINC01679-WT reporter luciferase activity, and the difference was not significant compared with the LINC01679-Mut reporter (**Figure 5H**). In addition, miR-3150a-3p mimics and miR-3150-3p inhibitors were transfected into PCa cell lines, respectively, to increase or decrease miR-3150a-3p levels

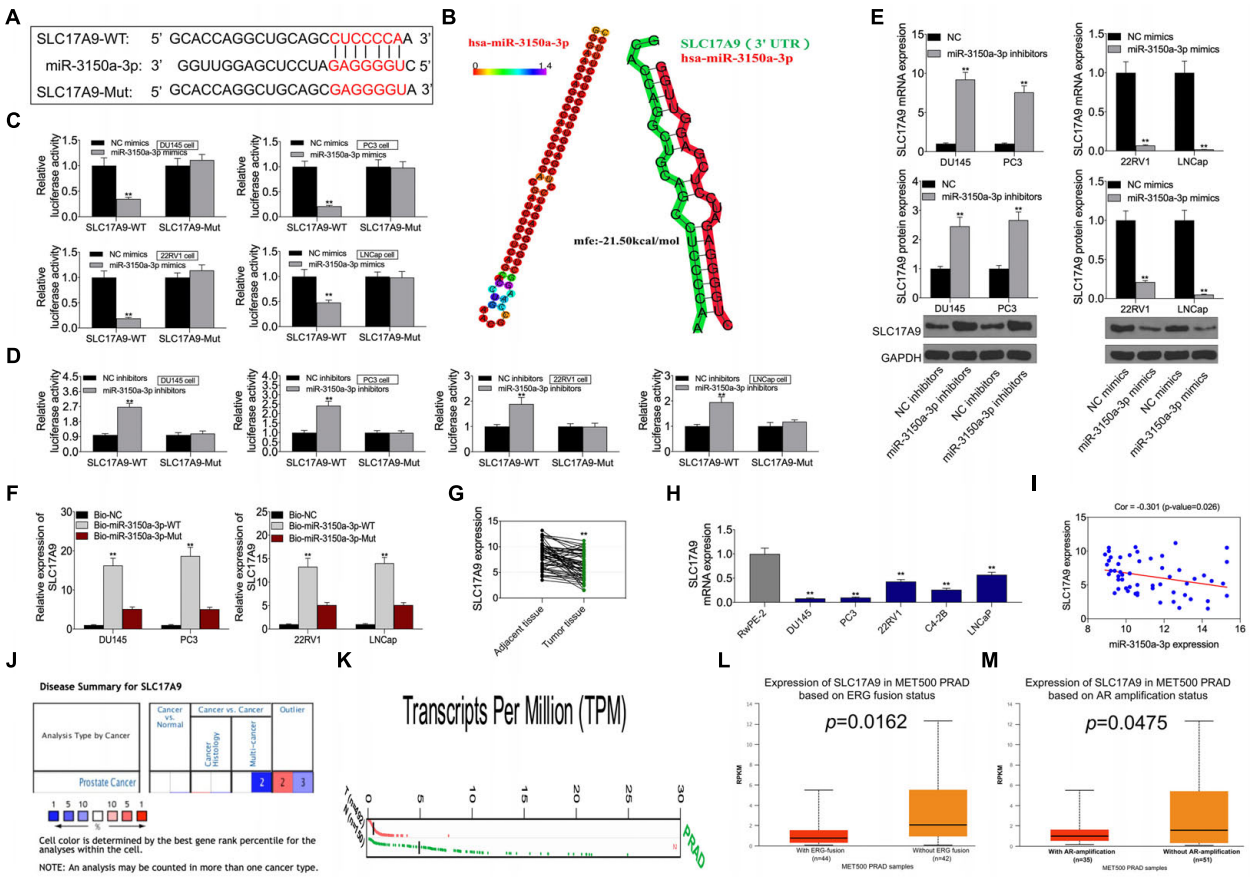

FIGURE 7 | (A) SLC17A9 acted as a target gene of miR-3150a-3p in PCa. SLC17A9 was predicted as a potential target of miR-3150a-3p by the starBase website. **(B)** The stem-loop structure of hsa-miR-3150a-3p was displayed using the RNAhybrid program, and the SLC17A9 target binding sites on the whole miR-3150a-3p sequences were predicted. **(C,D)** Binding of SLC17A9 to miR-3150a-3p verified by dual-luciferase reporter gene assay. **(E)** miR-3150a-3p expression in PCa cell lines transfected with miR-3150a-3p mimics or inhibitors determined by qRT-PCR and WB assays. **(F)** Dramatic enrichment of SLC17A9 was detected in biotinylated miR-3150a-3p by RNA pull-down assay. **(G,H)** SLC17A9 expression in PCa cell lines and patients measured by qRT-PCR. **(I)** The correlation analysis between SLC17A9 expression and miR-3150a-3p expression. SLC17A9 expression analysis in PCa samples based on Oncomine database **(J)**, GEPIA database **(K)**, and UALCAN database **(L,M)**. ** vs. NC mimics/inhibitors/Bio-NC/RwPE-2 group.

(**Figures 5I,J**). LINC01679 was dramatically enriched into the biotinylated miR-3150a-3p, as confirmed by RNA pull-down assay (**Figure 5K**). Moreover, LINC01679-KD increased miR-3150a-3p expression in 22RV1 and LNCap cells, whereas LINC01679-OE inhibited miR-3150a-3p expression in DU145 and PC3 cells (**Figure 5L**). Next, high miR-3150a-3p levels were measured within PCa cell lines and tissues (**Figures 5M,N**), which showed negative correlation with LINC01679 level among PCa cases (**Figure 5O**).

miR-3150a-3p Regulated Cell Proliferation, Invasion, Migration, and Apoptosis *in vitro*

According to CCK-8, flow cytometric, colony formation, scratch, and Transwell assays, miR-3150a-3p inhibitors inhibited PC3 and DU145 cell growth, migration, and invasion, and enhanced their apoptosis (**Figures 6A–F**). Besides, miR-3150a-3p mimics enhanced 22RV1 and LNCap cell growth, invasion, and migration, and suppressed their apoptosis (**Figures 6G–L**).

SLC17A9 Acted as an miR-3150a-3p Target Gene and Modulated Cell Growth, Invasion, Migration, and Apoptosis *in vitro*

This study predicted SLC17A9 as the candidate miR-3150a-3p target based on the starBase website, and it was confirmed that miR-3150a-3p contained the binding site for SLC17A9 (**Figure 7A**). Subsequently, hsa-miR-3150a-3p's stem-loop structure was revealed by the RNAhybrid program[9] and visualized using "RNAcofold" and "RNAfold" packages[10]. Then, the binding sites of SLC17A9 target on the whole miR-3150a-3p sequences were predicted (**Figure 7B**). Luciferase reporter assay

[9]https://bibiserv2.cebitec.uni-bielefeld.de/rnahybrid

[10]https://www.tbi.univie.ac.at/RNA

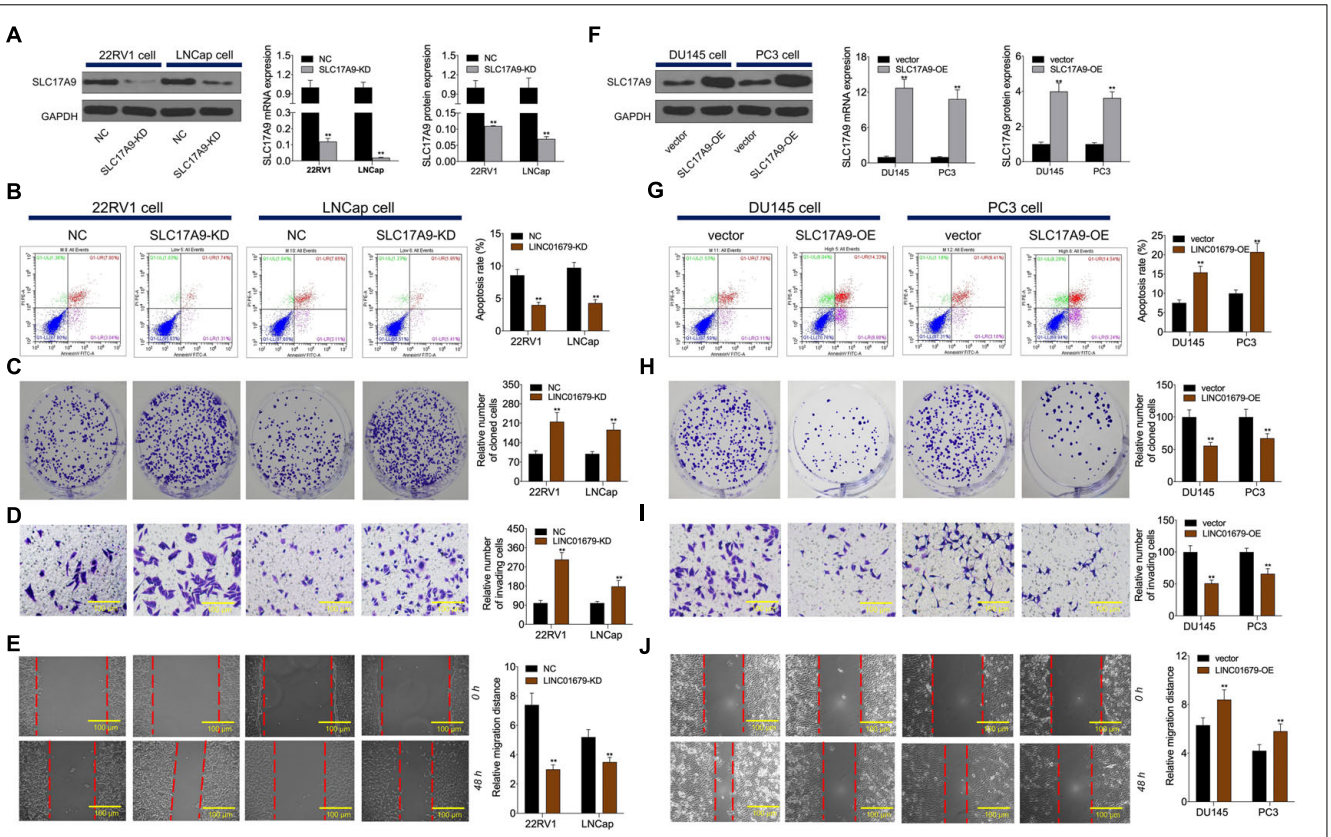

FIGURE 8 | SLC17A9 regulated cell proliferation, apoptosis, migration, and invasion *in vitro*. SLC17A9 expression **(A,F)**, cell apoptosis **(B,G)**, proliferation **(C,H)**, invasion **(D,I)**, and migration **(E,J)** of cells transfected with siRNA-SLC17A9 or SLC17A9-expressing vector determined by qRT-PCR, WB, flow cytometry, colony formation, Transwell, and scratch assays. The experiment was repeated thrice independently; ** vs. NC or vector group, $p < 0.01$.

confirmed that SLC17A9 directly interacted with miR-3150a-3p (**Figures 7C,D**). Moreover, miR-3150a-3p inhibitors increased SLC17A9 level within DU145 and PC3 cells, but miR-3150a-3p mimics inhibited that in 22RV1 and LNCap cells (**Figure 7E**). SLC17A9 was dramatically enriched into the biotinylated miR-3150a-3p, as revealed by the RNA pull-down assay (**Figure 7F**). In addition, SLC17A9 was significantly downregulated in PCa cells and tumor tissues (**Figures 7G,H**). SLC17A9 level showed significant negative correlation with the miR-3150a-3p level among PCa cases (**Figure 7I**). We wonder whether the expression level of SLC17A9 in castration-resistant prostate cancer (CRPC) tissues or metastatic tissues could be analyzed by using three public databases, including Oncomine, GEPIA, and UALCAN. However, the results of the Oncomine database do not have the data of SLC17A9 expression in PCa (**Figure 7J**). Then, the GEPIA database showed that SLC17A9 expression in tumor samples was significantly lower than that in normal samples (**Figure 7K**). SLC17A9 expression in metastatic PCa was decreased manifesting downregulated SLC17A9 expression in PCa patients with ERG fusion status and AR amplification status (**Figures 7L,M**).

To investigate whether SLC17A9 affected PCa cell growth, invasion, migration, and apoptosis, SLC17A9-KD and SLC17A9-OE were transfected into PCa cells to downregulate (**Figure 8A**) or upregulate (**Figure 8F**) their expression. The results showed that SLC17A9-KD inhibited cell apoptosis and promoted invasion and migration (**Figures 8B–E**), whereas SLC17A9-OE had opposite effects (**Figures 8G–J**).

miR-3150a-3p Regulated Cell Growth, Invasion, Migration, and Apoptosis by Targeting SLC17A9 *in vitro*

Functions of miR-3150a-3p inhibitors in promoting cell apoptosis and inhibiting proliferation, migration, and invasion were suggested using SLC17A9-KD (**Figures 9A,B**). In contrast, miR-3150a-3p mimics' role in inhibiting cell apoptosis and promoting proliferation, invasion, and migration was abolished by SLC17A9-OD (**Figures 9C,D**).

SLC17A9 Was Involved in LINC01679-mediated Inhibition of Prostate Cancer Progression

Then, SLC17A9 protein and mRNA expression was under the regulation by LINC01679 (**Figure 10A**). To further determine the interaction of LINC01679 with SLC17A9, we carried out luciferase reporter assay. The results showed that transfection with LINC01679-OE markedly upregulated

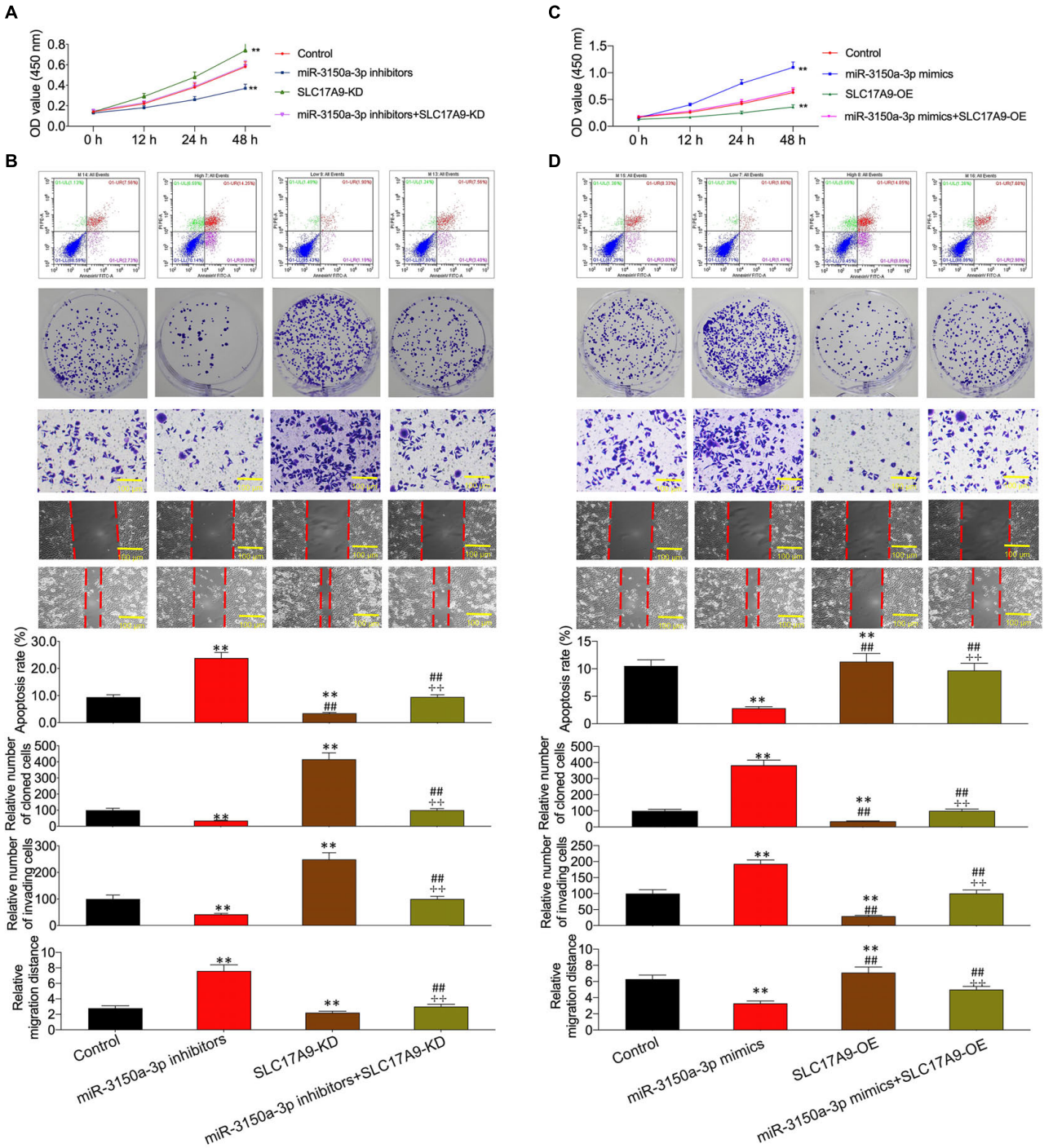

FIGURE 9 | miR-3150a-3p regulated cell proliferation, apoptosis, migration, and invasion *via* targeting SLC17A9 *in vitro*. Cell viability **(A,C)**, cell apoptosis, proliferation, invasion, and migration **(B,D)** of cells co-transfected with miR-3150a-3p inhibitors and siRNA-SLC17A9 or miR-3150a-3p mimics and SLC17A9-expressing vector determined by CCK-8, flow cytometry, colony formation, Transwell, and scratch assays. Each independent assay was conducted in triplicate; ** vs. control group, $p < 0.01$.

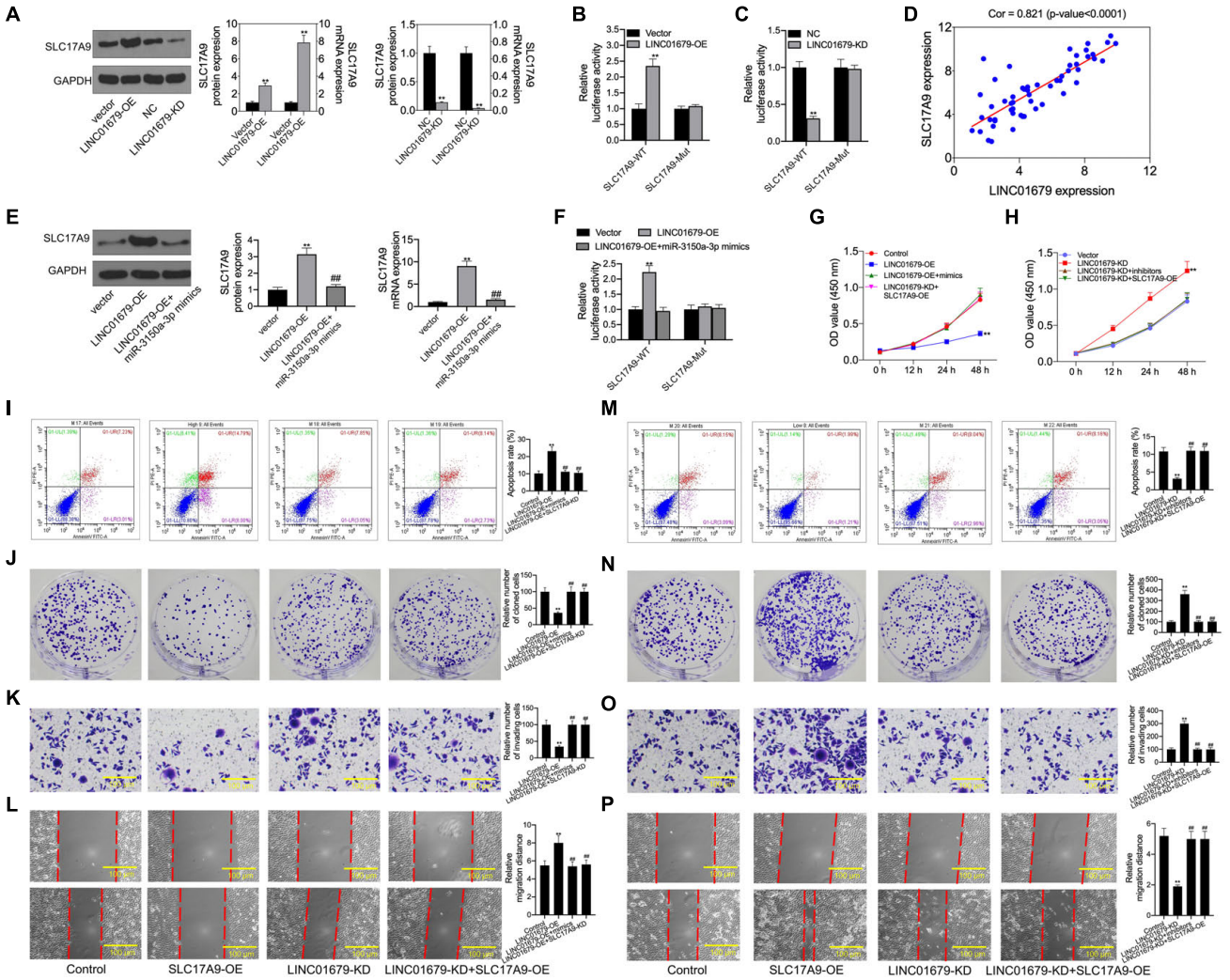

FIGURE 10 | SLC17A9 involved in the LINC01679-mediated inhibition of PCa progression. **(A)** SLC17A9 expression in PCa cell lines transfected with LINC01679-siRNA or LINC01679-expressing vector measured through qRT-PCR and Western blotting. **(B,C)** Binding of SLC17A9 to LINC01679 verified by dual-luciferase reporter gene assay. **(D)** The correlation analysis between LINC01679 expression and SLC17A9 expression. **(E)** SLC17A9 expression in PCa cell lines co-transfected with LINC01679-expressing vector and miR-3150a-3p mimics by measured through qRT-PCR and Western blotting. **(F)** The interaction among SLC17A9, miR-3150a-3p, and LINC01679 verified by dual-luciferase reporter gene assay. Cell viability **(G,H)**, cell apoptosis **(I,M)**, proliferation **(J,N)**, invasion **(K,O)**, and migration **(L,P)** of cells after transfection with LINC01679-expressing vector and siRNA-SLC17A9 or LINC01679-expressing vector and SLC17A9-expressing vector determined by CCK-8, flow cytometry, colony formation, Transwell, and scratch assays. Each independent assay was conducted in triplicate; ** vs. control group, $p < 0.01$; ## vs. LINC01679-OE group.

the SLC17A9-WT reporter luciferase activity, but still the difference was not significant compared with the SLC17A9-Mut reporter (**Figure 10B**), whereas transfection with LINC01679-KD markedly downregulated the SLC17A9-WT reporter luciferase activity (**Figure 10C**). SLC17A9 level showed a positive relationship with LINC01679 level within PCa cases (**Figure 10D**). Whether LINC01679 regulates SLC17A9 expression through targeting miR-3150a-3p needs to be further studied. The results of this study showed that SLC17A9 protein and mRNA expression saw a synchronous rise by transfection with LINC01679-OE, but this effect disappeared in cells co-transfected with LINC01679-OE and miR-3150a-3p mimics (**Figure 10E**). The effect of transfection with LINC01679-OE induced the SLC17A9-WT reporter luciferase activity, and the increase was reversed by miR-3150a-3p mimics (**Figure 10F**). According to the experimental results, upregulating miR-3150a-3p or downregulating SLC17A9 abolished the effect of LINC01679 overexpression on suppressing cell growth, invasion, and migration, and enhancing cell apoptosis (**Figures 10G–P**). However, the positive functions of LINC01679 knockdown in cell growth, migration, and invasion were attenuated in miR-3150a-3p inhibitor or SLC17A9-expressing vector transfected cells. Collectively, this study confirmed that LINC01679 was a ceRNA

that inhibited PCa development through modulating the miR-3150a-3p/SLC17A9 axis.

DISCUSSION

Some lncRNA-based prognosis prediction nomograms are established for PCa (Alahari et al., 2016). As far as we know, few lncRNA signatures are established for PCa cases. The present work was conducted among PCa cases for predicting their survival based on the mRNA and lncRNA signatures. In the present work, OS-related DEGs or DElncRNAs were completely selected through univariate and bioinformatics analyses. Then, the significant mRNAs and lncRNAs were incorporated for the construction of the prognosis prediction model. Later, Cox regression, KM, and ROC curve analyses were performed to confirm the value of the constructed mRNA and lncRNA signatures in prognosis prediction. A ceRNA network of PCa was established by lncRNA signature, mRNA signature, and their common miRNAs. Interestingly, the LINC01679/miR-3150a-3p/SLC17A9 axis was the only axis in the protection group in the network involving 4 DElncRNAs, 45 DEmiRNAs, and 4 DEmRNAs. lncRNAs have been well recognized to sponge candidate miRNAs as the ceRNAs, so as to regulate cancer development. For instance, lncRNA FOXD2-AS1 is the ceRNA that modulates thyroid cancer by combining with miR-7-5p (Liu et al., 2019). In addition, LINC-PINT suppresses the genesis of non-small cell lung cancer (NSCLC) as the miR-218-5p sponge through MAFG-AS1, and modulates miR-339-5p expression to promote breast cancer (BC) aggressiveness (Zhang L. et al., 2019). LINC01679's function in cancer together with the related mechanism has not been reported. Therefore, it was speculated that LINC01679 might function as the ceRNA in PCa. LINC01679 expression in PCa cells and tissues decreased significantly, compared with surrounding tissues or normal control cells, and the low LINC01679 expression group displayed a poor survival. Our results showed that LINC01679 overexpression inhibited cell proliferation, migration, invasion, and tumor growth, and induced cell apoptosis *in vitro* and *in vivo*. Therefore, LINC01679 might be an anti-oncogene in PCa. Therefore, the LINC01679/miR-3150a-3p/SLC17A9axis was used for follow-up research.

Many studies have suggested that miRNAs function as tumor suppressors or oncogenes to modulate cancer genesis and progression. For example, miR-193a-5p silencing enhances the chemosensitivity to docetaxel in PCa (Yang et al., 2017). miR-584-5p overexpression decreases gastric cancer (GC) cell growth and increases their apoptosis (Li et al., 2017). Nonetheless, as an important target of LINC01679, the role of miR-3150a-3p in tumor is still unclear.

Our results showed that miR-3150a-3p expression in PCa cells and tissues increased significantly, compared with matched surrounding tissues or normal control cells; besides, patients with high miR-3150a-3p expression displayed poor survival. According to our results, miR-3150a-3p mimics enhanced PCa cell growth, invasion, and migration, but inhibited their apoptosis. From the above, miR-3150a-3p was identified as an oncogene in PCa. Furthermore, miR-3150a-3p showed direct interaction with LINC01679. Rescue experiments proved that miR-3150a-3p upregulation abolished the suppression of LINC01679 overexpression on cell proliferation, invasion, and migration, and the promotion on cell apoptosis. Collectively, LINC01679 regulates PCa development by the sponge of miR-3150a-3p.

Solute carrier family 17 member 9 (SLC17A9) has been discovered as a vesicular nucleotide transporter (VNUT) in recent years, and it also belongs to the transmembrane protein family related to small-molecule transport (Wu et al., 2020). It has been reported that SLC17A9 upregulation is related to the dismal prognostic outcome of GC and colorectal cancer (CRC) (Li et al., 2019; Yang et al., 2019). However, this study indicated that SLC17A9 level was in direct proportion to LINC01679, and low expression of SLC17A9 predicted the poor prognosis of PCa. This showed that the same gene played different roles in different tumors. Interestingly, when survival time exceeds 115 months, the survival rate of PCa patients with high SLC17A9 expression and the rate of PCa patients with high LINC01679 expression are both significantly higher than that of PCa patients with low SLC17A9 expression and PCa patients with low LINC01679 expression. These also proved that the role of LINC01679 in OS of PCa patients was consistent with that of SLC17A9 in OS of PCa patients. The ERG gene in PCa is mainly regulated by the TMPRSS2-ERG fusion gene. It reported that nearly half of PCa cases express the TMPRSS2-ERC fusion gene (Wang et al., 2017). Therefore, the ERG gene should be an important marker of PCa, and its detection is helpful for the diagnosis and treatment of PCa. In addition, the early onset of PCa is dependent on the androgen receptor AR, and its pre-treatment is mainly AR deprivation therapy (ADT) (Tiwari et al., 2020). However, ADT does not cure PCa. Generally, after a median treatment time of 14–30 months, many patients will eventually develop CRPC (Fujita and Nonomura, 2019). Therefore, we also speculate on the expression level of SLC17A9 in CRPC tissues or metastatic tissues. We found that SLC17A9 expression in PCa patients with ERG fusion status and AR amplification status was decreased, manifesting downregulated SLC17A9 expression in PCa patients with ERG fusion status and AR amplification status. These studies showed that SLC17A9 plays a protective role in PCa patients. This result echoes the result of **Figure 2B**. Next, our experimental results proved that knockdown of SLC17A9 reversed the inhibition of LINC01679 overexpression or miR-3150a-3p inhibitors on cell proliferation, invasion, and migration, and enhancement of cell apoptosis. The above findings confirmed that LINC01679 was the ceRNA that competitively bound to miR-3150a-3p to positively regulate SLC17A9 expression, thereby inhibiting PCa progression.

In conclusion, the present work indicated that LINC01679 was a potential antitumor factor for PCa, which inhibited PCa development by competitively binding to miR-3150a-3p and the mediation of SLC17A9 level. As a result, the present work suggested that the LINC01679/miR-3150a-3p/SLC17A9 axis was possibly related to PCa treatment.

DATA AVAILABILITY STATEMENT

The datasets presented in this study can be found in online repositories. The names of the repository/repositories and accession number(s) can be found in the article/supplementary material.

ETHICS STATEMENT

The studies involving human participants were reviewed and approved by the Research Ethics Committee of the Affiliated Hospital of Jiangnan University. The patients/participants provided their written informed consent to participate in this study.

AUTHOR CONTRIBUTIONS

L-JZ and G-WX participated in the design of this study. Y-YM and L-FZ collected the clinical data. JW and C-YS worked on the analysis and interpretation of data. Y-YM and H-BS performed statistical analysis. Y-YM, L-FZ, and JW conducted experiments in this study. H-BS and FQ collected the background information. Y-YM drafted the manuscript. Y-YM, L-FZ, C-YS, and G-WX provided the funding support. All authors read and approved the final manuscript.

FUNDING

This work was supported by the National Natural Science Foundation of China (Nos. 81802576 and 81372316), the Jiangsu Provincial Central Administration Bureau (No. YB201827), the Wuxi City Medical Young Talent (No. QNRC043), the Wuxi Commission of Health and Family Planning (Nos. T202024, J202012, Z202011, and ZM001), the Science and Technology Development Fund of Wuxi (Nos. WX18IIAN024 and N20202021), the Jiangnan University Wuxi School of Medicine (No. 1286010242190070), and Wuxi "Taihu Talent Program"-High-end Talent in Medical and Health, Talent plan of Taihu Lake in Wuxi (Double hundred Medical Youth Professionals Program) from the Health Committee of Wuxi (No. BJ2020061).

REFERENCES

Alahari, S. V., Eastlack, S. C., and Alahari, S. K. (2016). Role of long noncoding RNAs in Neoplasia: special emphasis on prostate cancer. *Int. Rev. Cell Mol. Biol.* 324, 229–254. doi: 10.1016/bs.ircmb.2016.01.004

Athanasios, A., Charalampos, V., Vasileios, T., and Ashraf, G. M. (2017). Protein-Protein interaction (PPI) network: recent advances in drug discovery. *Curr. Drug Metab.* 18, 5–10. doi: 10.2174/1389200218011701920 4832

Chang, A. J., Autio, K. A., Roach, M. III, and Scher, H. I. (2014). High-risk prostate cancer-classification and therapy. *Nat. Rev. Clin. Oncol.* 11, 308–323. doi: 10.1038/nrclinonc.2014.68

Fujita, K., and Nonomura, N. (2019). Role of androgen receptor in prostate cancer: a review. *World J. Mens Health* 37, 288–295. doi: 10.5534/wjmh.180040

Grozescu, T., and Popa, F. (2017). Prostate cancer between prognosis and adequate/proper therapy. *J. Med. Life* 10, 5–12.

Hu, R., and Lu, Z. (2020). Long non-coding RNA HCP5 promotes prostate cancer cell proliferation by acting as the sponge of miR-4656 to modulate CEMIP expression. *Oncol. Rep.* 43, 328–336. doi: 10.3892/or.2019.7404

Jiang, J., Bi, Y., Liu, X. P., Yu, D., Yan, X., Yao, J., et al. (2020). To construct a ceRNA regulatory network as prognostic biomarkers for bladder cancer. *J. Cell. Mol. Med.* 24, 5375–5386. doi: 10.1111/jcmm.15193

Li, J., Su, T., Yang, L., Deng, L., Zhang, C., and He, Y. (2019). High SLC17A9 expression correlates with poor survival in gastric carcinoma. *Future Oncol.* 15, 4155–4166. doi: 10.2217/fon-2019-0283

Li, Q., Li, Z., Wei, S., Wang, W., Chen, Z., Zhang, L., et al. (2017). Overexpression of miR-584-5p inhibits proliferation and induces apoptosis by targeting WW domain-containing E3 ubiquitin protein ligase 1 in gastric cancer. *J. Exp. Clin. Cancer Res.* 36:59. doi: 10.1186/s13046-017-0532-2

Lingadahalli, S., Jadhao, S., Sung, Y. Y., Chen, M., Hu, L., Chen, X., et al. (2018). Novel lncRNA LINC00844 regulates prostate cancer cell migration and invasion through AR signaling. *Mol. Cancer Res.* 16, 1865–1878. doi: 10.1158/1541-7786.Mcr-18-0087

Liu, X., Fu, Q., Li, S., Liang, N., Li, F., Li, C., et al. (2019). LncRNA FOXD2-AS1 functions as a competing endogenous RNA to regulate TERT expression by sponging miR-7-5p in thyroid cancer. *Front. Endocrinol. (Lausanne)* 10:207. doi: 10.3389/fendo.2019.00207

Lou, W., Liu, J., Ding, B., Chen, D., Xu, L., Ding, J., et al. (2019). Identification of potential miRNA-mRNA regulatory network contributing to pathogenesis of HBV-related HCC. *J. Transl. Med.* 17:7. doi: 10.1186/s12967-018-1761-7

Prensner, J. R., Chen, W., Iyer, M. K., Cao, Q., Ma, T., Han, S., et al. (2014). PCAT-1, a long noncoding RNA, regulates BRCA2 and controls homologous recombination in cancer. *Cancer Res.* 74, 1651–1660. doi: 10.1158/0008-5472.Can-13-3159

Qi, X., Zhang, D. H., Wu, N., Xiao, J. H., Wang, X., and Ma, W. (2015). ceRNA in cancer: possible functions and clinical implications. *J. Med. Genet.* 52, 710–718. doi: 10.1136/jmedgenet-2015-103334

Shang, Z., Yu, J., Sun, L., Tian, J., Zhu, S., Zhang, B., et al. (2019). LncRNA PCAT1 activates AKT and NF-κB signaling in castration-resistant prostate cancer by regulating the PHLPP/FKBP51/IKKα complex. *Nucleic Acids Res.* 47, 4211–4225. doi: 10.1093/nar/gkz108

Soares, J. C., Soares, A. C., Rodrigues, V. C., Melendez, M. E., Santos, A. C., Faria, E. F., et al. (2019). Detection of the prostate cancer biomarker PCA3 with electrochemical and impedance-based biosensors. *ACS Appl. Mater. Interfaces* 11, 46645–46650. doi: 10.1021/acsami.9b19180

Tiwari, R., Manzar, N., Bhatia, V., Yadav, A., Nengroo, M. A., Datta, D., et al. (2020). Androgen deprivation upregulates SPINK1 expression and potentiates cellular plasticity in prostate cancer. *Nat. Commun.* 11:384. doi: 10.1038/s41467-019-14184-0

van Dam, S., Võsa, U., van der Graaf, A., Franke, L., and de Magalhães, J. P. (2018). Gene co-expression analysis for functional classification and gene-disease predictions. *Brief. Bioinform.* 19, 575–592. doi: 10.1093/bib/bbw139

Wang, G., Zhao, D., Spring, D. J., and DePinho, R. A. (2018). Genetics and biology of prostate cancer. *Genes Dev.* 32, 1105–1140. doi: 10.1101/gad.315739.118

Wang, J., Su, Z., Lu, S., Fu, W., Liu, Z., Jiang, X., et al. (2018). LncRNA HOXA-AS2 and its molecular mechanisms in human cancer. *Clin. Chim. Acta* 485, 229–233. doi: 10.1016/j.cca.2018.07.004

Wang, L., Cho, K. B., Li, Y., Tao, G., Xie, Z., and Guo, B. (2019). Long noncoding RNA (lncRNA)-mediated competing endogenous RNA networks provide novel potential biomarkers and therapeutic targets for colorectal cancer. *Int. J. Mol. Sci.* 20:5758. doi: 10.3390/ijms20225758

Wang, Z., Wang, Y., Zhang, J., Hu, Q., Zhi, F., Zhang, S., et al. (2017). Significance of the TMPRSS2:ERG gene fusion in prostate cancer. *Mol. Med. Rep.* 16, 5450–5458. doi: 10.3892/mmr.2017.7281

Wu, J., Yang, Y., and Song, J. (2020). Expression of SLC17A9 in hepatocellular carcinoma and its clinical significance. *Oncol. Lett.* 20:182. doi: 10.3892/ol.2020.12043

Wu, M., Huang, Y., Chen, T., Wang, W., Yang, S., Ye, Z., et al. (2019). LncRNA MEG3 inhibits the progression of prostate cancer by modulating miR-9-5p/QKI-5 axis. *J. Cell. Mol. Med.* 23, 29–38. doi: 10.1111/jcmm.13658

Wu, X., Xiao, Y., Zhou, Y., Zhou, Z., and Yan, W. (2019). LncRNA FOXP4-AS1 is activated by PAX5 and promotes the growth of prostate cancer by sequestering miR-3184-5p to upregulate FOXP4. *Cell Death Dis.* 10:472. doi: 10.1038/s41419-019-1699-6

Yang, L., Chen, Z., Xiong, W., Ren, H., Zhai, E., Xu, K., et al. (2019). High expression of SLC17A9 correlates with poor prognosis in colorectal cancer. *Hum. Pathol.* 84, 62–70. doi: 10.1016/j.humpath.2018.09.002

Yang, Z., Chen, J. S., Wen, J. K., Gao, H. T., Zheng, B., Qu, C. B., et al. (2017). Silencing of miR-193a-5p increases the chemosensitivity of prostate cancer cells to docetaxel. *J. Exp. Clin. Cancer Res.* 36:178. doi: 10.1186/s13046-017-0649-3

Yu, Y., Gao, F., He, Q., Li, G., and Ding, G. (2020). lncRNA UCA1 functions as a ceRNA to promote prostate cancer progression via sponging miR143. *Mol. Ther. Nucleic Acids* 19, 751–758. doi: 10.1016/j.omtn.2019.11.021

Zhang, L., Hu, J., Li, J., Yang, Q., Hao, M., and Bu, L. (2019). Long noncoding RNA LINC-PINT inhibits non-small cell lung cancer progression through sponging miR-218-5p/PDCD4. *Artif. Cells Nanomed. Biotechnol.* 47, 1595–1602. doi: 10.1080/21691401.2019.1605371

Zhang, Y., Zhang, D., Lv, J., Wang, S., and Zhang, Q. (2019). LncRNA SNHG15 acts as an oncogene in prostate cancer by regulating miR-338-3p/FKBP1A axis. *Gene* 705, 44–50. doi: 10.1016/j.gene.2019.04.033

Zhuang, C., Ma, Q., Zhuang, C., Ye, J., Zhang, F., and Gui, Y. (2019). LncRNA GClnc1 promotes proliferation and invasion of bladder cancer through activation of MYC. *FASEB J.* 33, 11045–11059. doi: 10.1096/fj.201900078RR

Conflict of Interest: The authors declare that the research was conducted in the absence of any commercial or financial relationships that could be construed as a potential conflict of interest.

Publisher's Note: All claims expressed in this article are solely those of the authors and do not necessarily represent those of their affiliated organizations, or those of the publisher, the editors and the reviewers. Any product that may be evaluated in this article, or claim that may be made by its manufacturer, is not guaranteed or endorsed by the publisher.

frontiers in Oncology

ORIGINAL RESEARCH
published: 14 January 2022
doi: 10.3389/fonc.2021.795302

Value of Contrast-Enhanced Ultrasound in the Preoperative Evaluation of Papillary Thyroid Carcinoma Invasiveness

Lei Chen, Luzeng Chen, Zhenwei Liang, Yuhong Shao, Xiuming Sun and Jinghua Liu*

Department of Ultrasound, Peking University First Hospital, Beijing, China

Objective: To evaluate the diagnostic performance of preoperative contrast-enhanced ultrasound (CEUS) in the detection of extracapsular extension (ECE) and cervical lymph node metastasis (LNM) of papillary thyroid carcinoma (PTC) and the added value of CEUS in the evaluation of PTC invasiveness to conventional ultrasound (US).

Materials and Methods: A total of 62 patients were enrolled retrospectively, including 30 patients with invasive PTCs (Group A, ECE or LNM present) and 32 patients with non-invasive PTCs (Group B). All patients underwent US and CEUS examinations before surgery. US and CEUS features of PTCs and lymph nodes were compared between groups. Sensitivity, specificity, positive predictive value (PPV), negative predictive value (NPV), and accuracy of US, CEUS, and the combination of the two in the detection of ECE and LNM of PTCs were calculated. Logistic regression was used to analyze relationships between variables.

Results: The PTC size was larger in group A on both US and CEUS (P = 0.001, P = 0.003). More PTCs showed hyper-enhancement in group A (P = 0.013) than in group B. More PTCs had >25% contact between PTC and the thyroid capsule and discontinued capsule on US and CEUS (all $P < 0.05$) in group A than in group B. More absent hilum and calcification of lymph nodes were observed in group A (both $P < 0.05$) than in group B on US. More centripetal perfusion and enlarged lymph nodes were observed in group A (both $P < 0.05$) than in group B on CEUS. CEUS alone and US combined with CEUS manifested higher diagnostic accuracy (79.0%) than US alone (72.6%) in the detection of ECE. The combination of US and CEUS manifested the highest diagnostic accuracy (95.2%) than CEUS alone (90.3%) and US alone (82.2%) in the detection of LNM. Diagnoses of ECE and LNM by the combination of US and CEUS were independent risk factors for PTC invasiveness [odds ratio (OR) = 29.49 and 97.20, respectively; both P = 0.001].

Conclusion: CEUS or US combined with CEUS is recommended for the detection of PTC ECE, while the combination of US and CEUS is most recommended for LNM detection. CEUS plays an essential role in the preoperative evaluation of PTC invasiveness.

Keywords: papillary thyroid carcinoma, extracapsular extension, lymph node metastasis, contrast-enhanced ultrasound, invasiveness

OPEN ACCESS

Edited by:
Hailong Pei,
Soochow University, China

Reviewed by:
Simona Censi,
University of Padua, Italy
Elisa Giannetta,
Sapienza University of Rome, Italy

****Correspondence:***
Luzeng Chen
chenluzeng@126.com

Specialty section:
This article was submitted to Molecular and Cellular Oncology, a section of the journal Frontiers in Oncology

Received: *14 October 2021*
Accepted: *17 December 2021*
Published: *14 January 2022*

Citation:
Chen L, Chen L, Liang Z, Shao Y, Sun X and Liu J (2022) Value of Contrast-Enhanced Ultrasound in the Preoperative Evaluation of Papillary Thyroid Carcinoma Invasiveness. Front. Oncol. 11:795302. doi: 10.3389/fonc.2021.795302

INTRODUCTION

Papillary thyroid carcinoma (PTC) accounts for approximately 80%–90% of thyroid cancers (1, 2). As the incidence of PTC is gradually increasing, overtreatment of low-risk disease has become a worldwide concern (1). Although PTC is considered a moderate subtype of thyroid cancer with a preferable prognosis (3), the presence of extracapsular extension (ECE) and lymph node metastasis (LNM) are adverse prognostic factors, associated with higher recurrence and mortality rate (4). The staging and therapy plan of PTC also vary according to the above two factors. Therefore, accurate preoperative diagnosis of ECE and LNM is essential for the stratified management and precise treatment of PTC.

Among all medical imaging tools, ultrasound (US) is the first-line choice for thyroid disease assessment. Several guidelines (5–7) have been developed to improve the diagnostic performance of US for thyroid cancer, as well as new modalities such as elastography (8, 9). However, US was found to be a useful tool in the evaluation of PTC invasiveness with certain limitations. The reported accuracy for ECE detection by US was around 64.7%–92.6% (10, 11), while the reported accuracy for LNM detection was around 51.9%–84.3% (12, 13). To generalize the use of US in PTC invasiveness assessment in clinical settings, improvement of diagnostic performance is required.

Contrast-enhanced ultrasound (CEUS) techniques have rapidly advanced in the diagnosis of endocrinological tumors, including thyroid cancer, testicular neoplasm, and paraganglioma (14–16). Superior in the detection of microvascularity of tissue, CEUS was proven to be a promising tool in the evaluation of ECE and LNM of PTC (17–23). However, most of the studies focused on either ECE or LNM of PTC. Comprehensive analysis of PTC invasiveness lacked. In addition, inconsistency was found among different studies.

In this study, we investigated the US and CEUS features of invasive PTC, analyzed the diagnostic performance of US and CEUS in the detection of ECE and LNM, and explored the relationship between imaging features and PTC invasiveness, aiming to verify the added value of CEUS in the evaluation of PTC invasiveness.

MATERIALS AND METHODS

Patients and Study Design

This study was approved by the ethics committee of our hospital. All patients signed an informed consent before examination. From February 2017 to December 2017, a total of 190 patients who underwent US and CEUS examinations of thyroid and cervical lymph nodes in our hospital were reviewed.

Inclusion criteria were as follows: 1) Surgical pathology-approved PTC; 2) US and CEUS examination within 1 month before surgery; 3) PTC size ≥0.5 cm; 4) Lymph node long-axis diameter + short-axis diameter ≥1.0 cm.

Exclusion criteria were as follows: 1) Patients with incomplete data; 2) Unsatisfied demonstration of PTC boundary; 3) Pathology-approved PTC could not be identified on US.

The presence of ECE and LNM was confirmed by surgical pathology. ECE was defined as positive if there was minimal microscopic extrathyroidal extension to surrounding soft tissues, strap muscles, or gross extrathyroidal extension to nerves, blood vessels, and other neighboring organs on pathology. Meanwhile, lymph nodes were considered benign if 1) Diagnosed as benign by surgical pathology or core needle biopsy (CNB); 2) There was a <20% increase in size and absence of US features suspicious for malignancy after a 2-year follow-up (18).

Finally, 62 patients were enrolled, including 51 females and 11 males, with an average age of 45.8 ± 13.4 years.

Ultrasound Examination

All conventional US and CEUS examinations were performed by three physicians with more than 9 years of experience in ultrasound diagnosis using a GE Logiq E9 (General Electric Healthcare, Waukesha, WI, USA) ultrasonic system equipped with a 6–15 MHz linear transducer according to a standard protocol in our department, which was consistent during the study period.

All conventional US images were reviewed and confirmed by two physicians with more than 5 years of experience, without knowing the histological information. Thyroid nodule features including size, the range of contact between PTC and thyroid capsule, and the presence of discontinued capsule were recorded. Nodule size was recorded as the maximum dimension in all planes. The range of contact between PTC and the thyroid capsule was divided into no contact (normal thyroid parenchyma existed between PTC and the thyroid capsule), <25% contact, 25%–50% contact, and >50% contact based on the ratio of contact part to the whole nodule perimeter. Discontinued capsule was recorded if there was the loss of normal thyroid capsule linear echo. The nodule nearest the thyroid capsule was enrolled in multifocal lesions.

For cervical lymph nodes, features including size, shape [long-axis diameter/short-axis diameter ratio (L/S ratio)], margin (well-defined/ill-defined), echogenicity (hypoechoic, isoechoic, or hyperechoic with respect to adjacent muscles), calcification (present/absent), and blood flow distribution (avascular/hilar/peripheral/mixed type) of cervical lymph nodes were recorded (21). In case the patient was present with several suspicious lymph nodes, the largest lymph node was enrolled. If no suspicious lymph node was present, the largest one of all non-suspicious lymph nodes was enrolled.

Contrast-Enhanced Ultrasound Examination

The mechanical index (MI = 0.08–0.10) was selected automatically by the ultrasonic system in relation to beam-focus depth. SonoVue (Bracco, Milan, Italy) was used as the ultrasound contrast agent. Here, 5.0 ml solution of 0.9% saline and SonoVue were mixed by oscillation. Then, 1.2 ml SonoVue was injected as a bolus followed immediately by 5.0 ml 0.9% saline flush *via* the cephalic vein. In this study, 90 s of CEUS was recorded in real time. TomTec workstation (TOMTEC Imaging

Systems GmbH, Unterschleissheim, Germany) was used for CEUS off-line analysis.

All CEUS images were reviewed and confirmed by two physicians with more than 10 years of experience without knowing the histological information.

For PTC, the size of the nodule, the degree of enhancement, the range of contact between PTC and thyroid capsule, and the presence of discontinued capsule were recorded. The degree of enhancement was divided into hyper-enhancement, iso-enhancement, and hypo-enhancement with respect to the surrounding normal thyroid parenchyma. The evaluation of the range of contact between PTC and thyroid capsule was similar to the evaluation on US. Discontinued capsule was noted when the thyroid capsule was discontinued in the early artery phase (17).

For cervical lymph nodes, enhancement direction (centripetal/centrifugal), enhancement type (no enhancement/homogeneous enhancement/peripheral enhancement/mixed enhancement), and enhancement range (enlarged or not) were recorded (21).

Diagnostic Criteria for Extracapsular Extension and Lymph Node Metastasis

If the contact range between PTC and the thyroid capsule was >25%, and discontinued thyroid capsule was observed on US or CEUS, ECE would be diagnosed respectively (20). When combining US and CEUS together, if three or more of the above four features (>25% contact on US, discontinued capsule on US, >25% contact on CEUS, discontinued capsule on CEUS) were observed, ECE would be diagnosed by US+CEUS.

If two or more of the following features (L/S ratio <2, ill-defined margin, hyper-echogenicity, absent hilum, calcification, peripheral or mixed vascularity) were observed on US, LNM would be diagnosed by US. If two or more of the following features (centripetal perfusion, peripheral or mixed enhancement, and enlarged size on CEUS compared to US) were found on CEUS, LNM would be diagnosed by CEUS. Combining US and CEUS together, if three or more of all the above features were observed, LNM would be diagnosed by US+CEUS (21).

Statistical Analysis

SPSS 16.0 software (IBM, Armonk, NY, USA) was used for statistical analysis. Continuous data of normal distribution were described by mean ± standard deviation, continuous data of non-normal distribution were described by median (interquartile range), and categorized data were described by percentage. Using independent-sample *t* test for the comparison of continuous data of normal distribution, Mann–Whitney test for continuous data of non-normal distribution, and chi-square test or Fisher's exact test for the proportion comparison of categorized data. Sensitivity, specificity, positive predictive value (PPV), negative predictive value (NPV), and overall accuracy of US and CEUS in the diagnosis of ECE and LNM were calculated. Logistic regression was used to explore the relationship between variables. $P < 0.05$ (two-tailed) was considered to be statistically significant.

RESULTS

Patients

Most enrolled patients were symptomless, with thyroid lesions accidentally discovered during physical examinations (49/62, 79.0%). The most common clinical symptom was painless neck mass (8/62, 12.9%), followed by hoarseness (4/62, 6.5%), cough (3/62, 4.8%), and palpitation (3/62, 4.8%). Among 59 patients (95.2%) with thyroid function test results, one had hyperthyroidism (1/62, 1.6%), while the others had normal thyroid function.

Based on pathology, 15 patients had multifocal PTCs (24.2%). Here, 16 patients had PTCs with ECE (25.8%), 11 patients had PTCs with LNM (17.7%), and 3 patients had PTCs with both ECE and LNM (4.8%). These 30 patients were group A (48.4%). The other 32 patients had PTCs without ECE or LNM (51.6%, group B). Among all patients with ECE, 3 presented with gross extrathyroidal extension (18.8%), and the others presented minimal extrathyroidal extension (13/16, 81.2%). No significant difference was found in age, gender, or multifocality between the two groups (all $P > 0.05$).

Ultrasound Examination

Most PTCs were solid (60/62, 96.8%), hypoechoic (54/62, 87.1%) nodules with microcalcifications (31/62, 50.0%) and lobulated or irregular margins (27/62, 43.5%). In addition, 18 PTCs (29.0%) showed taller-than-wide shape. Most PTCs (50/62, 80.6%) were grade 5 based on the 2017 American College of Radiology (ACR) Thyroid Imaging, Reporting and Data System (TI-RADS) (5), while the others were grade 4.

The average size of PTC on US was 0.95 (0.68, 1.30) cm, ranging from 0.5 to 6.8 cm. PTC size of group A was significantly larger than that of group B ($P = 0.001$). More PTCs showed >25% contact with the thyroid capsule and discontinued thyroid capsule in group A than in group B ($P < 0.001$, $P = 0.007$, respectively). More absent hilum and calcification were observed in lymph nodes in group A ($P = 0.02$, $P = 0.01$, respectively), while no significant difference was found in L/S ratio, ill-defined margin, hyper-echogenicity, or vascularity distribution of lymph nodes between groups, as shown in **Table 1**.

Contrast-Enhanced Ultrasound Examination

The average size of PTC on CEUS was 0.85 (0.60, 1.20) cm. As shown in **Table 1**, PTC size of group A was significantly larger than that of group B ($P = 0.003$). More PTCs with hyper-enhancement compared to the surrounding thyroid parenchyma were observed in group A, while more PTCs with hypo-enhancement were observed in group B ($P = 0.013$). More PTCs demonstrated >25% contact with the thyroid capsule and discontinued thyroid capsule in group A ($P < 0.001$). More centripetal perfusion and enlarged size of LNs were observed in lymph nodes in group A ($P < 0.001$, $P = 0.029$, respectively), while no significant difference was found in the enhancement type of LNs ($P > 0.05$).

TABLE 1 | US and CEUS features of PTCs and lymph nodes in the two groups.

		Group A (n = 30)	Group B (n = 32)	*P*
US	PTC size, cm	1.20 (0.88,1.45)	0.80 (0.60,1.00)	0.001*
	Contact between PTC and thyroid capsule, n (%)			<0.001*
	>25%	19 (63.3%)	4 (12.5%)	
	≤25%	11 (36.7%)	28 (87.5%)	
	Presence of discontinued capsule, n (%)			0.007*
	Yes	16 (53.3%)	6 (18.8%)	
	No	14 (46.7%)	26 (81.2%)	
	LN L/S ratio, n (%)			0.103
	≥2	17 (56.7%)	25 (78.1%)	
	<2	13 (43.3%)	7 (21.9%)	
	Margin of LN, n (%)			0.077
	Well-defined	23 (76.7%)	30 (93.8%)	
	Ill-defined	7 (23.3%)	2 (6.2%)	
	Hyper-echogenicity in LN, n (%)			0.099
	Present	25 (83.3%)	31 (96.9%)	
	Absent	5 (16.7%)	1 (3.1%)	
	Hilum structure, n (%)			0.020*
	Present	18 (60.0%)	28 (87.5%)	
	Absent	12 (40.0%)	4 (12.5%)	
	Calcification in LN, n (%)			0.010*
	Present	6 (20.0%)	0 (0.0%)	
	Absent	24 (80.0%)	32 (100%)	
	Peripheral or mixed blood flow, n (%)			0.249
	Present	5 (16.7%)	2 (6.2%)	
	Absent	25 (83.3%)	30 (93.8%)	
CEUS	PTC size, cm	1.15 (0.70, 1.45)	0.70 (0.50, 0.98)	0.003*
	Degree of enhancement, n (%)			0.013*
	Hyper-enhancement	6 (20.0%)	0 (0.0%)	
	Iso-enhancement	1 (3.3%)	2 (6.2%)	
	Hypo-enhancement	23 (76.7%)	30 (93.8%)	
	Contact between PTC and thyroid capsule, n (%)			<0.001*
	>25%	21 (70.0%)	3 (9.4%)	
	≤25%	9 (30.0%)	29 (90.6%)	
	Presence of discontinued capsule, n (%)			<0.001*
	Yes	17 (56.7%)	4 (12.5%)	
	No	13 (43.3%)	28 (87.5%)	
	Perfusion direction of LN, n (%)			<0.001*
	Centripetal	11 (36.7%)	0 (0.0%)	
	Centrifugal	19 (63.3%)	32 (100%)	
	Peripheral or mixed enhancement of LN, n (%)			0.125
	Present	17 (56.7%)	11 (34.4%)	
	Absent	13 (43.3%)	21 (65.6%)	
	Enlarged range on CEUS, n (%)			0.029*
	Yes	10 (33.3%)	3 (9.4%)	
	No	20 (66.7%)	29 (90.6%)	

LN, lymph node; PTC, papillary thyroid carcinoma; US, ultrasound; CEUS, contrast-enhanced ultrasound.
**Statistically significant.*

Diagnostic Performance Analysis

CEUS alone and the combination of US and CEUS were more accurate than US alone in the diagnosis of ECE of PTC. However, the combination of US and CEUS did not make much improvement in the diagnostic accuracy than CEUS alone. Meanwhile, the combination of US and CEUS was more accurate than US or CEUS alone in the diagnosis of LNM from PTC. CEUS alone was more accurate than US alone as well. The results are shown in **Tables 2**, **3** and **Figure 1**.

Logistic Regression Analysis

Based on the above statistical analysis results and clinical data, age, gender, PTC size, degree of enhancement, diagnosis of ECE by US+CEUS, and diagnosis of LNM by US+CEUS were used in binary logistic regression analysis. The results showed that the diagnoses of ECE and LNM by the combination of US and CEUS were independent risk factors for PTC invasiveness [odds ratio (OR) = 29.49, 97.20, respectively; both $P = 0.001$].

DISCUSSION

In this study, we found that the PTC size in group A was significantly larger than that in group B on both US and CEUS. Nodule size was reported to be an independent risk factor for differentiated thyroid cancer (22–25). This might be

TABLE 2 | Diagnostic performance of US, CEUS, and US combined CEUS for ECE of PTC.

Modalities	Sensitivity (%)	Specificity (%)	PPV (%)	NPV (%)	Accuracy (%)
US	52.6	81.4	55.6	79.5	72.6
CEUS	68.4	83.7	65.0	85.7	79.0
US+CEUS	73.6	81.4	63.6	87.5	79.0

PTC, papillary thyroid carcinoma; ECE, extracapsular extension; US, ultrasound; CEUS, contrast-enhanced ultrasound; PPV, positive predictive value; NPV, negative predictive value.

TABLE 3 | Diagnostic performance of US, CEUS, and US combined CEUS for LNM from PTC.

Modalities	Sensitivity (%)	Specificity (%)	PPV (%)	NPV (%)	Accuracy (%)
US	78.5	83.3	57.9	93.0	82.2
CEUS	78.5	93.8	78.6	93.8	90.3
US+CEUS	92.9	95.8	86.7	97.9	95.2

PTC, papillary thyroid carcinoma; LNM, lymph node metastasis; US, ultrasound; CEUS, contrast-enhanced ultrasound; PPV, positive predictive value; NPV, negative predictive value.

due to the aggressive nature of invasive PTC that the aggregation of tumor cells might be promoted at the gene or molecular level compared with non-invasive PTC (26). Meanwhile, more hyper-enhancement was observed in group A than in group B. Generally speaking, PTC tends to be hypo-enhanced compared to benign nodules of the thyroid, since they lack blood supply (27, 28), especially when the PTC size is small (29). However, we found that 20% of PTCs in group A were hyper-enhanced, even though two-thirds of them were smaller than 2.0 cm. Recently, intranodular vascularity evaluated by US has no longer been considered an independent risk factor for malignancy in PTCs (4). Nevertheless, we speculate that vascularity evaluated by CEUS might be associated with PTC invasiveness, consistent with other studies (22, 23, 30). Since angiogenesis is fundamental in the development, growth, and metastasis of PTC (23), this sign might suggest more active neovascularization and greater microvascular density in invasive PTC, which could be reflected by CEUS.

PTCs in group A had a larger contact range between PTC and the thyroid capsule and more presence of discontinued capsule than PTCs in group B. Meanwhile, lymph nodes in Group A showed more absent hilum and calcification on US, as well as more centripetal perfusion and enlarged size on CEUS than in group B. The above ultrasonic features were reported to be indicators for PTC ECE and LNM (17, 18, 21, 31), and our results consistently demonstrated its importance in PTC invasiveness evaluation. These findings helped us to obtain a better understanding of the ultrasonic characterization of invasive PTC.

Several studies have focused on the application of CEUS in the diagnosis of ECE or LNM from PTC (17–23, 28, 31). Most of them suggested that CEUS had better diagnostic performance than US. In this study, we had consistent findings. In both ECE and LNM diagnosis, CEUS showed higher sensitivity, specificity, PPV, NPV, and accuracy than those of US. CEUS is dominant in the detection of tissue perfusion. It is sensitive to microvascularity; hence, it has advantages in the display of lesion contour, thyroid capsule interruption, and hemodynamics of PTC and lymph nodes. These might be the fundamentals of the better diagnostic performance shown by CEUS. Interestingly, for ECE diagnosis, the combination of US and CEUS did not show much improvement in the diagnostic accuracy other than CEUS alone. This might be because for ECE diagnosis, the parameters obtained by US and CEUS were the same. CEUS was superior in the detection of PTC and capsule contact as well as capsule continuity (20), working more like a substitution than a supplement to US. However, for LNM diagnosis, US and CEUS showed different advantages. CEUS is more sensitive in the detection of perfusion direction and microvascularity structure than US (32), yet it has difficulty recognizing other features obtained by US, such as calcification and hyper-echogenicity. Thus, the combination of US and CEUS showed the highest accuracy, followed by CEUS and US alone.

The binary logistic regression analysis showed that the diagnoses of ECE and LNM by the combination of US and CEUS were independent risk factors for PTC invasiveness. The success of surgery for thyroid cancer hinges on thorough and accurate preoperative imaging. At present, US is recommended for the preoperative evaluation of thyroid cancer by the American Thyroid Association (ATA) (33). In commonly used guidelines for thyroid nodule management such as 2015 ATA guideline and 2017 ACR TI-RADS, PTC smaller than 1 cm without high-risk features is considered indolent, and active clinical diagnosis and treatment are not recommended (5, 33, 34). However, effective preoperative evaluation of PTC invasiveness lacks in traditional imaging methods. In our study, we found that the diagnosis of ECE and LNM by the combination of US and CEUS could significantly predict PTC invasiveness, even in subcentimeter PTCs. Thus, we state that the combination of US and CEUS could be a promising tool for the preoperative evaluation of PTC invasiveness and might benefit the optimal stratified management of PTC patients.

There are some limitations of this study: 1) This is a retrospective study with a relatively small sample size. Selection bias might exist because patients with non-invasive micro-PTC might take clinical and ultrasonic follow-up instead of surgery. Larger and prospective studies will be helpful to generalize the results in the future; 2) In this study, size thresholds were set for enrollment of PTC and LN because movement may lead to errors in measurement and difficulty existed in the CEUS feature observation for small lesions; 3) The value of CEUS in the

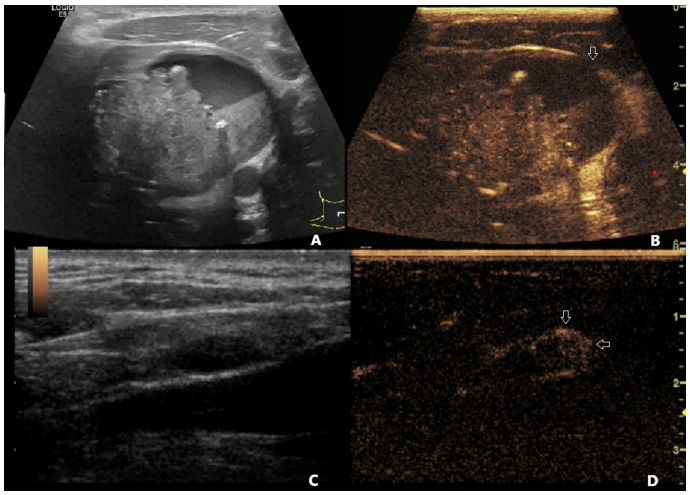

FIGURE 1 | **(A)** A 40-year-old male patient with pathology-confirmed PTC underwent preoperative US and CEUS examination. **(A)** One 6.8 cm * 4.7 cm mixed cystic and solid nodule was found in the left lobe of the thyroid. The contact range between PTC and the thyroid capsule was >50%. The capsule was continued on US. **(B)** On CEUS, the contact range between PTC and the thyroid capsule was >50%, and discontinued capsule was observed (white arrow). **(C)** A 1.2 cm * 0.5 cm hypoechoic lymph node with clear boundary and unclear hilum structure was found on US. **(D)** This lymph node demonstrated centripetal perfusion and peripheral enhancement on CEUS (white arrows). This patient was diagnosed with non-invasive PTC by US, PTC with ECE and LNM by CEUS and US+CEUS, and was finally confirmed to have PTC with ECE and LNM by pathology. PTC, papillary thyroid carcinoma; US, ultrasound; CEUS, contrast-enhanced ultrasound; ECE, extracapsular extension; LNM, lymph node metastasis.

evaluation of different degrees of ECE and different compartment lymph node metastasis will be further addressed in our future study.

CONCLUSION

US and CEUS features for invasive PTC include larger size, hyper-enhancement, >25% contact between PTC and thyroid capsule, discontinued capsule, absent hilum, calcification in lymph node, centripetal perfusion, and enlarged lymph node on CEUS. CEUS has added value in the evaluation of PTC invasiveness when compared to US. CEUS or US+CEUS is recommended for the evaluation of ECE, while US+CEUS is recommended for the evaluation of LNM. CEUS is a promising tool in the preoperative assessment of PTC invasiveness, which might benefit the clinical stratified management of PTC patients.

DATA AVAILABILITY STATEMENT

The raw data used to support the findings of this study are available from the corresponding author upon request.

ETHICS STATEMENT

The studies involving human participants were reviewed and approved by the Ethics Committee of Peking University First Hospital. The patients/participants provided their written informed consent to participate in this study.

AUTHOR CONTRIBUTIONS

LC conceived and designed the analysis, collected the data, contributed data or analysis tools, performed the analysis, and wrote the paper. LZC conceived and designed the analysis, collected the data, contributed data or analysis tools, and wrote the paper. ZL collected the data, contributed data or analysis tools, and wrote the paper. YS collected the data and wrote the paper. XS collected the data and wrote the paper. JL collected the data and wrote the paper. All authors contributed to the article and approved the submitted version.

FUNDING

This work was supported by Research Fund of Peking University First Hospital (grant nos. 2017CR05 and 2021CR02).

REFERENCES

1. Araque KA, Gubbi S, Klubo-Gwiezdzinska J. Updates on the Management of Thyroid Cancer. *Horm Metab Res* (2020) 52(8):562–77. doi: 10.1055/a-1089-7870
2. Sherman SI. Thyroid Carcinoma. *Lancet* (2003) 361(9356):501–11. doi: 10.1016/s0140-6736(03)12488-9
3. Cabanillas ME, McFadden DG, Durante C. Thyroid Cancer. *Lancet* (2016) 388(10061):2783–95. doi: 10.1016/s0140-6736(16)30172-6

4. Haugen BR, Alexander EK, Bible KC, Doherty GM, Mandel SJ, Nikiforov YE, et al. 2015 American Thyroid Association Management Guidelines for Adult Patients With Thyroid Nodules and Differentiated Thyroid Cancer: The American Thyroid Association Guidelines Task Force on Thyroid Nodules and Differentiated Thyroid Cancer. *Thyroid* (2016) 26(1):1–133. doi: 10.1089/thy.2015.0020
5. Tessler FN, Middleton WD, Grant EG, Hoang JK, Berland LL, Teefey SA, et al. ACR Thyroid Imaging, Reporting and Data System (TI-RADS): White Paper of the ACR TI-RADS Committee. *J Am Coll Radiol* (2017) 14(5):587–95. doi: 10.1016/j.jacr.2017.01.046
6. Shin JH, Baek JH, Chung J, Ha EJ, Kim JH, Lee YH, et al. Ultrasonography Diagnosis and Imaging-Based Management of Thyroid Nodules: Revised Korean Society of Thyroid Radiology Consensus Statement and Recommendations. *Korean J Radiol* (2016) 17(3):370–95. doi: 10.3348/kjr.2016.17.3.370
7. Russ G, Bonnema SJ, Erdogan MF, Durante C, Ngu R, Leenhardt L. European Thyroid Association Guidelines for Ultrasound Malignancy Risk Stratification of Thyroid Nodules in Adults: The EU-TIRADS. *Eur Thyroid J* (2017) 6(5):225–37. doi: 10.1159/000478927
8. Celletti I, Fresilli D, De Vito C, Bononi M, Cardaccio S, Cozzolino A, et al. TIRADS, SRE and SWE in INDETERMINATE Thyroid Nodule Characterization: Which has Better Diagnostic Performance? *Radiol Med* (2021) 126(9):1189–200. doi: 10.1007/s11547-021-01349-5
9. Cantisani V, Maceroni P, D'Andrea V, Patrizi G, Di Segni M, De Vito C, et al. Strain Ratio Ultrasound Elastography Increases the Accuracy of Colour-Doppler Ultrasound in the Evaluation of Thy-3 Nodules. A Bi-Centre University Experience. *Eur Radiol* (2016) 26(5):1441–9. doi: 10.1007/s00330-015-3956-0
10. Lee DY, Kwon TK, Sung MW, Kim KH, Hah JH. Prediction of Extrathyroidal Extension Using Ultrasonography and Computed Tomography. *Int J Endocrinol* (2014) 2014:351058. doi: 10.1155/2014/351058
11. Kim H, Kim JA, Son EJ, Youk JH, Chung TS, Park CS, et al. Preoperative Prediction of the Extrathyroidal Extension of Papillary Thyroid Carcinoma With Ultrasonography Versus MRI: A Retrospective Cohort Study. *Int J Surg* (2014) 12(5):544–8. doi: 10.1016/j.ijsu.2014.03.003
12. Choi JS, Kim J, Kwak JY, Kim MJ, Chang HS, Kim EK. Preoperative Staging of Papillary Thyroid Carcinoma: Comparison of Ultrasound Imaging and CT. *AJR Am J Roentgenol* (2009) 193(3):871–8. doi: 10.2214/ajr.09.2386
13. Hwang HS, Orloff LA. Efficacy of Preoperative Neck Ultrasound in the Detection of Cervical Lymph Node Metastasis From Thyroid Cancer. *Laryngoscope* (2011) 121(3):487–91. doi: 10.1002/lary.21227
14. Cantisani V, Bertolotto M, Weskott HP, Romanini L, Grazhdani H, Passamonti M, et al. Growing Indications for CEUS: The Kidney, Testis, Lymph Nodes, Thyroid, Prostate, and Small Bowel. *Eur J Radiol* (2015) 84(9):1675–84. doi: 10.1016/j.ejrad.2015.05.008
15. Isidori AM, Pozza C, Gianfrilli D, Giannetta E, Lemma A, Pofi R, et al. Differential Diagnosis of Nonpalpable Testicular Lesions: Qualitative and Quantitative Contrast-Enhanced US of Benign and Malignant Testicular Tumors. *Radiology* (2014) 273(2):606–18. doi: 10.1148/radiol.14132718
16. Puliani G, Sesti F, Feola T, Di Leo N, Polti G, Verrico M, et al. Natural History and Management of Familial Paraganglioma Syndrome Type 1: Long-Term Data From a Large Family. *J Clin Med* (2020) 9(2):588. doi: 10.3390/jcm9020588
17. Ding K, Cui Q, Yan K, Liu W, Wang T. Diagnostic Value of Conventional Ultrasound and Contrast Enhanced Ultrasound in Predicting Extrathyroidal Extension of Papillary Thyroid Cancer. *Chin J Ultrason* (2017) 26(3):243–8. doi: 10.2147/CMAR.S299157
18. Hong YR, Luo ZY, Mo GQ, Wang P, Ye Q, Huang PT. Role of Contrast-Enhanced Ultrasound in the Pre-Operative Diagnosis of Cervical Lymph Node Metastasis in Patients With Papillary Thyroid Carcinoma. *Ultrasound Med Biol* (2017) 43(11):2567–75. doi: 10.1016/j.ultrasmedbio.2017.07.010
19. Jiang W, Wei HY, Zhang HY, Zhuo QL. Value of Contrast-Enhanced Ultrasound Combined With Elastography in Evaluating Cervical Lymph Node Metastasis in Papillary Thyroid Carcinoma. *World J Clin Cases* (2019) 7(1):49–57. doi: 10.12998/wjcc.v7.i1.49
20. Chen L, Chen L, Liu J, Liang Z, Wang B. Contrast-Enhanced Ultrasound and BRAF Mutation in Diagnosis of Extracapsular Extension of Papillary Thyroid Carcinoma. *Chin J Med Imaging Technol* (2020) 36(1):50–4. doi: 10.13929/j.issn.1003-3289.2020.01.013
21. Chen L, Chen L, Liu J, Wang B, Zhang H. Value of Qualitative and Quantitative Contrast-Enhanced Ultrasound Analysis in Preoperative Diagnosis of Cervical Lymph Node Metastasis From Papillary Thyroid Carcinoma. *J Ultrasound Med* (2020) 39(1):73–81. doi: 10.1002/jum.15074
22. Tao L, Zhou W, Zhan W, Li W, Wang Y, Fan J. Preoperative Prediction of Cervical Lymph Node Metastasis in Papillary Thyroid Carcinoma *via* Conventional and Contrast-Enhanced Ultrasound. *J Ultrasound Med* (2020) 39(10):2071–80. doi: 10.1002/jum.15315
23. Zhan J, Zhang LH, Yu Q, Li CL, Chen Y, Wang WP, et al. Prediction of Cervical Lymph Node Metastasis With Contrast-Enhanced Ultrasound and Association Between Presence of BRAF(V600E) and Extrathyroidal Extension in Papillary Thyroid Carcinoma. *Ther Adv Med Oncol* (2020) 12:1758835920942367. doi: 10.1177/1758835920942367
24. Price DL, Wong RJ, Randolph GW. Invasive Thyroid Cancer: Management of the Trachea and Esophagus. *Otolaryngol Clin North Am* (2008) 41(6):1155–1168, ix-x. doi: 10.1016/j.otc.2008.08.002
25. Zhao Y, Zhang Y, Liu XJ, Shi BY. Prognostic Factors for Differentiated Thyroid Carcinoma and Review of the Literature. *Tumori* (2012) 98(2):233–7. doi: 10.1700/1088.11935
26. Xing M. BRAF Mutation in Papillary Thyroid Cancer: Pathogenic Role, Molecular Bases, and Clinical Implications. *Endocr Rev* (2007) 28(7):742–62. doi: 10.1210/er.2007-0007
27. Pang T, Huang L, Deng Y, Wang T, Chen S, Gong X, et al. Logistic Regression Analysis of Conventional Ultrasonography, Strain Elastosonography, and Contrast-Enhanced Ultrasound Characteristics for the Differentiation of Benign and Malignant Thyroid Nodules. *PloS One* (2017) 12(12):e0188987. doi: 10.1371/journal.pone.0188987
28. Peng Q, Niu C, Zhang M, Peng Q, Chen S. Sonographic Characteristics of Papillary Thyroid Carcinoma With Coexistent Hashimoto's Thyroiditis: Conventional Ultrasound, Acoustic Radiation Force Impulse Imaging and Contrast-Enhanced Ultrasound. *Ultrasound Med Biol* (2019) 45(2):471–80. doi: 10.1016/j.ultrasmedbio.2018.10.020
29. Zheng X, Zhang Y, Zhao C, Shi X, Li C, Jiang J, et al. Diagnosis of Thyroid Space-Occupying Lesions Using Real-Time Contrast-Enhanced Ultrasonography With Sulphur Hexafluoride Microbubbles. *Chin J Of Otorhinolaryngol Head And Neck Surg* (2009) 44(4):5. doi: 10.1016/j.ceramint.2007.09.109
30. Li W, Zhang Y, Song Q, Lan Y, He HY, Ma J, et al. [Correlation Between Contrast-Enhanced Ultrasound and Risk of Tumor Recurrence in Papillary Thyroid Carcinoma]. *Zhongguo Yi Xue Ke Xue Yuan Xue Bao* (2021) 43(3):343–9. doi: 10.3881/j.issn.1000-503X.13828
31. Wei X, Li Y, Zhang S, Gao M. Prediction of Thyroid Extracapsular Extension With Cervical Lymph Node Metastases (ECE-LN) by CEUS and BRAF Expression in Papillary Thyroid Carcinoma. *Tumour Biol* (2014) 35(9):8559–64. doi: 10.1007/s13277-014-2119-2
32. Zhang B, Jiang YX, Liu JB, Yang M, Dai Q, Zhu QL, et al. Utility of Contrast-Enhanced Ultrasound for Evaluation of Thyroid Nodules. *Thyroid* (2010) 20(1):51–7. doi: 10.1089/thy.2009.0045
33. Yeh MW, Bauer AJ, Bernet VA, Ferris RL, Loevner LA, Mandel SJ, et al. American Thyroid Association Statement on Preoperative Imaging for Thyroid Cancer Surgery. *Thyroid* (2015) 25(1):3–14. doi: 10.1089/thy.2014.0096
34. Stefanova DI, Bose A, Ullmann TM, Limberg JN, Finnerty BM, Zarnegar R, et al. Does the ATA Risk Stratification Apply to Patients With Papillary Thyroid Microcarcinoma? *World J Surg* (2020) 44(2):452–60. doi: 10.1007/s00268-019-05215-4

Conflict of Interest: The authors declare that the research was conducted in the absence of any commercial or financial relationships that could be construed as a potential conflict of interest.

this article, or claim that may be made by its manufacturer, is not guaranteed or endorsed by the publisher.

frontiers in Oncology

REVIEW
published: 28 February 2022
doi: 10.3389/fonc.2022.854773

An Overview of Epigenetic Methylation in Pancreatic Cancer Progression

Yuhao Zhao[1,2,3†], Mao Yang[1,2,3†], Shijia Wang[1,2,3†], Sk Jahir Abbas[1,2], Junzhe Zhang[1,2,3], Yongsheng Li[1,2,3], Rong Shao[4] and Yingbin Liu[1,2,3*]*

[1] Department of Biliary-Pancreatic Surgery, Renji Hospital Affiliated to Shanghai Jiao Tong University School of Medicine, Shanghai, China, [2] State Key Laboratory of Oncogenes and Related Genes, Shanghai Cancer Institute, Shanghai, China, [3] Shanghai Key Laboratory of Biliary Tract Disease Research, Shanghai, China, [4] Department of Pharmacology, Shanghai Jiao Tong University School of Medicine, Shanghai, China

Over the past decades, the aberrant epigenetic modification, apart from genetic alteration, has emerged as dispensable events mediating the transformation of pancreatic cancer (PC). However, the understanding of molecular mechanisms of methylation modifications, the most abundant epigenetic modifications, remains superficial. In this review, we focused on the mechanistic insights of DNA, histone, and RNA methylation that regulate the progression of PC. The methylation regulators including writer, eraser and reader participate in the modification of gene expression associated with cell proliferation, invasion and apoptosis. Some of recent clinical trials on methylation drug targeting were also discussed. Understanding the novel regulatory mechanisms in the methylation modification may offer alternative opportunities to improve therapeutic efficacy to fight against this dismal disease.

Keywords: Epigenetics, Pancreatic cancer, DNA methylation, Histone methylation, RNA methylation

OPEN ACCESS

Edited by:
Hailong Pei,
Soochow University, China

Reviewed by:
Xiaoqun Dong,
Brown University, United States
Rajeev Joshi,
T.N. Medical College & B.Y.L. Nair Ch.Hospital, India

****Correspondence:***
Yingbin Liu
laoniulyb@shsmu.edu.cn
Rong Shao
rongshao@sjtu.edu.cn

†These authors have contributed equally to this work

Specialty section:
This article was submitted to Molecular and Cellular Oncology, a section of the journal Frontiers in Oncology

Received: *14 January 2022*
Accepted: *07 February 2022*
Published: *28 February 2022*

Citation:
Zhao Y, Yang M, Wang S, Abbas SJ, Zhang J, Li Y, Shao R and Liu Y (2022) An Overview of Epigenetic Methylation in Pancreatic Cancer Progression. Front. Oncol. 12:854773. doi: 10.3389/fonc.2022.854773

INTRODUCTION

Pancreatic cancer (PC) is a type of tumor with high malignancy and aggressiveness. It is ranked the 8th leading causes of cancer death in the world in 2020 and its 5-year survival rate is less than 7% (1, 2). Although surgical radical resection remains the mainstay of PC treatment (3, 4), most PC patients are diagnosed at an advanced stage and miss the opportunity for surgery as they frequently appear to be atypical symptoms (5, 6). Even for the patients that undergo surgical resection, the rate of recurrence and death after surgery is particularly high. In the early diagnosis, the widely applied screening methods such as the detection of tumor marker CA19-9 and imaging yield minimal benefit as the measurement sensitivity does not give rise to the levels different from normal (7, 8). As a result, we need to further investigate the mechanisms of PC development to identify more molecules that can be detected at early stages to improve early diagnosis.

Increasing evidence shows that PC is associated with polygenic lesions, which include gene mutations and epigenetic modifications. Epigenetics proposed by Waddington, refers to reversible and heritable changes in gene function instead of the sequence alternations (9). Methylation modification are one of the main manifestations of epigenetics. The previous studies demonstrated that the methylation process is mainly regulated by writer, eraser and reader (10) (**Figure 1**). Writer

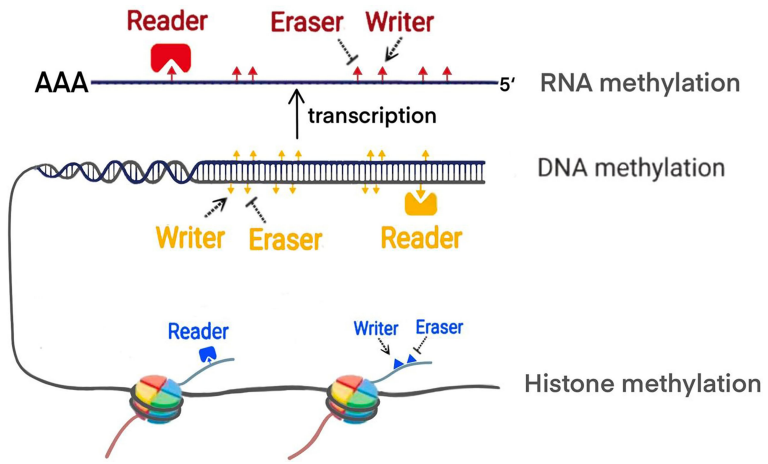

FIGURE 1 | The modification of methylation by writer, eraser and reader.

represents methyltransferase which can transfer the methyl group to specific site of DNA, RNA and histone. For example, DNA methylation mostly occurs in cytosine-phosphate-guanine (CpG) islands. In histone methylation, both lysine and arginine residues can be catalyzed. Various modifications of RNA methylation have been found, including N6-methyladenosine (m6A), 5-methylcytosine (m5C), andN1-methyladenosine (m1A). Eraser refers to demethylases which remove the methyl group. Reader is a class of proteins that are able to recognize methylation mark by their distinct domains and induce different biological functions. Up to date, the widespread application of methylation biomarkers detection and the emergence of epigenetic drug targets has brought new possibilities for the diagnosis and treatment of PC. Future therapy of PC will expectedly focus on some new targets revealed including epigenetic regulatory molecules. In this review, we particularly focus on the discussing the mechanism of the methylation modifications in PC from DNA methylation, histone methylation and RNA methylation modifications. Furthermore, we update recent clinical trials that target epigenetic methylation molecules.

DNA METHYLATION

DNA methylation, the most well-studied epigenetic modifications, often precedes before somatic cell mutation and occurs in early tumorigenesis. In the process of DNA methylation, S-adenosyl-L-methionine (SAM) provides the methyl group, which is transferred to specific site of DNA, including 5-methylcytosine, N6-methyladenine and 7-methylguanine. Methylation occurs mostly at the cytosine-C5 of the CpG dinucleotides which exists in two forms: CpG islands and CpG island shores. CpG islands, a region of the CpG dinucleotides cluster, are approximately located in 60% of gene promoters. CpG island shores, close to CpG islands, refer to a region that CpG dinucleotides disperse. In normal cells, only 5% of the CpG islands are methylated in the promoters; in contrast, all CpG island shores are usually methylated (11). DNA methylation modification does not alter the sequence or the composition of nucleotides; instead, it participates in the regulation of gene expression. For example, aberrant methylation of CpG islands in the promoter leads to downregulation of a variety of gene expression through the interaction with methylation-binding proteins. These proteins may act as transcriptional repressors to block the binding of the transcription factors, resulting in gene silencing.

Abnormal DNA methylation (hypermethylation and hypomethylation), mainly in CpG islands, is closely related to tumor development including PC. Overexpression of DNA methyltransferase (DNMT) leads to hypermethylation of gene promoters. The experimental evidence has shown that the genes with hypermethylation are tumor suppressors and are diminished or silenced due to hypermethylation in PC. DNA hypomethylation can be found not only in CpG islands, but also in CpG island shores when DNMT is inactivated, or demethylases are overexpressed. Currently, the most common genes with hypomethylation are oncogenes whose expression or activity is upregulated in tumor progression (12). Therefore, growing evidence has revealed on the specific mechanisms of methyltransferase (writer), demethylase (eraser) and DNA binding protein (reader) in the regulation of abnormal methylation during the development of PC (**Table 1**).

DNA Methyltransferase (Writer)

The degree of methylation, which is catalyzed by DNMT, is related to the activity and expression of DNMT. DNMT expression is closely associated with the prognosis of PC. DNMTs include DNMT1, DNMT2, DNMT3a, DNMT3b, DNMT3l and their isoforms.

DNMT1 acts as the most important DNMT for maintaining the methylation of genes (13). It has three domains, the catalytic domain at the C-terminus, the target region recognized by certain proteins at the N-terminal part and the unknown region. DNMT1 is overexpressed in PC and its expression

TABLE 1 | Major groups of DNA methylation regulators in PC.

Methylation enzymes	Family	Alias	Function in PC
Writer	DNMTs	DNMT1	pro-PC
		DNMT2	unclear
		DNMT3a	pro-PC
		DNMT3b	pro-PC
		DNMT3l	unclear
Eraser	TETs	TET1	anti-PC
		TET2	unclear
		TET3	unclear
Reader	MBDs	MeCP2	pro-PC
		MBD3	anti-PC
	SRA domain-containing proteins	UHRF1	pro-PC
		UHRF2	unclear
	Methyl-CpG binding zinc fingers	Kaiso	pro-PC
		KLF4	anti-PC

gradually increases with the transformation process from normal tissue, precancerous lesions to PC, indicating that the high expression of DNMT1 is associated with poor prognosis in patients (14). High DNMT1 expression is closely related to neural infiltration, tumor differentiation and TNM staging in PC, suggestive of a potential target for treatment of PC (15). Also, several studies showed that DNMT1 may regulate a variety of downstream genes to promote PC cell proliferation, migration and invasion as well as self-renewal of PC stem cells, such as suppressing the expression of Cyclin-dependent kinase inhibitors (CKIs) (16–18). Transfecting PC cells with siRNA DNMT1 reveals a significant decrease in cell proliferation and migration (19). In addition, n-butylidenephthalide (n-BP), a novel DNMT1 inhibitor, suppresses PC cell proliferation and blocks PC cells in G0/G1 phase (20). At present, phase I/II clinical trials of other DNMT1 inhibitors (Azacitidine, Decitabine) are ongoing (NCT01845805, NCT02959164) with the expectation of curing PC. DNMT3a and DNMT3b are the major *de novo* methylation enzymes, that affect the expression of target genes by regulating the level of DNA methylation (21). DNMT3a is highly expressed in PC and is closely associated with poor prognosis (22). Downregulation of DNMT3a in PC cell lines enhances their chemosensitivity to gemcitabine and oxaliplatin. Knocking out of DNMT3a inhibits cell proliferation, induces cell cycle arrest, and promotes apoptosis by decreasing cyclin D1 expression (22, 23). Studies about DNMT3b on PC are less reported compared to DNMT3a. For example, siRNA DNMT3b treatment of PC cells inhibit cell proliferation, while overexpression of miR-29b which targets DNMT3b promotes cell apoptosis (24). As a result, both DNMT3a and DNMT3b may become new targets for PC therapy. Neither DNMT2 nor DNMT3l possesses methyltransferase activity. However, DNMT3l is essential for *de novo* methylation, which interacts with DNMT3a and DNMT3b, stimulating their enzymatic activities (25, 26).

DNA Demethylase (Eraser)

DNA demethylation processes are divided into active demethylation and passive demethylation. Active demethylation is performed by demethylation enzymes which remove methylation marks, regulate gene expression and express different biological functions (27). Currently, the demethylases identified include the ten-eleven translocation family (TETs, TET1, TET2 and TET3) and ALKBH1 (27). Passive demethylation is a process which terminates due to the lack of DNMT1. In general, compared to DNMT, demethylase is less reported in PC. Several other demethylases need to be investigated apart from the TET1.

TETs

TETs were not recognized as demethylases until 2009. They convert 5-methylcytosine(5mC) to 5-hydroxymethylcytosine (5hmC), further generating 5-formylcytosine (5fC) and 5-carboxycytosine (5caC) to complete the demethylation process (28). TET1 is a 5mC hydroxylase that has been defined as a tumor suppressor in PC due to its low expression (29, 30). The overall survival of PC patients with low TET1 levels is shorter than those with high TET1 levels. TET1 is proved to suppress epithelial-mesenchymal transitions (EMT) in PC by inhibiting the Wnt signaling pathway (29). Other members of this family have similar function as TET1, but their mechanisms remain to be clarified in PC.

DNA Binding Protein (Reader)

Reader is a class of proteins or domains in the DNA methylation process, which can combine with different types of methylation modifications and interpret different biological functions. There is a mutual regulation between 'writer' and 'reader' (31). Familiar readers are divided into three categories, including the methyl-CpG-binding domain family (MBDs), SRA domain-containing proteins and Methyl-CpG binding zinc fingers (32–34).

MBDs

MBDs are key members in determining the transcriptional status of the epigenome, which bind to methylated CpG dinucleotides and exhibit various transcriptional regulatory effects (32). Up to date, there are eleven known members of the MBDs consisting of MeCP2, MBD1-6, SETDB1/2 and BAZ2A/B. But their roles in in PC are not well understood except a few members (35). MeCP is the first identified MBD domain-containing protein and considered to be an oncogene in PC, promoting EMT in PC cells (36). However, MBD3 plays a suppressive role in PC. Downregulation of MBD3 promotes the proliferation, migration and invasion of PC cells (37). Whether the opposite activities of MeCP2 and MBD3 present in PC are required to be further clarified. Nevertheless, both of them may become new targets for future treatment of PC.

SRA Domain-Containing Proteins

The SRA domain-containing proteins are another class of readers that contain SRA domain and are bound to the DNA hemi methylated regions (38). It consists of two main members: Ubiquitin-like with PHD and RING finger domain 1 (UHRF1) and Ubiquitin-like with PHD and RING finger domain 2 (UHRF2) (39). UHRF1 plays multiple roles in DNA methylation, which maintains DNA methylation during replication and is considered as a pivotal protein for integrating epigenetic information (40). UHRF1 is highly

expressed in variety of cancers and is associated with tumorigenesis, progression and invasion (41). UHRF1 mediates the silencing of PC suppressor genes and regulates the proliferation, metabolism and metastasis of PC cells through the UHRF1/SIRT4 axis (42). In addition, it can also regulate PC cell by other pathways (43).

Methyl-CpG Binding Zinc Fingers

Methyl-CpG binding zinc fingers are the third class of readers, which mainly binds to DNA methylation regions through c-terminal zinc finger motifs. This family has developed rapidly over the past few years, and there are eight members, including Kaiso, ZBTB4, ZBTB38, ZFP57, KLF4, EGR1, WT1, CTCF (44). However, studies of this family on PC are comparatively less and more worthy of exploration. Kaiso is the first member of the family that binds to both methylated and non-methylated regions of DNA, and its role in tumors may vary. Kaiso is overexpressed in aggressive and metastatic PC tissues, and its nuclear expression increases with aggressiveness and lymph node positivity (45). The underlying mechanisms involved in PC remain unclear. Only KLF4 is relatively well studied in PC and is similar to Kaiso in that it binds to both DNA methylated and DNA non-methylated regions (46). Nowadays, KLF4 has been reported to play either a promotive or inhibitory role in tumors, in which it is mostly considered as a tumor suppressor in PC. KLF4 limits PC metastasis by negatively regulating CD44, which provides theoretical evidence for KLF4-regulated therapy in advanced PC patients (47).

HISTONE METHYLATION

Histone modification is one of the most important post-translational epigenetic modifications, that can regulate multiple genetic events including transcription, DNA repair by influencing chromatin structure, recruiting remodeling enzymes or transcription complexes. Abnormal changes in a variety of histone modifications may promote the progression of PC. Histone modifications includes acetylation, methylation, phosphorylation, ubiquitination, and small ubiquitin-like modifier (SUMO). Histone methylation plays a primary role in regulating gene transcription.

Post-translational methylation in histone tails usually occurs in the lysine (K), and arginine(R) residues of histone H3 and H4. Residues of these amino acid can be mono-, di-, and trimethylated (only in lysine residues) to activate or inhibit gene transcription, depending on the specific situation (such as methylation site, state and number). For example, H3K4, H3K27, H3K36, H3K79and H4K12 in lysine residues largely promote transcriptional activation, while H3K7, H3K9, H3K56, H4K5 and H4K20 inhibit gene transcription (48). In arginine residues, H3R8, H3R17 and H4R3 activate transcription of downstream genes (48). Like DNA methylation, methyl group is dynamically added by methyltransferases-writers, removed by demethylase-erasers, and interpreted by proteins with methyl binding motifs-readers. These readers recognize histone methylation and help histone writers and erasers to locate appropriately. Different histone methylation sites are catalyzed by specific enzymes (**Table 2**). The balance between histone methylation and demethylation regulated by these enzymes has been shown to affect embryonic development and various physiological functions. Structural abnormalities or functional defects of these enzymes lead to a series of serious diseases (49). Numerous studies have confirmed that histone methylation has an impact on the progression of PC and related methyltransferases and demethylases inhibitors may be used as potential means to treat PC.

Lysine Methyltransferase (Writer)

Histone lysine methylation is catalyzed by lysine methyltransferases (KMTs) in the presence of SAM as the methyl donor. The two major writers, KMT3E (SET and MYND domain-containing protein 3, SMYD3) and KMT6 (enhancer of zeste homolog 2, EZH2) are known to function in PC.

SMYD3

SMYD3 belongs to the SET and myeloid-Nervy-DEAF-1 (MYND)-domain family that catalyzes lysine 4 of histone H3 (H4K5). SMYD3 has been widely explored because of its increased expression in many types of cancer, particularly those driven by the Ras signaling activation (50). SMYD3 is upregulated in PC and indicates a poor prognosis. Moreover, PC with a high expression of SMYD3 also has high caspase-3 and MMP-2 expressions (51). Decreased SMYD3 expression impairs cell growth and metastasis of PC *in vitro*. The MMP-2 mRNA and protein expressions are also downregulated in SMYD3 knock-down cell lines, but the expression of caspase-3 has not significantly changed. SMYD3 could be a candidate therapeutic target against tumorigenesis because of SMYD3 inhibitors discovered. There is a reported small molecule inhibitor targeting SMYD3 called piperidine-4-formamide-acetanilide compound, BCI-121 (52). It is a small molecule inhibitor that significantly reduces SMYD3 activity and inhibits proliferation in PC cell lines with SMYD3 overexpressed. However, this inhibitor has not been approved for clinical trials yet.

EZH2

EZH2 is the functional subunit of polycomb repressive complex 2 (PRC2), that epigenetically represses the expression of tumor suppressor gene through trimethylating lysine 27 of histone H3 (H3K27) in various cancer types. High expression of EZH2 is associated with PC (53). FBW7, an E3 ubiquitin ligase of EZH2, downregulates EZH2 through ubiquitination and degradation in PC cells. Activated CDK5 kinase can catalyze the EZH2 phosphorylation that is required for FBW7-mediated EZH2 degradation. Low expression of FBW7 causes an aberrant accumulation of EZH2 and induces tumorigenesis in PC (53). Non-coding RNAs can recruit EZH2 to modify histone H3 lysine 27 trimethylation (H3K27me3) of downstream target genes. For example, long non-coding RNA (lncRNA) BLACAT1 inhibits CDKN1C expression *via* EZH2-induced H3K27me3 and promotes proliferation, migration, and aerobic glycolysis of PC

TABLE 2 | Major groups of histone methylation regulators in PC.

Methylation enzymes	Family		Alias	Function in PC
Writer	KMTs		SMYD3	pro-PC
			EZH2	pro-PC
	PRMTs		PRMT1	pro- PC
			PRMT5	pro- PC
Eraser	KDMs	LSDs	KDM1	pro- PC
		JMJDs	KDM2B	pro- PC
			KDM3A	pro- PC
			KDM4A	anti- PC
			KDM4B	pro- PC
			KDM4D	unclear
			KDM5A	unclear
			KDM6B	anti- PC

cells (54). Highly-expressed EZH2 and low expressed miR-139-5p are detected in PC tissues and their expressions are associated with poor prognosis. Downregulation of EZH2 and upregulation of miR-139-5p impede EMT and lymph node metastasis (LNM) in PC cells. Mechanistically, EZH2 suppresses the expression of miR-139-5p through upregulating H3K27me3 (55). 3-Deazaneplanocin A (DZNeP) can reduce EZH2 and H3K27me3 expression. It shows that DZNeP/gemcitabine combination can significantly increase the apoptosis rate of PC cells, which seems to be promising anticancer reagents (56).

Lysine Demethylase (Eraser)

Histone lysine demethylases (KDMs) catalyze the removal of methyl groups on histone lysine residues, which is a reversible process. Based on the mechanism of action, KDMs are classified into two families: Flavin adenine dinucleotide (FAD)-dependent and Fe (II) and 2-oxoglutarate (2OG)-dependent.

KDM1

KDM1 is the only FAD-dependent KDM that is related to PC. The expression of two subtypes of KDM1, KDM1A (lysine-specific demethylase1, LSD1) and KDM1B (lysine-specific demethylase2, LSD2) are both elevated in PC tissues. The role of KDM1A in regulating PC progression is poorly understood. As for its homolog KDM1B, interfered KDM1B expression in PC cell lines reduces the cell proliferation and significantly increases the cell apoptosis (57).

JMJD Domain-Containing Protein Family

Another type of KDMs is from Jumonji C domain-containing (JMJD) protein family which is Fe (II) and α-ketoglutarate-dependent dioxygenases. Altered activity of JMJD protein family members is emerging as a common cause of tumor progression. In the study of PC, amplification or overexpression of the H3K9/H3K36 demethylases such as KDM2B、KDM3A and KDM4 exert positive roles in PC progression. KDM6B, an H3K27 demethylase, plays as a tumor suppressor.

KDM2B acts an active factor to drive the tumorigenicity. It mediates poorly differentiated PC through two different mechanisms. Occupancy of transcriptional start sites together with polycomb group (PcG) proteins represses developmental genes which function in cell cycle progression and senescence. In co-binding with the MYC oncogene and/or the histone demethylase KDM5A, KDM2B can activate the transcription of a module of genes involved broadly in metabolic homeostasis (58).

KDM3A participates in the epigenetic upregulation of DCLK1 expression which is correlated with PC morphology (59). DCLK1 is characteristic of a morphologically distinct subpopulation of stem-like cells in PC and its expression reveals the cellular and functional heterogeneity in PC (60).

The KDM4 subfamily mainly include 4 demethylases, including KDM4A, B, C and D. They are all studied and reported to play a role in PC, except KDM4C. Regulatory factor X-associated protein (RFXAP), a key transcription factor for MHC II molecules, binds to the promoter of KDM4A and promotes its transcription, thereby demethylating histone H3K36 (61). In PC, Fisetin induces DNA damage through RFXAP/KDM4A-dependent demethylation to inhibit proliferation *in vivo* and *in vitro* (62). KDM4B plays a crucial role in EMT process (63). It demethylates histone H3K9 to activate ZEB1 transcription (63). ZEB1 acts as an E-box binding transcription factor which is reported to epigenetically downregulate E-cadherin expression (64). High nuclear KDM4D expression in the specimens of pancreatic resection margins are significantly associated with dismal disease-free survival and can be an independent predictor of recurrence risk in PC patients (65). However, its physiological role in PC remains unknown.

It is known that oncogenic KRAS mutations can be detected in nearly all pancreatic lesions. KDM6B, the downstream of KRAS, is downregulated in PC cells with the lowest expression level in poorly differentiated PC (66). KDM6B knockdown can inhibit the expression of the CCAAT-enhancer binding protein alpha (CEBPA) gene and enhance tumor progression of PC cells both *in vitro* and *in vivo* (66).

The study of KDM5 family needs to be deepened in PC. KDM5A is a demethylase for histoneH3K4. KDM5A epigenetically suppresses the expression of mitochondrial pyruvate carrier-1 (MPC-1) and promotes the cell proliferation through mitochondria pyruvate metabolism in PC (67).

Arginine Methyltransferase (Writer)

Arginine residues can be methylated by protein arginine N-methyltransferases (PRMTs), which are classified as type I, II, or III enzymes according to their catalytic activity. PRMT1 from type I and PRMT5 from type II are related to PC.

PRMT1

Approximately 90% of total arginine methylation is catalyzed by PRMT1. As for histones, PRMT1 can catalyze the methylation of arginine 3 on histone H4(H4R3), which activates gene transcription. PRMT1 reported to be highly expressed in various cancer types, as well as in PC. Elevated expression level of PRMT1 is significantly associated with poor prognosis in PC patients. Functional experiments show that PRMT1 promotes PC cell proliferation *in vitro* and *in vivo*, and induces the upregulation of the β-catenin (68). The Wnt-β-catenin signaling pathway has already been highly implicated in pancreatic carcinogenesis and progression (69).

PRMT5

PRMT5 catalyzes the symmetrical dimethylation of arginine 8 on histone H3(H3R8) and arginine 3 on histone H4 (H4R3). Several studies show that PRMT5 plays a critical role in tumorigenesis and metastasis (70). As for PC, PRMT5 expression is highly expressed in tumor tissues. It promotes cell proliferation, migration, invasion, and EMT *via* activating EGFR/AKT/β-catenin signaling in PC cells (71). In addition, PRMT5 is proved to epigenetically suppress the promoter activity of FBW7 which controls the level of cMyc *via* ubiquitination and degradation (72). FBW7 is an E3 ubiquitin ligase that controls cMyc degradation. Mechanistically, PRMT5 post-translationally regulates c-Myc stability. Elevated c-Myc levels promote the proliferation of and aerobic glycolysis in PC cells (72). EZP015556, an inhibitor of PRMT5, is found to be effective in MTAP (a gene commonly lost in PC) negative tumors in preclinical experiments, and now there are a few clinical trials on this inhibitor ongoing (NCT03573310, NCT02783300, and NCT03614728) (73).

Arginine Demethylase (Eraser)

Corresponding to methylation, histone demethylation can occur in arginine residues and lysine residues. However, there is a large gap in research on arginine demethylases. To date, there have been no definite reports of specific arginine demethylases (74). In general, well-balanced arginine methylation is important for cellular proliferation and differentiation. Consequently, certain enzymes such as PRTMs, catalyze arginine methylation modifications and other enzymes acting as eraser of arginine methylation may participate in the demethylation, but remain to be established.

RNA METHYLATION

RNA methylation is a process that mediates RNA metabolism and gene expression. Over 150 modifications are identified in all types of RNA, in which RNA methylation is one of the most important forms of RNA modifications. These post-transcriptional RNA methylations include N6-methyladenosine (m6A), 5-methylcytosine (m5C) and N1-methyladenosine (m1A). RNA methylation can be dynamically and reversibly regulated by methyltransferase (writer), demethylase (eraser) and RNA binding protein (reader) (**Table 3**).

N6-Methyladenosine (m6A)

N6-methyladenosine (m6A) is the most abundant methylation modification of eukaryotic messenger RNA (mRNA) (75). The m6A site usually happens within the consensus sequence of RRm6ACH (R = G or A, H = A, C, or U) and are mainly enriched in 3′ untranslated regions (3′ UTRs) proximal to the stop codon. The evidence demonstrates that N6-methyladenosine (m6A) plays an important role in numerous physiological and pathophysiological processes by influencing pre-mRNA processing, splicing (76), nuclear export (77), decay (78), and translation (79).

m6A Methyltransferase (Writer)

The m6A writer, methyltransferase-like 3 and 14 proteins (METTL3 and METTL14) and their cofactors Wilms' tumor 1-associating protein (WTAP) form a highly conserved m6A methyltransferase complex (MTC).

METTL3 is the main component of the MTC, and it can be found both in cytoplasm and in nucleus. Given the different localization, it functions distinctively (80). In the nucleus, the METTL3 can interact with the activated transcription factor SMAD2/3 to promote co-transcription of m6A on selective transcripts through the TGFβ signaling pathway (81). Moreover, METTL3 can bind to the transcription factor CEBPZ and aggregate at the transcription initiation site, promoting tumor development (82). In the cytoplasm, METTL3 acts as an m6A binding protein rather than a methylation enzyme. It can interact with eIF3h to recognize and bind to the 3' end m6A site (83). It was showed that METTL3 is significantly overexpressed in PC and is related to poor prognosis. Knocking down METTL3 may reduce m6A levels and inhibits cell proliferation and invasion in PC (84). Furthermore, low METTL3 expression shows higher sensitivity to antitumor drugs such as gemcitabine, 5-fluorouracil, cisplatin and radiotherapy, suggesting that METTL3 could be a promising target for the treatment of PC patients (85).

METTL3 is the catalytic component in MTC, while METTL14 provides structural support for METTL3 close to its active site and also helps recognize METTL3 substrates (86). METTL14 are identified as a tumor suppressor in multiple types of cancers. However, METTL14 is overexpressed in PC. The upregulation of METTL14 can elevate the m6A level and decrease the expression of PERP, thereby promoting the proliferation and migration of PC cells both *in vivo* and *in vitro* (87). Loss of METTL14 can promote apoptosis induced by cisplatin in PC cells and enhance autophagy through an mTOR signaling-dependent pathway (88).

WTAP plays a crucial role in regulating the recruitment of the m6A methyltransferase complex to mRNA target proteins, acting as a regulatory subunit of the m6A MTC in the epitope regulation of RNA metabolism (89). WTAP also has a close relationship with tumor development. In PC, nuclear WTAP expression can be an independent prognostic indicator, where high expression is significantly correlated with poor overall survival and several pathological characteristics (90). Further studies show that WTAP can promote metastasis and suppress chemo-sensitivity to gemcitabine in PC cell lines *via* stabilizing Fak mRNA, and this function can be reversed by GSK2256098, a specific FAK inhibitor (91).

More co-factors of the m6A writer are also identified, such as viral-like m6A methyltransferase-associated protein (KIAAl429), RNA-binding motif protein 15/15B (RBM15/15B), and zinc finger CCCH domain protein 13 (ZC3H13). There are other independent m6A writers which do not work *via* the MTC, including methyltransferase-like 16 (METTL16), zinc finger CCHC-type containing 4 (ZCCHC4), and methyltransferase-like 5 (METTL5). However, the clinical impacts of them on PC are still unknown.

TABLE 3 | Major groups of RNA methylation regulators in PC.

Sites	Methylation regulators	Family	Alias	Function in PC
m6A	Writer	methyltransferase complex (MTC)	METTL3	pro-PC
			METTL14	pro-PC
			WTAP	pro-PC
	Eraser	AlkB homolog proteins	ALKBH5	anti-PC
		FTO		pro-PC
	Reader	YTH structural domain proteins	YTHDF2	anti-PC/pro-PC
		IGF2BPs	IGF2BP2	pro-PC
		hnRNP family		unclear
m5C	Writer	NOL1/NOP2/Sun domain family	NSUN6	anti-PC
	Eraser	TETs		unclear
	Reader	ALYREF		unclear
		YBX1		unclear
m1A	Writer	TRMTs		unclear
		NML		unclear
	Eraser	AlkB homolog proteins	ALKBH1	pro-PC

m6A Demethylase (Eraser)

m6A demethylases include AlkB homolog 5 (ALKBH5) and fat mass and obesity-associated protein (FTO) (92). ALKBH5 decreased in PC cell lines. It can inhibit PC progression by demethylating the lncRNA KCNK15-AS1 (93). Besides, ALKBH5 could serve as a PC suppressor by regulating the post-transcriptional activation of PER1 in an m6A-YTHDF2-dependent manner (94). Through demethylation of m6A-modified Wnt inhibitory factor 1 (WIF-1) transcripts, ALKBH5 can impair the Wnt pathway and sensitize PC cells to chemotherapy (95).

In contrast, FTO promotes the growth of various cancer types. However, the role of FTO is not well understood in PC. Up to now, only one study reported that high expression of FTO in PC. Downregulation of FTO can inhibit proliferation of PC cells. Mechanistically, FTO can interact with the MYC proto-oncogene and bHLH transcription factor, thereby regulating its stability *via* decreased m6A modification (96).

m6A Binding Protein (Reader)

The binding proteins of m6A include YTH structural domain proteins (YTHDF1, YTHDF2, YTHDF3, YTHDC1 and YTHDC2), members of the hnRNP family (hnRNPC and hnRNPA2B1), insulin-like growth factor 2 mRNA binding proteins (IGF2BP1, IGF2BP2, IGF2BP3), and eukaryotic initiation factor 3 (eIF3). Only YTHDF2 and IGF2BPs are involved in PC.

YTHDF2 expression is significantly upregulated in PC and related with poor survival in PC patients. Furthermore, YTHDF2 plays two different roles in cellular processes, including promoting proliferation and suppressing metastasis in PC cells, called the "migration-proliferation dichotomy". Mechanistically, it is because downregulation of YTHDF2 can increase total YAP expression but suppress TGF-β/Smad signaling (97).

Several studies showed that high expression of IGF2BP1, IGF2BP2 and IGF2BP3 is associated with a poor prognosis in PC (98–100). In addition, IGF2BP2 is also found to be significantly upregulated in pancreatic intraepithelial neoplasia (PanIN), a vital precursor of PC, implying the ability of IGF2BP2 to be a diagnostic marker for early-stage PC (98). Functionally, IGF2BP2 can increase cell proliferation and metabolism in PC by directly binding and stabilizing GLUT1 mRNA (101). IGF2BPs can also interact with various ncRNAs in order to function in PC progression (102).

5-Methylcytosine (m5C)

m5C methylation is the process by which the 5th carbon atom (C5) on cytosine is modified by methylation. m5C can be found in tRNA, rRNA, mRNA, miRNA, or lncRNA. The distribution of m5C differs among RNAs of different species. For example, m5C is not present in bacterial tRNA and mRNA, while it is found in eukaryotic and prokaryotic tRNA and mRNA (103, 104). The distribution of this modification in mRNA is not random and mostly enriched in the 5 ' and 3 ' UTR and AGO protein binding sites (105, 106). In tRNA, m5C is mostly present at the junction of the variable arm and the T-stem spanning positions (107). As for rRNA, m5C was found in the anticodon loop, and identified only in 28S rRNA but not in 18S RNA (103). This modification is mostly located at the center of peptidyl transferase or at the interface of large and small subunits in rRNA (108), and the location of this modified position is quite conserved (109). In the field of ncRNAs, Hao yuan et al, constructs an mRNA–lncRNA co-expression network between m5C-related mRNAs and lncRNAs and indicates that the m5C-related lncRNA risk model can be a biomarker of prognosis and plays an essential role in regulating PC immune cell distribution (110).

m5C Methyltransferase (Writer)

m5C methyltransferases include DNA methyltransferase 2 (DNMT2) and NOL1/NOP2/sun (NSUN) subgroups, which use SAM as a methyl donor. The NSUN family includes NSUN1, NSUN2, NSUN3, NSUN4, NSUN5, NSUN6, and NSUN7. The only one related to PC is NSUN6, which is found to be decreased in PC tissues. NSUN6 can suppress the proliferation of PC cell lines both *in vivo* and *in vitro*. However, the expression level of NSUN6 in PC patients is tightly correlated with clinicopathologic parameters and overall survival, which could be a potential marker of PC (111). The opposite function is still unknown mechanistically and remains further investigated.

DNMT2 was first thought to be a DNA methyltransferase, but a study found that DNMT2 does not catalyze DNA methylation, rather interestingly catalyzes tRNA methylation at C38 (112). Nonetheless, the role of DNMT2 in PC needs to be clarified.

m5C Binding Protein (Reader) and m5C Demethylase (Eraser)

Aly/REF export factor (ALYREF)is regarded as a specific binding protein for m5C-methylated mRNA. It can bind to m5C-enriched regions catalyzed by NSUN2, thereby regulating the out-of-nucleus movement of mRNA (113). Studies revealed that Y-box binding protein 1 (YBX1) may function as an m5C-binding protein which recognizes m5C binding sites and has a positive effect on mRNA stabilization and tumorigenesis (114, 115). The erasers of m5C methylation mainly include TET family members that identically act in DNA methylation. However, there is no study demonstrating the function of m5C readers and erasers in PC.

N1-Methyladenosine (m1A)

m1A modification refers to the modification method of adding a methyl group to the first nitrogen atom (N1) of adenine and it is found in tRNA (116), rRNA (117), mRNA (118, 119) and mitochondrial transcripts (120). m1A modification plays a critical role in maintaining tRNA structure and translation (119, 120). It occurs at positions 9, 14 and 58 of the tRNA, where m1A58 is indispensable for the stability of the tRNA structure (121). Compared with other RNA modifications, the level of m1A remains low in mRNA. m1A modification in the 5 ' cap region of mRNA may mediate translation (122). m1A modification of the mitochondrial mRNA coding region has been shown to affect the translation resistance of modified codons (120). m1A methyltransferases include tRNA methyltransferase (TRMTs) and NML. TRMT61A/6 is involved in modifying methylation at position 58 of tRNA in the cytoplasm (123), whereas the m1A methylation modification at positions 9 and 58 of mitochondrial tRNA is regulated by TRMT10C and TRMT61B (124, 125). In addition, m1A methylation was also found at position 1322 of 28s rRNA, catalyzed by nucleomethylin (NML) (126). ALKBH3 and ALKBH1 serve as erasers to remove m1A.

The significance of m1A for tumor development has been demonstrated in a variety of tumors. For example, knockdown of ALKBH3 can increase the m1A level of tRNA and decrease protein synthesis in cancer cells (127). ALKBH1 has also been confirmed to have an effect on tumorigenesis. In PC, it can promote cell proliferation through PI3K/AKT/mTOR and ErbB pathways (128).

However, compared with modifications such as m6A, our knowledge of m1A is far from adequate and the role of m1A in tumors needs to be established.

DISCUSSION

With recently rapid development of genome sequencing technologies, epigenetic changes have as essential events accounted for cancer progression and metastasis including PC. Methylation is the most common and important epigenetic modifications, including DNA methylation, histone methylation and RNA methylation, all of which are mediated by distinct writer enzymes, interpreted by reader proteins, and removed by eraser enzymes. Given the complicated mechanism of each modification in PC which has not been fully understood, the inconsistent evidence is reported. For example, in DNA methylation, hypermethylation catalyzed by writer can promote tumorigenesis; but in histone and RNA methylation, both writer and eraser can be oncogenes in PC, such as SMYD3 and KDM1, MELLT3 and FTO. This phenomenon is probably attributed to their distinct targets, in addition, other epigenetic regulators such as (de)acetylase, (de)phosphorylation and SUMO enzymes likely also participate in epigenetic modification, which co-occurs in the methylation modification, giving rise to divergent cellular outcomes. Therefore, the large effort is considerably taken into account in order to mechanistically illustrate the molecular network of epigenetic regulators that drive the malignancy of PC.

In the clinical aspects. there is strong evidence indicating the studies on methylation modification hold diagnostic and therapeutic value. Methylation signatures of cell free DNA *via* a non-invasive method can be tested for the identification of pre-neoplastic lesions and PC, assisting early diagnosis (129). At the present, this assay is only limited to DNA methylation, not for RNA or histone methylation because of the lack of detection technologies that analyze global methylation spectrum of RNAs or histones. The possibility in future of screening techniques detecting all of DNA, histone and RNA methylation will evidently assist the disease diagnosis. Some of methylation readers such as IGF2BP2 could serve as a diagnostic marker since its expression is significantly elevated in PanIN. Almost all regulators are reported to be independent prognosis indicators and are correlated with clinical outcomes. In addition, the therapeutic application has recently received significant attention, as those epigenetic regulators can be potential targets for anti-cancer therapy. Distinct inhibitors of epigenetic enzymes mainly targeting at DNA methyltransferases (DNMTs), histone methyltransferases (HMTs) and histone demethylases (HDMs) exhibit strong ability to interfere histone and DNA methylation process, thus some of these inhibitors have been used in clinical trials. Meanwhile, there have been many clinical studies on methylation in liver cancer, colorectal cancer which can provide ideas for the treatment of PC. Therefore, the discovery of methylation mechanisms and development of advanced technologies will be beneficial to the clinical diagnosis and treatment.

In conclusion, with recently intense focus on epigenetic methylation of varied key molecules that mediate pathogenesis of PC, the novel discovery including aberrant expression of dysfunctional factors as potential biomarkers, therapeutic targets, and methylation blockers will offer great value to assist the early diagnosis, prediction of recurrence and prognosis, and targeted therapy of PC. For example, many studies have identified the sensitivity and specificity of single locus promoter methylation in

tissue of PC, however, substantial large sample volume from multiple cancer centers with a variety of disease stages is essential to firmly establish the specific methylated single locus as a diagnostic or prognostic marker for PC. As the heterogeneity of PC, multigene methylations that regulate distinct signaling pathways in individual components of the tumor microenvironment coordinately promote the malignant transformation of PC. Therefore, the growing research will give rise to solid evidence favorable to lay the foundation of creating novel means to treat this lethal disorder. As expected, revealing the methylation function will encourage researchers to extensively focus on the mechanistic study, ultimately offering both potential biomarkers valuable for diagnosis and therapeutic strategy to treat this devastated disorder.

AUTHOR CONTRIBUTIONS

YZ, MY, and SW drafted the manuscript. JZ and YSL coordinated and edited the drafting of the manuscript. SJA, RS, and YBL revised and edited the final version of the manuscript. All authors contributed to the article and approved the submitted version.

FUNDING

This work was supported by the National Natural Science Foundation of China (32130036, 81874181).

REFERENCES

1. Sung H, Ferlay J, Siegel RL, Laversanne M, Soerjomataram I, Jemal A, et al. Global Cancer Statistics 2020: GLOBOCAN Estimates of Incidence and Mortality Worldwide for 36 Cancers in 185 Countries. *CA Cancer J Clin* (2021) 71(3):209–49. doi: 10.3322/caac.21660
2. Mizrahi JD, Surana R, Valle JW, Shroff RT. Pancreatic Cancer. *Lancet* (2020) 395(10242):2008–20. doi: 10.1016/s0140-6736(20)30974-0
3. Wu W, Wang X, Wu X, Li M, Weng H, Cao Y, et al. Total Mesopancreas Excision for Pancreatic Head Cancer: Analysis of 120 Cases. *Chin J Cancer Res* (2016) 28(4):423–8. doi: 10.21147/j.issn.1000-9604.2016.04.05
4. Gao Y, Chen MK, Chu YY, Yang L, Yu D, Liu Y, et al. Nuclear Translocation of the Receptor Tyrosine Kinase C-MET Reduces the Treatment Efficacies of Olaparib and Gemcitabine in Pancreatic Ductal Adenocarcinoma Cells. *Am J Cancer Res* (2021) 11(1):236–50.
5. Liu Y. Emphasis on Radical Pancreatic Cancer Resection Approach. *Chin J Gen Surg* (2018) 33(06):449–51. doi: 10.3760/cma.j.issn.1007-631X.2018.06.001
6. Liu Y, Li Y, Wang X. Application and Progress of Total Mesopancrease Excision in Radical Resection of Pancreatic Head Cancer. *J Abdom Surg* (2019) 32(5):315–318,323. doi: 10.3969/j.issn.1003-5591.2019.05.001
7. Azizian A, Rühlmann F, Krause T, Bernhardt M, Jo P, König A, et al. CA19-9 for Detecting Recurrence of Pancreatic Cancer. *Sci Rep* (2020) 10(1):1332. doi: 10.1038/s41598-020-57930-x
8. Su SB, Qin SY, Chen W, Luo W, Jiang HX. Carbohydrate Antigen 19-9 for Differential Diagnosis of Pancreatic Carcinoma and Chronic Pancreatitis. *World J Gastroenterol* (2015) 21(14):4323–33. doi: 10.3748/wjg.v21.i14.4323
9. Brune K, Hong SM, Li A, Yachida S, Abe T, Griffith M, et al. Genetic and Epigenetic Alterations of Familial Pancreatic Cancers. *Cancer Epidemiol Biomarkers Prev* (2008) 17(12):3536–42. doi: 10.1158/1055-9965.Epi-08-0630
10. Biswas S, Rao CM. Epigenetic Tools (the Writers, the Readers and the Erasers) and Their Implications in Cancer Therapy. *Eur J Pharmacol* (2018) 837:8–24. doi: 10.1016/j.ejphar.2018.08.021
11. Portela A, Esteller M. Epigenetic Modifications and Human Disease. *Nat Biotechnol* (2010) 28(10):1057–68. doi: 10.1038/nbt.1685
12. Gotoh M, Arai E, Wakai-Ushijima S, Hiraoka N, Kosuge T, Hosoda F, et al. Diagnosis and Prognostication of Ductal Adenocarcinomas of the Pancreas Based on Genome-Wide DNA Methylation Profiling by Bacterial Artificial Chromosome Array-Based Methylated Cpg Island Amplification. *J BioMed Biotechnol* (2011) 2011:780836. doi: 10.1155/2011/780836
13. Goyal R, Rathert P, Laser H, Gowher H, Jeltsch A. Phosphorylation of Serine-515 Activates the Mammalian Maintenance Methyltransferase Dnmt1. *Epigenetics* (2007) 2(3):155–60. doi: 10.4161/epi.2.3.4768
14. Zhang J-J, Zhu Y, Zhu Y, Wu J-L, Liang W-B, Zhu R, et al. Association of Increased DNA Methyltransferase Expression With Carcinogenesis and Poor Prognosis in Pancreatic Ductal Adenocarcinoma. *Clin Trans Oncol* (2012) 14(2):116–24. doi: 10.1007/s12094-012-0770-x
15. Wang W, Gao J, Man XH, Li ZS, Gong YF. Significance of DNA Methyltransferase-1 and Histone Deacetylase-1 in Pancreatic Cancer. *Oncol Rep* (2009) 21(6):1439–47. doi: 10.3892/or_00000372
16. Hong L, Sun G, Peng L, Tu Y, Wan Z, Xiong H, et al. The Interaction Between Mir−148a and DNMT1 Suppresses Cell Migration and Invasion by Reactivating Tumor Suppressor Genes in Pancreatic Cancer. *Oncol Rep* (2018) 40(5):2916–25. doi: 10.3892/or.2018.6700
17. Xie VK, Li Z, Yan Y, Jia Z, Zuo X, Ju Z, et al. DNA-Methyltransferase 1 Induces Dedifferentiation of Pancreatic Cancer Cells Through Silencing of Krüppel-Like Factor 4 Expression. *Clin Cancer Res* (2017) 23(18):5585–97. doi: 10.1158/1078-0432.Ccr-17-0387
18. Zagorac S, Alcala S, Fernandez Bayon G, Bou Kheir T, Schoenhals M, González-Neira A, et al. DNMT1 Inhibition Reprograms Pancreatic Cancer Stem Cells *via* Upregulation of the Mir-17-92 Cluster. *Cancer Res* (2016) 76 (15):4546–58. doi: 10.1158/0008-5472.Can-15-3268
19. Wang L, Mu N, Qu N. Methylation of the Mir−29b−3p Promoter Contributes to Angiogenesis, Invasion, and Migration in Pancreatic Cancer. *Oncol Rep* (2021) 45(1):65–72. doi: 10.3892/or.2020.7832
20. Huang MH, Chou YW, Li MH, Shih TE, Lin SZ, Chuang HM, et al. Epigenetic Targeting DNMT1 of Pancreatic Ductal Adenocarcinoma Using Interstitial Control Release Biodegrading Polymer Reduced Tumor Growth Through Hedgehog Pathway Inhibition. *Pharmacol Res* (2019) 139:50–61. doi: 10.1016/j.phrs.2018.10.015
21. Lyko F. The DNA Methyltransferase Family: A Versatile Toolkit for Epigenetic Regulation. *Nat Rev Genet* (2018) 19(2):81–92. doi: 10.1038/nrg.2017.80
22. Jing W, Song N, Liu Y, Qu X, Hou K, Yang X, et al. DNA Methyltransferase 3a Modulates Chemosensitivity to Gemcitabine and Oxaliplatin *via* CHK1 and AKT in P53−Deficient Pancreatic Cancer Cells. *Mol Med Rep* (2018) 17 (1):117–24. doi: 10.3892/mmr.2017.7923
23. Jing W, Song N, Liu YP, Qu XJ, Qi YF, Li C, et al. DNMT3a Promotes Proliferation by Activating the STAT3 Signaling Pathway and Depressing Apoptosis in Pancreatic Cancer. *Cancer Manag Res* (2019) 11:6379–96. doi: 10.2147/cmar.S201610
24. Wang LH, Huang J, Wu CR, Huang LY, Cui J, Xing ZZ, et al. Downregulation of Mir−29b Targets DNMT3b to Suppress Cellular Apoptosis and Enhance Proliferation in Pancreatic Cancer. *Mol Med Rep* (2018) 17(2):2113–20. doi: 10.3892/mmr.2017.8145
25. Aapola U, Kawasaki K, Scott HS, Ollila J, Vihinen M, Heino M, et al. Isolation and Initial Characterization of a Novel Zinc Finger Gene, DNMT3L, on 21q22.3, Related to the Cytosine-5-Methyltransferase 3 Gene Family. *Genomics* (2000) 65(3):293–8. doi: 10.1006/geno.2000.6168
26. Hata K, Okano M, Lei H, Li E. Dnmt3L Cooperates With the Dnmt3 Family of *De Novo* DNA Methyltransferases to Establish Maternal Imprints in Mice. *Development* (2002) 129(8):1983–93. doi: 10.1242/dev.129.8.1983

27. Bray JK, Dawlaty MM, Verma A, Maitra A. Roles and Regulations of TET Enzymes in Solid Tumors. *Trends Cancer* (2021) 7(7):635–46. doi: 10.1016/j.trecan.2020.12.011
28. Ito S, Shen L, Dai Q, Wu SC, Collins LB, Swenberg JA, et al. Tet Proteins can Convert 5-Methylcytosine to 5-Formylcytosine and 5-Carboxylcytosine. *Science* (2011) 333(6047):1300–3. doi: 10.1126/science.1210597
29. Wu J, Li H, Shi M, Zhu Y, Ma Y, Zhong Y, et al. TET1-Mediated DNA Hydroxymethylation Activates Inhibitors of the Wnt/β-Catenin Signaling Pathway to Suppress EMT in Pancreatic Tumor Cells. *J Exp Clin Cancer Res* (2019) 38(1):348. doi: 10.1186/s13046-019-1334-5
30. Fujikura K, Alruwaii ZI, Haffner MC, Trujillo MA, Roberts NJ, Hong SM, et al. Downregulation of 5-Hydroxymethylcytosine Is an Early Event in Pancreatic Tumorigenesis. *J Pathol* (2021) 254(3):279–88. doi: 10.1002/path.5682
31. Schübeler D. Function and Information Content of DNA Methylation. *Nature* (2015) 517(7534):321–6. doi: 10.1038/nature14192
32. Du Q, Luu PL, Stirzaker C, Clark SJ. Methyl-Cpg-Binding Domain Proteins: Readers of the Epigenome. *Epigenomics* (2015) 7(6):1051–73. doi: 10.2217/epi.15.39
33. Prokhortchouk A, Hendrich B, Jørgensen H, Ruzov A, Wilm M, Georgiev G, et al. The P120 Catenin Partner Kaiso Is a DNA Methylation-Dependent Transcriptional Repressor. *Genes Dev* (2001) 15(13):1613–8. doi: 10.1101/gad.198501
34. Sidhu H, Capalash N. UHRF1: The Key Regulator of Epigenetics and Molecular Target for Cancer Therapeutics. *Tumour Biol* (2017) 39(2):1010428317692205. doi: 10.1177/1010428317692205
35. Mahmood N, Rabbani SA. DNA Methylation Readers and Cancer: Mechanistic and Therapeutic Applications. *Front Oncol* (2019) 9:489. doi: 10.3389/fonc.2019.00489
36. Wang H, Li J, He J, Liu Y, Feng W, Zhou H, et al. Methyl-Cpg-Binding Protein 2 Drives the Furin/TGF-β1/Smad Axis to Promote Epithelial-Mesenchymal Transition in Pancreatic Cancer Cells. *Oncogenesis* (2020) 9(8):76. doi: 10.1038/s41389-020-00258-y
37. Wang H, Feng W, Chen W, He J, Min J, Liu Y, et al. Methyl-Cpg-Binding Domain 3 Inhibits Stemness of Pancreatic Cancer Cells *via* Hippo Signaling. *Exp Cell Res* (2020) 393(1):112091. doi: 10.1016/j.yexcr.2020.112091
38. Vaughan RM, Rothbart SB, Dickson BM. The Finger Loop of the SRA Domain in the E3 Ligase UHRF1 Is a Regulator of Ubiquitin Targeting and Is Required for the Maintenance of DNA Methylation. *J Biol Chem* (2019) 294(43):15724–32. doi: 10.1074/jbc.RA119.010160
39. Vaughan RM, Dickson BM, Cornett EM, Harrison JS, Kuhlman B, Rothbart SB. Comparative Biochemical Analysis of UHRF Proteins Reveals Molecular Mechanisms That Uncouple UHRF2 From DNA Methylation Maintenance. *Nucleic Acids Res* (2018) 46(9):4405–16. doi: 10.1093/nar/gky151
40. Li T, Wang L, Du Y, Xie S, Yang X, Lian F, et al. Structural and Mechanistic Insights Into UHRF1-Mediated DNMT1 Activation in the Maintenance DNA Methylation. *Nucleic Acids Res* (2018) 46(6):3218–31. doi: 10.1093/nar/gky104
41. Xue B, Zhao J, Feng P, Xing J, Wu H, Li Y. Epigenetic Mechanism and Target Therapy of UHRF1 Protein Complex in Malignancies. *Onco Targets Ther* (2019) 12:549–59. doi: 10.2147/ott.S192234
42. Hu Q, Qin Y, Ji S, Xu W, Liu W, Sun Q, et al. UHRF1 Promotes Aerobic Glycolysis and Proliferation *via* Suppression of SIRT4 in Pancreatic Cancer. *Cancer Lett* (2019) 452:226–36. doi: 10.1016/j.canlet.2019.03.024
43. Abu-Alainin W, Gana T, Liloglou T, Olayanju A, Barrera LN, Ferguson R, et al. UHRF1 Regulation of the Keap1-Nrf2 Pathway in Pancreatic Cancer Contributes to Oncogenesis. *J Pathol* (2016) 238(3):423–33. doi: 10.1002/path.4665
44. Hudson NO, Buck-Koehntop BA. Zinc Finger Readers of Methylated DNA. *Molecules* (2018) 23(10):2555. doi: 10.3390/molecules23102555
45. Jones J, Mukherjee A, Karanam B, Davis M, Jaynes J, Reams RR, et al. African Americans With Pancreatic Ductal Adenocarcinoma Exhibit Gender Differences in Kaiso Expression. *Cancer Lett* (2016) 380(2):513–22. doi: 10.1016/j.canlet.2016.06.025
46. Hashimoto H, Wang D, Steves AN, Jin P, Blumenthal RM, Zhang X, et al. Distinctive Klf4 Mutants Determine Preference for DNA Methylation Status. *Nucleic Acids Res* (2016) 44(21):10177–85. doi: 10.1093/nar/gkw774
47. Yan Y, Li Z, Kong X, Jia Z, Zuo X, Gagea M, et al. KLF4-Mediated Suppression of CD44 Signaling Negatively Impacts Pancreatic Cancer Stemness and Metastasis. *Cancer Res* (2016) 76(8):2419–31. doi: 10.1158/0008-5472.Can-15-1691
48. Tan M, Shen L, Hou Y. Epigenetic Modification of BDNF Mediates Neuropathic Pain *via* Mir-30a-3p/EP300 Axis in CCI Rats. *Biosci Rep* (2020) 40(11):BSR20194442. doi: 10.1042/bsr20194442
49. Liu XY, Guo CH, Xi ZY, Xu XQ, Zhao QY, Li LS, et al. Histone Methylation in Pancreatic Cancer and Its Clinical Implications. *World J Gastroenterol* (2021) 27(36):6004–24. doi: 10.3748/wjg.v27.i36.6004
50. Bottino C, Peserico A, Simone C, Caretti G. SMYD3: An Oncogenic Driver Targeting Epigenetic Regulation and Signaling Pathways. *Cancers (Basel)* (2020) 12(1):142. doi: 10.3390/cancers12010142
51. Zhu CL, Huang Q. Overexpression of the SMYD3 Promotes Proliferation, Migration, and Invasion of Pancreatic Cancer. *Dig Dis Sci* (2020) 65(2):489–99. doi: 10.1007/s10620-019-05797-y
52. Peserico A, Germani A, Sanese P, Barbosa AJ, Di Virgilio V, Fittipaldi R, et al. A Smyd3 Small-Molecule Inhibitor Impairing Cancer Cell Growth. *J Cell Physiol* (2015) 230(10):2447–60. doi: 10.1002/jcp.24975
53. Jin X, Yang C, Fan P, Xiao J, Zhang W, Zhan S, et al. CDK5/FBW7-Dependent Ubiquitination and Degradation of EZH2 Inhibits Pancreatic Cancer Cell Migration and Invasion. *J Biol Chem* (2017) 292(15):6269–80. doi: 10.1074/jbc.M116.764407
54. Zhou X, Gao W, Hua H, Ji Z. LncRNA-BLACAT1 Facilitates Proliferation, Migration and Aerobic Glycolysis of Pancreatic Cancer Cells by Repressing CDKN1C *via* EZH2-Induced H3k27me3. *Front Oncol* (2020) 10:539805:539805. doi: 10.3389/fonc.2020.539805
55. Ma J, Zhang J, Weng YC, Wang JC. EZH2-Mediated MicroRNA-139-5p Regulates Epithelial-Mesenchymal Transition and Lymph Node Metastasis of Pancreatic Cancer. *Mol Cells* (2018) 41(9):868–80. doi: 10.14348/molcells.2018.0109
56. Avan A, Crea F, Paolicchi E, Funel N, Galvani E, Marquez VE, et al. Molecular Mechanisms Involved in the Synergistic Interaction of the EZH2 Inhibitor 3-Deazaneplanocin a With Gemcitabine in Pancreatic Cancer Cells. *Mol Cancer Ther* (2012) 11(8):1735–46. doi: 10.1158/1535-7163.Mct-12-0037
57. Wang Y, Sun L, Luo Y, He S. Knockdown of KDM1B Inhibits Cell Proliferation and Induces Apoptosis of Pancreatic Cancer Cells. *Pathol Res Pract* (2019) 215(5):1054–60. doi: 10.1016/j.prp.2019.02.014
58. Tzatsos A, Paskaleva P, Ferrari F, Deshpande V, Stoykova S, Contino G, et al. KDM2B Promotes Pancreatic Cancer *via* Polycomb-Dependent and -Independent Transcriptional Programs. *J Clin Invest* (2013) 123(2):727–39. doi: 10.1172/jci64535
59. Dandawate P, Ghosh C, Palaniyandi K, Paul S, Rawal S, Pradhan R, et al. The Histone Demethylase KDM3A, Increased in Human Pancreatic Tumors, Regulates Expression of DCLK1 and Promotes Tumorigenesis in Mice. *Gastroenterology* (2019) 157(6):1646–59.e11. doi: 10.1053/j.gastro.2019.08.018
60. Bailey JM, Alsina J, Rasheed ZA, Mcallister FM, Fu YY, Plentz R, et al. DCLK1 Marks a Morphologically Distinct Subpopulation of Cells With Stem Cell Properties in Preinvasive Pancreatic Cancer. *Gastroenterology* (2014) 146(1):245–56. doi: 10.1053/j.gastro.2013.09.050
61. Hanna S, Etzioni A. MHC Class I and II Deficiencies. *J Allergy Clin Immunol* (2014) 134(2):269–75. doi: 10.1016/j.jaci.2014.06.001
62. Ding G, Xu X, Li D, Chen Y, Wang W, Ping D, et al. Fisetin Inhibits Proliferation of Pancreatic Adenocarcinoma by Inducing DNA Damage *via* RFXAP/KDM4A-Dependent Histone H3K36 Demethylation. *Cell Death Dis* (2020) 11(10):893. doi: 10.1038/s41419-020-03019-2
63. Li S, Wu L, Wang Q, Li Y, Wang X. KDM4B Promotes Epithelial-Mesenchymal Transition Through Up-Regulation of ZEB1 in Pancreatic Cancer. *Acta Biochim Biophys Sin (Shanghai)* (2015) 47(12):997–1004. doi: 10.1093/abbs/gmv107
64. Zhang Y, Xu L, Li A, Han X. The Roles of ZEB1 in Tumorigenic Progression and Epigenetic Modifications. *BioMed Pharmacother* (2019) 110:400–8. doi: 10.1016/j.biopha.2018.11.112
65. Isohookana J, Haapasaari KM, Soini Y, Karihtala P. KDM4D Predicts Recurrence in Exocrine Pancreatic Cells of Resection Margins From

Patients With Pancreatic Adenocarcinoma. *Anticancer Res* (2018) 38 (4):2295–302. doi: 10.21873/anticanres.12474
66. Yamamoto K, Tateishi K, Kudo Y, Sato T, Yamamoto S, Miyabayashi K. Loss of Histone Demethylase KDM6B Enhances Aggressiveness of Pancreatic Cancer Through Downregulation of C/Ebpα. *Carcinogenesis* (2014) 35 (11):2404–14. doi: 10.1093/carcin/bgu136
67. Cui J, Quan M, Xie D, Gao Y, Guha S, Fallon MB, et al. A Novel KDM5A/MPC-1 Signaling Pathway Promotes Pancreatic Cancer Progression *via* Redirecting Mitochondrial Pyruvate Metabolism. *Oncogene* (2020) 39 (5):1140–51. doi: 10.1038/s41388-019-1051-8
68. Song C, Chen T, He L, Ma N, Li JA, Rong YF, et al. PRMT1 Promotes Pancreatic Cancer Growth and Predicts Poor Prognosis. *Cell Oncol (Dordr)* (2020) 43(1):51–62. doi: 10.1007/s13402-019-00435-1
69. Farooqi AA, Nayyab S, Martinelli C, Berardi R, Katifelis H, Gazouli M, et al. Regulation of Hippo, Tgfβ/Smad, Wnt/β-Catenin, JAK/STAT, and NOTCH by Long Non-Coding RNAs in Pancreatic Cancer. *Front Oncol* (2021) 11:657965. doi: 10.3389/fonc.2021.657965
70. Kim H, Ronai ZA. PRMT5 Function and Targeting in Cancer. *Cell Stress* (2020) 4(8):199–215. doi: 10.15698/cst2020.08.228
71. Ge L, Wang H, Xu X, Zhou Z, He J, Peng W, et al. PRMT5 Promotes Epithelial-Mesenchymal Transition *via* EGFR-β-Catenin Axis in Pancreatic Cancer Cells. *J Cell Mol Med* (2020) 24(2):1969–79. doi: 10.1111/jcmm.14894
72. Qin Y, Hu Q, Xu J, Ji S, Dai W, Liu W, et al. PRMT5 Enhances Tumorigenicity and Glycolysis in Pancreatic Cancer *via* the FBW7/Cmyc Axis. *Cell Commun Signal* (2019) 17(1):30. doi: 10.1186/s12964-019-0344-4
73. Driehuis E, Van Hoeck A, Moore K, Kolders S, Francies HE, Gulersonmez MC, et al. Pancreatic Cancer Organoids Recapitulate Disease and Allow Personalized Drug Screening. *Proc Natl Acad Sci USA* (2019) 116 (52):26580–90. doi: 10.1073/pnas.1911273116
74. Zhang J, Jing L, Li M, He L, Guo Z. Regulation of Histone Arginine Methylation/Demethylation by Methylase and Demethylase (Review). *Mol Med Rep* (2019) 19(5):3963–71. doi: 10.3892/mmr.2019.10111
75. Li YL, Yu J, Song SH. [Recent Progresses in RNA N6-Methyladenosine Research]. *Yi Chuan* (2013) 35(12):1340–51. doi: 10.3724/sp.j.1005.2013.01340
76. Wang X, Lu Z, Gomez A, Hon GC, Yue Y, Han D, et al. N6-Methyladenosine-Dependent Regulation of Messenger RNA Stability. *Nature* (2014) 505(7481):117–20. doi: 10.1038/nature12730
77. Fustin JM, Doi M, Yamaguchi Y, Hida H, Nishimura S, Yoshida M, et al. RNA-Methylation-Dependent RNA Processing Controls the Speed of the Circadian Clock. *Cell* (2013) 155(4):793–806. doi: 10.1016/j.cell.2013.10.026
78. Molinie B, Wang J, Lim KS, Hillebrand R, Lu ZX, Van Wittenberghe N, et al. M(6)a-LAIC-Seq Reveals the Census and Complexity of the M(6)a Epitranscriptome. *Nat Methods* (2016) 13(8):692–8. doi: 10.1038/nmeth.3898
79. Meyer KD, Patil DP, Zhou J, Zinoviev A, Skabkin MA, Elemento O, et al. 5' UTR M(6)a Promotes Cap-Independent Translation. *Cell* (2015) 163 (4):999–1010. doi: 10.1016/j.cell.2015.10.012
80. Merkurjev D, Hong WT, Iida K, Oomoto I, Goldie BJ, Yamaguti H, et al. Synaptic N(6)-Methyladenosine (M(6)a) Epitranscriptome Reveals Functional Partitioning of Localized Transcripts. *Nat Neurosci* (2018) 21 (7):1004–14. doi: 10.1038/s41593-018-0173-6
81. Bertero A, Brown S, Madrigal P, Osnato A, Ortmann D, Yiangou L, et al. The SMAD2/3 Interactome Reveals That Tgfβ Controls M(6)a mRNA Methylation in Pluripotency. *Nature* (2018) 555(7695):256–9. doi: 10.1038/nature25784
82. Barbieri I, Tzelepis K, Pandolfini L, Shi J, Millán-Zambrano G, Robson SC, et al. Promoter-Bound METTL3 Maintains Myeloid Leukaemia by M(6)a-Dependent Translation Control. *Nature* (2017) 552(7683):126–31. doi: 10.1038/nature24678
83. Lin S, Choe J, Du P, Triboulet R, Gregory RI, et al. The M(6)a Methyltransferase METTL3 Promotes Translation in Human Cancer Cells. *Mol Cell* (2016) 62(3):335–45. doi: 10.1016/j.molcel.2016.03.021
84. Xia T, Wu X, Cao M, Zhang P, Shi G, Zhang J, et al. The RNA M6a Methyltransferase METTL3 Promotes Pancreatic Cancer Cell Proliferation and Invasion. *Pathol Res Pract* (2019) 215(11):152666. doi: 10.1016/j.prp.2019.152666
85. Taketo K, Konno M, Asai A, Koseki J, Toratani M, Satoh T, et al. The Epitranscriptome M6a Writer METTL3 Promotes Chemo- and Radioresistance in Pancreatic Cancer Cells. *Int J Oncol* (2018) 52(2):621–9. doi: 10.3892/ijo.2017.4219
86. Wang P, Doxtader KA, Nam Y. Structural Basis for Cooperative Function of Mettl3 and Mettl14 Methyltransferases. *Mol Cell* (2016) 63(2):306–17. doi: 10.1016/j.molcel.2016.05.041
87. Wang M, Liu J, Zhao Y, He R, Xu X, Guo X, et al. Upregulation of METTL14 Mediates the Elevation of PERP mRNA N(6) Adenosine Methylation Promoting the Growth and Metastasis of Pancreatic Cancer. *Mol Cancer* (2020) 19(1):130. doi: 10.1186/s12943-020-01249-8
88. Kong F, Liu X, Zhou Y, Hou X, He J, Li Q, et al. Downregulation of METTL14 Increases Apoptosis and Autophagy Induced by Cisplatin in Pancreatic Cancer Cells. *Int J Biochem Cell Biol* (2020) 122:105731. doi: 10.1016/j.biocel.2020.105731
89. Ping XL, Sun BF, Wang L, Xiao W, Yang X, Wang WJ, et al. Mammalian WTAP Is a Regulatory Subunit of the RNA N6-Methyladenosine Methyltransferase. *Cell Res* (2014) 24(2):177–89. doi: 10.1038/cr.2014.3
90. Li BQ, Huang S, Shao QQ, Sun J, Zhou L, You L, et al. WT1-Associated Protein Is a Novel Prognostic Factor in Pancreatic Ductal Adenocarcinoma. *Oncol Lett* (2017) 13(4):2531–8. doi: 10.3892/ol.2017.5784
91. Li BQ, Liang ZY, Seery S, Liu QF, You L, Zhang TP, et al. WT1 Associated Protein Promotes Metastasis and Chemo-Resistance to Gemcitabine by Stabilizing Fak mRNA in Pancreatic Cancer. *Cancer Lett* (2019) 451:48–57. doi: 10.1016/j.canlet.2019.02.043
92. Zheng G, Dahl JA, Niu Y, Fedorcsak P, Huang CM, Li CJ, et al. ALKBH5 Is a Mammalian RNA Demethylase That Impacts RNA Metabolism and Mouse Fertility. *Mol Cell* (2013) 49(1):18–29. doi: 10.1016/j.molcel.2012.10.015
93. He Y, Hu H, Wang Y, Yuan H, Lu Z, Wu P, et al. ALKBH5 Inhibits Pancreatic Cancer Motility by Decreasing Long Non-Coding RNA KCNK15-AS1 Methylation. *Cell Physiol Biochem* (2018) 48(2):838–46. doi: 10.1159/000491915
94. Guo X, Li K, Jiang W, Hu Y, Xiao W, Huang Y, et al. RNA Demethylase ALKBH5 Prevents Pancreatic Cancer Progression by Posttranscriptional Activation of PER1 in an M6a-YTHDF2-Dependent Manner. *Mol Cancer* (2020) 19(1):91. doi: 10.1186/s12943-020-01158-w
95. Tang B, Yang Y, Kang M, Wang Y, Wang Y, Bi Y, et al. M(6)a Demethylase ALKBH5 Inhibits Pancreatic Cancer Tumorigenesis by Decreasing WIF-1 RNA Methylation and Mediating Wnt Signaling. *Mol Cancer* (2020) 19(1):3. doi: 10.1186/s12943-019-1128-6
96. Tang X, Liu S, Chen D, Zhao Z, Zhou J. The Role of the Fat Mass and Obesity-Associated Protein in the Proliferation of Pancreatic Cancer Cells. *Oncol Lett* (2019) 17(2):2473–8. doi: 10.3892/ol.2018.9873
97. Chen J, Sun Y, Xu X, Wang D, He J, Zhou H, et al. YTH Domain Family 2 Orchestrates Epithelial-Mesenchymal Transition/Proliferation Dichotomy in Pancreatic Cancer Cells. *Cell Cycle* (2017) 16(23):2259–71. doi: 10.1080/15384101.2017.1380125
98. Dahlem C, Barghash A, Puchas P, Haybaeck J, Kessler SM. The Insulin-Like Growth Factor 2 mRNA Binding Protein IMP2/IGF2BP2 Is Overexpressed and Correlates With Poor Survival in Pancreatic Cancer. *Int J Mol Sci* (2019) 20(13):3204. doi: 10.3390/ijms20133204
99. Schaeffer DF, Owen DR, Lim HJ, Buczkowski AK, Chung SW, Scudamore CH, et al. Insulin-Like Growth Factor 2 mRNA Binding Protein 3 (IGF2BP3) Overexpression in Pancreatic Ductal Adenocarcinoma Correlates With Poor Survival. *BMC Cancer* (2010) 10:59. doi: 10.1186/1471-2407-10-59
100. Wan BS, Cheng M, Zhang L. Insulin-Like Growth Factor 2 mRNA-Binding Protein 1 Promotes Cell Proliferation *via* Activation of AKT and Is Directly Targeted by MicroRNA-494 in Pancreatic Cancer. *World J Gastroenterol* (2019) 25(40):6063–76. doi: 10.3748/wjg.v25.i40.6063
101. Huang S, Wu Z, Cheng Y, Wei W, Hao L. Insulin-Like Growth Factor 2 mRNA Binding Protein 2 Promotes Aerobic Glycolysis and Cell Proliferation in Pancreatic Ductal Adenocarcinoma *via* Stabilizing GLUT1 mRNA. *Acta Biochim Biophys Sin (Shanghai)* (2019) 51(7):743–52. doi: 10.1093/abbs/gmz048
102. Li J, Wang F, Liu Y, Wang H, Ni B. N(6)-Methyladenosine (M(6)a) in Pancreatic Cancer: Regulatory Mechanisms and Future Direction. *Int J Biol Sci* (2021) 17(9):2323–35. doi: 10.7150/ijbs.60115

103. Edelheit S, Schwartz S, Mumbach MR, Wurtzel O, Sorek R. Transcriptome-Wide Mapping of 5-Methylcytidine RNA Modifications in Bacteria, Archaea, and Yeast Reveals M5c Within Archaeal mRNAs. *PloS Genet* (2013) 9(6):e1003602. doi: 10.1371/journal.pgen.1003602
104. Huang W, Lan MD, Qi CB, Zheng SJ, Wei SZ, Yuan BF, et al. Formation and Determination of the Oxidation Products of 5-Methylcytosine in RNA. *Chem Sci* (2016) 7(8):5495–502. doi: 10.1039/c6sc01589a
105. Squires JE, Patel HR, Nousch M, Sibbritt T, Humphreys DT, Parker BJ, et al. Widespread Occurrence of 5-Methylcytosine in Human Coding and Non-Coding RNA. *Nucleic Acids Res* (2012) 40(11):5023–33. doi: 10.1093/nar/gks144
106. Amort T, Rieder D, Wille A, Khokhlova-Cubberley D, Riml C, Trixl L, et al. Distinct 5-Methylcytosine Profiles in Poly(a) RNA From Mouse Embryonic Stem Cells and Brain. *Genome Biol* (2017) 18(1):1. doi: 10.1186/s13059-016-1139-1
107. Trixl L, Lusser A. The Dynamic RNA Modification 5-Methylcytosine and Its Emerging Role as an Epitranscriptomic Mark. *Wiley Interdiscip Rev RNA* (2019) 10(1):e1510. doi: 10.1002/wrna.1510
108. Sharma S, Lafontaine DLJ. 'View From a Bridge': A New Perspective on Eukaryotic RRNA Base Modification. *Trends Biochem Sci* (2015) 40(10):560–75. doi: 10.1016/j.tibs.2015.07.008
109. Motorin Y, Lyko F, Helm M. 5-Methylcytosine in RNA: Detection, Enzymatic Formation and Biological Functions. *Nucleic Acids Res* (2010) 38(5):1415–30. doi: 10.1093/nar/gkp1117
110. Yuan H, Liu J, Zhao L, Wu P, Chen G, Chen Q, et al. Prognostic Risk Model and Tumor Immune Environment Modulation of M5c-Related LncRNAs in Pancreatic Ductal Adenocarcinoma. *Front Immunol* (2021) 12:800268. doi: 10.3389/fimmu.2021.800268
111. Yang R, Liang X, Wang H, Guo M, Shen H, Shi Y, et al. The RNA Methyltransferase NSUN6 Suppresses Pancreatic Cancer Development by Regulating Cell Proliferation. *EBioMedicine* (2021) 63:103195. doi: 10.1016/j.ebiom.2020.103195
112. Goll MG, Kirpekar F, Maggert KA, Yoder JA, Hsieh CL, Zhang X, et al. Methylation of Trnaasp by the DNA Methyltransferase Homolog Dnmt2. *Science* (2006) 311(5759):395–8. doi: 10.1126/science.1120976
113. Yang X, Yang Y, Sun BF, Chen YS, Xu JW, Lai WY, et al. 5-Methylcytosine Promotes mRNA Export - NSUN2 as the Methyltransferase and ALYREF as an M(5)C Reader. *Cell Res* (2017) 27(5):606–25. doi: 10.1038/cr.2017.55
114. Chen X, Li A, Sun BF, Yang Y, Han YN, Yuan X, et al. 5-Methylcytosine Promotes Pathogenesis of Bladder Cancer Through Stabilizing mRNAs. *Nat Cell Biol* (2019) 21(8):978–90. doi: 10.1038/s41556-019-0361-y
115. Zou F, Tu R, Duan B, Yang Z, Ping Z, Song X, et al. Drosophila YBX1 Homolog YPS Promotes Ovarian Germ Line Stem Cell Development by Preferentially Recognizing 5-Methylcytosine RNAs. *Proc Natl Acad Sci USA* (2020) 117(7):3603–9. doi: 10.1073/pnas.1910862117
116. Rajbhandary UL, Stuart A, Faulkner RD, Chang SH, Khorana HG. Nucleotide Sequence Studies on Yeast Phenylalanine SRNA. *Cold Spring Harb Symp Quant Biol* (1966) 31:425–34. doi: 10.1101/sqb.1966.031.01.055
117. Sharma S, Watzinger P, Kötter P, Entian KD. Identification of a Novel Methyltransferase, Bmt2, Responsible for the N-1-Methyl-Adenosine Base Modification of 25S RRNA in Saccharomyces Cerevisiae. *Nucleic Acids Res* (2013) 41(10):5428–43. doi: 10.1093/nar/gkt195
118. Dominissini D, Nachtergaele S, Moshitch-Moshkovitz S, Peer E, Kol N, Ben-Haim MS, et al. The Dynamic N(1)-Methyladenosine Methylome in Eukaryotic Messenger RNA. *Nature* (2016) 530(7591):441–6. doi: 10.1038/nature16998
119. Li X, Xiong X, Wang K, Wang L, Shu X, Ma S, et al. Transcriptome-Wide Mapping Reveals Reversible and Dynamic N(1)-Methyladenosine Methylome. *Nat Chem Biol* (2016) 12(5):311–6. doi: 10.1038/nchembio.2040
120. Safra M, Sas-Chen A, Nir R, Winkler R, Nachshon A, Bar-Yaacov D, et al. The M1a Landscape on Cytosolic and Mitochondrial mRNA at Single-Base Resolution. *Nature* (2017) 551(7679):251–5. doi: 10.1038/nature24456
121. Liu F, Clark W, Luo G, Wang X, Fu Y, Wei J, et al. ALKBH1-Mediated TRNA Demethylation Regulates Translation. *Cell* (2016) 167(3):816–28.e16. doi: 10.1016/j.cell.2016.09.038
122. Li X, Xiong X, Zhang M, Wang K, Chen Y, Zhou J, et al. Base-Resolution Mapping Reveals Distinct M(1)a Methylome in Nuclear- and Mitochondrial-Encoded Transcripts. *Mol Cell* (2017) 68(5):993–1005.e9. doi: 10.1016/j.molcel.2017.10.019
123. Ozanick S, Krecic A, Andersland J, Anderson JT. The Bipartite Structure of the TRNA M1a58 Methyltransferase From S. cerevisiae Is conserved in humans. *RNA* (2005) 11(8):1281–90. doi: 10.1261/rna.5040605
124. Vilardo E, Nachbagauer C, Buzet A, Taschner A, Holzmann J. A Subcomplex of Human Mitochondrial Rnase P Is a Bifunctional Methyltransferase–Extensive Moonlighting in Mitochondrial TRNA Biogenesis. *Nucleic Acids Res* (2012) 40(22):11583–93. doi: 10.1093/nar/gks910
125. Chujo T, Suzuki T. Trmt61B Is a Methyltransferase Responsible for 1-Methyladenosine at Position 58 of Human Mitochondrial TRNAs. *RNA* (2012) 18(12):2269–76. doi: 10.1261/rna.035600.112
126. Waku T, Nakajima Y, Yokoyama W, Nomura N, Kako K, Kobayashi A, et al. NML-Mediated RRNA Base Methylation Links Ribosomal Subunit Formation to Cell Proliferation in a P53-Dependent Manner. *J Cell Sci* (2016) 129(12):2382–93. doi: 10.1242/jcs.183723
127. Ueda Y, Ooshio I, Fusamae Y, Kitae K, Kawaguchi M, Jingushi K, et al. Alkb Homolog 3-Mediated TRNA Demethylation Promotes Protein Synthesis in Cancer Cells. *Sci Rep* (2017) 7:42271. doi: 10.1038/srep42271
128. Zheng Q, Yu X, Zhang Q, He Y, Guo W. Genetic Characteristics and Prognostic Implications of M1a Regulators in Pancreatic Cancer. . *Biosci Rep* (2021) 41(4):BSR20210337. doi: 10.1042/bsr20210337
129. Lee JS, Park SS, Lee YK, Norton JA, Jeffrey SS. Liquid Biopsy in Pancreatic Ductal Adenocarcinoma: Current Status of Circulating Tumor Cells and Circulating Tumor DNA. *Mol Oncol* (2019) 13(8):1623–50. doi: 10.1002/1878-0261.12537

Conflict of Interest: The authors declare that the research was conducted in the absence of any commercial or financial relationships that could be construed as a potential conflict of interest.

Publisher's Note: All claims expressed in this article are solely those of the authors and do not necessarily represent those of their affiliated organizations, or those of the publisher, the editors and the reviewers. Any product that may be evaluated in this article, or claim that may be made by its manufacturer, is not guaranteed or endorsed by the publisher.

frontiers in Oncology

ORIGINAL RESEARCH
published: 03 March 2022
doi: 10.3389/fonc.2022.773438

Gene Promoter-Methylation Signature as Biomarker to Predict Cisplatin-Radiotherapy Sensitivity in Locally Advanced Cervical Cancer

Carlos Contreras-Romero[1], Eloy-Andrés Pérez-Yépez[1,2], Antonio Daniel Martinez-Gutierrez[1], Alma Campos-Parra[1], Alejandro Zentella-Dehesa[3], Nadia Jacobo-Herrera[4], César López-Camarillo[5], Guillermo Corredor-Alonso[6], Jaime Martínez-Coronel[1], Mauricio Rodríguez-Dorantes[7], David Cantu de León[1] and Carlos Pérez-Plasencia[1,8]**

[1] Laboratorio de Genómica, Insituto Nacional de Cancerología, Ciudad de México, Mexico, [2] Cátedra CONACYT, Dirección de cátedras, Consejo Nacional de Ciencia y Tecnología (CONACYT), Mexico City, Mexico, [3] Programa Institucional de Cáncer de Mama, Dpto Medicina Genómica y Toxicología Ambiental, IIB, Universidad Nacional Autónoma de México (UNAM), Mexico City, Mexico, [4] Unidad de Bioquímica, Instituto Nacional de Ciencias Médicas y Nutrición Salvador Zubirán (INCMNSZ), Ciudad de México, Mexico, [5] Posgrado en Ciencias Genómicas, Universidad Autónoma de la Ciudad de México (UACM), Mexico City, Mexico, [6] Laboratorio de Patología, Hospital General de Zona #92, Ciudad Acuña, Mexico, [7] Laboratorio de Oncogenómica, Instituto Nacional de Medicina Genómica, Mexico City, Mexico, [8] Laboratorio de Genómica, Unidad de Biomedicina, FES-Iztacala, UNAM, Tlalnepantla, Mexico

Despite efforts to promote health policies focused on screening and early detection, cervical cancer continues to be one of the leading causes of mortality in women; in 2020, estimated 30,000 deaths in Latin America were reported for this type of tumor. While the therapies used to treat cervical cancer have excellent results in tumors identified in early stages, those women who are diagnosed in locally advanced and advanced stages show survival rates at 5 years of <50%. Molecular patterns associated with clinical response have been studied in patients who present resistance to treatment; none of them have reached clinical practice. It is therefore necessary to continue analyzing molecular patterns that allow us to identify patients at risk of developing resistance to conventional therapy. In this study, we analyzed the global methylation profile of 22 patients diagnosed with locally advanced cervical cancer and validated the genomic results in an independent cohort of 70 patients. We showed that BRD9 promoter region methylation and CTU1 demethylation were associated with a higher overall survival (p = 0.06) and progression-free survival (p = 0.0001), whereas DOCK8 demethylation was associated with therapy-resistant patients and a lower overall survival and progression-free survival (p = 0.025 and p = 0.0001, respectively). Our results suggest that methylation of promoter regions in specific genes may provide molecular markers associated with response to treatment in cancer; further investigation is needed.

Keywords: gene promoter methylation, chemoradioresistance, cervical cancer, biomarkers, Cisplatin-Radiotherapy sensitivity

OPEN ACCESS

Edited by:
Hailong Pei,
Soochow University, China

Reviewed by:
Beenish Rahat,
Eunice Kennedy Shriver National Institute of Child Health and Human Development (NICHD), United States
Daniel Hernández Sotelo,
Autonomous University of Guerrero, Mexico

****Correspondence:***
David Cantu de León
dfcantu@gmail.com
Carlos Pérez-Plasencia
carlos.pplas@gmail.com

Specialty section:
This article was submitted to Molecular and Cellular Oncology, a section of the journal Frontiers in Oncology

Received: *09 September 2021*
Accepted: *25 January 2022*
Published: *03 March 2022*

Citation:
Contreras-Romero C, Pérez-Yépez E-A, Martinez-Gutierrez AD, Campos-Parra A, Zentella-Dehesa A, Jacobo-Herrera N, López-Camarillo C, Corredor-Alonso G, Martínez-Coronel J, Rodríguez-Dorantes M, de León DC and Pérez-Plasencia C (2022) Gene Promoter-Methylation Signature as Biomarker to Predict Cisplatin-Radiotherapy Sensitivity in Locally Advanced Cervical Cancer. Front. Oncol. 12:773438. doi: 10.3389/fonc.2022.773438

1 INTRODUCTION

Cervical cancer (CC) is the fourth most common type of cancer in women worldwide (1). In developing countries, mainly in Latin America, about 30,000 deaths per year are caused by this disease (2). The high mortality rates are due to the fact that 50% of patients are diagnosed in locally advanced cervical cancer stages (LACC); the overall survival (OS) rate to 5 years is approximately 60% (1) and a recurrence rate from 15% to 40% (3). Conventional treatment for LACC patients consists of concomitant chemoradiotherapy. Unfortunately, treatment resistance is observed in approximately 30% of patients (4).

Treatment resistance involves several molecular alterations such as genetic mutations, dysregulated microRNAs, dysregulated long noncoding RNAs expression profiles, and epigenetic modifications (5–9). Several reports described that the aberrant DNA methylation that involves hypo- or hypermethylation is also associated with tumor progression and therapy resistance (10, 11). For example, the hypermethylation of PTEN, MYOD1, RASSF1A, APC1A, PTGS2, and VIM genes, which are associated with OS of CC patients, covered all stages (12–16). Nevertheless, the expanding knowledge about methylation profiles in patients with LACC is pertinent and is focused on the treatment resistance in these particular patients.

The goal of this study was to obtain the global methylation pattern of tumor biopsies from 92 LACC patients treated with chemoradiotherapy to identify the methylation status of specific gene promoters with predictive potential to the cisplatin-radiotherapy response. For this purpose, we analyzed the methylation profile in 22 patients and found global changes in methylation patterns in 7,957 gene promoter regions that distinguish responsive and resistant LACC patients to chemoradiation. Next, by means of bioinformatics tools, we selected promoter sequences with a CpG density higher than 60%; these regions corresponded to the promoters of the bromodomain containing 9 (BRD9), dedicator of cytokinesis 8 (DOCK8), and cytosolic thiouridylase subunit 1 (CTU1) genes. Then, promoter regions were experimentally validated by methylation-specific PCR (MSP) in an independent cohort of 70 LACC patients. Strikingly, we found a correlation between BRD9 promoter region methylation and CTU1 demethylation with complete response to chemoradiotherapy in addition to higher overall survival (OS) ($p = 0.06$) and progression-free survival (PFS) ($p = 0.0001$). Moreover, demethylation of DOCK8 promoter region was associated with patients who developed treatment resistance and lower OS and PFS ($p = 0.025$ and $p = 0.0001$, respectively). These data point to the methylation status of BRD9 CTU1 and DOCK8 as potential biomarkers for predicting survival and response to chemoradiotherapy in LACC patients.

2 MATERIAL AND METHODS

2.1 Tissue Samples

This study was approved by the Central Ethics and Scientific Committee at the National Cancer Institute in Mexico City (INCan) (015/012/ICI, CEI/961/15) and has been conducted in agreement with the ethical standards as laid down in the 1964 Declaration of Helsinki and its later amendments. A total of 92 biopsies from patients with LACC cancer were obtained. Tumor samples were collected from 2014 to 2018 by the Pathology Department, INCan, Mexico City. After confirmed diagnosis, all patients received concurrent chemoradiotherapy using cisplatin [weekly cis-diamminedichloroplatinum (II) at a dose of 40 mg/m^2] for a total of five or six cycles and radiation (external radiation and intracavitary brachytherapy, for a total dose of 64–66 Gy over 67 days) (17). The patients' therapy response was assessed according to RECIST criteria defined as follows: the disappearance of all target lesions was assigned as complete response (CR); meanwhile, patients with partial response, progressive disease, or stable disease were considered as therapy resistant (TR). The biopsies were divided into two cohorts: the first with 22 patients (12 CR and 10 TR) used as a discovery cohort to generate a microarray specific for CpG islands Array-Based Profiling of Reference-Independent Methylation Status (aPRIMES) (18); the second cohort, with 70 biopsies (40 CR and 30 TR), used for molecular data validation. The patient eligibility criteria consisted of (a) confirmed pathological diagnosis of CC stages from II-B to IV-B (LACC), (b) biopsies with a pathology report confirming more than 80% tumorous cells, (c) age range of 29–65 years, (d) high-quality DNA and RNA samples, (e) no other comorbidity, (f) no previous oncological treatment, and (g) patients able to receive the standard therapy based on concurrent chemotherapy and radiotherapy.

2.2 Nucleic Acid Extraction

The DNA extraction from the 92 biopsies was performed as follows: 20 mg of fresh tissue was placed in a Fisherbrand Bead Mill homogenizer, and 2 ml soft tissue homogenizing Mix Tube was preloaded with lysis buffer [10 mM Tris–HCl, 2 mM ethylenediaminetetraacetic acid (EDTA), 1% sodium dodecyl sulfate (SDS)]. The tissue was homogenized using the MagNA Lyser instrument at 6,000 rpm for 1 min. To purify the genomic DNA, the QIAamp DNA Blood Kit (Qiagen, CA, USA) was used according to the manufacturer's protocol. Finally, the purified DNA was stored at −20°C.

2.3 Microarray Differential Methylation Analysis (aPRIMES)

We employed the 3x720K CpG Island Plus RefSeq Promoter Arrays (Roche, Penzberg, Germany). These arrays cover the annotated CpG islands and the promoters of the RefSeq genes derived from the UCSC RefFlat files (Hg 38). Then, the hybridization probes were synthesized by aPRIMES assay. Briefly, genomic DNAs were digest by *Mse*I, and the fragments obtained were subjected to linker-mediated PCR as described by Klein and coworkers (19); later, through enzymatic digestion by methylated-sensitive and methylated-specific enzymes, we obtained a methylated and unmethylated fraction of DNA, which were labeled with Cy5 and Cy3 fluorophores, respectively, and competitive hybridizing in a Human DNA Methylation 3x720K CpG Island Plus (Roche) as shown in **Supplementary Figure 1**. Then, arrays were scanned in

an MS200 scanner (Roche). Finally, the alignment of the images and the extraction of data were carried out using the software DEVA Project Manager—1.2.1 (Roche). Next, for each region in the array, we obtained a continuous numerical ratio that represents if a region is hyper- or hypomethylated; we termed this ratio as bi-weight (BW) and is represented with the following formula:

$$BW = \frac{Log2(Cy3)}{Log2(Cy5)}$$

Finally, to determine the significative methylated regions between responsive and resistant tumors, we calculated the Student's t-test for each region between both groups and considered as statistical significance those methylated regions with a $p < 0.01$. Then, selected regions were ranked in ascending and descending orders accordingly to the difference of the means for both groups. All statistical analysis were executed in R environment.

2.4 Pathway Analysis

Differentially methylated regions were analyzed by Pathway enrichment analysis by using Webgestalt (20) and ReactomePA (21); we only considered pathways with a $p < 0.05$ as subject of regulation.

2.5 CpG Island Density Determination

We obtained from the Genome Browser database (22) a sequence of 2,000 bp (1,000 bp downstream; transcription start site, 1,000 bp upstream) that included the promoter region from each analyzed gene. These sequences were analyzed using MethPrimer web tool from Urogene to determine the CpG density (23).

2.6 Methylation-Specific PCR Assay

To determine the methylation status of selected genes (BRD9, CTU1, and DOCK8), genomic DNA from each sample was modified using Methylation-Direct EZ DNA Kit (ZYMO, CA, USA). DNA bisulfite treatment changed unmethylated cytosines to uracil, but the methylated bases remained as cytosines. Then, two PCR reactions were performed per sample using specific primers to determine the methylated (M) or unmethylated (U) DNA status. The list of primers and its characteristics are shown in **Supplementary Table S1**. The product of each reaction was analyzed in agarose gels and resolved in Minigel OWLTM Easy CastTM B2 system (Thermo Scientific, MA, USA). Later, the gel was stained with ethidium bromide and photo-documented using a Gel Doc EZ Imager transilluminator (Bio Rad, CA, USA).

2.7 Statistical Analysis

Chi-squared tests were employed to determine the differences in the distribution of the methylation status of the genes and the clinicopathological characteristics, considering $p < 0.05$ as statistically significant.

2.8 Survival Analysis

Kaplan–Meier plotter was calculated using the survival package in R, where the significance testing was assessed using the log-rank test. Significance was considered as $p < 0.05$.

3 RESULTS

3.1 Clinicopathological Characteristics of Patients

This study was approved by the Central Ethics and Scientific Committee at the National Cancer Institute in Mexico City (approval number 015/01271B/CEI/961/15). The 92 patients who were enrolled accepted and signed the informed consent. All patients received treatment based on cisplatin and radiotherapy as mentioned in *Material and Methods*. The median age was 48 years. Patients were classified following the last version of International Federation of Gynecology and Obstetrics (FIGO) staging criteria as II (51.8%), III (37%), and IV (11.2%) stages. According to the FIGO's guidelines, 52 patients (56.52%) showed complete response (CR) to therapy; meanwhile, 40 (43.48%) exhibited therapy resistance (TR). The HPV-genotype of all patients was determined by nested PCR (24). **Table 1** shows the clinicopathological characteristics; a supplementary table that compiles all clinical data is available as **Supplementary Table 2**.

3.2 Global Analysis of DNA Methylation in Locally Advanced Cervical Cancer Tumors

The determination of DNA methylation patterns has been proposed as a prognosis predictor in several types of cancer (25, 26). In this study, we employed aPRIMES arrays to obtain the genome-wide DNA methylation patterns on both groups, namely, responsive (CR) and therapy-resistant (TR) **LACC** patients. Next, to establish the differentially methylated regions (DMRs) on CR and TR groups, we compared the bi-weight ratio values from each analyzed region, using a Student's t-test. The results showed a methylated DNA profile between the two groups composed of 16,538 DMRs that corresponded to 7,957 unique regions, where 2,833 of them were hypermethylated, 5,881 were hypomethylated, and 757 regions had both hyper and hypomethylated DMRs regions ($p < 0.05$) (**Figure 1**). As expected, a global hypomethylation pattern across the genome was observed, where the distribution of these DMRs varied to a considerable extent depending on the chromosome (**Supplementary Figure S2**). We noticed that chromosomes 1 and 19 had the higher number of gene promoters with DMRs, 859 and 753, respectively (**Supplementary Figures S2**, **S3**). Next, we observed that clustering of these DMRs using the Euclidean distance algorithm could distinguish the TR (black bar) from CR LACC patients (green bar) (**Figure 1**). Since the bi-weight ratios are continuous variables, we transformed them to a Z-score to visualize the DMRs in a heatmap, which clearly shows a DNA methylation profile that includes 3,533 DMRs hypermethylated and 13,005 DRMs hypomethylated (**Figure 1**).

3.3 Gene Pathway Analysis

Furthermore, we were interested in evaluating the impact of the methylation profile in biological pathways. The gene set enrichment analysis using the Kyoto Encyclopedia of Genes and Genomes (KEGG) database revealed that multiple key carcinogenic pathways such as the PI3K-AKT signaling

TABLE 1 | Clinicopathological characteristics of LACC patients.

Clinicopathological characteristics N= 92 (%)		
Histological type		
Epidermoid	83 (90.27%)	
Adenocarcinoma	9 (9.73%)	
Clinical stage (FIGO)		
II	55 (59.78%)	Stage II: TR[a]=25.5% CR[b]=74.5%
III	27 (29.34%)	Stage III: TR= 57.1% CR=42.9
IV	10 (10.88%)	Stage IV: TR=100%
Age (29–63) years		
29-39	18 (19.56%)	
40-49	25 (27.17%)	
50-61	27 (29.34%)	
Older than 61	22 (23.93%)	
Tumor size		
≥5 cm	37	
< 5cm	55	
	Median= 4.01	
HPV genotype		
16	51 (55.43%)	
18	22 (23.91%)	
52	8 (8.69%)	
58	5 (5.46%)	
6	3 (3.26%)	
59	2 (2.17%)	
33	1 (1.08%)	

[a]*TR: percentage of patients who developed therapy resistance.*
[b]*CR: percentage of patients who had complete response to conventional treatment.*

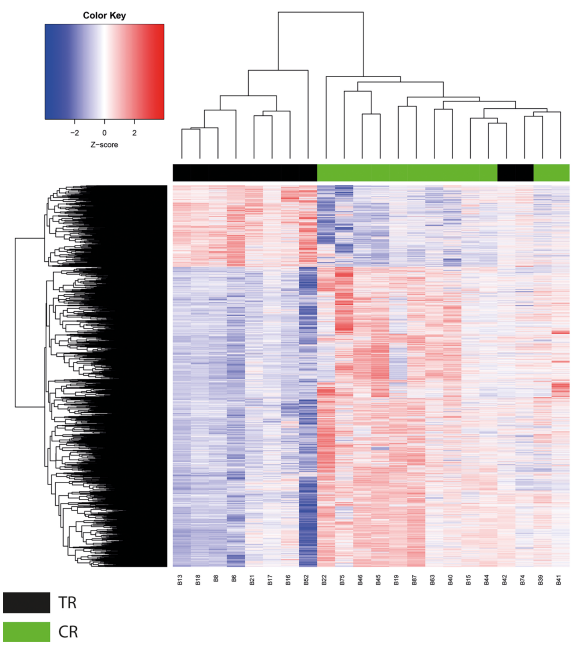

FIGURE 1 | Global methylation analysis. Unsupervised clustering analysis of 16,538 CpG regions differentially methylated between therapy resistance (TR) and complete response (CR) tumors. Red color regions represent high levels of methylation (Z score from 0 to 2), and blue color regions represent low methylation status (Z score from 0 to −2).

pathway, nuclear factor (NF)-kappa B pathway, RNA polymerase, and pathways associated with breast cancer were dysregulated as a consequence of differentially methylation profile (**Figure 2**). As the PI3K-Akt pathway was the most enriched, we focused on analyzing it in more detail. As shown in **Figure 2**, multiple key genes in this pathway were hypomethylated, including the insulin receptor substrate-1 (IRS-1) and oncogene JAK3. In contrast, genes such as RELA that inhibit the tumor growing were hypermethylated.

3.4 The Methylation Status of BRD9, CTU1, and DOCK8 Gene Promoter Regions Is Associated With Clinical Outcomes of LACC Patients

To select methylated genes as potential biomarkers of response to chemoradiation, we further narrowed the methylation profile by considering only those DMRs that showed hyper- or hypomethylation status for further analysis. The results showed 4,463 DMRs with these methylation patterns that correspond to 1,439 unique genes. Then, median bi-weight values of methylation from each gene in TR and CR tumors were compared to calculate the median difference (MD). Promoter regions with an MD upper than 1.4 times, corresponding to the 13 genes enlisted in **Table 2**, were chosen for further analysis. The promoter sequence of the selected genes was analyzed as mentioned in *Section CpG Island Density Determination*, and the three genes with highest CpG density were selected for validation. A CpG island is defined as a DNA region highest than 500 bp that contains 50% or more of CG

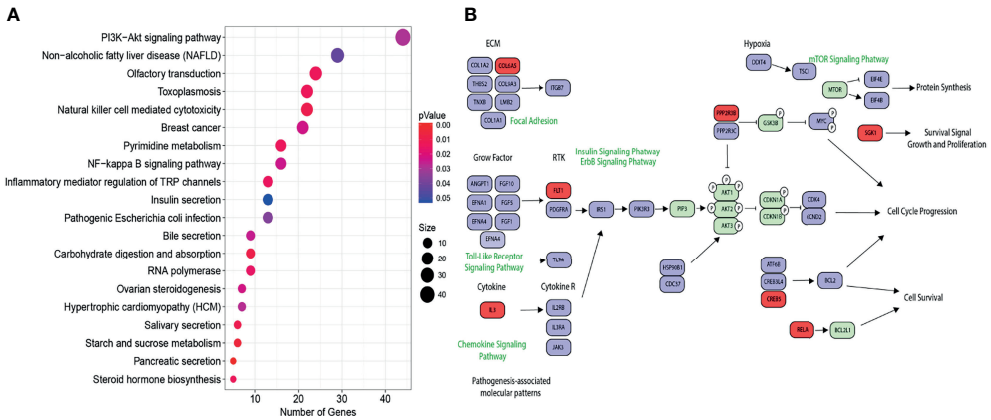

FIGURE 2 | **(A)** KEGG analysis. Signaling pathways with a $p < 0.05$ as subject of regulation by the methylated/unmethylated genes. The dot size is according to number of the related genes for each pathway. The color of the dots is represented by the range of colors from blue to red depending of the p-value. **(B)** The PI3K-AKT pathway, where blue represents hypomethylated genes and red represents hypermethylated genes.

dinucleotides (27). The promoter region of BRD9, CTU1, and DOCK8 genes showed 88%, 63%, and 90% of CpG density, respectively (**Figure 3**). Additionally, the MD for these promoter regions was 1.61, 2.25, and 1.73 for BRD9, CTU1, and DOCK8, respectively (**Figure 3**, boxplots). Interestingly, H3K4me3 mark (chromatin compaction mark) was found near to these promoter regions (**Figure 3**).

To validate the methylation levels of BRD9, DOCK8, and CTU1 promoter regions as therapy response biomarkers, an MSP assay was performed. Bisulfite-treated DNA from 30 TR and 40 CR tumors samples were used to analyze methylated status. The results showed that the BRD9 promoter region was methylated in all CR tumor samples (40 CR tumor samples, 100% of cases), whereas it was hemimethylated in 25 TR tumor samples and unmethylated in 5 TR tumor samples (83% and 17% of cases, respectively) (**Figure 4A**). Instead, the promoter region of CTU1 gene was detected to be unmethylated in all CR tumor samples (40 CR tumor samples, 100% of cases), while in 27 TR tumors samples, it was hemimethylated; in 2 TR tumor samples, it was unmethylated and only in 1 TR tumor sample that it was methylated (90%, 6.6%, and 3.4% of cases, respectively) (**Figure 4B**). On the other hand, the DOCK8 promoter region was unmethylated in 29 TR tumors samples (97% of cases), whereas in 31 CR tumors samples, it was hemimethylated, and in 9 CR tumors samples, it was unmethylated (77.5% and 22.5% of cases, respectively) (**Figure 4C**).

Additionally, a chi-square analysis was performed to compare the methylation status of BRD9, CTU1, and DOCK8 genes with demographic characteristics of LACC patients (**Table 3**). The methylation of the BRD9 gene was associated with tumor stages II and tumor size <5 cm. In contrast, unmethylation of the CTU1 promoter region gene was associate with stages II and with tumor size <5 cm. The unmethylation status of the DOCK8 promoter region showed an association with stages III–IV; however, no significant relationship was found between the methylation status of this promoter with tumor size.

TABLE 2 | Genes with the highest differential MD value.

Gen Name	MD
1. KIAA1539	2.4407
2. DCTPP1	2.3529
3. STAG3L3	2.3171
4. CTU1	2.2560
5. SLC17A7	2.2266
6. EPB41L1	1.7668
7. DOCK8	1.7396
8. PRPF40B	1.6712
9. HPS1	1.6231
10. TUBGCP2	1.6421
11. BRD9	1.6130
12. RNASEH2A	1.4513
13. SNX17	1.4315

3.5 A Gene Methylation Signature as Biomarker for Overall Survival and Progression-Free Survival in CC

Finally, we determined if the methylation status of BRD9, CTU1, and DOCK8 genes could be an OS and the PFS biomarker of LACC patients. The results showed a better OS ($p < 0.0041$) and PFS (2.28 months in the hemimethylated group, $p < 0.0001$) in patients with methylation of BRD9 promoter (**Figures 5A, D**). In contrast, worse OS ($p < 0.025$) and PFS (3.12 months in the unmethylated group $p < 0.0001$) was observed in patients with the methylation of the DOCK8 promoter (**Figures 5B, E**). Moreover, patients with a unmethylated CTU1 promoter showed a better OS and PFS (1.76 months in the hemimethylated group $p < 0.0001$) (**Figures 5C, F**). These data highlight that the methylation status of BDR9, CTU1, and DOCK8 have the potential as biomarkers of OS and PFS in LACC patients.

4 DISCUSSION

Despite global screening programs, CC remains a health problem in Latin American countries, with an estimated

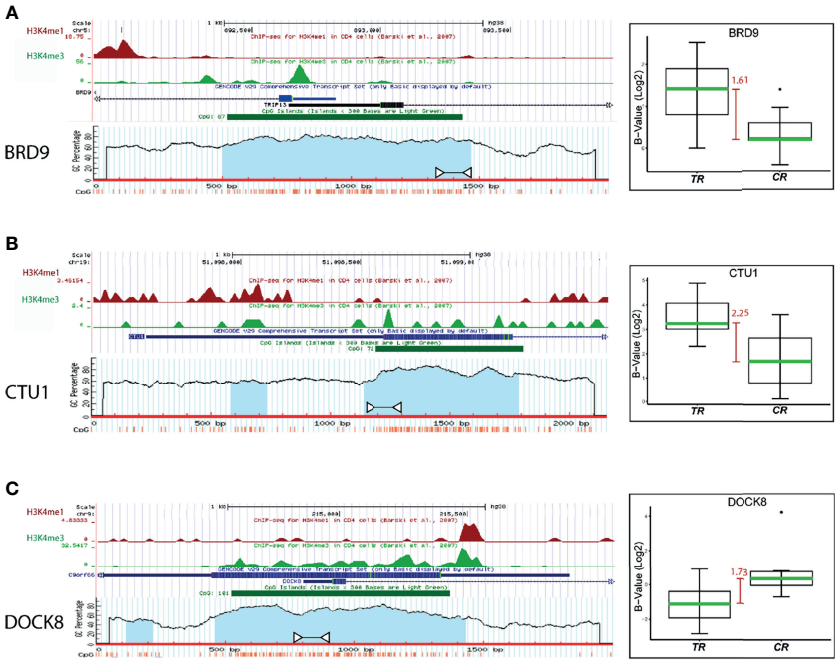

FIGURE 3 | Analysis of the promoter regions of **(A)** BRD9, **(B)** CTU1, and **(C)** DOCK8 genes. Blue bar represents the promoter region of each gene, the green bar points the CpG island location, and the blue shadow color indicates the CpG density of the island. White arrows indicate the amplification region for the MSP validation. The boxplot shows the median difference (MD, red bars) between TR and CR samples methylation levels from each promoter region.

56,000 new cases and 28,000 cervical cancer deaths (2). Unfortunately, more than 50% of CC patients are diagnosed at locally advanced stages with a 5-year survival rate of 60% (28). Epigenetic processes are crucial in cellular homeostasis, and their dysregulation leads to cancer and progression (29). DNA methylation is a tag for chromatin remodeling factors that have a crucial role in transcription regulation; DNA methylation in promoter regions is considered as a transcriptional repression mark of gene expression (30). The aberrant methylation of genes is a relevant event during carcinogenesis, which could be a diagnostic biomarker of the disease (31, 32). However, few studies are focused on associating the methylation status with the response to treatments in CC patients. Therefore, expanding knowledge about methylation profiles in patients is decisive to build knowledge focused on treatment resistance. In this regard, we aimed to find gene methylation as a biomarker of response to chemoradiotherapy in LACC. Consequently, we performed a global analysis of DNA methylation from chemoradiotherapy-responsive tumor biopsies to establish DNA methylation patterns. Hence, we identified a gene methylation profile that distinguished between responsive patients and resistance to chemoradiotherapy. As mentioned previously, prognostic biomarkers based on chemoradiotherapy-related aberrant DNA methylation are limited. However, a study in head and neck squamous cell carcinoma described a characteristic promoter methylation pattern of ZNF10, TMPRSS12, ERGIC2, and RNF215 genes, which was proposed as a biomarker of response to radiotherapy treatment (33). Another study performed in low-grade gliomas reported a consistent signature in the methylation of MGMT, MLH3, RAD21, and SMC4 promoter region predictive value for response to temozolomide (34). In breast cancer, the hypermethylation of IL15RA gene promoter induced the upregulation of genes involved in adhesion and ECM-interaction pathways correlating with the OS of patients (35). In CC, methylation patterns are used as biomarkers to distinguish between healthy and cancerous tissue (36–39). Besides, methylation of SOCS2 and hTERT promoter region was associated with early-stage tumors (40), while the methylation of the APC1A promoter was related to advanced stages (15). Therefore, methylation profiles could predict cancer stages. Elsewhere, reports indicated the role of gene methylation associated with survival, such as MYOD1 and VIM methylation status associated with more favorable disease-free survival and OS (12, 39, 41). Likewise, our results showed a correlation between the methylation status of BRD9, CTU1, and DOCK8 promoter regions with PFS, OS, and clinicopathological characteristics of LACC patients.

In the present work, we ascertained a signature to predict chemoradiotherapy response in LACC patients. This signature consisted of the methylation of the BRD9 promoter region, the unmethylation of the CTU1 gene, and the unmethylation of the promoter region of DOCK8. Fascinatingly, the methylation of the BRD9 promoter region and unmethylation of CTU1 were related to CR, and the unmethylation status of DOCK8 was

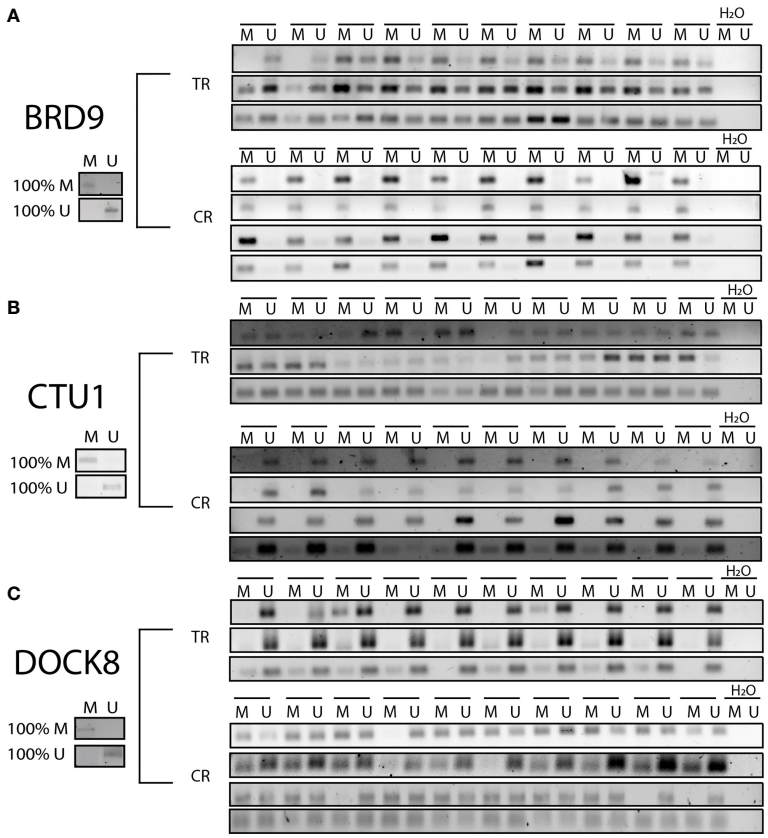

FIGURE 4 | Methylation status of BRD9, CTU1, and DOCK8 promoter regions. Products from methylation-specific PCR (MSP) assay were resolved in agarose gels. A representative gel to each evaluated gene is shows in the figure. Twenty biopsies TR and 20 CR were processed to verify the methylation (M), unmethylation (U), or hemimethylation (HM) status of promoter region to **(A)** BRD9, **(B)** CTU1, and **(C)** DOCK 8. As control for each PCR reaction, 100% methylated (100% M) and 100% unmethylated (100% U) DNA were used.

related to TR. Furthermore, the methylation signature was validated in an independent cohort, allowing us to propose it as a potential biomarker to predict the response capacity of LACC patients to chemoradiotherapy. In this regard, CpG island methylation from DNA promoter regions leads to the inactivation of genes, some of which are tumor suppressors, whereas the demethylation of those repeats elements induces the gene expression of oncogenes (5).

In our work, we detected the BRD9 gene promoter methylation pattern in CR tumors, suggesting low levels of expression of this gene, which could explain the response rates to chemoradiotherapy. The BRD9 gene encodes a protein that functions as a protein interaction module that recognizes lysine acetylation domains, a key event in the reading of epigenetic marks (40). The overexpression of this gene in lung cancer cells was associated with poor prognosis, and its oncogene role was demonstrated in synovial sarcoma (42).

In this work, we detected CTU1 unmethylated in LACC samples of patients that showed response to chemoradiotherapy and better OS. CTU1 plays a crucial role in the processing of transfer RNA by modifying nucleosides for the precise binding of the anticodon, thus guaranteeing the fidelity of the translation by the ribosome (43). However, its role in CC has not been analyzed yet, but in breast cancer, CTU1 overexpression promotes cell invasion (44). On the other hand, we found that the unmethylation of the promoter region of DOCK8 was detected in TR patients. The role of this gene is unknown in CC. Nevertheless, in a recent work, Biswas and colleagues (45) reported that DOCK8 is a gene that codifies to a nucleotide exchange factor (GEF) that activates the GTPase CdC42, participating in cell migration and invasion. In addition, it was shown acute in myeloid leukemia that its pharmacological inhibition attenuates cell survival (45).

Then, we performed a multi-pathway analysis using the differential methylation pattern established from the comparison between CR and TR tumors. The results showed dysregulated pathways such as PI3K-Akt-mTOR. This pathway regulates multiple cellular and molecular functions like cell cycle progression, cellular growth, and protein synthesis and is altered in various cancer types including CC, which are crucial for tumor initiation, invasion, and metastasis (46). These data suggested that this pathway could be hyperactivated in chemoradiotherapy-resistant LACC patients (**Figure 2**). This is

TABLE 3 | Chi-Square analysis of gene methylation status and clinical characteristics of patients.

	Methylated	**Hemi-methylated**	**Un-methylated**	***p* value**
BRD9				
Stage II	32	5	3	**0.00012**
Stage III – IV	8	20	2	
Tumor size < 5cm	30	11	2	**0.04984**
Tumor size ≥ 5cm	9	11	3	
	Methylated	**Hemi-methylated**	**Un-methylated**	***p* value**
CTU1				
Stage II	0	8	31	**0.00031**
Stage III – IV	1	20	9	
Tumor size < 5cm	0	14	29	**0.03959**
Tumor size ≥ 5cm	1	16	9	
	Methylated	**Hemi-methylated**	**Un-methylated**	***p* value**
DOCK8				
Stage II	0	25	15	**0.01189**
Stage III – IV	0	8	22	
Tumor size < 5cm	0	20	21	**0.563584**
Tumor size ≥ 5cm	0	9	16	

The bold values correspond to p value for each correlation chi-square analysis.

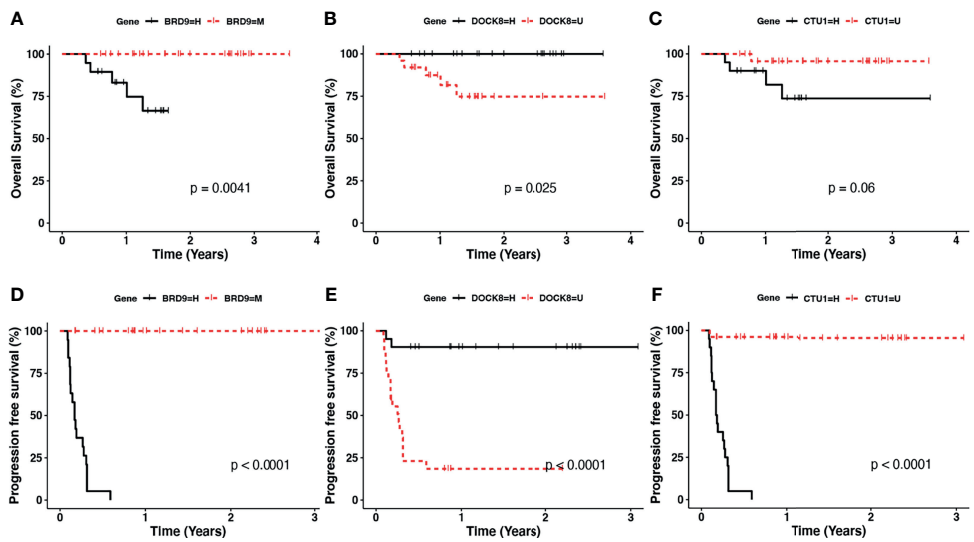

FIGURE 5 | Kaplan–Meier plotter for the methylation status of **(A, D)** BRD9, **(B, E)** DOCK8, and **(C, F)** CTU1 in the overall survival (upper panel) and progression-free survival (lower panel). Black lines correspond to hemimethylated (H) and red line to methylated (M) of analyzed gene promoter region.

the case of ovarian and breast cancers, where it was shown that hyperactivation of this pathway is related to chemoresistance and drug resistance, respectively (47, 48). There are no studies that corroborate the causality of hyperactivation of the pathway and chemoradiotherapy resistance in CC. Thus, the elucidation of molecular pathways altered by the differential methylation pattern between responsive and resistant cervical tumors remains a perspective to future studies.

In summary, this is the first study to report a molecular signature of promoter methylation of the BDR9, CTU1, and DOCK8 genes, which could distinguish LACC response patients to resistant to chemoradiotherapy. In this regard, we propose them as potential biomarkers of response to chemoradiotherapy in LACC patients. Extending this study to other cohorts and deepening the biological role of these genes are of great interest.

DATA AVAILABILITY STATEMENT

The datasets presented in this study can be found in online repositories. The names of the repository/repositories and accession number(s) can be found in the article/**Supplementary Material**.

ETHICS STATEMENT

The studies involving human participants were reviewed and approved by Ethics committees of the National Cancer Institute

of Mexico (015/012/ICI, CEI/961/15). The patients/participants provided their written informed consent to participate in this study.

AUTHOR CONTRIBUTIONS

Conceptualization, CC-R, CP-P; Experimentation CC-R, AM-G, GC-A; Analysis of results, CC-R, AM-G, E-AP-Y, AC-P, AZ-D, CP-P; Writing-Original Draft Preparation, CC-R, E-AP-Y, AM-G; Writing-Review & Editing, E-AP-Y; CP-P; AC-P, AZ-D Project Administration, CP-P; Funding Acquisition, CP-P. Clinical follow up: JMC. All authors contributed to the article and approved the submitted version

ACKNOWLEDGMENTS

This work was partially supported by Instituto Nacional de Cancerología Research Funds and CONACyT-scholarship 483149 to CRC and CONACyT-scholarship 628988 to MGAD. CC-R is a doctoral student from Programa de Doctorado en Ciencias Biológicas, Universidad Nacional Autónoma de México (UNAM) and was supported by CONACYT scholarship number 764158.

SUPPLEMENTARY MATERIAL

The Supplementary Material for this article can be found online at: https://www.frontiersin.org/articles/10.3389/fonc.2022.773438/full#supplementary-material

REFERENCES

1. Arbyn M, Weiderpass E, Bruni L, Sanjosé S, Saraiya M, Ferlay J, et al. Estimates of Incidence and Mortality of Cervical Cancer in 2018: A Worldwide Analysis. *Lancet Glob Heal* (2020) 8:e191–203. doi: 10.1016/S2214-109X(19)30482-6
2. Pilleron S, Cabasag CJ, Ferlay J, Bray F, Luciani S, Almonte M, et al. Cervical Cancer Burden in Latin America and the Caribbean: Where Are We? *Int J Cancer* (2020) 147:1638–48. doi: 10.1002/ijc.32956
3. Uppal S, Gehrig PA, Peng K, Bixel KL, Matsuo K, Vetter MH, et al. Recurrence Rates in Patients With Cervical Cancer Treated With Abdominal Versus Minimally Invasive Radical Hysterectomy: A Multi-Institutional Retrospective Review Study. *J Clin Onco* (2020) 38:1030–40. doi: 10.1200/JCO.19.03012.
4. Federico C, Sun J, Muz B, Alhallak K, Cosper PF, Muhammad N, et al. Localized Delivery of Cisplatin to Cervical Cancer Improves Its Therapeutic Efficacy and Minimizes Its Side Effect Profile. *Int J Radiat Oncol Biol Phys* (2021) 109:1483–94. doi: 10.1016/J.IJROBP.2020.11.052
5. Costello JF, Frühwald MC, Smiraglia DJ, Rush LJ, Robertson GP, Gao X, et al. Aberrant CpG-Island Methylation has Non-Random and Tumour-Type–Specific Patterns. *Nat Genet* (2000) 24(2):132–8. doi: 10.1038/72785
6. Fang J, Zhang H, Jin S. Epigenetics and Cervical Cancer: From Pathogenesis to Therapy. *Tumor Biol* (2014) 35(6):5083–93. doi: 10.1007/S13277-014-1737-Z
7. Filippova M, Filippov V, Williams VM, Zhang K, Kokoza A, Bashkirova S, et al. Cellular Levels of Oxidative Stress Affect the Response of Cervical Cancer Cells to Chemotherapeutic Agents. *BioMed Res Int* (2014) 2014:1–14. doi: 10.1155/2014/574659
8. Nahand JS, Taghizadeh-boroujeni S, Karimzadeh M, Borran S, Pourhanifeh MH, Moghoofei M, et al. microRNAs: New Prognostic, Diagnostic, and Therapeutic Biomarkers in Cervical Cancer. *J Cell Physiol* (2019) 234:17064–99. doi: 10.1002/JCP.28457
9. González-Quintana V, Palma-Berré L, Campos-Parra AD, López–Urrutia E, Peralta-Zaragoza O, Vazquez-Romo R, et al. MicroRNAs Are Involved in Cervical Cancer Development, Progression, Clinical Outcome and Improvement Treatment Response (Review). *Oncol Rep* (2016) 35:3–12. doi: 10.3892/OR.2015.4369
10. Feng C, Dong J, Chang W, Cui M, Xu T. The Progress of Methylation Regulation in Gene Expression of Cervical Cancer. *Int J Genomics* (2018) 2018:1–11. doi: 10.1155/2018/8260652
11. Lai H-C, Lin Y-W, Huang THM, Yan P, Huang R-L, Wang H-C, et al. Identification of Novel DNA Methylation Markers in Cervical Cancer. *Int J Cancer* (2008) 123:161–7. doi: 10.1002/IJC.23519
12. Cheung TH, Lo KW, Yim SF, Chan LK, Heung MS, Chan CS, et al. Epigenetic and Genetic Alternation of PTEN in Cervical Neoplasm. *Gynecol Oncol* (2004) 93:621–7. doi: 10.1016/J.YGYNO.2004.03.013
13. Lee Y, Ahn C, Han J, Choi H, Kim J, Yim J, et al. The Nuclear RNase III Drosha Initiates microRNA Processing. *Nat* (2003) 425(6956):415–9. doi: 10.1038/nature01957
14. Mitra S, Indra DM, Bhattacharya N, Singh RK, Basu PS, Mondal RK, et al. RBSP3 Is Frequently Altered in Premalignant Cervical Lesions: Clinical and Prognostic Significance. *Genes Chromosom Cancer* (2010) 49:155–70. doi: 10.1002/GCC.20726
15. Löf-Öhlin ZM, Sorbe B, Wingren S, Nilsson TK. Hypermethylation of Promoter Regions of the APC1A and P16ink4a Genes in Relation to Prognosis and Tumor Characteristics in Cervical Cancer Patients. *Int J Oncol* (2011) 39:683–8. doi: 10.3892/IJO.2011.1078
16. Widschwendter A, Gattringer C, Ivarsson L, Fiegl H, Schneitter A, Ramoni A, et al. Analysis of Aberrant DNA Methylation and Human Papillomavirus DNA in Cervicovaginal Specimens to Detect Invasive Cervical Cancer and Its Precursors. *Clin Cancer Res* (2004) 10:3396–400. doi: 10.1158/1078-0432.CCR-03-0143
17. Nicole McMillian N, Jillian Scavone M, Fisher CM, Frederick P, Gaffney DK, George S, et al. Continue NCCN Guidelines Panel Disclosures Ω Gynecologic Oncology Þ Internal Medicine † Medical Oncology § Radiotherapy/Radiation Oncology ≠ Pathology ¥ Patient Advocacy * Discussion Section Writing Committee Emily Wyse ¥ Patient Advocate. *J Nat Comprehensive Cancer Net* (2019) 17:64–84. doi: 10.6004/JNCCN.2020.0027
18. Pfister S, Schlaeger C, Mendrzyk F, Wittmann A, Benner A, Kulozik A, et al. Array-Based Profiling of Reference-Independent Methylation Status (aPRIMES) Identifies Frequent Promoter Methylation and Consecutive Downregulation of ZIC2 in Pediatric Medulloblastoma. *Nucleic Acids Res* (2007) 35:e51–1. doi: 10.1093/NAR/GKM094
19. Klein CA, Schmidt-Kittler O, Schardt JA, Pantel K, Speicher MR, Riethmüller G. Comparative Genomic Hybridization, Loss of Heterozygosity, and DNA Sequence Analysis of Single Cells. *Proc Natl Acad Sci* (1999) 96:4494–9. doi: 10.1073/PNAS.96.8.4494
20. Wang J, Vasaikar S, Shi Z, Greer M, Zhang B. WebGestalt 2017: A More Comprehensive, Powerful, Flexible and Interactive Gene Set Enrichment Analysis Toolkit. *Nucleic Acids Res* (2017) 45:W130–7. doi: 10.1093/NAR/GKX356
21. Yu G, He Q-Y. ReactomePA: An R/Bioconductor Package for Reactome Pathway Analysis and Visualization. *Mol Biosyst* (2016) 12:477–9. doi: 10.1039/C5MB00663E
22. Kent WJ, Sugnet CW, Furey TS, Roskin KM, Pringle TH, Zahler AM, et al. The Human Genome Browser at UCSC. *Genome Res* (2002) 12:996–1006. doi: 10.1101/GR.229102
23. Li L-C, Dahiya R. MethPrimer: Designing Primers for Methylation PCRs. *Bioinformatics* (2002) 18:1427–31. doi: 10.1093/bioinformatics/18.11.1427
24. Sotlar K, Diemer D, Dethleffs A, Hack Y, Stubner A, Vollmer N, et al. Detection and Typing of Human Papillomavirus by E6 Nested Multiplex PCR. *J Clin Microbiol* (2004) 42:3176. doi: 10.1128/JCM.42.7.3176-3184.2004
25. Jensen SØ, Øgaard N, Ørntoft M-BW, Rasmussen MH, Bramsen JB, Kristensen H, et al. Novel DNA Methylation Biomarkers Show High Sensitivity and Specificity for Blood-Based Detection of Colorectal Cancer—a Clinical Biomarker Discovery and Validation Study. *Clin Epigenet* (2019) 11(1):1–14. doi: 10.1186/S13148-019-0757-3
26. Fukushige S, Horii A. DNA Methylation in Cancer: A Gene Silencing Mechanism and the Clinical Potential of Its Biomarkers. *Tohoku J Exp Med* (2013) 229:173–85. doi: 10.1620/TJEM.229.173
27. Gardiner-Garden M, Frommer M. CpG Islands in Vertebrate Genomes. *J Mol Biol* (1987) 196:261–82. doi: 10.1016/0022-2836(87)90689-9

28. Naga Ch P, Gurram L, Chopra S, Mahantshetty U. The Management of Locally Advanced Cervical Cancer. *Curr Opin Oncol* (2018) 30:323–9. doi: 10.1097/CCO.0000000000000471
29. Momparler RL. Cancer Epigenetics. *Oncogene* (2003) 22(42):6479–83. doi: 10.1038/sj.onc.1206774
30. Jones PA, Baylin SB. The Epigenomics of Cancer. *Cell* (2007) 128:683–92. doi: 10.1016/J.CELL.2007.01.029
31. Paska AV, Hudler P. Aberrant Methylation Patterns in Cancer: A Clinical View. *Biochem Med* (2015) 25:161–76. doi: 10.11613/BM.2015.017
32. Belinsky SA, Nikula KJ, Palmisano WA, Michels R, Saccomanno G, Gabrielson E, et al. Aberrant Methylation of P16ink4a Is an Early Event in Lung Cancer and a Potential Biomarker for Early Diagnosis. *Proc Natl Acad Sci* (1998) 95:11891–6. doi: 10.1073/PNAS.95.20.11891
33. Ma J, Li R, Wang J. Characterization of a Prognostic Four−Gene Methylation Signature Associated With Radiotherapy for Head and Neck Squamous Cell Carcinoma. *Mol Med Rep* (2019) 20:622–32. doi: 10.3892/MMR.2019.10294
34. Wang Q, He Z, Chen Y. Comprehensive Analysis Reveals a 4-Gene Signature in Predicting Response to Temozolomide in Low-Grade Glioma Patients. *Sage J* (2019) 26:1-14. doi: 10.1177/1073274819855118
35. Yang H, Zhou L, Chen J, Su J, Shen W, Liu B, et al. A Four−Gene Signature for Prognosis in Breast Cancer Patients With Hypermethylated IL15RA. *Oncol Lett* (2019) 17:4245–54. doi: 10.3892/OL.2019.10137
36. Cardoso M de FS, Castelletti CHM, de Lima-Filho JL, Martins DBG, Teixeira JAC. Putative Biomarkers for Cervical Cancer: SNVs, Methylation and Expression Profiles. *Mutat Res Mutat Res* (2017) 773:161–73. doi: 10.1016/J.MRREV.2017.06.002
37. Farkas SA, Milutin-Gašperov N, Grce M, Nilsson TK. Genome-Wide DNA Methylation Assay Reveals Novel Candidate Biomarker Genes in Cervical Cancer. *Epigenetics* (2013) 8:1213–25. doi: 10.4161/EPI.26346
38. Jha AK, Nikbakht M, Jain V, Sehgal A, Capalash N, Kaur J. Promoter Hypermethylation of P73 and P53 Genes in Cervical Cancer Patients Among North Indian Population. *Mol Biol Rep* (2012) 39(9):9145–57. doi: 10.1007/S11033-012-1787-5
39. Widschwendter A, Müller HM, Fiegl H, Ivarsson L, Wiedemair A, Müller-Holzner E, et al. DNA Methylation in Serum and Tumors of Cervical Cancer Patients. *Clin Cancer Res* (2004) 10:565–71. doi: 10.1158/1078-0432.CCR-0825-03
40. Filippakopoulos P, Picaud S, Mangos M, Keates T, Lambert J-P, Barsyte-Lovejoy D, et al. Histone Recognition and Large-Scale Structural Analysis of the Human Bromodomain Family. *Cell* (2012) 149:214–31. doi: 10.1016/j.cell.2012.02.013
41. Mikeska T, Bock C, Do H, Dobrovic A. DNA Methylation Biomarkers in Cancer: Progress Towards Clinical Implementation. *Expert Rev Mol Diagn* (2012) 12:473–87. doi: 10.1586/erm.12.45
42. Brien GL, Remillard D, Shi J, Hemming ML, Chabon J, Wynne K, et al. Targeted Degradation of BRD9 Reverses Oncogenic Gene Expression in Synovial Sarcoma. *Elife* (2018) 7:132–8. doi: 10.7554/ELIFE.41305
43. Dewez M, Bauer F, Dieu M, Raes M, Vandenhaute J, Hermand D. The Conserved Wobble Uridine tRNA Thiolase Ctu1–Ctu2 Is Required to Maintain Genome Integrity. *Proc Natl Acad Sci* (2008) 105:5459–64. doi: 10.1073/PNAS.0709404105
44. Delaunay S, Rapino F, Tharun L, Zhou Z, Heukamp L, Termathe M, et al. Elp3 Links tRNA Modification to IRES-Dependent Translation of LEF1 to Sustain Metastasis in Breast Cancer. *J Exp Med* (2016) 213:2503–23. doi: 10.1084/JEM.20160397
45. Biswas M, Chatterjee SS, Boila LD, Chakraborty S, Banerjee D, Sengupta A. MBD3/NuRD Loss Participates With KDM6A Program to Promote DOCK5/8 Expression and Rac GTPase Activation in Human Acute Myeloid Leukemia. *FASEB J* (2019) 33:5268–86. doi: 10.1096/FJ.201801035R
46. Bahrami A, Hasanzadeh M, Hassanian SM, ShahidSales S, Ghayour-Mobarhan M, Ferns GA, et al. The Potential Value of the PI3K/Akt/mTOR Signaling Pathway for Assessing Prognosis in Cervical Cancer and as a Target for Therapy. *J Cell Biochem* (2017) 118:4163–9. doi: 10.1002/JCB.26118
47. Deng J, Bai X, Feng X, Ni J, Beretov J, Graham P, et al. Inhibition of PI3K/Akt/mTOR Signaling Pathway Alleviates Ovarian Cancer Chemoresistance Through Reversing Epithelial-Mesenchymal Transition and Decreasing Cancer Stem Cell Marker Expression. *BMC Cancer* (2019) 19(1):1–12. doi: 10.1186/S12885-019-5824-9
48. Dong C, Wu J, Chen Y, Nie J, Chen C. Activation of PI3K/AKT/mTOR Pathway Causes Drug Resistance in Breast Cancer. *Front Pharmacol* (2021) 118:143. doi: 10.3389/FPHAR.2021.628690

Conflict of Interest: The authors declare that the research was conducted in the absence of any commercial or financial relationships that could be construed as a potential conflict of interest.

Publisher's Note: All claims expressed in this article are solely those of the authors and do not necessarily represent those of their affiliated organizations, or those of the publisher, the editors and the reviewers. Any product that may be evaluated in this article, or claim that may be made by its manufacturer, is not guaranteed or endorsed by the publisher.

frontiers | Frontiers in Oncology

REVIEW
published: 08 April 2022
doi: 10.3389/fonc.2022.874645

The Status and Prospects of Epigenetics in the Treatment of Lymphoma

Jiaxin Liu[1,2†], *Jia-nan Li*[1,2†], *Hongyu Wu*[1,2] *and Panpan Liu*[1,2*]

[1] State Key Laboratory of Oncology in South China, Collaborative Innovation Center for Cancer Medicine, Sun Yat-sen University Cancer Center, Guangzhou, China, [2] Department of Medical Oncology, Sun Yat-Sen University Cancer Center, Guangzhou, China

The regulation of gene transcription by epigenetic modifications is closely related to many important life processes and is a hot research topic in the post-genomic era. Since the emergence of international epigenetic research in the 1990s, scientists have identified a variety of chromatin-modifying enzymes and recognition factors, and have systematically investigated their three-dimensional structures, substrate specificity, and mechanisms of enzyme activity regulation. Studies of the human tumor genome have revealed the close association of epigenetic factors with various malignancies, and we have focused more on mutations in epigenetically related regulatory enzymes and regulatory recognition factors in lymphomas. A number of studies have shown that epigenetic alterations are indeed widespread in the development and progression of lymphoma and understanding these mechanisms can help guide clinical efforts. In contrast to chemotherapy which induces cytotoxicity, epigenetic therapy has the potential to affect multiple cellular processes simultaneously, by reprogramming cells to achieve a therapeutic effect in lymphoma. Epigenetic monotherapy has shown promising results in previous clinical trials, and several epigenetic agents have been approved for use in the treatment of lymphoma. In addition, epigenetic therapies in combination with chemotherapy and/or immunotherapy have been used in various clinical trials. In this review, we present several important epigenetic modalities of regulation associated with lymphoma, summarize the corresponding epigenetic drugs in lymphoma, and look at the future of epigenetic therapies in lymphoma.

Keywords: epigenetics, lymphoma, DNA methylation, histone methylation, RNA methylation, histone acetylation

OPEN ACCESS

Edited by:
Hailong Pei,
Soochow University, China

Reviewed by:
Haiqing Ma,
Guangdong Provincial People's Hospital, China
Haopeng Yang,
University of Texas MD Anderson Cancer Center, United States

***Correspondence:**
Panpan Liu
liupp@sysucc.org.cn

[†]*These authors have contributed equally to this work*

Specialty section:
This article was submitted to Molecular and Cellular Oncology, a section of the journal Frontiers in Oncology

Received: *12 February 2022*
Accepted: *17 March 2022*
Published: *08 April 2022*

Citation:
Liu J, Li J-n, Wu H and Liu P (2022) The Status and Prospects of Epigenetics in the Treatment of Lymphoma. Front. Oncol. 12:874645. doi: 10.3389/fonc.2022.874645

1 INTRODUCTION

Lymphoma is the most common lymphoid malignancy and is among the ten most prevalent cancers worldwide. It can roughly be subclassified into Hodgkin's lymphoma (HL) and Non-Hodgkin's lymphoma (NHL) (1, 2). NHL accounts for about 90% of all lymphomas and the remaining 10% are referred to as HL (3). NHL is the sum of a group of independent diseases with strong heterogeneity

that can be divided into B cell, T cell, and NK cell lymphomas according to the lymphocyte type. While 90% of early-stage HL patients and more than 50% of NHL patients respond to first-line conventional treatment, the remaining ones and those with relapsed disease, are still challenging to treat (4, 5).

With the deepening in the understanding of tumor pathogenesis, it has become clear that the occurrence and development of tumors is not only related to gene mutations and deletions but also to the imbalance of epigenetic regulation. In the past, it was believed that tumors were diseases driven by the accumulation of gene mutations (6). In fact, epigenetic alterations in tumors are much more frequent than the existing identified genetic alterations. The epigenetic variations are not only associated with classical signaling pathways such as those for cell growth, proliferation and apoptosis but also lead to changes of new signal transduction pathways such as those for immune escape, energy metabolism disorders, activation of cellular phenotype transition, and promotion of tumor inflammation (6–10).

The core of epigenetic changes is the covalent modification of histones and nucleic acids to determine the chromatin configuration and unique transcription spectrum in cells (11). Chromatin is formed by a DNA measuring about 2 meters in length, wound around the nucleosome composed of four histones. The total chromatin is packed into 23 pairs of chromosomes by forming a quaternary structure, which is stored in about 7 μm in the nucleus of cells (7). The most common epigenetic modifications are histone modifications and DNA methylation at the fifth carbon atom of cytosines. DNA methylation and histone deacetylation result in a dense chromatin conformation, leading to gene transcriptional silencing. On the contrary, DNA demethylation and histone acetylation lead to a loose chromatin conformation and active gene transcription. In addition to covalent modification of histones and nucleic acids, epigenetic regulation also includes dynamic spatio-temporal positioning of nucleosomes, regulation of chromatin three-dimensional conformation and nuclear topology, regulation of non-coding RNA, microRNA and enhancer RNA (12, 13). In conclusion, the action of multiple epigenetic factors influence chromatin conformation, resulting in an anomalous interaction between DNA and transcription factors, abnormal regulation of gene transcription and signaling pathways. Abnormal inactivation of signaling pathways and tumor suppressor gene pathways may lead to tumorigenesis that may provide the possibility of using existing epigenetic regulators to restore normal gene expression.

2 EPIGENETIC TARGETS IN LYMPHOMA

2.1 DNA Methylation

2.1.1 DNMT

DNA methylation is an important epigenetic mechanism in normal cells as well as tumor cells that can affect gene expression by directly controlling the activity of DNA regulatory elements, including cytosine-phosphate-guanine (CpG) islands in the promoter region (14). DNA methylation occurring at the 5-carbon of cytosine residues in CpG dinucleotides is the first characteristic of an epigenetic modification of chromatin (15). 5-methylcytosine (5mC) is produced by the transfer of methyl groups to 5-cytosine using S-adenosyl methionine (SAM) as a methyl donor under the catalysis of DNA methyltransferase (DNMTs). DNMTs are multi-domain proteins in which two functional parts can be distinguished, a large N-terminal regulatory part and a smaller C-terminal part (16, 17). The C-terminal domains of DNMTs contain 10 conserved amino acid motifs that are characteristic for specific DNA-(cytosine-C5)-MTases. They are involved in DNA recognition and binding, target base flipping and catalysis, so they are called target recognition domains (TRD) (18). The N-terminal part of DNMTs includes several regulatory domains that guide the nuclear localization of enzymes, mediate their interaction with other proteins, regulatory nucleic acids (such as non-coding RNA) and chromatin, and perform post translational modification (PTM) (15, 19). They are classified into DNMT1, DNMT3A and DNMT3B according to the N-terminal regions. DNMT1 catalyzes DNA methylation retention that maintains the genetic stability of methylation sites during replication; DNMT3A and DNMT3B catalyze the *de novo* methylation of DNA (20, 21). The expression of *DNMT1* is up regulated in mantle cell lymphoma (MCL) (22) and can be inhibited by DNMT inhibitor decitabine (23). DNMT1 and DNMT3B show *MYC*-dependent overexpression in Burkitt's lymphoma (BL). MYC directly binds to DNMT1 and DNMT3B promoters, resulting in an increase in their transcription in the human BL model (24). All three DNMTs are overexpressed in diffuse large B-cell lymphoma (DLBCL), which is significantly correlated with advanced clinical stage and adverse reactions to chemotherapy and/or radiotherapy (25). For example, DNMT3A is overexpressed in 30% of angioimmunoblastic T-cell lymphoma (AITL) and 40% of DLBCL and is associated with reduced overall survival (OS) and event-free survival (EFS) in DLBCL patients (26). Mutations in *DNMT3A* are more common in patients with T-cell lymphoma (27–29).

2.1.2 TET

Unlike the DNMT family, which catalyzes and maintains DNA methylation, the ten–eleven translocation (TET) family of α-ketoglutarate (α-KG)-dependent dioxygenases indirectly drives DNA demethylation through 5mC oxidation catalysis (30). TET1, TET2, and TET3 in the TET family can gradually oxidize 5mC to 5-hydroxymethylcytosine (5hmC), 5-formylcytosine (5fC), and 5-carboxycytosine (5caC) (13). There are two main mechanisms by which TET protein promotes DNA demethylation: a passive (replication-dependent) DNA demethylation and an active DNA demethylation. All three oxidized methylcytosines (oxi-MC) are DNA demethylation intermediates. During DNA replication, if oxi-MC exists on the template chain, unmethylated cytosine on the newly synthesized chain will not be effectively recognized or methylated by DNMT1 complex, resulting in loss of DNA methylation during cell division (31). This passive (replication-dependent) DNA demethylation is

the main demethylation mechanism in most cells. Active DNA demethylation means that 5fC and 5caC can be removed from properly base-paired 5fC:G and 5caC:G base pairs by thymine DNA glycosylase, which normally excises T:G mismatches; then the base excision repair system replaces oxi-MC with unmodified cytosine (32). Among the three *TET* genes, *TET2* has repeated inactivation mutations in a wide range of bone marrow and lymphoid malignant tumors (33). *TET2* mutations include deletion, missense, nonsense, and frameshift mutations. Numerous studies have shown that most patients with AITL and peripheral T-cell lymphoma, not otherwise specified (PTCL-NOS) carry *TET2* mutations (28, 32, 34–36) and decreased OS of patients (37). Most AITL and some PTCL-NOS may come from follicular helper T (Tfh) cells, the T cells that facilitate B cell antibody responses by interacting with B cells in the germinal center (38). In AITL multistep tumor model, *TET2* and/or *DNMT3A* mutations occurred first, followed by specification into the Tfh lineage guided by expression of the $RHOA^{G17V}$ mutant and enhanced by hyper activation of the T-cell receptor signaling pathway (39). The expansion and/or dysfunction of Tfh can induce the production of cytokines, which play an important role in the early stage of lymphoma progression and the rich inflammatory components of AITL tumor lesions (39, 40). Similarly, TET2 mutations are common in B-cell lymphomas, especially in DLBCL (34).

2.3 IDH

As mentioned earlier, TET enzyme depends on the metabolic cofactor α-KG. However, in case isocitrate dehydrogenase (IDH) is mutated, α-KG might be converted into D-2-hydroxyglutarate (D-2-HG) which blocks TET2 function. A frequent mutation in the *IDH* family is $IDH2^{R172}$. The *IDH2* mutation often occurs in AITL and the D-2-HG, produced by the mutated enzyme, is a tumor metabolite (28, 41). *IDH2* mutation also affects histone lysine methylation. In AITL patients, in which the disease was caused by an $IDH2^{R172}$ mutation, the level of trimethylated H3 at lysine 27 (H3K27me3) increased significantly (29, 42).

2.1.2 Histone Methylation

Histone methylation is catalyzed by histone methyltransferase (HMT) and occurs at different lysine and arginine of histone, which may involve monobasic, dimethyl and trimethylation at the same residue. In addition, the dimethylation of arginine can be symmetric (me2s) or asymmetric (me2a) (43). Depending on the target residue, methylation level and symmetry, methylation corresponds to different gene expression and function, which affects the level of gene transcription and leads to gene transcriptional activation or inhibition. For example, trimethylated H3 at lysine 4(H3K4me3) and dimethylated H3 at lysine 79 (H3K79me2) are beneficial to transcription, while H3K27me3 and trimethylated H3 at lysine 9(H3K9me3) inhibit transcription (43, 44).

2.1.2.1 KMT2, DOT1L

Histone-lysine N-methyltransferase 2 (KMT2), which was initially named the mixed-lineage leukaemia (MLL) family, on the one hand, can directly H3K4me3 (45), on the other hand, it can change the chromatin state and DNA accessibility by recruiting demethylases to reduce H3K27me3. The KMT2 family includes KMT2A, KMT2B, KMT2C, KMT2D, KMT2F, and KMT2G. Nonsense or frameshift mutations frequently occur in DLBCL and follicular lymphoma (FL), resulting in down-regulation of KMT2D protein expression (46, 47). Zhang et al. demonstrated that FL and DLBCL-associated KMT2D mutations impair KMT2D enzyme activity, resulting in reduced global H3K4 methylation in germinal center (GC) B cells and DLBCL cells (48). Thus KMT2D is considered a tumor suppressor gene whose early deletion promotes lymphoma formation by remodeling the epigenetic landscape of cancer precursor cells. In MCL and Extra nodal NK/T-cell lymphoma, nasal type (ENKTL-NT), KMT2D mutation indicates a poor prognosis (49). KMT2D deficiency can lead to changes in a variety of genes, including *TNFAIP3* (*A20*), *SOCS3, SGK1, TRAF3, TNFRSF14 (HVEM)* and *ARID1A*, which in turn affect CD40, JAK-STAT, toll like receptor and the B-cell receptor pathway (47). Disruptor of telomeric silencing 1-like (DOT1L) is the only member of the KMT4 family. DOT1L can H3K79me2 and promote acetylation of H4, which in turn regulates the binding of bromodomain-containing protein 4 (BRD4) to chromatin (50). A potent and selective amino-nucleoside inhibitor of DOT1L histone methyltransferase activity, EPZ-5676, inhibited H3K79 methylation and MLL fusion target gene expression in cellular studies and showed selective and effective cell killing of acute leukemia lines carrying MLL translocations (51).

2.1.2.2 EZH2

The function of Enhancer of Zeste Homolog 2 (EZH2) is opposite to that of KMT2. EZH2 is a HMT of 746 amino acids and is a catalytic subunit of Polycomb Repression Complex 2 (PRC2) that can inhibit gene transcription by catalytic formation of H3K27me3, can also recruit histone deacetylase (HDAC) 1/2 and DNMTs to further inhibit transcription through its cofactor embryonic ectoderm development (EED) (52, 53). EZH2 is highly expressed in GC B cells and targeted by somatic mutations in B-cell lymphomas (54). In particular, activating mutations in EZH2 are frequently found in FL and germinal center DLBCL (GC-DLBCL) (55–57). *MYC* related EZH2 overexpression has been found in BL and double hit lymphoma (58). In DLBCL and FL, EZH2 catalyzes somatic heterozygous mutations of Y641 and A677 residues in the set domain (44, 59), thereby promoting transcriptional inhibition and tumorigenesis by increasing the level of H3K27me3 (60). Many experiments have confirmed that $Ezh2^{Y641}$ mutation and *Myc* synergistically promote the formation of lymphoma which has been shown in transgenic mouse models (61, 62). Similar to a Y641 mutant cell line, a $EZH2^{A677}$ mutant cell line showed abnormal increase of H3K27me3 and decrease of monomethylated H3K27 (H3K27me1) and dimethylated H3K27 (H3K27me2) (63). For T-cell lymphoma, it is reported that in 67.5% PTCL-NOS, 50% natural killer/T-cell lymphoma (NKTCL), in 73.3% anaplastic large-cell lymphoma (ALCL), and in 60% AITL cases EZH2 was strongly expressed, these patients with peripheral T-cell lymphoma (PTCL) overexpression were

often accompanied by more complications and displayed lower survival rates (64).

2.1.2.3 SETDB1

SET Domain, Bifurcated 1 (SETDB1) catalyzes the trimethylation of histone H3K9 (H3K9me3) and thereby promotes transcriptional silencing (65), the N-terminal of SETDB1 interacts directly with the plant homeodomain of DNMT3A and localizes to a silent promoter in cancer cells (66). A recent study showed that simultaneous inhibition of G9a (another methyltransferase of H3K9) and DNMTs with the dual inhibitor CM-272 enhanced antitumor immunity alone or in combination with anti-PD1 (67).

2.1.2.4 LSD1

Histone methylation is a dynamic equilibrium process and is a reversible histone modification. Lysine-specific demethylase 1 (LSD1/KDM1A) is a flavin adenine dinucleotide (FAD)-dependent demethylase that specifically removes monomethylated and dimethylated groups from H3K4 and H3K9 (H3K4me1, H3K4me2, H3K9me1, and H3K9me2) (68). In a mouse model, B-cell lymphoma 6 (Bcl6) was found to directly bind and recruit LSD1, and conditional deletion of *Lsd1* suppressed GC proliferation induced by constitutive expression of Bcl6 and significantly delayed Bcl6-driven lymphangiogenesis. This suggests that LSD1 plays a key role in lymphangiogenesis as an important BCL6 cofactor, as this classical lymphoma oncogene requires LSD1 to induce malignant transformation (69). *LSD1* is overexpressed in human DLBCL tissues and negatively correlates with the OS of DLBCL patients (70). *LSD1* was found to be upregulated and positively correlated with Ki67 in MCL patients, while H3K4me1 and H3K4me2 were downregulated (71).

2.1.2.5 PRMT

Arginine methylation is catalyzed by protein arginine methyltransferase (PRMT), that can be sub classified into type I and type II enzymes that are responsible for the formation of asymmetric and symmetric dimethylarginines, respectively. PRMT5 is the major type II enzyme that catalyzes the symmetrical dimethylarginine of histones and induces gene silencing by generating repressive histone tags, including the arginine asymmetric dimethylation of histones H2AR3, H3R8, and H4R3 (H2AR3me2s, H3R8me2s, and H4R3me2s) (72). In the cytoplasm, PRMT5 is involved in the formation of the 20S protein arginine methyltransferase complex, which forms the "methylome". The complex consists of the shedder Sm protein, PRMT5, pICln, and WD repeat protein (MEP50/WD45). PRMT5 methylates the Sm protein, which in turn regulates shedder activity and downstream gene expression (73). In *Eμ-myc* transgenic mice, MYC directly upregulates transcription of core small nuclear ribonucleoprotein particle assembly genes, including *Prmt5*, as a way to ensure splicing fidelity of exons with weak 5' donor sites-an important step in lymphomagenesis (74). PRMT5 is overexpressed in MCL, GC-DLBCL, and activated B cell-like DLBCL (ABC-DLBCL) cell lines and clinical samples as well as in mouse primary lymphoma cells. PRMT5 upregulates PRC2 expression by epigenetically silencing RBL2 and indirectly causing RB1 inactivation through phosphorylation (75, 76). PRMT5 knockdown reactivates the RB1/RBL2-E2F tumor suppressor pathway and antagonizes cyclin D1-CDK4/6 signaling, which in turn leads to lymphoma cell death. Another study found that PRMT5 directly silenced the expression of axin-related protein (AXIN2) and WNT inhibitory factor 1 (WIF1). This lead to a stimulation of WNT/β-catenin signaling and indirectly activated the AKT/GSK3β pathway, leading to an inhibition of the overexpression that induced lymphoma cell death (41).

2.1.3 RNA Methylation

According to the data analysis of the RNA modification database MODOMICS as of 2017, 163 different chemical RNA modifications have been identified in all organisms (77). Among them, N6-methyladenosine (m^6A) is considered to be the most common, rich and conservative internal PTM in eukaryotic messenger RNAs (mRNAs), microRNAs (miRNAs), and long non-coding RNAs (lncRNAs). M^6A usually occurs in adenine of the common sequence RRACH (R=A/G,H=A/C/U) (78), is enriched near the stop codon and the 3′ untranslated terminal region (UTR) and translated near the 5′ UTR in a cap-independent manner (79).

M^6A-RNA methylation modification is a reversible biological process participated by methyltransferases (writers), demethyltransferases (erasers) and methylation readers (readers), which affects RNA transcription, processing, translation and metabolism. Writers include methyltransferase-like 3 (METTL3) (80), METTL14 (81, 82), Wilms tumor 1-associated protein (WTAP) (83), RNA-binding motif protein 15/15B (RBM15/15B) (84), KIAA1429 (85), and zinc finger CCCH-type containing 13(ZC3H13) (86); readers comprise e.g. YT521-B homologue (YTH) protein family (87), insulin-like growth factor 2 mRNA-binding proteins (IGF2BP1/2/3) (88), eukaryotic initiation factor (eIF) 3 and heterogeneous nuclear ribonucleoprotein (hnRNP) family (86); whereas erasers include fat mass and obesity-associated protein (FTO) (89) and alkB homologue 5 (ALKBH5) (86, 90, 91).

METTL3 has a SAM-binding domain which can catalyze the transfer of methyl groups in SAM to adenine bases in RNA to produce S-adenosine homocysteine (SAH), while METTL14 is mainly used to stabilize the structure of the methyltransferase complex (MTC) and to determine a specific RNA sequence ("RRACH") as a catalytic substrate (92). Both of them were co-located in nuclear speckles and formed a stable complex at a ratio of 1:1 (81). WTAP, RBM15/15B, and KIAA1429 don't have a catalytic function. WTAP is responsible for recruiting METTL3-METTL14 heterodimers, which form the m^6A methyltransferase tricomplex (METTL3–METTL14–WTAP); RBM15/15B binds METTL3 and WTAP and directs these two proteins to specific RNA sites for m6A modification, which play important roles in cell growth and apoptosis, especially in blood cells, by regulating various signaling pathways such as Notch and Wnt; KIAA1429 recruits MTC and mediates methylation of adenine bases near the 3'UTR and stop codon regions in mRNA (83, 84, 86, 93). Through the interaction between ZC3H13 and WTAP, its low-complexity (LC) domain is

retained in nuclear speckles, thus improving its catalytic function (94).

FTO and ALKBH5 belong to the 2-oxoglutarate-dependent nucleic acid oxygenase (NAOX) family and catalyze the demethylation of m^6A in a Fe^{2+} and α-KG-dependent manner. The FTO in the nucleus mediates the demethylation of m^6A, whereas the FTO in the cytoplasm mediates the N6 and the dimethyladenosine (m^6Am) and m^6A in the cytoplasm. In addition, FTO can also combine with transfer RNA (tRNA) to mediate the demethylation of N1-methyladenosine (m^1A) in tRNA (95, 96). ALKBH5 colocalizes with nuclear speckles and influences mRNA processing factors' assembly/modification and regulates mRNA export and RNA metabolism (97).

Writers play a positive catalytic role in RNA methylation modification, which can be reversed by erasers. However, in this process, different readers need to identify the modified residues and transmit information to complete the downstream biological function and establish an efficient and orderly m^6A regulatory network. The YT521-B homology (YTH) domain family includes YTH domain family protein 1(YTHDF1), YTH domain family protein 2 (YTHDF2), YTH domain family protein 3 (YTHDF3), YTH domain containing 1(YTHDC1), and YTH domain containing 2 (YTHDC2) (98). YTHDF1/2/3 are located in the cytoplasm. The C-terminal region of YTHDF2 can identify specific m^6A sites, and its N-terminal region binds to the SH domain of CCR4-NOT transcription complex subunit 1 (CNOT1), thereby recruiting the CCR4-NOT deadenylase complex. After this series of processes, RNA is finally transported to the processing body (P-body) to accelerate RNA degradation. YTHDF1 interacts with eukaryotic translation initiation factor 3 (eIF3), eIF4E, and eIF4G to improve the translation efficiency of m^6A modified mRNA (86, 99); YTHDF3 promotes the translation of related mRNA through direct interaction with YTHDF2. YTHDC1 binds pre-mRNA and interacts with mRNA splicing factor, specifically recruiting serine- and arginine-rich splicing factor 3 (SRSF3) or antagonizing serine- and arginine-rich splicing factor 10 (SRSF10). Thereby promoting exon inclusion, splicing, as well as mRNA export from the nucleus to the cytoplasm (100). YTHDC2 selectively binds m^6A at its consensus motif, enhances the translation efficiency of its targets and also decreases their mRNA abundance (101). The YTH family is the most important type of m^6A readers, however, additional proteins are involved in this processing cascade. For example, IGF2BP1/2/3 rely on their K homology (KH) domains to recognize consensus GG (m^6A) C sequences, promote the stability and storage of their target mRNAs in an m^6A-depedent manner under normal and stress conditions and thus affect gene expression output (88). HNRNPA2B1 can bind to m^6A-bearing sites in the transcriptome and positively regulates primary miRNA transcript (pri-miRNA) processing in a similar manner as METTL3 (102).

In lymphoma, m^6A in DLBCL was studied the most. In DLBCL tissues and cell lines, the expression of METTL3 is up-regulated, which leads to the increase of the m^6A level of pigment epithelium-derived factor (PEDF) expression and transcription, and finally resulting in the activation of the Wnt pathway which accelerates cell proliferation. Down-regulation of METTL3 expression can inhibit the proliferation of DLBCL cells (103). Both knockdown and overexpression of METTL3 protein will lead to the upregulation of WTAP protein. The level of METTL3 is closely related to the homeostasis of WTAP, and in the absence of METTL3, the upregulation of WTAP is not enough to promote cell proliferation (104). Therefore, we speculate that WTAP plays a carcinogenic role in DLBCL and may be closely related to m^6A-RNA methylation co-participated by METTL3. WTAP forms a complex with heat shock protein 90 (HSP90) and BCL6 to maintain its stability, thus promoting the proliferation of DLBCL cells and improving the ability to resist apoptosis. After the use of the antineoplastic drug etoposide in a DLBCL cell line, the expression of WTAP decreased and the apoptosis rate of tumor cells increased significantly (105). Another study showed that WTAP enhances the hexokinase 2 (HK2) m^6A level by enhancing the expression of the *HK2* gene, a process regulated by PIWI-interacting RNAs (piRNAs)-30473 (106, 107). HK2 is the rate limiting enzyme of the glycolysis pathway which can enhance aerobic glycolysis and promote tumor cell proliferation. Previous studies have confirmed that HK2 is the key metabolic driver of the DLBCL phenotype (108). In addition, WTAP was obviously upregulated in human NKTCL cell lines (YTS and SNK-6 cells), compared with normal NK cells. More importantly, intervention of WTAP evidently prohibited NKTCL cell chemotherapy resistance to cisplatin (109).

Wu et al. found that MYC activates the expression of ALKBH5 and YTHDF3, reducing m^6A levels in the mRNA of the selected MYC-repressed genes (MRG) *SPI1* and *PHF12*. By inhibiting ALKBH5, or overexpression of SPI1 or PHF12, effectively suppresses the growth of MYC-deregulated B-cell lymphomas, both *in vitro* and *in vivo (*110). In addition, whole-exome sequencing (WES) showed deletions and mutations of YTHDF2 in PTCL (29). It was shown that Ki-67-related IGF2BP3 is the most strongly upregulated mRNA in MCL cases, and its high expression is closely related to the proliferation ability of tumor cell (111). In Zhang's study, 10 m^6A modulators were classified according to the risk ratio to predict the survival rate of patients with MCL (38).

2.1.4 Histone Acetylation

Chromatin histone acetylation and deacetylation are also key steps in epigenetic regulation. These two reversible processes are jointly regulated by histone acetyltransferase (HAT) and HDAC and are in dynamic equilibrium under normal physiological conditions (43).

2.1.4.1 HAT

HATs use acetyl coenzyme A as a cofactor and catalyze the transfer of acetyl groups to the ϵ-amino group of the lysine side chain. This leads to the neutralization of the positive lysine charge and thus potentially weakens the electrostatic interaction between the histone and the negatively charged DNA, which finally results in a more "open" chromatin conformation (112). HATs are classified into type A and B. Type A HATs are located

in the nucleus and are capable of modifying histones adulterated in chromatin. They are a very diverse family of enzymes that can be divided into three separate families: GNAT, MYST, and CREBBP/EP300 family (113). All of them not only modify multiple sites in the N-terminal tail of histones, but also acetylate the globular histone core (112). By establishing a mouse model, *Crebbp* and *Ep300* were found to be frequently mutated in B-cell lymphomas, mainly in DLBCL and FL (114). *CREBBP* mutations were found in 15-30% of DLBCL and 40% of FL, while *EP300* mutations were found in approximately 5% to 10% of DLBC and FL (115, 116). Mutations in HATs occur in a single allele and this mutation leads to inactivation of the HAT coding domain, which in turn affects on the one hand the acetylation of histones and non-histones, and on the other hand activates *BCL6* and the tumor suppressor *P53* involved in the development of B-cell lymphoma (117–119). *CREBBP* mutations were also found in 26% of patients with Sézary syndrome (SS) and primary cutaneous diffuse large B-cell lymphoma-leg type (PCLBCL-LT) (120, 121). Type B HATs are highly conserved and mainly acetylate free histones in the cytoplasm, but not acetylated and nucleosomal histones. Type B HATs rapidly acetylates newly synthesized histones H3 and H4, and this acetylation pattern is important for histone deposition. Moreover these modifications are removed during chromatin maturation (122).

2.1.4.2 HDAC

HDACs counteract the action of HATs and reverse lysine acetylation, restoring the positive charge of lysine which may facilitate the stabilization of local chromatin structure. In humans, there are 18 HDACs that can be divided into four classes: class I Rpd3-like proteins (HDAC1/2/3 and HDAC8), class II Hda1-like proteins (HDAC4-7, HDAC9, and HDAC10), class III Sir2-like proteins (SIRT1-7), and class IV protein (HDAC11) (123). Classes I, II, and IV HDACs are zinc dependent, while class III ones are sirtuins using NAD^+ as a reactant to deacetylate the acetyl lysine residue of the protein substrate to form nicotinamide, the deacetylation product and the metabolite 2'-O-acetyl-ADP-ribose (123, 124). The deacetylation of HDACs not only alters transcription but also other PTM such as methylation, ubiquitination and sumoylation. 55.8% PTCL-NOS, 57.1% NKTCL, 86.7% ALCL, and 50% AITL strongly expressed HDAC1; 58.1% PTCL-NOS, 57.1% NKTCL, 53.3% ALCL, and 60% AITL strongly expressed HDAC2 (64). As mentioned previously, *CREBBP* mutations disable acetylation and simultaneously enhance deacetylation of the HDAC3 complex, which may be the mechanism of GC lymphoma development (117). HDAC6 is either weakly expressed or undetectable in 96% of DLBCL cases (125) and HDAC6 may be an important prognostic marker associated with a good outcome in DLBCL or a more aggressive course in PTCL, respectively (126). HDAC7 has anti-cancer effects and expression is downregulated in BL (127). Increased *HDAC9* copy number was found in 50% of DLBCL cases and further genetic mouse models suggest that HDAC9 may contribute to lymphoma development by altering pathways related to growth and survival as well as regulating BCL6 activity and P53 tumor suppressor function (128).

2.1.4.3 BET

Bromodomain and extra terminal motif (BET) family is a reader used to detect acetylated lysine residues on histones and non-histone proteins. The BET family consists of BRD2, BRD3 and BRD4, which are widely expressed in tissues, and bromodomain testis-specific protein, which is mainly found in the testis (129). The BET protein consists of two amino-terminal bromodomains that bind to acetylated lysine residues of histones and other proteins, and an extra-terminal domain, which mediates further protein-protein interactions (130). BET acts as a chromatin "reader", transforming the chromatin state into a chromosome state by recruiting transcriptional regulatory complexes to their binding sites. In DLBCL, BL, and MCL, this action is always mediated by *MYC (*131). For example, BRD4 interacts with and activates positive transcription elongation factor-b (P-TEFb), which stimulates RNA Pol II into active elongation and activates transcription initiation and elongation (13, 131, 132).

2.2 Epigenetic Therapy

In the context of this complex epigenetic regulation of gene expression in tumors, the use of epigenetic therapies to reverse this aberrant gene expression can be effective in treating tumors. The development and testing of anti-tumor drugs targeting epigenetic factors is flourishing internationally, and a number of epigenetic drugs have been approved as drugs by the US Food and Drug Administration (FDA) in lymphoma (**Figure 1**).

2.2.1 DNMT Inhibitors

2.2.1.1 Decitabine

DNA demethylating agents, such as decitabine and azacitidine, have been approved by the U.S. Food and Drug Administration for the clinical treatment of myelodysplastic syndrome (MDS) and acute myeloid leukemia (AML). Decitabine is a deoxyribonucleoside that can be incorporated into DNA and occupy DNMTs to induce DNA hypomethylation. It displays cytotoxicity at high concentrations, whereas low doses can minimize toxicity and may improve the targeting effect of DNA hypomethylation through a re-expression of tumor suppressor genes during tumor therapy (133). A phase 4 clinical trial investigated the efficacy of a combination of decitabine together with a modified regimen of cisplatin, cytarabine, and dexamethasone (DHAP) in relapsed/refractory DLBCL (r/r DLBCL) (134). The results showed that overall response rate (ORR) reached 50% and complete response rate (CRR) reached 35%. Five patients (25%) showed a stable disease (SD) with a disease control rate (DCR) of 75% and the median progression-free survival (PFS) was 7 months. A randomized phase 2 study of anti-PD-1 camrelizumab plus decitabine in relapsed/refractory HL (r/r HL) achieved 79% ORR and prolonged the median PFS to 35.0 months (135). Many clinical trials are currently exploring the therapeutic efficacy of decitabine in combination with the HDAC inhibitor cidabendiamide in HL (NCT04514081, NCT04233294). The

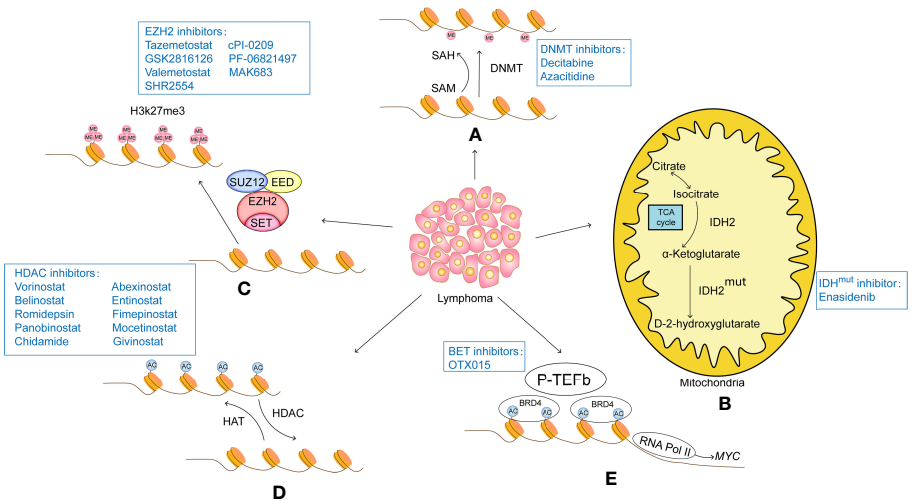

FIGURE 1 | **(A)** DNA methylation modifications usually turn off gene expression and therefore result in a lack of expression of tumor suppressors. Therefore, intervention with DNA methylesterase inhibitors can reduce the methylation level of the promoter region of the target gene, opening up the expression of these tumour suppressors and thus acting as a tumour suppressor. DNA methylesterase inhibitors that have been successfully marketed include azacitidine and decitabine, both of which are nucleoside analogues that cause genome-wide reductions in methylation levels and activate gene transcription. **(B)** IDH2 is the rate-limiting enzyme of the tricarboxylic acid cycle involved in cellular energy metabolism. Under normal conditions, IDH2 catalyzes the oxidation of isocitrate to produce a-KG. Mutant IDH2 loses its normal function and converts a-KG to D-2-HG. The accumulation of D-2-HG leads to histone hypermethylation. IDH2 inhibitors such as Enasidenib target mutant IDH2 to reduce D-2-HG, thereby inducing histone demethylation and slowing tumour progression. **(C)** Histone methylation modifications are highly site-specific and modifier-specific, and have very different effects on gene expression. EZH2 is the core component of PRC2, which acts as a histone methyltransferase to catalyse H3K27me3, causing tight binding of histones to DNA and inhibiting transcription of target genes, EZH2 inhibitors such as tazemetostat, GSK2816126, valemetostat, SHR2554, cPI-0209, PF-06821497 and MAK683 specifically act on EZH2, inhibiting its function and restoring transcription of oncogenes. **(D)** Histone acetylation is regulated by HAT and HDAC. HAT catalyzes the transfer of acetyl groups to the lysine side chain of histones, which neutralizes the positively charged lysine and weakens the affinity of histones for negatively charged DNA, loosening the structure of histones and facilitating the recruitment of transcription factors and the transcription of related genes. The HDAC-catalyzed deacetylation restores the positive electrical properties of histones, resulting in a stronger electrical interaction between histones and DNA, which acts as a repressor of gene expression. A number of HDAC inhibitors have been approved for marketing, among which, vorinostat and belistat of the hydroxamic acid class were approved by the US FDA for the treatment of CTCL and PTCL in 2006 and 2014 respectively; romidepsin of the cyclic tetrapeptide class was approved by the US FDA for the treatment of CTCL and PTCL in 2009 and 2011 respectively; and chidamycin of the benzylamine class was approved by the Chinese In addition, other HDAC inhibitors, such as panobinostat, abexinostat, entinostat, fimepinostat, mocetinostat and givinostat, are also in active clinical trials. **(E)** The BET family of proteins is an important class of proto-oncoproteins that contains the bromodomain, a histone acetylation recognition factor, and a member of the BET family, BRD4, which interacts with and activates positive transcription elongation factor-b (P-TEFb) to stimulate RNA Pol II into active elongation, activating transcription initiation and elongation. The BET inhibitor competes with the acetylation residues to bind to the bromine domain of BRD4, destabilizing the DNA repair machinery and inducing the accumulation of DNA changes until cell death.

effectiveness of camrelizumab in combination with decitabine in HL (NCT04510610) and NHL (NCT04337606) is also being evaluated. There has also been an explosion in the combination of novel CAR-T therapies with the traditional epigenetic drug decitabine. For example, decitabine-primed tandem CD19/CD20 CAR-T cells treatment in relapsed/refractory B-cell NHL (r/r B-cell NHL) (NCT04697940), sequential low-dose decitabine with PD-1/CD28, CD19 CAR-T in relapsed/refractory B-cell lymphoma (r/r B-cell lymphoma) (NCT04850560). Completed or all ongoing trials are listed in **Table 1**. From these trials we can look forward to DNA demethylating agents that show potential in the field of lymphoma therapy, such as in combination with immune checkpoint agents might being regimens that can improve ORR.

2.2.1.2 Azacitidine

Azacitidine is an analog of cytidine, which can replace nucleosides in DNA and RNA and covalently bind to DNMT to inhibit DNA methylation. The efficacy of azacitidine in the treatment of myelodysplasia is well known. A phase 1/2 study of azacitidine in combination with vorinostat in patients with r/r DLBCL resulted in a 6.7% ORR (NCT01120834). The regimen of azacitidine in combination with cyclophosphamide, doxorubicin, vincristine, and prednisone (CHOP) for PTCL-Tfh was presented at the 2021 Annual Meeting of the American Society of Hematology (ASH). Patients in the study received 300 mg azacitidine orally for 7 days before circle 1 and 14 days before circle 2-6 for a total of 6 cycles. This combination therapy achieved 88.2% CRR. In 17 Tfh patients, two-year OS and PFS reached 75.6% and 69.2%, respectively. A common grade ≥3 adverse event (AE) was neutropenia (2021 ASH Oral No.138). We also look forward to the performance of azacitidine in more lymphoma treatment cases. In the treatment of PTCL, different azacitidine combination therapy programs are in progress, such as azacitidine, romidepsin, belinostat, pralatrexate and emcitabine combined treatment protocols (NCT04747236),

TABLE 1 | Clinical trials of DNA methyltransferase inhibitors.

Regimen	Disease	n	Phases	Status	Clinical Result	Survival Benefit	NCT ID
Decitabine, Cisplatin, Cytarabin, Dexamethasone (134)	r/r DLBCL	21	Phase 4	completed	50% ORR, 25% SD	The median PFS was 7 months, one-year OS rate was 59.0%, two- year OS rate was 51.6%	NCT03579082
Decitabine, Camrelizumab (135)	r/r HL	61	Phase 2	completed	79% CRR	63% maintained a response at 24 months, the median PFS was 35.0 months	NCT02961101
Decitabine, Chidamide, Camrelizumab	HL		Phase 2	Recruiting			NCT04514081
Decitabine, Camrelizumab	HL		Phase 2/3	Recruiting			NCT04510610
Decitabine, Chidamide, Camrelizumab	HL		Phase 2	Recruiting			NCT04233294
Decitabine, SHR-1210	HL		Phase 2	Recruiting			NCT03250962
Decitabine, Chidamide, Camrelizumab	NHL		Phase 1/2	Recruiting			NCT04337606
Decitabine, Sintilimab	ENTKL		Phase 2	Recruiting			NCT04279379
Decitabine, Durvalumab, Pralatrexate, Romidepsin	T-Cell Lymphoma,		Phase 1/2	Recruiting			NCT03161223
Decitabine, Pembrolizumab, Pralatrexate	PTCL, CTCL		Phase 1	Not yet recruiting			NCT03240211
Decitabine, Cyclophosphamide, Rituximab, Doxorubicin, Vincristine, Prednisone, Ibrutinib, Lenalidomide, Chidamide	DLBCL		Phase 2	Recruiting			NCT04025593
Decitabine, Rituximab, Cyclophosphamide, Doxorubicin, Vincristine, Prednisone	DLBCL		Phase 1/2	Active, not recruiting			NCT02951728
Decitabine, CD19 PD-1/CD28 CAR-T	r/r DLBCL		Phase 1	Recruiting			NCT04850560
Decitabine, CD19/20 CAR-T	r/r B-cell NHL		Phase 1/2	Recruiting			NCT04697940
Decitabine, Chidamide, CD19/20 CAR-T	r/r B-cell NHL		Phase 1/2	Recruiting			NCT04553393
Azacitidine, Vorinostat	r/r DLBCL	18	Phase 1/2	completed	6.7% ORR		NCT01120834
Azacitidine, CHOP (2021 ASH Oral No.138)	PTCL	17		completed	88.2% CRR	Two-year OS rate was 75.6%, two-year PFS rate was 69.2%	
Azacitidine, Duvelisib	Lymphoma		Phase 1	Recruiting			NCT05065866
Azacitidine, Tucidinostat, CHOP	T-cell Lymphoma		Phase 3	Not yet recruiting			NCT05075460
Azacitidine, Cyclophosphamide, Doxorubicin, Vincristine, Prednisone, Etoposide, Duvelisib	T-cell Lymphoma		Phase 2	Recruiting			NCT04803201
Azacitidine, Durvalumab, Pralatrexate, Romidepsin	T-cell Lymphoma		Phase 1/2	Recruiting			NCT03161223
Azacitidine, Romidepsin, Gemcitabine	T-cell Lymphoma		Phase 3	Active, not recruiting			NCT03703375
Azacitidine, CHOP	T-cell Lymphoma		Phase 2	Active, not recruiting			NCT03542266
Azacitidine, Duvelisib, Romidepsin, Doxorubicin	T-cell Lymphoma		Phase 1	Not yet recruiting			NCT04639843
Azacitidine, Romidepsin, Bendamustine, Gemcitabine	r/r T-cell Lymphoma		Phase 3	Active, not recruiting			NCT03593018
Azacitidine, Tislelizumab, Lenalidomide, Etoposide, Pegaspargase	NKTCL-NT		Not Applicable	Recruiting			NCT05058755
Azacitidine, Dexamethasone, Pegaspargase, Tislelizumab	NKTCL		Phase 2	Not yet recruiting			NCT04899414
Azacitidine, Vorinostat	ENTKL-NT		Phase 1	Active, not recruiting			NCT00336063
Azacitidine, Romidepsin, Belinostat, Pralatrexate, Gemcitabine	PTCL		Phase 2	Recruiting			NCT04747236
Azacitidine, Chidamide	PTCL		Phase 2	Recruiting			NCT04480125
Azacitidine, Sintilimab, Chidamide	PTCL		Phase 2	Not yet recruiting			NCT04052659
Azacitidine, Romidepsin, Lenalidomide, Dexamethasone	PTCL, CTCL		Phase 1	Recruiting			NCT04447027
Azacitidine, Bendamustine, Piamprizumab	B-cell NHL		Phase 1/2	Recruiting			NCT04897477
Azacitidine, Cyclophosphamide, Doxorubicin Hydrochloride, Prednisone, Rituximab, Vincristine Sulfate	DLBCL		Phase 2/3	Recruiting			NCT04799275

(Continued)

TABLE 1 | Continued

Regimen	Disease	n	Phases	Status	Clinical Result	Survival Benefit	NCT ID
Azacitidine, Lenalidomide, Obinutuzumab	r/r B-cell Lymphoma		Phase 1	Recruiting			NCT04578600
Azacitidine, Venetoclax, Obinutuzumab	FL		Phase 1/2	Recruiting			NCT04722601
Azacitidine, R-GDP	DLBCL, r/r NHL		Phase 2	Not yet recruiting			NCT03719989
Azacitidine, R-ICE	DLBCL		Phase 1	Active, not recruiting			NCT03450343

azacitidine and chidamide combined treatment (NCT04480125). Relevant clinical trials have been listed in **Table 1**.

2.2.2 IDH2 Inhibitor

Enasidenib (AG-221) is an inhibitor of IDH2 mutations and has been approved for the treatment of AML. There is a phase 1/2 clinical trial of orally administered enasidenib (AG-221) in adults with AITL, displaying an IDH2 mutation (NCT02273739). However, the experimental results are not satisfactory. All AITL patients showed disease progression or died and had ≥ 1 treatment-emergent adverse event (TEAE).

2.2.3 EZH1/2 Inhibitors

2.2.3.1 Tazemetostat

On January 23, 2020, tazemetostat, the world's first EZH2 inhibitor, was approved by the FDA to treat patients aged 16 and over with metastatic or locally advanced unresectable epithelioid sarcoma. In a phase 1 trial, monotherapy with tazemetostat showed anticancer activity and a favorable safety profile in patients with relapsed/refractory NHL (r/r NHL) (136). In this trial, 38% of the patients with B-cell NHL had an objective response and the median duration of response (DOR) was 12.4 months. In another open-label, single-arm, multicenter, phase 2 trial, tazemetostat showed a good effect in treating patients with relapsed/refractory FL (r/r FL) (137). Patients were categorised by their EZH2 status: mutant ($EZH2^{mut}$) or wild type ($EZH2^{WT}$). The ORR was 69% (31 of 45 patients) in the $EZH2^{mut}$ cohort and 35% (19 of 54 patients) in the $EZH2^{WT}$ cohort and the median PFS was 13.8 months and 11.1 months, respectively. Secondary results of another phase 1 study showed that the ORR was only 15.4% of 13 subjects with B-cell lymphoma treated with tazemetostat which may be due to excessive (69.2%) missing data (NCT03028103). Tazemetostat monotherapy has shown satisfying results so far, but we hope to see effects of tazemetostat in combination with other therapies in the treatment of lymphoma as well. Many clinical trials, as listed in **Table 2**, are exploring the effect of tazemetostat combined with monoclonal antibodies, such as ublituximab, umbralisib (NCT05152459) or rituximab (NCT04224493) in r/r FL patients.

2.2.3.2 GSK2816126

GSK2816126 is a potent, highly selective, SAM-competitive, small-molecule inhibitor of EZH2 methyltransferase that decreases global H3K27me3 levels and reactivates silenced PRC2 target genes. In the proliferation assay using a group of B-cell lymphoma lines, those DLBCL origins with *Ezh2* activation mutations were the most sensitive to GSK2816126 (59). The ORR in a dose-escalation phase 1 study with tazemetostat was 38% in patients with B-cell lymphomas. One of these patients with germinal centre B-cell like DLBCL (GCB-DLBCL) treated with 1,800 mg dose had a partial response lasting 91 days, and 6 patients achieved SD (5 DLBCL and 1 FL) (138).

2.2.3.3 Valemetostat

Kagiyama et al. assessed the effect of a novel EZH1/2 dual inhibitor, named OR-S1, a close analog of valemetostat, also known as DS-3201 or (R)-OR-S2, on MCL tumor growth (139). In the mouse model, oral OR-S1 inhibited ibrutinib-resistant MCL tumor growth in patient-derived xenograft (PDX). Cyclin Dependent Kinase Inhibitor 1C (CDKN1C, also known as p57, KIP2) is a direct target of EZH1/2. OR-S1, through upregulation of CDKN1C, sharply inhibited cell proliferation which was accompanied by cell cycle arrest and B-cell differentiation. Valemetostat is being evaluated for its effectiveness in human lymphoma. Two phase 2 trials are evaluating valemetostat monotherapy in T-cell lymphoma (NCT04703192) and B-cell lymphoma (NCT04842877) (**Table 2**).

2.2.3.4 SHR2554, cPI-0209, PF-06821497, and MAK683

The therapeutic effect of other EZH2 inhibitors on lymphoma is still under further exploration. As shown in **Table 2**, a phase 1/2 study of SHR2554 in combination with SHR1701 in patients with B-cell lymphomas (NCT04407741), a study of cPI-0209 in patients with lymphoma (NCT04104776), PF-06821497 treatment of FL (NCT03460977), a study evaluating CPI-1205 in patients suffering from B-cell lymphoma (NCT02395601). A trial to evaluate the safety and efficacy of the EZH2 cofactor EED inhibitor MAK683 in DLBCL is also being recruited (NCT02900651).

2.2.4 HDAC Inhibitors

HDAC inhibitors can be classified into four categories based on their chemical structure: hydroxamate, short-chain fatty acid (carboxylate), benzamide, and cyclic peptide. Among them, hydroxamate acid-based vorinostat (SAHA) and belistat were approved by the FDA for the treatment of cutaneous T-cell lymphoma (CTCL) and PTCL in 2006 and 2014, respectively; cyclic tetra peptide-based romidepsin was approved by the FDA

TABLE 2 | Clinical trials of EZH1/2 inhibitors.

Regimen	Disease	n	Phases	Status	Clinical results	Survival benefit	NCT ID
Tazemetostat (136)	B-cell NHL	21	Phase 1/2	Completed	38% ORR	The median DOR was 12.4 months	NCT01897571
Tazemetostat (137)	r/r FL	99	Phase 2	Completed	$EZH2^{mut}$: 69% ORR; $EZH2^{WT}$: 35% ORR	$EZH2^{mut}$: the median PFS was 13.8 months; $EZH2^{WT}$: the median PFS was 11.1 months	NCT01897571
Tazemetostat, Fluconazole, Omeprazole, Repaglinide	B-cell Lymphoma		Phase 1				NCT03028103
Tazemetostat, Ublituximab, Umbralisib	r/r FL		Phase 1/2	Not yet recruiting			NCT05152459
Tazemetostat	FL		Phase 2	Recruiting			NCT04762160
Tazemetostat, Placebo, Lenalidomide, Rituximab	r/r FL		Phase 3	Recruiting			NCT04224493
Tazemetostat, CC-99282, Rituximab, Obinutuzumab, Tafasitamab,	NHL		Phase 1	Recruiting			NCT03930953
Tazemetostat	r/r B-cell NHL		Phase 2	Active, not recruiting			NCT03456726
Tazemetostat	NHL		Phase 2	Active, not recruiting			NCT03213665
Tazemetostat, Ensartinib, Erdafitinib, Larotrectinib, Olaparib, Palbociclib, Samotolisib, Selpercatinib, Selumetinib, Sulfate, Tipifarnib, Ulixertinib, Vemurafenib	NHL		Phase 2	Recruiting			NCT03155620
Tazemetostat, Rituximab, Cyclophosphamide, Vincristine, Doxorubicin, Prednisolone	DLBCL, FL		Phase 1/2	Recruiting			NCT02889523
Tazemetostat	DLBCL, FL		Phase 2	Active, not recruiting			NCT02875548
GSK2816126 (138)	DLBCL, FL, MZL	20	Phase 1	completed	38% ORR		NCT02082977
Valemetostat	B-cell Lymphoma		Phase 2	Recruiting			NCT04842877
Valemetostat	T-cell Lymphoma		Phase 2	Recruiting			NCT04703192
Valemetostat	T-cell Lymphoma		Phase 2	Active, not recruiting			NCT04102150
SHR2554, SHR1701	Lymphoma		Phase 1/2	Recruiting			NCT04407741
CPI-0209, Irinotecan	DLBCL, T-cell Lymphoma		Phase 1/2	Recruiting			NCT04104776
PF-06821497	FL		Phase 1	Recruiting			NCT03460977
CPI-1205	B-Cell Lymphoma		Phase 1	Completed			NCT02395601
MAK683	DLBCL		Phase 1/2	Recruiting			NCT02900651

for the treatment of CTCL and PTCL in 2009 and 2011, respectively.

2.2.4.1 Vorinostat

Vorinostat is a pan-HDAC inhibitor that has been shown to cause growth arrest and cystein-dependent apoptosis as well as cystein-independent autophagic cell death with an ORR of 29.7% in a phase 2B study of 74 patients with refractory CTCL (140). This led to FDA approval of vorinostat for CTCL in 2006. Compared to total skin electron beam therapy (TSEBT) monotherapy, the combination therapy of vorinostat together with TSEBT showed a dramatically better effect (100% ORR) in mycosis fungoide (NCT01187446). Vorinostat monotherapy has also been used to treat relapsed/refractory indolent B-cell NHL and MCL. In this phase 2 trial, 56 patients were recruited and 50 were available for ORR assessment with an ORR of 44% and a median PFS of 18 months. In 39 FL patients, the ORR reached 49% and the median PFS was 20 months. The primary toxicities were manageable grade 3/4 thrombocytopenia and neutropenia (141). More clinical trials have focused on the effects demonstrated by vorinostat in combination with other drugs in the treatment of lymphoma. Vorinostat combined with aurora kinase A inhibitor alisertib (MLN8237) in relapsed/refractory lymphoid malignancy showed that of the 34 patients included, two patients with DLBCL achieved durable complete response (CR) and two patients with HL achieved partial response (PR) (142). In a trail of vorinostat combined with gemcitabine, busulfan, and melphalan with autologous stem cell transplantation in patients with refractory lymphomas, the ORR among 28 patients with DLBCL and measurable disease was 96% (143). Treatment of patients suffering from indolent NHL with a combination of vorinostat together with rituximab, demonstrated a 46% ORR and a PFS of

29.2 months (144). In a phase 2 study of vorinostat for the treatment of FL, marginal zone lymphoma (MZL) or MCL, the ORR was 29%. The median PFS was 15.6 months for patients with FL, 5.9 months for MCL, and 18.8 months for MZL (145). Vorinostat, cladribine, and rituximab were used for treating patients with MCL, relapsed chronic lymphocytic leukemia (CLL), or relapsed B-cell NHL resulted in a 79% ORR and the median PFS for relapsed NHL and previously untreated MCL was 19.5 months and 84 months, respectively (146). Vorinostat monotherapy of DLBCL was not effective with only one patient that displayed a prolonged SD of 18 evaluable patients (147). Similarly, the effect of azacitidine combined with vorinostat for the treatment of DLBCL, was not satisfactory, with only 1 out of 15 patients achieving objective response (NCT01120834). In a trial of vorinostat in combination with cyclophosphamide, etoposide, prednisone, and rituximab for elderly patients with relapsed DLBCL, the results were reasonably good with the ORR reaching 32% (NCT00667615).

The trials currently being recruited are all combination therapies of vorinostat. A phase 2 trial is exploring the role of vorinostat, gemcitabine, clofarabine, busulfan combination therapy in the treatment of NHL (NCT04220008). A phase 1 trial is investigating the effectiveness of a combination therapy of vorinostat, other chemotherapy and biological drugs in lymphoma (NCT03259503, NCT00972478, and NCT01193842). A combination azacitidine and vorinostat therapy for ENKTL is also being recruited (NCT00336063). Given the role of vorinostat monotherapy in CTCL, we believe that additional clinical trials will reveal the effectiveness of vorinostat combination therapy in other types of lymphoma. All the clinical trials mentioned above are shown in **Table 3**

2.2.4.2 Belinostat

Belinostat is an isohydroxamic acid-derived pan-HDAC inhibitor that broadly inhibits all zinc-dependent HDAC enzymes (171). In a 2015 phase 2 study of relapsed/refractory PTCL (r/r PTCL), belinostat monotherapy demonstrated a completely durable response and manageable toxicity, showing an ORR in the 120 evaluable patients of 25.8% and a median PFS of 1.6 months (148). Based on this trial, belinostat monotherapy was approved by the FDA for the treatment of r/r PTCL patients in 2014. In a phase 2 trial for the treatment of r/r PTCL or relapsed/refractory CTCL (r/r CTCL), the ORR reached 25% in PTCL and 14% in CTCL (149). In a recent study, in patients with newly diagnosed PTCL, treatment with belinostat in combination with a standard cyclophosphamide, doxorubicin, vincristine, and prednisone (Bel-CHOP) regimen, resulted in an ORR of 86% (150). In addition, a randomized, phase 2B, multicentre, belinostat combination therapy trial for patients with r/r PTCL is recruiting (NCT04747236). The effect of belinostat in the treatment of B-cell lymphoma seems to be unsatisfactory. Among the 22 BL and DLBCL patients included, no patient achieved CR or PR (NCT00303953). The role of belinostat monotherapy or combination therapy in the treatment of B-cell lymphoma remains to be discussed. There is a phase 2 trial of belinostat as consolidation therapy with zidovudine for adult T-Cell leukemia-lymphoma (NCT02737046). Overall, the role of belinostat in the treatment of T-cell lymphoma is well established and its effectiveness in the treatment of B-cell lymphoma or other lymphoma needs to be further explored. Relevant clinical trials on belinostat are mentioned in **Table 3**.

2.2.4.3 Romidepsin

Romidepsin is a potent and selective inhibitor of HDAC, arrests the cell cycle, induces apoptosis and inhibits angiogenesis by enhancing acetylation, both of histones and non-histones (172). In a phase 2 trial, 96 patients with CTCL were included who had received at least one or more systemic therapies. Of these 71% had an advanced disease (≥ 2B) (151). The primary endpoint ORR was 34%, including 6 patients with CR. 26 of 68 patients (38%) with advanced disease achieved remission, including 5 CR. The median response time was 2 months and the median DOR was 15 months. In addition, a clinically meaningful improvement in pruritus was observed in the trial with a median duration of pruritus reduction of 6 months. In a phase 2 study in patients suffering from CTCL, romidepsin treatment resulted in a clinically meaningful reduction in pruritus (CMRP). The clinical benefit was evaluated by using a patient-assessed visual analog scale. A total of 44 of 96 patients (46%) achieved a significant clinical benefit, including objective response and/or defined CMRP, and 43% of 73 patients with moderate-to-severe pruritus experienced CMRP. The median time to CMRP was 1.8 months and the median duration of CMRP was 5.6 months (173). Based on these two phase 2 trials, romidepsin was approved by the FDA in November 2009 for the treatment of r/r CTCL patients. Foss et al. studied the efficacy and safety of romidepsin in patients with r/r CTCL with tumor stage and folliculotropic mycosis fungoides, where patients received 14 mg/m^2 of romidepsin on days 1, 8, and 15 of a 28-day cycle. The ORR to romidepsin treatment was found to be 45% (n = 20) in patients with skin tumors and 60% (n = 10) in patients with follicular disease involvement (149).

Two phase 2 studies examined the efficacy and safety of romidepsin in patients with PTCL. Of the 45 patients with PTCL included in the response analysis of the first study, 8 patients experienced CR and another 9 patients experienced PR with an ORR of 38% (152). The second phase 2 trial reported a 25% ORR, 15% CR/CR unconfirmed (CRu), a median of 1.8 months time to time to response (TTR), 17 months DOR (153). With a median PFS of 29 months, patients who achieved CR/CRu for ≥ 12 months had significantly longer survival versus those with CR/CRu for <12 months or <CR/CRu. For all patients, median PFS and OS were 4 months and 11.3 months, respectively (154). Based largely on these results, in 2011 the FDA accelerated approval of romidepsin for patients with ≥1 prior PTCL treatment. In a Japanese study of romidepsin in patients with r/r PTCL, the ORR was 43%, including 25% CR, with a median PFS of 5.6 months and a median DOR of 11.1 months (155). In a phase 3 trial comparing alisertib, gemcitabine, pralatrexate and romidepsin in patients with r/r PTCL, the ORRs were 33%, 35%, 43% and 43%, respectively, the median PFS were 115 days, 57 days, 101 days and 242 days, respectively (156).

TABLE 3 | Clinical trials of HDAC inhibitors.

Regimen	Disease	n	Phases	Status	Clinical results	Survival benefit	NCT ID
Vorinostat (140)	CTCL	74	Phase 2	Completed	29.7% ORR		NCT00091559
Vorinostat, Total skin electron beam therapy (TSEBT)	CTCL	28	Phase 1/2	Terminated	100% ORR	Duration of clinical benefit was 28 months	NCT01187446
Vorinostat (141)	Lymphoma	50	Phase 2	Completed	44% ORR	The median PFS was 18 months	NCT00875056
Vorinostat, Alisertib (142)	Lymphoma	34	Phase 1	Completed	12% ORR		NCT01567709
Vorinostat, Gemcitabine, Busulfan, Melphalan (143)	Lymphoma	78	Phase 1	Completed		DLBCL: the EFS rate was 61.5%, the OS rate was 73%; HL: the EFS rate was 40%, the OS rate was 80%	NCT01421173
Vorinostat, Rituximab (144)	NHL	30	Phase 2	Completed	46% ORR	The median PFS was 29.2 months	NCT00720876
Vorinostat (145)	FL, MZL, MCL	35	Phase 2	Completed	29% ORR	FL: the median PFS was 15.6 months; MCL: the median PFS was 5.9 months; MZL: the median PFS was 18.8 months	NCT00253630
Vorinostat, Cladribine, Rituximab (146)	relapsed B-cell NHL	57	Phase 2	Completed	79% ORR	The median PFS was 19.5 months	NCT00764517
Vorinostat, Azacitidine	DLBCL	15	Phase 1/2	Completed	6.7% ORR		NCT01120834
Vorinostat, Cyclophosphamide, Etoposide, Prednisone, Rituximab	r/r DLBCL	30	Phase 1/2	Completed	32% ORR		NCT00667615
Vorinostat, Gemcitabine, Clofarabine, Busulfan	NHL		Phase 2	Not yet recruiting			NCT04220008
Vorinostat, Busulfan, Gemcitabine, Melphalan, Olaparib, Rituximab	r/r Lymphoma		Phase 1	Recruiting			NCT03259503
Vorinostat, Pembrolizumab	r/r NHL		Phase 1	Recruiting			NCT03150329
Vorinostat, Cyclophosphamide, Doxorubicin Hydrochloride, Etoposide, Prednisone, Rituximab, Vincristine Sulfate	B-cell Lymphoma		Phase 1/2	Active, not recruiting			NCT01193842
Vorinostat, Cyclophosphamide, Doxorubicin Hydrochloride, Prednisone, Rituximab, Vincristine Sulfate	DLBCL		Phase 1/2	Active, not recruiting			NCT00972478
Vorinostat, Azacitidine	ENKTL-NT		Phase 1	Active, not recruiting			NCT00336063
Belinostat (148)	r/r PTCL	120	Phase 2	Completed	25.8% ORR	The median PFS was 1.6 months, OS was 7.9 months,	NCT00865969
Belinostat (149)	r/r CTCL, r/r PTCL	53	Phase 2	Terminated	PTCL: 25% (6/24) ORR; CTCL: 14% (4/29) ORR		NCT00274651
Belinostat, CHOP (150)	PTCL	23	Phase 1	Completed	86% ORR		NCT01839097
Belinostat	DLBCL, BL	22	Phase 2	Completed			NCT00303953
Belinostat, Azacitidine, Romidepsin, Pralatrexate, Gemcitabine	PTCL		Phase 2				NCT04747236
Romidepsin (151)	CTCL	96	Phase 2	Completed	34% ORR	The median time to response was 2 months; the median DOR was 15 months	NCT00106431
Romidepsin (151)	CTCL	30	Phase 2	Completed	Tumor stage: 45% ORR; folliculotropic mycosis fungoides: 60% ORR	Tumor stage: the median TTR was 1.9 months; folliculotropic mycosis fungoides: the median TTR was 2.1 months	NCT00106431
Romidepsin (152)	PTCL	45	Phase 2	Completed	38% ORR	The median DOR was 8.9 months	NCT00007345
Romidepsin (153, 154)	PTCL	130	Phase 2	Completed	25% ORR	The median PFS was 4 months; OS was 11.3 months	NCT00426764
Romidepsin (155)	PTCL	40	Phase 2	Completed	43% ORR	The median PFS was 5.6 months; the median DOR was 11.1 months	NCT01456039
Romidepsin (156)	PTCL	18	Phase 3	Completed	43% ORR	The median PFS was 242 days	NCT01482962
Romidepsin, Azacitidine (157)	PTCL	25	Phase 2	Completed	61% ORR	The median PFS was 8.0 month; the median DOR was 20.3 months	NCT01998035
Romidepsin, Gemcitabine (158)	PTCL	20	Phase 2	Completed	30% ORR	Two-year OS rate was 50%, two-year PFS rate was 11.2%	NCT01822886
Romidepsin, Chidamide	AITL		Phase 2	Not yet recruiting			NCT04831710
Romidepsin, Azacitidine, Bendamustine, Gemcitabine	r/r AITL		Phase 3	Active, not recruiting			NCT03593018

(Continued)

TABLE 3 | Continued

Regimen	Disease	n	Phases	Status	Clinical results	Survival benefit	NCT ID
Romidepsin	PTCL			Recruiting			NCT03742921
Romidepsin, Azacitidine, Belinostat, Pralatrexate, Gemcitabine	PTCL		Phase 2	Recruiting			NCT04747236
Romidepsin, Ixazomib	PTCL		Phase 1/2	Active, not recruiting			NCT03547700
Romidepsin, Pembrolizumab	r/r PTCL		Phase 1/2	Recruiting			NCT03278782
Romidepsin, Carfilzomib	r/r PTCL		Phase 1/2	Active, not recruiting			NCT03141203
Romidepsin, Lenalidomide	PTCL		Phase 2	Active, not recruiting			NCT02232516
Romidepsin, CHOEP	PTCL		Phase 1/2	Active, not recruiting			NCT02223208
Romidepsin, CHOP	PTCL		Phase 3	Active, not recruiting			NCT01796002
Romidepsin, Bortezomib, Duvelisib	r/r CTCL		Phase 1	Recruiting			NCT02783625
Romidepsin, Brentuximab vedotin	CTCL		Phase 1	Recruiting			NCT02616965
Romidepsin, Parsaclisib	r/r T-cell Lymphoma		Phase 1	Recruiting			NCT04774068
Romidepsin, Azacitidine, Duvelisib, Doxorubicin	T-cell Lymphoma		Phase 1	Not yet recruiting			NCT04639843
Romidepsin, Lenalidomide, Azacitidine, Dexamethasone	r/r T-cell Lymphoma		Phase 1	Recruiting			NCT04447027
Romidepsin, Azacitidine, Gemcitabine	T-cell Lymphoma		Phase 3	Active, not recruiting			NCT03703375
Romidepsin, Venetoclax	r/r T-cell Lymphoma		Phase 2	Recruiting			NCT03534180
Romidepsin, Carfilzomib, Lenalidomide	r/r T-cell Lymphoma		Phase 1/2	Active, not recruiting			NCT02341014
Romidepsin	T-cell NHL		Phase 2	Active, not recruiting			NCT01908777
Romidepsin, Lenalidomide	NHL		Phase 1/2	Active, not recruiting			NCT01755975
Panobinostat, Lenalidomide (159)	r/r HL	24	Phase 2	Completed	16.7% ORR	The median PFS was 3.8 months, the median OS was16.4 months	NCT01460940
Panobinostat, Ifosfamide, Carboplatin, Etoposide,	HL	40	Phase 1/2	Completed	85% ORR	65% Failure Free Survival	NCT01169636
Panobinostat, Everolimus	Lymphoma	61	Phase 1/2	Completed	33% ORR	20 mg panobinostat: the median PFS were 3.7 months; 30/40 mg panobinostat: the median PFS was 4.2 months	NCT00918333
Panobinostat, Rituximab	DLBCL	18	Phase 2	Terminated	11% ORR	The median PFS was 6 months	NCT01282476
Panobinostat, Rituximab (160)	DLBCL	40	Phase 2	Unknown status	28% ORR		NCT01238692
Panobinostat, Bortezomib (161)	PTCL	23	Phase 2	Completed	43% ORR	The median PFS was 2.59 months	NCT00901147
Panobinostat, Bexarotene (162)	CTCL	139	Phase 2	Completed	17.3% ORR	Bexarotene-exposed: the median PFS was 4.2 months; bexarotene-naïve: the median PFS was 3.7 months	NCT00425555
Panobinostat	r/r NHL	39	Phase 2	Active, not recruiting	21% ORR	The median PFS was 3.1 months, the median OS was 14.9 months	NCT01261247
Chidamide (163)	PTCL	79	Phase 2	completed	28% ORR	The median PFS was 2.1 months, the median OS was 21.4 months	
Chidamide, R-CHOP (164)	DLBCL	49	Phase 2	completed	94% ORR	Two-year PFS rate was 68%, two-year OS rate was 83%	NCT02753647
Chidamide (2021 ICML.Abstract No.209)	r/r PTCL	46	Phase 2	completed	46% ORR	The median PFS was 6 months, the medain OS was 23 months	
Chidamide, Cladribine, Gemcitabine, Busulfan (165)	r/r NHL	105	Phase 2	completed		Four-year PFS rate was 80.6%, four-year OS rate was 86.1%	NCT03151876
Chidamide, Sintilimab (2021 ASH Oral No.137)	ENKTL	30	Phase 2	completed	58% ORR, 47% CRR	The median PFS, OS, and DOR were 16.5, 28.5, and 20.6 months, respectively.	
Chidamide, Tislelizumab, Lenalidomid, Etoposide	r/r ENKTL	8	Phase 4	completed	87.5% ORR, 62.5% CRR		NCT04038411

(Continued)

TABLE 3 | Continued

Regimen	Disease	n	Phases	Status	Clinical results	Survival benefit	NCT ID
Chidamide, Azacitidine	AITL		Phase 2	Not yet recruiting			NCT05179213
Chidamide	DLBCL		Phase 2	Recruiting			NCT04661943
Chidamide, Cyclophosphamide, Rituximab, Doxorubicin, Vincristine, Prednisone, Ibrutinib, Lenalidomide, Decitabine	DLBCL		Phase 2	Recruiting			NCT04025593
Chidamide, Rituximab, Gemcitabine, Oxaliplatin	r/r DLBCL		Phase 2	Recruiting			NCT04022005
Chidamide, Anti-PD-1 Antibody, Rituximab	r/r DLBCL		Phase 2	Not yet recruiting			NCT05115409
Chidamide	r/r B-cell NHL		Phase 2	Recruiting			NCT03245905
Chidamide, Decitabine, CD19/20 CAR-T cells	r/r B-cell NHL		Phase 1/2	Recruiting			NCT04553393
Chidamide, Cyclophosphamide, Doxorubicin, Vincristine, Prednisone	AITL		Phase 2	Recruiting			NCT03853044
Chidamide, Sintilimab	r/r AITL		Phase 2	Not yet recruiting			NCT04831710
Chidamide, Sintilimab, Azacitidine, L-DEP	ENKTL		Phase 2	Not yet recruiting			NCT05008666
Chidamide, Sintilimab	ENKTL		Phase 2	Not yet recruiting			NCT04994210
Chidamide	ENKTL-NT		Not Applicable	Recruiting			NCT04511351
Chidamide, Sintilimab	ENKTL		Phase 1/2	Recruiting			NCT03820596
Chidamide, Etoposide	NKTCL		Phase 4	Recruiting			NCT04490590
Chidamide, PD-1 Antibody, Lenalidomide, Etoposide	NKTCL		Phase 4	Recruiting			NCT04038411
Chidamide, PD-1 antibody, Peg-Asparaginase	NKTCL		Phase 2	Recruiting			NCT04414969
Chidamide, Sintilimab	r/r CTCL		Phase 2	Recruiting			NCT04296786
Chidamide, Cyclophosphamide, Doxorubicin, Vincristine, Etoposide, Prednisone	PTCL		Phase 2	Recruiting			NCT03617432
Chidamide, Azacitidine, CHOP	PTCL		Phase 3	Not yet recruiting			NCT05075460
Chidamide, Cyclophosphamide, Epirubicin, Vindesine, Etoposide, Prednisone	PTCL		Phase 1/2	Recruiting			NCT02987244
Chidamide, Azacitidine	PTCL		Phase 2	Recruiting			NCT04480125
Chidamide, PD-1 antibody	PTCL		Phase 2	Recruiting			NCT04512534
Chidamide, CHOP	PTCL		Phase 2	Recruiting			NCT04480099
Chidamide, Sintilimab, Azacitidine	r/r PTCL		Phase 2	Not yet recruiting			NCT04052659
Chidamide, Lenalidomide	r/r PTCL		Phase 2	Recruiting			NCT04329130
Chidamide, Parsaclisib	r/r PTCL		Phase 1/2	Not yet recruiting			NCT05083208
Chidamide, Mitoxantrone Hydrochloride Liposome Injection	r/r PTCL		Phase 3	Not yet recruiting			NCT04668690
Chidamide	Lymphoma		Phase 2	Active, not recruiting			NCT03629873
Chidamide, Camrelizumab, Decitabine	HL		Phase 2	Recruiting			NCT04233294
Chidamide, Decitabine, Camrelizumab, Decitabine, Camrelizumab	HL		Phase 2	Recruiting			NCT04514081
Chidamide, Decitabine, Camrelizumab	NHL		Phase 1/2	Recruiting			NCT04337606
Chidamide, Chiauranib	r/r NHL		Phase 1/2	Recruiting			NCT03974243
Chidamide, APG-1252	r/r NHL		Phase 1/2	Not yet recruiting			NCT05186012
Abexinostat	FL, MCL	30	Phase 1/2	Completed	FL: 56.3% (9/16) ORR; MCL: 21.4% (3/14) ORR		NCT00724984
Abexinostat	NHL		Phase 1/2	Recruiting			NCT04024696

(Continued)

TABLE 3 | Continued

Regimen	Disease	n	Phases	Status	Clinical results	Survival benefit	NCT ID
Abexinostat, Ibrutinib	DLBCL, ML		Phase 1/2	Recruiting			NCT03939182
Abexinostat	r/r DLBCL		Phase 2	Recruiting			NCT03936153
Abexinostat	r/r FL		Phase 2	Recruiting			NCT03934567
Abexinostat	r/r FL		Phase 2	Active, not recruiting			NCT03600441
Entinostat (166)	r/r HL	49	Phase 2	Terminated	12% ORR, 24% DCR	The median PFS was 5.5 months, the medain OS was 25.1 months	NCT00866333
Entinostat, Pembrolizumab	r/r Lymphoma		Phase 2	Recruiting			NCT03179930
Entinostat, ZEN-3694	Lymphoma		Phase 1/2	Not yet recruiting			NCT05053971
Fimepinostat (167)	Lymphoma	33	Phase 1	Completed	24% ORR, 57% DCR		NCT01742988
Fimepinostat, Rituximab (168)	DLBCL	30	Phase 1	Completed	37% ORR	The medain DOR was 11.1 months, the median PFS was 2.9 months	NCT01742988
Fimepinostat (169)	r/r DLBCL and HGBL	66	Phase2	Completed	12% ORR, 30% DCR	The median PFS was 1.4 months	
Mocetinostat (170)	HL	51	Phase 2	Terminated	27% ORR		NCT00358982
Mocetinostat, Brentuximab Vedotin	r/r HL		Phase 1/2	Active, not recruiting			NCT02429375
Mocetinostat	r/r DLBCL, r/r FL		Phase 1/2	Active, not recruiting			NCT02282358
ITF2357, Mechlorethamine	HL	24	Phase 1/2	Completed			NCT00792467

More studies are currently focusing on the combined use of romidepsin. Combined oral azacitidine and a Tfh phenotype showed a higher ORR (80%) and CRR (67%) (157). In a phase 2 study on the role of gemcitabine plus romidepsin (GEMRO regimen) in the treatment of r/r PTCL patients, the ORR was 30% with 15% CRR, the two-year OS rate was 50% and the two-year PFS rate was 11.2% (158). Another important finding is that a pretreatment regimen of romidepsin combined with busulfan and fludarabine reduces the risk of relapse after allo-SCT in patients with aggressive T-cell tumors(2021 ASH Oral No.553).

At present, most clinical trials are still concerned with the role of romidepsin in T-cell lymphoma. For AITL patients, there have been clinical trials with romidepsin in combination with chidamide (NCT03593018) and also with romidepsin in combination with azacitidine, bendamustine, gemcitabine (NCT03593018). More types of combination drug regimens are being explored in patients with PTCL, such as romidepsin in combination with azacitidine, belinostat, pralatrexate, and gemcitabine (NCT04747236), romidepsin in combination with ixazomib (NCT03547700), and romidepsin in combination with pembrolizumab (NCT03278782) etc. The treatment options being tried in CTCL patients are romidepsin united brentuximab vedotin (NCT02616965) and romidepsin united bortezomib and duvelisib (NCT02783625). The performance of romidepsin in B-cell lymphoma is still unknown and it is hoped that more clinical trials in this area will be seen in the future. Relevant clinical trials on romidepsin are mentioned in **Table 3**.

2.2.4.4 Panobinostat

On February 23, 2015, the FDA approved panobinostat for the treatment of patients with multiple myeloma (MM). Panobinostat is a pan-HDACi with maximum potency against class I, II and IV histone deacetylases (174). The combination of panobinostat and the PI3K/mTOR inhibitor BEZ235 synergistically demonstrated effective inhibition of tumor growth and a prolonged survival in a mouse DLBCL xenograft model, demonstrating that PI3K inhibition enhances histone acetylation and enhances AKT dephosphorylation (175). In the trial of panobinostat and everolimus in the treatment of lymphoma, the combination treatment resulted in an ORR of 33% and the median PFS were 3.7 months and 4.2 months for patients treated with 20 mg and 30/40 mg panobinostat, respectively (NCT00918333). Panobinostat obtained a 21% ORR in NHL patients with a median PFS of 3.1 months (NCT01261247). In a phase 2 trial of panobinostat in combination with lenalidomide for the treatment of r/r HL, the ORR amounted up to 16.7%, which was lower than the ORR with either drug alone. The median PFS and OS were 3.8 and 16.4 months, respectively (159). In all 24 patients, grade 3 to 4 toxicities consisted of neutropenia (58%), throm-bocytopenia (42%), lymphopenia (25%), and febrile neutropenia (25%).These treatment results and adverse effects limited the further evaluation of this combination therapy. However, in a trial of panobinostat plus ifosfamide, carboplatin, and etoposide (ICE) against relapsed HL, the combination therapy demonstrated better results with an 85% ORR compared to ICE alone (75% ORR) (NCT01169636). Two clinical trials tested the efficacy of panobinostat in combination with rituximab in DLBCL. One of the trials was terminated due to slow accrual, and the results also showed that the combination therapy resulted in grade 3/4 thrombocytopenia in 44% of the patients (NCT01282476). The results of another trial were also unsatisfactory, with an overall remission rate of 29% for panobinostat and 26% for panobinostat plus rituximab. Moreover there appears to be a lacking benefit in adding rituximab to panobinostat (160).

In the treatment of T-cell lymphoma, panobinostat in combination with bortezomib performed well in the treatment of PTCL, reaching a 43% ORR (161). The greatest response was seen in patients with AITL, with 4 of 8 patients (50%) responding. Common treatment-related grade 3/4 AE continue to include thrombocytopenia (68%), and neutropenia (40%). In a CTCL setting, the benefit of a panobinostat with bexaroten combination therapy was greater than with panobinostat alone (20% ORR vs 15% ORR) (162). Clinical trials of panobinostat were stored in **Table 3**.

2.2.4.5 Chidamide

Chidamide, an original anti-cancer drug with Chinese intellectual property rights, was approved for global marketing as a benzylamine histone deacetylase inhibitor, designed to block the catalytic pocket of class I HDACs and to inhibit the activity of HDAC1, 2, 3, and 10, which results in growth arrest and apoptosis. In a phase 2 study of r/r PTCL, 79 patients were treated with chidamide monotherapy (163). The results were significant, with an ORR of 28%, of these, 14% had CR/CRu. Patients with AITL tend to have a higher ORR (50%) and CR/CRu rates (40%), as well as longer lasting responses to chidamide therapy. The median PFS and OS were 2.1 and 21.4 months, respectively. The majority of AE were of grade 1/2 and those that occurred in ≥10% of the patients were of grade ≥3: thrombocytopenia (22%), leukopenia (13%), and neutropenia (11%). In 2017, Shi et al. published a paper describing chidamide in the treatment of r/r PTCL: a multicenter real-world study in China (176). For the 256 patients receiving chidamide monotherapy, the ORR and DCR were 39.06% and 64.45%, respectively, with a median PFS of 129 days. In 127 patients receiving chidamide in combination with chemotherapy, the ORR and DCR were 51.18% and 74.02%, respectively, with a median PFS of 152 days. In a phase 2 study of chidamide in combination with rituximab plus cyclophosphamide, doxorubicin, vincristine, and prednisone (R-CHOP) in 49 elderly patients with no reported grade 4 non-hematologic toxicity, suffering from newly diagnosed DLBCL, the CRR was 86%, ORR was 94%, and 2-year PFS and OS rates were 68% and 83%, respectively (164). These results suggest that chidamide in combination with R-CHOP is effective and safe in elderly patients with newly diagnosed DLBCL. A Japanese phase 2 clinical study demonstrates the effectiveness of chidamide monotherapy for r/r PTCL. The ORR was 46% in 46 evaluable patients and up to 88% in AITL patients. The median PFS and OS were 6 months and 23 months, respectively (2021 ICML.Abstract No.209). A new conditioning regimen with chidamide, cladribine, gemcitabine and busulfan (ChiCGB), significantly improved the outcome of high-risk or relapsed/refractory NHL (r/r NHL) (165). All 105 patients with high-risk, relapsed/refractory lymphoma who received ChiCGB as a conditioning therapy after transplantation of autologous peripheral stem cells, achieved complete hematopoietic recovery. At a median follow-up of 35.4 months, 80.6% of the patients were free of tumor progression with a high PFS rate and OS rate of 80.6% and 86.1%, respectively, with 94.5% of patients with B-cell NHL and 75.4% of patients with NKTCL surviving. Huang et al. initiated a clinical trial of sintilimab in combination with chidamide (SC) for the treatment of ENKTL. All patients first received 2-3 cycles of sintilimab (200 mg) in combination with chidamide (30 mg twice weekly). For early stage (stage I-II) patients, 2 cycles of SC combined with sequential 2-4 cycles of pegaspargase plus gemcitabine and oxaliplatin (P-Gemox) followed by involved field radiotherapy (IFRT) were given; for late stage (stage III-IV) patients, 3 cycles of SC followed by sequential 3-6 cycles of P-Gemox treatment were used. Of the 30 patients whose efficacy could be evaluated, the ORR reached 58%, with a CRR of 47%. The median PFS, OS and DOR were 16.5 months, 28.5 months, and 20.6 months, respectively. The incidence of AE was 56%, mainly from sintilimab or chidamide alone, and recovered by dose reduction or discontinuation, with the SC regimen demonstrating promising efficacy and high safety in patients with ENKTL (2021 ASH Oral No.137). Another regimen used to treat relapsed/refractory ENKTL (r/r ENKTL) is tislelizumab combined with chidamide, lenalidomid and etoposide. In 8 evaluable patients, 87.5% ORR and 62.5% CRR were achieved (NCT04038411).

A very large number of clinical trials have been conducted to explore the therapeutic effects of chidamide in different types of lymphoma. In patients with DLBCL, clinical trials are currently underway with chidamide monotherapy (NCT04661943), chidamide in combination with R-CHOP and placebo (NCT04231448), and chidamide in combination with rituximab, gemcitabine, and oxaliplatin (NCT04022005). In patients with AITL, the treatment options being tried are chidamide in combination with cyclophosphamide, doxorubicin, vincristine, and prednisone (NCT03853044), chidamide in combination with azacitidine (NCT05179213), and chidamide in combination with sintilimab (NCT04831710). Chidamide in combination with sintilimab has also been used in ENKTL patients (NCT05008666, NCT04994210). In contrast, in patients with NKTCL, more clinical trials have opted for a combination regimen with PD-1 antibodies (NCT04038411, NCT04414969). There are also many studies on how well chidamide works in patients with PTCL. These include not only combinations with traditional chemotherapy regimens such as CHOP (NCT05075460, NCT04480099), but also with other epigenetic drugs such as azacidine (NCT04480125), and with targeted drugs such as sintilimab (NCT04052659) and PD-1 antibodies (NCT04512534). In HL patients, the drugs of choice in most clinical trials are chidamide, decitabine and camrelizumab (NCT04233294, NCT04514081). Chidamide, an emerging HDAC inhibitor, has achieved good results in the treatment of certain types of lymphoma, and we need to further explore its efficacy for more types of lymphoma in the future. The trials mentioned above and other chidamide related trials are shown in **Table 3**.

2.2.4.6 Abexinostat

Abexinostat (CRA-024781) is a broad-spectrum isohydroxamic acid-based HDAC inhibitor that demonstrated promising antitumor activity in a phase 1 clinical trial evaluating cancer (177). As shown in **Table 3**, the primary results reported in their phase 2 trial showed 56.3% ORR in FL and 21.4% ORR in MCL

(NCT00724984). As there are fewer evaluations of the efficacy of abexinostat, more clinical trials are still focusing on the efficacy of abexinostat alone in the treatment of DLBCL (NCT03936153) and FL (NCT03934567, NCT03600441).

2.2.4.7 Entinostat

Entinostat is a selective inhibitor of HDAC 1, 2, 3, and 11 (178). *In vitro* tests have shown that entinostat produces strong anti-proliferative and immunomodulatory signals through modulation of cytokine and chemokine levels, and displays synergistic effects when combined with immune checkpoint therapies (179, 180). In a phase 2 trial of entinostat against r/r HL, the ORR was 12% while the DCR was 24%, with a median PFS and OS of 5.5 and 25.1 months (166). Entinostat demonstrated good tolerability with significant clinical activity in a large number of pretreated HL patients. Based on these entinostat properties, combination applications with other drugs might be more promising in future trails. Clinical trials enrolling entinostat in combination with pembrolizumab (NCT03179930) or entinostat in combination with ZEN-3694 for lymphoma (NCT05053971). Relevant clinical trials mentioned are shown in **Table 3**.

2.2.4.8 Fimepinostat

Recent evidence suggests that both the PI3K-Akt-mTOR signaling pathway and HDAC are effective targets in blood cancers. Dual targeting can overcome primary resistance and block secondary resistance due to compensatory/feedback mechanisms in cancer cells. Fimepinostat (CUDC-907) is also a dual inhibitor of HDAC (class I and II) and PI3K (class I α, β, and δ). In a phase 1 trial evaluating CUDC-907, single agent use reached 24% ORR. Of the 9 DLBCL patients, 2 patients achieved CR and 3 patients achieved PR, and SD was observed in 19 (57%) out of 37 patients evaluable for response (167). In its phase 1 expansion trial, 30 DLBCL patients were evaluated for CUDC-907 alone or in combination with rituximab (168). The results shown that the ORR of the evaluable patient cohort was 37%, with 9 of 19 (47%) reporting objective remission with monotherapy and 2 of 11 (18%) reporting objective response with combination therapy. The median PFS for all DLBCL patients in the study was 2.9 months, with a median PFS of 5.7 months in patients treated with monotherapy and 1.3 months in patients treated with combination therapy. In the phase 2 study that included 66 r/r DLBCL and high-grade B-cell lymphoma (HGBL) patients, CUDC-907 monotherapy amounted up to 12% ORR and the PFS was 1.4 months (169). However, monotherapy in patients with r/r DLBCL and HGBL in the presence of *MYC* alterations achieved an extended duration of reflection, and combination therapies or biomarker-based patient selection strategies may lead to higher response rates in future clinical trials. The tests mentioned above are listed in **Table 3**.

2.2.4.9 Mocetinostat and Givinostat

Mocetinostat (MGCD0103) is an oral isotype-selective non-hydroxamic acid HDAC inhibitor targeting isotypes HDAC 1, 2, 3, and 11. It induces histone hyperacetylation, selectively induces apoptosis, and causes cell cycle arrest in a dose-dependent manner in various human cancer cell lines (181). In the phase 2 trial enrolling 51 patients with HL, the ORR for mocetinostat monotherapy was 27%, and 34 of 42 patients (81%) who completed at least 2 treatment cycles had decreases in tumor measurements (170). Another HDAC inhibitor against HL, givinostat (ITF2357), is also subject to clinical trials. These trails showed that ITF2357 in combination with mechlorethamine could achieve a 25% ORR and 28.66 months of PFS (NCT00792467). The above two drugs seem to have limited effect in the treatment of HL and hopefully in the future more epigenetic drugs will be available for the treatment of HL. There is now a clinical trial evaluating mocetinostat in combination with brentuximab vedotin in patients with HL (NCT02429375), and another study exploring mocetinostat alone in DLBCL and FL (NCT02282358). Relevant clinical trials mentioned are shown in **Table 3**.

2.2.5 BET Inhibitors

As readers of histone acetylation, BET proteins can bind to acetylated lysine residues in the histone tail, thereby carrying the extended complex to the promoter region and activating transcription in that region. Histone acetylation is prevalent in super enhancers of oncogene expression, therefore inhibiting the binding of BET proteins to chromatin has a significant impact on transcription, which in turn resulted in the studies of many bromodomain inhibitors. The BET inhibitor RVX2135 has been shown in mouse models to inhibit lymphoma proliferation and to induce apoptosis. Moreover, it sensitizes *Myc* overexpressing lymphocytes by inducing HDAC silencing genes that synergize with HDAC inhibitors to kill lymphocytes (182). The small molecule inhibitor OTX015 (MK-8628) specifically binds to the bromodomain motif BRD2, BRD3, and BRD4 of BET proteins and keeps them bound to acetylated histones and this binding occurs preferentially in the oncogene super enhancer region. Based on a phase 1 trial evaluating the safety and pharmacokinetics of OTX015, the recommended once-daily dose of oral single-agent oral OTX015 in lymphoma patients was 80 mg, with an additional 9.1% ORR observed in 33 lymphoma patients (183).

2.3 Discussions

There is no doubt that the therapeutic effect of epigenetic drugs in lymphoma is remarkable. In the future, on the one hand we are interested in the appropriate dosing regimen in the treatment of lymphoma. Combining laboratory data with clinical experience provides the most beneficial recommendations for patients. Combining epigenetic therapies with other currently prevailing therapies, such as with immunotherapy, to combat refractory or relapsed lymphomas in a common face. On the other hand, the development of drugs for epigenetic interventions is undoubtedly promising and challenging, as systematic functional genomic and molecular mechanistic studies will provide new pathways and targets for "synthetic lethal strategies"; the development of computer-aided tools, animal models and other technologies will also create better conditions for lead compounds to enter clinical studies. Increased investment in research and development and larger screening scales will also accelerate the process of new drug

development. We have every reason to believe that epigenetic therapies will fundamentally change the management of lymphoma patients and become an integral part of lymphoma treatment.

AUTHOR CONTRIBUTIONS

JXL, JNL, HW, and PL contributed to the conception and design of the study. JXL, JNL, and HW collected the data. JXL wrote the first draft of the manuscript. JNL and HW wrote parts of the manuscript. All authors contributed to the revision of the manuscript, read, and approved the submitted version.

FUNDING

This work was supported by grants from the National Natural Science Foundation of China (Grant No. 81972595).

ACKNOWLEDGMENTS

The work was supported by the Sun Yet-Sen University Cancer Center, State Key Laboratory of Oncology in South China, Collaborative Innovation Center for Cancer Medicine and Department of Medical Oncology, Sun Yat-Sen University Cancer Center, and I would like to show great gratitude to them all.

REFERENCES

1. Swerdlow AJ. Epidemiology of Hodgkin's Disease and Non-Hodgkin's Lymphoma. *Eur J Nucl Med Mol Imaging* (2003) 30 Suppl 1:S3–12. doi: 10.1007/s00259-003-1154-9
2. Siegel RL, Miller KD, Jemal A. Cancer Statistics, 2018. *CA Cancer J Clin* (2018) 68(1):7–30. doi: 10.3322/caac.21442
3. Shankland KR, Armitage JO, Hancock BW. Non-Hodgkin Lymphoma. *Lancet* (2012) 380(9844):848–57. doi: 10.1016/S0140-6736(12)60605-9
4. Hennessy BT, Hanrahan EO, Daly PA. Non-Hodgkin Lymphoma: An Update. *Lancet Oncol* (2004) 5(6):341–53. doi: 10.1016/S1470-2045(04)01490-1
5. Diefenbach CS, Connors JM, Friedberg JW, Leonard JP, Kahl BS, Little RF, et al. Hodgkin Lymphoma: Current Status and Clinical Trial Recommendations. *J Natl Cancer Inst* (2017) 109(4):djw249. doi: 10.1093/jnci/djw249
6. Hanahan D, Weinberg RA. Hallmarks of Cancer: The Next Generation. *Cell* (2011) 144(5):646–74. doi: 10.1016/j.cell.2011.02.013
7. Baylin SB, Jones PA. A Decade of Exploring the Cancer Epigenome - Biological and Translational Implications. *Nat Rev Cancer* (2011) 11(10):726–34. doi: 10.1038/nrc3130
8. Brabletz T. To Differentiate or Not–Routes Towards Metastasis. *Nat Rev Cancer* (2012) 12(6):425–36. doi: 10.1038/nrc3265
9. Baylin SB, Jones PA. Epigenetic Determinants of Cancer. *Cold Spring Harb Perspect Biol* (2016) 8(9):a019505. doi: 10.1101/cshperspect.a019505
10. Ozyerli-Goknar E, Bagci-Onder T. Epigenetic Deregulation of Apoptosis in Cancers. *Cancers (Basel)* (2021) 13(13):3210. doi: 10.3390/cancers13133210
11. Goldberg AD, Allis CD, Bernstein E. Epigenetics: A Landscape Takes Shape. *Cell* (2007) 128(4):635–8. doi: 10.1016/j.cell.2007.02.006
12. Achinger-Kawecka J, Clark SJ. Disruption of the 3D Cancer Genome Blueprint. *Epigenomics* (2017) 9(1):47–55. doi: 10.2217/epi-2016-0111
13. Hogg SJ, Beavis PA, Dawson MA, Johnstone RW. Targeting the Epigenetic Regulation of Antitumour Immunity. *Nat Rev Drug Discov* (2020) 19(11):776–800. doi: 10.1038/s41573-020-0077-5
14. Liu MK, Sun XJ, Gao XD, Qian Y, Wang L, Zhao WL. Methylation Alterations and Advance of Treatment in Lymphoma. *Front Biosci (Landmark Ed)* (2021) 26(9):602–13. doi: 10.52586/4970
15. Pan DS, Yang QJ, Fu X, Shan S, Zhu JZ, Zhang K, et al. Discovery of an Orally Active Subtype-Selective HDAC Inhibitor, Chidamide, as an Epigenetic Modulator for Cancer Treatment. *Medchemcomm* (2014) 5(12):1789–96. doi: 10.1039/C4MD00350K
16. Jeltsch A. Beyond Watson and Crick: DNA Methylation and Molecular Enzymology of DNA Methyltransferases. *Chembiochem* (2002) 3(4):274–93. doi: 10.1002/1439-7633(20020402)3:4<274::AID-CBIC274>3.0.CO;2-S
17. Hermann A, Gowher H, Jeltsch A. Biochemistry and Biology of Mammalian DNA Methyltransferases. *Cell Mol Life Sci* (2004) 61(19-20):2571–87. doi: 10.1007/s00018-004-4201-1
18. Jeltsch A, Jurkowska RZ. Allosteric Control of Mammalian DNA Methyltransferases - A New Regulatory Paradigm. *Nucleic Acids Res* (2016) 44(18):8556–75. doi: 10.1093/nar/gkw723
19. Hoang NM, Rui L. DNA Methyltransferases in Hematological Malignancies. *J Genet Genomics* (2020) 47(7):361–72. doi: 10.1016/j.jgg.2020.04.006
20. Subramaniam D, Thombre R, Dhar A, Anant S. DNA Methyltransferases: A Novel Target for Prevention and Therapy. *Front Oncol* (2014) 4:80. doi: 10.3389/fonc.2014.00080
21. Skvortsova K, Iovino N, Bogdanovic O. Functions and Mechanisms of Epigenetic Inheritance in Animals. *Nat Rev Mol Cell Biol* (2018) 19(12):774–90. doi: 10.1038/s41580-018-0074-2
22. Li XY, Li Y, Zhang L, Liu X, Feng L, Wang X. The Antitumor Effects of Arsenic Trioxide in Mantle Cell Lymphoma *via* Targeting Wnt/betacatenin Pathway and DNA Methyltransferase-1. *Oncol Rep* (2017) 38(5):3114–20. doi: 10.3892/or.2017.5945
23. Robaina MC, Mazzoccoli L, Arruda VO, Reis FR, Apa AG, de Rezende LM, et al. Deregulation of DNMT1, DNMT3B and miR-29s in Burkitt Lymphoma Suggests Novel Contribution for Disease Pathogenesis. *Exp Mol Pathol* (2015) 98(2):200–7. doi: 10.1016/j.yexmp.2015.03.006
24. Candace J, Poole1 WZ, Atul L, Yevtodiyenko Al, Liefwalker D, Li H, et al. DNMT3B Overexpression Contributes to Aberrant DNA Methylation and MYC-Driven Tumor Maintenance in T-ALL and Burkitt's Lymphoma. *Oncotarget* (2017) 8:76898–920. doi: 10.18632/oncotarget.20176
25. Amara K, Ziadi S, Hachana M, Soltani N, Korbi S, Trimeche M. DNA Methyltransferase DNMT3b Protein Overexpression as a Prognostic Factor in Patients With Diffuse Large B-Cell Lymphomas. *Cancer Sci* (2010) 101(7):1722–30. doi: 10.1111/j.1349-7006.2010.01569.x
26. Szablewski V, Bret C, Kassambara A, Devin J, Cartron G, Costes-Martineau V, et al. An Epigenetic Regulator-Related Score (EpiScore) Predicts Survival in Patients With Diffuse Large B Cell Lymphoma and Identifies Patients Who may Benefit From Epigenetic Therapy. *Oncotarget* (2018) 9(27):19079–99. doi: 10.18632/oncotarget.24901
27. Couronne L, Bastard C, Bernard OA. TET2 and DNMT3A Mutations in Human T-Cell Lymphoma. *N Engl J Med* (2012) 366(1):95–6. doi: 10.1056/NEJMc1111708
28. O'Connor OA, Bhagat G, Ganapathi K, Pedersen MB, D'Amore F, Radeski D, et al. Changing the Paradigms of Treatment in Peripheral T-Cell Lymphoma: From Biology to Clinical Practice. *Clin Cancer Res* (2014) 20(20):5240–54. doi: 10.1158/1078-0432.CCR-14-2020
29. Watatani Y, Sato Y, Miyoshi H, Sakamoto K, Nishida K, Gion Y, et al. Molecular Heterogeneity in Peripheral T-Cell Lymphoma, Not Otherwise Specified Revealed by Comprehensive Genetic Profiling. *Leukemia* (2019) 33(12):2867–83. doi: 10.1038/s41375-019-0473-1
30. Tahiliani M, Koh KP, Shen Y, Pastor WA, Bandukwala H, Brudno Y, et al. Conversion of 5-Methylcytosine to 5-Hydroxymethylcytosine in Mammalian DNA by MLL Partner TET1. *Science* (2009) 324(5929):930–5. doi: 10.1126/science.1170116
31. Hashimoto H, Liu Y, Upadhyay AK, Chang Y, Howerton SB, Vertino PM, et al. Recognition and Potential Mechanisms for Replication and Erasure of Cytosine Hydroxymethylation. *Nucleic Acids Res* (2012) 40(11):4841–9. doi: 10.1093/nar/gks155
32. Lio CJ, Yuita H, Rao A. Dysregulation of the TET Family of Epigenetic Regulators in Lymphoid and Myeloid Malignancies. *Blood* (2019) 134(18):1487–97. doi: 10.1182/blood.2019791475

33. Ko M, An J, Pastor WA, Koralov SB, Rajewsky K, Rao A. TET Proteins and 5-Methylcytosine Oxidation in Hematological Cancers. *Immunol Rev* (2015) 263(1):6–21. doi: 10.1111/imr.12239
34. Quivoron C, Couronné L, Della Valle V, Lopez CK, Plo I, Wagner-Ballon O, et al. TET2 Inactivation Results in Pleiotropic Hematopoietic Abnormalities in Mouse and Is a Recurrent Event During Human Lymphomagenesis. *Cancer Cell* (2011) 20(1):25–38. doi: 10.1016/j.ccr.2011.06.003
35. Lemonnier F, Couronné L, Parrens M, Jaïs JP, Travert M, Lamant L, et al. Recurrent TET2 Mutations in Peripheral T-Cell Lymphomas Correlate With TFH-Like Features and Adverse Clinical Parameters. *Blood* (2012) 120 (7):1466–9. doi: 10.1182/blood-2012-02-408542
36. Odejide O, Weigert O, Lane AA, Toscano D, Lunning MA, Kopp N, et al. A Targeted Mutational Landscape of Angioimmunoblastic T-Cell Lymphoma. *Blood* (2014) 123(9):1293–6. doi: 10.1182/blood-2013-10-531509
37. Guo YM, Liu XF, Jiao LJ, Yin SY, Wang Z, Li XX, et al. Angioimmunoblastic T-Cell Lymphoma: Histopathological Grading and Prognosis. *Zhonghua Bing Li Xue Za Zhi* (2019) 48(10):784–90. doi: 10.3760/cma.j.issn.0529-5807.2019.10.007
38. Zhang W, He X, Hu J, Yang P, Liu C, Wang J, et al. Dysregulation of N(6)-Methyladenosine Regulators Predicts Poor Patient Survival in Mantle Cell Lymphoma. *Oncol Lett* (2019) 18(4):3682–90. doi: 10.3892/ol.2019.10708
39. Cortés JR, Palomero T. The Curious Origins of Angioimmunoblastic T-Cell Lymphoma. *Curr Opin Hematol* (2016) 23(4):434–43. doi: 10.1097/MOH.0000000000000261
40. Sakata-Yanagimoto M, Enami T, Yoshida K, Shiraishi Y, Ishii R, Miyake Y, et al. Somatic RHOA Mutation in Angioimmunoblastic T Cell Lymphoma. *Nat Genet* (2014) 46(2):171–5. doi: 10.1038/ng.2872
41. Cairns RA, Iqbal J, Lemonnier F, Kucuk C, de Leval L, Jais JP, et al. IDH2 Mutations Are Frequent in Angioimmunoblastic T-Cell Lymphoma. *Blood* (2012) 119(8):1901–3. doi: 10.1182/blood-2011-11-391748
42. Wang C, McKeithan TW, Gong Q, Zhang W, Bouska A, Rosenwald A, et al. IDH2R172 Mutations Define a Unique Subgroup of Patients With Angioimmunoblastic T-Cell Lymphoma. *Blood* (2015) 126(15):1741–52. doi: 10.1182/blood-2015-05-644591
43. Peixoto P, Cartron PF, Serandour AA, Hervouet E. From 1957 to Nowadays: A Brief History of Epigenetics. *Int J Mol Sci* (2020) 21(20):7571. doi: 10.3390/ijms21207571
44. Bhat KP, Ümit Kaniskan H, Jin J, Gozani O. Epigenetics and Beyond: Targeting Writers of Protein Lysine Methylation to Treat Disease. *Nat Rev Drug Discov* (2021) 20(4):265–86. doi: 10.1038/s41573-020-00108-x
45. Rao RC, Dou Y. Hijacked in Cancer: The KMT2 (MLL) Family of Methyltransferases. *Nat Rev Cancer* (2015) 15(6):334–46. doi: 10.1038/nrc3929
46. Morin RD, Mendez-Lago M, Mungall AJ, Goya R, Mungall KL, Corbett RD, et al. Frequent Mutation of Histone-Modifying Genes in Non-Hodgkin Lymphoma. *Nature* (2011) 476(7360):298–303. doi: 10.1038/nature10351
47. Ortega-Molina A, Boss IW, Canela A, Pan H, Jiang Y, Zhao C, et al. The Histone Lysine Methyltransferase KMT2D Sustains a Gene Expression Program That Represses B Cell Lymphoma Development. *Nat Med* (2015) 21(10):1199–208. doi: 10.1038/nm.3943
48. Zhang J, Dominguez-Sola D, Hussein S, Lee JE, Holmes AB, Bansal M, et al. Disruption of KMT2D Perturbs Germinal Center B Cell Development and Promotes Lymphomagenesis. *Nat Med* (2015) 21(10):1190–8. doi: 10.1038/nm.3940
49. Ferrero S, Rossi D, Rinaldi A, Bruscaggin A, Spina V, Eskelund CW, et al. KMT2D Mutations and TP53 Disruptions Are Poor Prognostic Biomarkers in Mantle Cell Lymphoma Receiving High-Dose Therapy: A FIL Study. *Haematologica* (2020) 105(6):1604–12. doi: 10.3324/haematol.2018.214056
50. Gilan O, Lam EY, Becher I, Lugo D, Cannizzaro E, Joberty G, et al. Functional Interdependence of BRD4 and DOT1L in MLL Leukemia. *Nat Struct Mol Biol* (2016) 23(7):673–81. doi: 10.1038/nsmb.3249
51. Daigle SR, Olhava EJ, Therkelsen CA, Basavapathruni A, Jin L, Boriack-Sjodin PA, et al. Potent Inhibition of DOT1L as Treatment of MLL-Fusion Leukemia. *Blood* (2013) 122(6):1017–25. doi: 10.1182/blood-2013-04-497644
52. Chase A, Cross NC. Aberrations of EZH2 in Cancer. *Clin Cancer Res* (2011) 17(9):2613–8. doi: 10.1158/1078-0432.CCR-10-2156
53. Martin MC, Zeng G, Yu J, Schiltz GE. Small Molecule Approaches for Targeting the Polycomb Repressive Complex 2 (PRC2) in Cancer. *J Med Chem* (2020) 63(24):15344–70. doi: 10.1021/acs.jmedchem.0c01344
54. Béguelin W, Popovic R, Teater M, Jiang Y, Bunting KL, Rosen M, et al. EZH2 is Required for Germinal Center Formation and Somatic EZH2 Mutations Promote Lymphoid Transformation. *Cancer Cell* (2013) 23(5):677–92. doi: 10.1016/j.ccr.2013.04.011
55. Morin RD, Johnson NA, Severson TM, Mungall AJ, An J, Goya R, et al. Somatic Mutations Altering EZH2 (Tyr641) in Follicular and Diffuse Large B-Cell Lymphomas of Germinal-Center Origin. *Nat Genet* (2010) 42 (2):181–5. doi: 10.1038/ng.518
56. Bouska A, Zhang W, Gong Q, Iqbal J, Scuto A, Vose J, et al. Combined Copy Number and Mutation Analysis Identifies Oncogenic Pathways Associated With Transformation of Follicular Lymphoma. *Leukemia* (2017) 31(1):83–91. doi: 10.1038/leu.2016.175
57. Lue JK, Prabhu SA, Liu Y, Gonzalez Y, Verma A, Mundi PS, et al. Precision Targeting With EZH2 and HDAC Inhibitors in Epigenetically Dysregulated Lymphomas. *Clin Cancer Res* (2019) 25(17):5271–83. doi: 10.1158/1078-0432.CCR-18-3989
58. Tian X, Pelton A, Shahsafaei A, Dorfman DM. Differential Expression of Enhancer of Zeste Homolog 2 (EZH2) Protein in Small Cell and Aggressive B-Cell Non-Hodgkin Lymphomas and Differential Regulation of EZH2 Expression by P-ERK1/2 and MYC in Aggressive B-Cell Lymphomas. *Mod Pathol* (2016) 29(9):1050–7. doi: 10.1038/modpathol.2016.114
59. McCabe MT, Ott HM, Ganji G, Korenchuk S, Thompson C, Van Aller GS, et al. EZH2 Inhibition as a Therapeutic Strategy for Lymphoma With EZH2-Activating Mutations. *Nature* (2012) 492(7427):108–12. doi: 10.1038/nature11606
60. Yap DB, Chu J, Berg T, Schapira M, Cheng SW, Moradian A, et al. Somatic Mutations at EZH2 Y641 Act Dominantly Through a Mechanism of Selectively Altered PRC2 Catalytic Activity, to Increase H3K27 Trimethylation. *Blood* (2011) 117(8):2451–9. doi: 10.1182/blood-2010-11-321208
61. Berg T, Thoene S, Yap D, Wee T, Schoeler N, Rosten P, et al. A Transgenic Mouse Model Demonstrating the Oncogenic Role of Mutations in the Polycomb-Group Gene EZH2 in Lymphomagenesis. *Blood* (2014) 123 (25):3914–24. doi: 10.1182/blood-2012-12-473439
62. Souroullas GP, Jeck WR, Parker JS, Simon JM, Liu JY, Paulk J, et al. An Oncogenic Ezh2 Mutation Induces Tumors Through Global Redistribution of Histone 3 Lysine 27 Trimethylation. *Nat Med* (2016) 22(6):632–40. doi: 10.1038/nm.4092
63. McCabe MT, Graves AP, Ganji G, Diaz E, Halsey WS, Jiang Y, et al. Mutation of A677 in Histone Methyltransferase EZH2 in Human B-Cell Lymphoma Promotes Hypertrimethylation of Histone H3 on Lysine 27 (H3K27). *Proc Natl Acad Sci USA* (2012) 109(8):2989–94. doi: 10.1073/pnas.1116418109
64. Zhang H, Lv H, Jia X, Hu G, Kong L, Zhang T, et al. Clinical Significance of Enhancer of Zeste Homolog 2 and Histone Deacetylases 1 and 2 Expression in Peripheral T-Cell Lymphoma. *Oncol Lett* (2019) 18(2):1415–23. doi: 10.3892/ol.2019.10410
65. Sarkar D, Leung EY, Baguley BC, Finlay GJ, Askarian-Amiri ME. Epigenetic Regulation in Human Melanoma: Past and Future. *Epigenetics* (2015) 10 (2):103–21. doi: 10.1080/15592294.2014.1003746
66. Li H, Rauch T, Chen ZX, Szabó PE, Riggs AD, Pfeifer GP. The Histone Methyltransferase SETDB1 and the DNA Methyltransferase DNMT3A Interact Directly and Localize to Promoters Silenced in Cancer Cells. *J Biol Chem* (2006) 281(28):19489–500. doi: 10.1074/jbc.M513249200
67. Segovia C, San José-Enériz E, Munera-Maravilla E, Martínez-Fernández M, Garate L, Miranda E, et al. Inhibition of a G9a/DNMT Network Triggers Immune-Mediated Bladder Cancer Regression. *Nat Med* (2019) 25(7):1073–81. doi: 10.1038/s41591-019-0499-y
68. Michalak EM, Burr ML, Bannister AJ, Dawson MA. The Roles of DNA, RNA and Histone Methylation in Ageing and Cancer. *Nat Rev Mol Cell Biol* (2019) 20(10):573–89. doi: 10.1038/s41580-019-0143-1
69. Hatzi K, Geng H, Doane AS, Meydan C, LaRiviere R, Cardenas M, et al. Histone Demethylase LSD1 Is Required for Germinal Center Formation and BCL6-Driven Lymphomagenesis. *Nat Immunol* (2019) 20(1):86–96. doi: 10.1038/s41590-018-0273-1
70. Liu H, Wei J, Sang N, Zhong X, Zhou X, Yang X, et al. The Novel LSD1 Inhibitor ZY0511 Suppresses Diffuse Large B-Cell Lymphoma Proliferation by Inducing Apoptosis and Autophagy. *Med Oncol* (2021) 38(10):124. doi: 10.1007/s12032-021-01572-0

71. Zou ZK, Huang YQ, Zou Y, Zheng XK, Ma XD. Silencing of LSD1 Gene Modulates Histone Methylation and Acetylation and Induces the Apoptosis of JeKo-1 and MOLT-4 Cells. *Int J Mol Med* (2017) 40(2):319–28. doi: 10.3892/ijmm.2017.3032
72. Zhu F, Rui L. PRMT5 in Gene Regulation and Hematologic Malignancies. *Genes Dis* (2019) 6(3):247–57. doi: 10.1016/j.gendis.2019.06.002
73. Boisvert FM, Côté J, Boulanger MC, Richard S. A Proteomic Analysis of Arginine-Methylated Protein Complexes. *Mol Cell Proteomics* (2003) 2 (12):1319–30. doi: 10.1074/mcp.M300088-MCP200
74. Koh CM, Bezzi M, Low DH, Ang WX, Teo SX, Gay FP, et al. MYC Regulates the Core Pre-mRNA Splicing Machinery as an Essential Step in Lymphomagenesis. *Nature* (2015) 523(7558):96–100. doi: 10.1038/nature14351
75. Chung J, Karkhanis V, Tae S, Yan F, Smith P, Ayers LW, et al. Protein Arginine Methyltransferase 5 (PRMT5) Inhibition Induces Lymphoma Cell Death Through Reactivation of the Retinoblastoma Tumor Suppressor Pathway and Polycomb Repressor Complex 2 (PRC2) Silencing. *J Biol Chem* (2013) 288(49):35534–47. doi: 10.1074/jbc.M113.510669
76. Zhu F, Guo H, Bates PD, Zhang S, Zhang H, Nomie KJ, et al. PRMT5 Is Upregulated by B-Cell Receptor Signaling and Forms a Positive-Feedback Loop With PI3K/AKT in Lymphoma Cells. *Leukemia* (2019) 33(12):2898–911. doi: 10.1038/s41375-019-0489-6
77. Boccaletto P, Machnicka MA, Purta E, Piatkowski P, Baginski B, Wirecki TK, et al. MODOMICS: A Database of RNA Modification Pathways. 2017 Update. *Nucleic Acids Res* (2018) 46(D1):D303–d7. doi: 10.1093/nar/gkx1030
78. Dominissini D, Moshitch-Moshkovitz S, Schwartz S, Salmon-Divon M, Ungar L, Osenberg S, et al. Topology of the Human and Mouse M6a RNA Methylomes Revealed by M6a-Seq. *Nature* (2012) 485(7397):201–6. doi: 10.1038/nature11112
79. Chen XY, Zhang J, Zhu JS. The Role of M(6)A RNA Methylation in Human Cancer. *Mol Cancer* (2019) 18(1):103. doi: 10.1186/s12943-019-1033-z
80. Schumann U, Shafik A, Preiss T. METTL3 Gains R/W Access to the Epitranscriptome. *Mol Cell* (2016) 62(3):323–4. doi: 10.1016/j.molcel.2016.04.024
81. Liu J, Yue Y, Han D, Wang X, Fu Y, Zhang L, et al. A METTL3-METTL14 Complex Mediates Mammalian Nuclear RNA N6-Adenosine Methylation. *Nat Chem Biol* (2014) 10(2):93–5. doi: 10.1038/nchembio.1432
82. Weng H, Huang H, Wu H, Qin X, Zhao BS, Dong L, et al. METTL14 Inhibits Hematopoietic Stem/Progenitor Differentiation and Promotes Leukemogenesis *via* mRNA M(6)A Modification. *Cell Stem Cell* (2018) 22 (2):191–205.e9. doi: 10.1016/j.stem.2017.11.016
83. Ping XL, Sun BF, Wang L, Xiao W, Yang X, Wang WJ, et al. Mammalian WTAP Is a Regulatory Subunit of the RNA N6-Methyladenosine Methyltransferase. *Cell Res* (2014) 24(2):177–89. doi: 10.1038/cr.2014.3
84. Hu M, Yang Y, Ji Z, Luo J. RBM15 Functions in Blood Diseases. *Curr Cancer Drug Targets* (2016) 16(7):579–85. doi: 10.2174/1568009616666160112105706
85. Lan T, Li H, Zhang D, Xu L, Liu H, Hao X, et al. KIAA1429 Contributes to Liver Cancer Progression Through N6-Methyladenosine-Dependent Post-Transcriptional Modification of GATA3. *Mol Cancer* (2019) 18(1):186. doi: 10.1186/s12943-019-1106-z
86. Wang T, Kong S, Tao M, Ju S. The Potential Role of RNA N6-Methyladenosine in Cancer Progression. *Mol Cancer* (2020) 19(1):88. doi: 10.1186/s12943-020-01204-7
87. Haussmann IU, Bodi Z, Sanchez-Moran E, Mongan NP, Archer N, Fray RG, et al. M(6)A Potentiates Sxl Alternative Pre-mRNA Splicing for Robust Drosophila Sex Determination. *Nature* (2016) 540(7632):301–4. doi: 10.1038/nature20577
88. Huang H, Weng H, Sun W, Qin X, Shi H, Wu H, et al. Recognition of RNA N(6)-Methyladenosine by IGF2BP Proteins Enhances mRNA Stability and Translation. *Nat Cell Biol* (2018) 20(3):285–95. doi: 10.1038/s41556-018-0045-z
89. Su R, Dong L, Li Y, Gao M, Han L, Wunderlich M, et al. Targeting FTO Suppresses Cancer Stem Cell Maintenance and Immune Evasion. *Cancer Cell* (2020) 38(1):79–96.e11. doi: 10.1016/j.ccell.2020.04.017
90. Shen C, Sheng Y, Zhu AC, Robinson S, Jiang X, Dong L, et al. RNA Demethylase ALKBH5 Selectively Promotes Tumorigenesis and Cancer Stem Cell Self-Renewal in Acute Myeloid Leukemia. *Cell Stem Cell* (2020) 27(1):64–80.e9. doi: 10.1016/j.stem.2020.04.009
91. Yao L, Yin H, Hong M, Wang Y, Yu T, Teng Y, et al. RNA Methylation in Hematological Malignancies and Its Interactions With Other Epigenetic Modifications. *Leukemia* (2021) 35(5):1243–57. doi: 10.1038/s41375-021-01225-1
92. Wang X, Feng J, Xue Y, Guan Z, Zhang D, Liu Z, et al. Structural Basis of N (6)-Adenosine Methylation by the METTL3-METTL14 Complex. *Nature* (2016) 534(7608):575–8. doi: 10.1038/nature18298
93. Olsen SN, Armstrong SA. It's Not What You Say But How You Say It: Targeting RNA Methylation in AML. *Mol Cell* (2020) 78(6):996–8. doi: 10.1016/j.molcel.2020.05.027
94. Wen J, Lv R, Ma H, Shen H, He C, Wang J, et al. Zc3h13 Regulates Nuclear RNA M(6)A Methylation and Mouse Embryonic Stem Cell Self-Renewal. *Mol Cell* (2018) 69(6):1028–38.e6. doi: 10.1016/j.molcel.2018.02.015
95. Wei J, Liu F, Lu Z, Fei Q, Ai Y, He PC, et al. Differential M(6)A, M(6)A(m), and M(1)A Demethylation Mediated by FTO in the Cell Nucleus and Cytoplasm. *Mol Cell* (2018) 71(6):973–85.e5. doi: 10.1016/j.molcel.2018.08.011
96. Li Y, Wu K, Quan W, Yu L, Chen S, Cheng C, et al. The Dynamics of FTO Binding and Demethylation From the M(6)A Motifs. *RNA Biol* (2019) 16 (9):1179–89. doi: 10.1080/15476286.2019.1621120
97. Zheng G, Dahl JA, Niu Y, Fedorcsak P, Huang CM, Li CJ, et al. ALKBH5 Is a Mammalian RNA Demethylase That Impacts RNA Metabolism and Mouse Fertility. *Mol Cell* (2013) 49(1):18–29. doi: 10.1016/j.molcel.2012.10.015
98. Wang X, Lu Z, Gomez A, Hon GC, Yue Y, Han D, et al. N6-Methyladenosine-Dependent Regulation of Messenger RNA Stability. *Nature* (2014) 505(7481):117–20. doi: 10.1038/nature12730
99. Lan Q, Liu PY, Haase J, Bell JL, Huttelmaier S, Liu T. The Critical Role of RNA M(6)A Methylation in Cancer. *Cancer Res* (2019) 79(7):1285–92. doi: 10.1158/0008-5472.CAN-18-2965
100. Roundtree IA, Luo GZ, Zhang Z, Wang X, Zhou T, Cui Y, et al. YTHDC1 Mediates Nuclear Export of N(6)-Methyladenosine Methylated mRNAs. *Elife* (2017) 6:e31311. doi: 10.7554/eLife.31311
101. Hsu PJ, Zhu Y, Ma H, Guo Y, Shi X, Liu Y, et al. Ythdc2 is an N(6)-Methyladenosine Binding Protein That Regulates Mammalian Spermatogenesis. *Cell Res* (2017) 27(9):1115–27. doi: 10.1038/cr.2017.99
102. Alarcón CR, Goodarzi H, Lee H, Liu X, Tavazoie S, Tavazoie SF. HNRNPA2B1 Is a Mediator of M(6)A-Dependent Nuclear RNA Processing Events. *Cell* (2015) 162(6):1299–308. doi: 10.1016/j.cell.2015.08.011
103. Cheng Y, Fu Y, Wang Y, Wang J. The M6a Methyltransferase METTL3 Is Functionally Implicated in DLBCL Development by Regulating M6a Modification in PEDF. *Front Genet* (2020) 11:955. doi: 10.3389/fgene.2020.00955
104. Sorci M, Ianniello Z, Cruciani S, Larivera S, Ginistrelli LC, Capuano E, et al. METTL3 Regulates WTAP Protein Homeostasis. *Cell Death Dis* (2018) 9 (8):796. doi: 10.1038/s41419-018-0843-z
105. Kuai Y, Gong X, Ding L, Li F, Lei L, Gong Y, et al. Wilms' Tumor 1-Associating Protein Plays an Aggressive Role in Diffuse Large B-Cell Lymphoma and Forms a Complex With BCL6 *via* Hsp90. *Cell Commun Signal* (2018) 16(1):50. doi: 10.1186/s12964-018-0258-6
106. Cheng J, Guo JM, Xiao BX, Miao Y, Jiang Z, Zhou H, et al. piRNA, the New Non-Coding RNA, Is Aberrantly Expressed in Human Cancer Cells. *Clin Chim Acta* (2011) 412(17-18):1621–5. doi: 10.1016/j.cca.2011.05.015
107. Han H, Fan G, Song S, Jiang Y, Qian C, Zhang W, et al. piRNA-30473 Contributes to Tumorigenesis and Poor Prognosis by Regulating M6a RNA Methylation in DLBCL. *Blood* (2021) 137(12):1603–14. doi: 10.1182/blood.2019003764
108. Bhalla K, Jaber S, Nahid MN, Underwood K, Beheshti A, Landon A, et al. Author Correction: Role of Hypoxia in Diffuse Large B-Cell Lymphoma: Metabolic Repression and Selective Translation of HK2 Facilitates Development of DLBCL. *Sci Rep* (2018) 8(1):7221. doi: 10.1038/s41598-018-25251-9
109. Ma H, Shen L, Yang H, Gong H, Du X, Li J. M6a Methyltransferase Wilms' Tumor 1-Associated Protein Facilitates Cell Proliferation and Cisplatin Resistance in NK/T Cell Lymphoma by Regulating Dual-Specificity

Phosphatases 6 Expression *via* M6a RNA Methylation. *IUBMB Life* (2021) 73(1):108–17. doi: 10.1002/iub.2410
110. Wu G, Suo C, Yang Y, Shen S, Sun L, Li ST, et al. MYC Promotes Cancer Progression by Modulating M(6) A Modifications to Suppress Target Gene Translation. *EMBO Rep* (2021) 22(3):e51519. doi: 10.15252/embr.202051519
111. Hartmann EM, Beà S, Navarro A, Trapp V, Campo E, Ott G, et al. Increased Tumor Cell Proliferation in Mantle Cell Lymphoma Is Associated With Elevated Insulin-Like Growth Factor 2 mRNA-Binding Protein 3 Expression. *Mod Pathol* (2012) 25(9):1227–35. doi: 10.1038/modpathol.2012.84
112. Bannister AJ, Kouzarides T. Regulation of Chromatin by Histone Modifications. *Cell Res* (2011) 21(3):381–95. doi: 10.1038/cr.2011.22
113. Hodawadekar SC, Marmorstein R. Chemistry of Acetyl Transfer by Histone Modifying Enzymes: Structure, Mechanism and Implications for Effector Design. *Oncogene* (2007) 26(37):5528–40. doi: 10.1038/sj.onc.1210619
114. Meyer SN, Scuoppo C, Vlasevska S, Bal E, Holmes AB, Holloman M, et al. Unique and Shared Epigenetic Programs of the CREBBP and EP300 Acetyltransferases in Germinal Center B Cells Reveal Targetable Dependencies in Lymphoma. *Immunity* (2019) 51(3):535–47.e9. doi: 10.1016/j.immuni.2019.08.006
115. Pasqualucci L, Dominguez-Sola D, Chiarenza A, Fabbri G, Grunn A, Trifonov V, et al. Inactivating Mutations of Acetyltransferase Genes in B-Cell Lymphoma. *Nature* (2011) 471(7337):189–95. doi: 10.1038/nature09730
116. Schmitz R, Wright GW, Huang DW, Johnson CA, Phelan JD, Wang JQ, et al. Genetics and Pathogenesis of Diffuse Large B-Cell Lymphoma. *N Engl J Med* (2018) 378(15):1396–407. doi: 10.1056/NEJMoa1801445
117. Jiang Y, Ortega-Molina A, Geng H, Ying HY, Hatzi K, Parsa S, et al. CREBBP Inactivation Promotes the Development of HDAC3-Dependent Lymphomas. *Cancer Discov* (2017) 7(1):38–53. doi: 10.1158/2159-8290.CD-16-0975
118. Zhang J, Vlasevska S, Wells VA, Nataraj S, Holmes AB, Duval R, et al. The CREBBP Acetyltransferase Is a Haploinsufficient Tumor Suppressor in B-Cell Lymphoma. *Cancer Discov* (2017) 7(3):322–37. doi: 10.1158/2159-8290.CD-16-1417
119. Mondello P, Tadros S, Teater M, Fontan L, Chang AY, Jain N, et al. Selective Inhibition of HDAC3 Targets Synthetic Vulnerabilities and Activates Immune Surveillance in Lymphoma. *Cancer Discovery* (2020) 10(3):440–59. doi: 10.1158/2159-8290.CD-19-0116
120. da Silva Almeida AC, Abate F, Khiabanian H, Martinez-Escala E, Guitart J, Tensen CP, et al. The Mutational Landscape of Cutaneous T Cell Lymphoma and Sézary Syndrome. *Nat Genet* (2015) 47(12):1465–70. doi: 10.1038/ng.3442
121. Mareschal S, Pham-Ledard A, Viailly PJ, Dubois S, Bertrand P, Maingonnat C, et al. Identification of Somatic Mutations in Primary Cutaneous Diffuse Large B-Cell Lymphoma, Leg Type by Massive Parallel Sequencing. *J Invest Dermatol* (2017) 137(9):1984–94. doi: 10.1016/j.jid.2017.04.010
122. Parthun MR. Hat1: The Emerging Cellular Roles of a Type B Histone Acetyltransferase. *Oncogene* (2007) 26(37):5319–28. doi: 10.1038/sj.onc.1210602
123. Seto E, Yoshida M. Erasers of Histone Acetylation: The Histone Deacetylase Enzymes. *Cold Spring Harb Perspect Biol* (2014) 6(4):a018713. doi: 10.1101/cshperspect.a018713
124. Zhang Y, Sun Z, Jia J, Du T, Zhang N, Tang Y, et al. Overview of Histone Modification. In: D Fang and J Han, editors. *Histone Mutations and Cancer*. Singapore: Springer Singapore (2021). p. 1–16.
125. Gloghini A, Buglio D, Khaskhely NM, Georgakis G, Orlowski RZ, Neelapu SS, et al. Expression of Histone Deacetylases in Lymphoma: Implication for the Development of Selective Inhibitors. *Br J Haematol* (2009) 147(4):515–25. doi: 10.1111/j.1365-2141.2009.07887.x
126. Marquard L, Poulsen CB, Gjerdrum LM, de Nully Brown P, Christensen IJ, Jensen PB, et al. Histone Deacetylase 1, 2, 6 and Acetylated Histone H4 in B- and T-Cell Lymphomas. *Histopathology* (2009) 54(6):688–98. doi: 10.1111/j.1365-2559.2009.03290.x
127. Barneda-Zahonero B, Collazo O, Azagra A, Fernández-Duran I, Serra-Musach J, Islam AB, et al. The Transcriptional Repressor HDAC7 Promotes Apoptosis and C-Myc Downregulation in Particular Types of Leukemia and Lymphoma. *Cell Death Dis* (2015) 6(2):e1635. doi: 10.1038/cddis.2014.594
128. Gil VS, Bhagat G, Howell L, Zhang J, Kim CH, Stengel S, et al. Deregulated Expression of HDAC9 in B Cells Promotes Development of Lymphoproliferative Disease and Lymphoma in Mice. *Dis Model Mech* (2016) 9(12):1483–95. doi: 10.1242/dmm.023366
129. Shang E, Salazar G, Crowley TE, Wang X, Lopez RA, Wang X, et al. Identification of Unique, Differentiation Stage-Specific Patterns of Expression of the Bromodomain-Containing Genes Brd2, Brd3, Brd4, and Brdt in the Mouse Testis. *Gene Expr Patterns* (2004) 4(5):513–9. doi: 10.1016/j.modgep.2004.03.002
130. Belkina AC, Denis GV. BET Domain Co-Regulators in Obesity, Inflammation and Cancer. *Nat Rev Cancer* (2012) 12(7):465–77. doi: 10.1038/nrc3256
131. Reyes-Garau D, Ribeiro ML, Roué G. Pharmacological Targeting of BET Bromodomain Proteins in Acute Myeloid Leukemia and Malignant Lymphomas: From Molecular Characterization to Clinical Applications. *Cancers (Basel)* (2019) 11(10):1483. doi: 10.3390/cancers11101483
132. Hsu SC, Blobel GA. The Role of Bromodomain and Extraterminal Motif (BET) Proteins in Chromatin Structure. *Cold Spring Harb Symp Quant Biol* (2017) 82:37–43. doi: 10.1101/sqb.2017.82.033829
133. Römermann D, Hasemeier B, Metzig K, Göhring G, Schlegelberger B, Länger F, et al. Global Increase in DNA Methylation in Patients With Myelodysplastic Syndrome. *Leukemia* (2008) 22(10):1954–6. doi: 10.1038/leu.2008.76
134. Hu J, Wang X, Chen F, Ding M, Dong M, Yang W, et al. Combination of Decitabine and a Modified Regimen of Cisplatin, Cytarabine and Dexamethasone: A Potential Salvage Regimen for Relapsed or Refractory Diffuse Large B-Cell Lymphoma After Second-Line Treatment Failure. *Front Oncol* (2021) 11:687374. doi: 10.3389/fonc.2021.687374
135. Liu Y, Wang C, Li X, Dong L, Yang Q, Chen M, et al. Improved Clinical Outcome in a Randomized Phase II Study of Anti-PD-1 Camrelizumab Plus Decitabine in Relapsed/Refractory Hodgkin Lymphoma. *J Immunother Cancer* (2021) 9(4):e002347. doi: 10.1136/jitc-2021-002347
136. Italiano A, Soria JC, Toulmonde M, Michot JM, Lucchesi C, Varga A, et al. Tazemetostat, an EZH2 Inhibitor, in Relapsed or Refractory B-Cell Non-Hodgkin Lymphoma and Advanced Solid Tumours: A First-in-Human, Open-Label, Phase 1 Study. *Lancet Oncol* (2018) 19(5):649–59. doi: 10.1016/S1470-2045(18)30145-1
137. Morschhauser F, Tilly H, Chaidos A, McKay P, Phillips T, Assouline S, et al. Tazemetostat for Patients With Relapsed or Refractory Follicular Lymphoma: An Open-Label, Single-Arm, Multicentre, Phase 2 Trial. *Lancet Oncol* (2020) 21(11):1433–42. doi: 10.1016/S1470-2045(20)30441-1
138. Yap TA, Winter JN, Giulino-Roth L, Longley J, Lopez J, Michot JM, et al. Phase I Study of the Novel Enhancer of Zeste Homolog 2 (EZH2) Inhibitor GSK2816126 in Patients With Advanced Hematologic and Solid Tumors. *Clin Cancer Res* (2019) 25(24):7331–9. doi: 10.1158/1078-0432.CCR-18-4121
139. Kagiyama Y, Fujita S, Shima Y, Yamagata K, Katsumoto T, Nakagawa M, et al. CDKN1C-Mediated Growth Inhibition by an EZH1/2 Dual Inhibitor Overcomes Resistance of Mantle Cell Lymphoma to Ibrutinib. *Cancer Sci* (2021) 112(6):2314–24. doi: 10.1111/cas.14905
140. Olsen EA, Kim YH, Kuzel TM, Pacheco TR, Foss FM, Parker S, et al. Phase IIb Multicenter Trial of Vorinostat in Patients With Persistent, Progressive, or Treatment Refractory Cutaneous T-Cell Lymphoma. *J Clin Oncol* (2007) 25(21):3109–15. doi: 10.1200/JCO.2006.10.2434
141. Ogura M, Ando K, Suzuki T, Ishizawa K, Oh SY, Itoh K, et al. A Multicentre Phase II Study of Vorinostat in Patients With Relapsed or Refractory Indolent B-Cell Non-Hodgkin Lymphoma and Mantle Cell Lymphoma. *Br J Haematol* (2014) 165(6):768–76. doi: 10.1111/bjh.12819
142. Siddiqi T, Frankel P, Beumer JH, Kiesel BF, Christner S, Ruel C, et al. Phase 1 Study of the Aurora Kinase A Inhibitor Alisertib (MLN8237) Combined With the Histone Deacetylase Inhibitor Vorinostat in Lymphoid Malignancies. *Leuk Lymphoma* (2020) 61(2):309–17. doi: 10.1080/10428194.2019.1672052
143. Nieto Y, Valdez BC, Thall PF, Ahmed S, Jones RB, Hosing C, et al. Vorinostat Combined With High-Dose Gemcitabine, Busulfan, and Melphalan With Autologous Stem Cell Transplantation in Patients With Refractory Lymphomas. *Biol Blood Marrow Transplant* (2015) 21(11):1914–20. doi: 10.1016/j.bbmt.2015.06.003

144. Chen R, Frankel P, Popplewell L, Siddiqi T, Ruel N, Rotter A, et al. A Phase II Study of Vorinostat and Rituximab for Treatment of Newly Diagnosed and Relapsed/Refractory Indolent non-Hodgkin Lymphoma. *Haematologica* (2015) 100(3):357–62. doi: 10.3324/haematol.2014.117473
145. Kirschbaum M, Frankel P, Popplewell L, Zain J, Delioukina M, Pullarkat V, et al. Phase II Study of Vorinostat for Treatment of Relapsed or Refractory Indolent non-Hodgkin's Lymphoma and Mantle Cell Lymphoma. *J Clin Oncol* (2011) 29(9):1198–203. doi: 10.1200/JCO.2010.32.1398
146. Spurgeon SE, Sharma K, Claxton DF, Ehmann C, Pu J, Shimko S, et al. Phase 1-2 Study of Vorinostat (SAHA), Cladribine and Rituximab (SCR) in Relapsed B-Cell non-Hodgkin Lymphoma and Previously Untreated Mantle Cell Lymphoma. *Br J Haematol* (2019) 186(6):845–54. doi: 10.1111/bjh.16008
147. Crump M, Coiffier B, Jacobsen ED, Sun L, Ricker JL, Xie H, et al. Phase II Trial of Oral Vorinostat (Suberoylanilide Hydroxamic Acid) in Relapsed Diffuse Large-B-Cell Lymphoma. *Ann Oncol* (2008) 19(5):964–9. doi: 10.1093/annonc/mdn031
148. O'Connor OA, Horwitz S, Masszi T, Van Hoof A, Brown P, Doorduijn J, et al. Belinostat in Patients With Relapsed or Refractory Peripheral T-Cell Lymphoma: Results of the Pivotal Phase II BELIEF (CLN-19) Study. *J Clin Oncol* (2015) 33(23):2492–9. doi: 10.1200/JCO.2014.59.2782
149. Foss F, Advani R, Duvic M, Hymes KB, Intragumtornchai T, Lekhakula A, et al. A Phase II Trial of Belinostat (PXD101) in Patients With Relapsed or Refractory Peripheral or Cutaneous T-Cell Lymphoma. *Br J Haematol* (2015) 168(6):811–9. doi: 10.1111/bjh.13222
150. Johnston PB, Cashen AF, Nikolinakos PG, Beaven AW, Barta SK, Bhat G, et al. Belinostat in Combination With Standard Cyclophosphamide, Doxorubicin, Vincristine and Prednisone as First-Line Treatment for Patients With Newly Diagnosed Peripheral T-Cell Lymphoma. *Exp Hematol Oncol* (2021) 10(1):15. doi: 10.1186/s40164-021-00203-8
151. Whittaker SJ, Demierre MF, Kim EJ, Rook AH, Lerner A, Duvic M, et al. Final Results From a Multicenter, International, Pivotal Study of Romidepsin in Refractory Cutaneous T-Cell Lymphoma. *J Clin Oncol* (2010) 28 (29):4485–91. doi: 10.1200/JCO.2010.28.9066
152. Piekarz RL, Frye R, Prince HM, Kirschbaum MH, Zain J, Allen SL, et al. Phase 2 Trial of Romidepsin in Patients With Peripheral T-Cell Lymphoma. *Blood* (2011) 117(22):5827–34. doi: 10.1182/blood-2010-10-312603
153. Coiffier B, Pro B, Prince HM, Foss F, Sokol L, Greenwood M, et al. Results From a Pivotal, Open-Label, Phase II Study of Romidepsin in Relapsed or Refractory Peripheral T-Cell Lymphoma After Prior Systemic Therapy. *J Clin Oncol* (2012) 30(6):631–6. doi: 10.1200/JCO.2011.37.4223
154. Coiffier B, Pro B, Prince HM, Foss F, Sokol L, Greenwood M, et al. Romidepsin for the Treatment of Relapsed/Refractory Peripheral T-Cell Lymphoma: Pivotal Study Update Demonstrates Durable Responses. *J Hematol Oncol* (2014) 7:11. doi: 10.1186/1756-8722-7-11
155. Maruyama D, Tobinai K, Ogura M, Uchida T, Hatake K, Taniwaki M, et al. Romidepsin in Japanese Patients With Relapsed or Refractory Peripheral T-Cell Lymphoma: A Phase I/II and Pharmacokinetics Study. *Int J Hematol* (2017) 106(5):655–65. doi: 10.1007/s12185-017-2286-1
156. O'Connor OA, Ozcan M, Jacobsen ED, Roncero JM, Trotman J, Demeter J, et al. Randomized Phase III Study of Alisertib or Investigator's Choice (Selected Single Agent) in Patients With Relapsed or Refractory Peripheral T-Cell Lymphoma. *J Clin Oncol* (2019) 37(8):613–23. doi: 10.1200/JCO.18.00899
157. Falchi L, Ma H, Klein S, Lue JK, Montanari F, Marchi E, et al. Combined Oral 5-Azacytidine and Romidepsin are Highly Effective in Patients With PTCL: A Multicenter Phase 2 Study. *Blood* (2021) 137(16):2161–70. doi: 10.1182/blood.2020009004
158. Pellegrini C, Dodero A, Chiappella A, Monaco F, Degl'Innocenti D, Salvi F, et al. A Phase II Study on the Role of Gemcitabine Plus Romidepsin (GEMRO Regimen) in the Treatment of Relapsed/Refractory Peripheral T-Cell Lymphoma Patients. *J Hematol Oncol* (2016) 9:38. doi: 10.1186/s13045-016-0266-1
159. Maly JJ, Christian BA, Zhu X, Wei L, Sexton JL, Jaglowski SM, et al. A Phase I/II Trial of Panobinostat in Combination With Lenalidomide in Patients With Relapsed or Refractory Hodgkin Lymphoma. *Clin Lymphoma Myeloma Leuk* (2017) 17(6):347–53. doi: 10.1016/j.clml.2017.05.008
160. Assouline SE, Nielsen TH, Yu S, Alcaide M, Chong L, MacDonald D, et al. Phase 2 Study of Panobinostat With or Without Rituximab in Relapsed Diffuse Large B-Cell Lymphoma. *Blood* (2016) 128(2):185–94. doi: 10.1182/blood-2016-02-699520
161. Tan D, Phipps C, Hwang WY, Tan SY, Yeap CH, Chan YH, et al. Panobinostat in Combination With Bortezomib in Patients With Relapsed or Refractory Peripheral T-Cell Lymphoma: An Open-Label, Multicentre Phase 2 Trial. *Lancet Haematol* (2015) 2(8):e326–33. doi: 10.1016/S2352-3026(15)00097-6
162. Duvic M, Dummer R, Becker JC, Poulalhon N, Ortiz Romero P, Grazia Bernengo M, et al. Panobinostat Activity in Both Bexarotene-Exposed and -Naïve Patients With Refractory Cutaneous T-Cell Lymphoma: Results of a Phase II Trial. *Eur J Cancer* (2013) 49(2):386–94. doi: 10.1016/j.ejca.2012.08.017
163. Shi Y, Dong M, Hong X, Zhang W, Feng J, Zhu J, et al. Results From a Multicenter, Open-Label, Pivotal Phase II Study of Chidamide in Relapsed or Refractory Peripheral T-Cell Lymphoma. *Ann Oncol* (2015) 26(8):1766–71. doi: 10.1093/annonc/mdv237
164. Zhang MC, Fang Y, Wang L, Cheng S, Fu D, He Y, et al. Clinical Efficacy and Molecular Biomarkers in a Phase II Study of Tucidinostat Plus R-CHOP in Elderly Patients With Newly Diagnosed Diffuse Large B-Cell Lymphoma. *Clin Epigenetics* (2020) 12(1):160. doi: 10.1186/s13148-020-00948-9
165. Ji J, Liu Z, Kuang P, Dong T, Chen X, Li J, et al. A New Conditioning Regimen With Chidamide, Cladribine, Gemcitabine and Busulfan Significantly Improve the Outcome of High-Risk or Relapsed/Refractory non-Hodgkin's Lymphomas. *Int J Cancer* (2021) 149(12):2075–82. doi: 10.1002/ijc.33761
166. Batlevi CL, Kasamon Y, Bociek RG, Lee P, Gore L, Copeland A, et al. ENGAGE- 501: Phase II Study of Entinostat (SNDX-275) in Relapsed and Refractory Hodgkin Lymphoma. *Haematologica* (2016) 101(8):968–75. doi: 10.3324/haematol.2016.142406
167. Younes A, Berdeja JG, Patel MR, Flinn I, Gerecitano JF, Neelapu SS, et al. Safety, Tolerability, and Preliminary Activity of CUDC-907, a First-in-Class, Oral, Dual Inhibitor of HDAC and PI3K, in Patients With Relapsed or Refractory Lymphoma or Multiple Myeloma: An Open-Label, Dose-Escalation, Phase 1 Trial. *Lancet Oncol* (2016) 17(5):622–31. doi: 10.1016/S1470-2045(15)00584-7
168. Oki Y, Kelly KR, Flinn I, Patel MR, Gharavi R, Ma A, et al. CUDC-907 in Relapsed/Refractory Diffuse Large B-Cell Lymphoma, Including Patients With MYC-Alterations: Results From an Expanded Phase I Trial. *Haematologica* (2017) 102(11):1923–30. doi: 10.3324/haematol.2017.172882
169. Landsburg DJ, Barta SK, Ramchandren R, Batlevi C, Iyer S, Kelly K, et al. Fimepinostat (CUDC-907) in Patients With Relapsed/Refractory Diffuse Large B Cell and High-Grade B-Cell Lymphoma: Report of a Phase 2 Trial and Exploratory Biomarker Analyses. *Br J Haematol* (2021) 195(2):201–9. doi: 10.1111/bjh.17730
170. Younes A, Oki Y, Bociek RG, Kuruvilla J, Fanale M, Neelapu S, et al. Mocetinostat for Relapsed Classical Hodgkin's Lymphoma: An Open-Label, Single-Arm, Phase 2 Trial. *Lancet Oncol* (2011) 12(13):1222–8. doi: 10.1016/S1470-2045(11)70265-0
171. Furumai R, Matsuyama A, Kobashi N, Lee KH, Nishiyama M, Nakajima H, et al. FK228 (Depsipeptide) as a Natural Prodrug That Inhibits Class I Histone Deacetylases. *Cancer Res* (2002) 62(17):4916–21.
172. Smolewski P, Robak T. The Discovery and Development of Romidepsin for the Treatment of T-Cell Lymphoma. *Expert Opin Drug Discovery* (2017) 12 (8):859–73. doi: 10.1080/17460441.2017.1341487
173. Kim YH, Demierre MF, Kim EJ, Lerner A, Rook AH, Duvic M, et al. Clinically Meaningful Reduction in Pruritus in Patients With Cutaneous T-Cell Lymphoma Treated With Romidepsin. *Leuk Lymphoma* (2013) 54 (2):284–9. doi: 10.3109/10428194.2012.711829
174. Cheng T, Kiser K, Grasse L, Iles L, Bartholomeusz G, Samaniego F, et al. Expression of Histone Deacetylase (HDAC) Family Members in Bortezomib-Refractory Multiple Myeloma and Modulation by Panobinostat. *Cancer Drug Resist* (2021) 4(4):888–902. doi: 10.20517/cdr.2021.44
175. Rahmani M, Aust MM, Benson EC, Wallace L, Friedberg J, Grant S. PI3K/mTOR Inhibition Markedly Potentiates HDAC Inhibitor Activity in NHL Cells Through BIM- and MCL-1-Dependent Mechanisms *In Vitro* and In

Vivo. *Clin Cancer Res* (2014) 20(18):4849–60. doi: 10.1158/1078-0432.CCR-14-0034
176. Shi Y, Jia B, Xu W, Li W, Liu T, Liu P, et al. Chidamide in Relapsed or Refractory Peripheral T Cell Lymphoma: A Multicenter Real-World Study in China. *J Hematol Oncol* (2017) 10(1):69. doi: 10.1186/s13045-017-0439-6
177. Buggy JJ, Cao ZA, Bass KE, Verner E, Balasubramanian S, Liu L, et al. CRA-024781: A Novel Synthetic Inhibitor of Histone Deacetylase Enzymes With Antitumor Activity *In Vitro* and In Vivo. *Mol Cancer Ther* (2006) 5(5):1309–17. doi: 10.1158/1535-7163.MCT-05-0442
178. Saito A, Yamashita T, Mariko Y, Nosaka Y, Tsuchiya K, Ando T, et al. A Synthetic Inhibitor of Histone Deacetylase, MS-27-275, With Marked *In Vivo* Antitumor Activity Against Human Tumors. *Proc Natl Acad Sci U S A* (1999) 96(8):4592–7. doi: 10.1073/pnas.96.8.4592
179. Jóna A, Khaskhely N, Buglio D, Shafer JA, Derenzini E, Bollard CM, et al. The Histone Deacetylase Inhibitor Entinostat (SNDX-275) Induces Apoptosis in Hodgkin Lymphoma Cells and Synergizes With Bcl-2 Family Inhibitors. *Exp Hematol* (2011) 39(10):1007–17.e1. doi: 10.1016/j.exphem.2011.07.002
180. Oki Y, Buglio D, Zhang J, Ying Y, Zhou S, Sureda A, et al. Immune Regulatory Effects of Panobinostat in Patients With Hodgkin Lymphoma Through Modulation of Serum Cytokine Levels and T-Cell PD1 Expression. *Blood Cancer J* (2014) 4(8):e236. doi: 10.1038/bcj.2014.58
181. Fournel M, Bonfils C, Hou Y, Yan PT, Trachy-Bourget MC, Kalita A, et al. MGCD0103, a Novel Isotype-Selective Histone Deacetylase Inhibitor, has Broad Spectrum Antitumor Activity *In Vitro* and In Vivo. *Mol Cancer Ther* (2008) 7(4):759–68. doi: 10.1158/1535-7163.MCT-07-2026
182. Bhadury J, Nilsson LM, Muralidharan SV, Green LC, Li Z, Gesner EM, et al. BET and HDAC Inhibitors Induce Similar Genes and Biological Effects and Synergize to Kill in Myc-Induced Murine Lymphoma. *Proc Natl Acad Sci U S A* (2014) 111(26):E2721–30. doi: 10.1073/pnas.1406722111
183. Amorim S, Stathis A, Gleeson M, Iyengar S, Magarotto V, Leleu X, et al. Bromodomain Inhibitor OTX015 in Patients With Lymphoma or Multiple Myeloma: A Dose-Escalation, Open-Label, Pharmacokinetic, Phase 1 Study. *Lancet Haematol* (2016) 3(4):e196–204. doi: 10.1016/S2352-3026(16)00021-1

Conflict of Interest: The authors declare that the research was conducted in the absence of any commercial or financial relationships that could be construed as a potential conflict of interest.

Publisher's Note: All claims expressed in this article are solely those of the authors and do not necessarily represent those of their affiliated organizations, or those of the publisher, the editors and the reviewers. Any product that may be evaluated in this article, or claim that may be made by its manufacturer, is not guaranteed or endorsed by the publisher.

frontiers | Frontiers in Oncology

ORIGINAL RESEARCH
published: 11 April 2022
doi: 10.3389/fonc.2022.831268

CpG Site-Specific Methylation-Modulated Divergent Expression of *PRSS3* Transcript Variants Facilitates Nongenetic Intratumor Heterogeneity in Human Hepatocellular Carcinoma

Shuye Lin[1†], Hanli Xu[2†], Mengdi Pang[2], Xiaomeng Zhou[2,3], Yuanming Pan[1], Lishu Zhang[2], Xin Guan[2], Xiaoyue Wang[2], Bonan Lin[2], Rongmeng Tian[2], Keqiang Chen[4], Xiaochen Zhang[2], Zijiang Yang[2], Fengmin Ji[2], Yingying Huang[5], Wu Wei[5], Wanghua Gong[6], Jianke Ren[5], Ji Ming Wang[4], Mingzhou Guo[3] and Jiaqiang Huang[1,2,4*]*

[1] Cancer Research Center, Beijing Chest Hospital, Capital Medical University, Beijing Tuberculosis and Thoracic Tumor Institute, Beijing, China, [2] College of Life Sciences & Bioengineering, Beijing Jiaotong University, Beijing, China, [3] Department of Gastroenterology and Hepatology, Chinese People's Liberation Army of China (PLA) General Hospital, Beijing, China, [4] Laboratory of Cancer Immunometabolism, Center for Cancer Research, National Cancer Institute, Frederick, MD, United States, [5] Chinese Academy of Sciences (CAS) Key Laboratory of Computational Biology, Shanghai Institute of Nutrition and Health, University of Chinese Academy of Sciences, Chinese Academy of Sciences, Shanghai, China, [6] Basic Research Program, Leidos Biomedical Research, Inc., Frederick, MD, United States

Background: Hepatocellular carcinoma (HCC) is one of the most lethal human tumors with extensive intratumor heterogeneity (ITH). Serine protease 3 (PRSS3) is an indispensable member of the trypsin family and has been implicated in the pathogenesis of several malignancies, including HCC. However, the paradoxical effects of *PRSS3* on carcinogenesis due to an unclear molecular basis impede the utilization of its biomarker potential. We hereby explored the contribution of *PRSS3* transcripts to tumor functional heterogeneity by systematically dissecting the expression of four known splice variants of *PRSS3* (*PRSS3-SVs, V1~V4*) and their functional relevance to HCC.

Methods: The expression and DNA methylation of *PRSS3* transcripts and their associated clinical relevance in HCC were analyzed using several publicly available datasets and validated using qPCR-based assays. Functional experiments were performed in gain- and loss-of-function cell models, in which *PRSS3* transcript constructs were separately transfected after deleting *PRSS3* expression by CRISPR/Cas9 editing.

Results: *PRSS3* was aberrantly differentially expressed toward bipolarity from very low ($PRSS3^{Low}$) to very high ($PRSS3^{High}$) expression across HCC cell lines and tissues. This was attributable to the disruption of *PRSS3-SVs*, in which *PRSS3-V2* and/or *PRSS3-V1* were dominant transcripts leading to *PRSS3* expression, whereas *PRSS3-V3* and *-V4* were rarely or minimally expressed. The expression of *PRSS3-V2* or *-V1* was inversely associated with site-specific CpG methylation at the *PRSS3* promoter region that distinguished HCC cells and tissues phenotypically between hypermethylated low-

OPEN ACCESS

Edited by:
Hongquan Zhang, Peking University Health Science Centre, China

Reviewed by:
Haiwei Mou, Cold Spring Harbor Laboratory, United States
Jianxiang Chen, Hangzhou Normal University, China

***Correspondence:**
Jiaqiang Huang
jqhuang@bjtu.edu.cn
Mingzhou Guo
mzguo@hotmail.com

[†]These authors share first authorship

Specialty section:
This article was submitted to Molecular and Cellular Oncology, a section of the journal Frontiers in Oncology

Received: *08 December 2021*
Accepted: *16 March 2022*
Published: *11 April 2022*

Citation:
Lin S, Xu H, Pang M, Zhou X, Pan Y, Zhang L, Guan X, Wang X, Lin B, Tian R, Chen K, Zhang X, Yang Z, Ji F, Huang Y, Wei W, Gong W, Ren J, Wang JM, Guo M and Huang J (2022) CpG Site-Specific Methylation-Modulated Divergent Expression of PRSS3 Transcript Variants Facilitates Nongenetic Intratumor Heterogeneity in Human Hepatocellular Carcinoma. Front. Oncol. 12:831268. doi: 10.3389/fonc.2022.831268

expression (m*PRSS3-SV*^{Low}) and hypomethylated high-expression (um*PRSS3-SV*^{High}) groups. *PRSS3-SVs* displayed distinct functions from oncogenic *PRSS3-V2* to tumor-suppressive *PRSS3-V1*, *-V3* or *PRSS3-V4* in HCC cells. Clinically, aberrant expression of *PRSS3-SVs* was translated into divergent relevance in patients with HCC, in which significant epigenetic downregulation of *PRSS3-V2* was seen in early HCC and was associated with favorable patient outcome.

Conclusions: These results provide the first evidence for the transcriptional and functional characterization of *PRSS3* transcripts in HCC. Aberrant expression of divergent *PRSS3-SVs* disrupted by site-specific CpG methylation may integrate the effects of oncogenic *PRSS3-V2* and tumor-suppressive *PRSS3-V1*, resulting in the molecular diversity and functional plasticity of *PRSS3* in HCC. Dysregulated expression of *PRSS3-V2* by site-specific CpG methylation may have potential diagnostic value for patients with early HCC.

Keywords: liver cancer, hepatocellular carcinoma, *PRSS3*, transcript variant, intratumor heterogeneity, CpG methylation, epigenetics, biomarker

INTRODUCTION

Human primary liver cancer is one of the most lethal tumors with a dismal prognosis, featuring extensive intratumor heterogeneity (ITH) and aggressiveness in the context of genetic and epigenetic aberrations (1–5). Liver hepatocellular carcinoma (HCC or LIHC) accounts for approximately 75-85% of all primary liver cancers. Most HCCs (>90%) develop from chronic inflammation-induced liver cirrhosis contributed by multiple risk factors, such as hepatitis viruses, alcohol consumption, and nonalcoholic fatty liver disease, which trigger the molecular complexity of ITH, increasing HCC phenotypic diversity and therapeutic resistance (3, 5). Regardless of the many approaches developed for the management of HCC in the past decade, its incidence and mortality rate continue to increase worldwide (5).

Large-scale bioinformatics datasets generated with next-generation sequencing technologies reveal a comprehensive landscape of genomic and epigenetic heterogeneity among HCC cell lines and tissue specimens (1, 2, 4, 6, 7). These studies offer invaluable insight into the molecular basis of ITH to categorize HCC into proliferative and nonproliferative subclasses in favor of integrative molecular monitoring of malignant transformation and management of HCC. However, aside from most genetic alterations occurring in passenger genes that may be associated with aging and pollution, most genetic variants, such as driver mutations in *TP53, TERT* and *CTNNB1* detected in HCCs, are not clinically relevant or are not potentially targetable for the existing drugs (3). This gives rise to a growing drive to integrate nongenetic variations into ITH and to distinguish between functional and nonfunctional ITH (7, 8). PremRNA alternative splicing (AS), as a key co and posttranscriptional process, drives nongenetic phenotypic heterogeneity, the disruption of which generates aberrant transcript variants or splice variants (*SVs*) that contribute to ITH and functional divergence and are thus functionally important to carcinogenesis and oncotherapeutic resistance (9–12).

Proteases play critical roles in multiple biological processes and are associated with a wide variety of pathological conditions, including carcinogenesis (13). As a group of trypsin-family serine proteases, human trypsinogen gene, protease serine 3 (*PRSS3*), encodes PRSS3, also called mesotrypsinogen (MTG) (14–16). *PRSS3* possesses four experimentally validated *SVs*, referred to as trypsinogen transcript variants 1, 2, 3, and 4 (*PRSS3-V1*, *-V2*, *-V3* and *-V4*), encoding PRSS3 isoform 1 (also known as brain form or trypsinogen 4, TRY4) (15, 17), PRSS3-2 (form C or MTG) (14, 18), PRSS3-3 (form B or trypsinogen IV) (19), and PRSS3-4 (new form or trypsinogen 5), respectively (20). In addition to PRSS1 and PRSS2, as the major digestive enzymes in the pancreas, PRSS3 is a minor constituent trypsin isoform but is physiologically critical due to its resistance to common trypsin inhibitors (13, 14, 16). PRSS3 has long been implicated in the pathogenesis of several malignancies and is therefore a promising biomarker and potential therapeutic target for cancer (21–31). However, the functional roles associated with the expression of *PRSS3* in cancer development are debatable. On the one hand, PRSS3 was shown to be upregulated in association with cancer metastasis, recurrence and poor prognosis (21–24, 26–31).

Abbreviations: 5-aza-CR, 5 aza-2'-deoxycytidine; CCLE, Cancer Cell Line Encyclopedia; DEG, Differentially expressed gene; DepMap, The Cancer Dependency Map; FPKM, Fragments Per Kilobase Million; GTEx, Genotype-Tissue Expression; GEPIA, Gene Expression Profiling Interactive Analysis; HCC, Hepatocellular carcinoma; LIHC, Liver hepatocellular carcinoma; MeDIP-qPCR, Methylated DNA immunoprecipitation-qPCR; mPRSS3^{Low} lowly expressed *PRSS3-SVs* with hypermethylation; MS-qPCR, Methylation-specific qPCR; MTG, Trypsin-3 isoform 2/mesotrypsinogen; *PRSS3*, Serine protease 3 gene; PRSS3, Serine protease 3; *PRSS3*^{High} or *PRSS3*^{Low}, Highly or minimally expressed *PRSS3; PRSS3-V1~-V4*, *PRSS3* transcript variants 1, -2, -3 and -4; *PRSS3-SVs*, Splice transcripts of *PRSS3;* TCGA, The Cancer Genome Atlas; TPM, Transcripts Per Million; TRY4, Trypsin-3 isoform 1/trypsinogen 4; um*PRSS3*^{High}, highly expressed *PRSS3-SVs* with hypomethylation.

However, on the other hand, *PRSS3* was suggested to be a tumor suppressor gene due to epigenetic silencing (32–36). Although the evidence supports the dual roles of proteases in carcinogenesis depending on cellular sources and the cancer microenvironment (9, 12, 13, 22, 23, 26, 34–36), the underlying molecular basis of PRSS3 for its pro- and antitumorigenic roles shown in different cancer types, even reported in the same type of cancer, such as in esophageal adenocarcinoma (24, 32), lung cancer (29, 35) and liver cancer (21, 36), remains elusive, causing many miscellaneous aliases to *PRSS3* to impact its potential target-therapeutic applications (1, 12, 13, 23, 25, 36).

While *SVs* have emerged as new candidates for diagnostic and prognostic biomarkers and therapeutic targets (9, 10), the expression and function of *PRSS3-SVs* in cancer development have never been systematically addressed. Here, we hypothesized that the molecular basis of *PRSS3* exerts dual roles attributable to its different transcripts. We thereby investigated the functional expression and epigenetic alteration of *PRSS3-SVs* in relation to HCC heterogeneity. We found divergent expression of *PRSS3-SVs* in HCC, which were epigenetically dysregulated by site-specific abnormal CpG methylation. We also observed different functionalities and clinical relevance of *PRSS3-SVs*. Therefore, epigenetic dysregulation of the expression of *PRSS3-SVs* may integrate the molecular basis of *PRSS3* to exert divergent effects on hepatocarcinogenesis.

MATERIALS AND METHODS

Data Collection

The datasets used for this study are publicly available on the following websites: the Cancer Model Repository (LIMORE) (https://www.picb.ac.cn/limore/home) (6); the Cancer Genome Atlas (TCGA, https://www.cancer.gov/) (38); the Gene Expression Profiling Interactive Analysis (GEPIA, http://gepia.cancer-pku.cn/) (37); the Cancer Cell Line Encyclopedia (CCLE, http://www.broadinstitute.org/ccle) (39); the Cancer Dependency Map (DepMap, https://depmap.org/portal/, DepMap Public 20Q3) (40); and the Broad Genome Data Analysis Center (http://gdac.broadinstitute.org) (41). The expression of PRSS3 protein was analyzed using data obtained from the Clinical Proteomic Tumor Analysis Consortium (CPTAC) Confirmatory/Discovery dataset (http:ualcan.path.uab.edu) (42).

Cell Lines

Human HCC cell lines, including well differentiated (HepG2 and Huh7) and poorly differentiated (SK-Hep-1, SMMC-7721 and LM3) cell lines, were purchased from Cellcook Biotech Co. (Guangzhou, China) and authenticated by STR profiling (Additional files). The cell lines were grown in DMEM (Gibco, Life Technologies, USA) with 10% fetal bovine serum (Gibco, USA), penicillin/streptomycin and glutamine as described previously (36, 43). *TransSafe*™ Mycoplasma Prevention Reagent was used to prevent mycoplasma contamination (TransGene, China). The cells were split to low density (30% confluence) overnight culture and were then treated with 5 μM 5-aza-2'-deoxycytidine (5-aza-CR) (Sigma–Aldrich, USA) for 96 hours, with the medium exchanged every 24 hours.

Cell Line Construction

The establishment of stable cell lines with *PRSS3-V1* overexpression was described previously (36). The OmicsLink™ Expression clones of *PRSS3-V2, -V3* and *-V4* were purchased from GeneCopoeia (Rockville, MD, USA) (**Table S6**). The CRISPR/Cas9 bivector lentivirus was custom ordered from GeneChem (Shanghai, China). The sgRNA was GGCACTGAGTGCCTCATCTC. Genomic deletion of *PRSS3* transcripts ($PRSS3^{KO}$) by targeting the common exon 5-8 region in $PRSS3^{High}$ Huh7 cells was performed using the CRISPR/Cas9 system. Puromycin (Puro) (2 μg/ml) was used for selection of the transduced cells. $PRSS3^{KO}$ Huh7 cells were transfected with the *PRSS3-V1* to *-V4* constructs to establish stable re-expression of *PRSS3* transcripts dubbed the $PRSS3^{KO+V}$ cell model. Transfection was performed using Lipofectamine 2000 (Invitrogen, USA) following the manufacturer's instructions. Stable cell lines with *PRSS3-V2, -V3* or *-V4* were selected using 0.5 mg/ml G418 (Invitrogen) for 2 weeks.

Cell Viability

HepG2, SK-Hep-1 and Huh7 cells were seeded into 96-well plates at 2×10^3 cells/well. Cell viability was measured every day by using a 3-(4,5-dimethylthiazol-2-yl)-2,5-diphenyltetrazolium bromide (MTT) assay kit (KeyGEN Biotech, China). The absorbance at 490 nm was detected using a microplate reader (Thermo Multiskan MK3, Thermo Fisher Scientific Inc., USA) as described (36, 43).

Colony Formation

HCC cells were seeded in 6-well tissue culture plates (100 cells/well) in triplicate. Colonies with more than 50 cells were counted after 2 weeks. The cells were fixed with 75% ethanol for 30 minutes and stained with 0.2% crystal violet (Beyotime Biotech, China) for 20 minutes (36, 43).

Transwell Invasion Assay

A Transwell apparatus was used with 8-μm polyethylene terephthalate membrane filters (Corning Inc., USA). The upper chambers were seeded with 200 μl of serum-free medium containing serum-starved cells (HepG2 and SK-Hep-1: 1×10^4 cells; Huh7: 2×10^4 cells). The lower chambers were filled with 500 μl of 10% FBS-DMEM. After 24 hours, cells that invaded the lower chamber were fixed and stained with 0.2% crystal violet (Beyotime Biotech) as previously described (36). The invaded cell number from experiments in triplicate was counted in five randomly selected fields per chamber under an inverted microscope (Leica, Germany).

RNA Isolation and RT–qPCR

Cells were harvested for RNA isolation using an RNeasy Mini Kit (QIAGEN, USA), and first strand cDNA was synthesized with the Superscript First-Strand Synthesis System (Invitrogen). RT–qPCR was performed using primers as previously described (36).

The relative expression level of each mRNA was normalized to *β-actin* using the $2^{-\Delta\Delta Ct}$ method.

Methylation-Specific qPCR

DNA extraction, bisulfite modification and MSP-PCR were performed as previously described (36, 43). Genomic DNA was extracted from tissues using the QIAamp DNA Mini Kit (Qiagen), followed by quantitative analysis using a NanoDrop 2000 spectrophotometer (Thermo Fisher Scientific, USA). Bisulfite modification of DNA was performed using a Zymo DNA Methylation Kit (Zymo Research, USA). The positive and negative template controls were the Human Methylated & Nonmethylated DNA Set (Zymo Research). MSP-qPCR was performed by using methylated or unmethylated primer pairs specifically for *PRSS3* (36) and *β-actin* (43). The relative level of methylation and unmethylation of *PRSS3* was normalized to *β-actin* using the $2^{-\Delta\Delta Ct}$ method.

Methylated DNA Immunoprecipitation-qPCR

Genomic DNA was extracted from the HCC cells. The purified DNA was then sonicated into 200~1000 bp fragments. A 10% sonicated DNA sample was kept as an input control. The denatured DNA fragments (input fractions) were incubated with 2 μg anti-5-methylcytidine (5mC) (Active motif, USA) or 2 μg control IgG (Sigma–Aldrich) monoclonal antibodies at 4°C overnight, followed by precipitation using protein A beads. After washing, immunoprecipitated DNA (IP fractions) and the input control fraction were purified by using a QIAquick purification kit (QIAGEN) and analyzed by qPCR using the following primers: F: 5'- CTGTGATGGAGAGGGGGTTC -3'; R: 5'-GAGTAGTGTGCGCATCGGT-3'.

Western Blotting

HCC cells were lysed in RIPA buffer (Beyotime Biotech) containing protease and phosphatase inhibitors (Sigma–Aldrich). Equal amounts of total protein were loaded on and separated by sodium dodecyl sulfate–polyacrylamide gel electrophoresis (SDS–PAGE) and then transferred onto polyvinylidene difluoride membranes using a Bio–Rad Mini PROTEAN 3 system. The membranes were blocked for 1 h in PBS containing 5% milk (v/v) and 0.1% Tween-20 (v/v) and incubated with the indicated primary antibodies against PRSS3 (Cat. ab107430, Abcam) and PRSS3 isoforms (**Figure S1C**) overnight at 4°C, followed by incubation for 1 h with the appropriate secondary antibodies. Immunoreactive bands were visualized by using the Amersham ECL Western Blotting Detection Kit according to the manufacturer's instructions. β-Actin served as a loading control.

Tumorigenicity

The animal handling and all *in vivo* experimental procedures were approved by the Institutional Animal Ethics Committee of Beijing Chest Hospital. Huh7 cells (2×10^6) with or without constructs suspended in 0.1 ml PBS were injected into the subcutaneous flanks of 4-week-old Balb/c female athymic mice (Vital River Laboratories, Beijing, China). The tumor diameters and body weights of nude mice bearing HCC xenograft tumors were measured and documented every 3 days until the animals were sacrificed at day 15. HCC tumor xenografts were isolated and weighed. Tumor volume was calculated by measuring the longest (a) and shortest (b) diameters of the tumor and calculated by the formula: ab2/2.

Statistical Analysis

The data are expressed as the means ± standard deviation (SD) of at least three independent experiments. *PRSS3* transcript expression, epigenetic alterations and associated clinicopathological correlations were analyzed by using the two–tailed Student's t–test, Wilcoxon rank sum test, one–way analysis of variance (ANOVA) with Tukey's *post-hoc* test, Spearman rank test and Fisher's exact test, or χ^2 or Fisher's exact tests. Cancer-related survival was analyzed using the Kaplan–Meier method and was compared using log-rank tests. Statistical significance was considered when $P < 0.05$. All statistical analyses were performed using SPSS version 23.0 (IBM Corp.).

RESULTS

Aberrant Differential Expression of *PRSS3* in HCC Was Attributable to its Transcript Heterogeneity in Human HCC

The RNA-seq data from the Cancer Model Repository (LIMORE) and the DepMap portal revealed that *PRSS3* as a whole was differentially expressed in HCC cell lines (**Figure S1A**, **Figure 1A** and **Table S1**). RT–qPCR validation showed that the expression levels of *PRSS3* ranged from very low ($PRSS3^{Low}$) to very high ($PRSS3^{High}$) compared to human fetal liver L02 cells (**Figure 1B**). Western blot using an anti-PRSS3 antibody confirmed the differential expression of PRSS3 at protein level (**Figure 1C**). Comparative analysis using TCGA RNA-seq data from FIREHOSE Broad GDAC showed divergent features of *PRSS3* expression in HCC tissues compared to their matched nontumor tissues (n=50) (**Table S2** and **Figure 1D**). This was further evidenced by the analysis of more HCC tissue specimens (tumor =371) (**Table 1**, **Figure 1E**). The GEPIA portal combined TCGA with GTEx RNA-seq datasets showed that *PRSS3* expression was more varied in HCC tissues (n=369) than in normal controls (n=160) (**Figure S1B**) (38, 41). Although not statistically significant, the *PRSS3* mRNA level was lower but had an extraordinarily wide range in HCC tissues compared to normal tissues, consistent with the analysis of CPTAC data showing that PRSS3 protein was more highly expressed in normal human live tissues than in HCC tissues (**Figure 1F**). These results suggest that *PRSS3*, as a differentially expressed gene (DEG), was aberrantly and divergently expressed in HCC.

To explore the molecular basis of the divergent expression of *PRSS3* in HCC, we dissected the expression of *PRSS3-V1~-V4* in HCC (14, 15, 17–20) (**Figure 2A**). Analysis of the DepMap data revealed that in 24 HCC cell lines, *PRSS3-V2* and/or *-V1* were two major transcripts contributing to the expression of *PRSS3* because *PRSS3-V3* was infrequent and/or poorly expressed, while

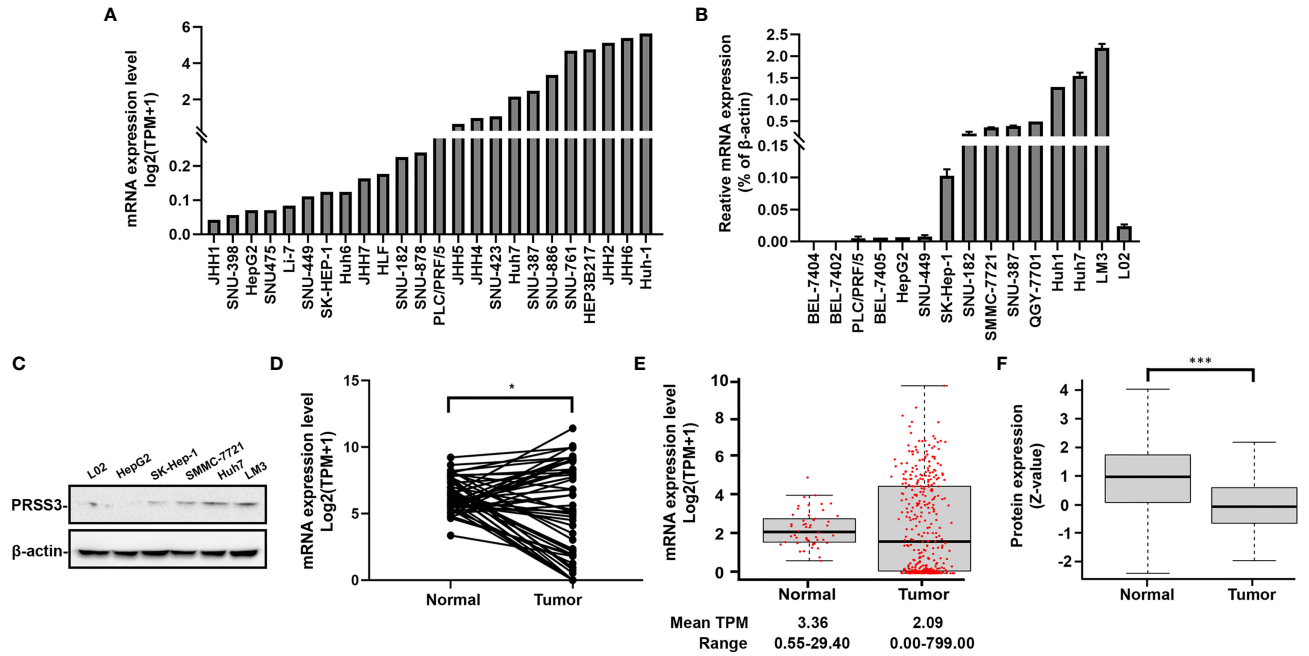

FIGURE 1 | *PRSS3* expression in human HCC cell lines and tissues. **(A)** The mRNA level of *PRSS3* expression in 24 HCC cell lines using RNA-seq data extracted from the DepMap website. The expression bar chart is sorted by *PRSS3* mRNA expression levels processed on a log2 (TPM+1) scale. TPM: transcripts per million. **(B)** RT–qPCR analysis of *PRSS3* expression in 14 HCC cell lines and the human fetal liver cell line L02. The relative expression of *PRSS3* mRNA was normalized to *β-actin*, presented as the mean ± SD from three independent experiments performed in triplicate. **(C)** Western blot analysis of PRSS3 in HCC cell lines and L02 cells. **(D, E)** The RNA-seq data were sourced from FIREHOSE (**Table 1**). *PRSS3* expression in 50 pairs of tumors and matched solid normal tissues from patients with HCC **(D)** or extensively in 371 tumor samples *versus* 50 normal tissues from HCC patients **(E)**. * $P < 0.05$, by Student's *t* test. **(F)** PRSS3 protein expression in human HCC (n = 165) in comparison with normal liver tissues (Normal) (n = 165), based on data from UALCAN portal analysis of CPTAC Confirmatory/Discovery dataset. Z-values represent the standard deviation from the median across samples for a given cancer type. Log2 spectral count ratio values from CPTAC were first normalized within each sample profile and normalized across samples. ***$P < 0.001$, by the Wilcoxon rank sum test.

TABLE 1 | Correlation between the mRNA levels of PRSS3 transcripts and clinicopathologic characteristics in patients with HCC.

Characteristics	N	*PRSS3* Expression		P
		High N (%)	Low N (%)	
Total	371	184 (49.6)	187 (50.4)	
Gender				
Male	250	123 (49.2)	127 (50.8)	
Female	121	61 (49.6)	60 (50.4)	0.9137
Cancer stage				
I	171	82 (47.9)	89 (52.1)	
II	86	43 (50.0)	43 (50.0)	0.8591
III	85	46 (54.1)	39 (45.9)	0.4259
IV	5	3 (60.0)	2 (40.0)	0.6736
Undefined	24	10 (41.7)	14 (48.3)	
Tumor grade				
I	55	21 (38.2)	34 (61.8)	
II	177	88 (49.7)	89 (50.3)	0.1794
III	122	67 (54.9)	55 (45.1)	0.0576
IV	12	5 (41.7)	7 (58.3)	1
Undefined	5	3 (60.0)	2 (40.0)	

The TCGA-LIHC data (version 28/01/2016) and clinical parameters of HCC patients were downloaded from the FIREHOSE Broad GDAC. After removing 2 samples of recurrent solid tumor tissues in the dataset, the remaining 421 samples included 50 matched pairs of primary solid normal and liver tumor tissues and 321 additional tumor specimens. The RNA level of PRSS3 expression was processed as TPM. High or low expression of PRSS3 ($PRSS3^{High}$ or $PRSS3^{Low}$) was classified based on the cutoff value of the median expression level of PRSS3 in the samples. The statistical significance of $PRSS3^{High}$ or $PRSS3^{Low}$ with clinicopathologic parameters of HCC patients was determined by $\chi 2$ tests.

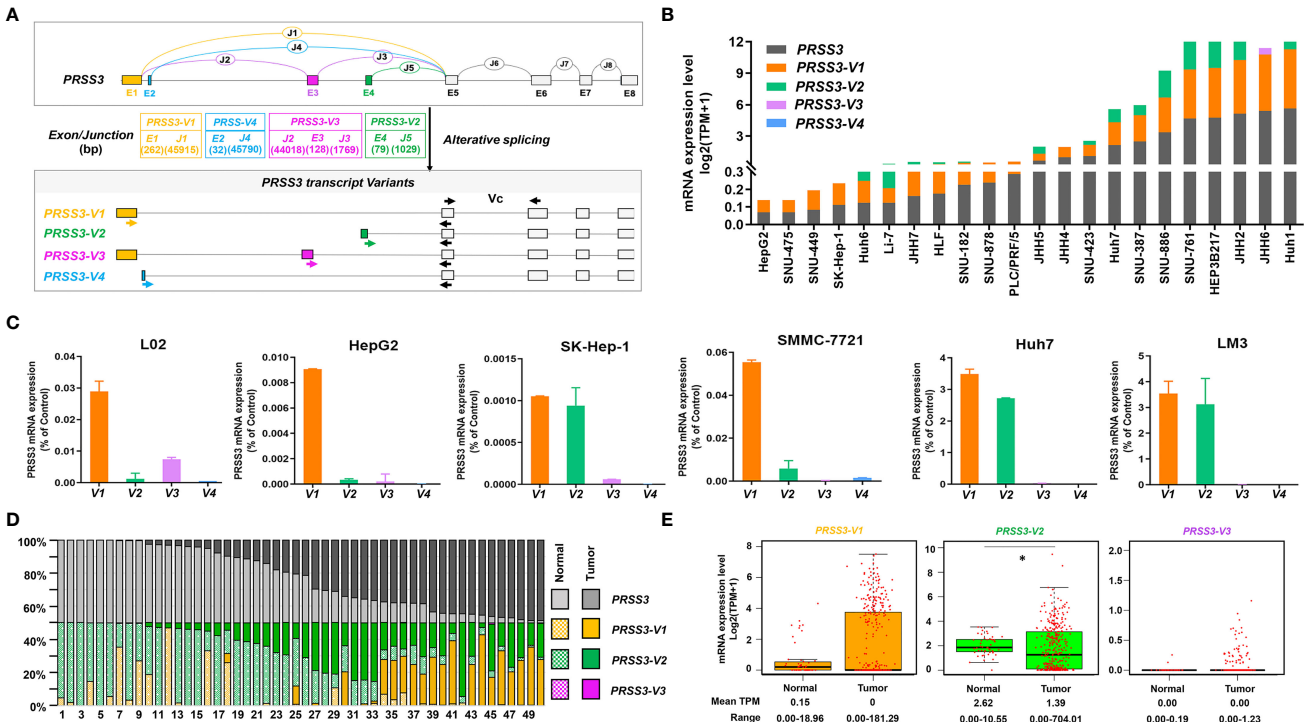

FIGURE 2 | The expression of *PRSS3* splice variants in human HCC cells and tissues. **(A)** A schematic overview of the human *PRSS3* gene structure and its splicing variants (*SVs*) and the designed RT–qPCR primers. The top diagram represents the genomic organization of *PRSS3*. Alternative splicing within the 5' region of the *PRSS3* gene leads to the creation of *PRSS3-V1* ~ *-V4*. The exons and introns are represented as boxes and lines (not drawn to scale). E1-E8: Exons; J1-J8: Junctions. E5-8: gray boxes common to all four variants. E1 to 4: sequence-specific for *PRSS3-V1* (brown), *-V4* (blue), *-V3* (purple), and *-V2* (green), respectively. Arrowheads indicate primer set locations used for amplification of *PRSS3-SVs*. Forward primers were designed specifically for *PRSS3-SVs*. Reverse primers were common to all. *Vc*: RT–qPCR primer set common to *PRSS3-SVs*. **(B)** Expression level of *PRSS3-SVs* in HCC cell lines. Data from the DepMap (**Table S1**). **(C)** RT–qPCR of *PRSS3* transcripts expressed in the human fetal liver cell line L02 and HCC cell lines. The relative expression level of each mRNA was normalized against *β-actin*. **(D)** Comparison of the mRNA expression of *PRSS3* and its transcript variants in 50 paired HCC and normal liver tissues (**Table S2**). The relative percentage of *PRSS3* transcripts expressed in each paired sample (TPM scale) was visualized by a 100% stacked bar graph. **(E)** The mRNA expression of *PRSS3* transcripts in HCC tissues (n=371) and normal liver tissues (n=50) based on data from FIREHOSE. The relative transcript level is presented as a log2 (TPM+1) scale. *$P < 0.05$ by Wilcoxon rank sum test.

PRSS3-V4 was absent (**Table S1** and **Figure 2B**). RT–qPCR showed that despite almost undetectable *PRSS3-V4* and very low expression of *PRSS3-V3* in all cell lines, *PRSS3-V1* was expressed at low levels in L02 cells, whereas *PRSS3-V1* and *-V2* were minimally expressed in HepG2, SK-Hep-1 and SMMC-7721 cells but highly expressed in Huh7 and LM3 cells (**Figure 2C**). Western blot using antibodies against PRSS3-V1 to -V4 showed that PRSS3-V1 and -V2 were detected in Huh7 and LM3 cells (**Figure S1C**), in parallel to their mRNA levels. Through comparative analysis of the expression levels of *PRSS3* transcripts, including *PRSS3* and its four *SVs*, in 50 paired tissue samples, we found that *PRSS3-V2* and *-V1* were predominantly present in both normal and tumor tissues (**Table S2** and **Figure 2D**). **Figure 2E** shows that the expression of *PRSS3-SVs* (no data available for *PRSS3-V4*) tended toward bipolarity in 371 HCC tissue samples compared to normal liver tissues, although only *PRSS3-V2* expression was significantly decreased. Coexpression analysis of both HCC cell lines and tissues summarized in **Table 2** further showed that the highest contributor of *PRSS3-SVs* to $PRSS3^{High}$ was *PRSS3-V2*, suggesting its expression dominance in $PRSS3^{High}$ in HCC. Moreover, $PRSS3^{Low}$ also resulted from decreased expression of *PRSS3-V2* and/or *-V1* because *PRSS3-V3* was minimally expressed in HCC and minimally affected the eventual expression of *PRSS3*, although $PRSS3\text{-}V3^{Low}$ was most frequently associated with $PRSS3^{Low}$. These results thereby revealed disruption of *PRSS3* transcripts toward bipolar expression contributing to aberrant and differential expression of *PRSS3* in HCC, in which *PRSS3-V2* and/or *PRSS3-V1* were dominant transcripts leading to *PRSS3* expression.

CpG Site-Specific Methylation Regulated the Expression Divergence of *PRSS3-SVs* in HCC

We previously observed epigenetic silencing of *PRSS3* in HCC (32, 34–36). However, methylation in association with the expression of its *SVs* has never been addressed. We next assessed the contribution of DNA methylation to the

TABLE 2 | Predominance and coexpression of *PRSS3* transcripts in HCC cell lines and tissues.

	Cell lines (n =24)				Tissue specimens (n =371)			
Transcript(s)	**High**	**%**	**Low**	**%**	**High**	**%**	**Low**	**%**
PRSS3	12	100	12	100.00	184	100.00	187	100.00
PRSS3-V1	9	75.00	9	75.00	163	88.59	166	88.77
PRSS3-V2	10	**83.33**	9	75.00	173	**94.02**	175	93.58
PRSS3-V3	1	8.33	11	**91.67**	48	26.09	185	**98.93**
PRSS3-V1+V2	8	**66.67**	6	50.00	153	**83.15**	156	83.42
PRSS3-V2+V3	0	0.00	9	75.00	45	24.46	173	92.51
PRSS3-V1+V3	1	8.33	9	75.00	46	25.00	165	88.24
PRSS3-V1+V2+V3	0	0.00	6	50.00	43	23.37	155	82.89

HCC cell lines and tumor samples were classified into high or low groups in accordance with the expression of PRSS3 transcripts (median expression level as cutoff value). The details are listed in ***Table 1***, ***Tables S1*** *and* ***S3****.*

Bold values show the highest frequency (%) of either highly or lowly expressed PRSS3-SV or coexpressed PRSS3-SVs in the HCC cell lines or tissues.

expression of *PRSS3-SVs* based on the data available from DepMap and FIREHOSE (39, 40) for three genomic regions in *PRSS3*. These were referred to as the promoter region and upstream and extended fragment, respectively (**Figure 3A**). The promoter region approximately 2400 bp (-1749 to 653 bp) around the TSS shared by *PRSS3-V1/3* contains 17 CpG sites (CpGs 1-17), including 5 CpGs (CpGs 2-7) in the 1 kb upstream fragment (-1000 bp to the TSS of *PRSS3-V1/3*), while the extended fragment includes 6 CpGs (defined as A, B, C, D, E and F) scattering around a broad genomic region approximately 34.5 kb in scale from -170 to 34,654 bp of the TSS of *PRSS3-V1/3* but still -10,643 bp upstream of the TSS of *PRSS3-V2*. The genomic position of each CpG site is shown in **Figure 3A** relative to the TSS of *PRSS3-V1/3* (**Table S4**).

Association analysis demonstrated an inverse association between the upstream methylation and mRNA expression of *PRSS3* and its transcripts *PRSS3-V1* and *-V2* that could distinguish HCC cell lines phenotypically between hypermethylation of $PRSS3^{Low}$ (m$PRSS3^{Low}$) and hypomethylation of $PRSS3^{High}$ (um$PRSS3^{High}$) groups (**Figure 3B**). The pattern of m$PRSS3^{Low}$ versus um$PRSS3^{High}$ was further confirmed in tumor samples showing more similarity between *PRSS3* and *PRSS3-V2*, whereas *PRSS3-V1* was more phenotypically defined with m$PRSS3^{Low}$ and um$PRSS3^{High}$ groups (**Figure 3C**). Together with the intragenic methylation associated with *PRSS3* expression shown in our previous study (35), these results support the regulatory effect of DNA methylation on *PRSS3* transcripts.

Unsupervised clustering combined with Spearman correlation analysis of CpG site methylation and expression of *PRSS3* transcripts in HCC cell lines revealed that among 17 CpGs distributed in the promoter region, methylation occurring at CpG sites 5-17 (-89~653 bp from the TSS of *PRSS3-V1/V3*) (**Table S4**) was inversely correlated with the mRNA expression level of *PRSS3-V1*, while methylation at CpG sites 12-16 (522 to 564 bp to *PRSS3-V1* TSS) was highly related to *PRSS3-V2* expression (**Figure 3D** and **Figure S2**, **Table S5**). No associative comparison was conducted on *PRSS3-V3* and *-V4* due to their rare expression in HCC. This result confirms the patterns of m$PRSS3^{Low}$ versus um$PRSS3^{High}$ in HCC cells. However, only CpG site 5 in the upstream was significantly associated with the expression of *PRSS3-V1* (**Figure 3D**, and **Figure S2**), suggesting CpG site-specific regulation of *PRSS3* transcript expression in HCC cells. Moreover, despite a positive association shown at CpG site F, methylation at CpG sites A-E was negatively correlated with *PRSS3* expression (**Figure 3E** and **Figure S3A**), in which the associative significance of site methylation with *PRSS3* and *PRSS3-V2* was B, C, D, E but reversed for *PRSS3-V1* (**Figure S3B**). CpG site methylation at the extended fragment of *PRSS3* was decreased at site A, increased at B, C and D, and then decreased at E and F in HCC tumors compared to normal controls (**Figure 3F**). The CpG site methylation in the *PRSS3* promoter region from -89 bp (CpG site 5) to 785 bp (CpG site E) to the TSS of *PRSS3-V1/3* associated with the expression of *PRSS3* transcripts suggests an epigenetic promoter contribution to divergent expression of *PRSS3* transcripts in HCC (**Figure 3A**).

We then examined the methylation-specific effect on *PRSS3* expression using qPCR-based assays (**Figure 3A**). MSP-qPCR showed that *PRSS3* was hypermethylated in $PRSS3^{Low}$ cell lines (HepG2, SK-Hep-1) but hypomethylated in $PRSS3^{high}$ Huh7 cells compared to L02 cells (**Figure 3G**), consistent with previous observations (36). **Figure 3H** reveals that treatment with the DNA methyltransferase inhibitor 5-aza-CR caused significant upregulation of *PRSS3* expression in $PRSS3^{Low}$ cell lines but had no effect on $PRSS3^{High}$ Huh7 cells. Notably, a bipolar expression pattern was observed in $PRSS3^{Low}$ cell lines upon 5-aza-CR treatment, showing significant upregulation of *PRSS3-V1* and *-V3* opposite to downregulation of *PRSS3-V2*, eventually integrative to the upregulation of *PRSS3*, whereas the treatment had no effect on $PRSS3^{high}$ Huh7 cells, actually due to integration between upregulation of *PRSS3-V2* and downregulation of *PRSS3-V1* and *-V3*. MeDIP-qPCR further showed that the anti-5-methylcytosine (5-mC) antibody significantly enriched fewer genomic DNA fragments in HepG2 cells but not in Huh7 cells upon 5-aza-CR treatment (**Figure 3I**), suggesting that 5-aza-CR was effective in the expression of *PRSS3* specifically by altering DNA methylation in this promoter region. Although the expression of *PRSS3-V3* in L02 or *PRSS3-V2* in HepG2 and SK-Hep-1 cells was too low to take into account its decreased significance level, these results are consistent with bioinformatic analysis of HCC cell lines and

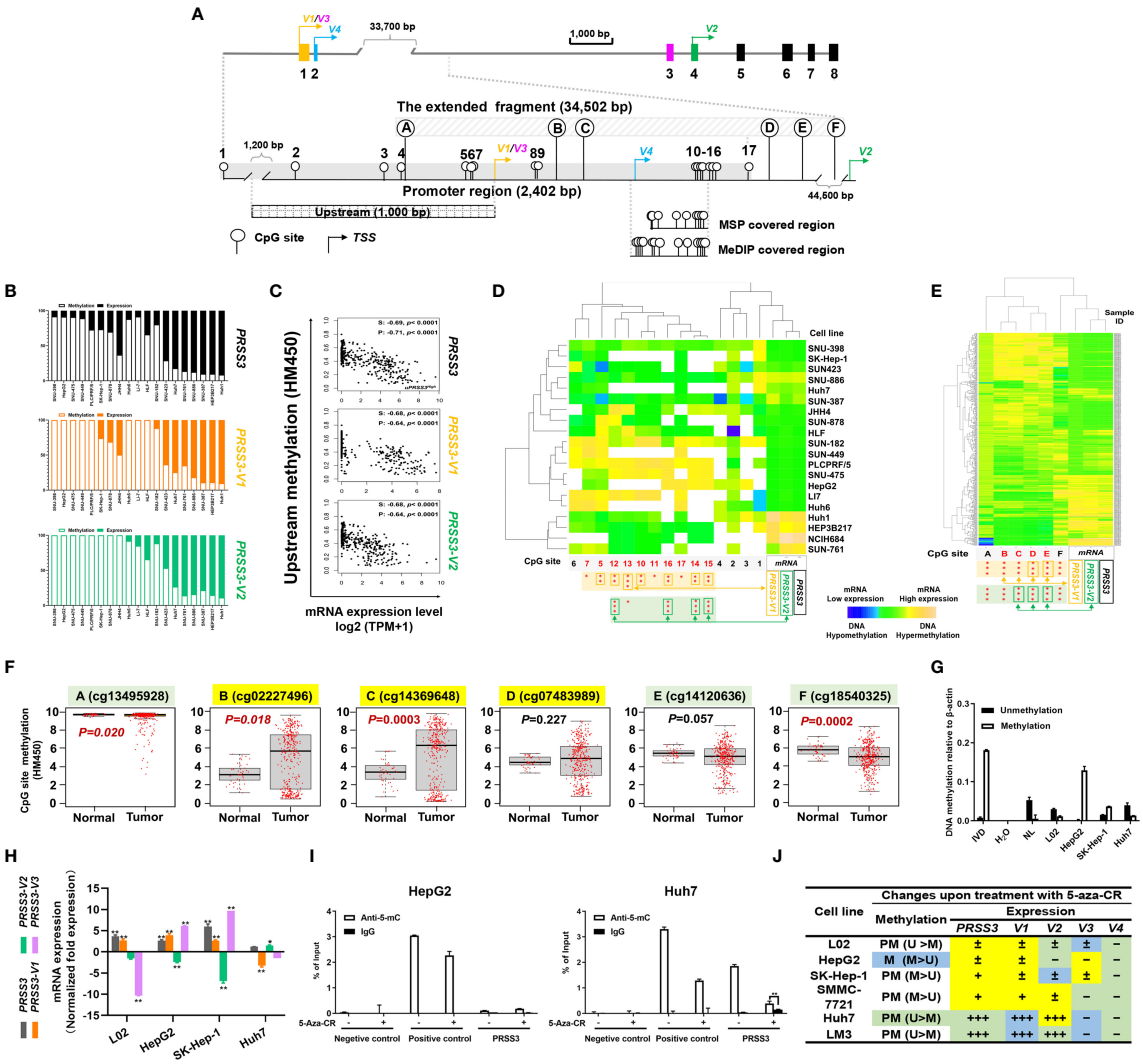

Cell line	Methylation	Changes upon treatment with 5-aza-CR				
		Expression				
		PRSS3	*V1*	*V2*	*V3*	*V4*
L02	PM (U >M)	±	±	±	±	–
HepG2	M (M>U)	±	±	–	–	–
SK-Hep-1	PM (M>U)	+	±	±	±	–
SMMC-7721	PM (M>U)	+	+	±	–	–
Huh7	PM (U>M)	+++	+++	+++	–	–
LM3	PM (U>M)	+++	+++	+++	–	–

FIGURE 3 | CpG methylation in the regulation of *PRSS3* transcript expression in HCC. **(A)** Schematic of the *PRSS3* 5'-genomic region including the extended promoter region and upstream and extended fragments. The promoter region (-1749 to 653 bp) shared by *PRSS3-V1/3* contains 17 CpG sites (CpGs), including 5 CpGs (CpG sites 2-7) in the 1 kb upstream fragment (-1000 bp from the TSS of *PRSS3-V1/3*). The extended fragment includes 6 CpGs (defined as **A–F**) scattering around a broad genomic region approximately 34.5 kb from -170 to 34,654 bp of the *PRSS3-V1/3* TSS but -10,643 bp from the TSS of *PRSS3-V2*. The genomic position of each CpG site is shown relative to the TSS of *PRSS3-V1/3* (**Table S4**). Primer-covered regions for MSP-qPCR and MeDIP-qPCR are shown. **(B)** 1 kb upstream methylation normalized as a percentage relative to *PRSS3* expression in HCC cell lines visualized by a 100% stacked bar graph. **(C)** Spearman and Pearson correlation analysis of 1 kb upstream methylation associated with *PRSS3* expression in human primary liver tumor samples (n=371). **(D, E)** Clustered heatmap of the correlation between CpG site methylation and *PRSS3* transcript expression. Data were visualized by using correlation as a distance function for heatmap cluster analysis of CpG methylation at the promoter in 20 HCC cell lines **(D)** and at the extended fragment in HCC tissue specimens (n=414) **(E)**. In the heatmap, blue indicates low, green indicates intermediate and yellow indicates high DNA methylation or mRNA values. Rows: CpG sites arranged based on the correlation between the methylation and mRNA expression levels of *PRSS3* transcripts. The values of DNA methylation levels were renormalized with mean=0 and standard deviation=1. Columns: HCC cell lines or tissue specimens. The statistical significance of correlation coefficients between CpG sites (red) and mRNA expression of *PRSS3* transcripts are shown at the bottom. $^{*}P < 0.05$, $^{**}P < 0.01$, $^{***}P < 0.001$ (**Figures S3, S4** and **Table S5**). **(F)** Association analysis of CpG site methylation with *PRSS3-SV* expression in 414 HCC tissue specimens compared with 41 normal controls (Wilcoxon rank sum test). **(G)** MS-qPCR of *PRSS3* methylation in HCC cell lines and L02 cells. *In vitro* methylated DNA (IVD) and normal human peripheral lymphocyte DNA (NL) served as positive and negative methylation controls, respectively. **(H)** RT–qPCR of the expression of *PRSS3* transcripts in HCC cell lines and L02 cells upon treatment with the epigenetic reagent 5-aza-CR (5 μM, 96 h). $^{*}P < 0.05$, $^{**}P < 0.01$ by Student's *t* test. **(I)** MeDIP-qPCR to analyze 5-mC-enriched genomic DNA associated with the extended promoter region in HCC cell lines and L02 cells after 5-aza-CR treatment. $^{**}P < 0.01$ by Student's *t* test. **(J)** In the summary table, the differential expression changes of *PRSS3* transcripts responding to treatment with 5-aza-CR are visualized with symbols and colors. Methylation was defined as partial methylation (PM) or methylation (M) based on the MSP results. *PRSS3* expression: "–", < 0.001%; "±", 0.001-0.05%; "+", > 0.05%; "+++", > 1%. The fold changes upon 5-aza-CR treatment are shown in color: yellow, upregulation; green, downregulation; blue, no change.

tissues, as well as our previous report (36), suggesting that methylation occurring at this region is more critical for epigenetically controlling *PRSS3* transcript activities in HCC. As shown in the summarized table (**Figure 3J**), the divergence of *PRSS3* transcript expression and their response to 5-aza-CR treatment was negatively associated with site-specific CpG methylation, which eventually determined the expression level of *PRSS3* as a whole. These results suggest that differential methylation of the promoter controls the expression of *PRSS3-SVs* in a site-specific manner in HCC.

PRSS3-V2 Exerts Oncogenic Functions Distinct From the Tumor-Suppressive Effects of *PRSS3-V1* and *PRSS3-V3* in HCC Cells

The functional role of *PRSS3-SVs* was assessed by transfecting *PRSS3-V1* to *-V4* into $PRSS3^{Low}$ HepG2 and SK-Hep-1 cells (defined as V1 to V4) (**Figure 4A** and **Figure S4A**). MTT assays showed that ectopic expression of *PRSS3-V1* or *PRSS3-V3* significantly inhibited HCC cell proliferation in contrast to notably enhancing the effect of ectopic *PRSS3-V2* expression or

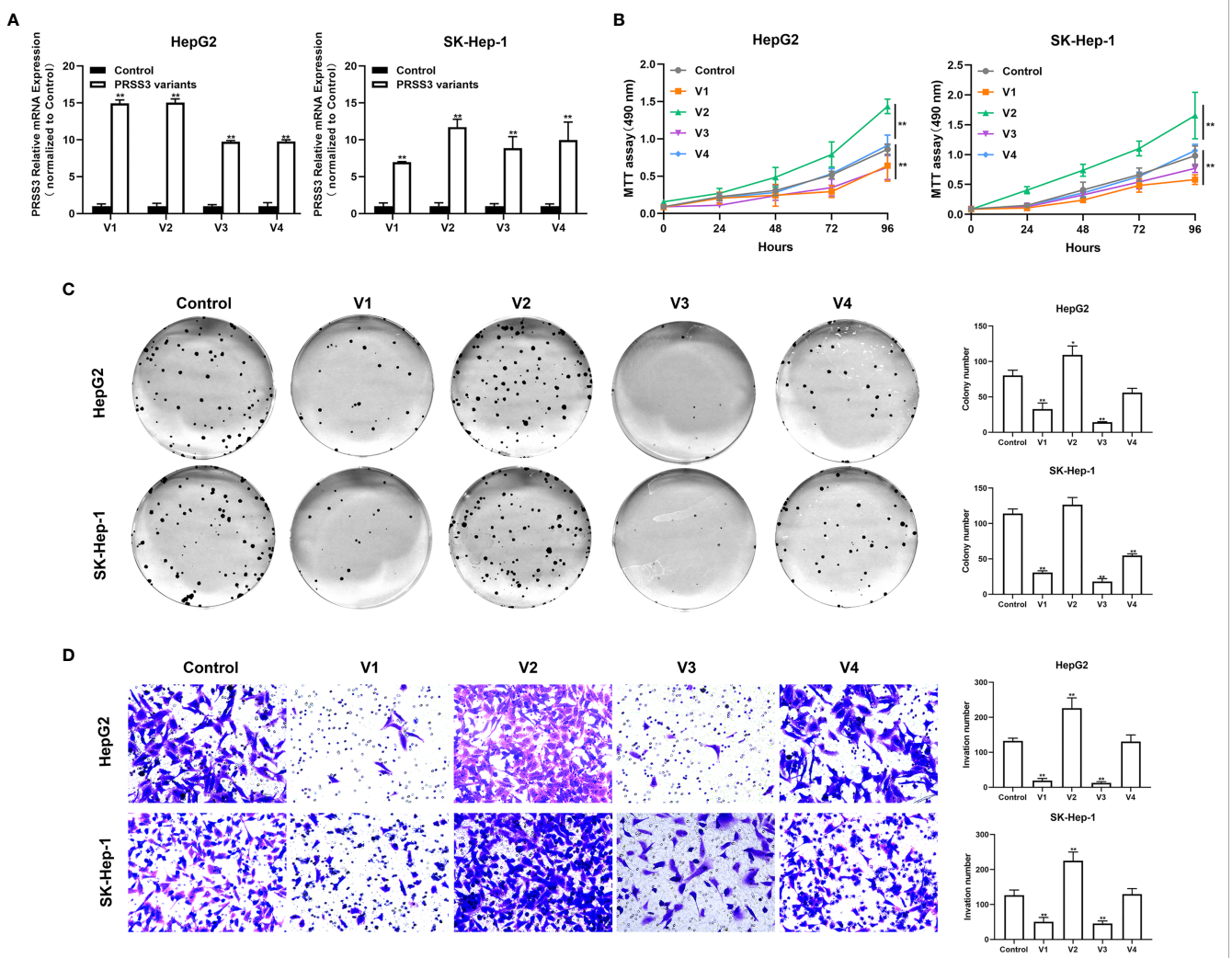

FIGURE 4 | Effects of ectopically expressed *PRSS3* transcripts on HCC cell malignancy. The *PRSS3* splicing variants were separately transfected into HepG2 and SK-Hep-1 cells to establish stable cell lines with individual overexpression of either *PRSS3-V1* to *-V4* (*V1* to *V4*) or vector control (Control). **(A)** The mRNA expression levels of *PRSS3* transcripts in the transfected cells were measured by RT–qPCR and quantified relative to the control cells (Student's *t* test). **(B)** Cell viability of HepG2 and SK-Hep-1 cells with ectopic expression of either *PRSS3* transcript was detected by MTT assays compared with the vector control (two-tailed Student's *t*-test). **(C)** Colony assays showing the colony formation of HepG2 and SK-Hep-1 cells after overgrowing for 2 weeks. Representative images are presented in the left panel; quantitation of the colony numbers is shown on the right. **(D)** Transwell invasion assay assessing cell invasion capacity following transfection of *PRSS3* transcripts. Left panel: representative image at 200× magnification; right panel: quantitation of the migrated cells. One–way ANOVA with Tukey's *post-hoc* test was calculated for the transfected cells compared with the vector control in **(C, D)**. $^{*}P < 0.05$, $^{**}P < 0.01$, *versus* control. Data are presented as the mean ± SD of three independent experiments performed in triplicate.

nonfunctional *PRSS3-V4* on HCC cell proliferation compared to the vector controls (**Figure 4B**). Moreover, the results of the clone formation assay showed that overexpression of *PRSS3-V1* or *PRSS3-V3* remarkably diminished the number of colonies of HCC cells compared with the control group, but *PRSS3-V2* overexpression resulted in an increased number of colonies only effectively in HepG2 cells. However, ectopic *PRSS3-V4* significantly reduced clone formation in SK-Hep-1 cells but had no effect in HepG2 cells (**Figure 4C**). Transwell assays further showed an inhibitory effect of *PRSS3-V1* or *PRSS3-V3* on HCC cell migration, in contrast to *PRSS3-V2*, which showed an enhanced effect in the cells (**Figure 4D**). These results suggest a tumor-suppressive effect of *PRSS3-V1*/*V3* versus an oncogenic effect of *PRSS3-V2* in HCC cells.

To further define the phenotypic properties of *PRSS3-SVs* in HCC cells, we established a $PRSS3^{KO+V}$ cell model in which each *PRSS3* transcript construct was separately transfected after endogenous *PRSS3* was deleted through the CRISPR/Cas9 system (**Figure 5A**). RT–qPCR showed that all the detected *PRSS3* transcripts were effectively deleted, and their constructs were stably expressed in Huh7 cells, designated $PRSS3^{KO+V1}$ to $PRSS3^{KO+V4}$, or the vector control ($PRSS3^{KO+V}$) (**Figure 5B**), which was further confirmed by Western blot analysis of PRSS3 protein isoforms (**Figure S4B**). Functional assays, as shown in **Figure 5C–E**, revealed that *PRSS3* deletion in Huh7 cells facilitated cell proliferation, colony formation and migration, which were abolished by re-expression of *PRSS3-V1* or *PRSS3-V3*. Ectopic re-expression of *PRSS3-V2* augmented the *PRSS3*-deletion effects on cell proliferation and, remarkably, on the migration of $PRSS3^{KO}$ Huh7 cells. Unexpectedly, *PRSS3-V4* re-expression did not affect Huh7 cell proliferation but resulted in significant inhibition of $PRSS3^{KO}$ Huh7 cell activity. To analyze the functional roles of the *PRSS3* variants in tumor growth *in vivo*, a tumor xenograft assay was performed by injecting $PRSS3^{KO+V}$ cells into nude mice (**Figure S5**). Consistent with *in vitro* findings, *PRSS3* deletion favored xenograft tumor growth formed by Huh7 cells, with a significant augmentation by re-expression of *PRSS3-V2* ($PRSS3^{KO+V2}$), whereas re-expressing either *PRSS3-V1* or *PRSS3-V3* ($PRSS3^{KO+V1/3}$) in the cells caused a marked inhibitory effect on xenograft tumor growth in contrast to a minimal role of $PRSS3^{KO+V4}$ (**Figure 5F**). These results exclusively demonstrate the dual roles of *PRSS-SVs* in HCC cells, and divergent disruption of *PRSS3* transcripts may be integrated to establish their functional heterogeneity in HCC cells.

To explore the possible mechanisms by which the *PRSS3* transcript variants exerted the dual effects on hepatocarcinogenesis, potential *PRSS3*-targeted downstream genes were sorted using network analysis of TCGA-LIHC tissue dataset available from SEEK (http://seek.princeton.edu) (**Figure S6A**), among which 8 key hub genes were shown in most association with *PRSS3* transcripts (except *PRSS3-V4*) either positively (*F2RL1, SMPDL3B, DUOX2, SLC43A3, TMEM45A* and *VNN1*) or negatively (*GLUL* and *NKD1*) in the network (**Figure S6B**), consistent with the validation in HCC cells using the CCLE dataset (**Tables S1, S7** and **S8**). In addition to a heatmap visualizing the differential expression of the hub genes (**Figure S6C**), **Figure S6D** shows significant upregulation of *F2RL1, SMPDL3B, DUOX2, SLC43A3, GLUL* and *NKD1*, but upregulation of *TMEM45A* and *VNN1* in HCC tissues compared with normal human live tissues. As shown in the summarized table based on the available data from UALCAN (https://www.ualcan.path.uab.edu/), there was a divergent association of the clinical significance between *PRSS3* and the hub genes (**Figure S6E**). For instance, the pattern of *PRSS3* downregulation associated with the clinical relevance of HCC patients was similar to that of *TMEM45A* and *VNN1*, which are positively co-expressed genes of *PRSS3* in HCC patients showing oncogenic effects on cancer-associated events (44, 45). However, *GLUL* and *NKD1*, completely opposite to *PRSS3*, showed increased expression related to clinical relevance, displaying the ability to regulate the invasion and migration of hepatocarcinoma cells (46–49). Importantly, PRSS3/MTG linked to F2RL1 (also known as PAR2), was reported to modulate inflammation and tumorigenesis in several cancer types, such as colon cancer and breast cancer (23, 24). In support of this point, Kaplan–Meier survival analysis showed divergent survival curves for HCC patients with high or low expression of the hub genes (**Figure S6F**). Kyoto Encyclopedia of Genes and Genomes (KEGG) pathway enrichment analysis indicated that these cancer-associated genes may be involved in the cell cycle and senescence through the *PRSS3-V1*-associated p53 signaling pathway, or *via* the PI3K-Akt pathway in association with *PRSS3-V2*/*PRSS3*, due to their corresponding pathways with more parallel lines (**Figure S6G**). These data therefore suggest that *PRSS3* transcripts are bifunctional, possibly *via* interplay with different cancer-associated gene pathways.

Epigenetic Alteration of *PRSS3-V2* Is Associated With Clinical Relevance in Patients With Early HCC

To further explore the contribution of *PRSS3* transcripts to tumor heterogeneity, we used the TCGA dataset to analyze their clinical relevance. We found that the expression of *PRSS3* and *PRSS3-V2* was similarly downregulated but with a gradually increasing tendency in HCC tumors compared with control tissues, following the progression of tumor stages (**Figure 6A**) and pathological grades (**Figure 6B**), in which $PRSS3\text{-}V2^{Low}$ was significantly detected in tumors of early HCC patients in contrast to $PRSS3\text{-}V2^{High}$ in advanced tumors. Kaplan–Meier (K-M) analysis revealed that $PRSS3\text{-}V2^{Low}$ was a favorable factor for the overall survival of HCC patients based on cancer stage (**Figure 6C**) and grade (**Figure 6D**), in which $PRSS3\text{-}V2^{Low}$ patient groups with low-grade tumors showed significantly favorable outcomes (P=0.011). Moreover, divergent disruption of CpG site methylation (A to F) was shown throughout the clinical progression of tumors but occurred more frequently and significantly in tumors of HCC patients with early-stage (**Figure 6E**) and lower-grade tumors (**Figure 6F**). In such tumors, alteration in CpG methylation at site D was most inversely correlated with the expression of *PRSS3* and *PRSS-V2*. Since the region located at site D was shown to be an important regulatory region specifically for epigenetic regulation

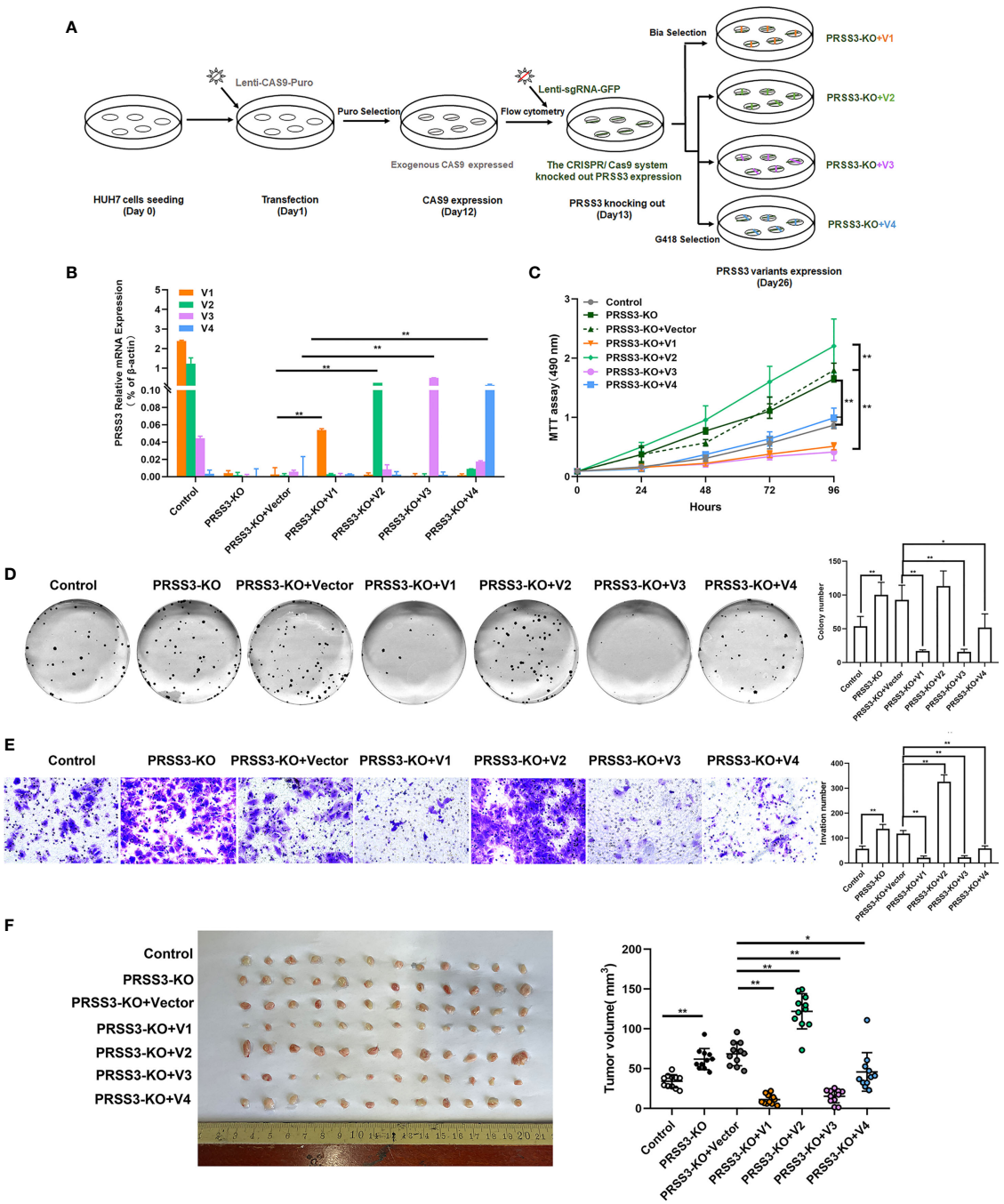

FIGURE 5 | Functional divergence of *PRSS3* transcript variants in a gain- and loss-of-function cell model. **(A)** Schematic of the workflow for the construction of a cell model by endogenous deletion and then ectopic expression of the *PRSS3* transcript in Huh7 cells (*PRSS3* $^{KO+V}$ cell model). Genomic deletion of *PRSS3* transcripts by targeting the common exon 5-8 region in *PRSS3*^{High} Huh7 cells was performed using the CRISPR/Cas9 system, followed by transfection with *PRSS3-V1* to *PRSS3-V4* constructs (*PRSS3* $^{KO+V1}$ to *PRSS3*$^{KO+V4}$) or vector control (*PRSS3*$^{KO+C}$). Puromycin (Puro), blasticidin (Bla) and geneticin (G418) were used for selection of the transduced cells. **(B)** RT–qPCR analysis of *PRSS3* mRNA expression in the transfected cells. The relative mRNA expression of *PRSS3* transcripts normalized to *β-actin* (Student's *t* test). **(C)** MTT assays showed the viability of Huh7 cells (two-tailed Student's *t*-test). **(D)** Colony formation of Huh7 cells for 2 weeks. Left panel: representative image; Right panel: The colony numbers counted. **(E)** Transwell invasion assay assessing the invasion capacity of Huh7 cells upon transfection. Left panel: representative images at 200× magnification; right panel: quantitation of the invaded cells. One–way ANOVA with Tukey's *post-hoc* test was calculated for the transfected cells compared with the vector control in **(C–F)**. $^{*}P < 0.05$, $^{**}P < 0.01$, versus control. Data are presented as the mean ± SD of three independent experiments performed in triplicate. **(F)** Effects of *PRSS-SVs* on HCC tumorigenicity using the *PRSS3* $^{KO+V}$ Huh7 cell model. Photographs (left panel) and tumor volumes (right panel) of dissected xenograft tumors from different groups of nude mice (n=12) after sacrifice. $^{*}P < 0.05$, $^{**}P < 0.01$, one–way ANOVA with Tukey's *post hoc* test.

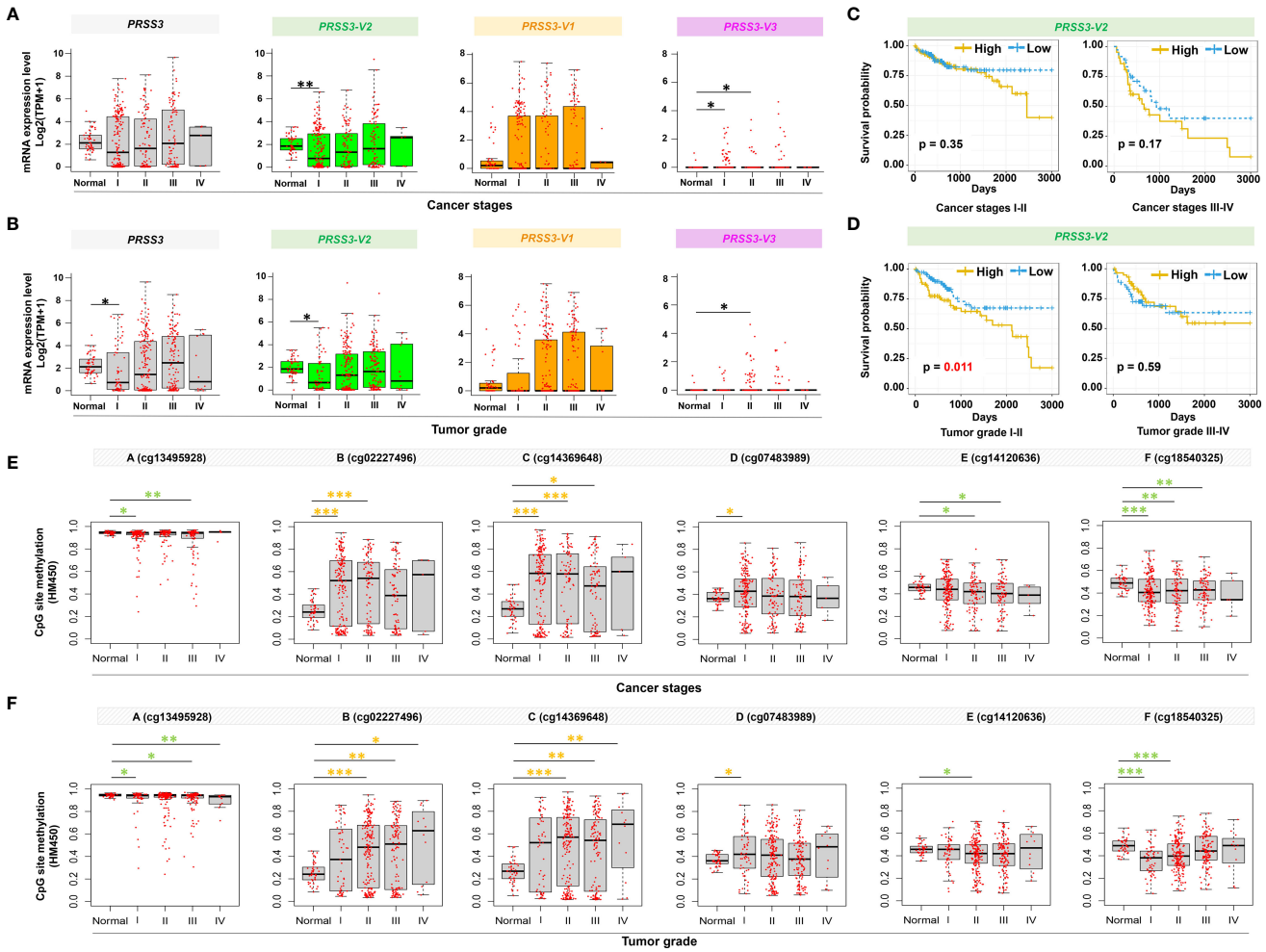

FIGURE 6 | Clinical relevance of epigenetic alteration of *PRSS3-SVs* in HCC patients. **(A, B)** Box-and-whisker plot with overlay of individual data points showing mRNA expression of *PRSS3* transcripts in HCC tissues (Tumor=371) and normal controls (Normal=50), based on **(A)** cancer stages (171 stage I, 86 stage II, 85 stage IIII, 5 stage IV) and **(B)** tumor grades (55 grade I, 177 grade II, 122 grade III, 12 grade IV) (**Table 1**). **(C, D)** HCC patients were grouped into *PRSS3-V2*^{High} and *PRSS3-V2*^{Low} groups based on the mean value of each transcript in tumors (**Table 1**). The Kaplan–Meier method was used to determine patient survival, and the log-rank (Mantel–Cox) test was used to compare survival rates. The results of HCC patient survival curves from left to right panels: cancer stages I-II and III-IV **(C)**, tumor grades I-II and tumor grades III-IV **(D)**. **(E, F)** The association of methylation of CpG sites **(A–F)** within the extended fragment with different clinical stages **(E)** and pathological grades **(F)** in HCC tissue specimens (n=414) in comparison with normal liver control tissues (Normal=41). The data were extracted from the FIREHOSE. Statistical significance was determined by the Wilcoxon rank sum test. Asterisks in green and yellow indicate the changes in hypermethylation and hypomethylation, respectively. *$P < 0.05$, **$P < 0.01$, ***$P < 0.001$.

of *PRSS3* transcripts (**Figure 3**), the data suggest that site-specific epigenetic alteration of *PRSS3-V2* in HCC tissues was distinct between mPRSS3-*V2*^{Low} in early HCC and um*PRSS3*^{High} in advanced HCC patients, in which early HCC patients with *PRSS3-V2*^{Low} tumors had better outcomes.

DISCUSSION

Paradoxical effects of many genes have been observed during tumorigenesis (13, 50, 51). The protease PRSS3 is the first to link the enzyme to prostate cancer, leading to the development of a compound to stop PRSS3 from promoting metastasis (13, 52). Since the high similarity in both sequences and structures to different trypsinogen isoenzymes made it difficult to delineate their functionally associated transcripts distributed in different tissues (13, 16), the protumor (21–31) or antitumor properties of PRSS3 (32–36) were too sophisticated to be deciphered. In this study, we found differentially expressed *PRSS3* in HCC due to CpG methylation-mediated epigenetic dysregulation of its splice variants. Different *PRSS3-SVs* were expressed in HCC, showing a dual role in hepatocarcinogenesis that may increase phenotypic diversity. Our study uncovered epigenetic-mediated *PRSS3* transcript variance contributing to the nongenetic phenotypic

diversity of HCC (50). To the best of our knowledge, this is the first study of functional dissection of the expression of *PRSS3-SVs* in cancer and thus has important implications in HCC patient-tailored management.

PRSS3 is a digestive protease with restricted expression in the pancreas. However, the preferential expression of *PRSS3-SVs* differs in human tissues, suggesting tissue-selective expression. For instance, *PRSS3-V2* was exclusively expressed in human pancreatic tissue and fluid encoding MTG (15, 53). Canonical *PRSS3-V1* was originally identified in the human brain (17, 53). *PRSS3-V3* shares the same TSS with *PRSS3-V1* but has a different in-frame exon with a deduced 261-amino acid sequence (formerly named isoform B) (19). *PRSS3-V4* was cloned from keratinocytes and shown to participate in keratinocyte terminal differentiation (20). Our study showed the differential expression of *PRSS3* as a DEG in HCC across a large expression range that could be used to phenotypically distinguish between $PRSS3^{Low}$ and $PRSS3^{High}$ HCC cells and tissues. Accordingly, we found divergent expression of *PRSS3-SVs* toward bipolarity following clinical progression from downregulation in early HCC to upregulation in advanced cancer, unveiling the molecular basis of *PRSS3* in tissue-selective expression of its splice transcripts in HCC. Despite the infrequent and/or minimal expression of *PRSS3-V3* and unexpressed *PRSS3-V4*, the divergent expression changes of *PRSS3-V2* and/or *-V1* were major contributors to the transcript heterogeneity of *PRSS3* in HCC. Notably, the expression of *PRSS3-SVs* was dynamically altered following clinical progression from downregulation in early HCC to upregulation in advanced cancer. *PRSS3* transcript heterogeneity was further evidenced by its divergent responses to 5-aza-CR treatment of HCC cells, distinguishing between upregulation of *PRSS3-V1* or *-V3* but downregulation of *PRSS3-V2* in $PRSS3^{Low}$ HCC and downregulation of *PRSS3-V1* but upregulation of *PRSS3-V2* in $PRSS3^{High}$ HCC. The divergent expression of *PRSS3* transcripts and their response to 5-aza-CR prompted our consideration of the effects of nongenetic heterogeneity on the chemotherapy response because this well-known anticancer drug has broad clinical applications and mis-splicing regulation, as a nongenetic mechanism is frequently linked to therapy escape (54–56). For precise evaluation of the clinical effectiveness and drug resistance by using a DEG, its functional splice variants, rather than its overall expression, need to be considered. Nevertheless, it was clear that differentially expressed *PRSS3* decreased as a whole, which was mainly attributable to its aberrant transcript variance expressed in HCC.

PRSS3 translocates from chromosome 7q34, the loci of *PRSS1* and *PRSS2*, to chromosome 9p11.2, a region frequently containing alterations (13, 57). However, frequent genetic variations occurring in *PRSS3* have not yet demonstrated disease-associated *PRSS3* variants (https://www.nextprot.org/entry/NX_P35030/medical). Alternative splicing forms a dynamic interactome offering precise therapeutic approaches to correcting cancer-specific defects caused by mis-splicing regulation, in which epigenetics plays an essential role (9, 11, 12, 55, 58–60). Our previous study showed epigenetic silencing of *PRSS3* in HCC (36), and we reasoned that epigenetic regulation of *PRSS3-SVs* contributes to nongenetic heterogeneity in HCC. The different TSSs and start codes in *PRSS3* suggest that *PRSS3*, like the majority of protein-coding genes, tends to be regulated by multiple or alternative promoters, the usage of which provides pretranscriptional control of gene activity to express its different isoforms in a tissue-specific manner (1, 6, 9, 24). Here, we found an extended promoter region covering the upstream and intragenic regions of *PRSS3-V1/V3* and *PRSS3-V4*, providing a site-specific way to regulate the expression of *PRSS3-SVs*. Both HCC cells and tissues were phenotypically classified as $mPRSS3^{Low}$ and $umPRSS3^{High}$ based on CpG methylation in association with the expression of *PRSS3* transcripts. Compared to consistent upstream hypermethylation, site-specific CpG methylation in the intragenic region was found to be more associated with the expression of *PRSS3-V1* and *PRSS3-V2*, suggesting that this extended promoter region played a central role in the regulation of both *PRSS3-V1* and *PRSS3-V2*. Given that epigenetic promoter alterations can change the chromatin accessibility of transcription regulatory elements binding to transcription factors (11, 12, 50, 60–63), the upstream hypermethylation of *PRSS3* may impact tissue-specific *cis*-regulatory modules that may alter the transcriptional activity of *PRSS3-SVs* in HCC. Dynamic disruption of methylation of different CpG sites within the extended promoter region may affect the occupancy of certain transcriptional regulators or splicing factors, resulting in an alteration in exon skipping to control the expression of *PRSS3-V1* or *-V3*. Meanwhile, site-specific epigenetic control of *PRSS3-V2* suggests that the extended promoter may be a distal regulatory region in the regulation of *PRSS3-V2* through a very different epigenetic pathway (64). Consistent with this, epigenetic silencing of *PRSS3* was found in several cancer types (32–35), and our previous study showed intragenic DNA methylation within the extended promoter region contributing to *PRSS3/TRY-4* downregulation in HCC (36). This study was the first to dissect epigenetic heterogeneity in the regulation of *PRSS3-SVs*, which may provide important implications for understanding epigenetic contributions to the genomic occupancy of transcription factors during transcription, in which many events may appear to be cospliced with distant events (58, 61–63).

Many transcript isoforms can exist per gene (9–11), most of which are thought not to be functionally relevant (65). Recently, comprehensive gain- and loss-of-function studies have shown the functional importance of *SVs* in tumor heterogeneity by linking genetic variants to individual phenotypes (58–60, 66, 67). *PRSS3* appears to be transcribed differentially to display heterogeneous functions in cancer, in which a dual role or contradictory effects reported might be due to MTG (PRSS3-V2) being functionally regarded as PRSS3 (13, 16, 22, 23, 29). We hereby deciphered *in vitro* and *in vivo* functional differences among the PRSS3 isoforms by using a constructed Huh7 cell model. Despite PRSS3-V2/MTG-mediated oncogenic effects in HCC in line with the promalignant activities of MTG shown in other cancer types (13, 16, 22, 23, 29), PRSS3-V1/TRY-4 or -V3 were found to be tumor suppressors in HCC cells, while ectopic

PRSS3-V4 showed an inhibitory effect on *PRSS3*^{ko} Huh7 cells. *PRSS3*^{ko} resulted in protumor effects in Huh7 cells, suggesting a tumor-suppressive role of PRSS3 in HCC that was attributed to the coexpression of PRSS3-V1 and PRSS3-V2, the two isoforms with opposite functionality. This is in line with our previous observations on *PRSS3/TRY-4* (36) and may explain some but not all cases of a similar phenotype with well-differentiated and/or low metastatic potential appearing in either *PRSS3*^{Low} (e.g., HepG2 and SK-Hep1 cells) or *PRSS3*^{High} (Huh7 cells) live cancer cell lines or a dual role of *PRSS3* contradictorily shown in carcinogenesis. To support this, corresponding clinicopathological analysis of HCC specimens compared to the normal tissue controls revealed that *PRSS3-V1* and *-V2* were main functional components of clinical relevance since *PRSS3-V1* and *-V2* were bipolarly present in either *PRSS3*^{Low} or *PRSS3*^{High} tissues; therefore, their abnormal coexpression could result in functional heterogeneity including insignificant or paradoxical clinical associations. However, a signature pattern of epigenetic regulation of *PRSS3* expression by site-specific CpG methylation was dynamically shown from m*PRSS3*^{Low} to um*PRSS3*^{High} through clinical progression, better matched to *PRSS3-V2*, suggesting PRSS3-V2 to be a more prevalent isoform functionally through clinical progression of HCC. Accordingly, significant epigenetic downregulation of *PRSS3-V2* was observed in early HCC with favorable patient outcomes. This finding supports an oncogenic role of PRSS3-V2/MTG predominantly in HCC, thus providing early diagnostic and prognostic value for HCC (16, 22, 23, 29). Thus, our study provides additional evidence supporting the hypothesis of functional hepato-heterogeneity attributed to genetic and epigenetic factors (1, 2, 4, 6).

Aberrant expression of *SVs* in cancer generates functional tumor heterogeneity resulting in cellular phenotype(s) or influencing cell fate determination (1, 4, 7, 8). In this regard, delineation of the heterogeneity of *PRSS3* expression and epigenetic regulation is critical for clarifying the molecular basis of *PRSS3* transcripts, thus facilitating functional interpretation of the paradoxical effects of *PRSS3* in cancer development. Functional classification and experimental dissection of *PRSS3-SVs* and their response to 5-aza-CR treatment distinct between *PRSS3*^{Low} and *PRSS3*^{High} HCC cells (such as Huh7 *versus* HepG2 cells) may be used as an experimental model for studying *PRSS3* splicing-mediated functional heterogeneity during hepatocarcinogenesis. In contrast to permanent genetic mutations, epigenetic disruptions frequently occur in early clinical stages and play an important role in modulating cell malignancy in a progressive and reversible manner. Therefore, delineation of the precise molecular mechanisms underlying epigenetic regulation of *PRSS3-SVs* could contribute to the molecular phenotypes of HCC.

This study on bioinformatic analysis of RNA sequencing data of *PRSS3-SVs* and their clinical relevance gave many insignificantly divergent results. For instance, *PRSS3*^{Low} was shown in 50 paired HCC tissues, consistent with our previous observation (36) and the analyses shown in the TCGA and UALCAN portals (38). However, its decrease was no longer statistically significant in more HCC tissue specimens due to different statistical methods or integration of the RNA-seq data with different median cutoff values for extensively divergent expression of *PRSS3-SVs* in HCC specimens. Therefore, conventional parameters, such as the median cutoff values, may need to be reevaluated for grouping a DEG with divergent expression levels. Moreover, functional heterogeneity could be caused by the microenvironment enhancing the coexpression diversity of *PRSS3-SVs*. As a result, further studies with larger sample sizes of paired HCC specimens are warranted to validate our observations. Moreover, due to the lack of commercial antibodies capable of discriminating well among PRSS3 isoforms, the functional pathways corresponding to PRSS3 isoforms could not be precisely distinguished from each other. This may yield inconsistent reports of *PRSS3* effects on

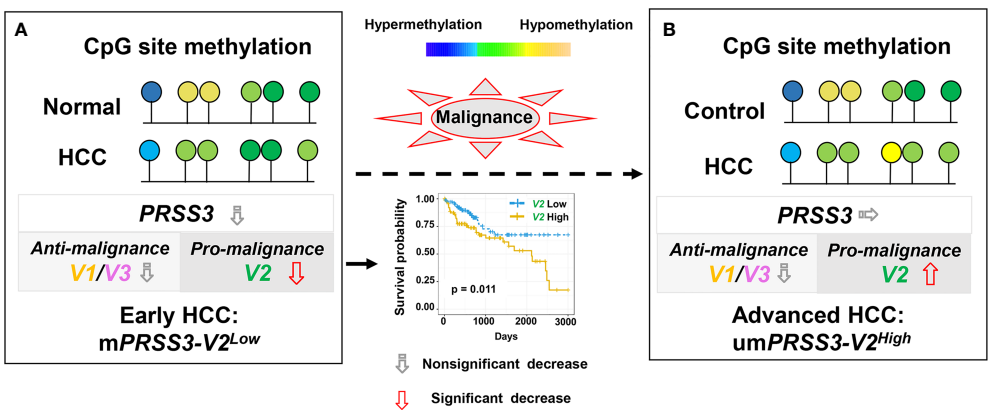

FIGURE 7 | A schematic model for epigenetic dysregulation of *PPRSS3* transcripts functionally contributing to hepatocarcinogenesis and its biomarker potential. **(A)** Epigenetic silencing of *PRSS3-SVs* by site-specific CpG methylation in the tumors of patients with early HCC, in which m*PRSS3*^{Low} was a potential biomarker favorable for patient survival. **(B)** Epigenetic disruption resulted in um*PRSS3*^{High} in tumors of advanced HCC patients.

carcinogenesis, resulting in inconclusive informatics analyses of the molecular mechanisms related to PRSS3 isoforms. Therefore, customized generation of more isoform-specific antibodies will be the subject of our future investigation to explore the molecular mechanisms underlying the dual role of *PRSS3* transcript isoforms in cancer development.

CONCLUSIONS

In summary, *PRSS3* was aberrantly expressed in HCC due to epigenetic dysregulation that was integrated with divergent expression of *PRSS3-SVs* by site-specific CpG methylation. The effects of oncogenic *PRSS3-V2* and tumor-suppressive *PRSS3-V1* in HCC cells may increase the molecular diversity and functional plasticity of hepatocarcinogenesis. Epigenetic dysregulation of *PRSS3-V2* distinct between $mPRSS3\text{-}V2^{Low}$ in early clinical stages and $umPRSS3^{High}$ in advanced tumors has potential diagnostic value for patients with early HCC (**Figure 7**).

DATA AVAILABILITY STATEMENT

The datasets presented in this study can be found in online repositories. The names of the repository/repositories and accession number(s) can be found in the article/**Supplementary Material**.

ETHICS STATEMENT

The animal handling protocols and all *in vivo* experimental procedures were approved by the Institutional Animal Ethics Committee of the Beijing Chest Hospital.

AUTHOR CONTRIBUTIONS

Conceptualization, SL, HX and JH; Formal analysis, SL, HX, MP, XG, XCZ, LZ, FJ, YH, WW, JR and JH; Funding acquisition, JW, MG and JH; Investigation, SL, HX, XMZ, MP, LZ, XG, YP and ZY; Methodology, SL, XMZ, HX, MP, XW, BL, RT, XCZ, ZY and JH; Resources, KC and WG; Supervision, MG and JH; writing-original draft, SL and JH; writing-review & editing, JW and JH. All authors have reviewed and agreed to the final version of the manuscript.

FUNDING

This study was funded by the Scientific Research Project of Beijing Educational Committee (Grant No. KM202110025004), the Intramural Research Funding Program from Beijing Tuberculosis and Thoracic Tumor Research Institute/Beijing Chest Hospital, National Key Research and Development Program of China (2018YFA0208902, 2020YFC2002705); Beijing Natural Science Foundation of China (7214242, 7171008), National Science Foundation of China (NSFC Grant No. 81872021, U1604281, 81672138); National Key Scientific Instrument Special Program of China (Grant No. 2011YQ03013405). KC, JH and JMW were also funded in part by Federal funds from the National Cancer Institute, National Institutes of Health, under Contract No. HHSN261200800001E and were supported in part by the Intramural Research Program of the NCI, CCR, LCIM, NIH.

ACKNOWLEDGMENTS

We thank all our laboratory members for technical help and helpful discussions.

SUPPLEMENTARY MATERIAL

The Supplementary Material for this article can be found online at: https://www.frontiersin.org/articles/10.3389/fonc.2022.831268/full#supplementary-material

REFERENCES

1. Cancer Genome Atlas Research Network. Comprehensive and Integrative Genomic Characterization of Hepatocellular Carcinoma. *Cell* (2017) 169 (7):1327–41.e1323. doi: 10.1016/j.cell.2017.05.046
2. Lin DC, Mayakonda A, Dinh HQ, Huang P, Lin L, Liu X, et al. Genomic and Epigenomic Heterogeneity of Hepatocellular Carcinoma. *Cancer Res* (2017) 77(9):2255–65. doi: 10.1158/0008-5472.Can-16-2822
3. Llovet JM, Montal R, Sia D, Finn RS. Molecular Therapies and Precision Medicine for Hepatocellular Carcinoma. *Nat Rev Clin Oncol* (2018) 15 (10):599–616. doi: 10.1038/s41571-018-0073-4
4. Dhanasekaran R. Deciphering Tumor Heterogeneity in Hepatocellular Carcinoma (HCC)-Multi-Omic and Singulomic Approaches. *Semin Liver Dis* (2021) 41(1):9–18. doi: 10.1055/s-0040-1722261
5. Sung H, Ferlay J, Siegel RL, Laversanne M, Soerjomataram I, Jemal A, et al. Global Cancer Statistics 2020: GLOBOCAN Estimates of Incidence and Mortality Worldwide for 36 Cancers in 185 Countries. *CA Cancer J Clin* (2021) 71(3):209–49. doi: 10.3322/caac.21660
6. Qiu Z, Li H, Zhang Z, Zhu Z, He S, Wang X, et al. A Pharmacogenomic Landscape in Human Liver Cancers. *Cancer Cell* (2019) 36(2):179–93.e111. doi: 10.1016/j.ccell.2019.07.001
7. Nam AS, Chaligne R, Landau DA. Integrating Genetic and non-Genetic Determinants of Cancer Evolution by Single-Cell Multi-Omics. *Nat Rev Genet* (2021) 22(1):3–18. doi: 10.1038/s41576-020-0265-5
8. Chan LK, Tsui YM, Ho DW, Ng IO. Cellular Heterogeneity and Plasticity in Liver Cancer. *Semin Cancer Biol* (2021) S1044-579X(21):00050-X. doi: 10.1016/j.semcancer.2021.02.015
9. Dvinge H, Guenthoer J, Porter PL, Bradley RK. RNA Components of the Spliceosome Regulate Tissue- and Cancer-Specific Alternative Splicing. *Genome Res* (2019) 29(10):1591–604. doi: 10.1101/gr.246678.118
10. Bonnal SC, López-Oreja I, Valcárcel J. Roles and Mechanisms of Alternative Splicing in Cancer - Implications for Care. *Nat Rev Clin Oncol* (2020) 17 (8):457–74. doi: 10.1038/s41571-020-0350-x
11. Sonneveld S, Verhagen BMP, Tanenbaum ME. Heterogeneity in mRNA Translation. *Trends Cell Biol* (2020) 30(8):606–18. doi: 10.1016/j.tcb.2020.04.008

12. Zhang J, Zhang YZ, Jiang J, Duan CG. The Crosstalk Between Epigenetic Mechanisms and Alternative RNA Processing Regulation. *Front Genet* (2020) 11:998. doi: 10.3389/fgene.2020.00998
13. Lópezotín C, Matrisian LM. Emerging Roles of Proteases in Tumour Suppression. *Nat Rev Cancer* (2007) 7(10):800–8. doi: 10.1038/nrc2228
14. Rinderknecht H, Renner IG, Abramson SB, Carmack C. Mesotrypsin: A New Inhibitor-Resistant Protease From a Zymogen in Human Pancreatic Tissue and Fluid. *Gastroenterology* (1984) 86(4):681–92. doi: 10.1016/S0016-5085(84)80117-1
15. Nyaruhucha CN, Kito M, Fukuoka SI. Identification and Expression of the cDNA-Encoding Human Mesotrypsin(Ogen), an Isoform of Trypsin With Inhibitor Resistance. *J Biol Chem* (1997) 272(16):10573–8. doi: 10.1074/jbc.272.16.10573
16. Salameh MA, Radisky ES. Biochemical and Structural Insights Into Mesotrypsin: An Unusual Human Trypsin. *Int J Biochem Mol Biol* (2013) 4(3):129–39.
17. Wiegand U, Corbach S, Minn A, Kang J, Müller-Hill B. Cloning of the cDNA Encoding Human Brain Trypsinogen and Characterization of its Product. *Gene* (1993) 136(1-2):167–75. doi: 10.1016/0378-1119(93)90460-k
18. Tóth J, Siklódi E, Medveczky P, Gallatz K, Németh P, Szilágyi L, et al. Regional Distribution of Human Trypsinogen 4 in Human Brain at mRNA and Protein Level. *Neurochem Res* (2007) 32(9):1423–33. doi: 10.1007/s11064-007-9327-8
19. Cottrell GS, Amadesi S, Grady EF, Bunnett NW. Trypsin IV, a Novel Agonist of Protease-Activated Receptors 2 and 4. *J Biol Chem* (2004) 279(14):13532–9. doi: 10.1074/jbc.M312090200
20. Nakanishi J, Yamamoto M, Koyama J, Sato J, Hibino T. Keratinocytes Synthesize Enteropeptidase and Multiple Forms of Trypsinogen During Terminal Differentiation. *J Invest Dermatol* (2010) 130(4):944. doi: 10.1038/jid.2009.364
21. Terada T, Ohta T, Minato H, Nakanuma Y. Expression of Pancreatic Trypsinogen/Trypsin and Cathepsin B in Human Cholangiocarcinomas and Hepatocellular Carcinomas. *Hum Pathol* (1995) 26(7):746–52. doi: 10.1016/0046-8177(95)90222-8
22. Jiang G, Cao F, Ren G, Gao D, Bhakta V, Zhang Y, et al. PRSS3 Promotes Tumour Growth and Metastasis of Human Pancreatic Cancer. *Gut* (2010) 59(11):1535–44. doi: 10.1136/gut.2009.200105
23. Hockla A, Miller E, Salameh MA, Copland JA, Radisky DC, Radisky ES. PRSS3/mesotrypsin Is a Therapeutic Target for Metastatic Prostate Cancer. *Mol Cancer Res* (2012) 10(12):1555–66. doi: 10.1158/1541-7786.Mcr-12-0314
24. Han S, Lee CW, Trevino JG, Hughes SJ, Sarosi GA Jr. Autocrine Extra-Pancreatic Trypsin 3 Secretion Promotes Cell Proliferation and Survival in Esophageal Adenocarcinoma. *PloS One* (2013) 8(10):e76667. doi: 10.1371/journal.pone.0076667
25. Radisky ES. PRSS3/mesotrypsin in Prostate Cancer Progression: Implications for Translational Medicine. *Asian J Androl* (2013) 15(4):439–40. doi: 10.1038/aja.2013.14
26. Ghilardi C, Silini A, Figini S, Anastasia A, Lupi M, Fruscio R, et al. Trypsinogen 4 Boosts Tumor Endothelial Cells Migration Through Proteolysis of Tissue Factor Pathway Inhibitor-2. *Oncotarget* (2015) 6(29):28389–400. doi: 10.18632/oncotarget.4949
27. Ma R, Ye X, Cheng H, Ma Y, Cui H, Chang X. PRSS3 Expression is Associated With Tumor Progression and Poor Prognosis in Epithelial Ovarian Cancer. *Gynecol Oncol* (2015) 137(3):546–52. doi: 10.1016/j.ygyno.2015.02.022
28. Qian L, Gao X, Huang H, Lu S, Cai Y, Hua Y, et al. PRSS3 is a Prognostic Marker in Invasive Ductal Carcinoma of the Breast. *Oncotarget* (2017) 8(13):21444–53. doi: 10.18632/oncotarget.15590
29. Ma H, Hockla A, Mehner C, Coban M, Papo N, Radisky DC, et al. PRSS3/Mesotrypsin and Kallikrein-Related Peptidase 5 are Associated With Poor Prognosis and Contribute to Tumor Cell Invasion and Growth in Lung Adenocarcinoma. *Sci Rep* (2019) 9(1):1844. doi: 10.1038/s41598-018-38362-0
30. Aboulouard S, Wisztorski M, Duhamel M, Saudemont P, Cardon T, Narducci F, et al. In-Depth Proteomics Analysis of Sentinel Lymph Nodes From Individuals With Endometrial Cancer. *Cell Rep Med* (2021) 2(6):100318. doi: 10.1016/j.xcrm.2021.100318
31. Schaid DJ, McDonnell SK, FitzGerald LM, DeRycke L, Fogarty Z, Giles GG, et al. Two-Stage Study of Familial Prostate Cancer by Whole-Exome Sequencing and Custom Capture Identifies 10 Novel Genes Associated With the Risk of Prostate Cancer. *Eur Urol* (2021) 79(3):353–61. doi: 10.1016/j.eururo.2020.07.038
32. Keishi Y, Koshi M, Hiroshi I, Masaki M, David S. A Tumor-Suppressive Role for Trypsin in Human Cancer Progression. *Cancer Res* (2003) 63(20):6575–8.
33. Marsit CJ, Karagas MR, Schned A, Kelsey KT. Carcinogen Exposure and Epigenetic Silencing in Bladder Cancer. *Ann N Y Acad Sci* (2006) 1076:810–21. doi: 10.1196/annals.1371.031
34. Marsit CJ, Houseman EA, Schned AR, Karagas MR, Kelsey KT. Promoter Hypermethylation is Associated With Current Smoking, Age, Gender and Survival in Bladder Cancer. *Carcinogenesis* (2007) 28(8):1745–51. doi: 10.1093/carcin/bgm116
35. Marsit CJ, Chinedu O, Hadi D, Kelsey KT. Epigenetic Silencing of the PRSS3 Putative Tumor Suppressor Gene in non-Small Cell Lung Cancer. *Mol Carcinog* (2010) 44(2):146–50. doi: 10.1002/mc.20125
36. Lin B, Zhou X, Lin S, Wang X, Zhang M, Cao B, et al. Epigenetic Silencing of PRSS3 Provides Growth and Metastasis Advantage for Human Hepatocellular Carcinoma. *J Mol Med (Berl)* (2017) 95(11):1237–49. doi: 10.1007/s00109-017-1578-5
37. Tang Z, Li C, Kang B, Gao G, Li C, Zhang Z. GEPIA: A Web Server for Cancer and Normal Gene Expression Profiling and Interactive Analyses. *Nucleic Acids Res* (2017) 45(W1):W98–w102. doi: 10.1093/nar/gkx247
38. Uhlen M, Zhang C, Lee S, Sjöstedt E, Fagerberg L, Bidkhori G, et al. A Pathology Atlas of the Human Cancer Transcriptome. *Science* (2017) 357(6352):eaan2507. doi: 10.1126/science.aan2507
39. Ghandi M, Huang FW, Jané-Valbuena J, Kryukov GV, Lo CC, McDonald ER, et al. Next-Generation Characterization of the Cancer Cell Line Encyclopedia. *Nature* (2019) 569(7757):503–8. doi: 10.1038/s41586-019-1186-3
40. Ben-David U, Siranosian B, Ha G, Tang H, Oren Y, Hinohara K, et al. Genetic and Transcriptional Evolution Alters Cancer Cell Line Drug Response. *Nature* (2018) 560(7718):325–30. doi: 10.1038/s41586-018-0409-3
41. Deng M, Brägelmann J, Kryukov I, Saraiva-Agostinho N, Perner S. FirebrowseR: An R Client to the Broad Institute's Firehose Pipeline. *Database (Oxf)* (2017) 2017:baw160. doi: 10.1093/database/baw160
42. Chen F, Chandrashekar DS, Varambally S, Creighton CJ. Pan-Cancer Molecular Subtypes Revealed by Mass-Spectrometry-Based Proteomic Characterization of More Than 500 Human Cancers. *Nat Commun* (2019) 10(1):5679. doi: 10.1038/s41467-019-13528-0
43. Lin S, Wang X, Pan Y, Tian R, Lin B, Jiang G, et al. Transcription Factor Myeloid Zinc-Finger 1 Suppresses Human Gastric Carcinogenesis by Interacting With Metallothionein 2a. *Clin Cancer Res* (2019) 25(3):1050–62. doi: 10.1158/1078-0432.Ccr-18-1281
44. Løvf M, Nome T, Bruun J, Eknaes M, Bakken AC, Mpindi JP, et al. A Novel Transcript, VNN1-AB, as a Biomarker for Colorectal Cancer. *Int J Cancer* (2014) 135(9):2077–84. doi: 10.1002/ijc.28855
45. Schmit K, Michiels C. TMEM Proteins in Cancer: A Review. *Front Pharmacol* (2018) 9:1345. doi: 10.3389/fphar.2018.01345
46. Zhang S, Li J, Wang X. NKD1 Correlates With a Poor Prognosis and Inhibits Cell Proliferation by Inducing P53 Expression in Hepatocellular Carcinoma. *Tumour Biol* (2016) 37(10):14059–67. doi: 10.1007/s13277-016-5173-0
47. Lin YY, Yu MW, Lin SM, Lee SD, Chen CL, Chen DS, et al. Genome-Wide Association Analysis Identifies a GLUL Haplotype for Familial Hepatitis B Virus-Related Hepatocellular Carcinoma. *Cancer* (2017) 123(20):3966–76. doi: 10.1002/cncr.30851
48. Wang C, Mou L, Chai HX, Wang F, Yin YZ, Zhang XY. Long non-Coding RNA HNF1A-AS1 Promotes Hepatocellular Carcinoma Cell Proliferation by Repressing NKD1 and P21 Expression. *BioMed Pharmacother* (2017) 89:926–32. doi: 10.1016/j.biopha.2017.01.031
49. Schmidt A, Armento A, Bussolati O, Chiu M, Ellerkamp V, Scharpf MO, et al. Hepatoblastoma: Glutamine Depletion Hinders Cell Viability in the Embryonal Subtype But High GLUL Expression is Associated With Better Overall Survival. *J Cancer Res Clin Oncol* (2021) 147(11):3169–81. doi: 10.1007/s00432-021-03713-4
50. Li Y, McGrail DJ, Xu J, Mills GB, Sahni N, Yi S. Gene Regulatory Network Perturbation by Genetic and Epigenetic Variation. *Trends Biochem Sci* (2018) 43(8):576–92. doi: 10.1016/j.tibs.2018.05.002
51. Belluti S, Rigillo G, Imbriano C. Transcription Factors in Cancer: When Alternative Splicing Determines Opposite Cell Fates. *Cells* (2020) 9(3):760. doi: 10.3390/cells9030760
52. Cohen I, Coban M, Shahar A, Sankaran B, Hockla A, Lacham S, et al. Disulfide Engineering of Human Kunitz-Type Serine Protease Inhibitors Enhances

Proteolytic Stability and Target Affinity Toward Mesotrypsin. *J Biol Chem* (2019) 294(13):5105–20. doi: 10.1074/jbc.RA118.007292
53. Tani T, Kawashima I, Mita K, Takiguchi Y. Nucleotide Sequence of the Human Pancreatic Trypsinogen III cDNA. *Nucleic Acids Res* (1990) 18 (6):1631. doi: 10.1093/nar/18.6.1631
54. Ramesh V, Ganesan K. Integrative Functional Genomic Analysis Unveils the Differing Dysregulated Metabolic Processes Across Hepatocellular Carcinoma Stages. *Gene* (2016) 588(1):19–29. doi: 10.1016/j.gene.2016.04.039
55. Urbanski LM, Leclair N, Anczuków O. Alternative-Splicing Defects in Cancer: Splicing Regulators and Their Downstream Targets, Guiding the Way to Novel Cancer Therapeutics. *Wiley Interdiscip Rev RNA* (2018) 9(4):e1476. doi: 10.1002/wrna.1476
56. Duchmann M, Itzykson R. Clinical Update on Hypomethylating Agents. *Int J Hematol* (2019) 110(2):161–9. doi: 10.1007/s12185-019-02651-9
57. Rowen L, Williams E, Glusman G, Linardopoulou E, Friedman C, Ahearn ME, et al. Interchromosomal Segmental Duplications Explain the Unusual Structure of PRSS3, the Gene for an Inhibitor-Resistant Trypsinogen. *Mol Biol Evol* (2005) 22(8):1712–20. doi: 10.1093/molbev/msi166
58. Sharma A, Merritt E, Hu X, Cruz A, Jiang C, Sarkodie H, et al. Non-Genetic Intra-Tumor Heterogeneity Is a Major Predictor of Phenotypic Heterogeneity and Ongoing Evolutionary Dynamics in Lung Tumors. *Cell Rep* (2019) 29 (8):2164–74.e2165. doi: 10.1016/j.celrep.2019.10.045
59. Calviello L, Hirsekorn A, Ohler U. Quantification of Translation Uncovers the Functions of the Alternative Transcriptome. *Nat Struct Mol Biol* (2020) 27 (8):717–25. doi: 10.1038/s41594-020-0450-4
60. Gopi LK, Kidder BL. Integrative Pan Cancer Analysis Reveals Epigenomic Variation in Cancer Type and Cell Specific Chromatin Domains. *Nat Commun* (2021) 12(1):1419. doi: 10.1038/s41467-021-21707-1
61. Yang X, Han H, De Carvalho DD, Lay FD, Jones PA, Liang G. Gene Body Methylation can Alter Gene Expression and is a Therapeutic Target in Cancer. *Cancer Cell* (2014) 26(4):577–90. doi: 10.1016/j.ccr.2014.07.028
62. Demircioğlu D, Cukuroglu E, Kindermans M, Nandi T, Calabrese C, Fonseca NA, et al. A Pan-Cancer Transcriptome Analysis Reveals Pervasive Regulation Through Alternative Promoters. *Cell* (2019) 178(6):1465–77.e1417. doi: 10.1016/j.cell.2019.08.018
63. Gomez L, Odom GJ, Young JI, Martin ER, Liu L, Chen X, et al. Comethdmr: Accurate Identification of Co-Methylated and Differentially Methylated Regions in Epigenome-Wide Association Studies With Continuous Phenotypes. *Nucleic Acids Res* (2019) 47(17):e98. doi: 10.1093/nar/gkz590
64. Schoenfelder S, Fraser P. Long-Range Enhancer-Promoter Contacts in Gene Expression Control. *Nat Rev Genet* (2019) 20(8):437–55. doi: 10.1038/s41576-019-0128-0
65. Gallego-Paez LM, Bordone MC, Leote AC, Saraiva-Agostinho N, Ascensão-Ferreira M, Barbosa-Morais NL. Alternative Splicing: The Pledge, the Turn, and the Prestige : The Key Role of Alternative Splicing in Human Biological Systems. *Hum Genet* (2017) 136(9):1015–42. doi: 10.1007/s00439-017-1790-y
66. eGTEx Project. Enhancing GTEx by Bridging the Gaps Between Genotype, Gene Expression, and Disease. *Nat Genet* (2017) 49(12):1664–70. doi: 10.1038/ng.3969
67. Louadi Z, Yuan K, Gress A, Tsoy O, Kalinina OV, Baumbach J, et al. DIGGER: Exploring the Functional Role of Alternative Splicing in Protein Interactions. *Nucleic Acids Res* (2021) 49(D1):D309–d318. doi: 10.1093/nar/gkaa768

Conflict of Interest: Author WG is employed by Basic Research Program, Leidos Biomedical Research, Inc.

The remaining authors declare that the research was conducted in the absence of any commercial or financial relationships that could be construed as a potential conflict of interest.

Publisher's Note: All claims expressed in this article are solely those of the authors and do not necessarily represent those of their affiliated organizations, or those of the publisher, the editors and the reviewers. Any product that may be evaluated in this article, or claim that may be made by its manufacturer, is not guaranteed or endorsed by the publisher.

frontiers | Frontiers in Oncology

ORIGINAL RESEARCH
published: 14 April 2022
doi: 10.3389/fonc.2022.862592

Chk1 Inhibition Hinders the Restoration of H3.1K56 and H3.3K56 Acetylation and Reprograms Gene Transcription After DNA Damage Repair

Nan Ding[1,2,3,4]*, *Zhiang Shao*[1,2], *Fangyun Yuan*[5], *Pei Qu*[1,2], *Ping Li*[1,2,3,4], *Dong Lu*[1,2], *Jufang Wang*[1,2]* and *Qianzheng Zhu*[3,4]*

[1] Key Laboratory of Space Radiobiology of Gansu Province and Key Laboratory of Heavy Ion Radiation Biology and Medicine of Chinese Academy of Sciences, Institute of Modern Physics, Chinese Academy of Sciences, Lanzhou, China, [2] College of Life Science, University of Chinese Academy of Sciences, Beijing, China, [3] Department of Radiology and Department of Molecular and Cellular Biochemistry, The Ohio State University, Columbus, OH, United States, [4] James Cancer Hospital and Solove Research Institute, The Ohio State University, Columbus, OH, United States, [5] Department of Oncology, The First Hospital of Lanzhou University, Lanzhou, China

OPEN ACCESS

Edited by:
Hailong Pei,
Soochow University, China

Reviewed by:
Meijuan Zhou,
Southern Medical University, China
Xiaobo Nie,
Henan University, China

***Correspondence:**
Nan Ding
dn@impcas.ac.cn
Jufang Wang
jufangwang@impcas.ac.cn
Qianzheng Zhu
zhu.49@osu.edu

Specialty section:
This article was submitted to Molecular and Cellular Oncology, a section of the journal Frontiers in Oncology

Received: 26 January 2022
Accepted: 15 March 2022
Published: 14 April 2022

Citation:
Ding N, Shao Z, Yuan F, Qu P, Li P, Lu D, Wang J and Zhu Q (2022) Chk1 Inhibition Hinders the Restoration of H3.1K56 and H3.3K56 Acetylation and Reprograms Gene Transcription After DNA Damage Repair. Front. Oncol. 12:862592. doi: 10.3389/fonc.2022.862592

H3K56 acetylation (H3K56Ac) was reported to play a critical role in chromatin assembly; thus, H3K56ac participates in the regulation of DNA replication, cell cycle progression, DNA repair, and transcriptional activation. To investigate the influence of DNA damage regulators on the acetylation of histone H3 and gene transcription, U2OS cells expressing SNAP-labeled H3.1 or SNAP-labeled H3.3 were treated with ATM, ATR, or a Chk1 inhibitor after ultraviolet (UV) radiation. The levels of H3.1K56ac, H3.3K56ac, and other H3 site-specific acetylation were checked at different time points until 24 h after UV radiation. The difference in gene transcription levels was also examined by mRNA sequencing. The results identified Chk1 as an important regulator of histone H3K56 acetylation in the restoration of both H3.1K56ac and H3.3K56ac. Moreover, compromising Chk1 activity *via* chemical inhibitors suppresses gene transcription after UV radiation. The study suggests a previously unknown role of Chk1 in regulating H3K56 and some other site-specific H3 acetylation and in reprograming gene transcription during DNA damage repair.

Keywords: posttranslational modification (PMT), H3K56 acetylation, radiation, Chk1, chromatin assembly

INTRODUCTION

The maintenance of genomic integrity and stability is crucial for the growth, development, homeostasis, and survival of all organisms. However, genomic instability is continually induced by various exogenous and endogenous factors such as radiation, ecotoxic chemicals, and DNA replication. DNA repair pathways and the subsequent associated processes have evolved universally in all eukaryotic organisms to limit genomic instability (1). In general, the cellular DNA damage response (DDR) originates from DNA lesion recognition, followed by the initiation of a complex cellular signaling cascade to promote DNA repair, and these cascades include cell cycle arrest, which

is aided by checkpoint activation. The DDR regulation is mainly organized by the following kinases in the phosphoinositide-3-kinase (PI3K)-related family of protein kinases (PIKKs): ataxia-telangiectasia mutated (ATM), ATM and RAD3-related (ATR), and DNA-dependent protein kinase, catalytic subunit (DNA-PKcs) (2). ATR-Chk1 and ATM-Chk2 are the two main signaling axes of the DDR network in mammals (3). For instance, the S317 and S345 residues of Chk1 are phosphorylated by the upstream kinase ATR when DNA damage is caused by radiation, replication stress or ecotoxic chemicals (4). Then, activated Chk1 will phosphorylate a variety of downstream substrates to modulate various cellular processes and the DNA damage response (DDR) (5).

In the DDR, posttranslational modifications (PTMs) of histones, such as acetylation, methylation, SUMOylation, and phosphorylation, play unique roles in controlling chromatin structure and gene activity (6, 7). Among these PTMs, the lysine acetylation of histones alters the accessibility of chromatin and offers a protein interaction platform during transcription, replication, and DNA repair (8, 9). Specifically, the acetylation of histone H3 at lysine 56 (H3K56ac) plays a critical role in regulating chromatin assembly during DNA synthesis and transcriptional activation, as this residue is located in the core of histone H3 at the nucleosome dyad (10, 11).

H3K56ac is a transient chromatin signal that turns over during transcription and DNA damage repair. In an unperturbed cell cycle, H3K56 of newly synthesized histones becomes acetylated during S-phase and disappears as cells progress through the G2 phase of the cell cycle (12). During the DDR, nucleosome destabilization and reassembly occur in response to genotoxic stress-induced DSBs (13). Because H3K56ac signals for the recovery of chromatin structure over repaired DNA, the presence of H3K56ac during DDR is a critical indicator that the DNA damage checkpoint is turning off, which allows cell cycle re-entry after DNA repair (9, 12). Tjeertes' research and our previous study identified that H3K56ac and H3K9ac are rapidly diminished and subsequently restored in U2OS cells and HeLa cells after ionizing radiation (IR) and ultraviolet radiation (UVR) (14–16). Furthermore, cells lacking H3K56ac may be sensitive to genotoxic agent due to defects in chromatin assembly (17). However, the cellular regulation of H3K56 acetylation in relation to DDR activation and termination is not fully understood.

In mammals, the key histone H3–H4 chaperone anti-silencing factor 1 (Asf1) is essential for the acetylation of H3K56. Asf1 functions in both DNA replication-dependent and replication-independent nucleosome assembly (18). In higher eukaryotes, the protein kinases in the Tousled-like family (TLKs) are the upstream regulators of Asf1 homolog (19). TLK signaling promotes cellular histone supply in S phase by targeting histone-free Asf1 and stimulating its ability to shuttle histones to sites of chromatin assembly (20, 21). Importantly, TLKs are rapidly inactivated in response to genotoxic stress through phosphorylation by the checkpoint kinase Chk1 (22, 23). However, the regulatory effect of Chk1 on the acetylation of H3K56 during the DDR remains unclear.

Mammalian histone H3 has several variants, namely, H3.1, H3.2, H3.3, H3t/H3.4, H3.5, H3.6, H3.8, H3.Y, H3.X, and CENP-A. The replicative variant H3.1 and the replacement variant H3.3 are arguably some of the better-studied histone variants (24, 25). The accumulation of both new H3.1 and H3.3 variants at UV-damaged DNA regions was detected in U2OS cells (26). However, the H3K56 acetylation status, levels, and functionality of individual histone variants H3.1 and H3.3 remain to be explored. Whether and how DDR regulators may be linked with the recovery of H3.1K56ac and H3.3K56ac to DDR termination and aftermath transcription recovery and cell cycle progression are critical and open questions.

In this study, we investigated the possible influence of the DDR regulators ATM, ATR and Chk1 on the acetylation of H3K56, H3K27, H3K14, and H3K9 after UVR. Our data revealed a previously unknown regulatory effect of Chk1 on H3K56 acetylation in response to UVR-induced DNA damage. Using chemical inhibition and mRNA sequencing as tools, we further explored transcriptional reprogramming during UVR-induced DDR and revealed a regulatory role of Chk1 in cellular transcription linked to H3K56 acetylation.

MATERIALS AND METHODS

Cell Lines, Chemicals, and Antibodies

The stable U2OS cell lines expressing H3.1-SNAP or H3.3-SNAP were generated and previously described by Dunleavy et al. (27). Of note, SNAP tag is a 20 kilo-Dalton (kDa) mutant of the DNA repair protein O6-alkylguanine-DNA alkyltransferase, and the SNAP-tagged histone variants enable visualization and detection of histones and their modifications in cooperation in chromatin, for example, the H3.3 and H3K4Me2 at centromere.

Human U2OS cells (ATCC) were cultured in Dulbecco's modified Eagle medium (DMEM) (Thermo Fisher Scientific, Waltham, MA 02451, USA) supplemented with 10% fetal bovine serum (FBS) (Thermo Fisher Scientific) and 1% penicillin and streptomycin at 37°C in a humidified atmosphere of 5% CO_2. The H3.1- and H3.3-SNAP U2OS cell lines were also cultured in DMEM under the same conditions. For the serum starvation experiment, cells were seeded and grown to 70% confluence and then the medium was changed to serum-free DMEM medium for 24 h.

The ATM inhibitor KU55933, the Chk1 inhibitor UCN-01, and the Chk1&Chk2 inhibitor AZD7762 were obtained from Sigma-Aldrich (St. Louis, MO 63103, USA), while the ATR inhibitor VE-821, the Chk1 inhibitor MK8776, and the ATM & ATR inhibitor AZD6738 were obtained from Cayman Chemical company (Ann Arbor, Michigan 48108, USA). The Chk1 inhibitor Ly2606368 was obtained from Selleck Chemicals (Houston, TX 77014, USA).

The anti-H3K56ac, anti-H3K27ac, and anti-H3K9ac antibodies were purchased from GeneTex (Irvine, CA 92606, USA). Anti-H3K14ac antibodies from Millipore (Billerica, MA 01821, USA), whereas anti-Chk1 antibodies, anti-pChk2 antibodies, anti-TLK1 antibodies, anti-Asf1a, and anti-Asf1b

antibodies were purchased from Cell Signaling (Danvers, MA 01923, USA). Antibodies against β-actin and GAPDH were purchased from Santa Cruz Biotechnology (Dallas, TX 75220, USA). The anti-SNAP antibody was obtained from New England Biolabs (Ipswich, MA 01938, USA).

Cellular Protein Fractionation, Immunoprecipitation, and Western Blotting Analysis

The cellular protein fractionation experiments were conducted as described by Anindya et al. (28), with modifications. Briefly, cells (~10^7) were lysed with 1 ml (~5× cell volume) of cytoplasmic lysis buffer (10 mM Tris-HCl [pH 7.9], 0.34 M sucrose 3 mM $CaCl_2$, 2 mM magnesium acetate, 0.1 mM EDTA, 1 mM DDT, 0.5% NP-40, and a protease inhibitor cocktail). Nuclei were pelleted by centrifugation at 3,500 *g* for 15 min and washed with cytoplasmic lysis buffer without NP-40 and then lysed in 1 ml of nuclear lysis buffer (20 mM HEPES [pH 7.9], 3 mM EDTA, 10% glycerol, 1.5 mM $MgCl_2$, 150 mM KOAc, and protease inhibitors). The nucleoplasmic fractions were separated by centrifugation at 15,000 *g* for 30 min and the pellets were designated as chromatin fraction. For further processing, the chromatin fraction pellets were resuspended in 0.2 ml of nuclease incubation buffer (150 mM HEPES [pH 7.9], 1.5 mM $MgCl_2$, 150 mM KOAc, and protease inhibitors) and incubated with 50 U Benzonase (25 U/μl) for 30 min at room temperature. The soluble chromatin fraction was collected by centrifugation at 20,000 *g* for 30 min, while the insoluble chromatin fraction was dissolved by boiling in SDS sample buffer. Soluble chromatin fractions may be kept frozen in storage buffer (10 mM Tris-HCl, 300 mM NaCl, 1 mM DTT, 0.1 mM EDTA, and 50% glycerol) at −20°C short term/or −80°C.

The immunoprecipitation was done at 4°C overnight in RIPA buffer (50 mM Tris-HCl [pH 8.0], 150 mM NaCl, 1% NP40, 0.5% deoxycholate, and protease inhibitors) using nuclease-releasable chromatin containing ~200–500 μg protein, with proper amount of desired antibody and Protein A plus G beads. After 4°C incubation, the beads were washed 1 time with RIPA buffer and then 3 times with TBS buffer (50 mM Tris-HCl [pH 7.4] and 150 mM NaCl), and the bound proteins were eluted by boiling in SDS loading buffer.

The Western blotting analysis was done using SDS-PAGE, followed immuno-detection. To analyze histone, tagged histone variants, and their acetylation levels, the immunoprecipitation samples or chromatin fraction samples containing ~10–30 μg protein in SDS sample buffer were separated by 14% acrylamide gel, Western transferred to PVDF membrane, and immuno-detected with anti-SNAP, or acetylation site-specific histone antibodies and chemiluminescence.

mRNA Sequencing

The RNA samples were extracted using a TRIzol reagent (Invitrogen, Thermo Fisher Scientific) from ~5 × 10^6 cells according to the manufacturer's instructions. The concentration of RNA was measured using a Qubit® RNA Assay Kit and a Qubit® 2.0 Fluorometer (Life Technologies, Thermo Fisher Scientific). The RNA integrity was assessed by the RNA Nano 6000 Assay Kit of the Bioanalyzer 2100 system (Agilent Technologies Santa Clara, CA 95051, USA).

Sequencing libraries were constructed using the NEB Next®Ultra®Directional RNA Library Prep Kit for Illumina® (NEB) according to the manufacturer's instructions by Biomarker Technologies Co. (Beijing, China). Briefly, mRNA was denatured by heating to 94°C for 15 min in 5× NEB Next First Strand Synthesis Reaction Buffer. Random primers, reverse transcriptase, and murine RNase inhibitor were then added, and first-strand cDNA was synthesized at 42°C for 30 min. Then, second-strand cDNA was synthesized using a synthesis enzyme mix for 60 min at 16°C and then for 30 min at 20°C. The resulting dsDNA fragments were purified using Agencourt AMPure XP Beads (Beckman Coulter, Beverly, CA, USA). The overhangs were digested to blunt ends with NEB Next End Prep Enzyme Mix and then adaptors linked to the USER Enzyme were ligated to the cDNA. The cDNA was then purified using AMPure XP Beads. Finally, the DNA fragments were amplified using Hot Start HiFi PCR Master Mix, and the products were re-purified using the AMPure XP system and library quality was analyzed using an Agilent Bioanalyzer 2100 and qRT-PCR. TruSeq PE Cluster Kitv3-cBot-HS was adopted to construct clusters of index-coded samples on an acBot Cluster Generation System (Illumina Inc., San Diego, CA, USA). The RNA library was then sequenced on an Illumina Hiseq platform and paired-end reads were generated.

The resultant raw reads were further cleaned by eliminating adapter sequences, low-quality reads, and poly-N sequences. The GC content and sequence duplication levels of the clean data were then calculated to confirm the quality of the data. For further analysis, Clean Reads of each sample were compared with reference annotation (ftp://ftp.ensembl.org/pub/release-95/fasta/homo_sapiens/dna/). Cufflinks package was used to calculate expression of genes depending on fragments per kilobase of exon per million reads (FPKM) values. DESeq R package (version 1.18.0) was used for statistical analysis of differential gene expression between samples. The *p*-values were set to <0.05 based on Benjamini and Hochberg's method to reduce the false discovery rate. Genes with a log2 fold expression variation value > 1.5 were considered to be differentially expressed.

Reverse Transcription and Quantitative Real-Time PCR

Reverse transcription was conducted with All-in-One™ First-Strand cDNA Synthesis kit (AORT-0060, GeneCopoeia, Shenzhen, China). To quantify the mRNA expression of HOXB6, DTX3L, SSTR2, MYC, and HOXC10, real-time PCR was performed on CFX96 Touch™ Real-Time PCR Detection System (Bio-Rad, Hercules, CA 94547, USA) using All-inOne™ mRNA Detection kit (AOPR-0200, GeneCopoeia) based on SYBR-Green. PCR primers for GAPDH (HQP006940), HOXB6 (HQP008992), DTX3L (HQP003638), SSTR2 (HQP017744), MYC (HQP117877), and HOXC10 (HQP009003) were all purchased from GeneCopoeia. In each qRT-PCR, GAPDH mRNAs were used as internal reference for normalization,

respectively. The relative expression was calculated using the $2^{-\Delta\Delta Ct}$ method.

Quantitative Analysis and Statistics

Quantitative analysis was done on digitalized Western blotting images by ImageJ software and the relative protein amounts were calculated based on gray density. The Student's *t*-test was performed using Sigma Plot.

RESULTS

UV Radiation Transient Suppresses H3.1K56ac and H3.3K56ac Levels and Their Restoration Following DNA Damage Repair

We previously demonstrated that the nucleotide excision repair factor $CRL4^{DDB2}$ ubiquitin ligase preferentially regulates post-repair chromatin restoration of H3K56Ac (16). To distinguish between acetylated H3.1 and H3.3, two variants of histone H3 in such a post-repair chromatin restoration of H3K56Ac, we took advantage of the system, in which SNAP-tagged H3.1 and H3.3 were expressed in U2OS cells. This system was used to visualize H3.1 and H3.3 at UV damage repair sites (26). In such a study, the accumulation of new H3.1 at UV damage repair sites was demonstrated to be dependent on the H3.1 histone chaperone CAF1, while the accumulation of new H3.3 was dependent on H3.3 histone chaperone HIRA. In our study, H3.1-SNAP-tagged and H3.3-SNAP-tagged U2OS cells were cultured and verified by anti-SNAP and anti-H3K27ac antibodies. As shown in **Figure 1A**, the acetylated H3K27 band at approximately 14 kDa was detected in all three kinds of cells. SNAP-tagged H3.1 and H3.3 were detected as ~37-kDa bands only in H3.1- and H3.3-SNAP-tagged U2OS cells but not in SNAP-free U2OS cells. As expected, a similar pattern was found for SNAP-tagged H3K27ac. As for the difference in expression levels in SNAP-tagged H3.1 and H3.3, the band of SNAP-tagged H3.3 was more intense than that of SNAP-tagged H3.1. Similarly, the band of SNAP-tagged H3.3K27ac was also heavier than SNAP-tagged H3.1K27ac. Furthermore, the bands of histone H3 were also much heavier than the band of SNAP-tagged histone H3, presumably due to the low expression levels of SNAP-tagged H3.1 and H3.3 in U2OS cells.

After 20 J/m^2 UV radiation, the time courses of H3.1K56ac and H3.3K56ac were investigated by Western blotting in H3.1- and H3.3-SNAP-tagged U2OS cells at 0, 2, 4, 8, 16, and 24 h after radiation. The acetylation levels of K27, K14, and K9 on histone H3.1 and H3.3 were measured at the same time points with the levels of SNAP-tagged H3.1 or H3.3 tested as the internal reference.

As shown in **Figures 1B, D**, the levels of H3.1K56ac, H3.1K27ac, and H3.1K9ac were decreased at the beginning after UV radiation, while the levels of H3.1K14ac were not significantly affected. The lowest acetylation level of H3.1K56 appeared at approximately 8 h after irradiation while the lowest H3.1K27ac and H3.1K9ac levels appeared at approximately 4 h after irradiation. After reaching the lowest point, the levels of H3.1K56ac and H3.1K9ac started increasing, which coincides with our previous study (16). The acetylation of H3.1K27 remained steady after reaching the lowest level until 24 h after radiation (**Figures 1B, D**). On the other hand, the acetylation levels of H3.3K56, H3.3K27, H3.3K14, and H3.3K9 were decreased by UV radiation, as shown in **Figures 1C, D**. The lowest H3.3K56ac and H3.3K9ac appeared 4–8 h after irradiation and then started to reverse, while the levels of H3.3K27ac and H3.3K14ac continued to decrease until 24 h after radiation.

Singular ATM Inhibitor or ATR Inhibitor Treatment Did Not Influence the Patterns of H3.1K56ac and H3.3K56ac After UV Radiation

To determine the influence of ATM and ATR on the acetylation of H3.1K56 and H3.3K56 after UV radiation, the ATM inhibitor Ku55933 (10 μM) and the ATR inhibitor VE-821 (10 μM) were used, respectively. Both H3.1- and H3.3-SNAP expressing U2OS cells were treated with inhibitors individually and cellular fractionation samples were collected at 0, 2, 4, 8, 16, and 24 h after 20 J/m^2 UV radiation. Histone acetylation was then examined in chromatin fractions.

After Ku55933 treatment, the levels of H3.1K9ac decreased continually until 24 h after UV radiation (**Figures 2A, C**). At the same time, the acetylation of H3.1K14 showed a decrease after radiation and the lowest level appeared at approximately 4 h after radiation. Then, the H3.1K14ac levels were restored and remained steady until 24 h (**Figures 2A, C**). Combined with Ku55933 and UV radiation treatment, levels of H3.1K27ac and H3.1K56ac were also decreased, while the patterns of H3.1K27ac and H3.1K56ac were the same as those in radiation samples from treated cells, which are shown in **Figures 1B, D**. The H3.1K27ac level has bottomed out at approximately 4 h after radiation and then remained steady at this level for 24 h. The lowest H3.1K56ac also appeared at approximately 4 h after UV irradiation and then the acetylation levels started rising and returned to normal levels at approximately 16 h after radiation and continued to rise slowly for 24 h (**Figures 2A, C**).

As shown in **Figures 2B, D**, in the ATM inhibitor Ku55933-treated SNAP-tagged H3.3 U2OS cells, the levels of H3.3K9ac, H3.3K14ac, H3.3K27ac, and H3.3K56ac all decreased after UV radiation. However, H3.3K14ac and H3.3K27ac transiently decreased at 2 h after radiation and quickly recovered. The decrease in H3.3K9ac also began 2 h after radiation, while the acetylation levels showed a slight increase at 4 h and then continued to decrease until 24 h after UV radiation. The acetylation of H3.3K56 decreased 2 h after radiation and then continued to slowly rise until 24 h after radiation. This pattern was quite similar in simple irradiated cells without the Ku55933 treatment.

In the ATR inhibitor VE-821-treated H3.1-SNAP-tagged U2OS cells, the levels of H3.1K9ac, H3.1K14ac, H3.1K27ac, and H3.1K56ac all decreased during the first 4 h after UV radiation. The levels of H3.1K9ac, H3.1K14ac, and H3.1K27ac

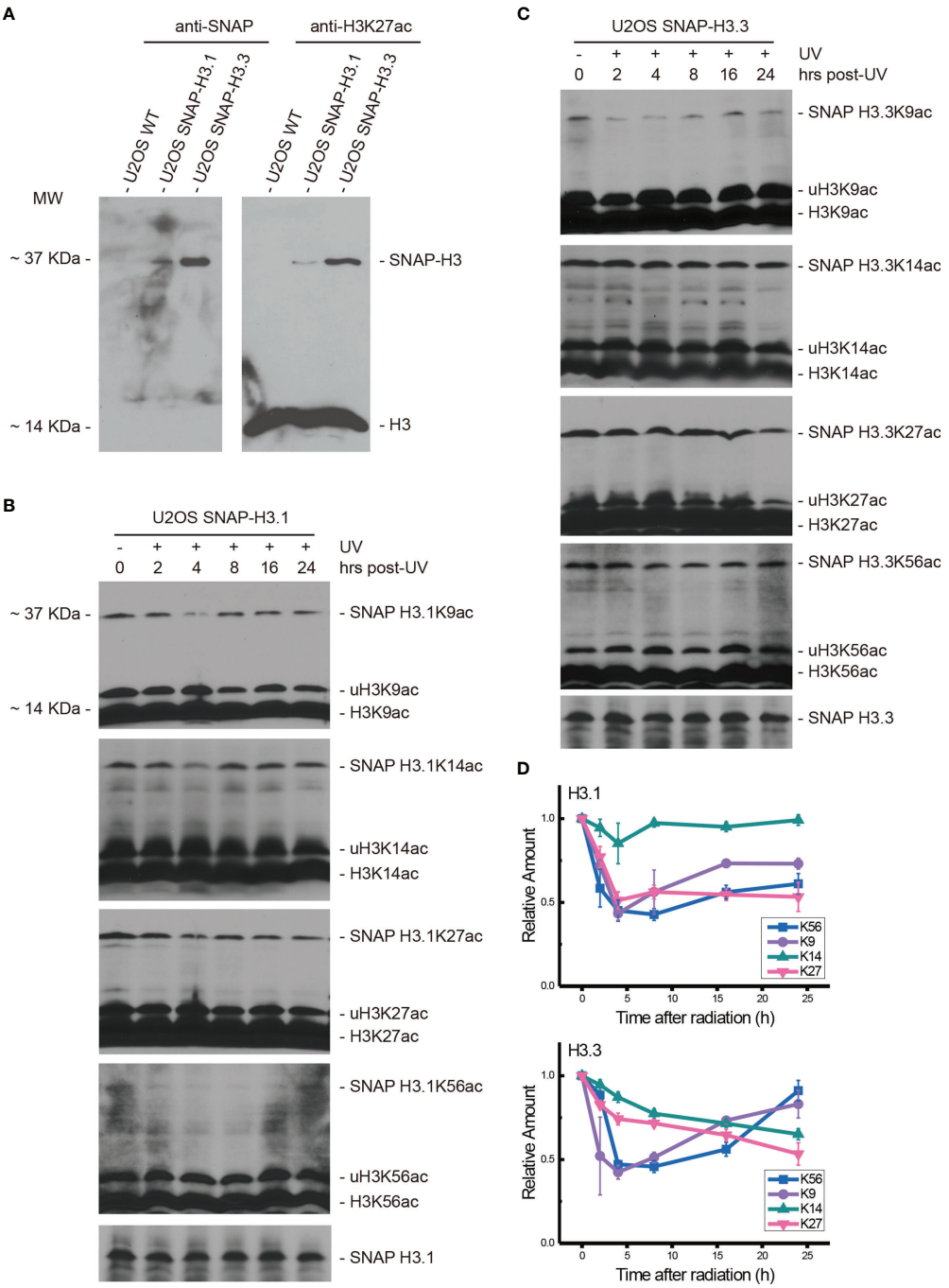

FIGURE 1 | Both H3.1K56ac and H3.3K56ac were transiently suppressed by UV radiation and restored following DNA damage repair. **(A)** SNAP-tagged histone H3.1 and H3.3 were investigated in wild-type U2OS cells and H3.1-SNAP U2OS and H3.3-SNAP U2OS cells by an anti-SNAP antibody and anti-H3K27ac antibody. Bands at approximately 37 kDa indicate SNAP-tagged histone H3 or SNAP-tagged lysine 27 acetylated histone H3, respectively. **(B)** H3.1-SNAP U2OS cells were treated with 20 J/m^2 UV radiation. The insoluble nuclear protein samples were collected at 0 h, 2 h, 4 h, 8 h, 16 h, and 24 h after radiation treatment. The acetylation levels of H3K9, H3K14, H3K27, and H3K56 were examined. SNAP-tagged histone H3 was used as an internal reference. **(C)** H3.3-SNAP U2OS cells were treated with 20 J/m^2 UV radiation. The insoluble nuclear protein samples were collected at different time points after radiation treatment. The acetylation levels of H3K9, H3K14, H3K27, and H3K56 were investigated, and SNAP-tagged histone H3 was used as an internal reference. **(D)** Time-course alteration of acetylated K9, K14, K27, and K56 of H3.1 or H3.3 after 20 J/m^2 UV radiation. The data are normalized immunoblotting results by ImageJ analysis from three separate experiments.

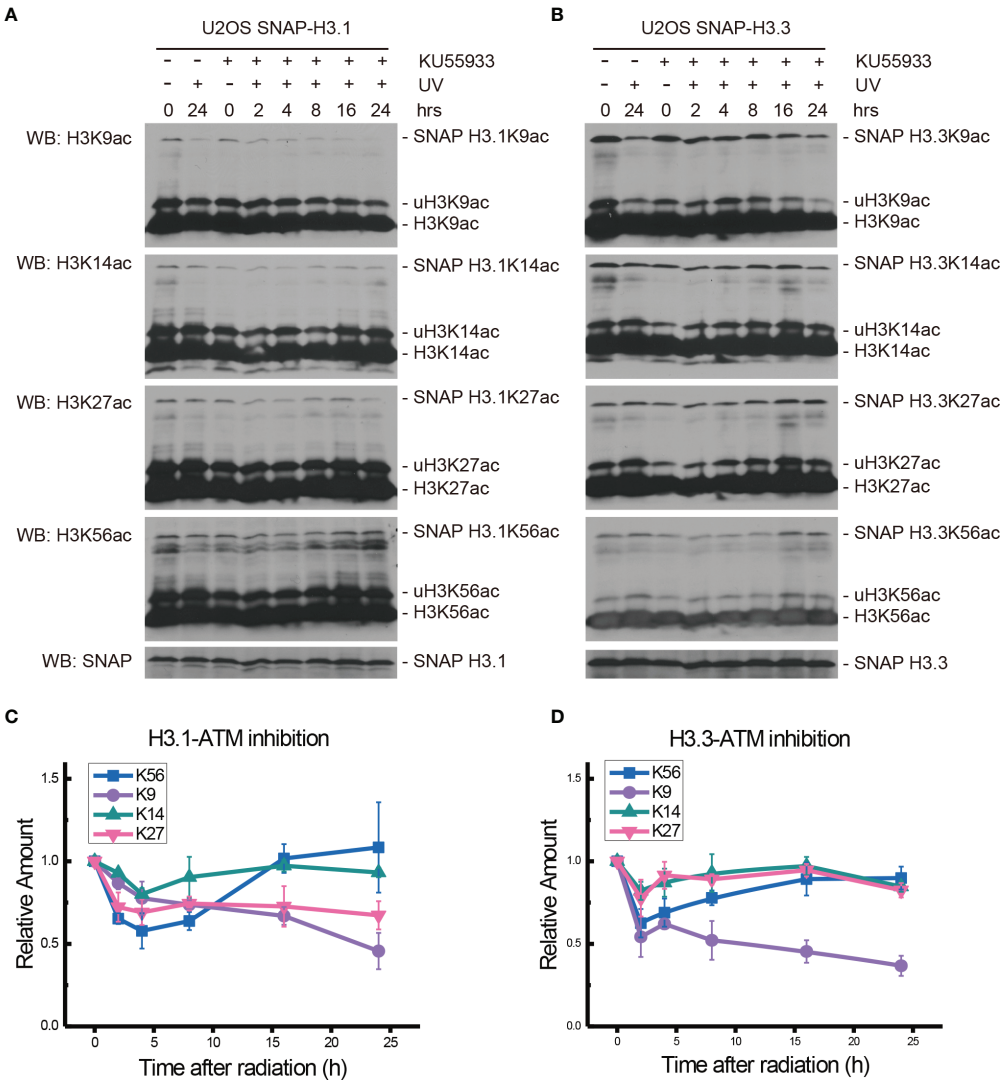

FIGURE 2 | Modulation of acetylated K9, K14, K27, and K56 of histone H3.1 or H3.3 by the ATM inhibitor KU55933 and UV radiation. **(A)** H3.1-SNAP U2OS cells were pretreated with DMSO (-) or KU55933 (+) for 1 h and then irradiated with 20 J/m^2 UV radiation. The insoluble nuclear protein samples were collected at 0 h, 2 h, 4 h, 8 h, 16 h, and 24 h after radiation. The acetylation levels of H3K9, H3K14, H3K27, and H3K56 were examined. SNAP-tagged histone H3 was used as an internal reference. **(B)** H3.3-SNAP U2OS cells were pretreated with DMSO or KU55933 and then irradiated with 20 J/m^2 UV radiation. The insoluble nuclear protein samples were collected, and the acetylation levels of H3K9, H3K14, H3K27, and H3K56 were examined. SNAP-tagged histone H3 was used as an internal reference. **(C)** Time-course alteration of acetylated K9, K14, K27, and K56 of histone H3.1 after 20 J/m^2 UV radiation and KU55933 treatment. The data are normalized immunoblotting results by ImageJ analysis from three separate experiments. **(D)** Time-course alteration of acetylated K9, K14, K27, and K56 of histone H3.3 after 20 J/m^2 UV radiation and KU55933 treatment. The data are normalized immunoblotting results by ImageJ analysis from three separate experiments.

continued to decrease until 24 h after UV radiation, while H3.1K56ac started to rise from 8 h to 24 h after radiation (**Figures 3A, C**).

As shown in **Figures 3B, D**, the levels of H3.3K9ac, H3.3K14ac, H3.3K27ac, and H3.3K56ac in VE-821 treated H3.3-SNAP-tagged U2OS cells all decreased at 2 h after UV radiation. After that, the levels of H3.3K14ac continued to decrease until 24 h while the acetylation of H3.3K9 and H3.3K27 showed a slight increase and then continued to decrease. On the other hand, the decrease in H3.3K56ac continued for 8 h and then started to rise until 24 h after radiation.

ATM and ATR Double Inhibition Suppressed the Restoration of H3.1K56ac and H3.3K56ac After UV Radiation

The ATM inhibitor Ku55933 and ATR inhibitor VE-821 were then used together to further probe the function of ATM and ATR in the acetylation of H3.1 and H3.3 in SNAP-tagged H3 U2OS cells. One hour after inhibitor pretreatment, cells were

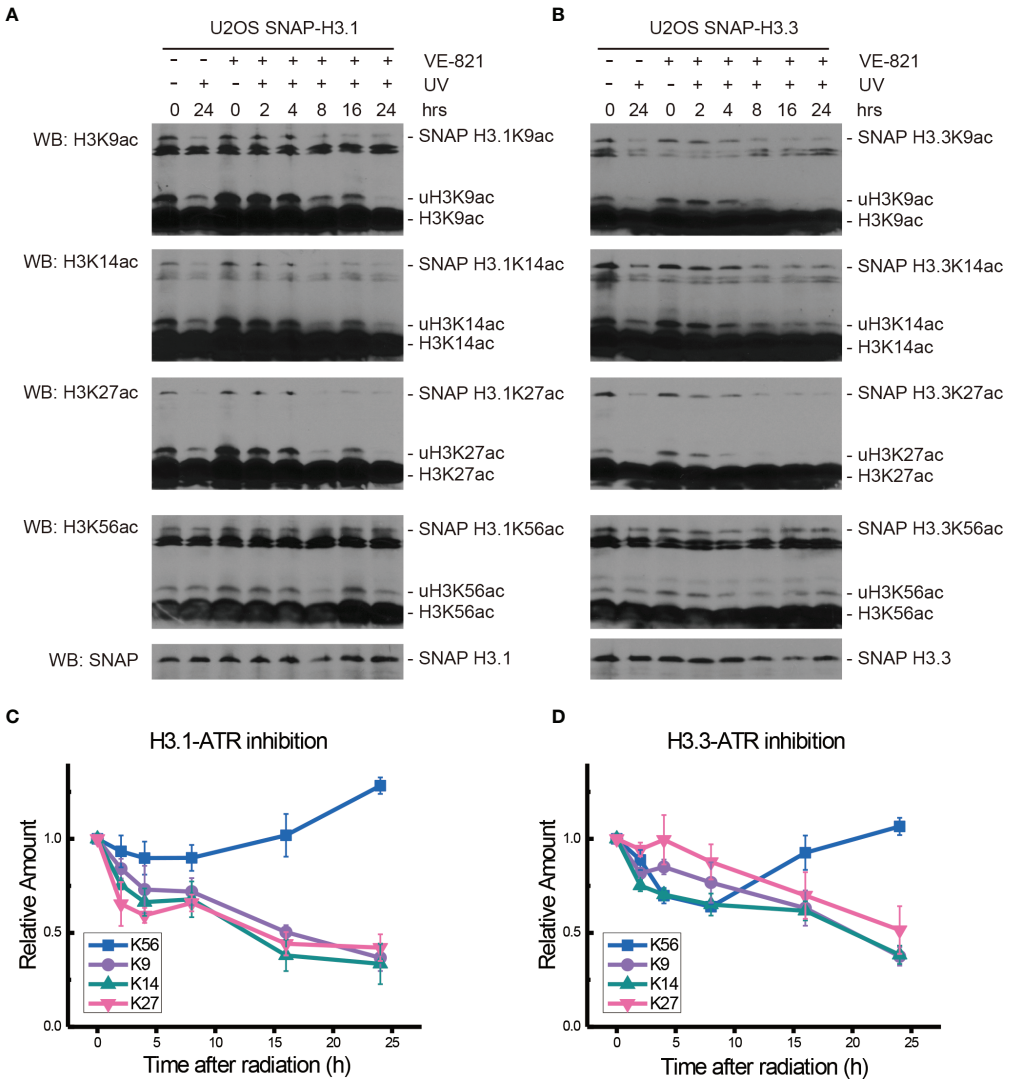

FIGURE 3 | Modulation of acetylated K9, K14, K27, and K56 of histone H3.1 or H3.3 by the ATR inhibitor VE-821 and UV radiation. **(A)** H3.1-SNAP U2OS cells were pretreated with DMSO (-) or VE-821 (+) for 1 h and then irradiated with 20 J/m^2 UV radiation. The insoluble nuclear protein samples were collected at 0 h, 2 h, 4 h, 8 h, 16 h, and 24 h after radiation. The acetylation levels of H3K9, H3K14, H3K27, and H3K56 were examined. SNAP-tagged histone H3 was used as an internal reference. **(B)** H3.3-SNAP U2OS cells were pretreated with DMSO or VE-821 and then irradiated with 20 J/m^2 UV radiation. The insoluble nuclear protein samples were collected, and the acetylation levels of H3K9, H3K14, H3K27, and H3K56 were examined. SNAP-tagged histone H3 was used as an internal reference. **(C)** Time-course alteration of acetylated K9, K14, K27, and K56 of histone H3.1 after 20 J/m^2 UV radiation and VE-821 treatment. The data are normalized immunoblotting results by ImageJ analysis from three separate experiments. **(D)** Time-course alteration of acetylated K9, K14, K27, and K56 of histone H3.3 after 20 J/m^2 UV radiation and VE-821 treatment. The data are normalized immunoblotting results by ImageJ analysis from three separate experiments.

irradiated with 20 J/m^2 UV and histone acetylation in U2OS cells was then examined in chromatin fractions.

As shown in **Figures 4A, C**, after double inhibitor treatment, the acetylation of H3.1K9, H3.1K14, H3.1K27, and H3.1K56 under UV radiation decreased for 4 h after radiation. The levels of H3.1K9ac increased at approximately 8 h after radiation and quickly decreased at 16 h after radiation. The levels of H3.1K14ac and H3.1K27ac also showed a slight increase at approximately 8 h after radiation and then continued to slowly decrease for 24 h. In contrast, the levels of H3.1K56ac continued to decrease for 24 h after UV radiation, and the recovery of H3.1K56ac was absent. As shown in **Figures 4B, D**, the levels of H3.3K9ac, H3.3K14ac, H3.3K27ac, and H3.3K56ac all decreased 2 h after a double inhibitor treatment plus UV radiation. After that, the levels of H3.3K9ac, H3.3K14ac, and H3.3K27ac continued to decrease slowly until 24 h after radiation. However, H3.3K56ac showed a short increase at 4 h after UV irradiation and then continued to decrease slowly for 24 h. The recovery of H3.3K56ac under double inhibition was again absent.

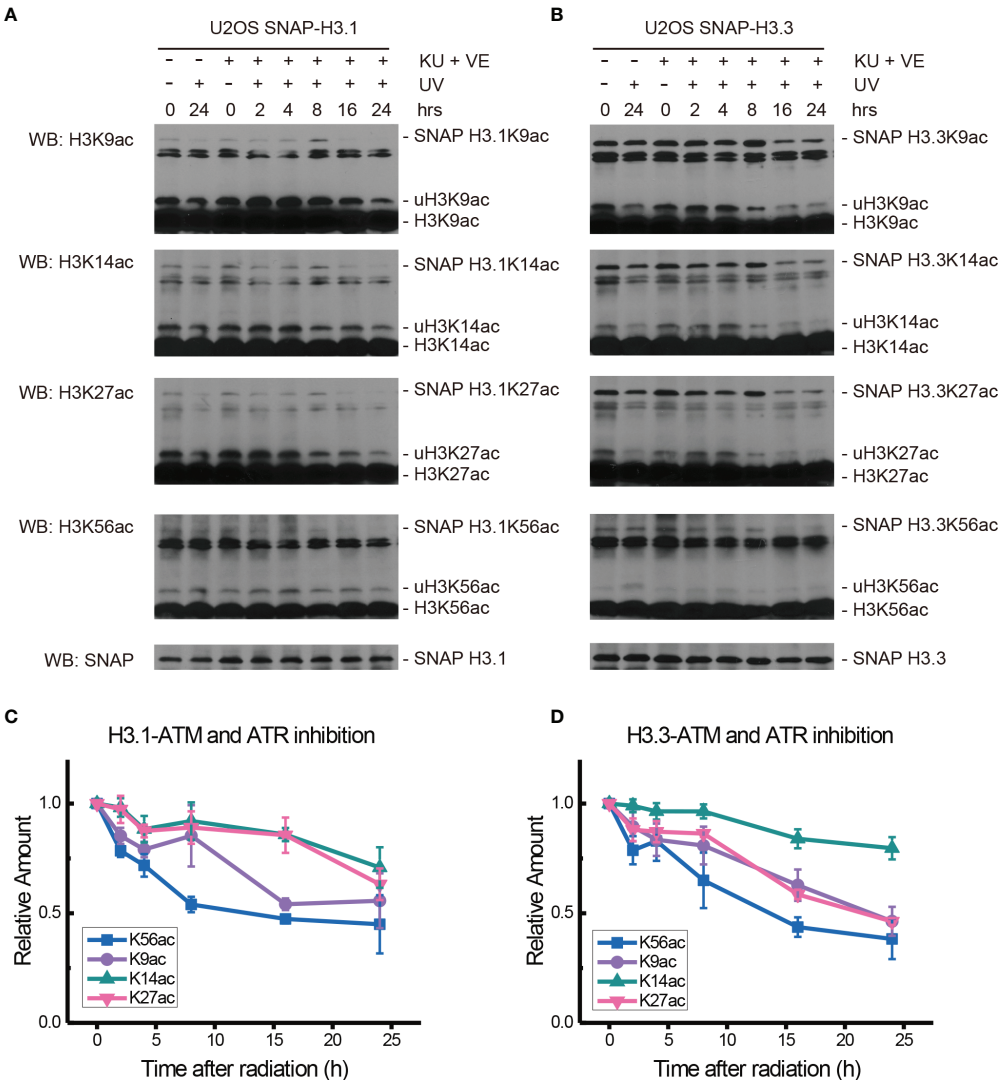

FIGURE 4 | Modulation of acetylated K9, K14, K27, and K56 of histone H3.1 or H3.3 by an ATM inhibitor, ATR inhibitor, and UV radiation. **(A)** H3.1-SNAP U2OS cells were pretreated with DMSO (-) or KU55933 and VE-821 (+) for 1 h and then irradiated with 20 J/m^2 UV radiation. The insoluble nuclear protein samples were collected at 0 h, 2 h, 4 h, 8 h, 16 h, and 24 h after radiation. The acetylation levels of H3K9, H3K14, H3K27, and H3K56 were examined. SNAP-tagged histone H3 was used as an internal reference. **(B)** H3.3-SNAP U2OS cells were pretreated with DMSO or two inhibitors and then irradiated with 20 J/m^2 UV radiation. The insoluble nuclear protein samples were collected, and the acetylation levels of H3K9, H3K14, H3K27, and H3K56 were examined. SNAP-tagged histone H3 was used as an internal reference. **(C)** Time-course alteration of acetylated K9, K14, K27, and K56 of histone H3.1 after 20 J/m^2 UV radiation and two inhibitor treatments. The data are normalized immunoblotting results by ImageJ analysis from three separate experiments. **(D)** Time-course alteration of acetylated K9, K14, K27, and K56 of histone H3.3 after 20 J/m^2 UV radiation and two inhibitor treatments. The data are normalized immunoblotting results by ImageJ analysis from three separate experiments.

Chk1 Inhibition Blocked the Restoration of H3.1K56ac and H3.3K56ac Levels After UV Radiation

To explore the possible effectors downstream of ATM and ATR, the Chk1 inhibitor MK8776 at 0.5 μM was added 2 h before 20 J/m^2 UV radiation, cellular fractionation samples were collected, and histone acetylation in chromatin fractions was again examined, as shown in **Figure 5**.

After MK8776 treatment and UV irradiation, the acetylation of H3.1K14, H3.1K27, and H3.1K56 all decreased remarkably, while the change in H3.1K9 was not obvious at 2 h after UV radiation (**Figures 5A, C**). The levels of H3.1K9, H3.1K27, and H3.1K56 sharply decreased at 4 h and then continued to decrease slowly until 24 h after radiation. The acetylation of H3.1K14 continued to decrease at 4 h and remained low until 24 h after UV radiation (**Figures 5A, C**). As shown in **Figures 5B, D**, the levels of H3.3K9ac and H3.3K56ac decreased while the levels of H3.3K14ac and H3.3K27ac increased at 1 h after UV radiation. Then, the levels of H3.3K27ac and H3.3K56ac continued to decrease for 24 h. The levels of H3.3K9ac experienced a short

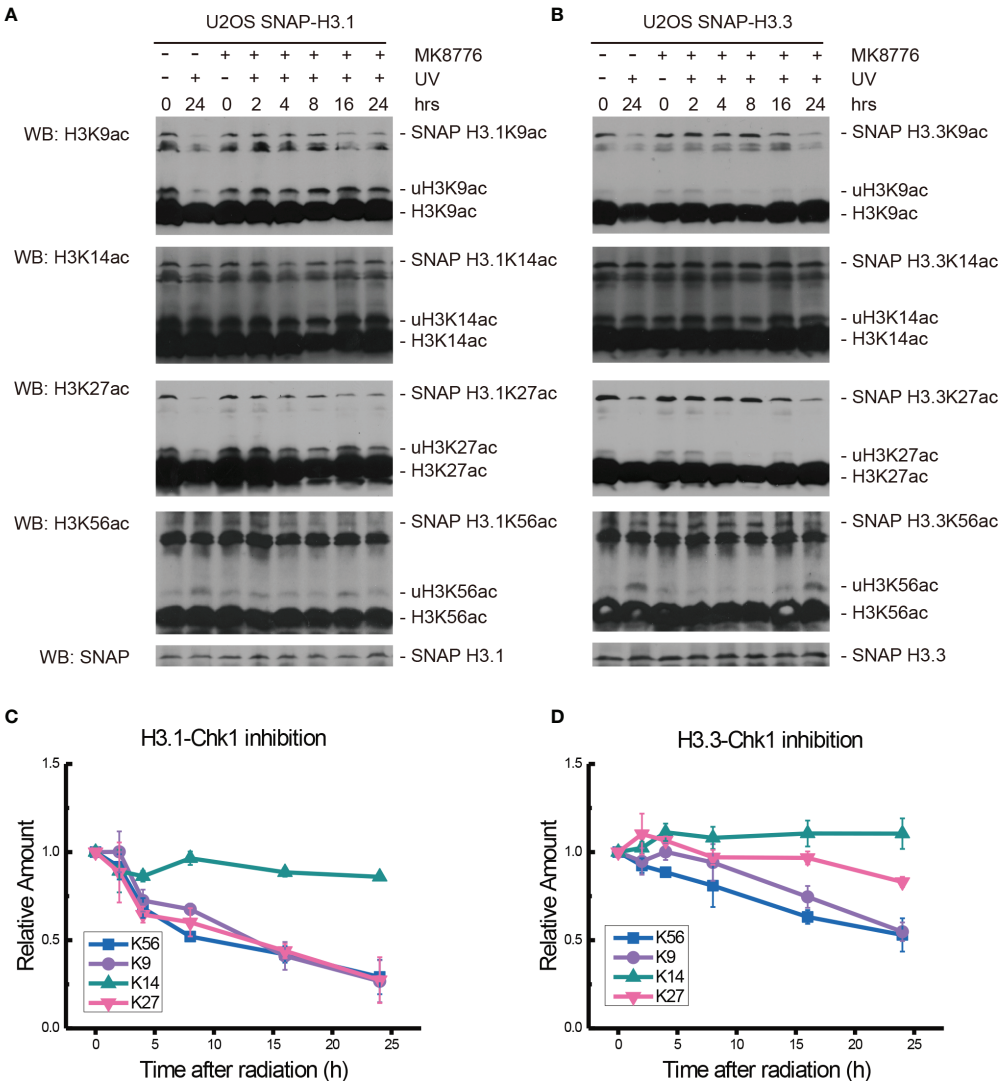

FIGURE 5 | Modulation of acetylated K9, K14, K27, and K56 of histone H3.1 or H3.3 by the Chk1 inhibitor MK8776 and UV radiation. **(A)** H3.1-SNAP U2OS cells were pretreated with DMSO (-) or MK8776 (+) for 1 h and then irradiated with 20 J/m^2 UV radiation. The insoluble nuclear protein samples were collected at 0 h, 2 h, 4 h, 8 h, 16 h, and 24 h after radiation. The acetylation levels of H3K9, H3K14, H3K27, and H3K56 were examined. SNAP-tagged histone H3 was used as an internal reference. **(B)** H3.3-SNAP U2OS cells were pretreated with DMSO or MK8776 and then irradiated with 20 J/m^2 UV radiation. The insoluble nuclear protein samples were collected, and the acetylation levels of H3K9, H3K14, H3K27, and H3K56 were examined. SNAP-tagged histone H3 was used as an internal reference. **(C)** Time-course alteration of acetylated K9, K14, K27, and K56 of histone H3.1 after 20 J/m^2 UV radiation and MK8776 treatment. The data are normalized immunoblotting results by ImageJ analysis from three separate experiments. **(D)** Time-course alteration of acetylated K9, K14, K27, and K56 of histone H3.3 after 20 J/m^2 UV radiation and MK8776 treatment. The data are normalized immunoblotting results by ImageJ analysis from three separate experiments.

increase at 4 h and then continued to decrease slowly for 24 h. The levels of H3.3K14ac increased slightly at 4 h and then remained steady until 24 h after UV radiation (**Figures 5B, D**).

While the individual ATM inhibition by Ku55933 or ATR inhibition by VE-821 did not suppress the restoration of histone H3K56 acetylation levels, both individual inhibitions indeed suppressed the decrease in H3.1K9ac, H3.3K9ac, H3.1K27ac, H3.3K27ac, H3.1K56ac, and H3.3K56ac after UV radiation, especially in the first 8 h after radiation (**Figure 6**). In contrast, Chk1 inhibition by MK8776 resulted in a decrease in acetylation at all tested sites. The acetylation levels were higher than those in cells without inhibitor treatment and the influence of MK8776 on H3.3 was more serious than that on H3.1. However, this phenomenon was not observed under the Ku55933 plus VE-821 treatment (**Figure 6**).

Chk1 Inhibition Results in Cellular Transcription Suppression

We further examined the influence of Chk1 inhibition on patterns in cellular gene expression during UV DNA damage repair.

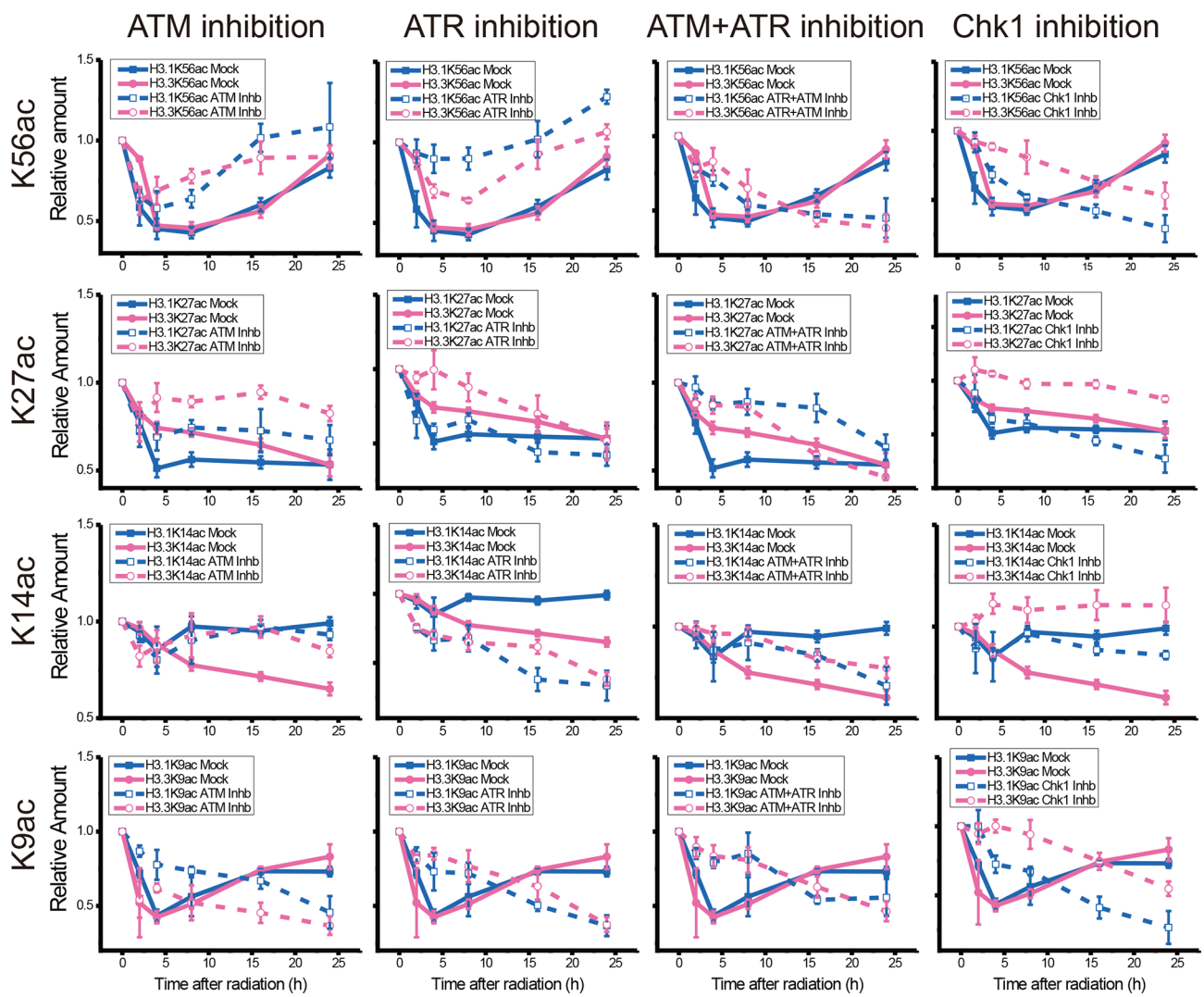

FIGURE 6 | Comparison of the acetylation levels of K9, K14, K27, and K56 of histone H3.1 and H3.3 in irradiated U2OS cells. For each acetylation site, the relative amounts of H3.1 and H3.3 acetylation before and after chemical treatment were compared separately.

The U2OS cells were pretreated with vehicle DMSO or the Chk1 inhibitor Ly2606368 at 10 nM 1 h before 20 J/m^2 UV radiation. At 2, 8, and 24 h after UV radiation, RNA samples were collected for RNA sequencing. Nineteen libraries were generated from our experimental groups (Sequencing ID: BMK190830-U285-0102), and summaries of the RNA sequencing analyses are shown in **Tables S1**, **S2**. More than 38,339,762 reads (from 38,339,762 to 50064758) were sequenced from each library, and more than 96.44% (from 96.44% to 97.38%) clean reads were unique reads, of which more than 89.79% (from 89.79% to 94.59%) reads were paired reads that mapped to the human genome.

There were 105 genes that were expressed in all 19 libraries. The relative expression levels of these 105 genes are listed in a heatmap (**Figure 7A** and **Table S3**). Compared with the controls, approximately two-thirds of the genes were upregulated at 2 h following UV radiation in both the DMSO-mock group and the Ly2606368-treated group. At 8 and 24 h, more genes were downregulated in the Ly2606368-treated group. However, expression resumed for more genes in the mock, and small sections of them were even upregulated at 8 h and 24 h. The numbers of upregulated or downregulated genes among these 105 genes were calculated (**Figure 7B**). Several genes with expression that increased at least two times showed little difference between the DMSO-mock group and the Ly2606368-treated group. When the threshold was extended to 1.5 times, the number of upregulated genes in the DMSO-mock group was slightly higher than that in the Ly2606368-treated group. On the other hand, there were more downregulated genes at the 8- and 24-h time points in the Ly2606368-treated group than in the DMSO-mock group under either 0.66- or 0.5-times threshold. The sequencing results were confirmed by qRT real-time PCR, and the trends of DNA repair- or translation-

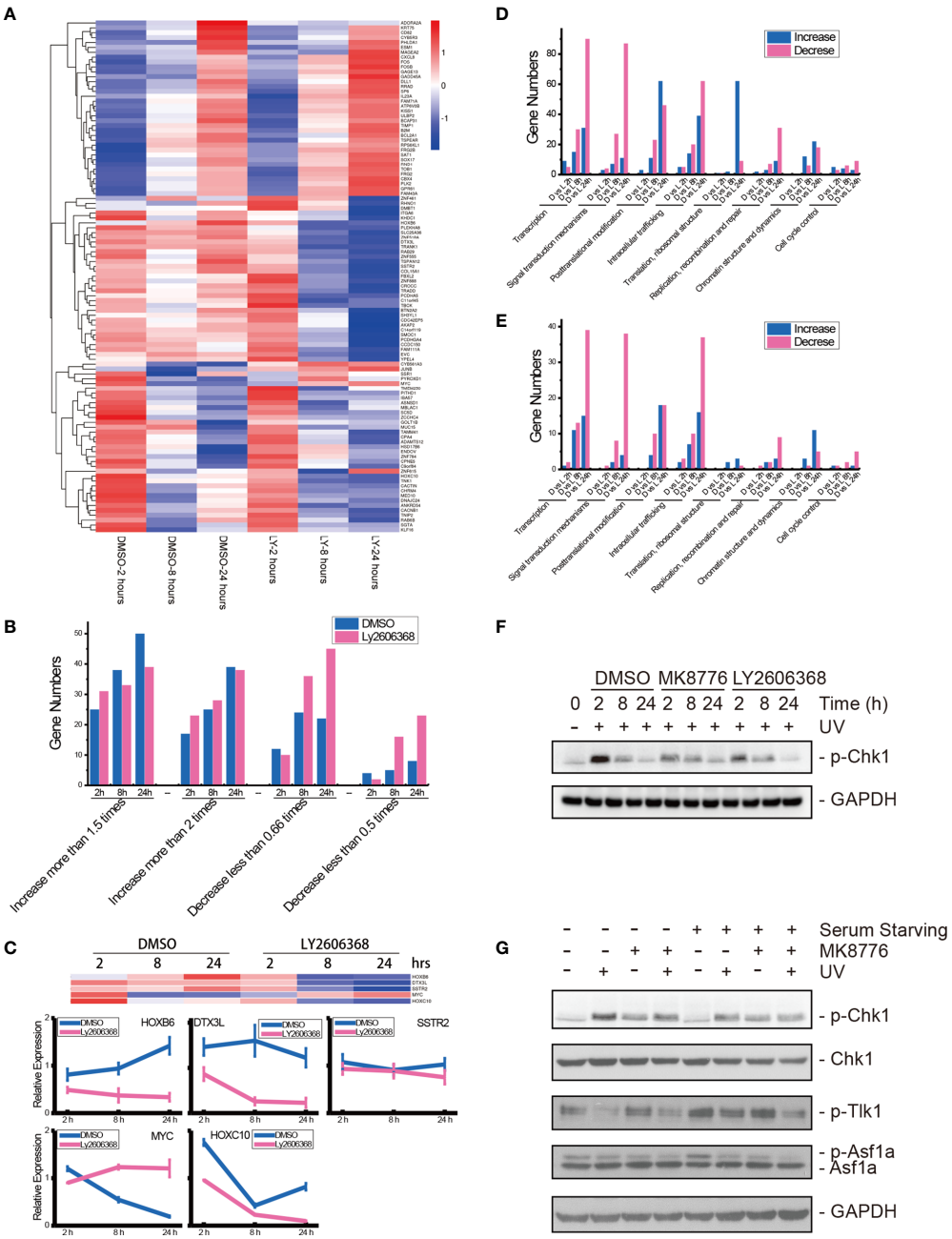

FIGURE 7 | mRNA sequencing of Chk1-inhibited samples after UV radiation and verification of Chk1 inhibition. **(A)** Heatmap visualization of 105 genes that were expressed in all libraries. Data are expressed as the mean FPKM, standardized, and visualized by the DESeq R package (version 1.18.0). Columns: samples; rows: genes; red: relatively high expression; blue: relatively low expression. DMSO: DMSO mock group; LY: Ly2606368 treated group; 2 hours: 2 h after UV radiation; 8 hours: 8 h after UV radiation; 24 hours: 24 h after UV radiation. **(B)** Calculations of differentially expressed genes in the 105 genes. **(C)** qRT-PCR results of HOXB6, DTX3L, SSTR2, MYC, and HOXC1 mRNA expression levels after DMSO or Ly2606368 treatment and UV radiation. **(D)** Numbers of changed genes after chemical treatment and UV radiation. At 2 h, 8 h, and 24 h after UV radiation and chemical treatment, the normalized gene expression of Ly2606368-treated U2OS cells and DMSO-mock U2OS cells was compared, and the numbers of differentially expressed genes classified by functional annotation are shown. **(E)** Numbers of genes that changed more than 2-fold after chemical treatment and UV radiation. The numbers of genes that increased more than 2-fold or decreased more than 0.5-fold were calculated. **(F)** Western blot detection of phosphorylated Chk1 after DMSO, MK8776, or Ly2606368 treatment after UV radiation. The data are normalized immunoblotting results by ImageJ analysis from three separate experiments. **(G)** Western blot detection of phosphorylated Chk1, Tlk-1, and Asf1a after DMSO or MK8776 treatment under serum starvation conditions and UV radiation. For the serum starvation experiment, U2OS cells were seeded and grown to 70% confluence, and then the medium was changed to serum-free DMEM for 24 h.

related genes such as HOXB6, DTX3L, SSTR2, MYC and HOXC10 were coincident with the mRNA sequencing results (**Figure 7C**).

We further compared the expression of genes in the Ly2606368-treated group with that in the DMSO-mock group at the same time point after UV radiation, and the number of differentially expressed genes (DEGs) was calculated and categorized by eggNOG class annotation (**Figures 7D, E** and **Table S4**). Analysis of the functional gene distribution showed that transcription-, signal transduction mechanism-, posttranslational modification-, and intracellular trafficking-related genes were the most common DEGs. The transcription-related DEGs were the most abundant, and there were 90 decreased and 30 increased genes in the Ly2606368-treated group as compared with the DMSO-mock group at 24 h, 30 decreased and 15 increased genes at 8 h, and 5 decreased and 9 increased genes at 2 h. The number of decreased genes at 24 h was the highest (**Figure 7D**). In addition, a significant change (log2 more than 1 or less than −1) was also detected in transcription-related DEGs, and among these DEGs, there were 39 decreased and 15 increased genes (**Figure 7E**). The second most abundant DEGs were signal transduction mechanism-related genes, and among them, the number of decreased genes was higher than increased genes in the Ly2606368-treated group compared with the DMSO mock group at all time points (**Figures 7D, E**).

The changing status of Chk1 activation after inhibitor treatment and the influence of the Chk1 inhibitor on Tlk1 and Asf1 were verified by Western blotting. The levels of phosphorylated Chk1 (p-Chk1) were significantly upregulated after UV radiation and declined gradually until 24 h after UV radiation and the levels of p-Chk1 were remarkably suppressed by two special Chk1 inhibitors, MK8776 and Ly2606368. In addition, the levels of Chk1 remained stable under the same treatments (**Figure 7F**). Additionally, when the activation of Chk1 was induced by UV radiation, the levels of p-Tlk1 were suppressed, as were the levels of p-Tlk1 and p-Asf1a. As expected, the inhibition of p-Chk1 by MK8776 resulted in the upregulation of p-Tlk1 and p-Asf1a (**Figure 7G**).

DISCUSSION

Since the discovery of the unique H3K56 acetylation pathway by genetic screening in budding yeast (12), the acetylation of H3K56 has become an increasingly important phenomenon for understanding the mechanisms of chromatin dynamics in various cellular processes, such as transcription, DNA replication, and DNA damage response. In this study, we investigated the regulation of acetylation restoration at the 56 lysine residues of both histone H3.1 and H3.3 by ATM, ATR, and Chk1 after UV radiation. According to our results, neither ATM nor ATR inhibition is capable of fully suppressing the restoration of either H3.1K56ac or H3.3K56ac after UV radiation. However, the Chk1 inhibition is abundant to suppress the restoration. Furthermore, total genome transcription was suppressed, and the expression of transcription-related genes was decreased by Chk1 inhibition. Given that ATM, ATR, and Chk1 are not directly involved in nucleotide excision repair of UV-induced DNA photolesions, our data suggest the key function of Chk1 in histone PTMs, chromatin dynamics and transcription regulation and recovery during DNA damage repair.

A large body of studies has revealed that histone acetylation, in addition to its role in transcriptional regulation, belongs to a broad repertoire of histone modifications involved in the DDR (14, 16, 29, 30). We and others have reported that H3K9ac and H3K56ac are highly responsive to DNA damage and repair (14, 16). Both H3K9ac and H3K56ac are rapidly and reversibly reduced after DNA damage, including UV radiation, ionizing radiation, and phleomycin. Furthermore, both histone H3.3 and H3.1 variants have been observed to be recruited to sites of DSB and UV damage (26, 31, 32). These findings revealed the participation of K9ac and K56ac of both H3.1 and H3.3 in nucleosome disassembly and reassembly during UV damage repair. As expected, we detected a rapid decrease and gradual restoration of H3.1K9ac, H3.3K9ac, H3.1K56ac, and H3.3K56ac after UV radiation (**Figure 1**). Our data confirmed that both H3.1-associated DNA synthesis-dependent and H3.3-associated DNA synthesis-independent but transcription-dependent chromatin dynamics occur during UV damage repair. Our data further revealed that both H3.1 and H3.3 are regulated by acetylation, and the latter are further controlled by Chk1 and by ATM and ATR kinases, upstream of Chk1, in a redundant manner.

It has been reported that DNA damage triggers a decrease in cellular H3K27ac levels (33) or induces an enrichment of H3K27ac at specific promoter regions (34). Accordingly, our data showed that the levels of both H3.1K27ac and H3.3K27ac decreased after UV radiation. H3K14ac is a non-DNA damage-responsive histone modification (14). Our results (**Figure 1**) showed that the levels of H3.1K14ac were steady after radiation while the levels of H3.3K14ac slightly decreased. However, it remains unclear whether such a subtle change is related to transcription-related chromatin dynamics. Taken together, our data verified the decrease and restoration of H3K56ac and H3K9ac after UV radiation. Our SNAP-based H3.1 and H3.3 PTMs detection system faithfully uncovered the changes in histone acetylation in these H3 variants and the possible regulation of acetylation by checkpoint kinases.

It is generally recognized that H3K56ac incorporation into repaired chromatin signals the completion of DNA repair as well as termination of checkpoint signaling activation. To relate H3.1 and H3.3 acetylation to these events, we examined the effect of kinase inhibition on H3 acetylation using the ATM inhibitor KU55933, ATR inhibitor VE-821, ATM and ATR inhibitor AZD6738, Chk1 inhibitor UCN-01, MK8776, Ly2606368, and Chk1 and Chk2 inhibitor AZD7762. In our experiments (**Figures 2–5** and summary **Figure 6**), the restoration of both H3.1K56ac and H3.3K56ac was not hindered by single ATM or ATR inhibition, while the ATM–ATR dual inhibition and Chk1 inhibition successfully suppressed the H3K56Ac restoration.

Chk1 is conventionally phosphorylated and activated by ATR, which is recruited by RPA-coated single-stranded DNA, and Chk1 acts downstream. ATM, however, is phosphorylated and activated by single DNA breaks, and Chk2 acts downstream of ATM upon single- and double-DNA breaks. However, Cep164 is phosphorylated by ATR/ATM both *in vivo* and *in vitro* which can induce phosphorylation of Chk1 upon replication stress and radiation (35). Our results suggest that Chk1 is a converging point through which ATM and ATR redundantly regulate the restoration of H3K56ac.

DNA damage is known to induce the rapid transcriptional repression and activation of a variety of genes related to cell cycle arrest, DNA damage repair, senescence, and apoptosis; Chk1 was reported to influence histone posttranslational modifications. For instance, Chk1 is responsible for the phosphorylation of H3T11 as the kinase that suppresses gene transcription following DNA damage *in vitro* (36). In our study, when the UV radiation-induced activation of Chk1 was suppressed by Ly2606368, the downregulation of gene expression was slow but continuous, especially at 24 h after treatment (**Figure 7**). Importantly, the largest group of downregulated genes were transcription-related genes (**Figures 7D, E**). These data revealed that Chk1 inhibition aggravated the inhibition of transcription related to cell cycle recovery. Moreover, UV radiation induced a rapid decrease in *c-myc* expression and then increased until 24 h after UV radiation, while Ly2606368 plus UV treatment strongly induced a decrease in *c-myc* expression. The data coincided with an earlier report that revealed the function of Ly2606368 in the suppression of both Chk1 and *c-myc* activity (37).

Taken together, the results of the present study identified Chk1 as an important histone H3K56 acetylation regulator during the DDR, by regulating the restoration of both H3.1K56ac and H3.3K56ac. More in-depth future studies to gain informative insights into how Chk1, Tlk1, and Asf1a interact with each other and function in histone PTMs would further clarify the mechanistic nature of these complex interactions in DNA damage processing.

DATA AVAILABILITY STATEMENT

The datasets presented in this study can be found in online repositories. The names of the repository/repositories and accession number(s) can be found in the article/**Supplementary Material**.

AUTHOR CONTRIBUTIONS

ND and QZ participated in the design of this study. ND, ZS, FY, and PQ conducted the experiments and analyzed and interpreted the data in this study. PL and DL performed statistical analysis. JW and QZ collected the background information. ND drafted the manuscript. ND, JW, and QZ provided funding support. All authors contributed to the article and approved the submitted version.

FUNDING

This research was funded by the National Institute of Health of the USA (no. ES012991, QZ), the National Natural Science Foundation of China (no. U1932208, Kai Yang), the Science and Technology Research Project of Gansu Province (no. 17JR5RA307 and 145RTSA012, JW), and the Science and Technology Research Project of Gansu Province (no. 21JR7RA108, ND).

ACKNOWLEDGMENTS

H3.1 SNAP-labeled U2OS cells and H3.3 SNAP-labeled U2OS cells were gifts from Dr. Gray H Karpen's lab in the Lawrence Berkeley National Laboratory, Berkeley, CA. We would like to thank the Heavy Ion Research Facility in Lanzhou (HIRFL) for their support. We also want to thank the biomedical platform of the Public Technical Service Center, Institute of Modern Physics, Chinese Academy of Sciences for experimental support.

SUPPLEMENTARY MATERIAL

The Supplementary Material for this article can be found online at: https://www.frontiersin.org/articles/10.3389/fonc.2022.862592/full#supplementary-material

Supplementary Table 1 | Sequencing summary of all samples.

Supplementary Table 2 | Normalized reads of detected genes in each sample.

Supplementary Table 3 | Fold changes in genes detected in all samples.

Supplementary Table 4 | Relative expression of genes at 2 h, 8 h, and 24 h after radiation.

REFERENCES

1. Ciccia A, Elledge SJ. The DNA Damage Response: Making It Safe to Play With Knives. *Mol Cell* (2010) 40:179–204. doi: 10.1016/j.molcel.2010.09.019
2. Mladenov E, Fan X, Dueva R, Soni A, Iliakis G. Radiation-Dose-Dependent Functional Synergisms Between ATM, ATR and DNA-PKcs in Checkpoint Control and Resection in G2-Phase. *Sci Rep* (2019) 9:8255. doi: 10.1038/s41598-019-44771-6
3. Sancar A, Lindsey-Boltz LA, Unsal-Kacmaz K, Linn S. Molecular Mechanisms of Mammalian DNA Repair and the DNA Damage Checkpoints. *Annu Rev Biochem* (2004) 73:39–85. doi: 10.1146/annurev.biochem.73.011303.073723
4. Zhao H, Piwnica-Worms H. ATR-Mediated Checkpoint Pathways Regulate Phosphorylation and Activation of Human Chk1. *Mol Cell Biol* (2001) 21:4129–39. doi: 10.1128/MCB.21.13.4129-4139.2001
5. Cheng YC, Shieh SY. Deubiquitinating Enzyme USP3 Controls CHK1 Chromatin Association and Activation. *Proc Natl Acad Sci USA* (2018) 115:5546–51. doi: 10.1073/pnas.1719856115
6. Ruthenburg AJ, Li H, Patel DJ, Allis CD. Multivalent Engagement of Chromatin Modifications by Linked Binding Modules. *Nat Rev Mol Cell Biol* (2007) 8:983–94. doi: 10.1038/nrm2298
7. Bryant L, Li D, Cox SG, Marchione D, Joiner EF, Wilson K, et al. Histone H3.3 Beyond Cancer: Germline Mutations in Histone 3 Family 3A and 3B Cause a Previously Unidentified Neurodegenerative Disorder in 46 Patients. *Sci Adv* (2020) 6(49). doi: 10.1126/sciadv.abc9207

8. Han J, Zhou H, Horazdovsky B, Zhang K, Xu RM, Zhang Z. Rtt109 Acetylates Histone H3 Lysine 56 and Functions in DNA Replication. *Science* (2007) 315:653–5. doi: 10.1126/science.1133234
9. Chen CC, Carson JJ, Feser J, Tamburini B, Zabaronick S, Linger J, et al. Acetylated Lysine 56 on Histone H3 Drives Chromatin Assembly After Repair and Signals for the Completion of Repair. *Cell* (2008) 134:231–43. doi: 10.1016/j.cell.2008.06.035
10. Simoneau A, Ricard E, Weber S, Hammond-Martel I, Wong LH, Sellam A, et al. Chromosome-Wide Histone Deacetylation by Sirtuins Prevents Hyperactivation of DNA Damage-Induced Signaling Upon Replicative Stress. *Nucleic Acids Res* (2016) 44:2706–26. doi: 10.1093/nar/gkv1537
11. Das C, Lucia MS, Hansen KC, Tyler JK. CBP/p300-Mediated Acetylation of Histone H3 on Lysine 56. *Nature* (2009) 459:113–7. doi: 10.1038/nature07861
12. Masumoto H, Hawke D, Kobayashi R, Verreault A. A Role for Cell-Cycle-Regulated Histone H3 Lysine 56 Acetylation in the DNA Damage Response. *Nature* (2005) 436:294–8. doi: 10.1038/nature03714
13. Polo SE. Reshaping Chromatin After DNA Damage: The Choreography of Histone Proteins. *J Mol Biol* (2015) 427:626–36. doi: 10.1016/j.jmb.2014.05.025
14. Tjeertes JV, Miller KM, Jackson SP. Screen for DNA-Damage-Responsive Histone Modifications Identifies H3K9Ac and H3K56Ac in Human Cells. *EMBO J* (2009) 28:1878–89. doi: 10.1038/emboj.2009.119
15. Zhu Q, Battu A, Ray A, Wani G, Qian J, He J, et al. Damaged DNA-Binding Protein Down-Regulates Epigenetic Mark H3K56Ac Through Histone Deacetylase 1 and 2. *Mutat Res* (2015) 776:16–23. doi: 10.1016/j.mrfmmm.2015.01.005
16. Zhu Q, Wei S, Sharma N, Wani G, He J, Wani AA, et al. Human CRL4(DDB2) Ubiquitin Ligase Preferentially Regulates Post-Repair Chromatin Restoration of H3K56Ac Through Recruitment of Histone Chaperon CAF-1. *Oncotarget* (2017) 8:104525–42. doi: 10.18632/oncotarget.21869
17. Wurtele H, Kaiser GS, Bacal J, St-Hilaire E, Lee EH, Tsao S, et al. Histone H3 Lysine 56 Acetylation and the Response to DNA Replication Fork Damage. *Mol Cell Biol* (2012) 32:154–72. doi: 10.1128/MCB.05415-11
18. Zhang L, Serra-Cardona A, Zhou H, Wang M, Yang N, Zhang Z, et al. Multisite Substrate Recognition in Asf1-Dependent Acetylation of Histone H3 K56 by Rtt109. *Cell* (2018) 174:818–30.e811. doi: 10.1016/j.cell.2018.07.005
19. Sillje HH, Nigg EA. Identification of Human Asf1 Chromatin Assembly Factors as Substrates of Tousled-Like Kinases. *Curr Biol* (2001) 11:1068–73. doi: 10.1016/S0960-9822(01)00298-6
20. Carrera P, Moshkin YM, Gronke S, Sillje HH, Nigg EA, Jackle H, et al. Tousled-Like Kinase Functions With the Chromatin Assembly Pathway Regulating Nuclear Divisions. *Genes Dev* (2003) 17:2578–90. doi: 10.1101/gad.276703
21. Klimovskaia IM, Young C, Stromme CB, Menard P, Jasencakova Z, Mejlvang J, et al. Tousled-Like Kinases Phosphorylate Asf1 to Promote Histone Supply During DNA Replication. *Nat Commun* (2014) 5:3394. doi: 10.1038/ncomms4394
22. Groth A, Lukas J, Nigg EA, Sillje HH, Wernstedt C, Bartek J, et al. Human Tousled Like Kinases Are Targeted by an ATM- and Chk1-Dependent DNA Damage Checkpoint. *EMBO J* (2003) 22:1676–87. doi: 10.1093/emboj/cdg151
23. Krause DR, Jonnalagadda JC, Gatei MH, Sillje HH, Zhou BB, Nigg EA, et al. Suppression of Tousled-Like Kinase Activity After DNA Damage or Replication Block Requires ATM, NBS1 and Chk1. *Oncogene* (2003) 22:5927–37. doi: 10.1038/sj.onc.1206691
24. Talbert PB, Henikoff S. Histone Variants–Ancient Wrap Artists of the Epigenome. *Nat Rev Mol Cell Biol* (2010) 11:264–75. doi: 10.1038/nrm2861
25. Scott WA, Campos EI. Interactions With Histone H3 & Tools to Study Them. *Front Cell Dev Biol* (2020) 8:701. doi: 10.3389/fcell.2020.00701
26. Adam S, Polo SE, Almouzni G. Transcription Recovery After DNA Damage Requires Chromatin Priming by the H3.3 Histone Chaperone HIRA. *Cell* (2013) 155:94–106. doi: 10.1016/j.cell.2013.08.029
27. Dunleavy EM, Almouzni G, Karpen GH. H3.3 Is Deposited at Centromeres in S Phase as a Placeholder for Newly Assembled CENP-A in G(1) Phase. *Nucleus-Phila* (2011) 2:146–57. doi: 10.4161/nucl.2.2.15211
28. Anindya R, Aygun O, Svejstrup JQ. Damage-Induced Ubiquitylation of Human RNA Polymerase II by the Ubiquitin Ligase Nedd4, But Not Cockayne Syndrome Proteins or BRCA1. *Mol Cell* (2007) 28:386–97. doi: 10.1016/j.molcel.2007.10.008
29. Ozdemir A, Spicuglia S, Lasonder E, Vermeulen M, Campsteijn C, Stunnenberg HG, et al. Characterization of Lysine 56 of Histone H3 as an Acetylation Site in Saccharomyces Cerevisiae. *J Biol Chem* (2005) 280:25949–52. doi: 10.1074/jbc.C500181200
30. Simoneau A, Delgoshaie N, Celic I, Dai J, Abshiru N, Costantino S, et al. Interplay Between Histone H3 Lysine 56 Deacetylation and Chromatin Modifiers in Response to DNA Damage. *Genetics* (2015) 200:185–205. doi: 10.1534/genetics.115.175919
31. Luijsterburg MS, de Krijger I, Wiegant WW, Shah RG, Smeenk G, de Groot AJL, et al. PARP1 Links CHD2-Mediated Chromatin Expansion and H3.3 Deposition to DNA Repair by Non-Homologous End-Joining. *Mol Cell* (2016) 61:547–62. doi: 10.1016/j.molcel.2016.01.019
32. Li X, Tyler JK. Nucleosome Disassembly During Human Non-Homologous End Joining Followed by Concerted HIRA- and CAF-1-Dependent Reassembly. *Elife* (2016) 5. doi: 10.7554/eLife.15129
33. Escarda-Castro E, Herraez MP, Lombo M. Effects of Bisphenol A Exposure During Cardiac Cell Differentiation. *Environ Pollut* (2021) 286:117567. doi: 10.1016/j.envpol.2021.117567
34. Wang J, Sun Y, Zhang X, Cai H, Zhang C, Qu H, et al. Oxidative Stress Activates NORAD Expression by H3K27ac and Promotes Oxaliplatin Resistance in Gastric Cancer by Enhancing Autophagy Flux *via* Targeting the miR-433-3p. *Cell Death Dis* (2021) 12:90. doi: 10.1038/s41419-020-03368-y
35. Sivasubramaniam S, Sun XM, Pan YR, Wang SH, Lee EYHP. Cep164 is a Mediator Protein Required for the Maintenance of Genomic Stability Through Modulation of MDC1, RPA, and CHK1. *Gene Dev* (2008) 22:587–600. doi: 10.1101/gad.1627708
36. Shimada M, Niida H, Zineldeen DH, Tagami H, Tanaka M, Saito H, et al. Chk1 is a Histone H3 Threonine 11 Kinase That Regulates DNA Damage-Induced Transcriptional Repression. *Cell* (2008) 132:221–32. doi: 10.1016/j.cell.2007.12.013
37. Sen T, Tong P, Stewart CA, Cristea S, Valliani A, Shames DS, et al. CHK1 Inhibition in Small-Cell Lung Cancer Produces Single-Agent Activity in Biomarker-Defined Disease Subsets and Combination Activity With Cisplatin or Olaparib. *Cancer Res* (2017) 77:3870–84. doi: 10.1158/0008-5472.CAN-16-3409

Conflict of Interest: The authors declare that the research was conducted in the absence of any commercial or financial relationships that could be construed as a potential conflict of interest.

Advantages of publishing in Frontiers

OPEN ACCESS
Articles are free to read for greatest visibility and readership

FAST PUBLICATION
Around 90 days from submission to decision

HIGH QUALITY PEER-REVIEW
Rigorous, collaborative, and constructive peer-review

TRANSPARENT PEER-REVIEW
Editors and reviewers acknowledged by name on published articles

Frontiers
Avenue du Tribunal-Fédéral 34
1005 Lausanne | Switzerland

Visit us: www.frontiersin.org
Contact us: frontiersin.org/about/contact

REPRODUCIBILITY OF RESEARCH
Support open data and methods to enhance research reproducibility

DIGITAL PUBLISHING
Articles designed for optimal readership across devices

FOLLOW US
@frontiersin

IMPACT METRICS
Advanced article metrics track visibility across digital media

EXTENSIVE PROMOTION
Marketing and promotion of impactful research

LOOP RESEARCH NETWORK
Our network increases your article's readership